LIST OF EFFECTIVE PAGES

CHAPTER 4

REACTOR

Page	Amendment	Page	Amendment
4-1	30	4.2-17	0
4-2	30	4.2-18	0
4-3	30	4.2-19	0
4-4	30	4.2-20	0
4-5	30	4.2-21	25
		4.2-22	25
4-i	30	4.2-23	22
4-ia	28	4.2-24	0
4-ii	28	4.2-25	0
4-iii	26	4.2-26	25
4-iv	30	4.2-27	0
4-v	28	4.2-28	26
4-vi	22	4.2-29	26
4-vii	30	4.2-30	26
4-viia	30	4.2-31	26
4-viii	22	4.2-32	26
4-ix	0	4.2-32a	22
4-x	22	4.2-33	22
4-xi	28	4.2-33a	25
4-xii	22	4.2-34	22
4-xiii	22	4.2-35	25
		4.2-36	30
4.1-1	30	4.2-37	30
4.1-2	22	4.2-38	20
4.1-3	26	4.2-39	0
4.1-4	30	4.2-40	25
4.1-5	26	4.2-41	28
4.1-5a	27	4.2-42	22
4.1-6	25	4.2-43	22
4.1-7	0	4.2-44	8
4.1-8	28	4.2-45	25
		4.2-46	26
F4.1-1	22	4.2-47	26
F4.1-2	3	4.2-48	30
		4.2-49	25
4.2-1	30	4.2-50	25
4.2-1a	7	4.2-51	0
4.2-2	22	4.2-52	30
4.2-3	22	4.2-53	0
4.2-4	25	4.2-54	23
4.2-5	25	4.2-55	23
4.2-6	22	4.2-56	25
4.2-7	23	4.2-57	21
4.2-8	17	4.2-58	25
4.2-9	25	4.2-59	25
4.2-10	0	4.2-60	21
4.2-11	25	4.2-60a	30
4.2-12	16	4.2-60aa	30
4.2-13	0	4.2-60b	30
4.2-14	0	4.2-60c	26
4.2-15	0	4.2-60d	30
4.2-16	0	4.2-60e	30

Page	Amendment
4.2-60f	30
4.2-60g	27
4.2-60h	26
4.2-60i	26
4.2-60j	26
4.2-60k	30
4.2-60l	27
4.2-60m	30
4.2-60n	30
4.2-60o	27
4.2-61	16
4.2-62	15
4.2-63	16
4.2-64	3
4.2-65	0
4.2-66	22
4.2-67	0
4.2-68	0
4.2-69	22
4.2-70	30
4.2-71	22
4.2-72	27
4.2-73	27
4.2-74	27
4.2-75	30
4.2-75a	30
F4.2-1	3
F4.2-1A	3
F4.2-2	10
F4.2-3	3
F4.2-4	3
F4.2-5	3
F4.2-5A	0
F4.2-5B	0
F4.2-5C	0
F4.2-5D	0
F4.2-5E	0
F4.2-6	3
F4.2-7	26
F4.2-8	0
F4.2-9	0
F4.2-10	26
F4.2-11	22
F4.2-12	16
F4.2-13	25
F4.2-14	0
F4.2-15A	26
F4.2-15B	26
F4.2-15C	26
F4.2-16a	17
F4.2-16B	21
F4.2-16c	10
F4.2-16d	10
F4.2-16e	25
F4.2-17	0
F4.2-17A	0
F4.2-17B	0
F4.2-17C	0
F4.2-17D	0
F4.2-17E	0
F4.2-17F	0
F4.2-18	30
F4.2-19	30
F4.2-20	30
F4.2-21	30
F4.2-22	30
F4.2-23	30
F4.2-24	30
4.3-1	28
4.3-2	0
4.3-3	27
4.3-3a	28
4.3-3b	28
4.3-4	22
4.3-5	26
4.3-6	25
4.3-7	0
4.3-8	24
4.3-9	25
4.3-9a	4
4.3-10	4
4.3-11	25
4.3-12	25
4.3-13	27
4.3-14	0
4.3-15	22
4.3-16	25
4.3-17	25
4.3-18	26
4.3-19	22
4.3-20	26
4.3-21	22
4.3-22	29
4.3-23	22
4.3-23a	4
4.3-24	22
4.3-25	22
4.3-26	22
4.3-27	22
4.3-28	22
4.3-29	25

Page	Amendment
4.3-30	25
4.3-31	26
4.3-31a	29
4.3-32	3
4.3-33	4
4.3-34	0
4.3-35	0
4.3-36	25
4.3-37	0
4.3-38	22
4.3-39	22
4.3-40	25
4.3-41	25
4.3-42	0
4.3-43	26
4.3-44	26
4.3-45	25
4.3-46	16
4.3-47	16
4.3-48	16
4.3-49	16
4.3-50	16
4.3-51	0
4.3-52	16
4.3-53	16
4.3-54	16
4.3-55	16
4.3-56	19
4.3-57	0
4.3-58	0
4.3-59	0
4.3-60	0
4.3-61	26
4.3-62	23
4.3-63	22
4.3-64	30
4.3-65	21
4.3-66	28
4.3-67	28

Page	Amendment
F4.3-1	3
F4.3-2	3
F4.3-3	3
F4.3-4	3
F4.3-5	3
F4.3-6	3
F4.3-7	3
F4.3-8	0
F4.3-9	0
F4.3-10	0
F4.3-11	0
F4.3-12	0
F4.3-13	0
F4.3-14	0
F4.3-15	0
F4.3-16	0
F4.3-17	0
F4.3-18	0
F4.3-19	16
F4.3-20	0
F4.3-20A	16
F4.3-21	0
F4.3-21A	3
F4.3-22	3
F4.3-23	16
F4.3-23A	16
F4.3-24	16
F4.3-25	3
F4.3-26	3
F4.3-26A	3
F4.3-26B	3
F4.3-26C	3
F4.3-26D	3
F4.3-26E	3
F4.3-26F	3
F4.3-26G	3
F4.3-26H	3
F4.3-26I	3
F4.3-27	0
F4.3-27A	0
F4.3-27B	0
F4.3-27C	0
F4.3-27D	0
F4.3-27E	0

Page	Amendment
F4.3-27F	0
F4.3-27G	3
F4.3-28	0
F4.3-29	0
F4.3-30	0
F4.3-31	0
F4.3-32	0
F4.3-33	0
F4.3-34	0
F4.3-35	0
F4.3-36	0
F4.3-37	0
F4.3-38	0
F4.3-38A	0
F4.3-39	0
F4.3-40	0
F4.3-41	0
F4.3-42	19
F4.3-43	28
F4.3-44	28
F4.3-45A	28
F4.3-46	17
F4.3-47	22
4.4-1	30
4.4-1a	7
4.4-2	8
4.4-3	25
4.4-4	8
4.4-5	25
4.4-6	3
4.4-7	0
4.4-8	0
4.4-9	0
4.4-10	0
4.4-11	0
4.4-12	0
4.4-13	0
4.4-14	0
4.4-15	0
4.4-16	0
4.4-17	0
4.4-18	0
4.4-19	0
4.4-20	0
4.4-21	0
4.4-22	0
4.4-23	0
4.4-24	25
4.4-25	0
4.4-26	0
4.4-27	27
4.4-28	0
4.4-29	0
4.4-30	0
4.4-31	0
4.4-32	0
4.4-33	22
4.4-34	22
4.4-34a	8
4.4-34b	4
4.4-35	3
4.4-36	27
4.4-37	3
4.4-38	26
4.4-38a	26
4.4-38b	30
4.4-38c	26
4.4-39	3
4.4-39a	3
4.4-39b	26
4.4-39c	30
4.4-40	16
4.4-41	17
4.4-42	7

CHAPTER 4

Page	Amendment
4.4-43	7
4.4-44	11
4.4-45	19
4.4-46	16
4.4-47	17
4.4-48	16
4.4-49	16
4.4-50	3
4.4-51	3
4.4-52	16
4.4-53	27
4.4-53a	26
F4.4-1	0
F4.4-2	0
F4.4-3	0
F4.4-4	0
F4.4-5	0
F4.4-6	0
F4.4-7	0
F4.4-8	0
F4.4-9	0
F4.4-10	0
F4.4-11	0
F4.4-12	0
F4.4-13	0
F4.4-14	0
F4.4-15	0
F4.4-16	0
F4.4-17	0
F4.4-18	0
F4.4-19	0
F4.4-20	3
F4.4-21	3
F4.4-22	8
F4.4-23	15
F4.4-24	0
F4.4-25	0
F4.4-26	0
F4.4-27	15
F4.4-28	16
F4.4-29	4

REACTOR

CHAPTER 4

TABLE OF CONTENTS

EC292529

CHAPTER 4

TABLE OF CONTENTS

TABLE OF CONTENTS (Cont'd)

REACTOR

CHAPTER 4

LIST OF TABLES

CHAPTER 4

LIST OF TABLES

CHAPTER 4

LIST OF FIGURES

LIST OF FIGURES (Cont'd)

LIST OF FIGURES (Cont'd)

LIST OF FIGURES (Cont'd)

LIST OF FIGURES (Cont'd)

LIST OF FIGURES (Cont'd)

LIST OF FIGURES (Con't)

LIST OF FIGURES (Cont'd)

LIST OF FIGURES (Cont'd)

CHAPTER 4

REACTOR (1)

4.1 SUMMARY DESCRIPTION

This chapter was originally prepared to describe the Cycle 1 core. Much of the original text is retained in the update for historical record, however, current cycle information has been added in the text. Physical changes, where applicable, are reflected in the text. Where information is not applicable in subsequent cycles it is identified as "Cycle 1."

The reactor is of the pressurized water type using two reactor coolant loops. Vertical and horizontal cross sections of the reactors are shown on Figures 4.1-1 and 4.1-2, respectively. The reactor core is composed of 217 fuel assemblies and 73 control element assemblies. The fuel assemblies are arranged to approximate a right circular cylinder with an equivalent diameter of 136 inches and an active length of 136.7 inches. The fuel assemblies are comprised of a structure, fuel rods, and, in some assemblies, poison rods. The structure which provides for 176 fuel rod positions consists of 5 guide tubes welded to spacer grids and the top and bottom end fittings. The guide tubes each displace four fuel rod positions and provide channels which guide the CEA's over their entire length of travel. In selected fuel assemblies, the central guide tube houses incore instrumentation. Figure 4.1-2 shows the reactor core cross section and dimensional relations between fuel assemblies, fuel rods and CEA guide tubes.

The fuel is low enrichment natural or depleted UO_2 in the form of ceramic pellets and is encapsulated in pre-pressurized zirconium alloy tubes which form a hermetic enclosure.

The core also contained two plutonium 238 antimony beryllium neutron sources for initial and subsequent startups through Cycle 9. The sources have been removed from the core and are stored in the spent fuel pool. Irradiated fuel from previous cycles now provides the source of neutrons.

The reactor coolant enters the upper section of the reactor vessel, flows downward between the reactor vessel wall and the core barrel, and passes through the flow skirt and into the lower plenum where the flow distribution is equalized. The coolant then flows upward through the core removing heat from the fuel rods, and exits from the reactor vessel and passes through the tube side of the vertical "U" tube steam generators where heat is transferred to the secondary system. The reactor coolant pumps return the coolant to the reactor vessel.

(1) The fuel loaded in Cycles 1-5 was manufactured by Combustion Engineering. The fuel loaded in Cycles 6 through the present cycle was manufactured by Exxon Nuclear Company and its successors, Advanced Nuclear Fuels (ANF), Siemens Power Corporation, Nuclear Division (SPC-ND), Framatome-ANP (FRA-ANP), AREVA NP and Framatome. EC292529

The reactor internals support and orient the fuel assemblies, control element assemblies, and incore instrumentation and guide the reactor coolant through the reactor vessel. They also absorb the static and dynamic loads and transmit the loads to the reactor vessel flange. They safely perform their functions during normal operating and upset conditions. The internals are designed to safely withstand the forces due to dead weight, handling, pressure differentials, flow impingement, temperature differentials, vibration and seismic acceleration. All reactor components are Class 1 seismic design. The reactor internals limit deflection where required by function. The stress values of all structural members under normal operating and expected transient conditions are not greater than those established by Section III of the ASME Pressure Vessel Code. The effect of neutron irradiation on the materials is included in the design evaluation. The effect of accident loadings on the internals is included in the design analysis.

During the end of Cycle 5 refueling outage, difficulties were encountered during core reload when a fuel assembly would not seat properly on the core support plate. Subsequent inspection determined there was debris of unknown origin on the plate. The fuel was unloaded and the core support barrel was removed to investigate the source of the debris. A visual examination of the core support barrel/thermal shield assembly disclosed the thermal shield support system to be severely damaged. A number of thermal shield support pins were fractured and/or missing and damage to the core support barrel was visible. An evaluation of the thermal shield support system concluded that refurbishment was impractical. Therefore, a decision was made to remove the thermal shield. Analyses performed to evaluate operation of the plant without a thermal shield for its remaining design life indicated that replacement of the thermal shield was not necessary.

A structural evaluation of the repaired core support barrel and the reactor internals without the thermal shield was performed. The component stresses under normal, upset and faulted conditions were evaluated and found to be within the limits of Section III, Subsection NG 1972, Draft Edition of the ASME Nuclear Components Code. A reanalysis of the revised reactor internals was performed and is discussed in Section 4.2.2.2.

Reactivity control is provided by two independent systems, the control element drive system and the chemical and volume control system. The control element drive system controls short term reactivity changes and is used for rapid

shutdown. The chemical and volume control system is used to compensate for long term reactivity changes and can make the reactor subcritical without the benefit of the control element drive system.

The control element assemblies (CEAs) consist of five (5) poison rods assembled in a square array, with one rod in the center. The rods are connected to a spider structure which couples to the control element drive mechanism (CEDM) extension shaft. There are a total of 73 CEAs of which 65 are of full length full poison strength and 8 are of full length reduced poison strength. Twenty-four of the 65 full length full strength CEAs are joined in pairs and are called dual CEAs.

The design life for the CEAs are originally set at approximately 10 years. This life was based on the swelling characteristics of the boron carbide pellets in the center finger. The lower portions of all five fingers now contain Ag-In-Cd, which does not swell significantly under irradiation. CEA inspections at both St. Lucie Units 1 and 2 were used to develop CEA life criteria specific to St. Lucie Unit 1 (Reference 30 and 31).

The CEAs are positioned by magnetic jack type CEDMs mounted on the reactor vessel head.

The maximum reactivity worth of the CEAs and the associated reactivity addition rate are limited by system design to prevent sudden large reactivity increases. The design restraints are such that reactivity increases will not result in violation of the fuel design limits, rupture of the reactor coolant pressure boundary, or disruption of the core or other internals sufficient to impair the effectiveness of emergency core cooling.

Boric acid dissolved in the coolant is used as a neutron absorber to provide long term reactivity control. In order to reduce the boric acid concentration required at beginning-of-cycle operating conditions and thus ensure that the moderator coefficients of reactivity have appropriate magnitudes and algebraic signs, burnable poison rods (also called shims) are provided in certain fuel assemblies. The poison is gadolinia, integral with the fuel.

A three batch fuel management scheme is employed, where approximately one-third of the core is replaced at each refueling. The average burnup will be about 45,000 MWD/MTU over the three-cycle life of the fuel. Sufficient margin is provided to ensure that peak burnups are within acceptable limits.

The nuclear design of the core will ensure that the combined response of all reactivity coefficients in the power operating range will meet Technical Specifications for the moderator temperature coefficient.

Control element assemblies are moved in groups to satisfy the requirements of shutdown, power level changes and operational maneuvering. The control system is designed to produce power distributions that are within the acceptable limits on overall nuclear heat flux factor (F_q^n) and departure from nucleate boiling ratio (DNBR). The reactor protective system and administrative controls ensure that these limits are not exceeded.

Axial xenon oscillations, should they occur, can be manually controlled by a variety of methods, including RCS boration / dilution, RCS temperature, and regulating bank 7 CEA'S, using information provided by the out-of-core detectors.

The core mechanical design is discussed in Section 4.2; the nuclear design of the core is discussed in Section 4.3; the thermal and hydraulic design is discussed in Section 4.4. Summary lists of significant core parameters are presented in Tables 4.2-1, 4.2-8, 4.3-1 and 4.4-2.

Structural analysis of the reactor internals is performed by use of mathematical models developed to represent the internals. The models are constructed in terms of lumped masses elastic beam and bar elements, and thin elastic shell elements. Verified computer codes in conjunction with generally accepted applied mechanics techniques are used to derive the load-deflection characteristics and stresses of the internal structures. Table 4.1-1 is a tabulation of the analysis techniques, load conditions and computer codes utilized in the analyses of the internals.

The St. Lucie Unit 1 Reload consists of a combination of fresh and burned fuel for a total of 217 fuel assemblies. The active fuel height for all the fuel assemblies is 136.7 inches.

Typical reload enrichments and burnable absorber characteristics are given in Table 4.1-2. Cycle specific values can be found in the respective Reload Engineering Change Package. The core contains only Framatome-manufactured fuel assemblies. EC292529

The characteristics of the fuel and the reload core are in conformance with Technical Specification limits as amended to reflect the LPD LCO shown in Section 15.6. A review of Chapter 15 event analyses is provided on Table 15.1.6-6. The referenced safety analyses support an average steam generator tube plugging level of 10% (References 23 and 25) and 15.0 kW/ft LHR limit independent of axial position (References 23 and 25).

REFERENCES FOR SECTION 4.1

1. Gliosh S., Wilson E., "Dynamic Stress Analysis of Axisymmetric Structures under Arbitrary Loading," Dept. No. EERC 69-10, University of California, Berkeley, September 1969.

2. Cabrielson V. K., "SHOCK - A Computer Code for Solving Lumped-Mass Dynamic Systems," SCL-DR-65-34, January 1966.

3. "MRI/STARDYNE - Static and Dynamic Structural Analysis System: User Information Manual," Control Data Corporation, June 1, 1970.

4. MRI/STARDYNE User Manuel, Computer Methods Department, Mechanics Research, Inc., Los Angeles, California, January 1, 1970.

5. Tillerson J. R. , Haisler W. E., "SAMMSOR II - A Finite Element Program to Determine Stiffness and Mass Matrices of Shells-Revolution," Texas A&M University, TEES-RPT-70-18, October, 1970. "DYNASOR II - A Finite Element Program for the Dynamic Non-Linear Analysis of Shells-of-Revolution," Texas A&M University, TEES-RAPT-70-19, October, 1970.

6. Nieh, L. C., "SAAS - Finite Element Stress Analysis of Axisymmetric Solids with Orthotropic Temperature Dependent Material Properties, AVCO Digital Computer Program 2663 User's Manual," AVCO Missiles, Space and Electronics Group, Missile Systems Division, April 1968.

7. Dunham, R. S., Nickell, R. E., et.al., "NAOS - Finite Element Analysis of Axisymmetric Solids with Arbitrary Loadings," Structural Engineering Laboratory, University of California, Berkeley, California, June, 1967.

8. ICES STRUDL II, “The Structural Design Language. Engineering User’s Manual, Volume I,” Structures Dvision and Civil Engineering Systems Laboratory, Department of Civil Engineering, MIT, Second Edition, June 1970.

9. EASE, "Elastic Analysis for Structural Engineering," Control Data Corporation Publication No. D0001200602, March 1970.

10. Computer Program No. WIN 12100, "Heat Transfer by Relaxation," T. R. McCormack, Combustion Engineering Inc., Windsor Connecticut, 1968.

11. SHELL ***, "Analysis of Thin Shells of Revolution," General Electric Mark II Time-Sharing Service User's Guide No. 910369.

12. XN-NF-82-09 (A), "Generic Mechanical Design Report Exxon Nuclear 14x14 Fuel Assemblies for Combustion Engineering Reactors," Exxon Nuclear Company, November 1982.

13. XN-NF-82-97, "St Lucie Unit 1 Addendum to Generic Mechanical Design Report Exxon Nuclear 14x14 Fuel Assemblies for Combustion Engineering Reactors," Exxon Nuclear Company, December 1982.

REFERENCES FOR SECTION 4.1 (continued)

14. XN-NF-82-99, "Plant Transient Analysis for St Lucie Unit 1 Reactor," Exxon Nuclear Company, January 1983.

15. XN-NF-84-11, "St Lucie Unit 1 Transient and Setpoint Analyses for Cycle 6," Exxon Nuclear Company, April 1984.

16. Deleted.

17. XN-NF-78-44 (A), "A Generic Analysis of the Control Rod Ejection Transient for Pressurized Water Reactors," Exxon Nuclear Company, January 1979.

18. XN-NF-66-23, Rev 1, "St Lucie Unit 1 LOCA/ECCS Analysis with 11% Steam Generator Tube Plugging," Exxon Nuclear Company, March 1986.

19. Letter, J M Ross (ENC) to A R Morse (FPL), "Drawing of Lower End Cap for St Lucie Unit 1, XN-3," JMR:228:86, dated September 23, 1986.

20. ANF-87-149, "Mechanical Design Report for St Lucie Unit 1, Batches XN-1 through XN-4," December 1987.

21. Letter, T. J. Helbling (ANF) to A. R. Morse (FPL) TJH:157:88, dated June 13, 1988.

22. XN-NF-84-85(P), Revision 1, "St Lucie Unit 1 Radiological Assessment of Postulated Accidents," April 1985.

23. ANP-3199(P), Revision 0, "St. Lucie Nuclear Plant Unit 1 EPU Realistic Large Break LOCA Summary Report with M5 Fuel Cladding," March 2013.

24. ANP-3000(P), Revision 0, "St. Lucie Unit 1 EPU – Information to Support License Amendment Request," May 2011.

25. ANP-3198P, Revision 0, "St. Lucie Unit 1 EPU Small Break LOCA Summary Report with M5 Fuel Cladding," March 2013.

26 ANF-88-113(P), "St Lucie Unit 1 Assessment of Radiological and Rod Bow Effects for Increased Burnup," July 1988.

27. ANF-88-125(P), "Extended Burnup for St Lucie Unit 1 24-Month Cycle Analysis for Reload ANF-5 and Beyond," March 1989.

28. ANF-90-116(P), "St. Lucie Unit 1 High Burnup Customer Mechanical Design Report for Reload ANF-6 and Beyond," February 1991.

29. Not used.

30. PSL-ENG-SEFJ-02-005, "St. Lucie Unit 1 Control Element Assembly (CEA) Lifetime Determination."

31. PSL-ENG-SEFJ-05-011, "Evaluation of Framatome ANP-Designed Control Element Assemblies for St. Lucie Unit 1."

TABLE 4.1-1

REACTOR INTERNALS STRESS ANALYSES METHODS SUMMARY

Component	Load Conditions	Analysis Technique	Computer Code
Core Support Barrel	Axial & Lateral Loads	Shell Analysis Beam Analysis	ASHSD[1] SHOCK [2] STARDYNE [3][4]
	Dynamic Buckling	Shell Analysis	SAMMSOR - DYNASOR [5]
Upper & Lower Core	Lateral Loads	Finite Element Analysis	SAAS [6]
Support Barrel Flanges	Axial Loads Bending Moments		NAOS [7]
Lower Support Structure - Beams		Plane grid structure analysis. Simply supported beams.	STRUDL [8]
- Columns	Axial Loads Bending Loads	Column analysis.	SHOCK [2] STARDYNE[3][4]
Upper Guide Structure CEA Shrouds	Lateral Loads Axial Loads	Beam Analysis Column analysis	SHOCK [2] STARDYNE [3][4]
- Beam Structure	Uniform Lateral Loading	Plane grid structure	STRUDL [8]
- Support Plate Flange	Axial Loads Bending Moments	Finite element analysis	SAAS [6] NAOS[7]

TABLE 4.1-1(Cont'd)

Component	Load Conditions	Analysis Technique	Computer Code
Core Shroud	Thermal & Pressure Loading	Finite element analysis	EASE [9]
Expansion Compensating Ring	Torsional & Bending Moments	Finite element analysis	SAAS[6]
CEDM and PLCEDM	Pressure, fatigue and thermal loads	Finite Element Analysis	SAAS[6]
CEDM and PLCEDM	Seismic Loading	Framed Structure Analysis	STRUDL[8]
CEDM and PLCEDM Nozzles	Thermal Loading	Relaxation Analysis	WIN 12100[10]
CEDM and PLCEDM Omega Seal	Pressure, thermal, rotational and displacement loadings	Shell Analysis	SHELL*** [11]

TABLE 4.1-2

TYPICAL ST. LUCIE UNIT 1 RELOAD FUEL
ENRICHMENTS AND BURNABLE ABSORBER CHARACTERISTICS

Batch Type	Number of assemblies	Rods/Assembly	Rod Central* Zone Enrichment (w/o U-235)	Gd_2O_3 Concentration (w/o)
HH1	20	128 40 8	4.6 4.2 3.6	 4.0
HH2	4	124 40 12	4.6 4.2 3.6	 4.0
HH3	4	120 40 16	4.6 4.2 2.4	 8.0
HH4	12	124 40 8 4	4.1 3.7 2.4 2.4	 6.0 4.0
HH5	8	120 40 4 12	4.1 3.7 2.4 2.4	 2.0 8.0
HH6	40	120 40 8 8	4.6 4.2 2.4 2.4	 8.0 4.0

* The top 6 inches and bottom 6 inches of the fuel rods, which do not contain Gd_2O_3, contain 2.6 w/o U-235 pellets. The central zone length for these rods is 124.7 inches. For the fuel rods containing Gd_2O_3 the top and bottom 11.4 inches contain 2.6 w/o U-235 pellets. The central zone length for these Gd_2O_3 bearing rods is 113.9 inches.

Note that the values represented in the above table are from SLU1-26 (BATCH HH).

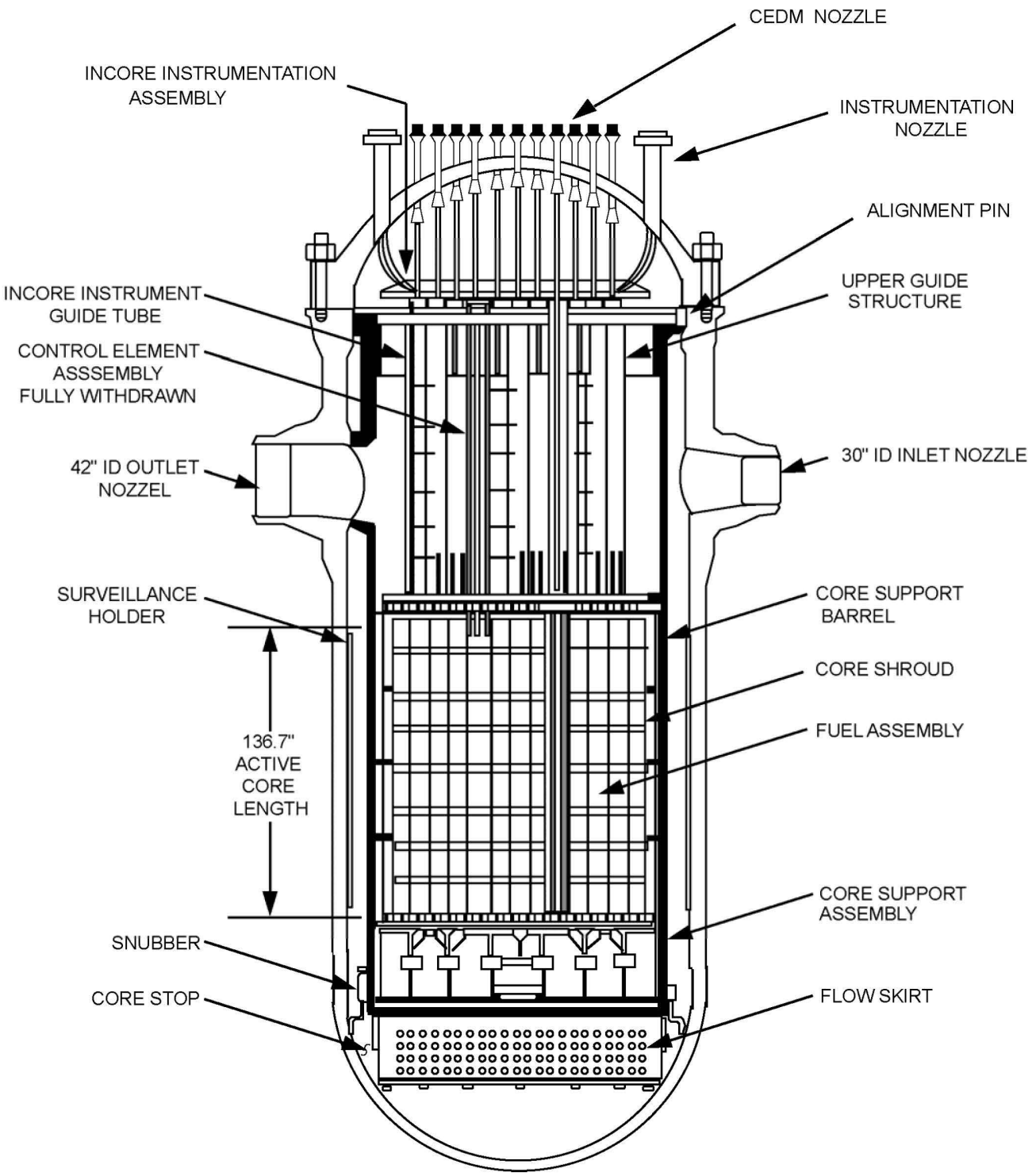

Florida Power & Light Company
St. Lucie Plant Unit 1

Reactor Arrangement - Vertical Section
Figure 4.1-1

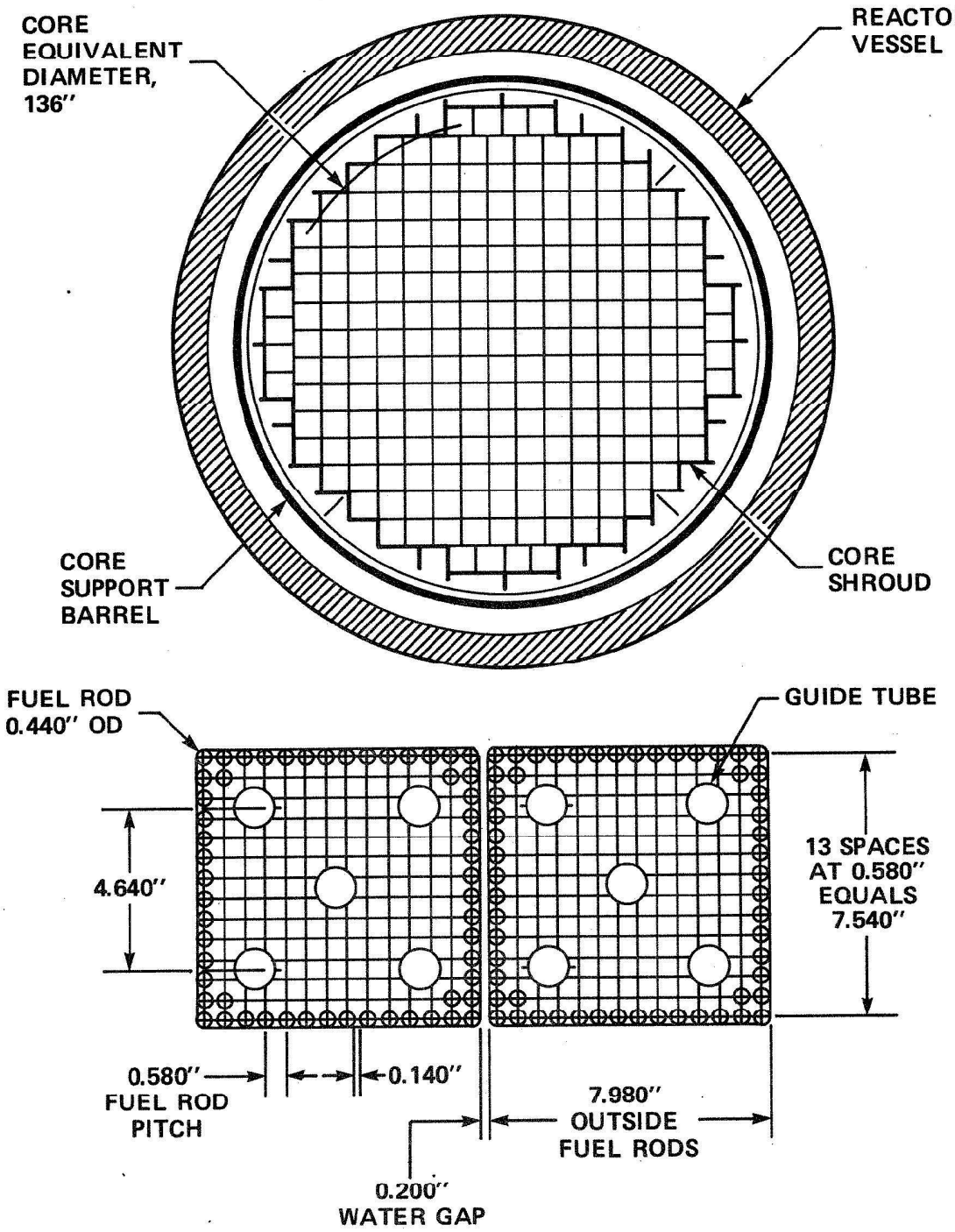

Am. 3-7/85

FLORIDA POWER & LIGHT CO. St. Lucie Plant Unit 1	REACTOR CORE CROSS-SECTION	Figure 4.1-2

4.2 MECHANICAL DESIGN

A summary of the core mechanical design is presented in Table 4.2-1. A summary of Advanced Nuclear Fuel mechanical design is presented in Table 4.2-8. These data are intended to be descriptive of the design; limiting values of these and other parameters will be discussed in the appropriate sections. Also, Table 4.2-1 represents fuel of Combustion Engineering design employed in Cycles 1 through 7. Exxon fuel was employed beginning with Cycle 6 which had nearly 1/3 core of Exxon design and 2/3 of Combustion. Cycle 7 had 2/3 Exxon fuel and 1/3 Combustion. Cycle 8 and later cycles are manufactured by Exxon Nuclear Company and its successors, Advanced Nuclear Fuels (ANF), Siemens Power Corporation, Nuclear Division (SPC-ND), Framatome-ANP (FRA-ANP), AREVA NP, and Framatome. EC292529 EC292529

4.2.1 FUEL (COMBUSTION ENGINEERING)

The descriptions provided in the following text of Section 4.2.1 and its subsections are descriptive of Combustion Engineering fuel design and manufacture. Combustion Engineering fuel was used in Cycles 1 through 7. Section 4.2.4 describes the design of Framatome fuel. EC292529

4.2.1.1 Fuel Assembly Design Bases

The following summarizes the primary stress limited corresponding to three plant conditions:

a) Normal Operating and Upset Conditions

The fuel assembly shall be designed with sufficient margin to ensure safe operation during normal operating conditions, the operational basis earthquake, and those accidents which may occur with moderate frequency.

$P_m \leq S_m$
$P_m + P_B \leq F_s S_m$

Where: P_m = Calculated general primary membrane stress*

P_B = Calculated primary bending stress*

S_m = Design stress intensity value as defined by Section III, ASME Boiler and Pressure Vessel Code

F_S = Shape factor corresponding to the cross section being analyzed

With the exception of zirconium base alloys, the design stress intensity values of materials not specified by the code are determined in the same manner as the code, classifying the materials into two groups according to their unirradiated properties. The design stress intensity of zirconium base alloys shall not exceed two-thirds of the unirradiated minimum yield strength at temperature.

*P_m and P_B are defined by Article NB-300, Section III, ASME Boiler and Pressure Vessel Code, 1971

b) Emergency Conditions

The fuel assembly shall be designed to permit some local yielding during the postulated design basis earthquake and those accidents which have a low probability of occurrence. A small number of fuel elements may be damaged. However, deflections are limited so that the CEA's can function and adequate core cooling is preserved.

$P_m \leq 1.5\ S_m$
$P_m + P_B \leq 1.5\ F_s S_m$

c) Faulted Conditions

Permanent deformation of the fuel assembly is permitted during postulated LOCA accidents in conjunction with the design basis earthquake. Quantitative primary stresses of the fuel assembly end fittings (excluding holddown springs) are limited by the following:

$P_m \leq 2.4S_m$; $0.7S_u$ $P_m+P_B \leq 2.4\ F_S\ S_m$; $0.7\ F_S\ S_u$

S_u = minimum unirradiated ultimate tensile strength

F_s = shape factor corresponding to the particular cross section being analyzed. F_s = 1.5 for a rectangular section

The shape factor, F_S is defined as the ratio of the fully plastic moment to the maximum elastic moment for a material which behaves in an elastic-perfectly plastic manner. The value of a shape factor is determined by the cross-sectional geometry. Table A-9221(a)-1 in the Winter, 1972, Addenda to ASME Section III of the Boiler and Pressure Vessel Code lists the shape factors for various cross-sectional geometries. The fuel assembly end fittings are comprised of cylindrical posts and rectangular plates; the corresponding maximum shape factors for these components are 1.44 and 1.5, respectively.

The values of Su in the faulted condition for the cast 304 stainless steel plates and for the wrought 304 stainless steel posts are 44.6 KSI and 57.0 KSI, respectively.

Appendix F (Rules for Evaluation of Faulted Conditions) was added to Section III of the ASME Boiler and Pressure Vessel Code in 1972. For the elastic analysis, the design limit for the primary stress in the faulted condition was changed to the lowest of either 2.4 Sm or 0.7 Su.

Because the minimum ultimate strength values for a ASTM-A296 Grade CF8 metal are not specified for high temperatures (100 - 600 °F), the minimum specified value of Su is calculated using a conservative extrapolation of the procedure discussed in the ASTM Data Series DS-5S2. The ASTM Data Series DS-5S2 establishes a procedure to calculate the tensile strengths of wrought 304, 321 and 347 stainless steel at elevated temperatures. Using a conservative extrapolation of this procedure gives the specified minimum ultimate tensile strengths for ASTM-A296 Grade CF8 listed below:

Temperature °F	Specified Minimum UTS (ksi)
100	65.0
200	54.6
300	48.4
400	45.3
500	44.6
600	45.3

Because 44.6 ksi is the lowest value in the operating temperature range, it is selected as the value for Su in the faulted condition.

The cylindrical posts are made from ASTM-A276 bar stock. Because the ASTM-A276 bar stock is equivalent to SA-479-304 bar stock, the results of the ASTM study presented in the ASTM Data Series DS-5S2 is valid for the ASTM-A276 bar stock. In this ASTM publication is a table which permits calculation of the specified minimum UTS at temperature for any bar stock. The results of the calculation for ASTM-A276-304 Bar Stock are given below:

Temperature °F	Specified Minimum UTS(ksi)
100	72.0
200	63.0
300	58.5
400	57.0
500	57.0
600	57.0

Because 57.0 ksi is the lowest value in the operating temperature range, it is selected as the value for Su in the faulted condition.

Deformations are limited to the following:

1) If the pipe break does not exceed the largest line connected to the reactor coolant system, the fuel assembly deformation is limited to a value not exceeding the loss of function deformation limit which would preclude satisfactory insertion of the CEAs.

2) For reactor coolant system (LOCA) pipe breaks, CEA insertion is not required for a safe and orderly shutdown; deformation of structural components is limited to maintain the fuel in a coolable array.

4.2.1.2 Fuel Rod Cladding Design Bases

Margin shall be provided to prevent fuel rod damage under steady state and transient operating conditions. The fuel rod design accounts for external pressure, differential expansion of fuel and clad, fuel swelling, clad creep, fission and other gas releases, initial helium pressure thermal stress, pressure and temperature cycling and flow induced vibrations. The structural criteria are based on the following:

a) The maximum tensile stress in the Zircaloy clad shall not exceed 2/3 of the minimum unirradiated yield strength of the material at the applicable temperature.

b) Net unrecoverable circumferential strain shall not exceed I percent as predicted by computations considering clad creep and fuel-clad interaction effects.

c) The clad shall be initially pressurized with helium to an amount sufficient to prevent gross clad deformation under the combined effects of external pressure and long term creep. The clad design shall not rely on the support of fuel pellets or the holddown spring to prevent gross deformation.

d) Cummulative strain cycle usage factor, defined as the sum of the ratios of the number of cycles at a given effective strain range (Δε) to the permitted number (N) at that range as taken from Figure 4.2-1 is less than 1.0.

The minimum unirradiated yield strength is used as a design basis since it is lower than the irradiated value at the same temperature (WCAP-3269-41, "Physical and Mechanical Properties of Zircaloy 2 & 4," D. B. Scott, May 1965). The 2/3 factor on yield strength for establishing the maximum allowable tensile stress provides a safety factor against permanent clad strain.

The cyclic strain limit design curve, shown on Figure 4.2-1 is based upon the "Method of Universal Slopes" developed by S. S. Manson(1) and has been adjusted to provide a strain cycle margin for the effects of irradiation and uncertainty. The resulting curve has been compared with known data on the cyclic loading of Zircaloy and has been shown to be conservative. Specifically, it encompasses all the data of Reference 2.

4.2.1.3 Fuel Assembly Description

4.2.1.3.1 Fuel Rod

The fuel rod shown in Figure 4.2-2 consists of UO_2 pellets, a compression spring and spacer discs, all encapsulated within a Zircaloy-4 tube. The UO_2 pellets have a density of 10.30 g/cc and are dished at both ends. Dishing is used to accommodate the effects of thermal expansion and swelling and results in a pellet column density of approximately 10.20 g/cc.

A value of 50,000 Mwd/MTU is set as the local exposure limit for the fuel. Previous burnup experience (see Section 4.2.1.4.14) has shown this to be an acceptable limit.

The fuel cladding is slightly cold worked (less than 15%) Zircaloy-4 tubing. The cold nominal diametral gap between the pellet and clad I. D. has been set taking into account clad stresses and strains, transfer of heat from the pellets and fuel loading considerations. The compression spring located at the top of the fuel pellet column is 302 stainless steel and maintains the column in its proper position during handling and shipping. It also provides support for the clad in the plenum region to prevent local buckling. The adequacy of the spring to perform its function has been demonstrated in a series of long term creep buckling tests on the fuel rod cladding with plenum clad temperatures above those expected in the reactor. The purpose of these tests was to determine if the cladding on an unpressurized fuel rod would collapse between the coils of the compression spring located at the top of the fuel pellets. After 23,500 hours of testing, samples with and without precollapsed clad did not collapse between the spring coils.

These tests are conservative relative to the design and the operational history that the fuel rods will be subjected to for the following reasons:

	Test Samples	Fuel Rod
Ratio of clad thickness to the clad outside diameter	0.054	0.059
Internal pressure	Atmospheric Pressure	Pressurized
Plenum temperatures, °F	650	580-650
Calculated maximum hoop stress, psi	21,500	14,000

Each fuel rod is internally pressurized with helium. The internal helium improves the thermal conductance between fuel pellets and the claddings, and the resulting decrease in fuel temperatures is attended by a significant reduction in released fission pores and an increase in the margins between operating temperatures and allowable thermal limits. In addition, by reducing the differential pressure across the clad, internal pressurization affords a substantial reduction in the adverse effects of fuel-clad interaction and ensures that the fuel clad will be free standing against the possibility of collapsing under the effects of long-term creep due to differential pressure. The initial helium pressure is sufficient to prevent cladding collapse at the peak power location for the full design life of the fuel rod.

There are two alumina spacers in each fuel rod. The spacers are located at each end of the fuel pellet stack. The lower spacer reduces the lower end cap temperature while the upper spacer prevents UO_2 chips from entering the plenum region. The plenum above the pellet column provides space for axial thermal expansion of the fuel column, and to accommodate the initial helium loading and fission gases.

4.2.1.3.2 Burnable Poison Rods (Cycle 1)

To make the first cycle beginning-of-life moderator coefficient negative, poison rods are included in batch B and C fuel assemblies. The poison rods are mechanically similar to fuel rods except that they each contain a slightly shorter column of burnable poison pellets instead of the fuel pellets. The balance of the column length is made up of alumina pellets. The poison material is alumina with uniformly dispersed boron carbide particles.

On July 10, 1976, St. Lucie Unit 1 was shutdown to investigate neutron flux anomalies in the St. Lucie Unit 1 reactor. A comprehensive investigatory program disclosed that the anomaly was caused by accelerated depletion of the boron content from the poison shims. The accelerated boron loss resulted from perforations in the shim cladding and subsequent leaching of the boron. Subsequently, all burnable poison shims (batch B and C) were replaced using improved manufacturing processes and the addition of a retention assembly on top of the upper end fitting flow plate. Details of the fuel assembly repairs, including evaluation of potential effects of the repair, was submitted to the NRC in Reference 25. Analysis of the repair, as reported, shows no significant impact on the existing Safety Analysis and was bounded conservatively by the limits established in the FSAR, the plant Technical Specifications, 10 CFR 20 and 10 CFR 100.

4.2.1.3.3 Fuel Assembly (Combustion Engineering) - Historical

The fuel assembly is shown in Figure 4.2-3 and consists of fuel rods, burnable poison rods, five CEA guide tubes; eight fuel spacer grids, a fuel rod retention grid and upper and lower end fittings. Batch A assemblies consist of 176 fuel rods; Batch B assemblies contain 164 fuel rods and twelve poison rods. Batch C assemblies consist of three types; an unshimmed assembly similar to Batch A, and two shimmed assemblies having different B_4C loadings in the shim rods.

The CEA guide tubes, spacer grids and end fittings form the structural frame of the assembly. The four outer CEA guide tubes are mechanically attached to the stainless steel end fittings and the spacer grids are welded to all five CEA guide tubes.*

The lower end fitting is Type 304 stainless steel consisting of an end plate containing flow holes and holes for positioning the guide tubes, and support legs with precision machined holes for accepting the alignment pins.

The upper end fitting shown in Figure 4.2-4 is an assembly consisting of two stainless steel cast structures, five machined posts, and helical holddown springs and serves as an attachment for the guide tubes and as the lifting fixture. The machined posts mate with precision drilled holes in the fuel alignment plate and align the upper ends of the fuel assembly.

The fuel rod spacer grids (Figure 4.2-5) maintain the fuel rod pitch over the full length of the fuel rods. The grids are fabricated from preformed Zircaloy strips interlocked in an egg crate fashion and welded together. Each fuel rod is supported by two leaf springs and two arches which are opposite each leaf spring. The leaf springs press the rod against the arches to restrict relative motion between the grids and the fuel rods. The spring and arch positions are reversed from grid to grid to provide additional restriction to relative motion. The perimeter strips also contain springs and arches in addition to special lead-in features to prevent hangup of grids during refueling operations.

A retention grid fabricated of Ni-Cr-Fe is welded to the lower end fitting. The grid consists of strips interlocked in egg crate fashion and welded to perimeter strips. Overlapping spring fingers formed within the spring strips engage a machined groove in the fuel rod lower end cap. In this manner, all rods are retained laterally and vertically at their lower end.

The fuel assembly holddown device shown in Figure 4.2-4 prevents lifting of the fuel assembly by hydraulic forces under high flow conditions. The holddown device consists of a spring-loaded plate which is integral to the fuel assembly. The springs are compressed as the upper guide structure is lowered into place. The added spring load, together with the weight of the fuel assembly, prevents axial motion of the fuel assembly during Operation.

*Stainless steel sleeves have been installed in CEA guide tubes in assemblies that are installed in CEA locations to prevent guide tubewear by CEA'S.

The holddown device features a moveable spider which acts on the underside of the fuel alignment plate. The springs are positioned at the upper end of the assembly so that the spring load combines with the assembly weight in counteracting the upward hydraulic forces. The springs are sized and the spring preload selected, such that a net downward force will be maintained for all normal and anticipated transient flow and temperature conditions. The moveable spider also serves as the lifting surface during handling of the fuel assembly.

The spider and end fitting are fabricated of Type 304 stainless steel and the coil springs are fabricated of Ni-Cr-Fe X750. The design criteria limit the maximum stress to below the yield strength of the spring material. The maximum stress occurs during a cold startup condition and decreases as the reactor heats up. The reduction in stress is due to a decrease in spring deflection resulting from differential thermal expansion between the Zircaloy fuel bundles and the stainless steel internals. A number of different stress cycles-occur in going from cold startup to operating condition, during normal operation, and from normal operation to cold shutdown conditions. The maximum stress range in the springs occurs for a plant heatup or plant cooldown, which will occur less than 50 times over the life of a fuel assembly. The number of cycles at operating conditions is estimated to be less than 1500. The operating stress is less than the maximum stress at cold conditions, and the operating stress range is relatively small.

During normal operation, a spring will never be compressed to its solid height. However, if the fuel assembly were loaded in an abnormal manner such that a spring were compressed to its solid height, the spring would continue to serve its function when the loading condition returned to normal.

A series of tests has been conducted to verify the holddown design. Load deflection tests, tensile tests, as well as simulation of various loading conditions, have been run to demonstrate the adequacy of the device. The holddown device has been subjected to hot loop performance testing to ensure its adequacy under reactor operating conditions.

Improper loading of a fuel assembly into the core, such that a fuel assembly is laterally displaced from its designated position, could conceivably occur if the lower end fitting, shown in Figure 4.2-3, does not engage the four fuel alignment pins, shown in Figure 4.2-7, which position each assembly. Should this occur, it would not be possible to correctly load one or more adjacent assemblies. Also, the design of the core shroud assembly, shown in Figure 4.2-9, and the arrangement of fuel alignment pins makes it physically impossible to laterally mislocate a fuel assembly and still load all 217 assemblies into the core.

There is no preferred orientation of the fuel assemblies for the first burnup cycle. Once or twice burned fuel may, however, be preferentially oriented in subsequent cycles as a means of flattening fuel assembly burnup and as a secondary means of reducing local power peaking. Since there is no physical means of insuring the desired orientation of the assemblies, a record of the orientation of the assembly identification numbers, stamped on the upper end fitting (see Figure 4.2-4), must be recorded for each core configuration.

4.2.1.4 Fuel Design Evaluation

4.2.1.4.1 Deflections

Axial load compression tests of the fuel assembly have been performed to determine the lateral and vertical deflections due to normal handling and refueling operations, steady state and transient operating conditions and postulated accident conditions.

The lateral stability of a fuel assembly has been measured to determine the stability and resiliency under laterally applied loads at the top of the fuel assembly which are expected during refueling.

Under hot operating conditions, the fuel assembly can be deflected approximately 1 inch at its center without exceeding the yield stress of the structural members. However, if the bundles were deflected to this point, some residual deflection would remain due to the interaction of the fuel rods with the spacer grids. This deflection is small and can be easily overcome by small lateral loads. Tests have been conducted which demonstrate that the functioning of the CEA is not adversely affected with the guide tubes bowed 1 inch.

The maximum possible bow occurs in a fuel assembly located on the periphery of the core and is approximately 0.9 inches. This assumes an extremely unlikely condition where all fuel assemblies are bowed in the same direction at the same time and that all clearances between fuel assemblies and the core shroud are reduced to zero. The loss of function deformation is that value which precludes satisfactory insertion of the CEAs and which results in difficulty in refueling of the core. Since testing has been performed with a guide tube bowed one inch (bow of the CEA finger was also present) without adversely affecting CEA gravity drop within the 2.5 seconds specified, this limit is in excess of one inch. Testing has also shown that, although residual deflection does occur for large deflections, these deflections will not preclude handling or refueling of the assembly.

In December 1975 the applicant was notified by the NRC that a study was underway to determine the advisability of assessing a rod bowing penalty on St. Lucie Unit 1. The NRC requested and was provided with the following information to assist them in making that determination.

Average Linear Heat Generation Rate	6.09 Kw/ft.
Max expected assembly burn-up	16,300 MWD/T
Power Measurement Uncertainty	2%
Rod Radial Peaking Factor	1.33
Peaking Factor Uncertainty	8%
Densification Effects Uncertainty	1%

In addition, with reference to Table 4.4-2, the nominal steady state DNBR is 2.30 and a rod pitch and bow factor of 6.5% is assumed in the DNB calculations.

While this information was submitted in order that the applicant may be in full compliance with NRC requests for information, the inference

should not be made that the applicant expects any significant fuel rod bowing to occur with C-E fuel. On the contrary, C-E has-made extensive examinations of irradiated fuel and has not found any significant fuel rod bowing. This position and supportive data have been transmitted to the NRC with C-E letter DF-573 of 2/13/75 and more recently with DF-692 of 12/15/75. The applicant's position is that no significant fuel rod bowing will occur with C-E fuel and, furthermore, that existing thermal hydraulic calculations include sufficient margin to account for any insignificant fuel rod bowing which might occur.

4.2.1.4.2 Cycling and Fatigue

A fatigue analysis has been performed to determine the cumulative fatigue damage fraction of fuel rod cladding exposed to lifetime power cycling conditions. The fatigue cycle was determined by considering combinations of events that would produce maximum strain in the clad. The major, conservative calculational assumptions are as follows:

a) Hot spot fuel rod radii,

b) The most adverse tolerance conditions of fuel and cladding dimensions to produce maximum interactions and hence maximum clad strains, and

c) Primary creep rate data for the clad tensile and compressive strains.

The chosen fatigue cycle represents daily operation at both full and reduced power. Clad strains calculated from tile primary creep rate of the clad were used to calculate the effective strain ranges. The cumulative fatigue damage fraction was determined by summing the ratios of the number of cycles at a given effective strain range to the permitted number at that range as taken from the fatigue curve in Figure 4.2-1. The results of the analysis showed that the maximum cumulative fatigue damage fraction (described in paragraph NB-3222.4 (e) in ASME Boiler and Pressure Vessel Code, Section III) representing the worst anticipated condition in fuel rods is 0.64. This is well below the maximum allowable value of 1.0 selected as a design basis to be consistent with ASME Section III Code.

The linear cumulative damage theory, with a maximum allowable cumulative, damage fraction of 1.0, is the basis for clad cyclic fatigue analysis. Conservatism results by constructing the design fatigue curves for the fatigue life of irradiated and unirradiated Zircaloy to show the maximum allowable number of cycles for a loading to occur at ninety percent of the fatigue life. This method is equivalent to using the actual fatigue life curves and a maximum cumulative fatigue damage fraction of 0.9. The basis for using a value of 1.0 as the upper limit cumulative fatigue damage fraction is to comply with Section III analyses and to decrease the level of uncertainty by reducing the actual life curves by ten percent.

The cumulative fatigue damage fraction of 0.64 does not include a worst case accident condition. As discussed in Section 15.4, some damage to the fuel rods may occur during a worst case however, the effects from such an accident are analyzed separately and it is not appropriate to include a worst case accident situation in the cyclic cumulative fatigue damage analysis.

Fatigue tests shown on Figure 4.2-1A have been conducted by KAPL (Reference CONF-446-35, "Effects of 1.0% Superimposed Mean Strain on the Bending Fatigue Strength of Zircaloy 4," D. F. Mowbray, 1964) on Zircaloy strip material at room temperature in the hydrided and unhydrided conditions to establish the endurance limit. Autoclave vibration tests which act as fatigue tests were run at fuel rod deflections which are greater than expected in reactor operation. The resulting stress in the grid springs based on measured deflections was calculated. The cyclic stress caused by fuel rod vibration is significantly lower than the endurance limit.

4.2.1.4.3 Fuel Rod Internal Pressure

The fuel rod internal gas pressure and cladding stresses at end of life are discussed in Section 4.4. The results of the analysis show that the structural criteria for normal operating conditions have been satisfied.

An analysis has also been performed to determine the maximum stress in the clad which occurs in the event of a rapid depressurization transient at end of life. The most severe secondary steam line rupture was chosen and the resulting clad stresses due to pressure differential across the clad were calculated and found to be below the minimum clad yield strength.

The variation of fuel rod internal pressure at 100 percent with burnup for the initial three cycles of operation are presented in quartercore cross section on Figures 4.2-17A through 4.2-17F. The results presented are maximum and minimum fuel rod internal pressure for six different conditions as follows:

Beginning of cycle 1, equilibrium xenon - Figure 4.2-17A

End of cycle 1, equilibrium xenon - Figure 4.2-17B

Beginning of cycle 2, no xenon - Figure 4.2-17C

End of cycle 2, equilibrium xenon - Figure 4.2-17D

Beginning of cycle 3, no xenon - Figure 4.2-17E

End of cycle 3, equilibrium xenon - Figure 4.2-17F

The above figures are presented for illustrative purposes only and are maintained as historical information. The maximum pressure is based on the predicted 1-pin peaking factor, the maximum initial fill helium pressure, worst case internal rod dimensions and includes the effect of the predicted fission gas release. Minimum pressure is based on worst case internal dimensions, minimum initial fill gas pressure and no fission gas release.

4.2.1.4.4 Clad Physical Properties

Table 4.2-2 is a list of unirradiated physical properties of Zircaloy-4 fuel rod cladding at room temperature and at 675F.

4.2.1.4.5 Radiation Damage to Fuel Cladding

Zircaloy-4 fuel cladding has been utilized in PWR reactors at temperatures and burnups anticipated in current designs with no failures attributable to radiation damage. Mechanical property tests on cladding exposed to neutron irradiation in excess of 2×10^{21} nvt (beyond saturation) have revealed that the cladding retains a significant amount of ductility (in excess of 6% elongation). Typical results of irradiation studies are presented in Table 4.2-3. Lower temperature irradiation (below 600F) has consistently shown decreased ductility and increased strength. At higher irradiation temperatures, typical of PWR reactors, the effect of irradiation is not as deleterious, tending to partially anneal the irradiation damage.

4.2.1.4.6 Shock and Seismic Loading

The fuel assemblies are capable of withstanding the effects of both operational and design basis earthquakes. During an operational basis

earthquake, the reactor is capable of continuing normal operation. During a design basis earthquake, the reactor can be shut down, and no loss of function with respect to safety will result. The fuel assemblies are designed to meet the following seismic criteria:

Operational basis earthquake (OBE):

a) The fuel assemblies must be capable of sustaining an OBE without exceeding limits imposed by the structural criteria.

b) The CEA's can be scrammed during the OBE within the allowable scram time.

c) No inspection of fuel or CEA's is required for continued operation.

Design basis earthquake (DBE)

a) The fuel assemblies must be capable of sustaining DBE with no loss of function with respect to safety.

b) The CEA's will scram during a DBE, but not necessarily within the prescribed time.

c) After a DBE, tests and inspection may be required before resuming normal operation.

4.2.1.4.7 Fuel Cladding Strain Limits

Data from O'Donnell [3] and Weber[4] were used to determine the one percent strain limit. O'Donnell developed an analytical failure curve for Zircaloy cladding based upon the maximum strain of the material at its point of plastic instability. O'Donnell compared his analytical curve to circumferential strain data obtained on irradiated coextruded Zr-U metal fuel rods tested by Weber. The correlation was good, thus substantiating O'Donnell's instability theory. Since O'Donnell performed analysis, additional data have been derived at Bettis[5,6,7] and AECL [8, 9]. These new data are shown in Figure 4.2-6, along with O'Donnell's curve and Weber's data. This curve was then adjusted because of differences in anisotropy, stress states and strain rates. It also takes into consideration all test data available to date. Thus, based on this curve, the design limit was set at one percent.

4.2.1.4.8 Results of Vibration Analysis

Several analyses have been performed to determine the effects of flow induced vibration on the fuel assembly under normal operating conditions. Possible damage resulting from fuel rod interactions was investigated.

An analysis has been performed to determine the effects of vibration of fuel rods due to parallel flow. Natural frequency and amplitude of a fuel rod were determined and the value was used as an input for the autoclave tests described in Section 4.2.1.4.9. The rods were excited at the computed natural frequency to determine the extent of fretting resulting from fuel rod and spacer grid interactions. The test concluded that the wear due to fretting in the components is insignificant.

The effect of the vibration of the core support barrel on the entire fuel assembly has also been examined. The frequency of the core barrel excitation was determined and used as an input in the dynamic flow tests described in Section 4.2.1.4.9. The tests showed that under normal operating flow conditions and simulated core barrel vibration, there would be no long term damage to the fuel assemblies.

The effect of reactor coolant pump startup/shutdown transients on vessel internals vibrations has been experimentally determined in the conduct of the precritical vibration programs for the Maine Yankee (CENPD-93, Precritical Vibration Monitoring Program, February 1973) and Fort Calhoun reactors. The experimental evidence shows that there is no dynamic magnification of structural response during pump startup and shutdown transients but rather a gradual transition from one steady state mode of operation to another resulting in a low potential for increased wear during such transients.

4.2.1.4.9 Fretting Corrosion

The phenomenon of fretting corrosion in Zircaloy clad fuel rods supported by Zircaloy spacer grids has been extensively investigated. Since a reduction in grid spring load resulting from irradiation induced stress relaxation, in combination with certain vibratory forces, may cause fretting, an extensive test program involving autoclave vibration tests, dynamic flow tests, and fatigue tests were undertaken.

The autoclave tests were performed by vibrating a fuel rod sample supported by two rigidly held spacer grid sections. Test conditions simulate reactor coolant temperature and pressure. Testing conditions provide data to evaluate the effects of time, frequency of fuel rod vibration, amplitude of fuel rod vibration, spacer grid spring preset load, and axial rod movement simulating reactor load following conditions.

Two years of actual test time have been accumulated under autoclave conditions. Results show that fretting starts with a brief break-in period, then proceeds at a negligible rate. Changes in frequency, spring preset including zero preset and amplitude within representative limits do not significantly alter fretting characteristics. At no time under any conditions was fretting significant.

The dynamic flow tests were performed on 4 x 4 (16 fuel rods) and full cross section fuel bundles at simulated reactor conditions. Test conditions established for the 4 x 4 bundles included coolant flow velocity expected in reactor, parallel and maximum expected cross flow, forced bundle vibration representing vibratory forces imparted by the internals, spring preset, and time. A total of 18,000 hours of test time has been accumulated with the longest single test run of 3,000 hours.

Three separate flow tests at simulated reactor conditions were run with full size fuel assemblies. A large number of fuel rods in the fuel assemblies were tested with zero preset grid spring loads to conservatively represent end-of-life grid conditions. A total of more than 10,000 hours of-test time has been accumulated with the longest single test run of >3500 hours.

The maximum fretting depths from both the 4 x 4 and full size bundles follow the same trends found in autoclave vibration tests. Based on the above tests, a very conservative estimate of maximum wear expected for lifetime operation is less than 3 mils, representing only 12 percent of the cladding wall thickness.

4.2.1.4.10 Potential for Chemical Reaction

a) Corrosion Tests

Corrosion tests of Zircaloy fuel rod cladding were conducted in excess of 4000 hours exposure and include 600F and 650F autoclave tests and 600F loop tests with borated lithium hydroxide additives in the water. The test results agree with long term corrosion tests in lithium hydroxide reported by Bettis (WAPD-MRP-108), Pressurized Water Reactor Project, Period January 24, 1964 to April 23, 1964. No deleterious effects have occurred.

b) Hydriding

During operation of the reactor with exposure to high temperature, high pressure water, Zircaloy-4 cladding will react to form a protective oxide film in accordance with the following equation:

$$Zr + 2H_2O \rightarrow ZrO_2 + 2H_2$$

Approximately 20 percent of the hydrogen is absorbed by the Zircaloy. Based on data described in "Quarterly Progress Report, PWR Project," October 1963 to January 1964, the cladding is expected to contain up to 250 ppm of hydrogen following three years of exposure.

A series of 600F hydride burst tests have been performed on Zircaloy- 4 tubes containing 200 to 250 and 400 ppm of hydrogen precipitated as hydride platelets in various orientations from radial to circumferential. Little difference in burst test ductility was evident. Therefore hydrogen normally absorbed in Zircaloy-4 tubing will not prove deleterious to the cladding integrity.

4.2.1.4.11 Effect of Swelling

Fuel swelling due to accumulation of solid and gaseous fission products and thermal expansion results in an increase in the fuel pellet diameter. The fuel rod design makes provision for accommodating both forms of pellet growth. The fuel-clad diametral gap is more than sufficient to accommodate the thermal expansion of the fuel. To accommodate irradiation induced swelling, it is conservatively assumed that the fuel-clad gap is used up by the thermal expansion and that only the fuel porosity and the dishes on each end of the pellets are available. Enough free volume, 8 percent of the fuel volume for nominal dimensions, is provided to take advantage of thermal and irradiation induced creep of the restrained fuel.

At a total fission-products-induced swelling rate of 0.7 percent change in volume (ΔV) per 10^{20} f/cm^3, 0.54 percent would be accommodated by the fuel porosity and dishes through fuel creep and 0.16 percent would increase the fuel diameter. Assuming peak burnup, this would correspond to using up a void volume equal to approximately 6.5 percent of the fuel volume and increasing the fuel rod diameter by a maximum of < 0.003 inch which corresponds to < 0.72 percent clad strain. It is concluded that sufficient accommodation volume has been provided even under the most adverse burnup and tolerance conditions.

Demonstration of the margin which exists is seen in the Large Seed Blanket Reactor (LSBR) irradiation. Two rods which operated in the B-4 loop of the MTR offer an interesting simulation for current PWR design[6, 10]. Both rods were comprised of 95 percent theoretical density pellets with dished ends and clad in Zircaloy. The first of these, No. 79-21, was operated successfully to a burnup of 12.41 x 10^{20} f/CM^3 (> 48,000 Mwd/MTU). The second fuel rod, No. 79-25, operated successfully to 15.26 x 10^{20} f/CM^3 (>60,000 Mwd/MTU). The linear heat rating ranged from 7.1 to 16.0 kw/ft. The wall thickness for the latter rod was 0.028 inch (t/OD = 0.058) as compared with 0.016 inch (t/OD = 0.033) for the former. All other parameters were essentially identical. The two rods were assembled by shrinking the cladding onto the fuel. The maximum diametral increase measured at ridge heights for rod 79-21, low t/OD ratio was 0.005 inch, while it was less than 0.002 inch for rod 79-25. From post-irradiation examination, it was concluded that approximately 84 percent of the total fuel swelling was accommodated by the porosity and dishes, while 16 percent caused diametral expansion of the clad and ridging at pellet interfaces. These results indicate that a comparable irradiation of the fuel elements for the C-E design, cold diametral gap 0.0085 inch, t/OD = 0.059 density 93 percent TD would allow a considerable increase in swelling life at a given clad strain.

The successful combined VBWR-Dresden irradiation of Zircaloy-clad oxide pellets provides additional confidence with respect to the design conditions for the fuel rods for the core[11, 12]. Ninety eight rods which had been irradiated in VBWR to an average burnup of about 10,700 Mwd/MTU were assembled in fuel bundles and irradiated in Dresden to a peak burnup greater than 48,000 Mwd/MTU. The reported maximum heat rating for these rods is 17.3 kw/ft which occurred in VBWR. Post irradiation examination [13] revealed that diametral increases in the fuel rods ranged from 0.001 to 0.003 inches maximum. The maximum diametral change corresponds to 1.42 percent ΔV (or 0.12 percent $\Delta V/V$ per 10^{20} f/cm^3) for these 0.424 inch diameter rods. The relevant fuel parameters are listed below for the above test and the C-E design:

	Fuel Density % TD	Cold Diametral Gap (inch)	Clad t/OD Ratio	Coolant Pressure (psia)
VBWR-Dresden	95	0.004 to 0.008	.052	1000
C-E Design	93	0.0085	.059	2250

A comparison of the design parameters above relative to the test results provide a conservative demonstration of the clad strains resulting from swelling of the fuel.

4.2.1.4.12 Variation of Melting Point and Fuel Conductivity with Burnup

This information is covered in Section 4.4.3.5.

4.2.1.4.13 Potential for Water Logging Rupture

The potential for water logging rupture is considered remote. Basically, the necessary factors, or combination of factors, include the presence of a small opening in the cladding, time to permit filling of the fuel rod with water, and, finally a rapid power transient. The size of the opening necessary to cause a problem falls within a fairly narrow band. Below a certain defect size, it takes a relatively long time to fill a fuel rod with water. Above a certain defect size, the rod can fill rapidly, but during a power increase it also expels water or steam readily without a large pressure buildup. Holes or defects which could result in an opening in cladding are scrupulously checked during the fuel rod manufacturing process by both ultrasonic and helium leak testing. Clad defects which could develop during reactor operation due to hydriding are also controlled by limiting those factors, e.g., moisture content of fuel pellets, which contribute to hydriding. The most likely time for a water logging rupture accident would occur after an abnormally long shutdown period. After this time, however, the startup rate is controlled so that even if a fuel rod were filled with coolant, it could "bake out" thus minimizing additional cladding rupture. The combination of control and inspection during the manufacturing process and the limits on the rate of power change restrict the potential for water logging to a very small number of fuel rods.

4.2.1.4.14 Fuel Burnup Experience

Design bases for the Zircaloy-4 cladding have been established which are conservative with respect to the reported data. Evidence currently available indicates that zirconium and UO_2 fuel performance is satisfactory to exposures in excess of 50,000 Mwd/MTU.

a) High Linear Heat Rating Irradiation Experience

The determination of the effect of linear heat rating and fuel cladding gap on the performance of 0.032 inch thick Zircaloy clad UO_2 fuel rods was the object of two experimental capsule irradiation programs conducted in the Westinghouse Test Reactor (WTR) [14]. In the first program, 18 rods containing 94 percent theoretical density UO_2 pellets were irradiated at 11, 16, 18 and 24 kw/ft with cold diametral gaps of 0.006 inch, 0.012 inch and 0.025 inch. The wall thickness to diameter ratio (t/OD) of the Zircaloy cladding was 0.064 which is slightly higher than the value of 0.059 in this design. Although these irradiations were of short duration (about 40 hours), significant results applicable to this design were obtained. No significant dimensional changes were found in any of the fuel rods. Only one rod, which operated at a linear heat rate of 24 kw/ft with an initial diametral gap of 0.025 inch, experienced center melting. Rods which operated at 24 kw/ft with cold gaps of 0.006 inch and 0.012 inch did not exhibit center melting. On these bases, the initial gap of 0.0085 inch and the maximum linear heat ratings for this design provide adequate margin against center melting, even when 112 percent overpower conditions are considered. These results also indicate that an initial diametral gap of 0.0085 inch is adequate to accommodate radial thermal expansion without inducing cladding dimensional changes even at a linear heat rate of 24 kw/ft. This margin with respect to thermal expansion will be diminished with increasing burnup at a rate of

0.16 percent ΔV per 10^{20} fissions/cm^3. However, the linear heat rating will decrease with burnup. Since the diametral thermal expansion, assuming BOL maximum heat ratings, is almost twice as great as the swelling diametral growth at the EOC burnup, these data add considerable weight to the conservative treatment of the influence of transients on fuel rod integrity.

Further substantiation of the capability of operation at maximum linear heat ratings in excess of those in this design is obtained from later irradiation tests in WTR [14]. Thirty eight inch long and six inch long fuel rods were irradiated at linear heat ratings of 19 kw/ft and 22.2 kw/ft to burnups of 3450 and 6250 Mwd/MTU. The cold diametral gaps in these Zircaloy clad rods containing 94 percent dense UO_2 were 0.002 inch, 0.006 inch and 0.012 inch. The cladding t/OD was 0.064 inch. No measurable diameter changes were noted for the 0.006 inch or 0.012 inch fuel clad gap rods. Only small changes were observed for the rods with a 0.002 inch diametral gap.

b) Shippingport Irradiation Experience

Zircaloy clad fuel rods have operated successfully (three defects have been observed which were a result of fabrication defects) in the Shippingport blanket with burnups of about 37,000 Mwd/MTU and maximum linear heat ratings of about 13 kw/ft. [14,15,16]. Although higher linear heat ratings will be experienced, swelling primarily burnup dependent and thermal expansion linear heat rate dependent provide the primary forces for fuel cladding strain at the damage limit. Thus, the Shippingport irradiations have demonstrated that Zircaloy clad rods with a cladding t/OD comparable to that for this plant (0.059), can successfully contain the swelling associated with 37,000 Mwd/MTU burnup while at the same time containing the radial thermal expansion associated with moderate heat ratings. Irradiation test programs in support of Shippingport in in-reactor loops demonstrated successful operation of burnups of 40,000 Mwd/MTU and linear heat ratings of 11 kw/ft with cladding t/OD ratios as low as 0.053 as compared to 0.059 for this plant. [17]

c) Saxton Irradiation Experience

Zircaloy-4 clad fuel rods containing UO_2-PuO_2 pellets of 94 percent theoretical density have been successfully irradiated in Saxton to peak burnups of 31,800 Mwd/MTU at 16 kw/ft linear heat rate under USAEC Contract AT (30-1)-3385 [18]. The t/OD of the cladding was 0.059 which is equal to that of this design. The amount of PuO_2, 6.6 percent, is considered as insignificant with respect to providing any difference in performance when compared with that for UO_2. In fact, the higher thermal expansion coefficient for PuO_2-UO_2 compared to that of UO_2 would induce greater cladding strain under equivalent irradiation conditions. Subsequent tests on two of the above rods, 18,600 Mwd/MTU at 10.5 kw/ft, successfully demonstrated the capability of these rods to undergo power transients from 16.8 kw/ft to 18.7 kw/ft.

d) Vallecitos Boiling Water Reactor (VBWR) - Dresden Experience

The combined VBWR - Dresden irradiation of Zircaloy clad oxide pellets provides additional confidence with respect to the design conditions for the fuel rods for this core. [11,19] Ninety eight rods which were irradiated in VBWR to an average burnup of about 10,700 Mwd/MTU were assembled in fuel bundles and irradiated in Dresden to a peak burnup greater than 48,000 Mwd/MTU. The reported maximum heat ratings for these rods is 17.3 kw/ft which occurred in VBWR. The t/OD cladding ratio of 0.052, and the external pressure of about 1000 psia are conditions which are all in the direction of less conservatism with respect to fuel rod integrity when compared with the design values of 0.059 cladding t/OD ratio and an external pressure of 2250 psia. Ten of these VBWR - Dresden rods representing maximum combinations of burnup, linear heat rating and pellet density have been examined in detail and found to be in satisfactory condition. The remaining eighty eight rods were returned to Dresden and successfully irradiated to the termination of the program.

e) Large Seed Blanket Reactor (LSBR) Rods Experience

Two rods operated in the B-4 loop at the Materials Testing Reactor MTR) provide a very interesting simulation for current PWR designs [6,10]. Both rods were comprised of 95 percent theoretical density pellets with dished ends, clad in Zircaloy. The first of these No. 79-21, was operated successfully to a burnup of 12.41×10^{20} f/cc (48,000 Mwd/MTU) through several power cycles which included linear heat rates from 5.6 to 13.6 kw/ft. The second fuel rod No. 79-25, operated successfully to 15.26×10^{20} f/cc. (~60,000 Mwd/MTU). The basic difference in this rod was the 0.028 inch wall thickness, as compared to 0.016 inch (t/OD = 0.058) in the first rod. All other parameters were essentially identical. The linear heat rating ranged from 7.1 to 16.0 kw/ft. After the seventh interim examination, the rod operated at a peak linear power of 12.9 kw/ft at a time when the peak burnup was 49,500 Mwd/MTU. These high burnups were achieved with fuel rods which were assembled by shrinking the cladding onto the fuel and indicate that a comparable irradiation of the fuel rods for this reactor, cold diametral gap of 0.0085 inch, would allow a considerable increase in swelling life at a given clad strain.

f) Central Melting in Big Rock Experience

As part of a Joint U. S. - Euratom Research and Development Program, Zircaloy-clad UO_2 pellet rods, 95 percent theoretical density, were irradiated under conditions designed to induce central melting in the Big Rock Point Reactor[20]. The test includes 0.7 inch diameter fuel rods, cladding t/OD= 0.057, fuel-clad gap of about 0.012 inch, at maximum linear heat ratings of about 27 kw/ft and 22 kw/ft with peak burnups up to 30,000 Mwd/MTU. Results of these irradiations provide a basis for incorporating linear heat ratings well in excess of those calculated for this reactor, and show that the presence of localized regions of fuel melting is not catastrophic to the fuel assembly.

g) Peach Bottom 2 Experience

General Electric has successfully irradiated fuel rods of the Peach Bottom 2 design to burnups in excess of 42,000 Mwd/MTU at peak linear heat ratings of 23 kw/ft. An interim examination at 32,500 Mwd/MTU indicated a satisfactory condition.[21]

4.2.1.4.15 Effects of Fuel Densification

The effects of fuel densification should be considered for their influence on the safety evaluation for normal operation, operation during various transient conditions and postulated accident situations (Reference 22). The C-E Fuel Evaluation Model (Reference 23) provides an analytical method of predicting fuel pellet temperature, fuel rod internal pressure and pellet/clad gap conductivity, based on experimental data, for various as-fabricated properties, core lifetimes and linear heat generation rates. Results of the analysis are used as input to the safety analysis.

Reference 23 describes the analytical fuel thermal performance model and the experimental data used to develop that model; provides a comparison of predicted performance with actual performance for applicable cases; describes input parameters and assumptions; discusses correction factors applied to account for fuel pellet densification and clad collapse; and shows the interfaces between the Fuel Evaluation Model analysis and the safety analysis. This model has been reviewed and approved by the NRC staff for licensing calculations. Application of the model and results of the evaluation are discussed in Section 4.3.3.4 (Augmentation Factors) and in Sections 6.3.3.6, 15.1.5 and 15.4 (Safety Analysis) and in Section 4.2.1.4.16 (Prevention of Cladding Creep Analysis).

Input parameters used in the St. Lucie Plant No. 1 fuel evaluation, for the most limiting fuel (Batch B) are given in Table 4.2-3a.

4.2.1.4.16 Prevention of Cladding Creep Collapse

Summary and Conclusions

In the St. Lucie Unit 1 reactor, long-term creep collapse of the fuel rod cladding is prevented by internal pressurization with all fuel rods at the time of manufacture with 100% helium, or with a mixture of helium and argon gases. The effect of internal pressurization is to reduce cladding stresses (and, hence, creep rates) during operation to such an extent that the cladding remains stable and does not callapse during a period of time equal to the expected service life of the fuel. The St. Lucie Unit 1 fuel rod fill pressure is given in Reference 24, CENPD-187-P.

The St. Lucie Unit 1 fuel rod collapse time predictions reported herein were calculated using these fill pressures and the CEPAN computer code (Reference 24). The results show that the fuel rods will operate for their entire lifetime without collapse. The details of the calculations are discussed in the following paragraphs.

Calculation of Cladding Creep Collapse

The calculations of the minimum times to collapse for fuel rods in the St. Lucie Unit 1 reactor represent the results of two independent analyses performed in sequence; the first to determine the minimum fuel rod internal pressure as a function of burnup, and the second to determine clad ovalities versus time. The two calculations are discussed separately in the following paragraphs.

Calculation of Fuel Rod Internal Pressures

Fuel rod internal pressure is calculated using the FATES computer code (Reference 23). FATES is a digital program which determines internal volume and pressure variation with burnup. The computer model divides the fuel rod into twenty axial segments, and also divides the rod operating lifetime into a number of burnup steps, each of which has local power level inputs for the axial segments. For each axial position, and for each burnup step, FATES calculates fuel and cladding temperatures, fuel and cladding thermal expansion, axial and radial fuel pellet swelling and cladding elastic deformation and creep. FATES then calculates the effective internal volume within the fuel rod, including specific accounting for upper end plenum, fuel-clad annulus, pellet end dish volume and pellet internal porosity. The model also includes specific steps to account for the effects of helium solubility, assumed fuel densification to 96.5 percent, and cladding elongation due to irradiation.

Figures 4.2-5A to 4.2-5E depict the variation in minimum internal pressure with time in St. Lucie Unit 1 rods, as predicted by the FATES code. These curves are based on combinations of fuel rod properties and dimensions which lead to the minimum pressure condition. As an added conservatism, the minimum pressure calculation did not take credit for the release of gaseous fission products from the fuel. The power histories used to generate the curves represent envelopes around the expected power levels of all rods of each fuel type during Cycle 1, and a best estimate of these envelopes, during subsequent cycles.

Collapse Analysis Description

Fuel rod cladding collapse calculations were performed with the CEPAN computer code (Reference 24). Input values to the cases covering operation of the various fuel types are summarized in Table 4.2-3b.

Collapse Analysis Results

Based on CEPAN cases using the conservative input values listed above, the cladding of St. Lucie Unit 1 fuel rods is not subject to collapse during its operating lifetime.

4.2.1.5 Verification of Mechanical Characteristics by Inspection and Test

Fuel assembly quality assurance is attained by adherence to the quality assurance requirements specified and evaluated in accordance with the FPL Quality Assurance Topical Report described in Section 17.2. Vendor product certifications, process surveillance, inspections, tests and material check analyses are performed to ensure conformity of all fuel assembly components to the design requirements from material procurement through loading of the completed assembly onto the shipping carrier. The following are basic quality assurance measures which are performed in addition to dimensional inspections and material verifications:

a) Fuel Pellets

A sampling test procedure is performed to provide assurance that the enrichment requirements are met and that the total adsorbed and absorbed gas content does not exceed the specified limit. Pellet density is measured and calculated; visual inspections of the pellets are required.

b) Fuel Cladding

Mechanical and physical properties of the cladding are verified by testing samples selected at random from each finished tubing lot. Flare, metallographic, burst, and ultrasonic tests are performed in addition to verification of corrosion resistance, determination of hydride orientation and surface finish inspection.

c) Fuel Rod

Fuel stack weight and length are verified prior to loading. The loading process is such that cleanliness and dryness of the components are maintained until after the final end cap weld is completed. The loaded fuel rods are evacuated and back filled with helium, a controlled purity and quantity. End cap welds are visually inspected and leak tested. Quality of the end cap welds is ensured by evaluating longitudinal sections cut from weld samples. The finished fuel rods are fluoroscoped to ensure a continuous pellet stack, and visually inspected to ensure a proper surface finish. Each fuel rod is marked to provide a means of identifying the pellet enrichment, pellet lot, and stack weight.

d) Spacer Grids, Retention Grid, Guide Tubes

The welds and surface finish of these components are inspected to ensure conformance with approved standards.

e) Upper and Lower End Fittings

The upper end fitting posts are ultrasonically and visually inspected and the flow plate and hold down plate are radiographically inspected to ensure conformance with approved standards. The lower end fitting is visually inspected.

f) Fuel Assembly

The quality of welds joining guide tubes to spacer grids are verified by corrosion tests and visual inspection. All guide tubes are ball gaged ensuring free passage within the tubes between the upper flange and the reduced buffer region. An alpha smear test is performed on the exterior surface of the fuel rods. Guide tube to end fitting joints are inspected in accordance with an approved standard. The spacer grid to fuel rod relationship is carefully examined at each grid location.

Each completed fuel assembly is inspected for cleanliness, wrapped to preserve its cleanliness, and loaded within shipping containers which are later purged and filled with dry air.

Protection of the fuel assembly in transit is ensured through proper design of the shipping container. Clamping and support surfaces are provided at each support grid and end fitting location. Design of the container will prevent shock loads to the fuel assembly from exceeding 5 g's in any direction when the shipping container assembly is subjected to handling and shipping peak loads typical of the carriers used in accomplishing delivery. Impact recorders are contained within each shipment to determine if shock loads in the axial, vertical and lateral directions have exceeded 5 g's in transit. The fuel assembly will be visually inspected for evidence of damage and repaired if necessary.

Guidelines for visual inspection of the conveyance vehicle, shipping container and fuel assembly are provided. Instructions are also given for unloading the fuel assemblies. A check list is provided for visual inspection of exterior fuel assembly components for shipping damage and cleanliness.

REFERENCES FOR SECTION 4.2.1

1. Manson, S. S., "Fatigue: A Complex Subject - Some Simple Approximations," Experimental Mechanics, Vol. 22, No. 2, pp. 193 - 226, July 1965.

2. O'Donnell, W. J. And B. F. Langer, "Fatigue Design Basis for Zircaloy Components," Nuclear Science and Engr., Vol. 20, pp. 1 - 12, 1964.

3. O'Donnell, W. J., "Fracture of Cylindrical Fuel Rod Cladding due to Plastic Instability," WAPD-TM-651, April 1967.

4. Weber, J. M., "Plastic Stability of Zr-2 Fuel Cladding, Effects of Radiation on Structural Metals," ASTM STP 426, American Society of Testing Materials, 1967, pp. 653 – 669.

5. Engel, J. T. and H. B. Meieran, "Performance of Fuel Rods Having 97 Per Cent Theoretical Density UO_2 Pellets Sheathed in Zircaloy-4 and Irradiated at Low Thermal Ratings," WAPD-TM-631, July 1968.

6. Duncombe, E., J. E. Meyer, and W. A. Coffman, "Comparisons with Experiment of Calculated Dimensional Changes and Failure Analysis of Irradiated Bulk Oxide Fuel Test Rods Using the CYGRO-1 Computer Program," WAPD-TM-583, Sept. 1966.

7. McCauley, J. E., R. C. Daniel, B. B. Meieran, and J. T. Engel, "Evaluation of the Irradiation Performance of Zircaloy-4 Clad Test Rod Containing Annular UO_2 Fuel Pellets (Rod 79-19)," WAYD-TM-595, December 1966.

8. Notley, M. J. F., A. S. Bain and J. A. L. Robertson, "The Longitudinal and Diametral Expansion of UO_2 Fuel Elements," AECL-2143, November 1964.

9. Notley, M. J. F., "The Thermal Conductivity of Columnar Grains in Irradiated UO_2 Fuel Elements," AECL-1822, July 1962.

10. Berman, R. M., H. B. Meieran and P. Patterson, "Irradiation Behavior of Zircaloy-Clad Fuel Rods Containing Dished End UO_2 Pellets," (LWBR-LSBR Development Program), WAPD-TM-629, July 1967.

11. Baroch, C. J., J. P. Hoffmann, H. E. Williamson, and T. J. Pashos, "Comparative Performance of Zircaloy and Stainless Steel Clad Fuel Rods Operated to 10,000 Mwd/T in the VBWR," GEAP-4849, April 1966.

12. Megerth, F. H., "Zircaloy-Clad UO_2 Fuel Rod Evaluation Program," Quarterly Progress Report No. 8, August 1969 - October 1969, GEAP-10121, November 1969.

13. Megerth, F. H., "Zircaloy-Clad UO_2 Fuel Rod Evaluation Program," Quarterly Progress Report No. 1, November 1967 to January 1968, GEAP-5598, March 1968.

14. Indian Point Nuclear Generating Unit No. 2, PSAR, Appendix A.

REFERENCES FOR SECTION 4.2.1

15. Stiefel, J. T., H. Feinroth and G. M. Oldnam, "Shippingport Atomic Power Station Operating Experience, Development and Future Plans," WAPD-TM-390, April, 1963.

16. Question V. B. 2, Prairie Island Nuclear Generating Plant, Preliminary Safety Analysis Report (Docket No. 50-306)

17. Anderson, T. D., "Effects of High Burnup on Bulk UO_2 Fuel Elements," Nuclear Safety, Vol. 6, No. 2, Winter 1964 - 65, pp. 164-169.

18. Miller, R. S. et al, "Operating Experience with the Saxton Reactor Partial Plutonium Core - II," paper presented at AEC Plutonium Meeting in Phoenix (August 1967).

19. Megerth, F. H., "Zircaloy-Clad $U0_2$ Fuel Rod Evaluation Program, Quarterly Progress Report No. 2, February 1968 - April 1968," GEAP-5624 (May 1968).

20. Blakely, J. P., "Action on Reactor and Other Projects Undergoing Regulatory Review or Consideration," Nuclear Safety, Vol. 9, No. 4, p. 326 (July - August 1968).

21. Summary Description of Peach Bottom Atomic Power Station Units No. 2 and No. 3 and Review of Considerations Important to Safety, (Docket No. 50-277 and 50-278).

22. Regulatory Staff, U S Atomic Energy Commission, "Technical Report on Densification of Light Water Reactor Fuels," November 14, 1972.

23. "CE Fuel Evaluation Model," CENPD-139-P-A (Proprietary) and CENPD-139-A (Non-Proprietary), July 1, 1974.

24. "CEPAN - Method of Analyzing Creep Collapse of Oval Cladding," CENPD-187-P (Proprietary) and CENPD-187 (Non-Proprietary), June 1975.

25. R. E. Uhrig (FPL) to V. Stello (NRC) Re: St. Lucie Unit No 1, Docket No 50-335, St. Lucie Unit No. 1 Repair Report, CEN-35(F)-P, Revision 1, L-76-368 dated 10/25/76.

4.2.2 REACTOR VESSEL INTERNALS

4.2.2.1 Design Bases

The reactor vessel internals are designed to meet the loading conditions listed in Section 4.2.2.1.1 and the design limits specified in Section 4.2.2.1.2. The details of the dynamic analyses are described in Section 3.9.1. The materials of the reactor internal structures are primarily Type 304 stainless steel. The flow skirt is fabricated from Ni-Cr-Fe. Welded connections are used where feasible; however, in locations where mechanical connections are required, structural fasteners are designed to remain captured in the event of a single failure. Structural fastener material is typically a high strength austenitic stainless steel, however, in less critical applications, Type 316 stainless steel is employed. Hardfacing of Stellite material is used at wear points. The effect of irradiation on the properties of the materials is considered in the design of the reactor internal structures.

4.2.2.1.1 Categorization and Combination of Loadings

a) Normal Operating and Upset Conditions

The reactor vessel internals are designed to perform their normal functions while experiencing the following combination of loadings:

Normal operating temperature differentials
Normal operating pressure differentials
Flow impingement load
Weights, reactions and superimposed loads
Vibration loads
Shock loads, including operating basis earthquake OBE
Transient loadings not requiring forced shutdown
Handling loads (not combined with above).

b) Emergency Conditions

The internals are designed to permit an acceptable amount of local yielding while experiencing the loadings listed above with the design basis earthquake (DBE) load replacing the operating basis earthquake load.

c) Faulted Conditions

Permanent deformation of the reactor internal structures is permitted. The loadings for these conditions include all the loadings given for emergency conditions plus the loadings resulting from the postulated LOCA.

4.2.2.1.2 Design Limits

Reactor internal components are designed to ensure that the stress levels and deflections are within an acceptable range. The allowable stress values for core support structures are not greater than those given in the May 1972 draft of Section III of the ASME Boiler and Pressure Vessel Code, Subsection

NG, Appendix F, "Rules for Evaluation of Faulted Conditions." Stress limits for the reactor vessel core support structures are presented in Table 4.2-4. In the design of reactor vessel internal components which are subject to fatigue, the stress analysis is performed utilizing the design fatigue curve of Figure 1-9.2 of Section III of the ASME Boiler and Pressure Vessel Code and a cumulative usage factor of less than 1.0 as the limiting criteria. In addition, to properly perform their functions, the reactor internal structures will satisfy the deformation limits listed below.

a) Under design loadings plus operating basis earthquake forces or normal operating loadings plus design basis earthquake forces, deflections will be limited so that the CEAs can function and adequate core cooling is preserved.

b) Under normal operating loadings plus design basis earthquake forces plus pipe rupture loadings resulting from a break of the largest line connected to the reactor coolant system piping, deflections will be limited so that the core will be held in place, adequate core cooling is preserved, and all control element assemblies can be inserted. Those deflections which would influence CEA movement will be limited to less than 80 percent of the deflections required to prevent CEA insertion.

c) Under normal operating loadings plus design basis earthquake forces plus the maximum pipe rupture loadings resulting from the full spectrum of pipe breaks, deflections will be limited so that the core will be held in place and adequate core cooling is preserved. Although CEA insertion is not required for the largest reactor coolant system pipe break, calculations show that the CEAs can be insertable except for a few CEAs located near the vessel outlet nozzle which is feeding the postulated break.

4.2.2.2 Reactor Vessel Internals Description

4.2.2.2.1 Reactor Internal Structures

The reactor internals are divided into four major parts consisting of the core support barrel, the lower core support structure and core shroud, the upper guide structure and CEA shrouds, and the incore instrumentation guide tubes. The flow skirt, although functioning as an integral part of the coolant flow path, is separate from the internals and is affixed to the bottom head of the reactor vessel. These components are shown in Figure 4.2-7. The incore instrumentation structure is described in Section 4.2.2.2.7.

4.2.2.2.2 Core Support Structure

The major support member of the reactor internals is the core support structure. The core support structure consists of the core support barrel and the lower support structure. The material for the assembly is Type 304 stainless steel.

a) Core Support Barrel

The core support barrel is a right circular cylinder with a heavy ring flange at the top end and an internal ring flange at the lower end. The core barrel is supported from a ledge on the reactor vessel. The core support barrel, in turn, supports the lower support structure upon which the fuel assemblies rest. Press fitted into the flange of the core support barrel are four alignment keys located 90 degrees apart. The reactor vessel, closure head, expansion compensating ring and upper guide structure assembly flange are slotted in locations corresponding to the alignment key locations to provide alignment between these components in the vessel flange region.

The upper section of the barrel contain two outlet nozzles contoured to minimize coolant bypass leakage.

Since the weight of the core support barrel is supported at its upper end, it is postulated that coolant flow could induce vibrations in the structure. Therefore, amplitude limiting devices, or snubbers, are installed on the outside of the core support barrel near the bottom end. The snubbers consist of six equally spaced lugs around the circumference of the barrel and act as a tongue and groove assembly with the mating lugs on the reactor vessel. Minimizing the clearance between the two mating pieces limits the amplitude of vibration. During assembly, as the internals are lowered into the reactor vessel, the reactor vessel lugs engage the core support barrel lugs in an axial direction. Radial and axial expansion of the core support barrel are accommodated, but lateral movement of the core support barrel is restricted. The reactor vessel lugs have bolted, captured Ni-Cr-Fe shims and the core support barrel lug mating surfaces are hardfaced with Stellite to minimize wear. The shims are machined during initial installation to provide a minimum clearance. The snubber assembly is shown in Figure 4.2-8.

b) Core Support Plate and Lower Support Structure

The core support plate is a Type 304 stainless steel plate into which the necessary flow distributor holes for the fuel assemblies have been machined. Fuel assembly locating pins, four for each assembly, are shrunk-fit into this plate.

The fuel assemblies and core shroud are positioned on the core support plate which forms the top support member of a welded assembly consisting of a cylinder, a bottom plate, support columns and support beams as shown in Figure 4.2-7. The cylinder guides the main coolant flow and limits the core shroud bypass flow by means of holes located near the base of the cylinder.

4.2.2.2.3 Core Shroud

The core shroud provides an envelope for the core and limits the amount of coolant bypass flow. The shroud consists of two Type 304 stainless steel ring sections secured to each other and to the core support plate by pre-tensioned tie rods. A small gap is provided between the core shroud outer perimeter and the core support barrel in order to provide coolant flow between the core shroud and core support barrel, thereby minimizing thermal stresses in the core shroud and eliminating stagnant flow pockets. The core shroud is shown in Figure 4.2-9.

4.2.2.2.4 Flow Skirt

The Ni-Cr-Fe flow skirt is a right circular cylinder, perforated with flow holes, and reinforced at the top and bottom with stiffening rings. The flow skirt function is to reduce inequalities in core inlet flow distribution and to prevent formation of large vortices in the lower plenum. The skirt provides a nearly equalized pressure distribution across the bottom of the core support barrel. The skirt is supported by nine equally spaced sections which are welded to the bottom head of the reactor vessel.

4.2.2.2.5 Upper Guide Structure Assembly

This assembly shown in Figure 4.2-10, consists of the upper support structure, control element assembly shrouds, fuel assembly alignment plate and a hold down ring. The upper guide structure assembly aligns and laterally supports the upper end of the fuel assemblies, maintains the CEA spacing, holds down the fuel assemblies during operation, prevents fuel assemblies from being lifted out of position during a severe accident condition, protects CEAs from the effect of coolant crossflow in the upper plenum, and supports the ICI plate assembly. The upper guide structure is handled as one unit during installation and refueling.

The upper end of the assembly is a structure consisting of a support plate welded to a grid array of beams and a cylinder, which encloses and is welded to the ends of the beams. The periphery of the plate contains four accurately machined equally spaced alignment keyways, which engage the core barrel alignment keys. This system of keys and slots provides an accurate means of aligning the core with the closure head and with the CEDMs.

The CEA shrouds extend from the fuel assembly alignment plate to above the upper guide structure support plate. The single CEA shrouds consist of cylindrical upper sections welded to integral bottom sections, which are shaped to provide flow passages for the coolant through the alignment plate while shrouding the CEAs from cross flow. Dual CEA shrouds accommodate two adjacent and interconnected CEAs. These shrouds have an oval shaped upper section welded to a flow diverting base section. The shrouds are bolted and lockwelded to the fuel assembly alignment plate. At the upper guide structure support plate, the single shrouds are connected to the plate by spanner nuts. The spanner nuts are tightened to specified torque to assure a rigid connection and lockwelded. The dual shrouds are attached to the upper plate by welding.

The fuel assembly alignment plate is designed to align the upper ends of the fuel assemblies and to support and align the lower ends of the CEA shrouds. Precision machined holes in the fuel assembly alignment plate align the fuel assemblies. The fuel assembly alignment plate also has four equally spaced slots on its outer edge which engage with Stellite hardfaced pins protruding from the core shroud to limit lateral motion of the upper guide structure assembly during operation. The fuel alignment plate bears the upward force of the fuel assembly holddown devices. This force is transmitted from the alignment plate through the CEA shrouds to the upper guide structure support plate and thence to the expansion compensating ring.

The hold down ring is positioned on the upper guide structure and engaged with the reactor vessel head. The expansion compensating ring functions to resist axial upward movement of the upper guide structure assembly and to accommodate axial differential thermal expansion between the core barrel flange, upper guide structure flange and reactor vessel flange support ledge and head flange recess.

The hold down ring design has been revised based on the experience gained at the Palisades plant (Docket 50-255) with the loss-of-holddown and resulting vibration of the core support barrel. Both the design configuration and the material of the ring have been changed from stainless 304 to 403 to provide holddown loading that is approximately 500,000 pounds greater than before the revision to the ring.

To account for zircaloy neutron irradiation growth of the fuel assemblies with burnup, as was evidenced by the growth measured in the Palisades and Maine Yankee reactors, a stainless steel shim of 0.200 inch thickness will be installed between the top of the upper guide structure and the compensating ring and one of 0.100 inch between the upper guide structure and the core support barrel flanges. This initial core installation allows for a zircaloy growth of up to 0.100 inch during the first cycle. For subsequent cycles the zircaloy growth is accommodated by stacking the two shims between the upper guide structure and the core support barrel flanges. The current configuration is one 0.200 inch thick shim between the upper guide structure and core support barrel flange.

4.2.2.2.6 Thermal Shield

A historical description of the thermal shield is as follows:

The thermal shield is a cylindrical structure which reduces the neutron flux and radiation heating in the reactor vessel wall. The thermal shield is fabricated from Type 304 stainless steel. At the upper end, the shield is supported by nine equally spaced lugs on the outer periphery of the core support barrel which restrict axial and tangential motion of the shield. Directly under each support lug is a preloaded positioning pin which is threaded radially through the thermal shield and butts against the core barrel. The lower end of the thermal shield is similarly restrained radially by seventeen positioning pins.

During the March 1983 refueling outage, visual examination of the core support barrel/thermal shield assembly disclosed the thermal shield support system to be severely damaged. A number of thermal shield support pins were fractured and/or missing and damage to the core support barrel was visible.

An evaluation of the thermal shield support system concluded that refurbishment was impractical. Therefore, a decision was made to remove the thermal shield. Analyses performed to evaluate operation of the plant without a thermal shield for its remaining design life indicated that replacement of the thermal shield was not necessary.

Upon removal of the thermal shield from the core support barrel, a nondestructive examination of the core support barrel was conducted. Damage of varying degrees was in evidence at eight of the nine thermal shield support lug locations. Four lugs were separated from the core support barrel and through wall cracks were confirmed adjacent to some damaged lug areas.

The repair process for the core support barrel was formulated. Underwater machining of the core support barrel in the damaged areas was used to reduce stress concentrations. Through wall cracks were arrested by crack arrestor holes appropriately sized for each crack; non-through-wall cracks were removed by machining away all material around the crack, and lug tear out areas were machined and patched as necessary. The crack arrestor holes were sealed by inserting expandable plugs.

A structural evaluation of the repaired core support barrel without the thermal shield was performed. The component stresses under normal, upset and faulted conditions were evaluated and found to be within the limits of Section III, Subsection NG 1972, Draft Edition of the ASME Nuclear Components Code.

In addition to the effects of thermal shield removal on the repaired core support barrel the effects on the reactor internals were investigated and determined to be:

(a) A small change in the hydraulic loads on the reactor internals.

(b) A negligible change in the frequency of the core support barrel assembly.

Evaluation of the above effects were considered in combination with the site specific seismic and asymmetric loads analysis. A seismic analysis was performed considering the thermal shield had been removed and asymmetric LOCA load data were derived based on no thermal shield. The analysis showed that the reactor internals with the thermal shield removed meet the ASME Code allowable stresses using the original design criteria for normal operation, upset (Level A and B), and LOCA (Level D) conditions.

4.2.2.2.7 Incore Instrumentation Support System

The function of the incore instrumentation system is described in Section 4.2.2.2.8. The incore instrumentation system begins outside of the reactor vessel, penetrates the vessel boundary and terminates in the fuel assembly. This section describes the mechanical components which support the incore instrumentation inside the reactor vessel (see Figure 4.1-1).

The support system provides guidance for each instrument and protects them from turbulent cross flow. The guidance path consists of a conduit above the incore instrument support plate and incore thimbles which extend into

the center of selected fuel assemblies. The conduit and incore thimbles are attached to and supported by the instrument plate assembly shown in Figure 4.2-11. The instrumentation plate assembly fits within the confines of the reactor vessel head and rests in the recessed section of the upper guide structure assembly. Its weight is supported by four bearing pins. The upper guide structure CEA shrouds extend through the instrumentation plate clearance holes. Above the instrument plate, the conduits bend and are gathered to form instrument stalks which extend into the reactor vessel head instrumentation nozzles. The instrumentation plate assembly is raised and lowered during refueling to insert or withdraw all instruments and their thimbles simultaneously.

The incore instrument thimbles are designed such that the temperature of the coolant surrounding the incore instruments at the location of the thermocouples is representative of fuel assembly outlet temperatures. The incore instruments lengths and the thimbles are designed to locate individual neutron detectors within ±2 inches of their nominal position relative to the fuel under operating conditions. Smooth paths are provided for insertion and withdrawal of each instrument. All mechanical fasteners are positively locked into place.

4.2.2.2.8 Incore Instrumentation

a) Design Bases

The primary function of the incore instrumentation is to provide measured data which may be used in evaluating the gross core power distribution in the reactor core as an aid to reactor operations. This data may be used to evaluate thermal margins and to estimate local fuel burnup. No credit is taken for this system in the accident analysis of Chapter 15. The incore detectors will be used to periodically calibrate the out-of-core detectors as defined in the Technical Specifications, monitor the azimuthal power tilt, calibrate the power level neutron flux channels and monitor the linear heat rate.

The incore instrumentation system, when used to perform functions listed above, must meet the appropriate operability requirements of Section 13.8.1.2.1.

If these minimum conditions are not met, the incore instrumentation system is not used for the above listed applicable monitoring or calibration functions.

The incore detector monitoring system may be used for monitoring the core power distribution when the incore detector Local Power Density alarms have appropriately included the uncertainty allowances specified in Section 13.8.1.2.2 in the setting of these alarms.

Operability of the incore detector system is demonstrated by performance of the surveillance requirements specified in Section 13.8.1.2.2.

This information on the incore detector monitoring system was removed from Technical Specifications and relocated into the UFSAR by Technical Specification Amendment 136.

b) Design Criteria

1) Detector assemblies are installed in the reactor core at selected locations to measure core neutron flux and coolant temperature information during reactor operation in the power range;

2) Flux detectors of the self-powered type with proven capabilities for incore service are used;

3) The information obtained from the detector assemblies may be used for fuel management purposes and to assess the core performance. It is not used for automatic protective or control functions;

4) The output signal of the flux detectors will be corrected for changes in sensitivity due to emitter material burnup and for radiation induced background interference;

5) Axial spacing of the detectors in each assembly and radial spacing of the assemblies permit an evaluation of the gross core power distribution.

c) System Description

The incore instrumentation system consists of up to 45 available locations for fixed incore detector assemblies to be inserted into selected fuel assemblies. The incore detector assembly design contains one full-core length background detector, four 40 cm long rhodium detectors, and one Cr-Al thermocouple.

Assemblies are inserted into the core through instrumentation nozzles in the reactor vessel head. Each assembly is guided into the position in the center of the fuel assembly via a fixed guide tube and instrument thimble assembly. The locations of the incore detectors in the core are shown in Figure 4.2-13.

The rhodium detectors produce a current proportional to neutron flux by a neutron-beta reaction in the detector wire. The expected useful life of the rhodium detectors is about 3 cycles at full power, after which the detector assemblies will be replaced by new units.

The data from the thermocouples and detectors are read by the data processor which scans all assemblies, processes and prints out the data periodically or on demand. In the case of the rhodium detectors, the data processor periodically computes integrated flux at each detector to update detector sensitivity factors to compensate for detector burnout.

4.2.2.2.9 Neutron Source

Two plutonium 238 - antimony - beryllium startup sustainer source assemblies were installed in the reactor through operating cycle 9. The purpose of neutron sources is to provide sufficient subcritical neutron multiplication for positive indication on the out-of-core neutron detectors.

Irradiated fuel reloaded into the core from previous operating cycles produces a sufficient neutron source and is now used as the startup neutron source. The startup sustainer source assemblies are stored in the spent fuel pool.

4.2.3 REACTIVITY CONTROL SYSTEM

Reactivity control of the reactor is achieved by two independent systems. The first is the Reactor Control System (discussed in Section 7.7.1.1) which directs the CEDMs to insert, hold, withdraw or trip the CEAs. Figure 4.2-16c shows the CEA location by bank and Figure 4.2-16d shows the CEDM numbering sequence. The chemical and volume control system provides the second means, by varying the concentration of boric acid in the coolant to affect relatively slow reactivity changes. The chemical and volume control system is discussed in more detail in Section 9.3.4.

4.2.3.1 Control Element Drive Mechanism

The control element drive mechanism (CEDM) are magnetic jack drives shown in Figure 4.2-14 used to vertically position and indicate the position of the control element assemblies (CEA) in the core. Each CEDM is capable of withdrawing, inserting, holding or tripping the CEA from any point within its travel in response to operating signals. Each CEDM is connected to the CEA by an extension shaft.

4.2.3.1.1 CEDM Design Bases

The CEDMs are designed to function during and after all normal plant transients of temperature and pressure. The CEA trip time for 90 percent insertion is 3.1 seconds maximum where trip time is defined as the interval between the opening of the CEDM coil power circuit breakers and the time the CEA has reached 90 percent of fully inserted position.

The CEDMs are designed to function during and after an operational basis earthquake. The CEDM is capable of tripping or inserting the CEAs after a design basis earthquake. For pipe break accident loads, the CEDMs are designed to maintain the position of the CEAs in the core. The CEDM is capable of inserting the CEA to the full position from the fully withdrawn position and transmitting all position indication signals for 15 minutes after a postulated LOCA. During the application of the accident loads, ejection of the CEA are prevented in the event of a split of the upper portion of the pressure housing above the operating mechanism, or a major pipe rupture.

The CEDM pressure housings are an extension of the reactor vessel and a part of the reactor coolant boundary, and designed to meet the requirements of Section III, of the ASME Boiler and Pressure Vessel Code Class A. Pressure and thermal transients and steady-state loadings are evaluated in the design analysis. A summary of the reactor vessel stress limits is provided in Section 5.2.1.

4.2.3.1.2 Design Description

The CEDMs are mounted and welded to nozzles on top of the reactor vessel closure head. The CEDMs consist principally of the

motor assembly, upper pressure housing, and coil stack assembly. The drive power is supplied by the coil stack assembly which is positioned around the CEDM housing. The CEDMs are forced air cooled.

The lifting operation consists of a series of magnetically operated step movements. Two sets of mechanical latches are utilized engaging a notched drive shaft. The magnetic force is obtained from DC magnet coils mounted on the outside of the motor tube.

Power for the electromagnets is from two separate power supplies. The CEA control system actuates the stepping cycle thereby raising or lowering the CEA by a forward or reverse stepping sequence. CEDM hold is accomplished by energizing one coil at a reduced current while all other coils are deenergized. The CEDMs are tripped upon interruption of electrical power to the coils. EC291158

a) CEDM Pressure Housing

The CEDM pressure housing consists of the motor housing assembly and the upper pressure housing assembly. The motor housing assembly is attached to the reactor vessel head nozzle by means of a threaded joint and seal welded. Once the motor housing assembly is seal welded to the head nozzle, it need not be removed since all servicing of the CEDM is performed from the top of the housing. The upper pressure housing is threaded into the top of the motor housing assembly and seal welded. The upper pressure housing encloses the CEDM extension shaft, supports the reed switch and coil power assembly and contains the vent valve. The top opening of the upper pressure housing is closed by means of a threaded cap which can be seal welded.

b) Motor Assembly

The motor assembly is an integral unit which fits into the motor housing assembly through an opening in the top of the housing and consists of a motor tube, magnets and lift, hold and anti-ejection latches.

The anti ejection device utilizes three grippers which are operated through a three bar linkage. When deenergized, they are spring loaded into engagement with the drive shaft. The drive shaft ratchets through these grippers with a minimum retarding force during CEA insertion on trip.

c) Coil Stack Assembly

The coil stack assembly consists of electromagnetic coils mounted on the outside of the motor housing assembly. The coils supply magnetic force to actuate mechanical latches utilized in engaging and driving the notched drive shaft. The CEA control system actuates the stepping cycle and obtains the correct CEA EC291158

location by a forward or reverse stepping sequence. CEDM hold is obtained by energizing one coil at a reduced current while all other coils are deenergized. The scrammable CEAs are tripped upon interruption of electrical power to all coils. Redundant logic power for the control system is provided by the use of two power supplies connected in parallel, with isolation provided by blocking diodes in an auctioneered circuit, to insure against inadvertent CEA trips due to power failure. Step in and step out digital signals are totalized within the CEA control system to provide a means for determining CEA position indication. A conduit assembly containing the lead wires for the coil stack assembly is routed along the upper pressure housing, as shown on Figure 4.2-14. EC291158 EC291158

d) Reed Switch Assembly

The reed switch assembly provides two additional separate means for transmitting CEA position information. One method utilizes reed switches and a voltage divider network to provide an output voltage proportional to the CEA position. The second method utilizes three pairs of reed switches spaced at discreet axial locations. The reed switch assembly is positioned so as to utilize the permanent magnet in the top of the extension shaft. The permanent magnet actuates the reed switches one at a time as it passes by them.

e) Extension Shaft and CEA Coupling System

The extension shaft assemblies connect the CEDMs to the CEAs. The assemblies are of two types: the single, which is coupled to only one CEA and the dual, which is coupled to two CEAs. An extension shaft assembly consists of an operating rod assembly and an outer sleeve assembly. The operating rod assembly is a stepped 304 stainless steel rod consisting of a permanent magnet assembly at the top for actuating reed switches in the reed switch assembly as a means of position indication, a center section called the drive shaft which is notched to be compatible with the mechanical latches that are magnetically operated in step movements for lifting and lowering operations, and a lower end consisting of a gripper plunger.

The outer sleeve assembly consists of a gripper assembly, extension shaft, drive shaft, top extension shaft and the extension sleeve. The gripper assembly consists of a gripper, spring, sleeve and end fitting. The sleeve and end fitting act as the outer sleeve with the gripper, spring and plunger in the center of the assembly. The plunger is spring-loaded to remain in the center of the gripper.

In the coupled position the operating rod assembly is preloaded torsionally relative to the outer sleeve assembly to preclude inadvertent uncoupling. With the plunger in the center of the gripper, it is expanded sufficiently to maintain engagement with the CEA. The dual CEA differs in that the operating rod engages a yoke assembly, which in turn mates to the two grippers.

Near the bottom of the extension shaft is a larger diameter section which allows the upper guide structure to pick up the extension shafts as the upper guide structure is removed from the reactor vessel.

The drive shaft is a long tube made of 304 stainless steel. It is threaded and pinned to the extension shaft. The drive shaft has circumferential notches along the shaft to provide the means of engagement to the control element drive mechanism.

The magnet assembly consists of a housing, magnet and plug. Two, 2-inch cylindrical Alnico-V magnets with a minimum flux density of 325 gauss are used in the assembly. This magnet assembly is used to actuate the reed switch position indication. The magnets are contained in a housing which is plugged at the bottom. The housing provides a means of attaching the lifting tool for disengaging the CEA from the extension shaft.

In order to engage or disengage a CEA to or from the extension shaft, a special gripper operating tool is attached to the top of the extension shaft assembly when the reactor vessel head has been removed. One part of the tool is attached to the extension sleeve to hold this portion of the extension shaft assembly fixed. Another part of the tool is attached to the operating rod at the magnet assembly and is used to raise the operating rod to conform to the pattern of the slot in the extension sleeve. Withdrawing of the operating rod raises the plunger which in turn allows the fingers of the collet type gripper to collapse to a smaller diameter and allows separation of the extension shaft assembly from the CEA.

4.2.3.1.3 Design Evaluation

(a) Prototype Tests

A prototype magnetic jack type standard CEDM was subjected to accelerated life tests accumulating 100,000 feet of travel equivalent to a 60-year lifetime.

The first phase of the accelerated life test consisted of continuous operation of the mechanism at 40 in/min over a 137 inch stroke lifting and lowering 230 pounds for a total travel of 32,500 feet. This test was performed at simulated normal reactor operating conditions of 600°F and 2200 psig. Upon completion of the test, the motor bearing surfaces were inspected and measured. A maximum bearing wear of .003-inch was measured. This degree of wear is considered acceptable based on the 60-year design life.

The second phase of the accelerated life test also conducted at simulated normal reactor condition consisted of (a) 200 full height gravity drops and (b) 20,000 reversals at 40 in/min one extension shaft position with 230 pounds lift weight. The additional travel accumulated during this phase of testing was 5,400 feet for a total travel of 38,400 feet for the 40 in/min mechanism operation. All drops were completed satisfactorily. Inspection of the extension shaft after this test showed no excessive wear on the shaft in the area of the reversals.

In the third phase of the test program the prototype magnetic jack was coupled to a Dual CEA and extension shaft assembly (335 lbs dry). The test was conducted under operating conditions of 600°F and 2200 psig and water chemistry adjusted to 1100 ppm boron. The mechanism was operated lifting and lowering the Dual CEA and extension shaft assembly at 20 in/min for a total of 15,625 feet and 200 full-height drops. Post test inspections again showed that motor bearing wear was negligible. No motor failures were encountered during this test phase. Total accumulated travel up to this phase of testing of the mechanism was 60,000 feet of travel or 24 years of design life.

Two inadvertent drops occurred during the third test phase. These were encountered during CEA drop testing when the mechanism was primarily operated in the withdrawal mode of operation. Driving the mechanism in the insertion mode after each series of ten drops corrected this condition. It was concluded that crud buildup under the pull down magnet caused difficulty in resetting the mechanism during withdrawal since the pull down force on this magnet is less in the withdrawal cycle than in the insertion cycle. However, it was discovered that by driving the CEA in occasionally, instead of continuously dropping the CEAs, the crud under the pull down magnet was displaced and the malfunction eliminated.

The mechanism was installed on a high temperature test facility and coupled to a test CEA having a total weight of 230 pounds dry. Its operating speed was increased to 30 inches per minute. The test loop conditions were set at 600°F and 2200 psig and a fourth phase of the accelerated life test was initiated. The object of this accelerated life test was to accumulate an additional 30,000 feet of continuous operation utilizing the prototype mechanism as a part-length drive. After a total of 15,000 feet of operation had been accumulated, the holding latch spring in the motor assembly failed. The total travel accumulated on this particular component to that point was 75,000 feet or an equivalent of 30 years of design life. The spring design was reviewed and an improved spring design incorporated into the production units with a design life of twice that of the failed spring. The holding latch spring was replaced and the life test continued without modification to the other parts.

During the latter half of the fourth phase of the accelerated life test, the drive shaft distorted. The cause of the distortion was attributed to the operating rod in the extension shaft assembly having been pinned at its upper end, causing differential growth between the drive shaft and the operating rod. This design was changed for the production units to allow for the differential thermal expansion between the drive shaft and operating rod. Drive shaft bowing has not occurred with the new design. This distortion of the drive shaft caused the mechanism to occasionally fail to complete a step. At no time did the CEA drop due to this distortion. Under these test conditions, an additional 18,000 feet was completed for a total accumulated travel on the prototype mechanism as a part-length unit of 33,000 feet. Total travel on the drive shaft and major components of the motor assembly was 92,000 feet. Upon disassembly and inspection, no additional failures were found. Upon completion of the non-tripping accelerated life test, the prototype mechanism was converted back to a tripping drive by removal of the non-tripping device.

The mechanism was again operated in the high temperature test facility at normal reactor temperature and pressure. The driven weight was 230 pounds (dry) including drive shaft and CEA. Limit switches were positioned to give a total stroke of 120 inches over the upper end of the mechanism travel. The remainder of the life test consisted of operating the mechanism for 7,000 feet continuously up and down over the 120 inch stroke. Upon completion of this travel, the facility was shutdown and the ring surfaces remeasured. The measurements were recorded and the wear was found to be within acceptable limits.

The fast shutdown capability of the tripping magnetic jack mechanism was verified by dropping the minimum effective weight of 130 lbs (dry) with the prototype mechanism. A curve showing CEA position versus time was generated utilizing the reed switch position transmitter. The facility test conditions were set at 40 psi pressure, ambient temperature with no flow. Six drops were completed with acceptable insertion times. Time deviations between the various drops were less than 0.1 second.

A preproduction mechanism was installed on a full flow test facility for drop testing under reactor operating conditions including flow. Two hundred and six full height scrams and one hundred and twenty-six partial height scrams were completed under reactor operating conditions including flow. Drop times for 90 percent insertion at full flow reactor operating conditions met the required drop criteria and time displacement curve.

The magnetic jack type drive mechanism (CEDM) is designed to operate in reactor coolant water at temperatures up to 650°F and 2500 psia. The design temperature of the coils surrounding the mechanism pressure housing (see Figure 4.2-14) is 350°F (except for the upper gripper coils which are designed for 392°F). To maintain the coils below the design temperature forced air cooling is required.

The control element drive mechanism is designed to withstand a complete loss of cooling air for a four hour period with the plant at normal operating temperature and pressure. Upon restoration of cooling air, the mechanism is capable of normal operation. The mechanism is not required to be operated during loss of cooling service. A test was performed to verify the mechanism's ability to meet this requirement.

The mechanism was tested at reactor operating fluid conditions of 600°F and 2250 psia. Cooling air was stopped and the upper end of the cooling shroud blocked to prevent convective cooling. In addition, the cooling shroud was insulated to minimize radiant heat loss from the shroud. The upper gripper current was maintained so that the CEA was held in the withdrawn position. This condition was maintained for four hours. The maximum coil temperature measured was in the upper gripper coil which reached 535°F. Cooling air flow was restored and after one hour of cooling, coil temperature was reduced sufficiently to allow the magnetic jack to operate reliably without dropping the CEA assembly.

An inspection of the coils after test completion showed no electrical deterioration. Some cracking in the encapsulating insulation material was found. Most of these defects appeared to propagate from depressions caused by test thermocouple installation. These thermocouples are not installed in coils used for reactor systems and, therefore, this condition is not expected to occur in reactor service.

Prior to the loss of air cooling test, the coils utilized in the test had operated the mechanism for a total footage estimated to be equivalent to sixteen years of service. During this period, the coils had been at operating temperature for a total of sixty days. After completion of the loss of air cooling test, the coils were subjected to a steam environment for fifteen minutes without affecting their electrical capabilities.

Coil life may be shortened if the mechanism must remain in the hot reactor head environment without air cooling for an extended period of time. Degradation of coil and electrical properties that may result from a loss of cooling air can be detected during the yearly coil current trace evaluation and insulation resistance measurements (megger readings) performed every refueling outage, as part of the mechanism maintenance program.

The CEDM switch position transmitters and cabling are located outside of the CEDM cooling shroud and in the free circulating air environment of the containment. Loss of the CEDM cooling system described in Section 9.4.8.3 will not appreciably affect the environment to which hey are exposed nor cause any functional degradation. For additional assurance, a long term elevated temperature test has been conducted on a small scale reed switch position transmitter which was built from identical production reed switch components. The transmitter has not suffered any operational degradation at a temperature of 300°F for a period of more than a year.

The incore detector assemblies are designed for the reactor vessel temperature environment of 650°F and are therefore unaffected by any change in the head area environment. The connectors are rated for service at 500°F. The cables from the incore detector connectors on the instrument flanges and with in the cooling shroud are rated at 90°C continuous service based on the fact that the CEDM cooling system consists of redundant fans with one unit in service and the other on standby duty. The standby unit is manually started on annunciation in the control room following stoppage of the running unit.

(b) First Production Test

A qualification test program was completed on the first production CE magnetic jack design CEDM. During the course of this program, over 4,000 feet of travel was accumulated and 30 full height gravity drops without mechanism malfunction or measurable wear
on operating parts. The program included the following:

(1) Operation at 40 in/min lifting and lowering 230 lbs (dry) at ambient temperature and 2000 psig pressure for 800 feet.

(2) Six full height 230 lbs dry weight gravity drops at ambient temperature and 2000 psig.

(3) Operation at simulated reactor operating conditions (600°F and 2200 psig) at 40 in/min lifting and lowering 230 lbs for 1700 feet.

(4) Six full height drops at simulated reactor operating conditions (600°F and 2200 psig) with 230 lbs weight.

(5) An operational test at ambient temperature and 2300 psig pressure, lifting 335 lbs at 20 in/min for 500 feet.

(6) Six full height drops of the 335 pound weight.

(7) Operation at simulated reactor conditions for 1700 feet at 20 in/min lifting 335 pounds.

(8) Operation at ambient temperature and 2300 psi for 1100 feet and 20 full height drops with an attached dry weight of 130 lbs.

(c) Preoperational Tests

After installation of the CEDMs and prior to power operation the CEDMs are Tested following fuel loading.

4.2.3.2 Control Element Assembly

4.2.3.2.1 Design Bases

The CEA has been designed to ensure that the stress intensities in the individual structure components do not exceed the allowable limits for the materials specified in Section III of the ASME Boiler and Pressure Vessel Code. The exceptions to this criterion are that (a) the N_i-C_r-F_e 625 cladding is permitted to sustain plastic strain up to one percent due to irradiation induced expansion of the filler materials; (b) where compressive stress occurs, the stress limits are revised to take into account critical buckling; and (c) the allowable stress for the CEA springs are based on values which have been proven in practice. The CEA stress analyses evaluate the following loads:

a) Internal helium pressure buildup due to the effect of irradiation of B_4C

b) External pressure of reactor coolant

c) Dynamic stresses produced by seismic loading

d) Dynamic loads produced by stepping motion of the CEDM

e) Mechanical and hydraulic loads produced during reactor trip

f) Cladding loads produced by differential expansion between clad and filler material

g) Loads produced by LOCA

In addition to the comparison of calculated stress levels with allowable stresses, the fatigue usage factor for significant cyclic stresses is also determined. It is a design requirement that the calculated cumulative damage factor for any location may not be equal to or greater than 1.0. The fatigue usage factor calculations are based on the fatigue curves, stress range vs number of cycles, contained in Section III of the ASME Boiler and Pressure Vessel Code.

4.2.3.2.2 CEA Mechanical Design

The CEA is shown in Figures 4.2-15A through 4.2-15C. Each of the five poison rods consists of an Inconel 625 tube loaded with a cylindrical stack of neutron absorbing poison material.

The St. Lucie Unit 1 reactor utilizes 73 CEAs. Of these 73 CEAs, 65 are full strength (5 poison fingers), 4 are reduced strength with 4 poison fingers, and 4 are reduced strength with three poison fingers. Reduced strength CEAs are used in the lead CEA bank.

For all of the full strength CEAs currently residing in the reactor, the poison stack in all five fingers consists of boron carbide pellets with a silver-indium-cadmium slug in the lower end. The slug provides dimensional stability to the lower portion of the CEA fingers.

The original full strength CEAs used in the reactor have a complete stack of boron carbide pellets in the center finger of the CEA. The poison stack in the four outer CEA fingers of these CEAs consists of boron carbide pellets with silver-indium-cadmium alloy slugs in the lower portion of the CEA fingers.

The 4 poison finger reduced strength CEA is designed as follows. The neutron absorber material in the 4 outer fingers consists of boron carbide pellets with a silver-indium-cadmium slug in the lower end. The center finger contains either Al_2O_3 pellets or stainless steel spacers.

The 3 poison finger reduced strength CEA is designed as follows. The neutron absorber material in the 3 diagonal fingers consists of boron carbide pellets with a silver-indium-cadmium slug in the lower end. The two outer poison fingers contain all Al_2O_3 pellets with stainless steel slugs in the tip regions.

Figure 4.2-16b shows the material composition in the fingers of the St. Lucie Unit 1 CEAs.

In each poison rod, there is a plenum volume above the poison material which provides expansion room for gases generated in the poison. This gas space contains a holddown spring which prevents shifts in the poison location while allowing for differential expansion between the poison and the clad.

The lower end of each rod is sealed with a welded end cap, and the upper end is sealed with a welded end fitting. The upper end fittings in turn are joined to a common support member called a spider. The functions of the spider are to provide rigid lateral and axial support for the poison rods and to provide a point of attachment for the CEA extension shaft, through which the CEA is controlled.

In addition to the CEA discussed above, there are several other types of CEAs used for special purposes and are discussed below.

a) Reduced worth CEAs are CEAs in which the rod reactivity worth has been reduced by the substitution of a low neutron absorbing filler material for poison. Reduced worth CEAs are identical to CEAs except for filler materials and external identification features. The use of reduced worth CEAs in certain locations allows more favorable power distribution than would exist if all CEAs were identical. Reduced worth CEAs are used in the lead group (Bank 7).

b) Dual CEA is two CEAs which are connected so as to be operated in unison by a single drive mechanism. The use of dual CEAs permits an increase in shutdown rod worth without overcrowding the closure head with additional CEDMs. Dual CEAs are used in the shutdown groups (Banks A and B).

   Each single or dual CEA is positioned by a CEDM. The CEA extension shaft joins and connects the CEA to the CEDM. Mechanical reactivity control is achieved by operational maneuvering of the CEAs by the CEDMs. Above the top of the core, each CEA is enclosed in a shroud which ensures lateral alignment of the CEA and prevents coolant cross flow around the withdrawn portion of the poison rods. Within the core, each poison rod travels in a Zircaloy guide tube. In addition, the lower ends of the four outer guide tubes are tapered gradually to form a region of reduced diameter[1] which, in conjunction with the CEA outer poison rods, constitutes an effective hydraulic buffer for reducing the loads produced by the sudden CEA deceleration at the end of a scram stroke. This purely hydraulic damping action is augmented by an additional spring and piston arrangement on the CEA spider. The composition of the various types of CEAs are shown in Figures 4.2-16a and b.

[1] The guide tube design beginning Cycle 25 differs from that of the existing CE14 HTP as it includes the MONOBLOC™ feature. The MONOBLOC™ guide tube has two inside diameters (ID) and a single outside diameter (OD) as opposed to two inside and outside diameters as present in the standard (swaged) guide tubes.

Wear of the CEA cladding was evaluated as part of a CEA/CEDM accelerated life test program which included over 30,000 feet of CEA travel, 332 CEA trips and over 1000 hours of flow testing at reactor operating conditions. Post test examination of the CEA revealed insignificant wear of the cladding which was determined by measurement to be less than .001 inch deep in all cases.

The build up of internal pressure within the cladding due to the release of helium is one of two more relevant parameters in determining useful life. At the beginning of life, the prime concern is that of cladding collapse due to external coolant pressure. The cladding is free standing against the external pressure with sufficient margin to prevent collapse. As CEA life progresses, the internal pressure increases. At end-of-life, the criterion which has been established is that the CEA cladding primary stress levels shall not exceed 2.4 S_m (where S_m = 2/3 minimum unirradiated yield strength at temperature) when exposed to maximum internal gas pressure combined with a rapid removal of external coolant pressure. A second consideration in CEA design life is the cladding strain which may occur as burn-up and swelling of the poison material progresses. Based primarily on these two considerations, the design life of the CEA was originally set at approximately 10 years.

The original 10 year limit CEA lifetime limit was determined primarily on internal material swelling considerations of each CEA finger. The lower portion of the center fingers of the original CEAs utilized boron carbide or alumina (Al_2O_3) against the center finger endcap. Current CEAs now contain silver-indium-cadmium and/or stainless steel slugs at the CEA finger tips (except Type-2 center finger), which do not swell significantly under neutron irradiation. The Type-2 CEA continues to use alumina at the tip of the center finger, which greatly reduces its lifetime due to increased alumina swelling from a higher neutron flux and subsequent cladding strain. Starting with Cycle 19, the Type 2 CEA design incorporates a long slug at the tip of the CEA effectively raising the boron carbide and alumina away from the end cap. Life limits have been developed (References 30 and 31 of Section 4.1) considering fuel management strategies and CEA positioning programs to mitigate wear. These limits were determined considering the effects of poison depletion, clad strain, clad wear, fast fluence, and EPU conditions for Cycle 24 and beyond.

Figures 4.2-15A through 4.2-15C show the types of CEAs utilized for reactivity control and illustrate the identifying features that enable distinguishing each type during refueling activities and CEA handling operations. Table 4.2-5 further describes the CEA identification system which consists of two methods of distinguishing each CEA type. The spider web serialization system provides the primary method of visual indication of CEA type while specially machined corner posts on the spider provide a secondary system for CEA identification.

The composition of the neutron absorber materials over the CEA poison rod length varies with the type of CEA. Figures 4.2-16a and b show the type of absorber material used in the poison rods of the different types of CEAs and Section 4.2.3.2.3(i) describes the method of identifying each poison rod type during fabrication and assembly.

4.2.3.2.3 Control Element Assembly Design Evaluation

a) Mechanical Clearances

There are two basic categories into which the clearances associated with the CEA can be divided:
clearances between the CEA and the guide structure, and clearances between internal components of the CEA.

The clearances between the CEA and its guide structure, both in the fuel assembly and in the upper guide structure, have been established to meet the following requirements:

1) assure adequate flow of coolant past CEA poison rods;

2) assure sufficient freedom of CEA axial motion to meet scram time requirements under conditions of worst case bowing of fuel assemblies; most adverse alignment between fuel assemblies, upper guide structure, and CEDMs; adverse locating and dimensional tolerances of poison rod cladding and CEA guide tube; and radial growth of poison rods due to irradiation effects;

3) assure proper lateral positioning of CEA poison rods relative to adjacent fuel rods;

4) assure proper hydraulic damping action at the lower end of the four outer poison rods to prevent damage to the CEA or related components when the CEA is tripped.

The spacing and clearance gaps between the CEA hold down spring, stainless steel spacers, B_4C pellets, Al_2O_3 pellets, and Ag-In-Cd rods assure adequate heat transfer capability between internal components and CEA cladding tubes and prevent excessive filler/clad interaction.

b) CEA Insertion Requirements

1) For single and dual CEAs, the design maximum time required to drop at normal reactor operating and upset conditions from any withdrawn position to 90 percent of full insertion does not exceed 2.6 seconds measured from the start of CEA insertion (see Figure 4.2-17). The 2.6 second drop time is not a requirement under emergency and faulted conditions. Not shown on Figure 4.2-17 but assumed in the safety analysis is a 0.5 second delay time from the time of trip breaker opening to the start of CEA insertion, which is an allowance for collapse of the CEDM gripper coil magnetic field. See Section 15.1.3 for a discussion on the CEA drop time assumed in the accident analyses. EC291158 EC291158

2) The CEAs can be inserted under emergency and faulted conditions, except for those CEAs located near the vessel outlet nozzle which is feeding the postulated rupture in the faulted condition.

The CEA insertion requirements for power operation discussed above have been established on the basis of providing sufficient negative reactivity insertion rates to enable the reactor to follow

design power reduction transients without exceeding operational limits. In addition, they satisfy the requirements for CEA insertability imposed by the safety analysis.

c) CEA Material Selection

The selection of materials for the CEAs is based on the following considerations:

1) Neutron absorption cross section;

2) Whether the material has been used successfully in similar applications;

3) Physical properties as they affect suitability for the intended use;

4) Irradiated properties of the material;

5) Dimensional stability under irradiation;

6) Compatibility with other CEA materials and with the reactor environment.

The materials used in the CEA are listed below.

1) The spider is a 304 stainless steel casting. Selection of this material is based on its proven acceptability for use in reactor structural applications.

2) Cladding tube, upper end fitting, and end cap are Ni-Cr-Fe 625. The selection of this material is based on its high strength, including creep resistance, good corrosion resistance, and excellent dimensional stability under irradiation at the temperatures and neutron fluences to which it will be subjected. In addition, tests have shown that the Ni-Cr-Fe 625 cladding material will sustain less than 0.001 inch of wear during the design life of the CEA.

3) The hold down springs are made from 302 stainless steel. This selection is based on the proven special characteristics of this material.

4) The primary poison material in the CEA is low density boron carbide (B_4C) in the form of cylindrical pellets. This selection is based on the excellent neutron absorption capabilities of B_4C and the proven acceptability of B_4C for reactor control applications. It should be noted that, under irradiation, the B_4C pellets may swell diametrally up to 3.0 percent and some boron is transmuted to lithium and helium. However, the resulting effects on clad strain and rod reactivity worth are accounted for in the CEA design.

5) Each of the poison rods of the CEA contains a solid cylinder of Ag-In-Cd alloy at the lower end. The use of Ag-In-Cd

alloy in these positions is based on its high neutron absorption capability and its proven acceptability for reactivity control applications. However, the primary reason for using this material is its good dimensional stability under irradiation (less than 0.5 percent diametral expansion) which is an important factor because the lower ends of the outer poison rods are an integral part of the hydraulic trip buffer and swelling of the poison rods, which might occur if B_4C were used, could alter the buffer characteristics.

6) Selective reduction in CEA worth is accomplished in the reduced strength CEAs by substitution of solid stainless steel 304 cylinders or rods for B_4C poison fingers (see Figures 4.2-16a and 16b). Stainless steel has good dimensional stability and is a proven reactor grade material.

7) The primary non-absorbing filler material used in reduced strength CEAs is aluminum oxide (Al_2O_3) in the form of cylindrical pellets. Under irradiation, the high density Al_2O_3 pellets may swell diametrally as much as 3.0 percent.. However, this effect is accounted for and has no adverse effect on CEA performance.

8) The secondary filler material is 304 stainless steel, used in cylinders in place of B_4C pellets in locations where good dimensional stability is important. The reason is analogous to that given for substituting Ag-In-Cd for B_4C in standard poison rods.

9) The spring mounted on the spider is made from Ni-Cr-Fe X-750. Selection of this material is based on its excellent strength and corrosion resistance.

The swelling of B_4C and Al_2O_3 filler materials has been accounted for in the design of the CEA in three ways.

a. Diametral gaps have been provided between the pellets and the cladding to accommodate growth of the pellets. The diametral gaps provided are 8 mills for the B_4C and 18 mills for the Al_2O_3.

b. A design limit has been established at 1% plastic strain of the CEA cladding due to radiation induced swelling of the filler materials. For the burnup to be experienced during approximately 8 full power years the swelling of the B_4C will not exceed the 1.0 percent clad strain limit.

C. The anticipated small increase in clad diameter due to swelling of the B_4C and Al_2O_3 will not impair the movement of the CEAs within the fuel assembly guide tubes, since sufficient diametral clearance exists.

d) Radiation Effects

The effects of neutron irradiation on the integrity and performance of the CEA can be divided into three categories.

Neutron interactions with boron carbide produce helium which causes the poison rod internal pressure to increase. However, the poison rod contains sufficient plenum volume to prevent the internal pressure from having any adverse effect during the design life of the CEA.

No significant quantity of gas is produced in any other CEA material.

Neutron irradiation causes volumetric expansion in the B_4C, Al_2O_3, and Ag-In-Cd materials. The maximum expansions are on the order of one-half to three percent increases in length and diameter of the above materials over the design life of the CEA. However, the CEA design is based on allowing for the maximum expected expansions.

For the temperatures and integrated neutron fluxes encountered by the CEA, the dimensional changes in CEA materials other than those discussed above are insignificant.

Long term neutron irradiation tends to increase the tensile strength and decrease the ductility of reactor structural materials. The only CEA structural material which receives significant irradiation (from the standpoint of producing changes in the strength and ductility properties) is the cladding. For the temperatures and fluences seen by the cladding, the maximum strength increase is approximately ten percent of the unirradiated value, and the ductility is reduced from approximately 30 percent to about 6 percent. However, the allowable primary stress limit in the cladding assumes no increase in yield strength, and the maximum allowable strain for cladding is established at one percent.

e) CEA Positioning Requirements

The vertical position of the CEAs in the core is controlled by CEDMs, which move the CEA in a series of 0.75 inch steps. The selection of the step size was originally based on a requirement that the reactivity insertion produced by a single step not be sufficient to produce effects in the reactor which would cause the automatic regulation system to signal an opposite step. The position of a CEA in the core is indicated by three independent readout systems. One counts the CEDM steps electronically, and the other two consist of magnetically actuated reed switches located at regular intervals along the CEDM. These systems are designed to indicate CEA position to within two inches of the true location. This accuracy requirement is based on ensuring that the axial alignment between CEAs in a group is maintained within acceptable limits (7.5 inch maximum axial alignment with alarm at 3 inch misalignment). Details of the design and logic of the CEDM instrumentation is discussed in Section 7.5. EC291158 EC291158

f) Pressure Forces Tending to Eject CEAs

Under normal operating conditions and during all abnormal and accident conditions, except failures of the reactor coolant pressure boundary, the pressure forces pushing upward on the CEA are much less than the weight (in water) of the CEA and extension shaft.

The CEDMs are designed with anti-ejection latches with a 3500 pound minimum holddown capability.

During the period of blowdown following a LOCA, the combination of the weight of the CEA and with extension shaft and the holddown capability of the CEDM anti-ejection latches will operate against the upward forces on the CEA. Therefore, a rod ejection accident is possible only in the event of a failure of the CEDM pressure boundary structure which causes the CEDM to separate from the closure head or a LOCA combined with an override of the CEDM anti-ejection latches. The probability for such events is considered to be very small. The rod ejection accident is analyzed and discussed in Chapter 15.

g) Potential for and Consequences of CEA/CEDM Functional Failure

The probability of a functional failure of the CEA or CEDM is considered to be very small. This conclusion is based on the conservatism in design, the quality control procedures and quality assurance program used during manufacturing, and the fact that a full size CEA/CEDM combination has been successfully tested under simulated reactor conditions for a length of travel and number of scrams considerably greater than what is expected to occur during the design life of the CEDM. The consequences of a CEA/CEDM functional failure are discussed in Chapter 15.

Another possible CEA failure mode is cladding failure. In the event that a poison rod cladding failure occurred, the CEA could fill with water. If a failed poison rod is assumed to fill with water under low or zero power conditions, it can be postulated that, upon returning to power, the path of the water to the outside could be blocked and the expansion of the water could cause the poison rod to swell to such a degree that axial motion of the CEA is prevented. The consequences of "stuck rod" are discussed in Chapter 15. However, in tests, a waterlogged poison rod was welded shut and heated to 750F without causing any significant rod swelling. This test result, coupled with the low probability of a poison rod cladding failure leading to a sealed waterlogged rod, demonstrates that the probability for a CEA functional failure from this cause is low.

Other possible consequences of failed poison rod cladding are the release of small quantities of CEA filler materials, helium and lithium from the neutron-boron reaction. However, the amounts which could be released are too small to have significant effects on coolant chemistry or rod worth.

In addition to the failure modes discussed above, it is possible that a small object carried with the coolant could be swept into the CEA guide tube where it could interfere with normal operation of the CEA. In order to minimize the probability for such an occurrence, the guide tube flow inlet holes are of small diameter and are oriented with axes perpendicular to the coolant flow direction. However, in the event that an object did enter the guide tube and did interfere with CEA operation, the most serious consequence would be a stuck rod.

h) Effect of Violent Fuel Rod Failure on CEA Operation

As discussed in Chapter 15, there are several postulated accident conditions (e.g., LOCA, rod ejection) which can produce rapid failure of the cladding, either by swelling or splitting of some of the fuel rods. Since some of the fuel rods are adjacent to the CEA guide tubes, it is necessary to consider the possible effect of such fuel rod failures on CEA operation.

Since the CEA poison rods travel within individual Zircaloy guide tubes in the fuel assembly it is therefore impossible for swelled

or split fuel rods to interfere with CEA operation unless the swelling or splitting has first caused significant deformation of the guide tubes. The probability that a rod failure would deform the guide tube sufficiently to prevent CEA operation is considered extremely small. This conclusion is based on the following considerations:

1) The minimum clearance between a fuel rod and a guide tube in the fuel assembly is approximately 0.130 inches. Thus, the fuel rod diameter would have to swell by approximately sixty percent before it contacted the guide tube;

2) The guide tube has much greater (~10 times) resistance to lateral deflection than a fuel rod. The fuel rod therefore could not exert a lateral force sufficient to cause a significant deflection of the guide tube except at a support grid location. However, at a support grid, the fuel rod would first have to overcome the additional restraining effects of the support grid before it contacted the guide tube.

In conclusion, even in the event of a major failure of fuel rods adjacent to CEA guide tubes, the probability that such failures would deform the guide tubes enough to affect CEA operation is small.

i) Verification of Component Characteristics by Inspection and Test

The basic measures employed to ensure that the CEAs conform to the design requirements are as follows:

1) The loading of each CEA poison rod is monitored to ensure that the amounts and types of filler materials are correct for the application in which the poison rod will be used (e.g., full length full strength, and reduced CEA; central or corner rod position). The filler materials are uniquely identified by either color or geometry (e.g., B_4C pellets are dark gray, Al_2O_3 pellets are white).

2) All CEA poison rod types differ in outward appearance such that they may be visually identified during handling and assembly. The "Zones" referred to are shown in Figure 4.2-16a and b.

   a. All corner Poison rods are readily differentiated from center rods by the Poison rod end fitting design. The center rod has a stepped diameter which serves as a guide for the buffer spring housing, and is, therefore, different in appearance from the corner poison rods.

   b. Corner Poison rods having necked down end fittings and no grooves (see Figures 4.2-15A, 4.2-15B, and 4.2-15C) are for full length applications and contain the following filter material:

Zone A	Ag-In-Cd
Zone B	B_4C pellets
Zone C	B_4C pellets

c. Corner rods having a necked down end fitting plus three grooves (see Figure 4.2-15C) are for full length applications and contain the following filler material:

Zone A	Stainless Steel
Zone B	Al_2O_3 pellets
Zone C	Al_2O_3 pellets

d. Center poison rods having no grooves (see Figures 4.2-15A and 4.2-15C) are for full length applications and contain the following filler material:

Zone A	B_4C pellets or Ag-In-Cd
Zone B	B_4C pellets
Zone C	B_4C pellets

e. Center poison rods having three grooves (see Figure 4.2-15B) are for full length applications and contain the following filler material:

Zone A	Al_2O_3 pellets or stainless steel spacers (starting with Cycle 20)
Zone B	Al_2O_3 pellets or stainless steel spacers (starting with Cycle 20)
Zone C	Al_2O_3 pellets or stainless steel spacers (starting with Cycle 20)

3) Each type of completed CEA has a unique identification system (Table 4.2-5) which distinguishes it from all other types of CEA.

4) Each completed CEA is checked for proper positioning and alignment of the poison rods using a special inspection fixture. The alignment check ensures that the frictional force that could result from adverse tolerances is well below the force which could significantly increase insertion time.

5) After installation in the reactor, but prior to criticality, each CEA/CEDM combination is checked for proper operation under the temperature, pressure, and flow conditions which will be encountered when the reactor is at power.

In addition to the basic measures discussed above, the manufacturing process includes numerous other quality control and quality assurance steps for ensuring that the individual CEA components satisfy design requirements as to material quality, detail dimensions, process control and similar considerations.

j) Results of CEA Stress Analysis

The results of the CEA stress analyses presented below show that in all cases the calculated stresses are less than the allowable stresses. Certain aspects of the CEA design are best verified by actual hardware tests. Such test activity is identified where it has been conducted in support of the design.

1) Internal Helium Pressure Build-up due to B_4C Irradiation.

During the life of a CEA, pressure within the cladding continues to build-up in proportion to burnup due to the release of helium from the B_4C and the dissociation of moisture.

Changes in differential clad pressure are determined for full-length CEAs. The results, shown in Table 4.2-6, are based on conservative assumptions which include an adverse accumulation of dimensional tolerances contributing to the smallest possible gas expansion space, the maximum B_4C pellet B_{10} density contributing to the greatest helium generation, and use of peak B_{10} burn-ups, rather than average values. Clad stresses shown represent the values associated with minimum wall clad.

2) External Pressure of Reactor Coolant

The CEA clad experiences full reactor coolant pressure of 2250 psia at beginning of life. No credit is taken for the presence of the filler materials or holddown springs within the cladding. When analyzed as an infinitely long tube (no end supports), the pressure required to cause elastic instability of the clad tube has been determined to be 3,605 (3,730)**psi. This value is based on a maximum diameter, minimum wall tube. The beginning of life margin between reactor operating pressure and the calculated pressure required for elastic instability of the tube is, therefore, 1,355 (1,480)** psi. Moreover, in short term collapse tests performed on typical sections of clad tubing at 750°F, the external pressures required for collapse were significantly higher than the calculated value. The clad hoop stress associated with 2250 psia reactor coolant pressure is 26.9 (26.2)** ksi for zero internal pressure and beginning of life, which is well below the allowable stress limit of 43.3 (33.5)** ksi.

3) Stresses Produced by Seismic Loading

Horizontal Seismic, CEA Withdrawn into Upper Guide Structure

In the withdrawn position, the CEA is supported at the upper end by the extension shaft while the lower ends of the control elements are positioned by the fuel assembly guide tubes. The lateral acceleration required to produce a clad bending: stress of 1.5 Sm is on the order of 10 g. Horizontal accelerations of this magnitude are not predicted for the CEA. Tests have been

** The results in parenthesis are applicable to the redesigned CEAs implemented in Cycle 20.

performed with the control element drive mechanism skewed at an angle sufficient to cause the control element fingers to contact the insides of the Upper guide structure CEA shrouds. The misalignment employed in this test represented a condition which is more adverse than either the operating basis or design basis earthquakes are expected to produce. No structural damage resulted to the CEA as a result of these tests.

Horizontal Seismic, CEA Inserted in Fuel

When fully inserted, the maximum lateral excursion of the CEA poison rods is limited by the motion of the fuel assembly guide tubes which contain the poison rods. The maximum possible lateral deflection of a fuel assembly is approximately 0.9 inch. (Refer to Section 4.2.1.4.1). The conservative assumption applied to the CEA poison rod is that it is forced to conform to the deflection of the fuel assembly guide tube, with no credit taken for the diametral clearance between the poison rod O.D. and guide tube I.D. Results of this analysis show the CEA poison rod clad stress to be 5,300 (23.7 ksi)** psi which is well within the elastic range for Inconel 625.

Vertical Seismic

Vertical Seismic loads are transmitted to the CEA through the extension shaft, which is held by the CEDM latches. The same load path acts during normal stepping motion of the CEA.

A test was conducted to determine the nature and magnitude of the accelerations and decelerations imposed on the extension shaft and CEA by the CEDM during a typical life cycle. The resultant accelerations were then applied to a spring-mass model of the extension shaft and CEA. Member forces derived from this analysis were then applied to the CEA using conventional stress analysis techniques.

Of significance is that when the peak OBE response spectra acceleration at the CEDM nozzle/closure head interface is compared with the acceleration produced by the CEDM during the driving of the CEA, it is found that the peak OBE acceleration is only 15 percent of the normal driving acceleration. Therefore, vertical seismic loads are not significant to the structural integrity of the CEA. The results of the stress analysis for vertical OBE and DBE are given in Table 4.2-7.

4) Stresses Produced by Stepping Motion of the CEDM

Results of the CEA stress analysis for loads induced by stepping motion of the CEDM are given in Table 4.2-7. These stresses are well below the allowable limits for the component materials.

5) Mechanical and Hydraulic Loads Produced during Reactor Trip

Mechanical Loads

The largest loads imposed on the CEA occurs during a reactor trip and towards the end of the stroke when the CEA decelerates as it passes through the tapered buffer zone in the fuel assembly guide tubes and is further decelerated by the spring and piston

** The results in parenthesis are applicable to the redesigned CEAs implemented in Cycle 20.

arrangement mounted on the CEA spider. The contact load at the end of the stroke was determined using a simple energy balance on the system, wherein the kinetic energy of the CEA and extension shaft was assumed to be absorbed entirely by the fuel assembly guide tubes. CEA stresses which result are as follows:

Spider web shear stress	0.66 ksi
CEA end fitting tensile stress	1.8 ksi
Clad tensile stress	3.0 ksi
Spider hub compressive stress	3.2 ksi

Hydraulic Loads

The vertical decelerating forces produced by the hydraulic buffer in the guide tubes acts on the bottom ends of the poison rods. At the time deceleration begins, the poison rods are approximately 90 percent inserted. Buckling of the poison rods due to the upward hydraulic force at the tips is, therefore, precluded since they are guided essentially over their entire length.

The shock absorber action of the buffer results in a pressure rise of short duration within the lower portion of the fuel assembly guide tube as the poison rod enters the buffer region. When this pressure is applied to the CEA cladding, the resultant compressive circumferential stress is approximately 8,900 psi. In the course of accelerated life testing performed on the control rod drive mechanism at operating temperatures and pressures and on related cold water tests of the buffer, the CEA was subjected to over 300 simulated trips with no adverse effect on the clad.

6) Cladding Loads Produced by Differential Expansion between Clad and Filler Materials

Of the four filler materials employed in the CEAs, only the B_4C and Al_2O_3 contribute significantly to clad strain as a result of differential expansion. As exposure of the filler materials progresses, contact with the clad inside diameter is expected to occur in those CEAs which experience the highest burnups, since the end of life pellet diameter may exceed the beginning of life clad inside diameter. Test data of irradiated Inconel show an increase in tensile properties accompanied by a decrease in elongation. After fast fluences of 1.3×10^{21} NVT, the uniform elongation appears to remain approximately 3.0 percent. Extrapolation of the same test data shows a decrease in total elongation to approximately 6.0 percent above 1×10^{22} NVT. On this basis, a criteria of 1.0 percent maximum allowable end of life plastic strain is conservative for the CEA cladding design.

7) Loads Produced by LOCA

For large reactor coolant system pipe breaks greater than the largest line connected to the system, CEA insertion is not required for a safe and orderly shutdown. However, consideration is given to the CEA clad integrity when it experiences a sudden removal of external pressure. Burst tests of typical sections of unirradiated CEA cladding have been performed at approximately 750°F and have demonstrated that the minimum burst pressure is approximately 8900 psig.

Additional room temperature tests were performed on typical sections of tube, some of which were deliberately defected by introducing a surface flaw .005 inch deep by .001 inch wide. The minimum burst pressure for the defect free samples was 11,300 psig. Defected samples exhibited an average 6 percent decrease in burst pressure.

Analysis on the basis that the average volumetric temperature within the poison rods remain essentially constant during a small break in the reactor coolant system shows ample margin between the calculated clad stress and the allowable stress as shown in Table 4.2-5.

8) Fatigue Analysis due to Cyclic Loads

A fatigue analysis was performed to determine the cumulative fatigue damage factor for the significant points in the structure subjected to cyclic loading. The conservative assumptions utilized in this analysis include:

a. The number of stepping load cycles considered in the analysis of the spider is twice the anticipated number of steps during the CEA lifetime.

b. Clad cyclic loading is based on 1000 full plant depressurizations at B.O.L. and 1000 plant depressurizations at E.O.L., the latter of which is applied to the poison rod having the highest internal pressure.

A maximum allowable fatigue utilization factor of 1.0 is allowed by the methods of analysis for cyclic operation given by NB-3222.4, Section III of the ASME Boiler and Pressure Vessel Code, 1971 Edition.

The cyclic stresses for the CEA spider are below the endurance limit for 300 series stainless steels, as presented in Figure I-9.2 of the ASME Boiler and Pressure Vessel Code, Section III, 1971 Edition.

For the Inconel 625 end fittings and clad, the cyclic stresses are less than the Published endurance limits for unirradiated Inconel 625.

0n this basis, the fatigue damage over the CEA lifetime insignificant. In addition, accelerated life tests of CEA/ CEDM combinations produced no damage to the CEA.

9) CEA Spring Stress Limits

Spider Mounted Spring

The spring is prevented from reaching solid height by the spring housing hardstop design. Stress limits utilized in the design of the spring material (AMS 5699 Inconel X-750 spring temper wire) are less than the conservative values normally allowed for spring applications. The maximum torsional shear stress, as obtained by conventional spring analysis techniques, is less than the unirradiated design allowables shown below:

Shear Stress, ksi	Temperature F
100.0	to 500
90.0	500 to 600
85.0	600 to 700

Poison Rod Springs

These springs provide a means of absorbing pellet stack height dimensional tolerances within the poison rods and exert a nominal preload against the stack. In tests, a production loaded CEA was subjected to approximately 500,000 simulated control element drive mechanism stepping cycles (equivalent to over 30,000 feet of travel). At the conclusion of the test, it was observed that wear of the components was insignificant, and the orientation of the poison material has not changed. The initial spring torsional shear stress is approximately 73.5 ksi, which is less than the published allowables for 302 stainless steel wire. For the redesigned CEAs implemented in Cycle 20, the spring torsional shear stress at the end of life, cold conditions, is approximately 96.6 ksi, which is less than the published allowable for 302 stainless steel wire.

4.2.4 FUEL (Framatome) EC292529

The descriptions provided in the following subsections are descriptive of Framatome design and manufacture. Framatome was previously AREVA, and prior to that it was Siemens Power Corporation (SPC-ND). EC292529

4.2.4.1 Summary

SPC-ND fuel was first used in Cycle 6. The initial fuel design was used in Cycles 6 and 7. The fuel design for the St. Lucie Unit 1 plant was modified starting with the ANF-3 Reload (Cycle 8) to achieve a peak assembly average discharge burnup of 44,500 MWd/MTU. Subsequent analyses were performed for Reloads ANF-3 and ANF-4 to increase the peak assembly burnups to 48,000 MWd/MTU. Analyses to support peak assembly burnups out to 52,500 MWd/MTU were reported for assemblies fabricated for Reload ANF-5 and beyond to accommodate the present core and fuel management plan. The use of natural uranium axial blankets provides improved uranium utilization. The neutron absorber used is gadolinia, integral with the fuel in 4, 8, 12, 16 or 20 rods/assembly and concentrations of 4.0, 6.0-8.0 w/o. The mechanical design was revised for ANF-3, 4 and 5 (Cycles 8, 9 and 10) and differs from the previous design in two (2) major ways:

1) The lower end cap design was revised to a long solid design for the prevention of debris damage to the fuel rods. This change required the cladding and active fuel lengths to be reduced. The fuel rod overall length was not affected.

2) The natural blankets in the bottom end of the fuel rods were reduced in length to accommodate the long lower end cap. The plenum length in the fuel rods was, therefore, not affected.

The fuel rod design was revised for reload ANF-6 to improve neutronic and thermal performance. The pellet diameter was increased from 0.370 inch to 0.377 inch, the pellet density was increased from 94 to 95% TD, and clad thickness was reduced from 0.031 to 0.028 inches. The active fuel length was increased to 136.7 inches by adding 2.64 inches to the top natural blanket.

Fuel rod design was revised for Cycle 16 (Batch X) to have equal length (6 inches) top and bottom enriched (2.6 w/o) uranium blankets. The central zone length of 124.7 inches and the active fuel length of 136.7 inches remained unchanged.

Additional improvements to Cycles 8, 9, 10, 11 and 12 fuel were made to improve the fuel resistance to handling damage. Spacer springs were improved and backup dimples were added to peripheral rod locations. The new springs were included in all nine spacers in each fuel assembly. The backup dimples were included for the top and bottom spacers.

The improved spacer spring design provided increased spacer spring width at the rod contact location. The design increased spring strength to assure more positive rod centering should the rods be inadvertently moved due to external forces, (i.e., fuel handling).

The peripheral backup dimples which were added to the top and bottom spacers of the fuel assemblies provide protection to the spacer springs from external rod forces. Spring function is critical at the top and bottom spacers because the rods are cantilevered in these positions. Corner rods, in particular, are susceptible to handling damage.

The thermal-hydraulic impact of the spacer design changes was assessed, and will not significantly affect the performance of the fuel. This is due to the fact that the increase in pressure drop due to these changes is small.

The mechanical design beginning with SLA-12 (Cycle 17) reload fuel for St. Lucie Unit 1 was changed from previously supplied reload fuel. Specifically, the differences for SLA-12 were:

- HTP™* spacers (8 Zircaloy-4 HTP™ spacers in the upper locations, and Alloy 718 HMP™* spacer at the lowest axial location) instead of 9 Bimetallic spacers
- A welded cage instead of having the spacers mechanically attached to the guide tubes
- A FUELGUARD™* LTP instead of a standard LTP
- A shorter fuel rod because of a shorter lower end cap
- An increase in the nominal pellet density of 95.35% TD from 95% TD
- The length of the axial blankets on the NAF rods was increased
- A shorter UTP center nut

The use of the HTP™ spacers allowed the spacers to be welded directly to the guide tubes instead of being mechanically attached. This welded attachment improved the control of the spacer location, reducing the potential for damage during rod insertion. It also increased the bundle stiffness.

The FUELGUARD™* LTP provided increased protection to the fuel from debris in the reactor coolant system. The tie plate design was slightly taller (0.232 inch) than the standard LTP on previous reloads. The pressure drop was also slightly less than the standard tie plate used on the previous reloads. The guide tube attachments were unchanged as was the interface with the fuel alignment pins on the lower core support plate. The attachment surface on the FUELGUARD™* LTP was recessed so that the guide tube lengths were unchanged from previous reloads.

Because the SLA-12 LTP was taller than the previous reloads, the lower end cap length was reduced from 3.04 inches to 2.81 inches. This length reduction maintained the same beginning-of-life position for the axial position of the fuel stack. The reduction also maintained the same beginning-of-life allowance for the differential fuel rod/fuel assembly irradiation growth. The geometry interior to the fuel rod was unchanged; that is, the total stack length, the cladding ID/OD, the pellet OD, and the plenum volume were unchanged.

Besides the fuel rod length, the nominal pellet density was increased from 95% TD to 95.35 % TD. This increase provided a slight increase in the assembly weight (less than 5 pounds) and provided an improvement in the neutronic efficiency. The other change in the fuel rod design was that the axial blanket length in the fuel rods containing UO_2-Gd_2O_3 was increased. This increase was made for neutronic reasons and was explicitly considered in the mechanical analyses.

The other major design change was the reduction in height of the center nut on the UTP. This height for the SLA-12 fuel was 0.125 inch shorter than the height on the previous reloads. The reduction resulted in a decrease in the overall fuel assembly length. For the previous reloads, the peak assembly burnup limit was 52.5 MWd/kgU due to the assembly irradiation growth. With the reduction in the assembly length, the SLA-12 design could reach the peak assembly burnup.

The guide tube design beginning Cycle 25 differs from that of the existing CE14 HTP™ as it includes the MONOBLOC™ feature. The MONOBLOC™ guide tube has two inside diameters (ID) and a single outside diameter (OD) as opposed to two inside and outside diameters as present in the standard (swaged) guide tubes.

For Cycle 26, the Zircaloy-4 fuel rod cladding was replaced with the Framatome (formerly AREVA) Zirconium-Niobium alloy, M5®* material. The dimensions are unchanged. The advantage of the M5 cladding is the greatly improved corrosion resistance and reduced hydrogen uptake over the life of the fuel. EC292529

* Footnote: HTP, HMP, FUELGUARD, and MONOBLOC are trademarks of Framatome (formerly AREVA). M5 is a registered trademark of Framatome (formerly AREVA). EC292529

Mechanical design analyses for high burnup included cladding steady-state strain, transient stress and strain, fatigue, creep collapse, corrosion, hydrogen absorption, fuel rod internal pressure, elongation, and fuel assembly growth. Design criteria consistent with approved Framatome (formerly AREVA) methodology were used in the analyses. These criteria and methods were explicitly reviewed and accepted by the USNRC for M5® material. Bounding power histories were used and the results indicate that the mechanical design criteria are satisfied for all of the cases evaluated. EC292529

a) The maximum end-of-life (EOL) steady-state cladding strain and positive strain increment are below the design limit.

b) The cladding stress and strain during power ramps, calculated under different overpower conditions, do not exceed the design stress corrosion cracking threshold or the strain limit.

c) The cladding fatigue usage factor is within the design limit.

d) The end-of-life fuel rod internal pressure is less than the approved design limit.

e) The criterion for the prevention of creep collapse is satisfied.

f) The maximum calculated EOL thickness of the oxide corrosion layer and the maximum calculated concentration of hydrogen in the cladding are within the design limits.

g) The clearance between the upper and lower tie plate will accommodate the maximum differential fuel rod and fuel assembly growth to the design burnups.

h) The fuel assembly growth does not exceed the minimum space between the upper and lower core plates in the reactor cold condition (70°F).

Table 4.2-8 is a summary of the fuel assembly design parameters for Framatome (formerly AREVA) fuel. Figures 4.2-18 and 4.2-19 show the fuel assembly and guide tube structure (cage) prior to HTP™ / FUELGUARD™ implementation. Figures 4.2-21 and 4.2-22 show the fuel assembly and cage for the HTP™ / FUELGUARD™ design. EC292529

Mechanical design analyses of the St. Lucie Unit 1 reload fuel design have been performed using U.S. Nuclear Regulatory Commission (NRC)-approved mechanical design analysis methodology (References 1, 2, 3, 17 and 18). These analysis evaluate the mechanical criteria presented in the Reference 17 and 18 topical reports. Reference 18 is the implementation of the M5® properties into the criteria.

The analyses demonstrate that the mechanical design criteria for the fuel rod and fuel assembly design are satisfied for the fuel design to the peak assembly discharge exposure of 55 MWd/MTU and a peak rod exposure of 62 MWd/kgU when the fuel is operated within the peaking limits given in the Technical Specifications.

Analyses were also repeated, as necessary, for the other fuel which will be used in the current cycle. These analyses and evaluations of previous analyses confirm that all of the fuel will continue to meet the approved design criteria.

Table 4.2-10 is a summary of the fuel assembly design parameters for Framatome (formerly AREVA) Fuel starting with Cycle 17. Figures 4.2-21 and 4.2-22 show the fuel assembly and components. EC292529

4.2.4.2 Fuel Rod Design Basis

4.2.4.2.1 Cladding Physical and Mechanical Properties

Zircaloy-4 combines a low neutron absorption cross section, high corrosion resistance, and high strength ductility at operating temperatures. Physical and mechanical properties including irradiation effects on Zircaloy-4 are well known and accommodated in the fuel rod design.

M5® is a Zirconium-Niobium alloy with very similar properties as Zircaloy-4. However, M5® has much lower corrosion (oxidation) throughout its operating life and much lower hydrogen uptake levels. Therefore, the degradation of the properties due to oxidation and hydrogen is greatly reduced.

4.2.4.2.2 Cladding Stress Limits

The design basis for the fuel cladding stress limits is that the fuel system will not be damaged due to fuel cladding stresses exceeding material capability. Conservative limits shown in Table 4.2-9 are derived from the ASME Boiler and Pressure Vessel Code, Section III, Article III-2000 (Reference 4).

The cladding may also be damaged by the combination of volatile fission products and high cladding tensile stresses which may lead to stress corrosion cracking. Stress corrosion cracking of fuel rod cladding is considered the principal failure mechanism for pellet-cladding interaction (PCI) failures encountered during changes in reactor operating conditions (Reference 5).

The concept used to avoid failures from the stress corrosion crack failure mechanism from power ramps is to keep the fuel rods from operating above the stress threshold associated with the nucleation of a propagating stress corrosion crack.

4.2.4.2.3 Cladding Strain Limits

Tests on irradiated tubing (References 6 and 7) indicate potential for failure at relatively low mean strains. The data on tensile, burst and split ring tests, indicate a ductility ranging between 1.2 percent and 5 percent at normal reactor operating temperatures. The failures are usually associated with unstable or localized regions of high deformation after some uniform deformation. To prevent cladding failure due to plastic instability and localization of strain, the total mean hoop cladding strain for steady-state conditions is limited, and the increment of the thermal creep during a transient is also limited.

4.2.4.2.4 Strain Fatigue

Cyclic PCI loading combined with other cyclic loading associated with relatively large changes in power can cause cumulative damage which may eventually lead to fatigue failure. Cyclic loading limits are established to prevent fuel failures due to this mechanism. The design life is based on correlations which give a safety factor of 2 on stress amplitude or a safety factor of 20 on the number of cycles, whichever is more conservative (Reference 8).

4.2.4.2.5 Fretting Corrosion and Wear

The design basis for fretting corrosion and wear is that fuel rod failures due to fretting shall not occur. Since significant amounts of fretting wear can eventually lead to fuel rod failure, the spacer grid assemblies are designed to prevent such wear.

4.2.4.2.6 Corrosion

Cladding oxidation and corrosion product buildup are limited in order to prevent significant degradation of clad strength. A PWR clad external temperature limit is chosen so that corrosion rates are very slow below this temperature and therefore overall corrosion is limited. An external corrosion

layer limit is also specified so that this amount of corrosion will not significantly affect thermal and mechanical design margins. This decrease in clad thickness does not increase clad stresses above allowable levels. M5® reduces the amount of corrosion.

4.2.4.2.7 Hydrogen Absorption

The as-fabricated cladding hydrogen level and the fuel rod cladding hydrogen level during life are limited to prevent adverse effects on the mechanical behavior of the cladding due to hydriding. Hydrogen can be absorbed on either the outside or the inside of the cladding. Excessive absorption of hydrogen can result in premature cladding failure due to reduced ductility and the formation of hydride platelets. M5® has lower hydrogen uptake and therefore reduces the amount of hydrogen adsorbed by cladding over its lifetime.

4.2.4.2.8 Creep Collapse

The design basis for creep collapse of the cladding is that significant axial gaps due to fuel densification shall not occur and therefore that fuel failure due to creep collapse shall not occur. Creep collapse of the cladding can increase nuclear peaking, inhibit heat transfer, and cause failure due to localized strain.

If significant gaps form in the pellet column due to fuel densification, the pressure differential between the inside and outside of the cladding can act to increase cladding ovality. Ovality increase by clad creep to the point of plastic instability would result in collapse of the cladding. During power changes, such collapse could result in fuel failure.

Through proper design, the formation of axial gaps and the probability of creep collapse can be significantly reduced. Framatome pellets are stable dimensionally. EC292529

A compressive Inconel plenum spring is included in the Framatome fuel rod design and the rods are pressurized with helium to help prevent the formation of gaps in the pellet column and reduce the differential pressure causing the cladding creepdown and ovalization. EC292529

An analysis is performed in order to guard against the unlikely event that sufficient densification occurs to allow pellet column gaps of sufficient size for clad flattening to occur.

4.2.4.2.9 Fuel Rod Internal Pressure

The internal gap pressure of the fuel rods may exceed the external coolant pressure up to the NRC approved design limit (Reference 1). Significant outward circumferential creep which may cause an increase in pellet-to-cladding gap must be prevented since it would result in higher fuel temperature and higher fission gas release.

4.2.4.2.10 Creep Bow

Differential expansion between the fuel rods and lateral thermal and flux gradients can lead to lateral creep bow of the rods in the span between spacer grids. The design basis for fuel rod bowing is that lateral displacement of the fuel rods shall not be of sufficient magnitude to impact thermal margins. Framatome fuel has been designed to minimize creep bow. Extensive post-irradiation examinations have confirmed that such rod bow has not reduced spacing between adjacent rods by more than 50 percent. The potential effect on thermal margins is negligible. EC292529

4.2.4.2.11 Overheating of Cladding

The design basis for fuel rod cladding overheating is that transition boiling shall be prevented. Prevention of potential fuel failure from overheating of the cladding is accomplished by minimizing the probability that boiling transition occurs on the peak fuel rods during normal operation and anticipated operational occurrences.

4.2.4.2.12 Overheating of Fuel Pellets

Prevention of fuel failure from overheating of the fuel pellets is accomplished by assuring that the peak linear heat generation rate (LHGR) during normal operation and anticipated operational occurrences does not result in fuel centerline melting. The melting point of the fuel is adjusted for burnup and gadolinia loading in the centerline temperature analysis.

4.2.4.3 Fuel Assembly Design Bases

4.2.4.3.1 Structural Design

The structural integrity of the fuel assemblies is assured by setting design limits on stresses and deformations due to various handling operational and accident loads. These limits are applied to the design and evaluation of upper and lower tie plates, grid spacers, guide tubes, holddown (reaction) springs, and locking hardware. The design bases for evaluating the structural integrity of the fuel assemblies are:

a) Fuel Assembly Handling - Dynamic axial loads approximately 2.5 times assembly weight.

b) For all applied loads for normal operation and anticipated operational events - The fuel assembly component structural design criteria are established for the two primary material categories, austenitic stainless steels (tie plates) and Zircaloy (guide tubes, grids, spacer sleeves). The stress categories and strength theory for austenitic stainless steel presented in the ASME Boiler and Pressure Vessel Code, Section III, (Reference 4) are used as a general guide.

c) Loads during postulated accidents - Deflections or failure of components shall not interfere with reactor shutdown or emergency cooling of the fuel rods.

d) The fuel assembly structural component stresses under faulted conditions are evaluated using primarily the methods outlined in Appendix F of the ASME Boiler and Pressure Vessel Code, Section III.

4.2.4.3.2 Fuel Rod and Assembly Growth

The design basis for fuel rod and assembly growth is that adequate clearance shall be provided to prevent any interference which might lead to buckling or damage. Cladding and guide tube growth measurements of Framatome fuel are used in establishing the growth correlations used for calculations. EC292529

4.2.4.3.3 Assembly Holddown

The design basis for fuel assembly holddown is that the holddown (reaction) springs, as compressed by the fuel alignment plate during reactor operation, will provide a net positive downward force during steady-state operation, based on the most adverse combination of component dimensional and material property tolerance. In addition, the holddown springs are designed to accommodate the additional load associated with a flow increase transient (resulting in possible temporary uplift of the fuel assemblies), and to continue to ensure fuel assembly holddown following such an occurrence.

4.2.4.4 Fuel Assembly Design Description

Framatome reload assemblies consist of a 14x14 square array occupied by 176 fuel rods, and five Zircaloy-4 guide tubes. Nine bi-metallic Zircaloy-4, Inconel 718 spacers are positioned along the length of the fuel bundle in positions compatible with the existing fuel residing in the core. The spacers are held in position by Zircaloy springs which engage sharp edges formed by flats machined on the O.D. of the guide tubes which are mechanically attached and secured to the upper and lower tie plates. The spacers, guide tubes and tie plates form the structural skeleton of the fuel bundle. Fuel assembly characteristics are summarized in Table 4.2-8. The fuel assembly is shown in Figures 4.2-18 and 4.2-19. EC292529

The upper tie plates are designed to be mechanically dismountable by underwater remote handling techniques. Proper orientation of fuel assemblies is controlled by designing the upper tie plate in a manner consistent with the existing fuel handling equipment and orientation schemes for PSL-1.

Beginning with SLA-12 (Cycle 17), the mechanical fuel design contains several differences from the previous supplied reloads contained in the cycle. The SLA-12 design changes are:

- High Thermal Performance (HTP™) spacers (8 Zircaloy-4 HTP™ spacers in the upper locations, and Alloy 718 HMP™ spacer at the lowest axial location) instead of 9 Bimetallic spacers
- A welded cage instead of having the spacers mechanically attached to the guide tubes
- A FUELGUARD™ lower tie plate (LTP) instead of a standard LTP
- A shorter fuel rod because of a shorter lower end cap
- An increase in the nominal pellet density of 95.35% theoretical density (TD) from 95% TD
- The length of the axial blankets in the neutron absorber fuel (NAF) rods was increased
- A shorter upper tie plate (UTP) center nut

The guide tube design beginning Cycle 25 differs from that of the existing CE14 HTP™ as it includes the MONOBLOC™ feature. The MONOBLOC™ guide tube has two inside diameters (ID) and a single outside diameter (OD) as opposed to two inside and outside diameters as present in the standard (swaged) guide tubes.

For Cycle 26, the Zircaloy-4 fuel rod cladding was replaced with the Framatome M5® material. The dimensions are unchanged. EC292529

4.2.4.4.1 Fuel Assembly Material Properties

The material properties used in the design evaluation are described in this section.

4.2.4.4.2 Zircaloy-4 Chemical Properties

Zircaloy-4 is used in three forms: (a) cold worked and stress relieved cladding; (b) recrystallized annealed tubing; and (c) recrystallized annealed strip.

4.2.4.4.3 Fissile Material (Uranium Dioxide)

Chemical composition is as follows:

a) Uranium Content - The uranium content shall be a minimum of 87.7 percent by weight of the uranium dioxide on a dry weight basis.

b) Stoichiometry - The oxygen-to-uranium ratio of the sintered fuel pellets shall be within the limits of 1.99 and 2.01.

Mechanical properties are as follows:

a) Mechanistic Fuel Swelling Model - The irradiation environment and fissioning events cause the fuel material to alter its volume and, consequently, its dimensions.

b) Fission Gas Release - For design evaluations of end-of-life pressures, pellet-cladding interactions and general thermal mechanical conditions, a physically based two-stage release model is used. First stage fission gas release is to grain boundaries, and then the second stage release is from the grain boundaries to the interconnected free gas volume.

c) Melting Point - The value used for the UO_2 melting point (unirradiated) is 2805°C (5081°F). Based on measurements by Christensen, et. al., (Reference 9), the melting point is reduced linearly with irradiation at the rate of 12.2°C (22.0°F) per 10^{22} fission/cm^3 or 32°C (57.6°F) per 10^4 MWd/MTU.

4.2.4.4.4 Alloy X-750 Springs

Coil springs are fabricated from Alloy X-750 wire or rod with an alloy composition in accordance with AMS 5699B.

4.2.4.5 Fuel Rod Design Description

For Cycle 25 and prior reloads, the fuel rods consist of cylindrical UO_2 pellets in Zircaloy-4 tubular cladding. In Cycle 26, the cladding was changed to M5®.

The Zircaloy-4 fuel rod cladding is cold worked and lightly stress relieved. The M5® cladding is in the fully recrystallized condition. Zirconium alloy plug type end caps are welded to each end. The upper end cap has external features to allow remote underwater fuel rod handling. The lower end cap has a truncated cone exterior to aid fuel rod reinsertion into the fuel assembly during inspection and/or reconstitution.

The fuel rod upper plenum contains an Alloy X-750 compression spring to prevent fuel column separation during fabrication and shipping, and during operation.

Fuel rods are pressurized with helium which provides a good heat transfer medium and assists in the prevention of clad creep collapse.

The fuel rod is shown in Figure 4.2-20.

The fuel rod design starting with Cycle 20 is shown in Figure 4.2-23.

The fuel rod design starting with Cycle 22 is shown in Figure 4.2-24.

4.2.4.6 Reactor Operating Conditions for Design

The fuel assembly design is based on the following nominal reactor operating at the following Extended Power Uprate conditions:

.	Nominal Heat Output	3020 MWt
.	Heat Output Uncertainty	±54 MWt
.	Nominal Pressurizer Pressure	2250 psia
.	Total Coolant Flow (Min.)	3.75×10^5 gpm
.	Total Coolant Flow (Best Estimate)	4.1×10^5 gpm
.	Maximum Measured Coolant Flow (Ref. 15) (Holddown Spring Design)	4.4×10^5 gpm
.	Maximum Allowed Inlet Temperature	551°F
.	Measured Inlet Temperature Uncertainty	±2°F
.	No. of Assemblies in Core	217

4.2.4.7 Fuel Rod Design Evaluation

4.2.4.7.1 Design Criteria

a) Cladding steady state stresses shall not exceed the established limits.

b) Maximum cladding strain shall not exceed limits at end-of-life (EOL), or during power transients.

c) During power transients, the maximum hoop stress in the cladding shall be limited to avoid failure by stress corrosion cracking.

d) The cumulative usage factor for cyclic stresses shall not exceed the design limit.

e) The fuel rod internal pressure at the end of the design life may exceed the system operating pressure up to the NRC approved design limit (Reference 1).

f) Cladding creep collapse shall not occur.

g) The hydrogen absorption of the cladding and thickness of the corrosion layer shall not exceed design limits.

h) The fuel elongation must be accommodated by the clearance between fuel rods and tie plates.

i) Fuel rod creep bow throughout the design life of the assemblies shall be limited so as to maintain licensing and operational limit restraints.

j) The fuel rod plenum spring shall maintain a positive compression on the fuel column during shipping and during the fuel densification stage.

k) Cladding temperatures shall not exceed the design limits.

l) Pellet temperatures shall not exceed the melting temperature during normal operation and anticipated transients.

4.2.4.7.2 Fuel Rod Analysis

a) Steady-State Stresses - The cladding steady-state stresses are highest at beginning-of-life except for a bending stress due to ovality. Since the cladding eventually is supported by the pellets, the ovality bending stress is eliminated as a factor for the end-of-life condition at higher burnup. The cladding stresses are within the established limits.

The stress analysis is performed at the lower end cap since the maximum temperature gradients occur at this end.

The mechanical stress is caused by the pressure differential across the rod wall and by the axial load of the pellet stack weight and the plenum spring force. The thermal stress is caused by the temperature gradient between the end cap and the heat generating pellets.

The ANSYS code (Reference 10), which allows thermal as well as stress analyses, was used to model the subject rod region. The maximum weld stress intensity is well below the design limit.

b) Steady-State Strain Analyses - The cladding steady-state strain was evaluated with the RODEX2 code (Reference 11). The code calculates the thermal, mechanical and compositional state of the fuel, and cladding for a given duty history. Conservative input values were used in the strain analysis. Bounding dimension values covering all reloads were selected for the calculations.

The design limit at EOL is satisfied (Reference 1).

c) Ramp Stress and Strain Analysis - The clad response ramping power changes is calculated with the RAMPEX code (Reference 12). This code calculates the pellet-cladding interaction during a power ramp. The initial conditions are obtained from RODEX2 output. The RAMPEX code considers the thermal condition of the rod in its flow channel and the mechanical interactions that result from the fuel creep, crack healing, and cladding creep at any desired axial section in the rod during the power ramp.

The power histories assumed for these analyses were enveloping for the designs with maximum exposure rod and arbitrary power histories with low and intermediate powers for the first cycle, followed by high power second and third cycles. The arbitrary cycles were used to evaluate large power swings resulting from fuel shuffling.

The conditions at the end of each cycle obtained with the RODEX2 code are used as input data for the RAMPEX code. The rods under consideration were ramped to the maximum power. The peak stresses obtained are below the threshold Stress for stress corrosion cracking, thus complying with the design requirements. In addition, the maximum clad strains due to each ramp were examined. The maximum strains, including primary and secondary thermal creep, were less than the design limit.

d) Cladding Fatigue Usage Factor - In addition to the ramp strain analyses, a fatigue usage factor for cladding was calculated. The calculations were based upon the typical duty cycles. Cladding stress amplitudes for the various power cycles were determined from RAMPEX analyses. RAMPEX analyses were run for each cycle at the plane of maximum contact pressure which resulted in conservatively high stresses for the fatigue analysis. The overall fatigue usage factor is within the design limit.

e) Internal Pressure - A RODEX2 analysis was performed to evaluate the end-of-life (EOL) internal fuel rod pressure. To prevent cladding instability, the rod internal pressure cannot exceed the approved design limit (References 1 and 3) or else the cladding may creep away from the pellet, which increase the fuel rod pellet temperatures. Higher fuel temperatures result in increased fission gas release and, therefore, higher internal rod pressures. The results of these analyses show the internal rod pressure does not exceed the design criteria at any time during irradiation. The fuel rod will, therefore, remain stable throughout the expected power history.

f) Creep Collapse - The collapse calculation is done using the RODEX code to determine the temperature and pressure conditions throughout the fuel rod lifetime, and to determine the clad creepdown. These conditions are used as input for COLAPX. The COLAPX code then predicts the time dependent creep ovality deformations in an infinite length tube subjected to external pressure, internal pressure, and linearly varying temperature gradients through the thickness of the cylinder.

If significant gaps are not allowed to form, then tube ovality, as predicted by the COLAPX evaluation, cannot occur beyond the point of fuel support.

In order to guard against the highly unlikely event that enough densification occurs to form pellet column gaps of significant size to allow clad flattening, an evaluation was performed. The cladding ovality increase was calculated with COLAPX, and the creepdown was calculated with RODEX2. The combined creepdown at the cladding minor axis was determined not to exceed the minimum level to allow the fuel column to relocate axially without the formation of axial gaps.

g) Hydrogen Absorption - The RODEX2 fuel performance code is used to calculate the oxide thickness of fuel rods in PWR fuel as a function of burnup.

The waterside corrosion and hydrogen pick-up in the cladding are evaluated with RODEX2 for power histories used in the steady-state strain analysis. The results show that the peak oxide thickness and the hydrogen level are below the design limit.

h) Fuel Elongation - Fuel rod growth projected to occur during irradiation is based on measurements made showing the gap between the fuel rods and the upper and lower tie plates on Framatome 14x14 fuel. The maximum assembly growth projection is based on assembly length measurements. The maximum rod growth minus the minimum assembly growth is compared with the clearance within the assembly for fuel rod growth. Maximum and minimum projections bound the applicable growth data. EC292529

The calculations show that there is ample clearance between the tie plates to accommodate rod growth through end-of-life (EOL). The minimum EOL clearance is conservatively calculated at hot conditions considering maximum for growth, minimum bundle growth, and minimum initial clearances. There is adequate space between the upper core plate and the assembly to accommodate fuel assembly growth. The remaining clearance at cold reactor conditions (78 degrees F) is based on the as-built core plate spacing for St. Lucie Unit 1.

i) Fuel Rod Creep Bow - In support of Framatome methodology to determine the effects of fuel rod bowing upon pressurized water reactor limits, pre- and post-irradiation rod spacing measurements have been obtained for Framatome reload fuel. The spacing measurements are used to obtain an empirical relationship between rod bow (gap closure) as a function of assembly exposure. The detailed development of these empirical relationships have previously been approved by the NRC along with appropriate models to determine the impact of rod bow upon DNB margins and LOCA margins. EC292529 EC292529

The results envelope the relationship describing rod bow as a function of exposure. The lateral displacement of the fuel rods will not impact thermal margins.

j) Plenum Spring (See item f above) - The cladding ovality increase and creepdown at a minimum level are summed to show that they are less than the design criteria of the initial minimum pellet clad gap. This will prevent pellet hangups due to cladding creep, allowing the plenum spring to close axial gaps until densification is substantially complete, thus assuring that clad collapse will not occur.

k&l) Fuel Temperature - The fuel temperature and the cladding total uniform strain are analyzed in order to simulate an anticipated operational occurrence (AOO) which could be reached in the rod was at the maximum allowable power, defined by F_r. This AOO level is the level defined by F_q with a conservative overpower value. The ratio of these values corresponds to a local peaking factor which is applied to each power history. This local peaking factor is used at each successive axial node as a spike and successive burnups. The RODEX2 computer model is used to establish the conditions of the rod prior to each power spike. It then calculates the temperatures in the fuel and cladding for very node separately during the overpower spike assuming steady-state conditions. This analysis is performed using the most conservative parameters from the thermal and strain analyses. The results of the AOO total uniform strain analysis and the AOO fuel temperature calculations show that the design criteria are met.

4.2.4.8 Fuel Assembly Design Evaluation

4.2.4.8.1 Design Criteria

a) The fuel assembly cage formed by the guide tubes and spacers shall support the rods considering loads and stresses due to mechanical holddown and differential thermal expansion.

b) The fuel assembly shall support the fuel rod, providing sufficient spring force to minimize flow-induced vibrations and to prevent fretting corrosion at the spacer-fuel rod contact points.

c) The assembly shall be designed to provide clearance for irradiation induced guide tube growth without exceeding the core plate-to-core spacing.

d) The fuel assembly holddown, consisting of the upper tie plate reaction springs and the immersed assembly weight shall exceed the maximum hydraulic loads so as to provide positive seating of the assembly against the lower core plate.

4.2.4.8.2 Fuel Assembly Analysis

a) Guide Tube Stresses

The guide tubes along with the upper and lower tie plates and grid spacers provide the principal structure for the fuel assembly. Guide tubes are considered as restrained columns and are analyzed accordingly, using appropriate load combinations. Column deflection is permissible within constraints of allowable bending stress, allowable displacement, and allowable approach to column instability. The allowable total stress, primary plus bending, is less than the yield strength of the material at the temperature of the load conditions (Reference 1).

As the power level of the reactor is increased, differential thermal expansion between the Zircaloy guide tubes and the hotter fuel rod would tend to put the guide tube in tension. Therefore, there is no concern as to the stability of the guide tube on approach to

normal operating conditions. After some period at power, vibration loads would tend to reduce or eliminate loads caused by differential thermal expansion. Upon reduction in power, differences in temperature between the guide tubes and fuel rods would decrease causing compression loading on the guide tube. Thus, the stability of Zircaloy guide tubes is evaluated as the power level is reduced.

Guide tube stresses and loads considering holddown forces and spacer to rod axial friction forces are within the maximum stress criteria and the critical buckling limit of the guide tube.

b) Fuel Rod Support

The spacer springs are known to relax during irradiation and the fuel rod cladding tends to creepdown. Together, these two characteristics combine to reduce the spacer spring force on a fuel rod during its lifetime. These characteristics have been considered in the design of the spring to assure an adequate holding force when the assembly has completed its design operating life.

Spacer spring relaxation and rod creepdown characteristics are modeled and the resulting gaps between the rod and the spacer grid are shown not to exceed values which have demonstrated acceptable fretting wear performance.

c) Fuel Assembly Growth

The limiting condition for fuel assembly growth is at end of life after cooldown. Because of the higher coefficient of thermal expansion for the stainless steel core structure relative to the zirconium alloy guide tubes, differential thermal expansion increases the assembly/internals structure clearance during heatup and reduces the clearance upon cooldown. The guide tube growth data for SNP irradiated fuel assemblies includes data for the Framatome 14x14 design. EC292529
Allowing for measurement error and other uncertainties, the maximum EOL fuel assembly length predicted from the upper limits of the data leaves a clearance with the minimum as-built core plate to core plate separation.

d) Holddown

The design for fuel assembly holddown is such that the holddown springs, as compressed by the fuel alignment plate during reactor operation, provide a net positive downward force during steady-state operation, based on the most adverse combination of component dimensional and material property tolerances.

4.2.4.9 Testing and Inspection Plan

4.2.4.9.1 Quality Assurance/Control

Fuel assembly quality control is achieved by a component inspection program which has the following features consistent with Framatome Design Control procedures: EC292529

a) An enrichment verification program which covers incoming UF_6 gas to completed fuel rod

b) Verification of cladding integrity by testing and inspection of each lot of tubing received

c) Inspection of fuel pellets for conformity to specification

d) Inspection of each fuel assembly for cleanliness, straightness, envelope, rod-to-rod spacing, length and fuel rod axial position, and

e) On-site inspection for fuel rod axial position, rod-to-rod spacing, and cleanliness.

REFERENCES FOR SECTION 4.2.4

1. XN-NF-82-09(NP)(A), "Generic Mechanical Design Report, Exxon Nuclear 14x14 Fuel Assemblies for Combustion Engineering Reactors," November 1983.

2. XN-NF-82-97, "St. Lucie Unit 1 Addendum to Generic Mechanical Design Report, Exxon Nuclear 14x14 Fuel Assemblies for Combustion Engineering Reactors," December 1983.

3. XN-NF-82-06(P)(A), "Qualification of Exxon Nuclear Fuel for Extended Burnup (PWR), Rev. 1, Supplements 2,4,5, October 1986.

4. ASME Boiler and Pressure Code, Section III, 1971 Edition, ASME, New York, NY.

5. EPRI-NASA Cooperative Project on Stress Corrosion Cracking of Zircaloy, SRI International, EPRI NP-717, March 1978.

6. A.A. Bauer, L.M. Lowry, and J.S. Perrin, Process on Evaluating Strength and Ductility of Irradiated Zircaloy During July through September 1975. BMI1938, September 1975.

7. A.A. Bauer, L.M. Lowry, W.J. Gallaugher, and A.J. Markworth, Evaluating Strength and Ductility of Irradiated Zircaloy - Quarterly Progress Report January through March 1978, NUREG/CR-0085, BMI-2000, June 1978.

8. W.J. O'Donnel and B.F. Langer, "Fatigue Design Bases for Zircaloy Components," Nuclear Science and Engineering, Volume 20, January 1964.

9. J.A. Christensen, et al., "Melting Point of Irradiated UO_2," WCAP-6065, February 1965.

10. ANSYS Engineering Analysis System Theoretical Manual, P.C. Kohnke, 1977. ANSYS User's Guide, 1979. Swanson Analysis System, Houston, PA.

11. K.R. Merckx, RODEX2 Fuel Rod Thermal-Mechanical Response Evaluation Model, XNNF-81-58(NP), Rev. 2, Supplement 3.

12. RAMPEX Pellet-Clad Interaction Evaluation Code for Power Ramps, XN- NF-573, May 1982.

13. Deleted.

14. PSL-ENG-SEMS-97-054, Review of Plant Operation with Replacement Steam Generators, Rev. 0.

15. Deleted.

16. ANF-88-133(P)(A) and Supplement 1, *Qualification of Advanced Nuclear Fuels' PWR Design Methodology for Rod Burnups of 62 GWd/MTU*, Advanced Nuclear Fuels Corporation, December 1991.

17. EMF-92-116(P)(A) Revision 0, *Generic Mechanical Design Criteria for PWR Fuel Designs*, Seimens Power Corporation, February, 1999.

18. BAW-10240(P)(A) Revision 0, "Incorporation of M5™ Properties in Framatome ANP Approved Methods," May, 2004.

TABLE 4.2-1

MECHANICAL DESIGN PARAMETERS - CE FUEL AND CEAs
(Historical Information)

Cycle 1
Fuel Assemblies

Batch	No. of Assemblies	Fuel Rods No./Assy.	Poison Rods No./Assy.	Poison Rods No./Batch	Enrichment Wgt. % U-M
A	69	176	0	0	1.93
B	80	164	12	960	2.33
C	40	176	0	0	2.82
C*	12	164	12	144	2.82
C**	16	164	12	192	2.82
	217			1296	2.35 avg.

C* - Low concentration B_4C Loading
C** - High concentration B_4C Loading

Fuel Rod Array, square	14 x 14	
Fuel Rod Pitch, inches	0.580	
Spacer Grid		
Type	Leaf Spring	
Material	Zircaloy-4	
Number per Assembly	8	
Weight, each, lb	1.5	
Retention Grid		
Type	Leaf Spring	
Material	Ni-Cr-Fe	
Number per Assembly	1	
Weight, each, lb	1.5	
Weight of Fuel Assembly, lb	1280	(unshimmed)
	1220	(shimmed)
Weight of Contained Uranium, kg U per assembly		
Batch A	395	
Batch B	368	
Batch C (shimmed)	368	
Batch C (unshimmed)	395	
Outside Dimensions		
Fuel Rod to Fuel Rod, inches	7.980 x 7.980	

TABLE 4.2-1 (Con't)

Fuel Rod	
Fuel material (Sintered Pellets)	UO_2
Pellet Diameter, inches	0.3805(batch A), 0.3795(batch B), 0.3765 (batch C)
Pellet Dish Depth,inches	0.015 (B), 0.029 (A and C)
Pellet Dish Diameter, inches	0.2725(A), 0.2915(B),0.2685(C)
Pellet Length, inches	0.650 (B), 0.450 (A and C)
Pellet Density, g/cc	10.193(B), 10.41 (A and C)
Pellet Theoretical Density, g/cc	10.96
Pellet Density (%theoretical)	93.0 (B), 95.0 (A and C)
Stack Height Density, g/cc	10.05
Clad Material	Zircaloy-4
Clad I. D., inches	0.388(A and B), 0.384 (C)
Clad O. D., inches	0.440
Clad Thickness, inches	0.026 (A and B),0.028 (C)
Diametral Gap, (cold), inches	0.0085(B),0.0075 (A and C)
Active Length, inches	136.7
Plenum Length, inches	8.6
Burnable Poison Rod (Cycle 1)	
Active Length,inches	122.7
Material	B_4C - Al_2O_3
Pellet Diameter, inches	0.376
Clad Material	Zircaloy-4
Clad I. D., inches	0.388
Clad O. D., inches	0.445
Clad Thickness, inches	0.026
Diamtral Gap, (cold), inches	0.012
Control Element Assembly (CEA)	
Number	73
No. of Absorber Elements per Assy.	5
Type	Cylindrical Rods
Clad Material	Ni-Cr-Fe 625
Clad thickness, inches	0.040
Clad O. D., inches	0.948
Diametral Gap, inches	0.008
Poison Material	*
Corner Element Pitch, inches	4.64
Total Element Length, inches	161
Poison Length	*
CEA Dry Weight, (standard) pounds	81
Total Operating Assembly Dry Weight, pounds	
Single	195
Dual	299
B_4C Pellet	
Diameter,inches	0.860
Density, % of theoretical density of 2.52 g/cc	73
Weight % Boron, minimum	78

*See Figures 4.2-16a, 16b, 16c, 16d

TABLE 4.2-1 (Con't)

Control Element Drive Mechanisms (CEDM)

	Single CEA	Dual CEA
Number of drive mechanisms	49	12
Stroke, inches	137	137
Speed, inches per minute	30	20
Drop time, seconds (90% insertion)	3.1	3.1

Core Arrangement

Number of Fuel Assemblies in Core, Total	217
Number of CEA's	73
Number of Fuel Rods	36,896***
Number of Poison rods	1,296
CEA Pitch, Min., inches	11.57
Spacing Between Fuel Assemblies, Fuel Rod Surface to Surface, inches	0.200
Spacing,Outer Fuel Rod Surface to Core Shroud,inches	0.204
Hydraulic Diameter, Nominal Channel, feet	0.0444
Total Flow Area (Excluding Guide Tubes), sq ft	53.5
Total Core Area, sq ft	101.1
Core Equivalent Diameter, inches	136
Core Circumscribed Diameter, inches	142.5
Core Volume, liters	32,600
Total Fuel Loading, kg U	82,850
Total Fuel Weight, pounds $U0_2$	207,200**
Total Weight of Zircaloy Clad, pounds	44,700
Total Heat Transfer Area, sq ft	48,420**
Fuel Volume (Including pellet dished ends), cu ft	330.2**

**Cycle 1 values.

***Cycle 6 values.

TABLE 4.2-2

CLAD PHYSICAL PROPERTIES (CE FUEL)

	Room Temperature	675F
Modulus of Elasticity, psi	15.0×10^6	10.0×10^6
Poisson's Ratio	0.296	0.252
Ultimate Tensile Strength		
Minimum, psi	79,000	45,000
Average, psi	94,000	62,000
Yield Strength (Tensile)		
Minimum, psi	52,000	32,000
Average, psi	70,000	48,000
Total Elongation		
Minimum, percent	18.0	10.0
Average, percent	22.0	19.0
Uniform Elongation		
Minimum, percent	7.0	3.0
Average, percent	8.0	5.0
Reduction in Area		
Minimum, percent	38	42
Average, percent	50	54

TABLE 4.2-3

TENSILE TEST RESULTS ON IRRADIATED SAXTON CORE II CLADDING[C]

Sample Rod Number	Identification Axial Location (Inches)a	Fluence (>I Mev) (n/cm^2)[b]	Test Temperature (F)	0.2% Yield Strength (kpsi)	Ultimate Strength (kpsi)	Uniform Elongation (percent)	Total Elongation (percent)	Reduction of Area (percent)
TE	9.8 - 16.8	3.2×10^{21}	675	46.2	54.2	3.6	9.3	27
TI	3.0 - 9.0	2.3×10^{21}	675	54.2	61.7	5.2	9.3	48
TP	7.0 - 14.0	3.1×10^{21}	675	52.0	59.6	2.5	6.0	44
TT	2.0 - 8.0	2.3×10^{21}	675	49.1	57.9	6.0	11.3	31
TT	8.0 - 14.0	3.3×10^{21}	675	48.4	54.6	2.6	8.0	53
LA	3.0 - 9.0	2.3×10^{21}	675	48.4	58.1	7.1	15.1	50
LA	19.8 - 25.8	3.1×10^{21}	675	52.5	60.4	4.9	9.8	26
NI	8.0 - 14.0	3.1×10^{21}	675	51.6	64.8	5.6	18.4	46
N3	8.0 - 14.0	3.1×10^{21}	675	54.3	65.3	5.7	14.9	56
TE	2.0 - 8.8	2.1×10^{21}	675	67.0	73.1	2.9	12.2	48
JF	2.0 - 8.8	1.7×10^{21}	675	40.1	45.9	11.5	13.6	44
RI	2.8 - 8.8	2.0×10^{21}	675	56.9	65.9	6.1	19.5	53
S1	2.8 - 8.8	2.0×10^{21}	675	48.2	58.2	7.2	19.3	37
S1	9.8 - 16.8	3.2×10^{21}	675	56.7	67.8	3.6	7.9	37
PO	2.0 - 8.8	2.0×10^{21}	675	53.2	72.4	7.3	12.5	65
PO	9.8 - 16.8	3.2×10^{21}	675	42.3	62.0	3.5	11.1	67
PO	29.8- 37.0	1.5×10^{21}	675	52.2	61.6	4.0	8.9	49
K4	30.3- 36.5	1.8×10^{21}	675	48.3	52.0	3.3	10.4	64
NI	2.0 - 8.0	2.1×10^{21}	675	49.3	63.3	4.8	8.6	37
N3	2.0 - 8.0	2.1×10^{21}	675	45.8	59.2	4.1	10.1	58
TI	19.8 - 25.8	3.1×10^{21}	700	53.8	57.3	4.3	9.0	36
TP	1.0 - 7.0	1.9×10^{21}	700	44.8	53.8	4.2	18.2	60

[a] Distance of specimen ends from bottom of rod.

[b] Interpolated fluence at center of sample.

[c] W. R. Smalley, "Saxton Plutonium Program, Semi annual Progress Report for the Period Ending December 31, 1969," WCAP-3385-22, March 1970.

TABLE 4.2-3a

EVALUATION INPUT PARAMETERS (CE FUEL)

Parameter		Value
Pellet O.D., Design,	in.	.3795
Clad 0. D., Design,	in.	.440
Clad I.D., Design,	in.	.388
$U0_2$ Pellet Density		
Design Nominal,	% TD	93.0
Active Fuel Length, Design,	in.	136.7

TABLE 4.2-3b
Cycle 1
CEPAN INPUT VALUES**

	Batch A	Batch B-1	Batch B-2	Batch C
1. Cladding Type (Dimensions listed below)	1 and 2	1	2	3
2. Coolant Pressure - psia	2250	2250	2250	2250
3. Operating Lifetime - hours	(See Reference 24, CENPD- 187-P)			(4)‡
4. Internal Pressure History	Fig.4.2-5A	Fig.4.2-5B(2-cycle) Fig.4.2-5C(3-cycle)	Fig.4.2-5A (2-cycle) Fig.4.2-5D (3-cycle)	Fig.4.2-5E
5. Cladding Temperature - °F*	626	626(2-cycle) 620(3-cycle)	626 (2-cycle) 620 (3-cycle)	626
6. Fast Flux History (>1.0 Mev)	1	1(2-cycle) 2(3-cycle)	1 (2-cycle) 2 (3-cycle)	1

* Temperatures and fluxes are calculated to be consistent with the power histories described in Section 2.2.1 at an axial elevation equal to 80% of the active length. Minimum cladding yield strength @ 620-626°F is given in Reference 24, CENPD - 187-P. (4)

Cladding Dimensions	Type I	Type 2	Type 3	
1. O.D. (upper 2 σ) - inches				
2. Wall thickness (lower 2 σ)- inches	(See Reference 24, CENPD -187-P)			(4)
3. Initial ovality (upper 2 σ) - inches				
Fast Flux Histories				
(See Reference 24, CENPD - 187-P)				(4)

‡ Indicates proprietary information

**A new CEPAN analysis was performed for Cycle 5; See Cycle 5 RSE Section 2.1 and Table 2.1-l, Appendix 4A.

TABLE 4.2-4

ASME III STRESS LIMITS FOR REACTOR VESSEL INTERNAL STRUCTURES

Operating Condition		Stress Categories and Limits of Stress Intensities
1.	Normal and Upset	Figure NG 3221.1 including notes.
2.	Emergency	Figure NG 3224.1 including notes.
3.	Faulted	Appendix F, Rules for Evaluating Faulted Conditions.

TABLE 4.2-5

CONTROL ELEMENT ASSEMBLY IDENTIFICATION SYSTEM

CEA Type	Designation	Spider Web Serialization	Identifying Feature Machined on Spider Corner Post	Applicable Figure
Full length Full strength (a)	CEA-1	Numerical 01 thru 65,74 thru 199, F01 and F02, L1 thru L9, The "400" Series (401-499)	Conical taper - 4 places	4.2-15A
Full length Reduced strength (b)	CEA-2	Numerical 66 thru 69, The “200” Series (200 thru 299)	Single notch - 4 places	4.2-15B
Full length Reduced strength (c)	CEA-3	Numerical 70 thru 73, The “300” Series (300 thru 399)	Double notch - 2 places over stainless steel, Al_2O_3 rods Single notch - 2 places over Ag, B_4C rods	4.2-15C

NOTE: See Figure 4.2-16b for CEA Design

(a) F01 and F02 were purchased from Maine Yankee, to replace damaged PSL CEAs, which accounts for the “non-PSL” serialization convention (F, prefix). The "L" prefix designation has been established to assist in tracking the lifetimes of CEA Type 1's used in the lead bank.
(b) Four corner poison rods contain identical filler materials.
(c) Only diagonally opposite poison rods contain identical filler materials.

TABLE 4.2-6

CEA CLADDING DIFFERENTIAL PRESSURES AND STRESSES

Operating Condition	CEA Type	Internal Pressure, psia	External Pressure, psia	Clad ΔP, psi	Calculated Stress, ksi	Allowable Stress,ksi At 650°F
Normal Operation (beginning of life)	Full Length	0 (524)***	2250	-2250 (-1726)***	-26.9 (-22.9)***	S_m = 43.3 (33.5)***
Normal Operation (end of life)	Full Length	3352	2250	+1102	+13.1	S_m = 43.3
	(The internal pressure at the end of life is calculated to be 1925. This case is bounded by the Normal Operation scenario at beginning of life)***					
*Loss-of-Coolant small breaks, (end of life)	Full Length	3352 (1925)***	0	+3352 (+1925)***	+40.0 (23.0)***	2.4S_m=103.9 (80.4)***
**Normal Plant Depressurization (end of life)	Full Length	1596	0	+1596	+19.1	2.4S_m=103.9
	(This case is bounded by the Loss-of-Coolant scenario at the end of life)***					

* CEA insertion is not required for a safe and orderly shutdown of the reactor for large breaks of the reactor coolant system.

** Internal pressure computed at 150°F.

*** The results in parenthesis are applicable to the redesigned Framatome (formerly AREVA) CEAs implemented in Cycle 20 and EPU cycles.

EC 292529

TABLE 4.2-7

CEA STRESSES RESULTING FROM CEDM STEPPING MOTION AND VERTICAL SEISMIC ACCELERATIONS

Location	Stress due to CEDM Stepping Motion (ksi)	Stress Due to OBE Vertical Seismic (ksi)	Stress Due to DBE Vertical Seismic (ksi)
Spider Web (Shear)	± 4.3	± .7	± 1.4
Clad (Tensile)	± 18.9	± 2.9	± 5.8
End Fitting (Tensile)	± 15.6	± 2.4	± 4.8
Poison Rod to Spider Threaded Connections	The preload at these joints is greater than the load developed by CEDM stepping motion or seismic events.		

TABLE 4.2-8

FUEL ASSEMBLY DESIGN (AREVA FUEL prior to Cycle 17)

Item	Value
FUEL ASSEMBLY DESIGN PARAMETERS:	
Total Number of Fuel Assemblies	217
Number of Fuel Rod Positions/Assembly	176
Total Number of Fuel Rods	38192
Rod Array	14x14
Assembly Pitch	8.180 in.
Cycle Length (Annual, 18-Month, etc.)	18 Month
Number of Spacers	9
Spacer Span (Max.)	18.859 in.
Materials of Spacers	Zircaloy Grid with Inconel Spring
Material of Upper and Lower Tie Plates	Stainless Steel
Material of Holddown Springs	Inconel
Number of Guide Tubes/Assembly	5
Material of Guide Tubes	Zircaloy-4
Guide Tube I.D., Upper Part	1.035 in.
Guide Tube I.D., Lower Part	0.968 in.
Guide Tube O.D., Upper Part	1.115 in.
Guide Tube O.D., Lower Part	1.048 in.
Assembly Weight (Dry) (All Fueled Rods)	1315 lbs.

TABLE 4.2-8

FUEL ASSEMBLY DESIGN (AREVA FUEL prior to Cycle 17) (CONT.)

Item	Value
FUEL ROD DESIGN PARAMETERS:	
Cladding O.D.	0.440 in.
Cladding I.D.	0.384 in.
Cladding Material	Zircaloy-4
Rod Pitch	0.580 in.
Total Active Fuel Length	136.70 in.
Fuel Length, UO_2 Rods	
Upper End, Natural UO_2	8.64 in.[1]
Enriched UO_2	124.7 in.
Lower End, Natural UO_2	3.36 in.[1]
Fuel Length, UO_2-Gd_2O_3 Rods	
Upper End, Natural UO_2	14.04 in.[2]
Enriched UO_2	113.9 in.[3]
Lower End, Natural UO_2	8.76 in.[4]
Plenum Spring Material	Inconel X-750
FUEL PELLET DESIGN PARAMETERS:	
Enriched UO_2 Fuel Pellet Parameters	
Pellet Material	UO_2
Pellet O.D.	0.3770 in.
Density, % Theoretical	95.0%

1 For Batch X these are 6 in. blankets of 2.6 w/o U-235
2 For Batch X this is 11.4 in. 2.6 w/o U-235
3 For Batch X this is 116.54 in.
4 For Batch X this is 2.6 w/o U-235

TABLE 4.2-8

FUEL ASSEMBLY DESIGN (AREVA FUEL prior to Cycle 17) (CONT.)

Item	Value
FUEL PELLET DESIGN PARAMETERS (cont.):	
UO_2-Gd_2O_3 Fuel Pellet Parameters	
Pellet Material	UO_2-Gd_2O_3
Pellet O.D.	0.3770 in.
Density, % Theoretical	95.0%
Natural Fuel Pellet Parameters	
Pellet Material	UO_2
Pellet O.D.	0.3770 in.
Density, % Theoretical	95.0%

TABLE 4.2-9

STRESS INTENSITY UNITS

Framatome (formerly AREVA) Zircaloy-4 FUEL EC292529

STRESS CATEGORY	Yield Strength	Ultimate Tensile Strength
General Primary Membrane	2/3 σ_y	1/3σ_u
Local Primary Membrane	1.0 σ_y	1/2σ_u
Primary Membrane Plus Primary Bending	1.0 σ_y	1/2σ_u
Primary Plus Secondary	2.0 σ_y	1.0σ_u

For M5® clad fuel, Sm based on hoop yield stress.

Table 4.2-10
Fuel Assembly Design (Framatome (AREVA) Fuel Starting Cycle 17) EC292529

Characteristic	Material	Value
Fuel Assembly		
Fuel Assembly Pitch, in.		8.18
Array		14 x 14
Number of fuel rods		176
Number of non-fueled elements		
Guide Tubes	Zircaloy-4	4
Outside Diameter, in		1.115
Inside Diameter, in		1.035
Dashpot Outside diameter, in		1.048[1]
Dashpot inside diameter, in		0.968
Instrument Tube	Zircaloy-4	1
Outside Diameter, in		1.115
Inside Diameter, in		1.035
Overall Assembly Length, in		157.115
Spacers		
Number of spacers		
HTP™	Zircaloy-4	8
HMP™	Alloy 718	1 (lowest axial location)
Envelope (Zircaloy-4 HTP™), in		8.105
Envelope (Alloy 718 HMP™), in		8.105
Fuel Rod pitch, in		0.580
LTP envelope, in (FUELGUARD)	Stainless Steel	8.109
UTP envelope, in	Stainless Steel	8.030
Holddown springs	Alloy X-750	
Fuel Rod		
Cladding	Zircaloy-4[2]	
Cladding outside diameter, in		0.440
Cladding inside diameter, in		0.384
Fuel column	UO_2 or UO_2/Gd_2O_3	
Pellet diameter, in		0.377
Active fuel length, in		136.7
Density, % of theoretical		95.35
Fill gas pressure, psia	Helium	330
Plenum spring	Alloy X-750	
Overall fuel rod length, in		145.77

[1] The guide tube OD is 1.115 inches for the MONOBLOC™ guide tube feature (starting with Cycle 25).
[2] The cladding material changed to M5® starting with Cycle 26.

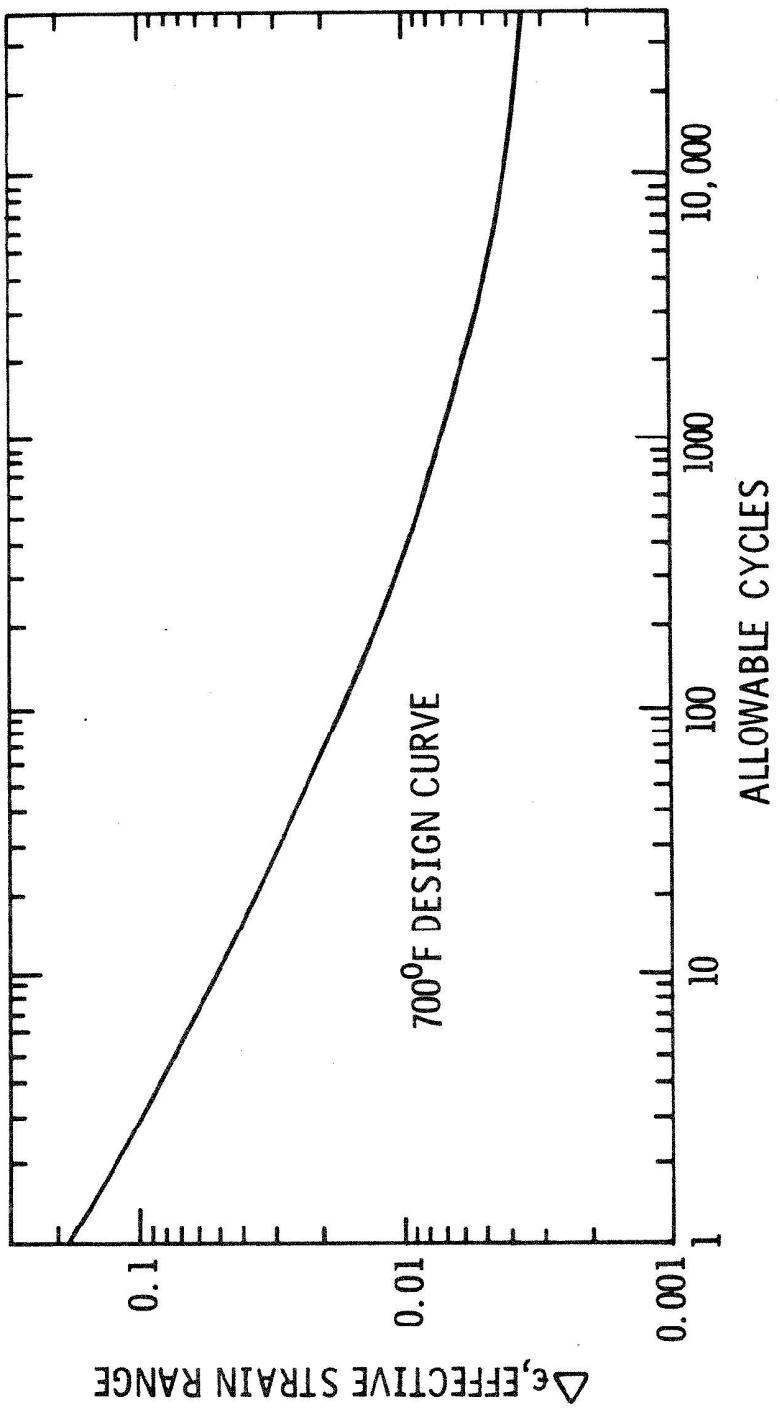

Am. 3-7/85

FLORIDA POWER & LIGHT CO. St. Lucie Plant	Design Curve for Cyclic-Strain Usage of Zircaloy-4 at 700F CE FUEL	Figure 4.2-1

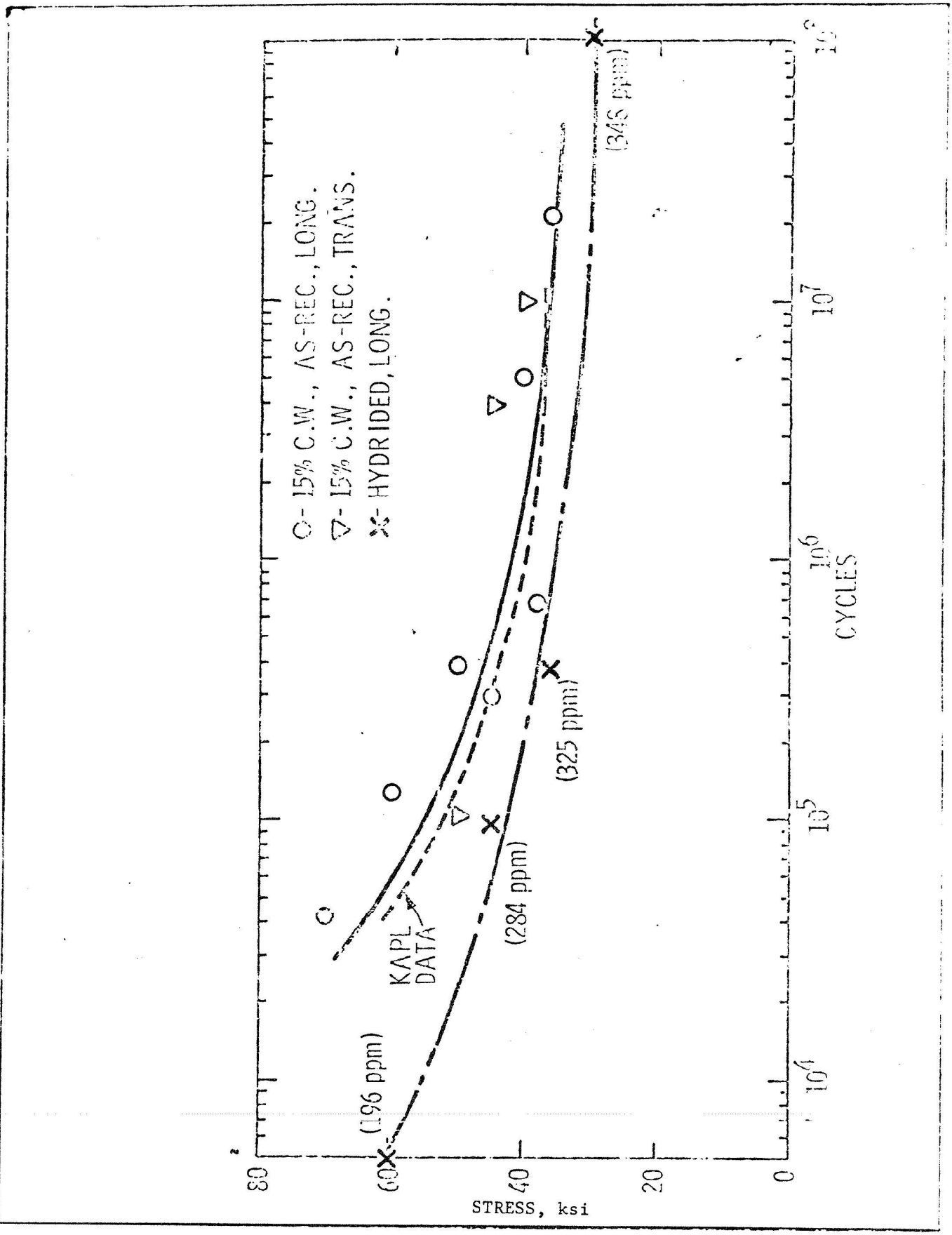

Am. 3-7/85

ROOM TEMPERATURE FATIGUE DATA FOR ZR-4 SHEET, REVERSE BENDING

CE FUEL

FIGURE 4.2-1A

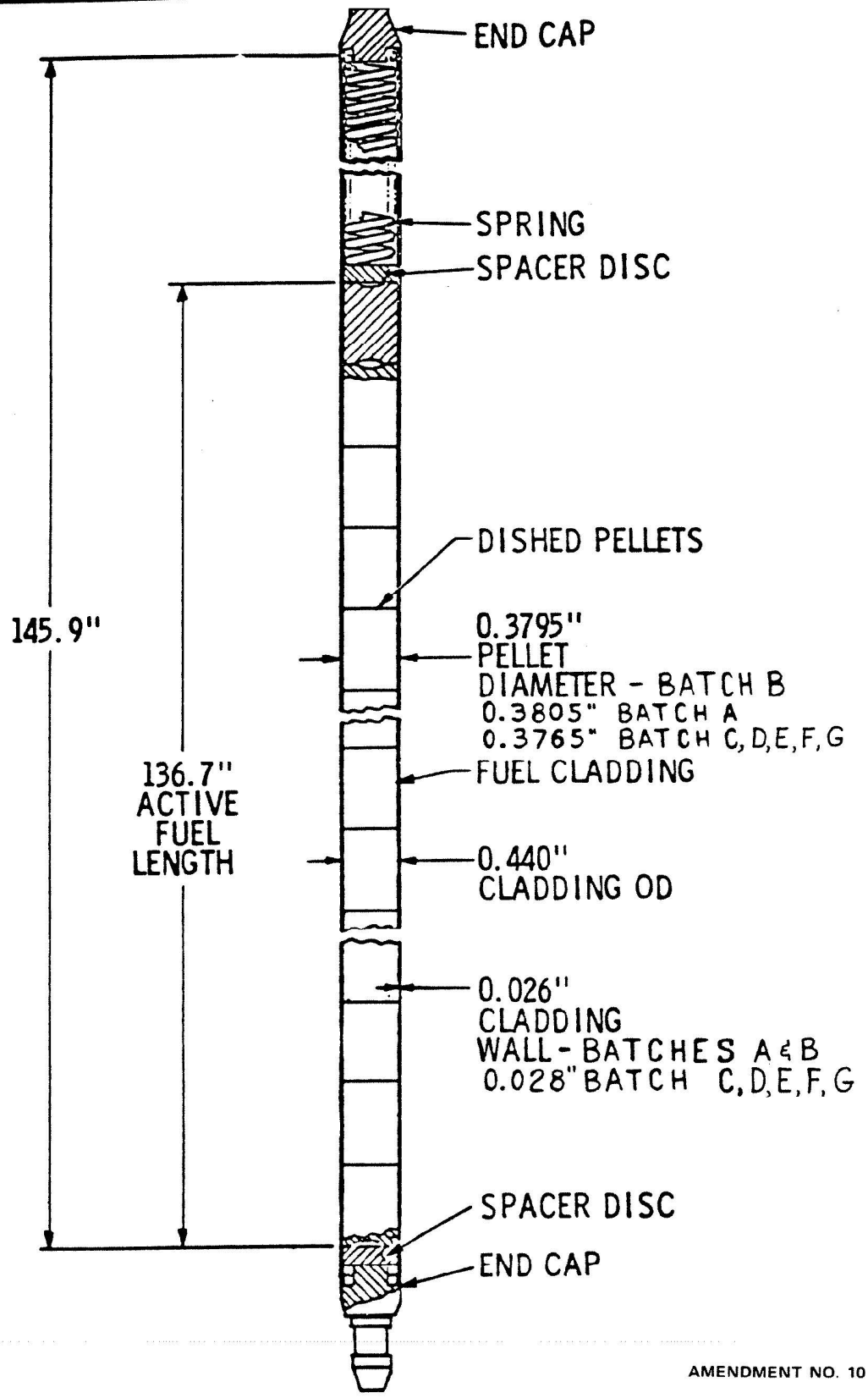

AMENDMENT NO. 10 (7/91)

FLORIDA POWER & LIGHT CO. St. Lucie Plant	Fuel Rod CE FUEL	Figure 4.2-2

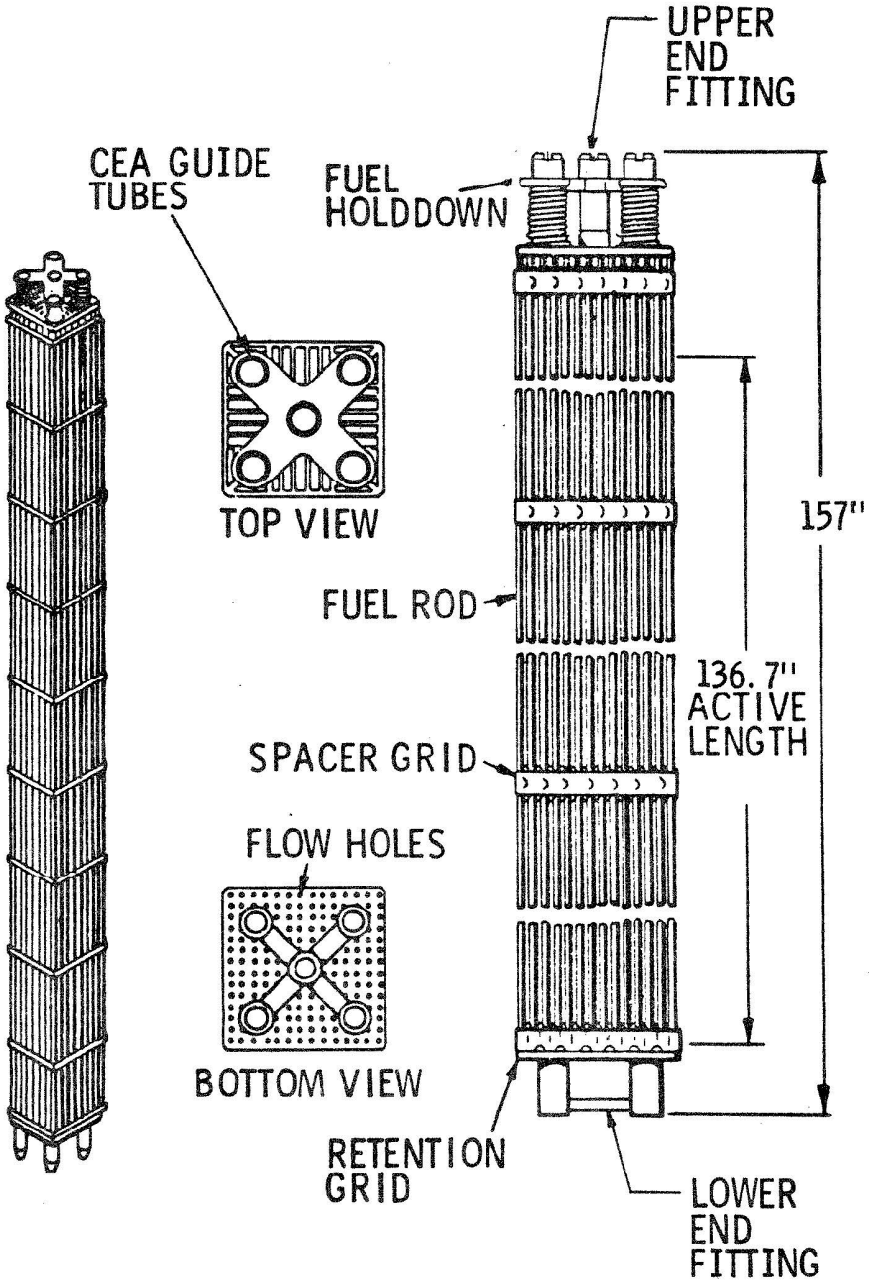

Am. 3-7/85

FLORIDA POWER & LIGHT CO. St. Lucie Plant	Fuel Assembly CE FUEL	Figure 4.2-3

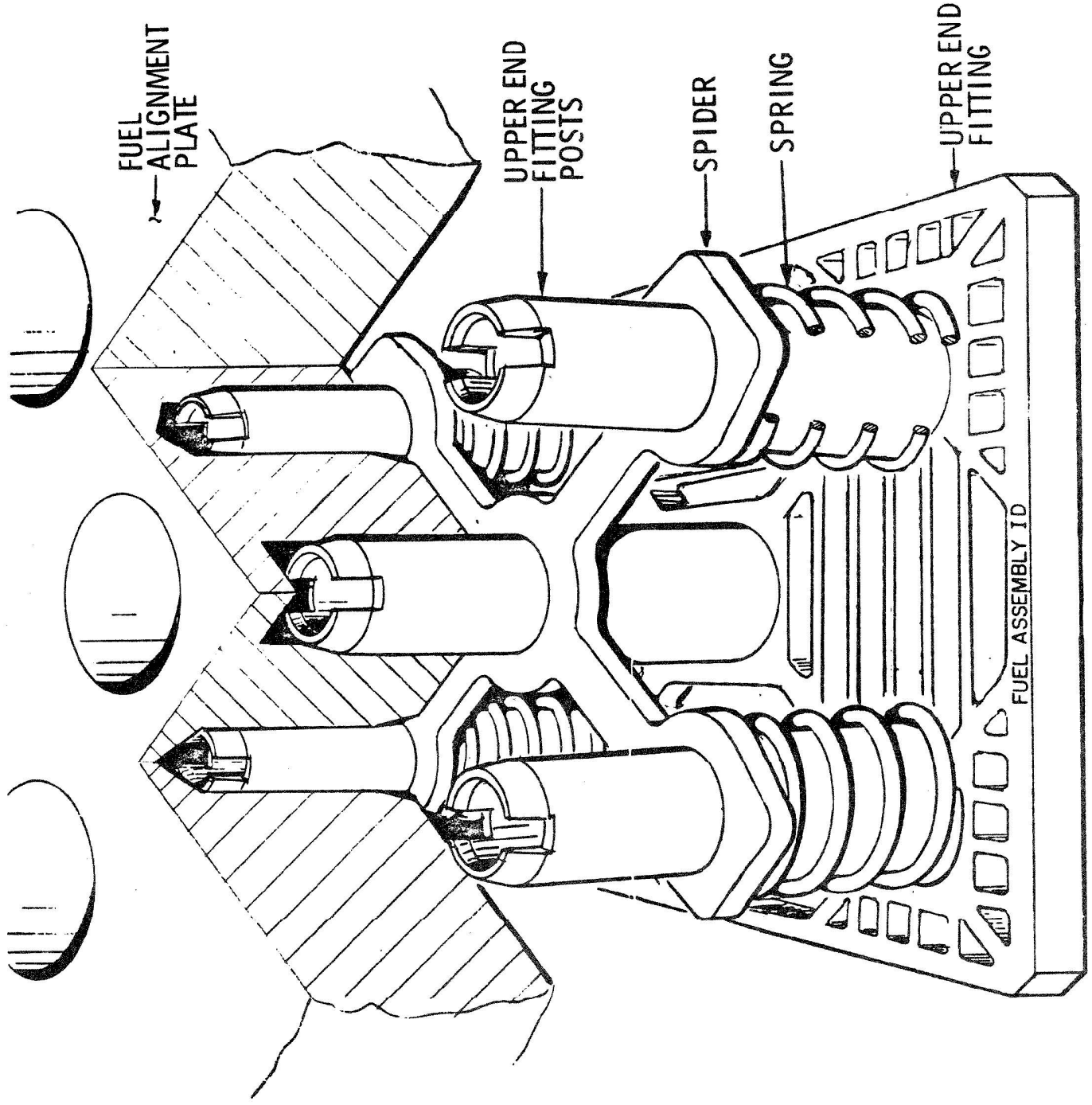

Am. 3-7/85

FLORIDA POWER & LIGHT CO. St. Lucie Plant Unit I	Fuel Assembly Hold Down CE FUEL	Figure 4.2-4

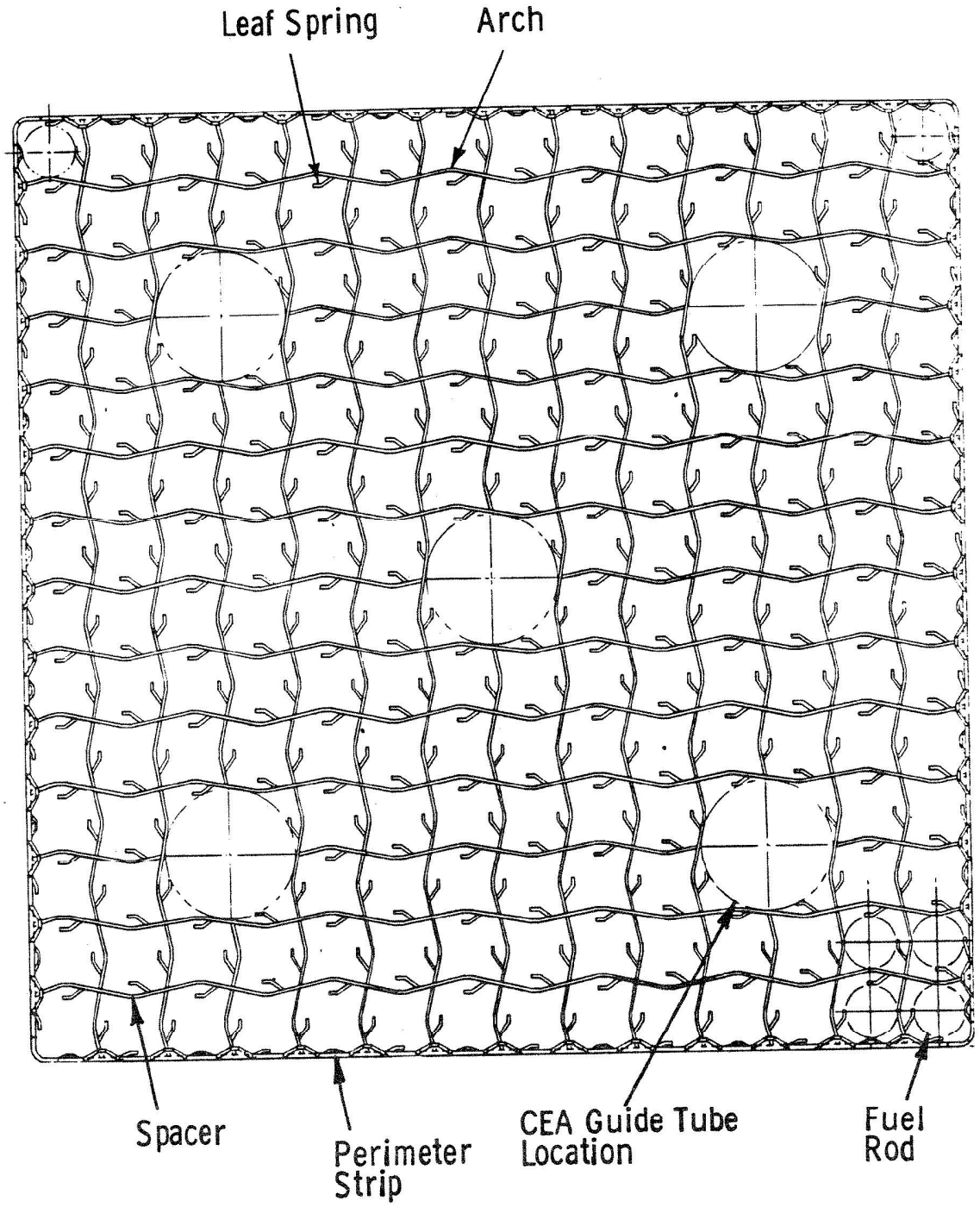

Am. 3-7/85

FLORIDA POWER & LIGHT CO. St. Lucie Plant Unit 1	Fuel Spacer Grid CE FUEL	Figure 4.2-5

Figure 4.2-5A*

St. Lucie Minimum Rod Internal Pressure vs Time
Batches A & B 2 Fuel Cycles 95% Nominal Initial Density

Figure 4.2-5B*

St. Lucie Minimum Rod Internal Pressure vs Time
Batch B 2 Fuel Cycles 93% Nominal Initial Density

Figure 4.2-5C*

St. Lucie Minimum Rod Internal Pressure vs Time
Batch B 3 Fuel Cycles 93% Nominal Initial Density

Figure 4.2-5D*

St. Lucie Minimum Rod Internal Pressure vs Time
Batch B 3 Fuel Cycles 95% Nominal Initial Density

Figure 4.2-5E*
St. Lucie Minimum Rod Internal Pressure vs Time
Batch C 3 Fuel Cycles

---

* Reference 24, CENPD- 187-P

FLORIDA POWER & LIGHT CO.
St. Lucie Plant

Circumferential Strain vs Temperature

CE FUEL

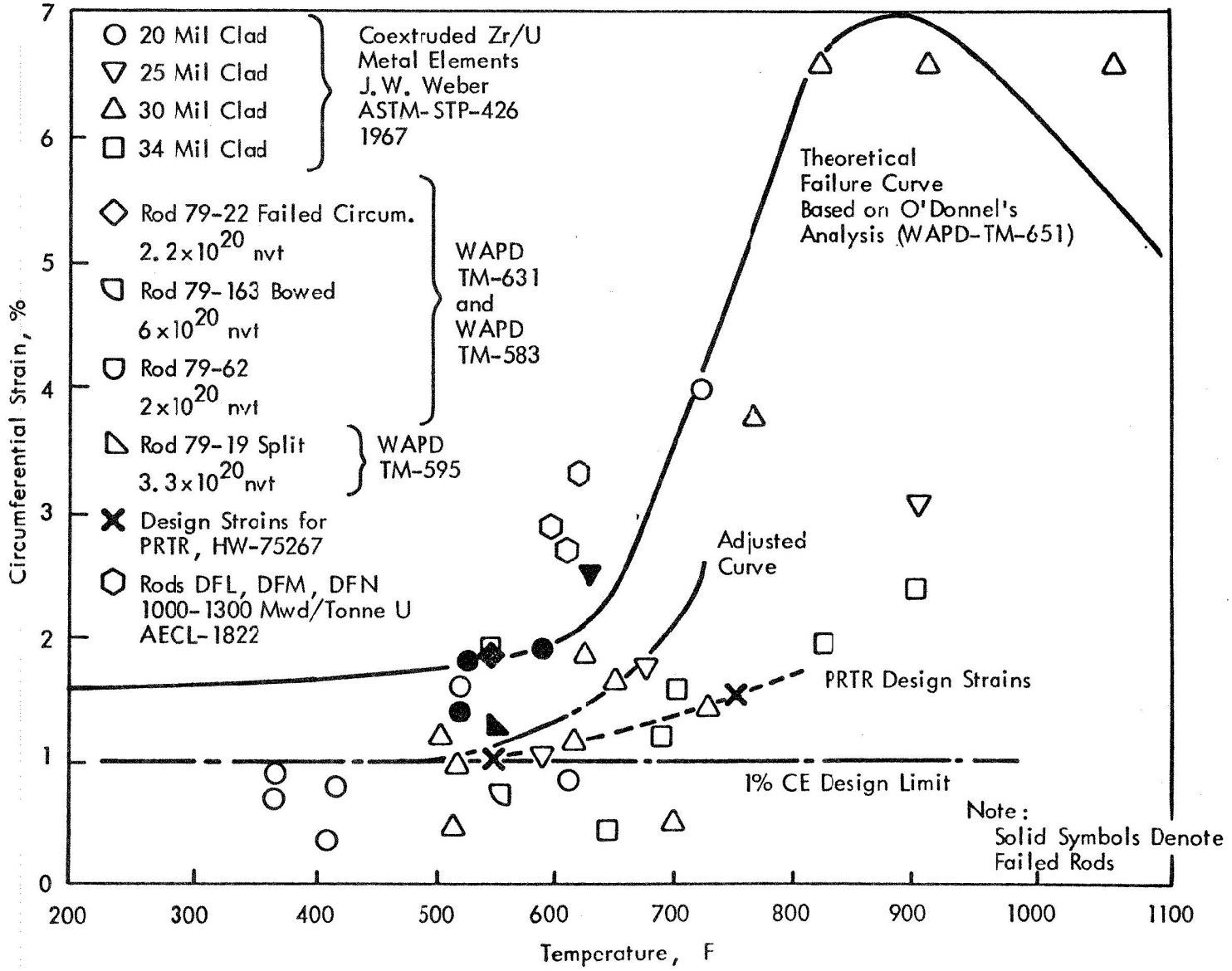

Figure 4.2-6

Am. 3-7/85

REFER TO DRAWING 8770-2050

Florida Power & Light Company
St. Lucie Plant Unit 1

Reactor Internals Assembly

Figure 4.2-7

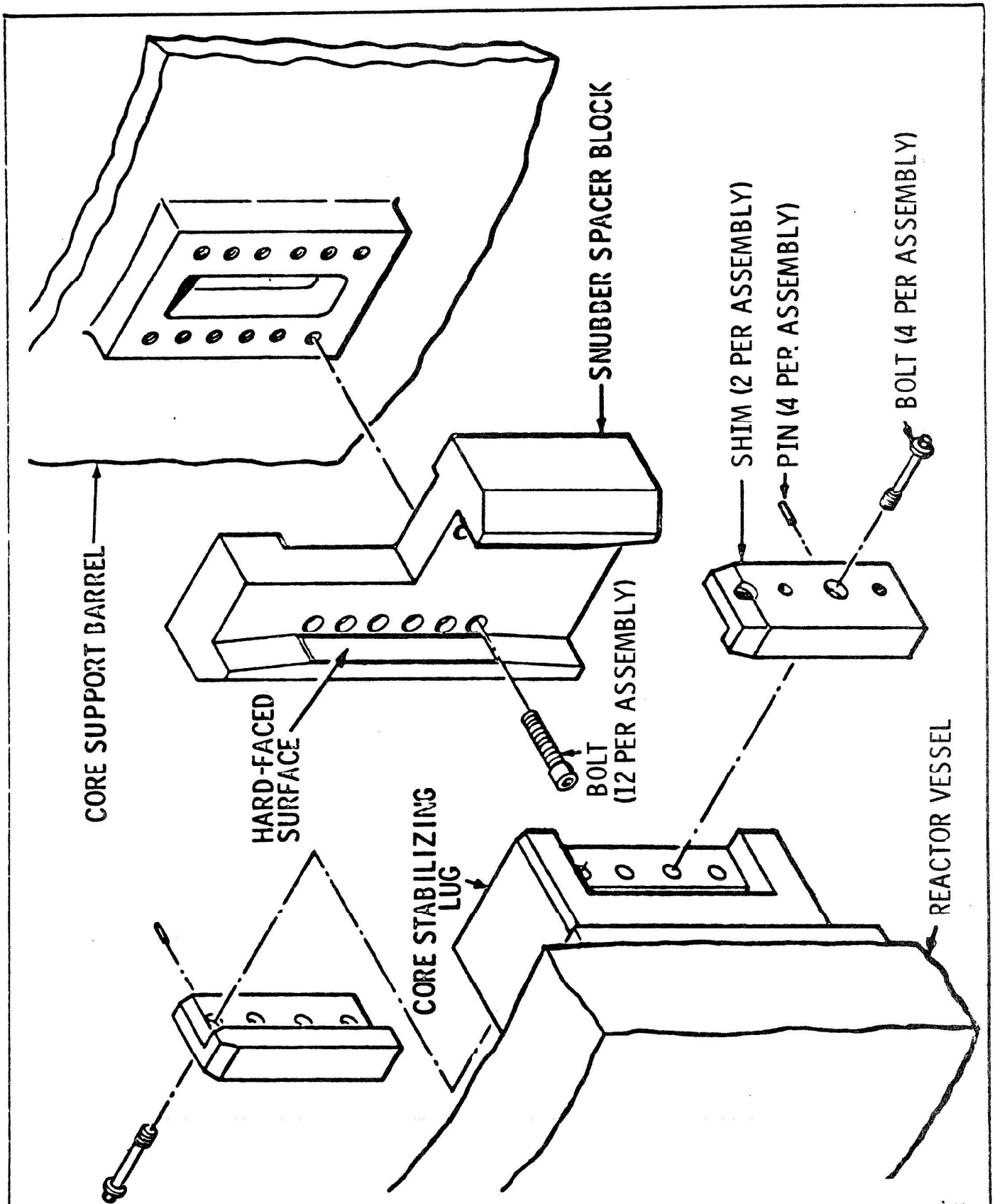

FLORIDA POWER & LIGHT CO. St. Lucie Plant Unit 1	Reactor Vessel - Core Support Barrel Snubber Assembly	Figure 4.2-8

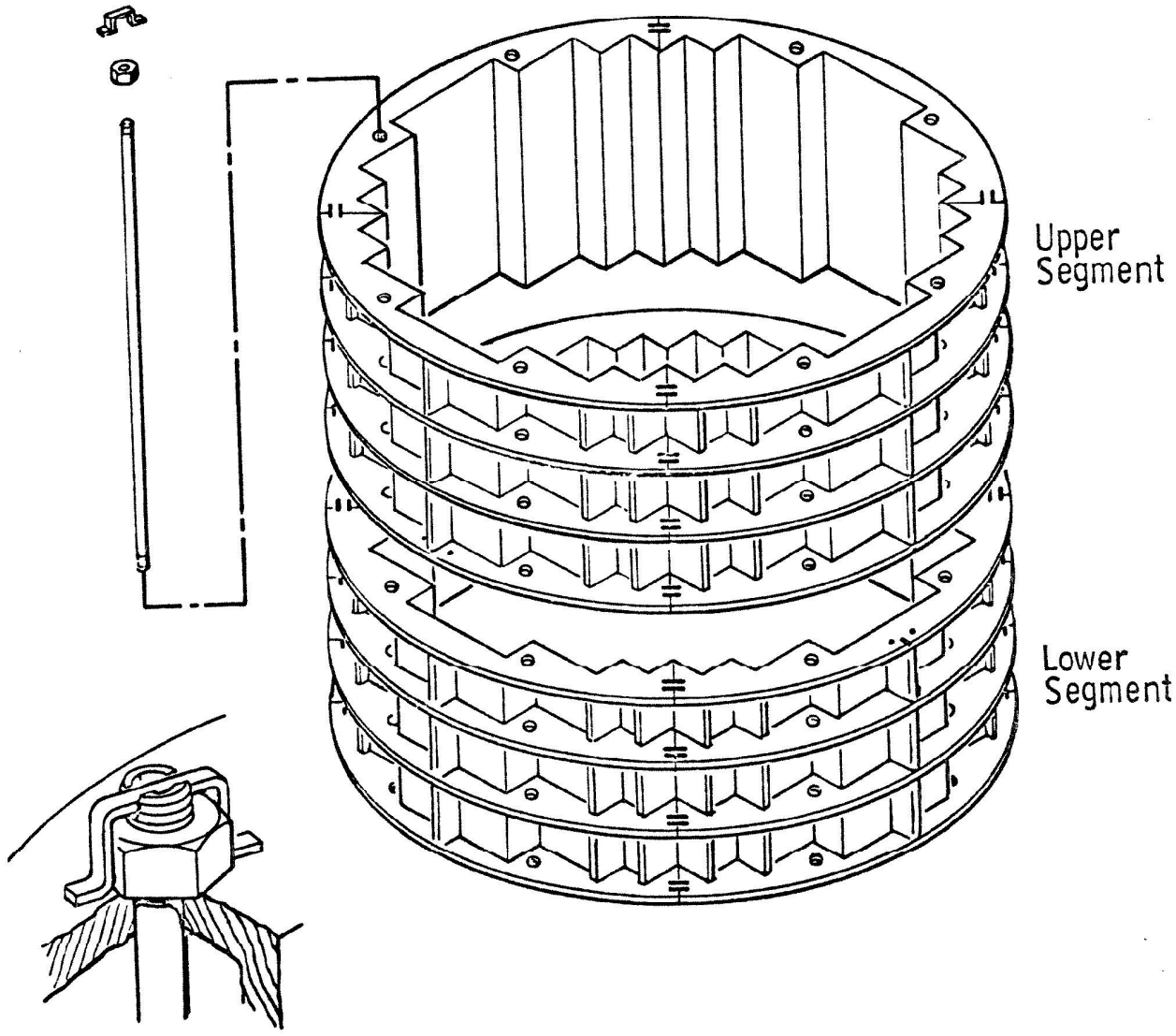

13-67

FLORIDA POWER & LIGHT CO. St. Lucie Plant	Core Shroud Assembly	Figure 4.2-9

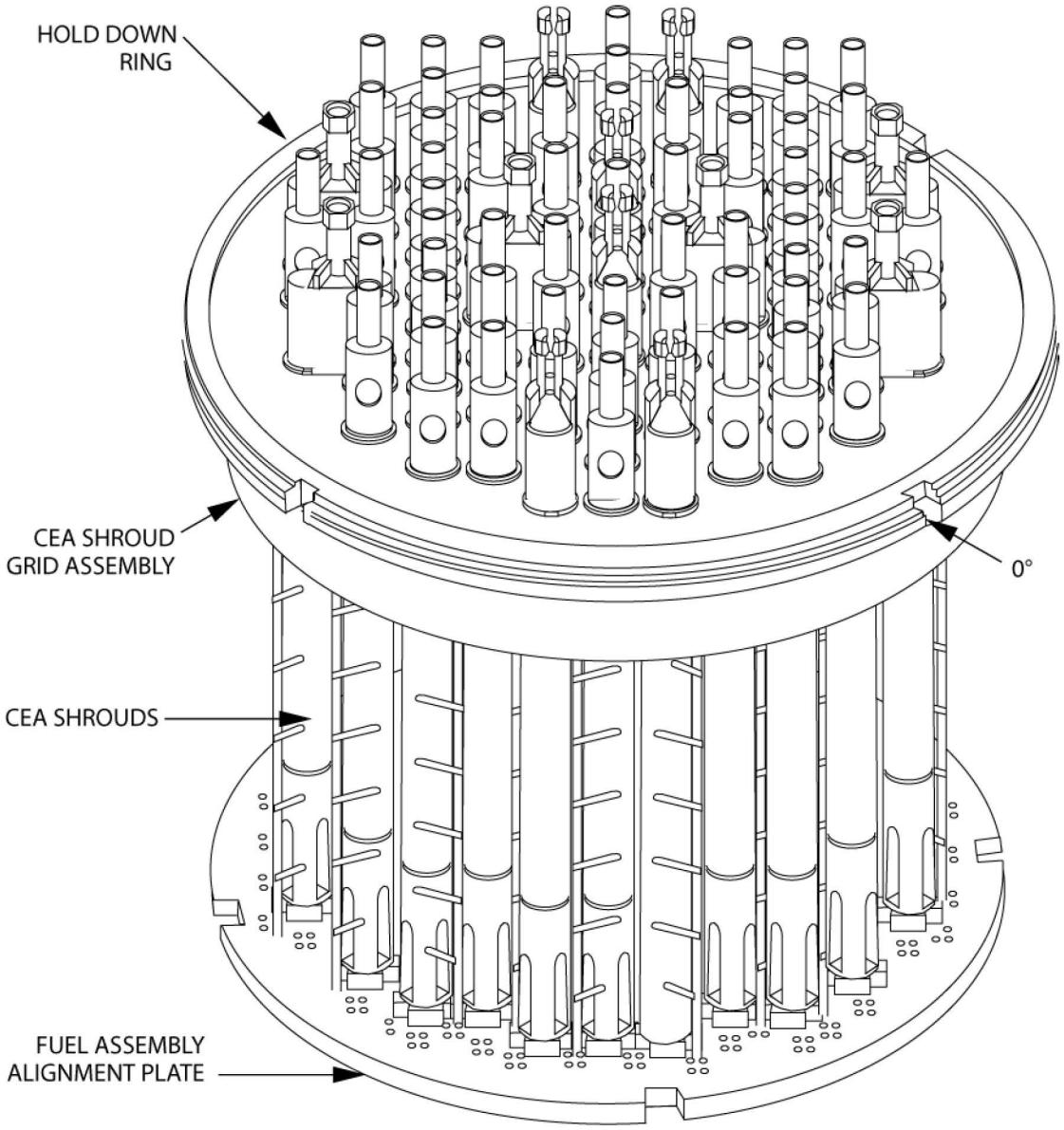

Florida Power & Light Company
St. Lucie Plant Unit 1

Reactor Internals Assembly

Figure 4.2-10

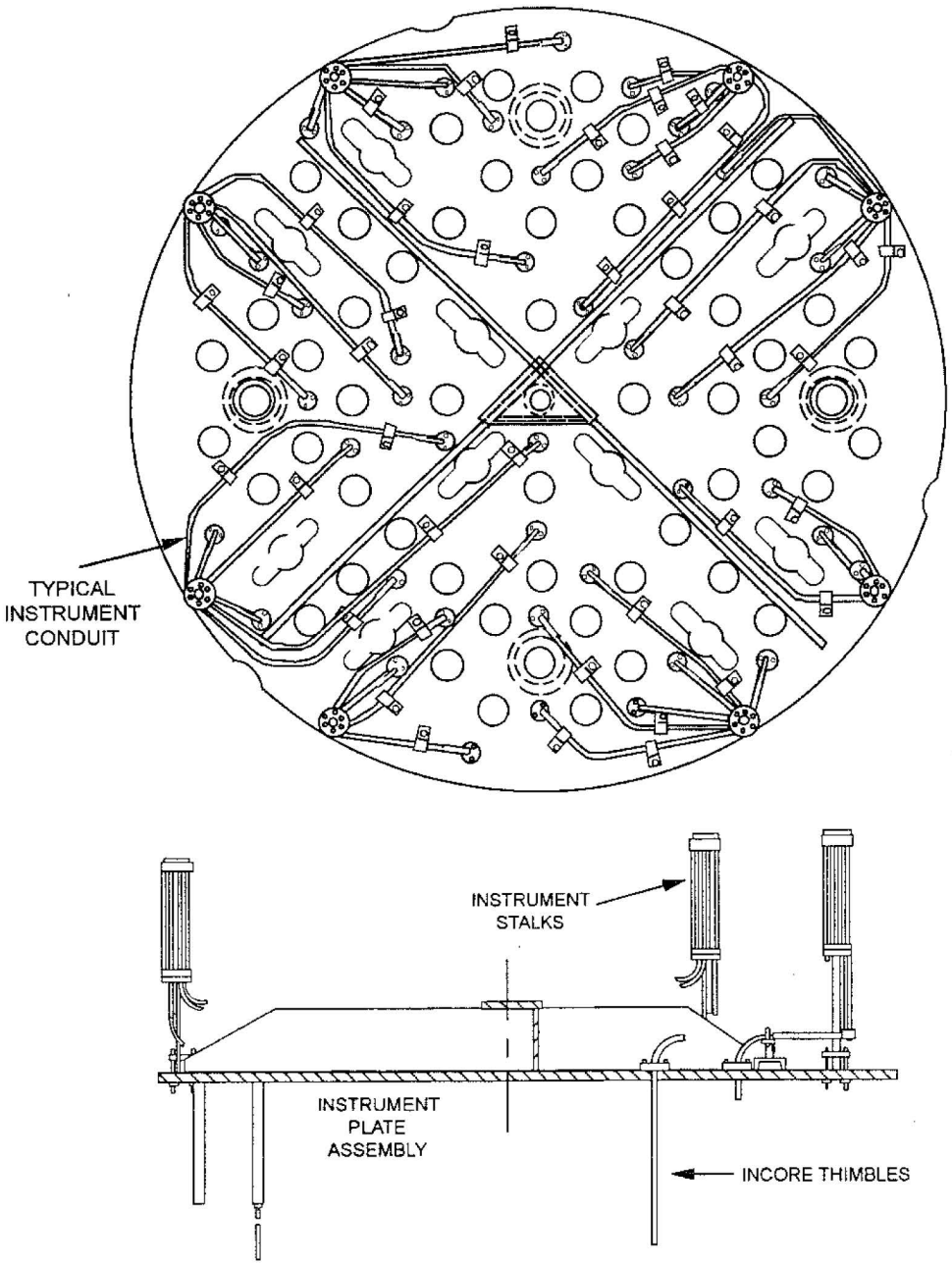

Florida Power & Light Company
St. Lucie Plant Unit 1

Incore Instrumentation Assembly

Figure 4.2-11

THIS FIGURE HAS BEEN DELETED

Amendment No. 16, (1/98)

FLORIDA POWER & LIGHT COMPANY
ST. LUCIE PLANT UNIT 1

IN-CORE NUCLEAR DETECTOR ASSEMBLY

FIGURE 4.2-12

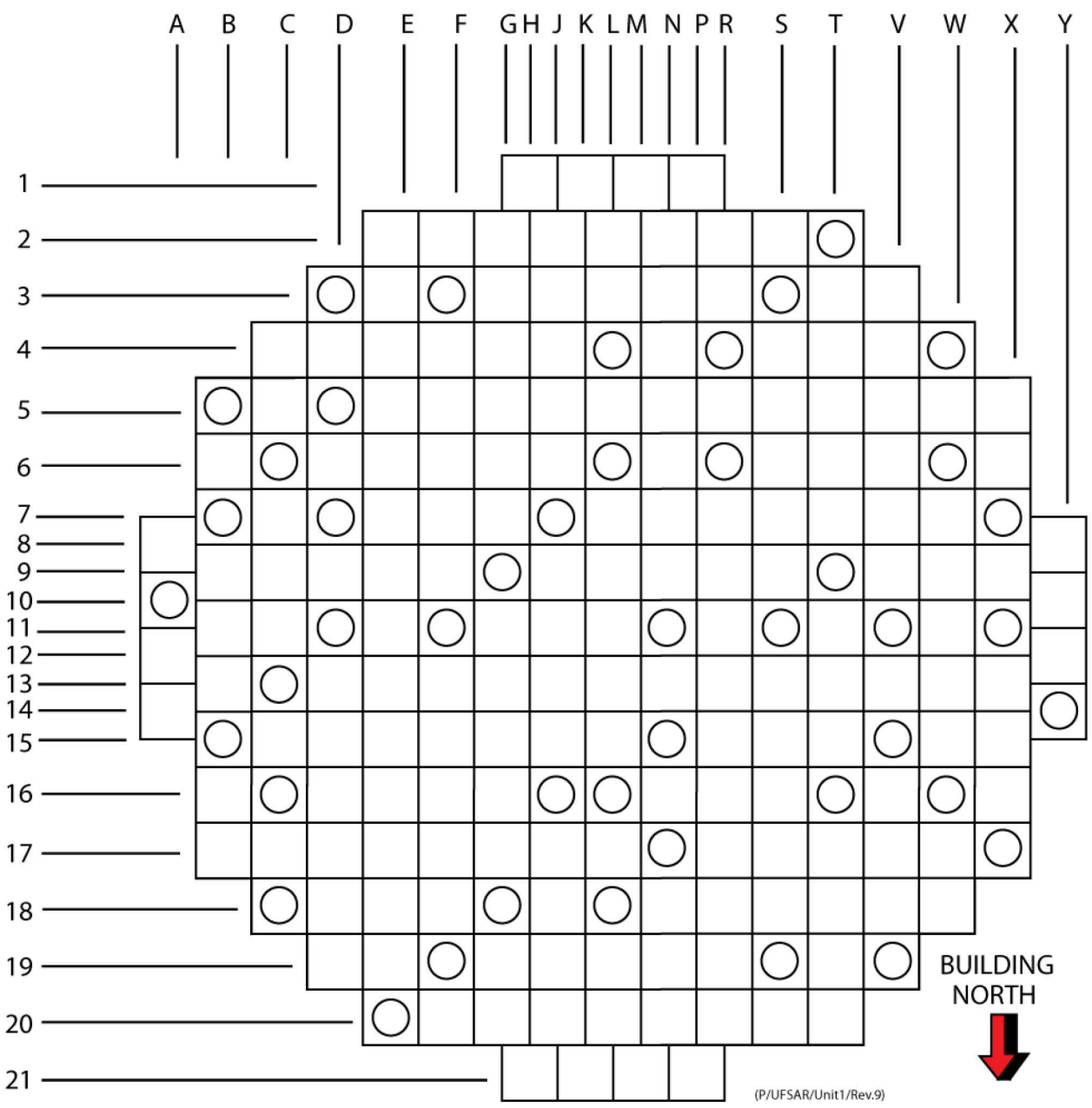

Florida Power & Light Company
St. Lucie Plant Unit 1

Incore Detector Locations

Figure 4.2-13

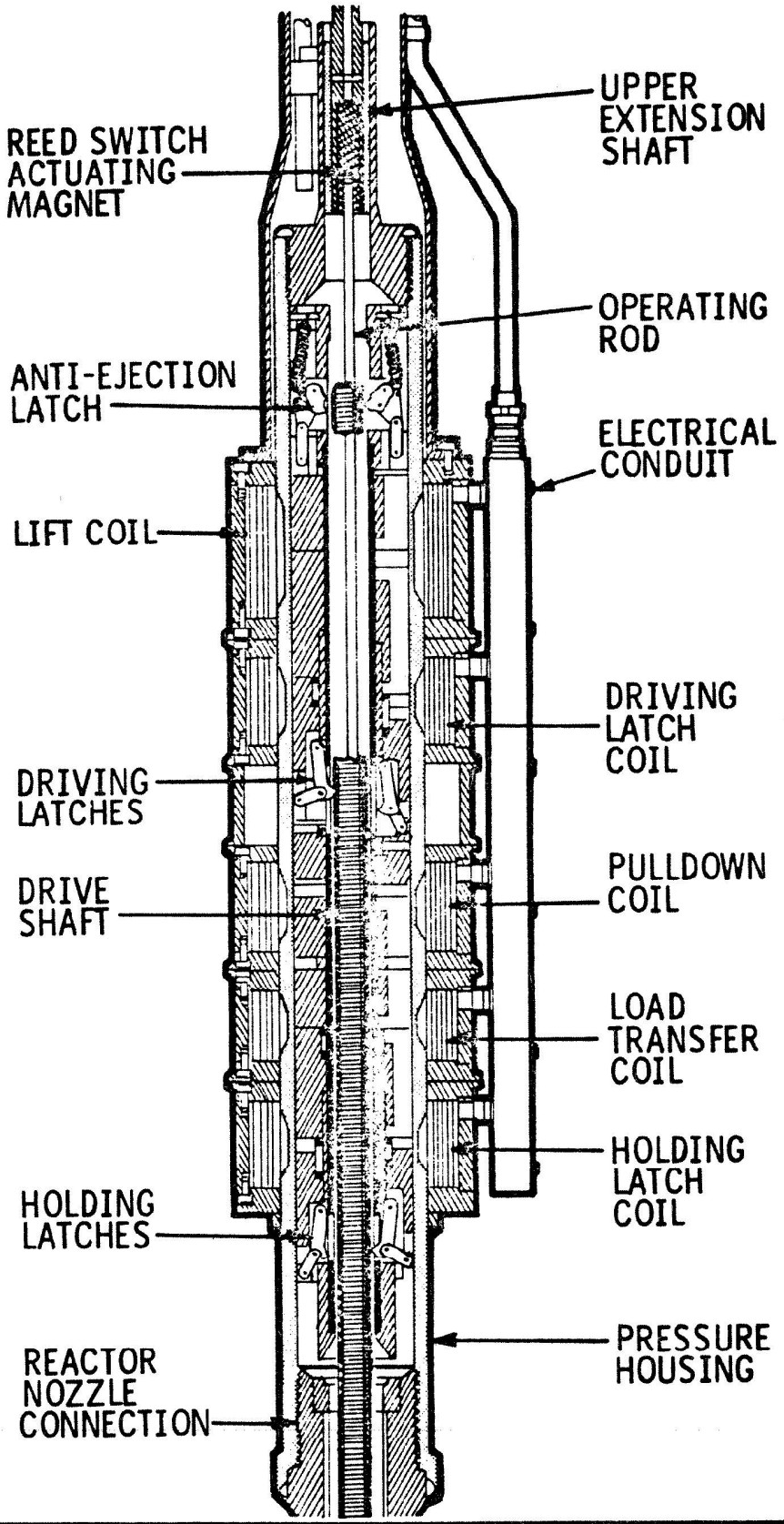

FLORIDA POWER & LIGHT CO. St. Lucie Plant	Control Element Drive Mechanism	Figure 4.2-14

Refer to Drawing
8770-15165

Florida Power & Light Company
St. Lucie Plant Unit 1

CEA-1 Full Length-Full Strength CEA
Figure 4.2-15A

Refer to Drawing
8770-15142

Florida Power & Light Company
St. Lucie Plant Unit 1

CEA-2 Full Length-Reduced Strength CEA
Figure 4.2-15B

Refer to Drawing
8770-15143

Florida Power & Light Company
St. Lucie Plant Unit 1

CEA-3 Full Length-Reduced Strength CEA
Figure 4.2-15C

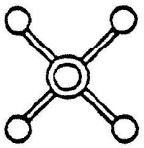

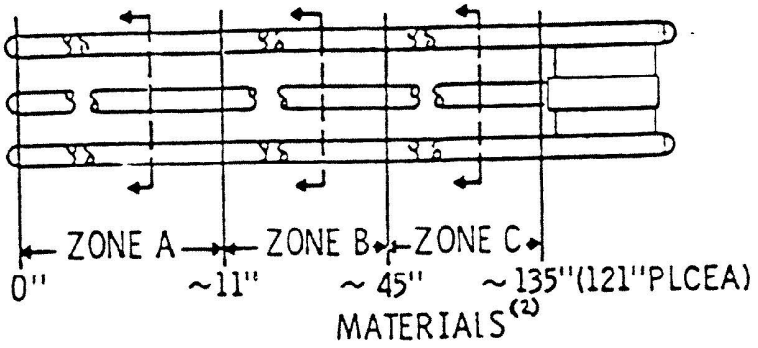

ABBREVIATIONS	CEA NUMBER	LOCATIONS(1)	ZONE A	ZONE B	ZONE C
CEA1	65	ALL OTHERS	Ag Ag / B / Ag Ag	B B / B / B B	B B / B / B B
CEA2	4	GROUP 7 POSITION D-4 AND SYMETRICAL POSITIONS	Ag Ag / Al / Ag Ag	B B / Al / B B	B B / Al / B B
CEA3	4	GROUP 7 POSITION L-3 AND SYMETRICAL POSITIONS(3)	Ag S / B / S Ag	B Al / B / Al B	B Al / B / Al B

NOTES: (1) See Figure 4.3-25 for Cycle 1 locations and Figure 4.2-16c for current locations

B= B_4C S= Stainless Steel Ag= Ag-In-Cd Al= Al_2O_3

(3) See Figure 4.2-16e for orientation of Type CEA-3 CEAs in the core

Amendment No. 17, (10/99)

FLORIDA POWER & LIGHT COMPANY
ST. LUCIE PLANT UNIT 1

CEA MATERIALS
CYCLES 1 THROUGH 8

FIGURE 4.2-16a

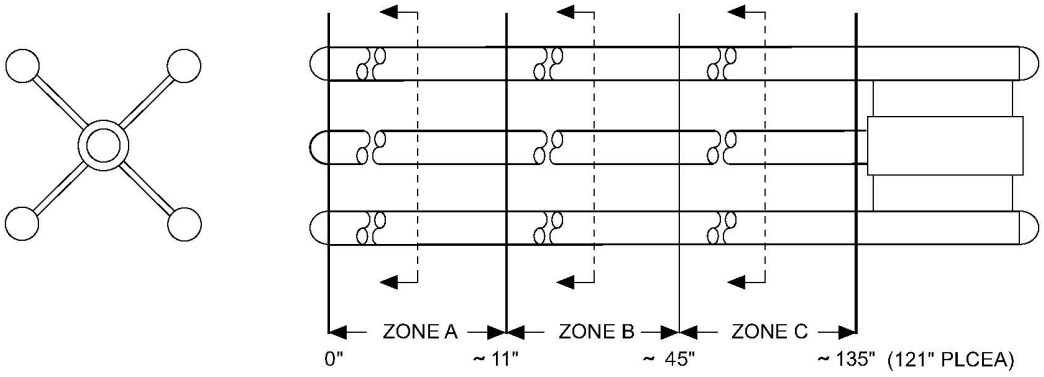

ABBREVIATIONS	NUMBER	CEA LOCATIONS (1)	MATERIALS (2) ZONE A	ZONE B	ZONE C
CEA 1	65	ALL OTHERS	Ag Ag B (3,6) Ag Ag	B B B B B B	B B B B B B
CEA 2	4	GROUP 7 POSITION D-4 AND SYMETRICAL POSITIONS	Ag Ag Al (5,6) Ag Ag	B B Al (6) B B	B B Al (6) B B
CEA 3	4	GROUP 7 POSITION L-3 AND SYMETRICAL POSITIONS(4)	Ag S B (3) S Ag	B Al B Al B	B Al B Al B

NOTES:

(1) See Figure 4.3-25 for Cycle 1 locations

(2) B = B_4C S = Stainless Steel Ag = Ag-In-Cd Al = Al_2O_3

(3) Tip region (lower 8 in.) can be B or Ag. CEAs with I.D.s less than 80 (and not a type 2 CEA) have B in the tip region of the center finger. See Table 4.2-5.

(4) See Figure 4.2-160 for orientation of Type CEA-3 CEAs in the core.

(5) Starting in Cycle 19, the tip region of new Type 2 CEA incorporates a stainless steel(S) slug in the center finger.

(6) Starting in Cycle 20, the tip region of the new Type 1 CEAs (401 and higher) incorporates 12.5 inch lengths of Ag-In-Cd. Also, the new Type 2 CEAs incorporate full length of stainless steel in the center finger.

Florida Power & Light Company
St. Lucie Plant Unit 1

CEA Materials Starting With Cycle 9
Figure 4.2-16B

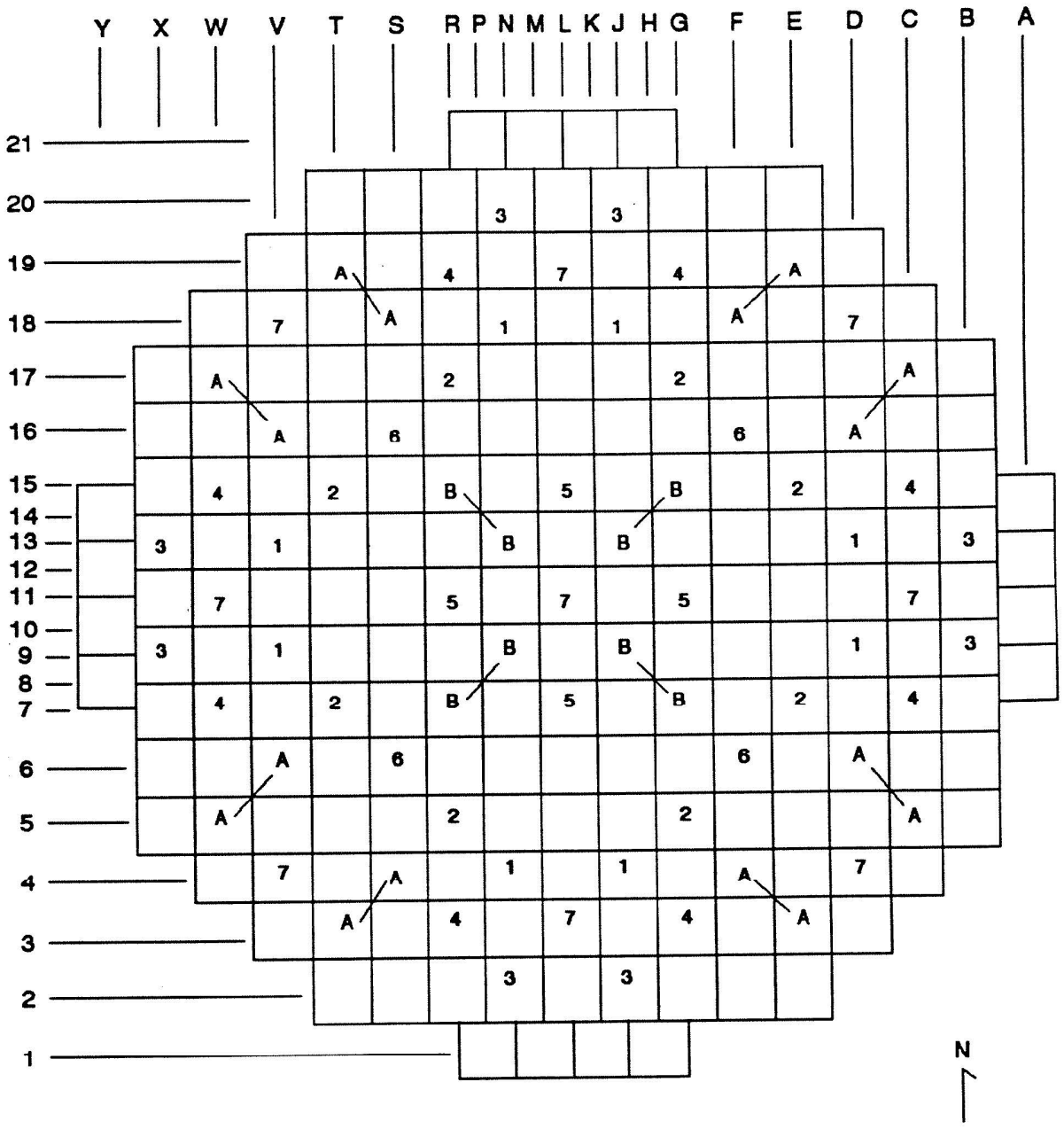

AMENDMENT NO. 10 (7/91)

FLORIDA POWER & LIGHT COMPANY
ST. LUCIE PLANT UNIT 1

CEA LOCATION BY BANK

FIGURE 4.2-16c

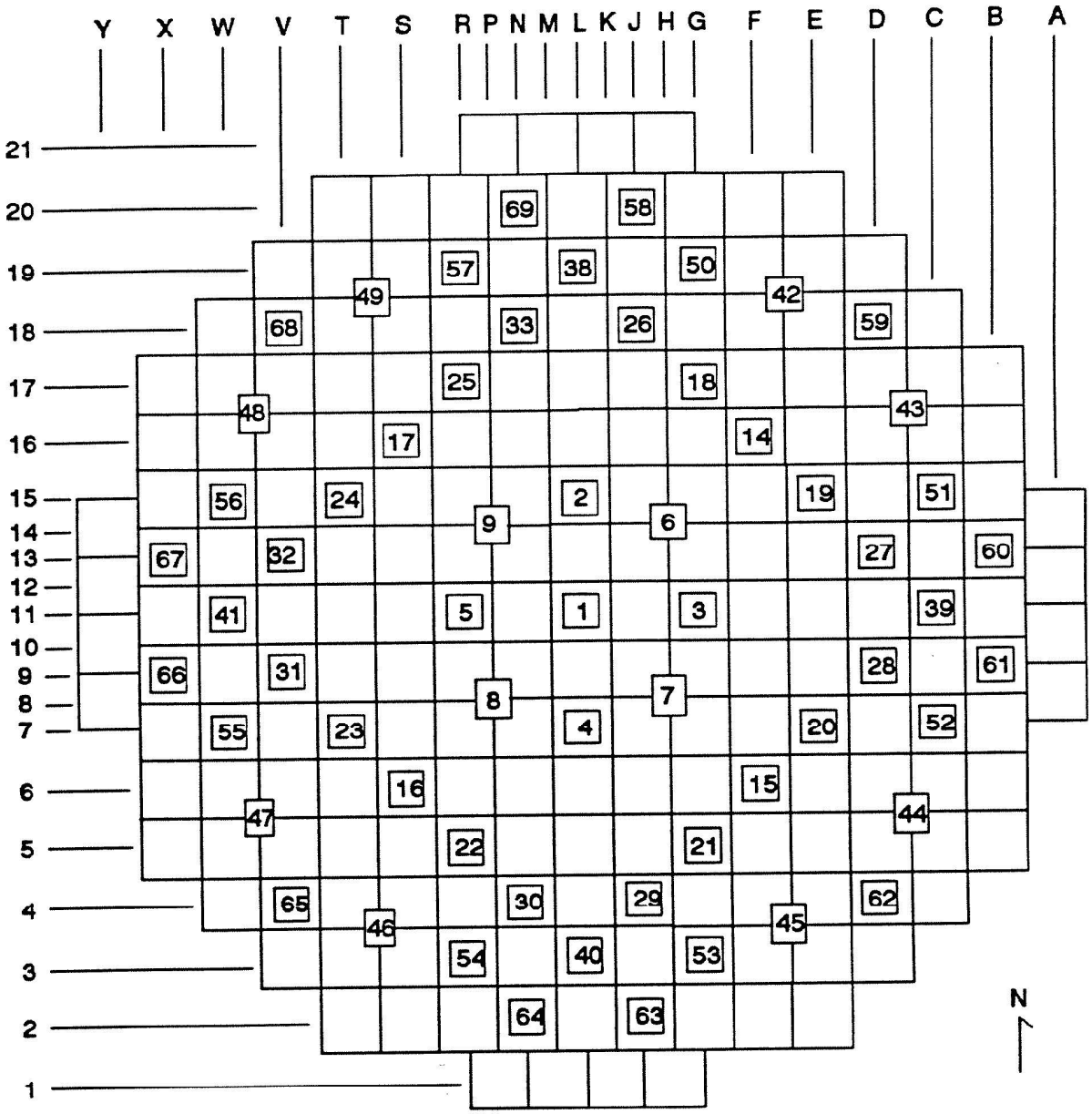

AMENDMENT NO. 10 (7/91)

FLORIDA POWER & LIGHT COMPANY
ST. LUCIE PLANT UNIT 1

CEDM NUMBERING SEQUENCE

FIGURE 4.2-16d

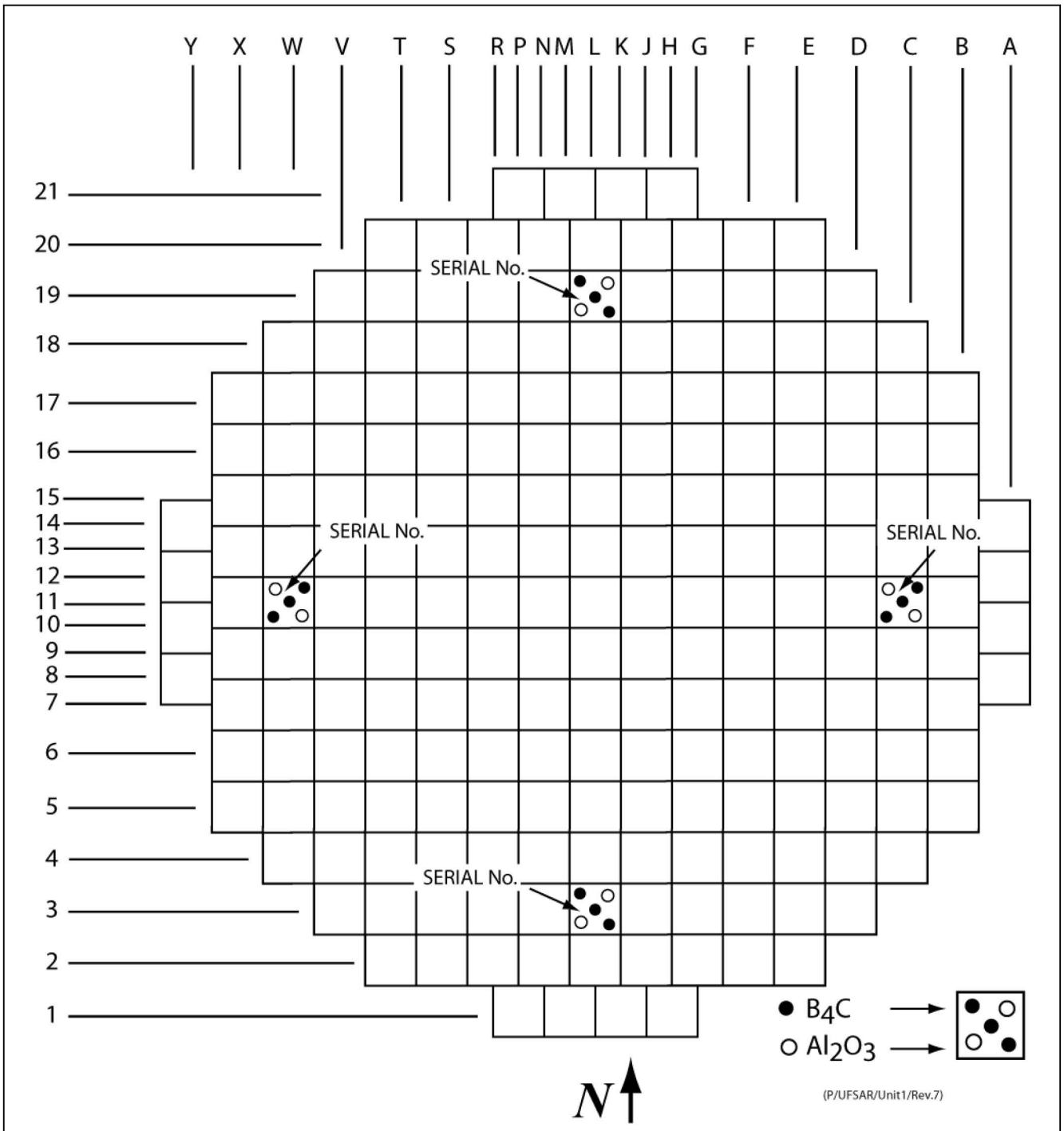

Florida Power & Light Company St. Lucie Plant Unit 1
Orientation of Type CEA-3 CEAs In Lead Bank Figure 4.2-16e

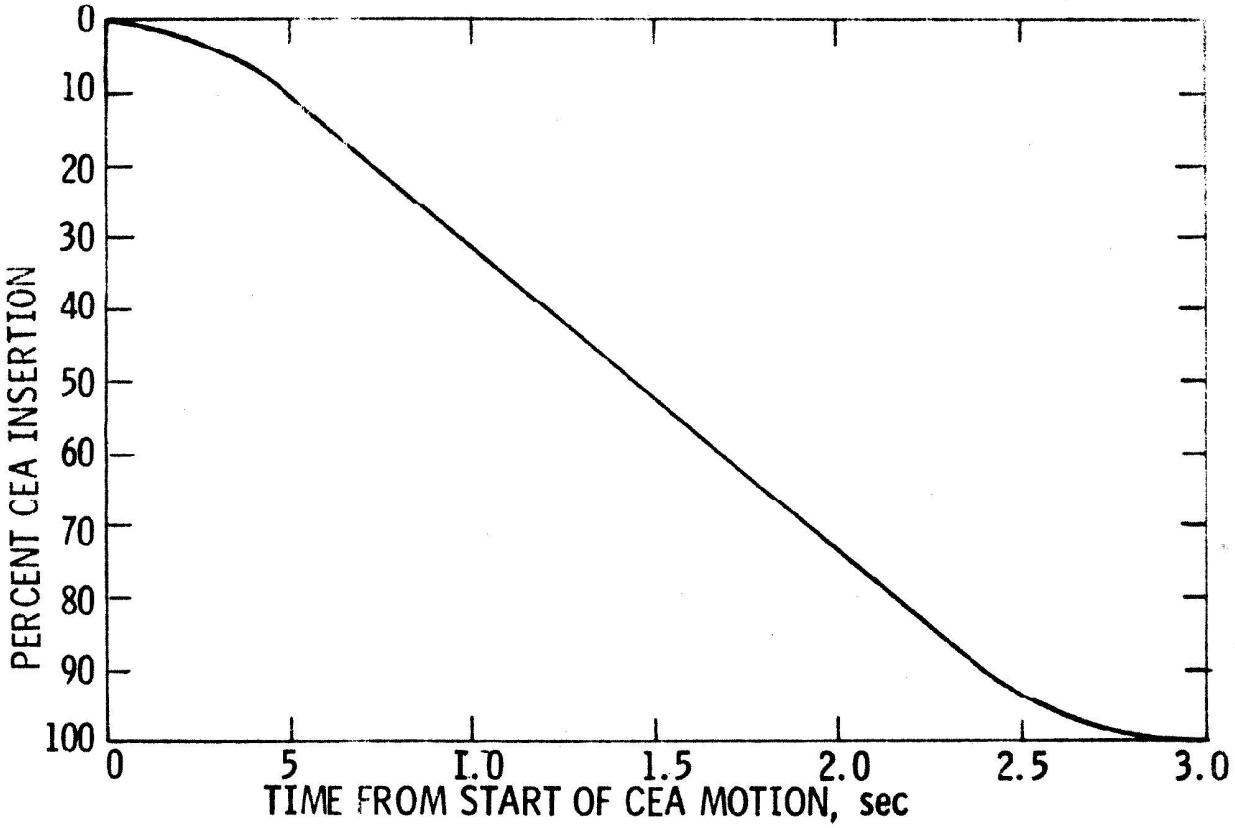

FLORIDA POWER & LIGHT CO. St. Lucie Plant	CEA POSITION vs TIME FROM START OF ROD MOTION FAST SHUTDOWN	Figure 4.2-17

FLORIDA POWER & LIGHT CO.
St. Lucie Plant
Unit 1

FUEL ROD INTERNAL PRESSURE

BEGINNING OF CYCLE 1, EQUILIBRIUM XENON, 2560Mwt

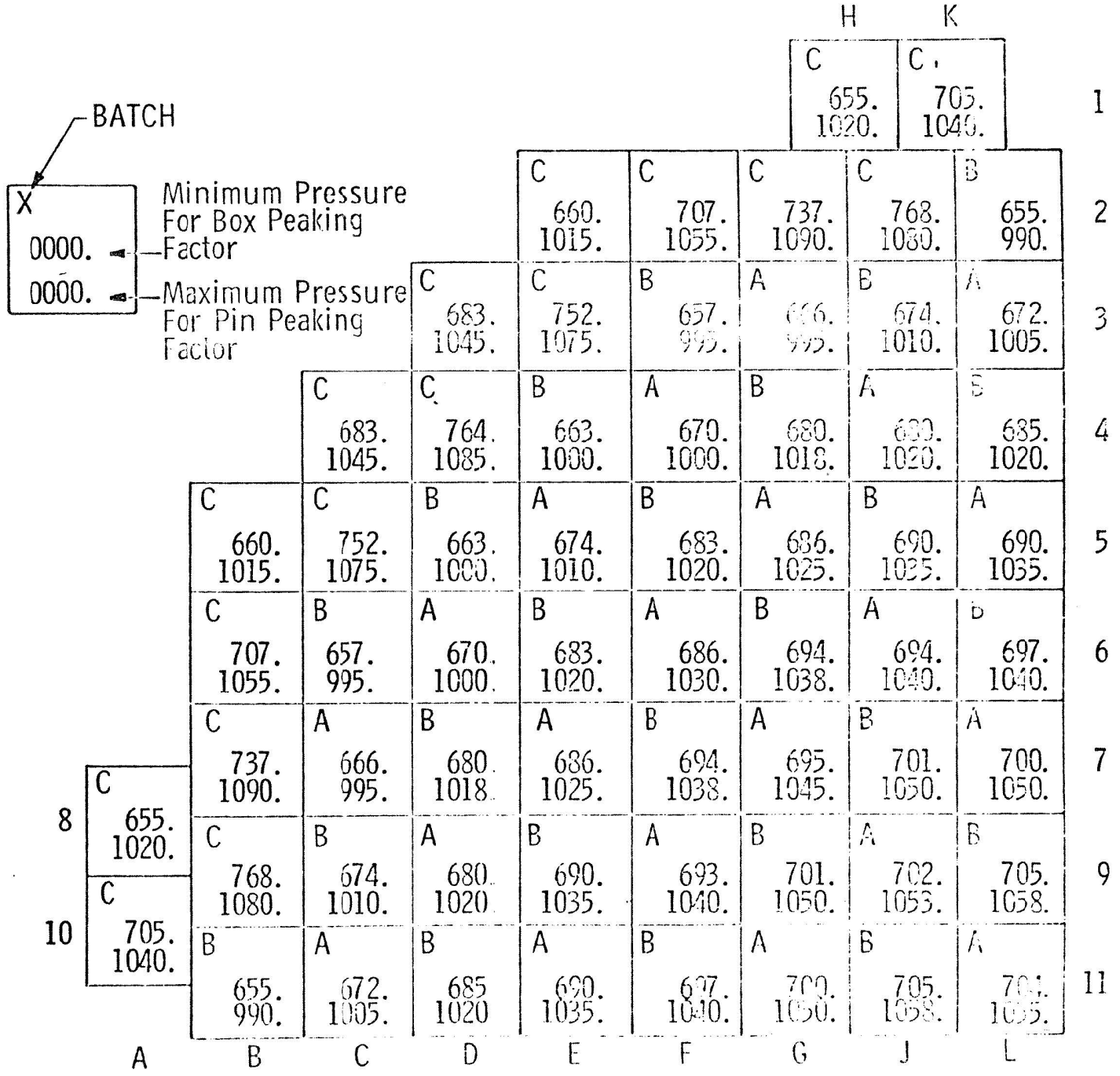

Figure 4.2-17A

FLORIDA POWER & LIGHT CO.
St. Lucie Plant
Unit 1

FUEL ROD INTERNAL PRESSURE
END OF CYCLE 1, EQUILIBRIUM XENON, 2560 Mwt

Figure 4.2-17B

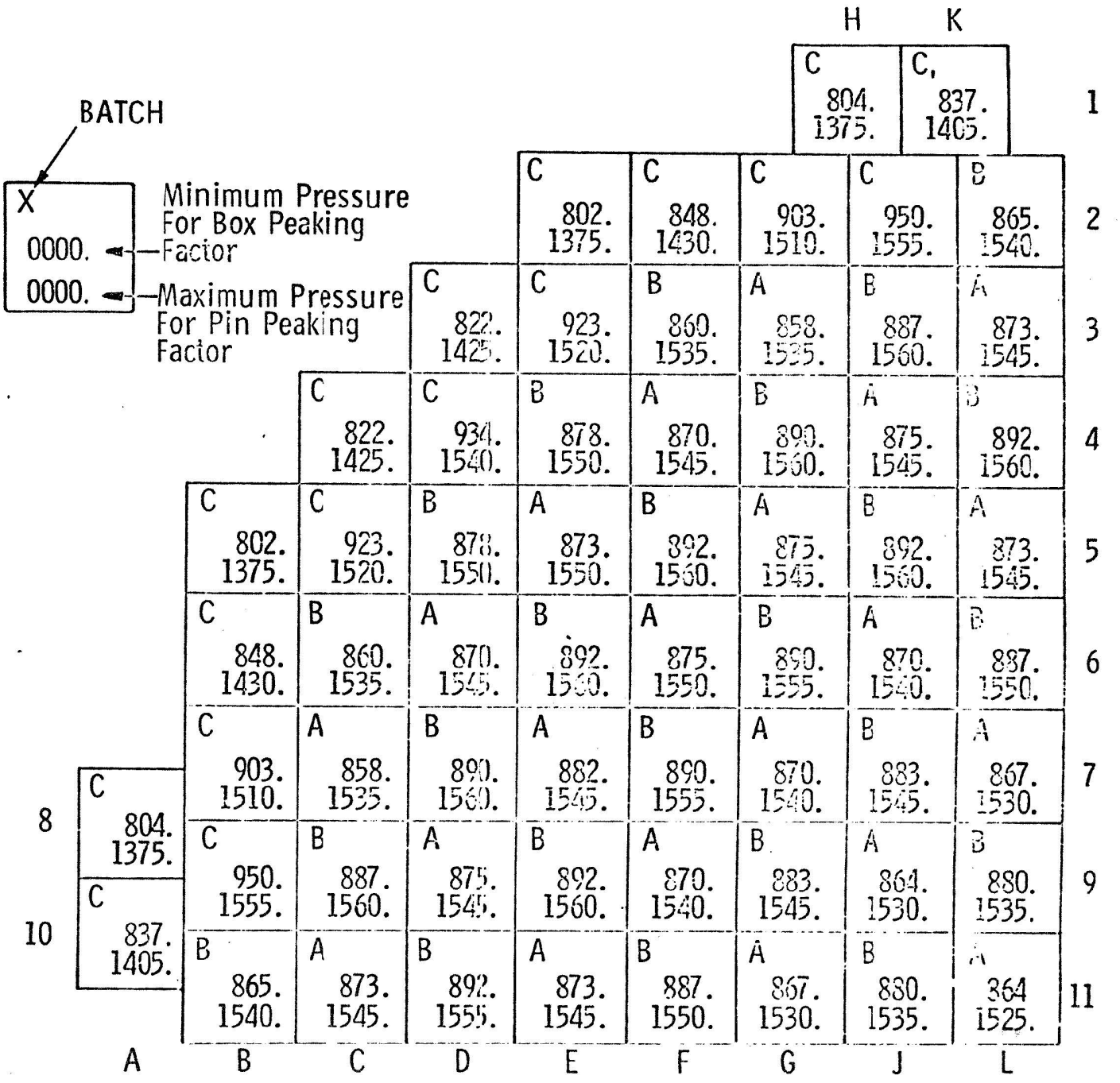

FLORIDA POWER & LIGHT CO.
St. Lucie Plant
Unit 1

FUEL ROD INTERNAL PRESSURE
BEGINNING OF CYCLE 2, NO XENON, 2560 Mwt

Figure 4.2-17C

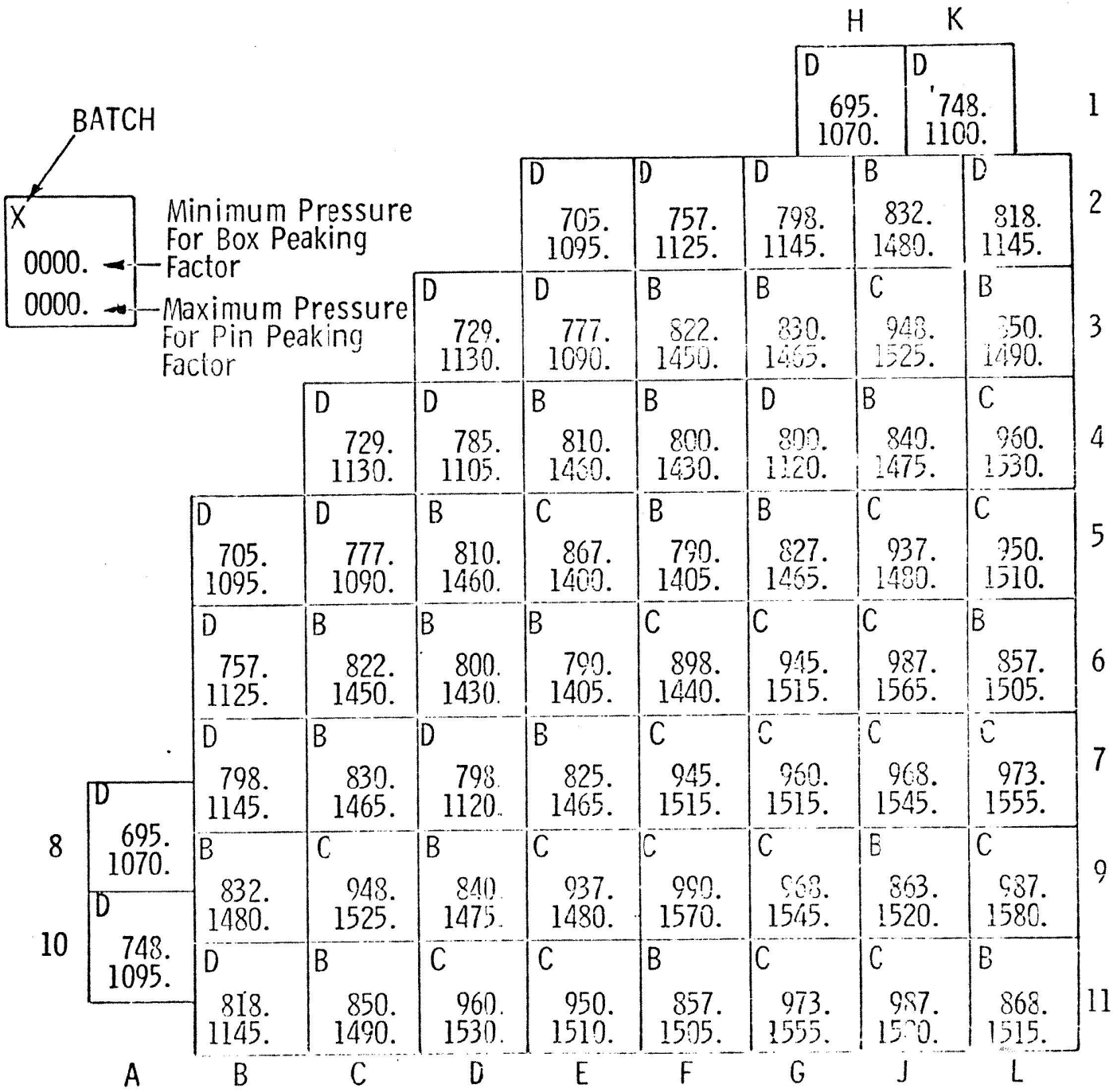

FLORIDA POWER & LIGHT CO.
St. Lucie Plant
Unit 1

FUEL ROD INTERNAL PRESSURE

END OF CYCLE 2, EQUILIBRIUM XENON, 2560 Mwt

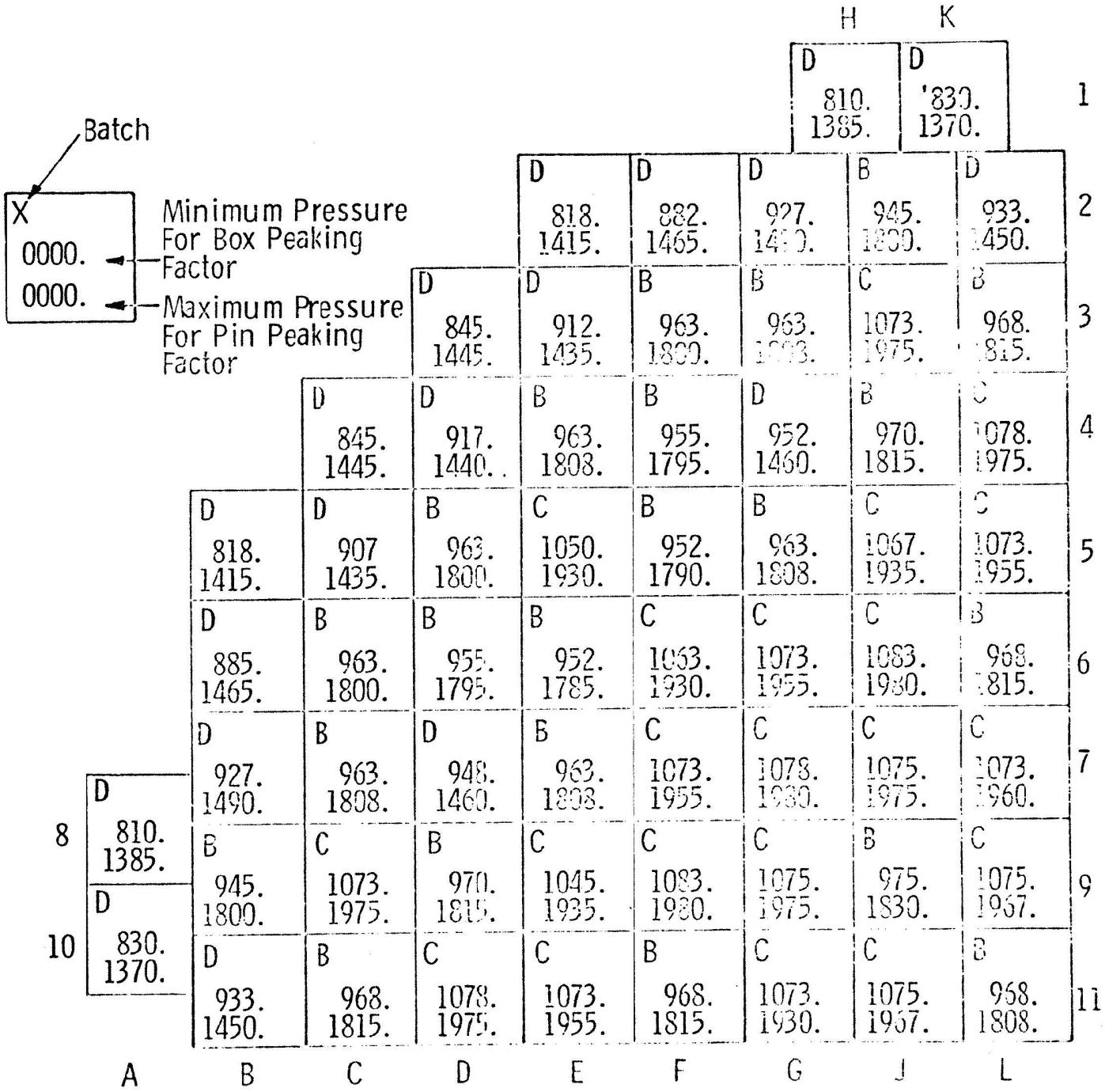

Figure 4.2-17D

FLORIDA POWER & LIGHT CO.
St. Lucie Plant
Unit 1

FUEL ROD INTERNAL PRESSURE

BEGINNING OF CYCLE 3, NO XENON, 2560 Mwt

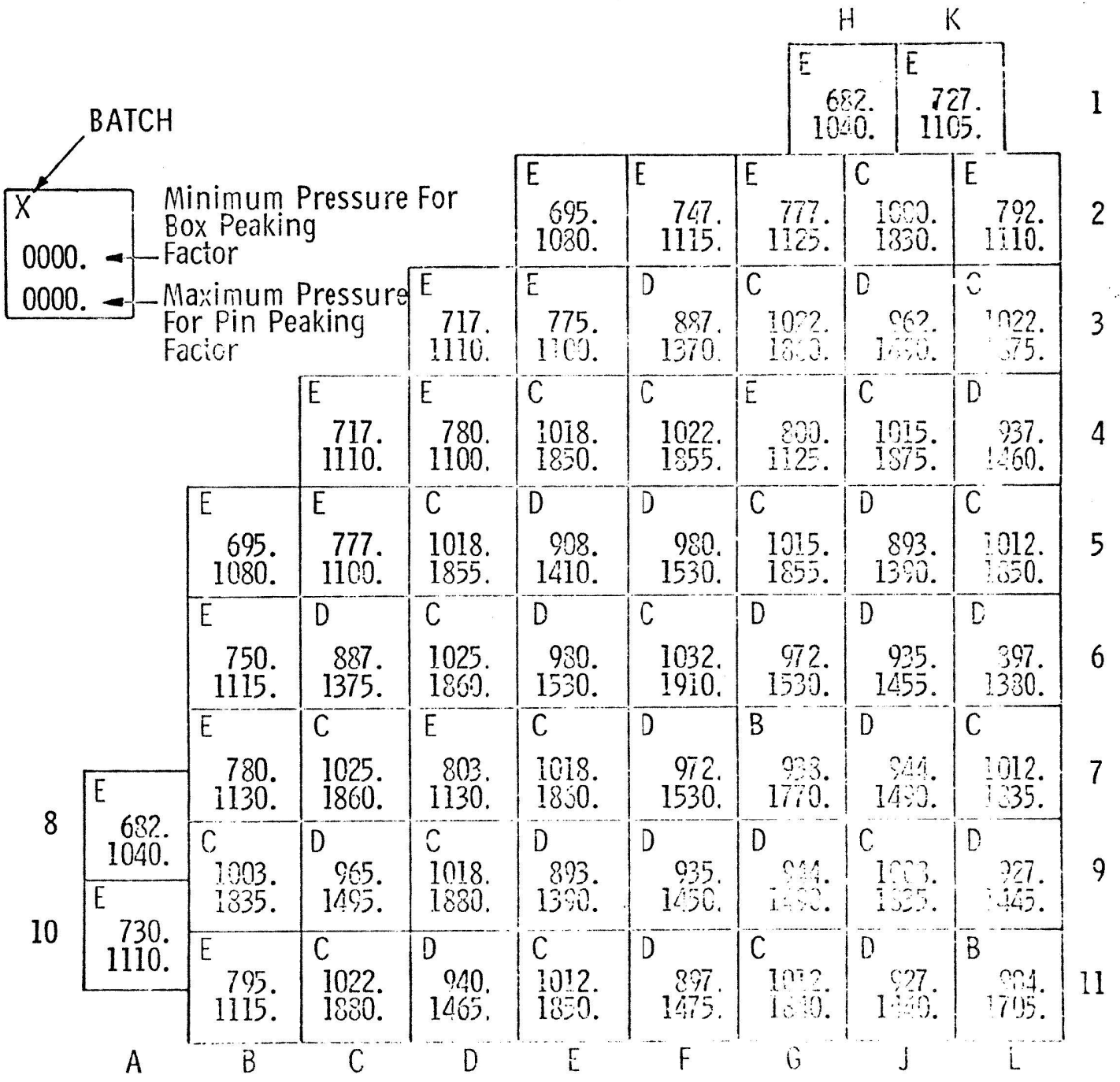

Figure 4.2-17E

FLORIDA POWER & LIGHT CO.
St. Lucie Plant
Unit 1

FUEL ROD INTERNAL PRESSURE
END OF CYCLE 3, EQUILIBRIUM XENON, 2560 Mwt

Figure 4.2-17F

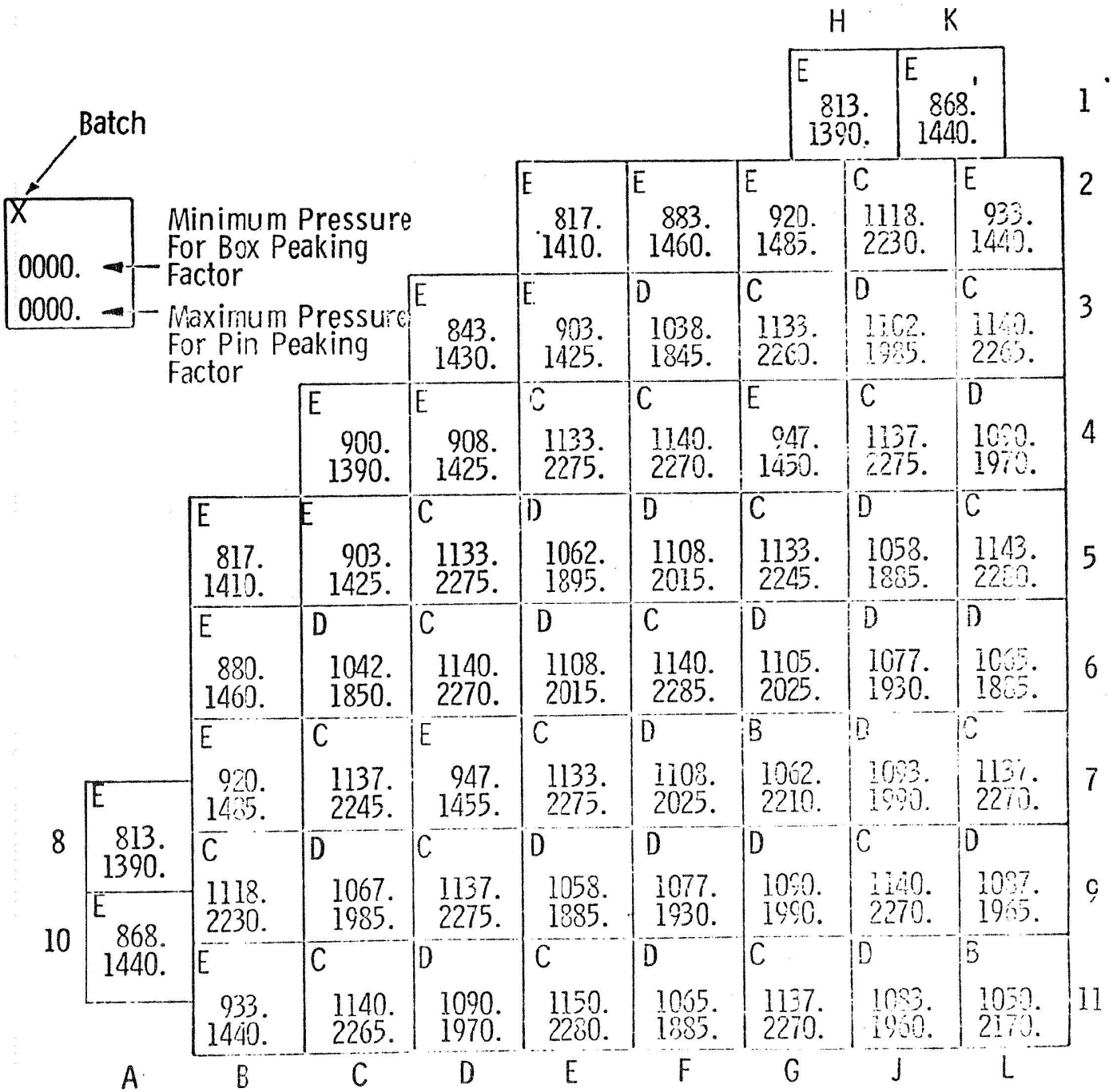

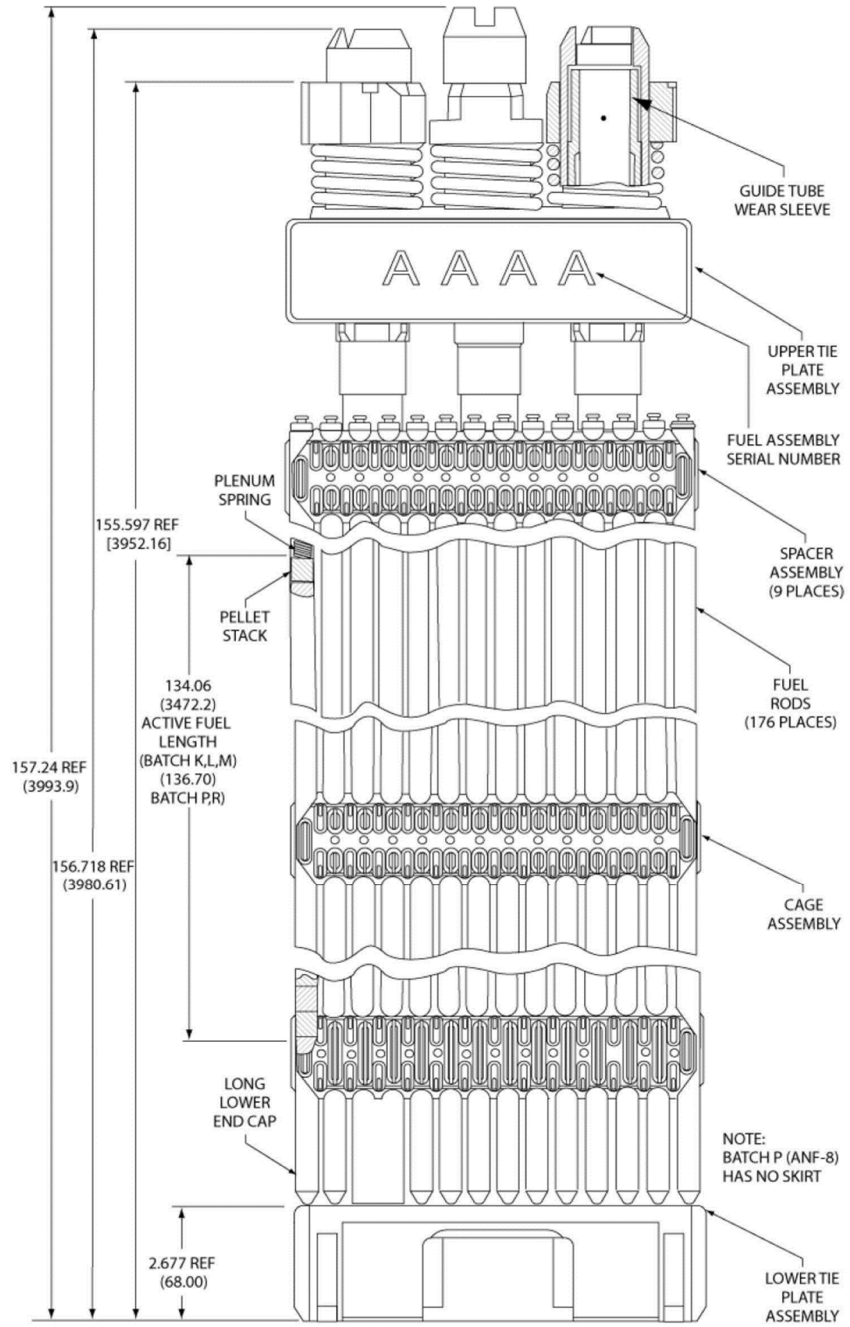

FLORIDA POWER & LIGHT COMPANY
ST. LUCIE PLANT UNIT 1

FRAMATOME (FORMERLY AREVA)
FUEL ASSEMBLY
FIGURE 4.2-18

EC292529

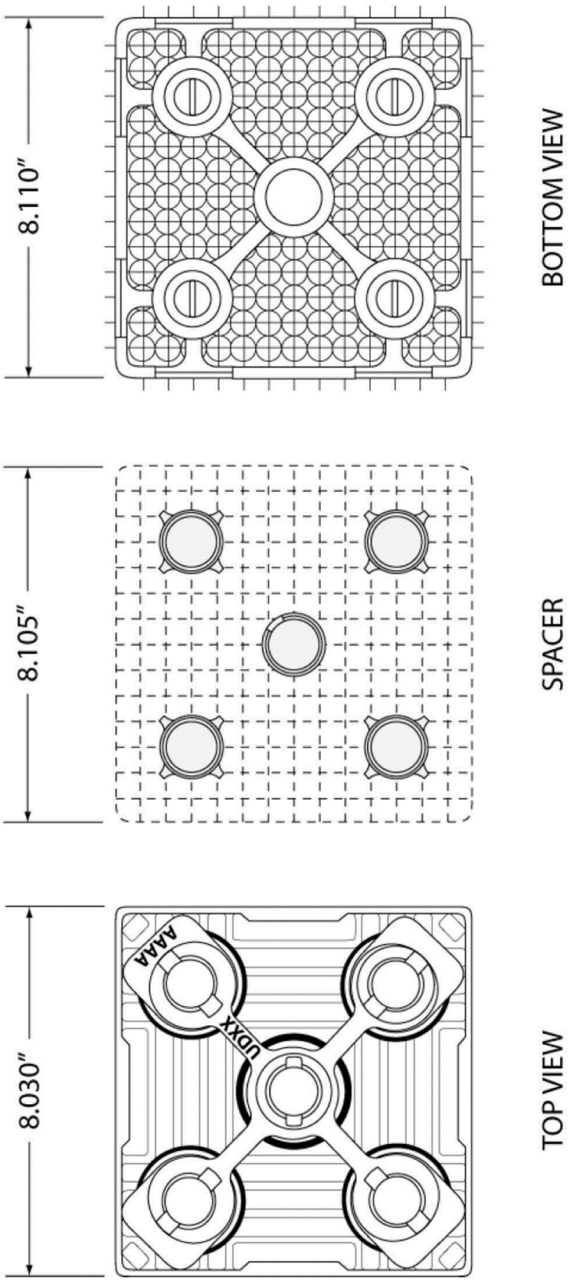

FLORIDA POWER & LIGHT COMPANY
ST. LUCIE PLANT UNIT 1

FRAMATOME (FORMERLY AREVA)
FUEL ASSEMBLY
FIGURE 4.2-19

EC292529

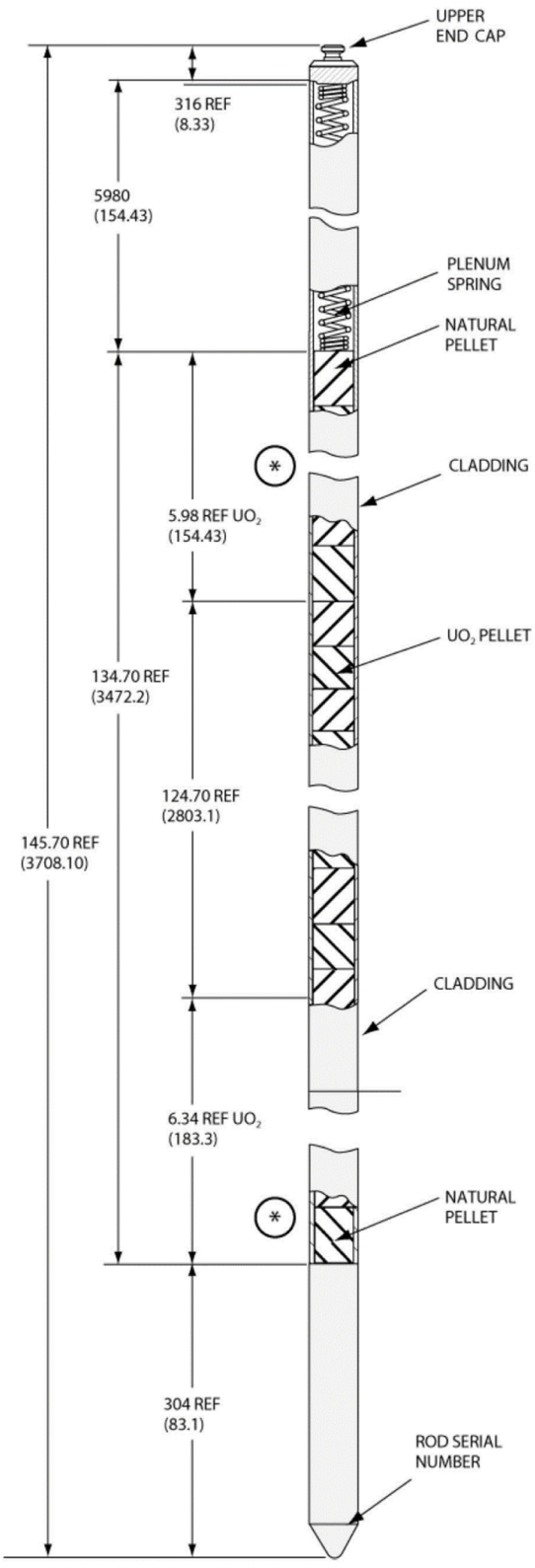

(*) For Batch X, these are 6 in. 2.6 w/o U-235.

FLORIDA POWER & LIGHT COMPANY
ST. LUCIE PLANT UNIT 1

TYPICAL BATCH S, T, U AND X
FRAMATOME (FORMERLY AREVA)
FUEL ROD
FIGURE 4.2-20

EC292529

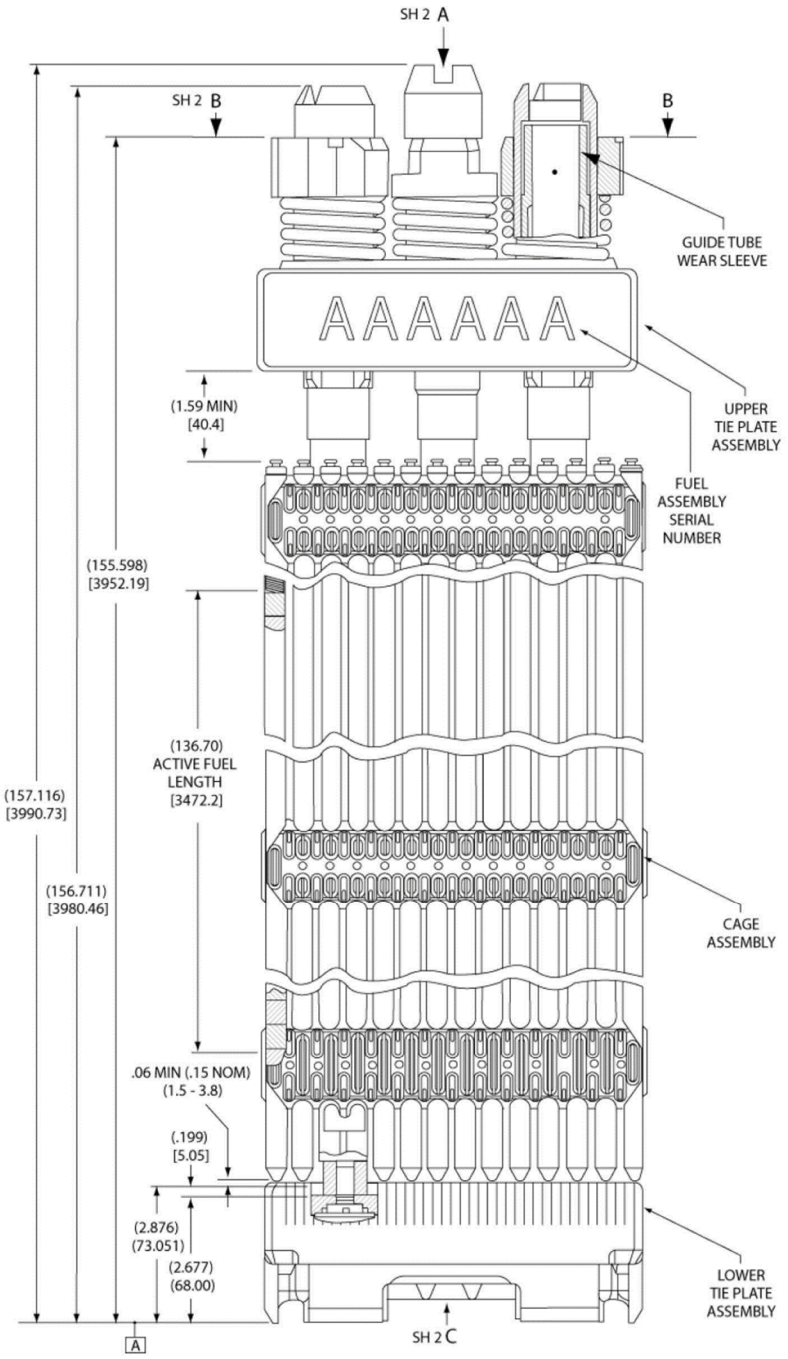

FLORIDA POWER & LIGHT COMPANY
ST. LUCIE PLANT UNIT 1

FRAMATOME (FORMERLY AREVA)
FUEL ASSEMBLY
STARTING WITH CYCLE 20
FIGURE 4.2-21

EC292529

Amendment No. 30 (05/20)

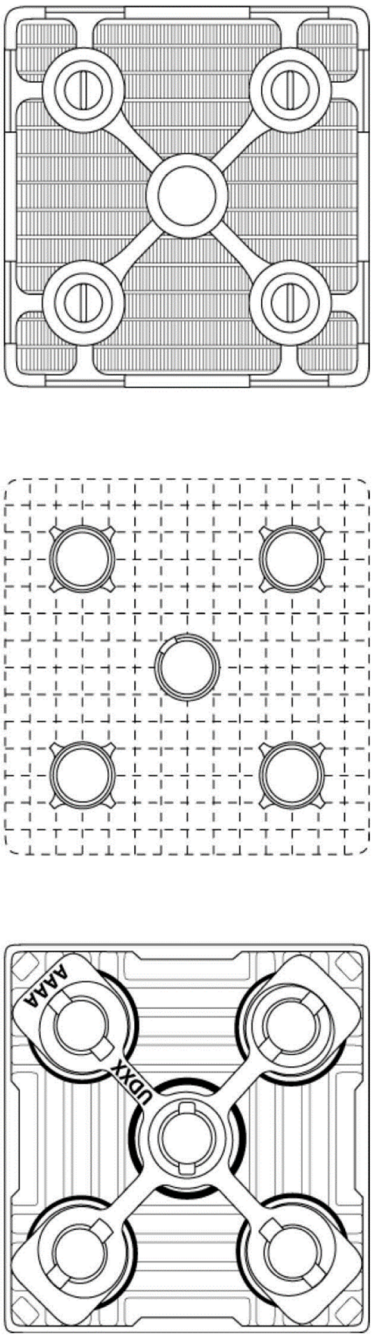

FLORIDA POWER & LIGHT COMPANY
ST. LUCIE PLANT UNIT 1

FRAMATOME (FORMERLY AREVA)
FUEL ASSEMBLY
STARTING WITH CYCLE 17
FIGURE 4.2-22

EC292529

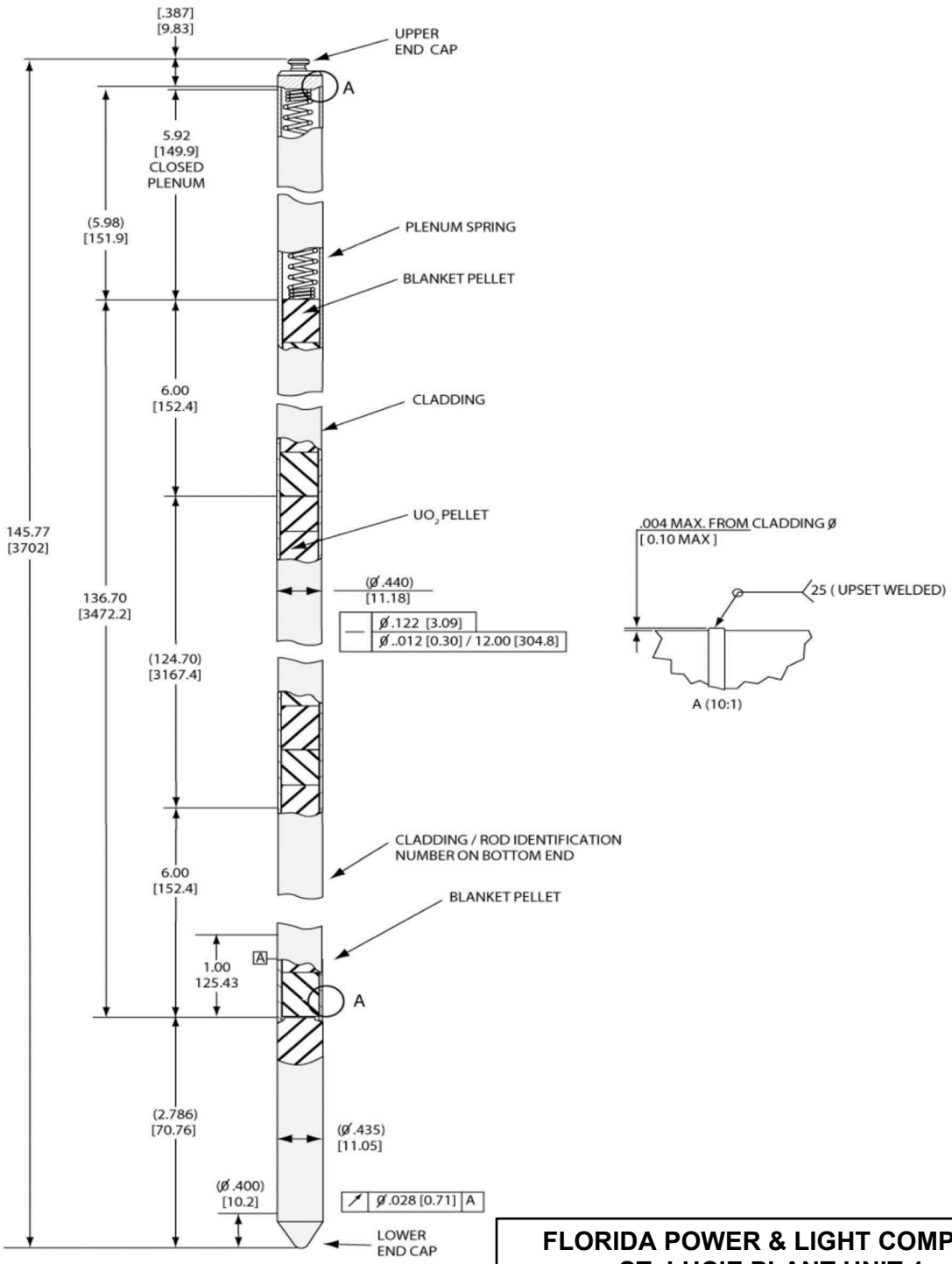

FLORIDA POWER & LIGHT COMPANY
ST. LUCIE PLANT UNIT 1

TYPICAL FRAMATOME (FORMERLY AREVA) FUEL ROD
STARTING WITH CYCLE 20
FIGURE 4.2-23

EC292529

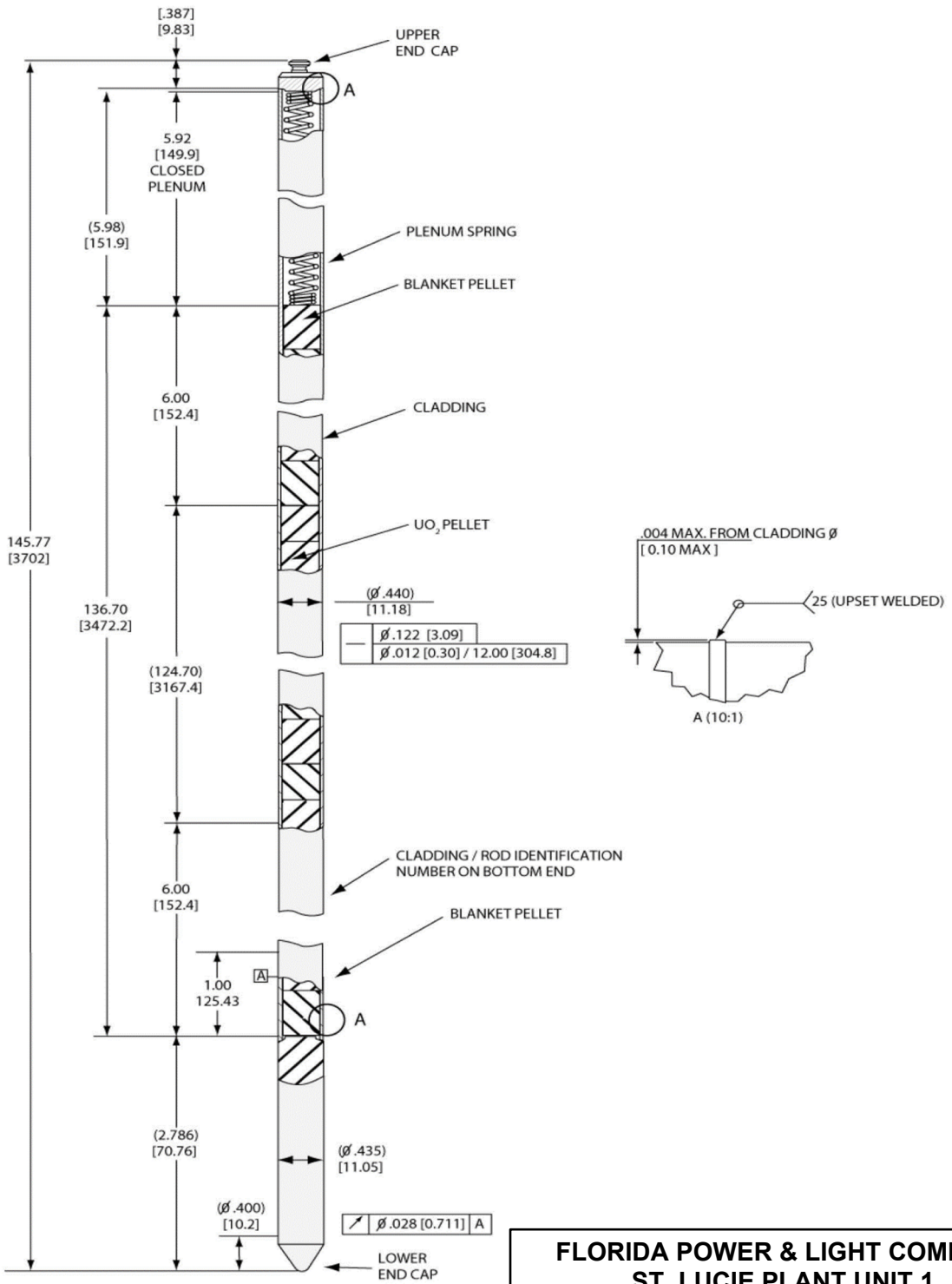

FLORIDA POWER & LIGHT COMPANY
ST. LUCIE PLANT UNIT 1

TYPICAL FRAMATOME (FORMERLY AREVA) FUEL ROD
STARTING WITH CYCLE 22
FIGURE 4.2-24

EC292529

4.3 NUCLEAR DESIGN

4.3.1 DESIGN BASES

The full power thermal rating of the core is 3020 Mwt for an extended power uprate. The core was rated at 2700 MWT. This is a stretch rating which was first put into effect during Cycle 5.

At the reactivity end of life (end of cycle), the reactor is shut down for refueling. A portion of the fuel assemblies comprising the core are discharged, fresh fuel assemblies are added and, based on the design calculations, a new core loading pattern is implemented. The core configuration following refueling operations comprises the reload core which will be operated until its respective end of reactivity life.

Nuclear design calculations are performed for each reload core to determine a proper core loading pattern which satisfies the cycle energy and safety analysis requirements. Particular attention is paid to peaking factors and core kinetics characteristics. If core characteristics fall outside of the range of values covered by the previous nuclear design or safety analysis, those core conditions or accidents so affected are reanalyzed or evaluated for compliance with the acceptance criteria.

As part of the reload evaluation, the mechanical, nuclear, and thermal hydraulic characteristics of the reload core are assessed. Special conditions such as off-normal operating conditions, LOCA limits, or special operational limitations are also addressed. Thus, each reload core is designed and provided with the same or better safety margins than the initial core analysis presented in the FSAR.

The design bases for the nuclear design of the fuel and reactivity control systems are:

a) Excess Reactivity and Fuel Burnup

The excess reactivity provided for each cycle is based on the depletion characteristics of the fuel and burnable poison and on the desired burnup for each cycle. The desired burnup is based on an economic analysis of both the fuel cost and the projected operating load cycle for the plant. The average burnup is chosen so as to ensure that the peak burnup is within limits discussed in Section 4.2.

b) Core Design Lifetime and Fuel Replacement Program

The core design lifetime and fuel replacement program are based on a four region core with approximately 18 month refueling and with approximately one third of the fuel assemblies replaced at each refueling.

c) Negative Reactivity Feedback and Reactivity Coefficients

The negative reactivity feedback provided by the design is based on the requirement of AEC General Design Criterion 11 stated in Section 3.1.11. In the power operating range, the inherent combined response of the reactivity feedback characteristics (fuel temperature coefficient, moderator temperature coefficient, and moderator pressure coefficient) to an increase in reactor thermal power will be a decrease in the reactivity.

d) Burnable Poison Requirements

The burnable poison reactivity worth provided in the design will be sufficient to ensure that moderator coefficients of reactivity have magnitudes and algebraic signs consistent with the requirements for negative reactivity feedback and acceptable consequences in the event of postulated accidents or anticipated operational occurrences, viewed in conjunction with the characteristics of the reactor protective system.

e) Stability Criteria

The design of the reactor and the instrumentation and control systems is based on meeting the requirements of AEC General Design Criterion 12, Section 3.1.12, with respect to spatial xenon oscillations and stability. Sufficient CEA worth is available to suppress xenon-induced spatial oscillations.

f) Maximum Controlled Reactivity Insertion Rates

The maximum reactivity addition rates are limited by core, CEA, reactor regulating and boron charging system design based on preventing increases in reactivity which would result in the violation of specified acceptable fuel design limits, damage to the reactor coolant pressure boundary, or disruption of the core or other internals sufficient to impair the effectiveness of emergency core cooling.

g) Power Distribution Control

Acceptable steady state and anticipated transient operation of the reactor depends on maintaining a relationship among many parameters, some of which depend on the power distribution. The power distribution is controlled such that, in conjunction with other controlled parameters, limiting conditions for operation are not violated. Limiting conditions for operation are at least as conservative as the initial conditions used in the accident analyses in Chapter 15. Limiting conditions for operation and limiting safety system settings are determined such that specified acceptable fuel design limits are not violated as a result of anticipated operational occurrences and such that specified predicted acceptable consequences are not exceeded for other postulated accidents.

h) Shutdown Margins and Stuck Rod Criteria

The amount of reactivity available from insertion of withdrawn CEAs is sufficient, under all power operating conditions, to ensure that the reactor can be brought to the greater of: (a) one percent $\Delta\rho$ subcritical from existing conditions, or (b) that amount of reactivity assumed in the safety analysis; including the effects of cooldown to hot zero power temperature conditions, even when the highest worth CEA fails to insert.

i) Chemical Shim Control

The chemical and volume control system (Section 9.3.4) is used to adjust dissolved boron concentration in the moderator. After a reactor shutdown, this system is able to compensate for the reactivity changes associated with xenon decay and reactor coolant temperature decreases to ambient temperature, and it provides adequate shutdown margin during refueling. This system also has the capability of controlling long term reactivity changes due to fuel burnup, and reactivity changes during xenon transients resulting from changes in reactor load independently of the CEAs. In particular, any xenon burnout transient may be accommodated at any time in the fuel cycle.

j) Maximum CEA Speeds

Maximum CEA speeds are consistent with the accident analyses bases discussed in Chapter 15 and with the requirements noted in Section 4.3.1-f.

4.3.2 DESCRIPTION

4.3.2.1 Nuclear Design Description

This section summarizes the nuclear characteristics of the core and discusses the design parameters that are of significance to the performance of the core in steady state and normal transient operation. The numerical values presented are based primarily on the first core. However, sufficient analyses has been completed to ensure that reload fuel can be designed to keep nuclear power peaking within design limits, to accommodate essential reactivity requirements with the control system provided, and to meet other requirements for safe operation. A summary of nuclear design parameters is presented in the following tables and figures. These data are intended to be descriptive of the design. Limiting values for these and other parameters are discussed in the appropriate sections.

Fuel enrichment and burnable poison distributions for one quadrant are shown in Figure 4.3-1. The other three quadrants of the core are symmetrically arranged. Physical features of the lattice and fuel assemblies are described in Section 4.2.

Assembly enrichments, core burnup, critical soluble boron concentrations and worths, plutonium buildup, maximum deboration rates and neutron lifetime are shown in Table 4.3-1 (historical data). Delayed neutron fractions are given in Section 15.4.5.2. K_{eff}, reactivity and reactivity defect data associated with the cold zero power, hot standby, hot full power-no xenon or samarium, and hot full power-equilibrium xenon and samarium conditions are shown in Table 4.3-2. Soluble boron insertion is discussed in Subsection 9.3.4.2.1 and is sufficient to compensate for the maximum reactivity addition due to xenon burnout and core cooldown.

4.3.2.1.1 Nuclear Core Design

The nuclear design bases for the core are as follows:

1) The design shall permit operation within the Technical Specification for St. Lucie Unit 1 Nuclear Plant.

2) The loading pattern shall be designed to achieve power distribution and control rod reactivity worths according to the following constraints:

   a) The peak LHR shall not exceed 15 kW/ft and the F_r peaking factor shall not exceed 1.65 in any single fuel rod through the cycle under nominal full power operating conditions.

   b) The scram worth of all rods minus the most reactive rod shall exceed the shutdown requirement.

The neutronic design methods used to ensure the above requirements are consistent with those described in References 1, 2, 3, 6, 7 and 8.

The fresh assemblies loaded in the core interior contain gadolinia-bearing fuel in order to control power peaking and reduce the initial boron concentration to maintain the MTC within its Technical Specification/COLR limit. The exposed fuel is also loaded in a manner to control the power peaking.

4.3.2.1.2 Physics Characteristics

Typical St. Lucie Unit 1 neutronics characteristics of the core are presented in Table 4.3-16. The safety analysis typically supports an end of cycle temperature/power coastdown beyond the nominal energy used in the design of each cycle. The typical boron letdown curve is shown in Figure 4.3-42.

4.3.2.2 Power Distribution

4.3.2.2.1 General

The power distribution is one of many items that affect the margins (difference between actual core conditions and specified acceptable fuel design limits) of the reactor. The acceptability of a particular combination of parameters, e.g., power distribution, power level and coolant conditions, depends upon the situation in which it is required to be acceptable.

Power distributions are monitored on a continuing basis as described in Section 4.3.2.5 by the monitoring of (a) CEA positions, which affect radial and axial power distributions, (b) quadrant power tilt, and (c) axial shape index by the out-of-core neutron detectors, which provides a measure of the axial power distribution.

Under normal conditions, the power distribution may be improved relative to the limiting power distribution at existing coolant conditions and power level by appropriate action. Methods of improving the power distribution include (a) decreasing CEA insertion by boration, and thereby improving the radial power distribution, and (b) correcting off-optimum conditions which cause margin degradations (e.g., CEA misalignments). These methods do not change power level or coolant state conditions. Section 7.7.1.1 addresses the reactor control systems used to maintain power distributions within the limiting conditions for operation.

4.3.2.2.1.1 Power Distribution Considerations

The power distributions are obtained from a three-dimensional ANC (Ref 8) model within moderator density and Doppler feedback effects incorporated.

The calculated hot full power (HFP) equilibrium xenon nuclear peaking factor F_r is ≤1.65. The peak linear heat rate (LHR) including uncertainties is calculated to be <15.0 kW/ft. The uncertainties include 7.419% for measurement, 3% for engineering and 0.3% for thermal power. These reported LHR values incorporate an axially dependent augmentation factor to account for the fact that the current LHR limit is not a constant with core height. Because this factor is incorporated, these LHR values can be compared (once the appropriate uncertainties are included) to a constant LHR of 15 kW/ft.

4.3.2.2.2 Expected Power Distribution

The detailed power distribution depends on the following parameters: (a) CEA insertion, (b) power level, (c) fuel exposure, (d) coolant conditions, and (e) boron concentration. During the fuel cycle, variations in the foregoing parameters are expected, but at all times the combination of power distribution and other variables is maintained within limiting conditions for operation.

Figures 4.3-2 through 4.3-18 show typical planar radial and unrodded core average axial power distributions. They illustrate conditions expected at full power at various times in the fuel cycle as specified on the figures. The normal operation of the reactor will be with limited CEA insertion so that these distributions represent the expected power distribution during most of the cycle.

Calculational uncertainties in the predicted power distributions and non-separable effects are taken into account by allowances applied to the appropriate limiting quantity. The magnitudes of these uncertainty allowances are based on comparisons of predicted and measured power distributions in operating reactors. Startup testing provided information in support of these allowances.

A typical power distribution within a fuel assembly is shown in Figure 4.3-19. This is typical of an intra-assembly power distribution that would be used to evaluate intra-assembly mixing and cross flow; it represents the minimum local peaking in any assembly at any time during the cycle. It should be noted that the local peaking during most of the cycle and for most of the assemblies is substantially larger than the local peaking shown on Figure 4.3-19, as shown in Figures 4.3-2 through 4.3-13.

In allowed operating modes the power distribution together with other parameters is required to be within limiting conditions for operation. These limiting conditions for operation are such that, when the entire system is considered, no anticipated operational occurrence will result in violation of specified acceptable fuel design limits and no other postulated accident will result in consequences more severe than the specified acceptable predicted consequences reported in Chapter 15.

The maximum allowable axial and radial peaking factors are determined from the axial shape analysis described in Section 4.3.2.6 which also describes the method of accounting for allowances and uncertainties in the shape analysis. Based on the results of the shape analysis peaking factor limits are established which insure that:

a) the peak linear heat rate at any power level is no higher than the allowable peak linear heat rate determined by the LOCA analysis in Chapter 15.

b) the allowable full power three-dimensional peaking factors (Fq's) are no higher than the Fq inferred from the design peaking factors given in Table 4.4-2.

c) the allowable axial power distributions do not result in DNB margins less conservative than those required to assure valid protection against the most DNB limited anticipated operational occurrence, i.e. loss of coolant flow described in Section 15.2.5.

Assurance that these limits are not violated is provided by power level dependent axial shape index monitoring limits in conjunction with limits on:

a) the power dependent rod insertions (PDIL's)

b) CEA misalignment, sequencing and overlap

c) quadrant power tilt

d) coolant conditions (i.e., reactor coolant system flow, pressure and inlet temperature).

The reactor protective system, described in Section 7.2, is designed to prevent exceeding specified acceptable fuel design limits as a result of anticipated operational occurrences and to limit the consequences of certain highly improbable postulated accidents. It is clear that to guarantee the effectiveness of the protective system, there must be provided a means to assure that under all allowed operating modes the

state of the reactor is confined to conditions not more severe than the initial conditions assumed in the design and analysis of the protective system, i.e., the limiting conditions for operation. The following discusses the various power distributions that are considered in setting the limiting conditions for operation.

Since the reactor will not be operated under conditions which would imply instability with respect to azimuthal xenon oscillations, as discussed in Section 4.3.2.8, no special protective system equipment is needed to accommodate azimuthal mode oscillations. Nevertheless, a maximum quadrant tilt is prescribed in the Technical Specifications along with prescribed operating restrictions. Thus, in order to satisfy the foregoing requirements, the maximum allowed azimuthal (quadrant) tilt is considered in design and analysis of the reactor protective system. Also, as mentioned in Section 4.3.2.8, means are provided for monitoring azimuthal tilt.

The axial shape monitoring system provides assurance that fuel design conditions will not be exceeded due to abnormal axial power distributions. The axial power distribution input to the axial shape monitoring system takes into account allowed operating conditions and abnormal conditions. These axial power distributions are used in combination with all radial power distributions associated with CEA configurations allowed at a given power level by the CEA insertion limits to determine the margins between actual core conditions and specified acceptable fuel design limits. These margins take into account the variation of allowable peaking factors with axial position and burnup and include allowances for uncertainties in calculated parameters. It is not meaningful to specify any of these limits separately. It is the combination of these variables that determines safety margins.

The presence of axial gaps in the fuel pellet column which may form as a result of densification results in an increase in the local peaking factors. This effect is accounted for by axially dependent local power peaking augmentation factors, calculated in accordance with the requirements of the AEC staff, "Technical Report on Densification of Light Water Reactor Fuels," dated November 14, 1972. The calculation of these augmentation factors is discussed in Section 4.3.3.4.

The types of axial power distributions that are considered in evaluating the monitoring system include allowable conditions and abnomal conditions. For example, as discussed in Section 4.3.2.8, the core may be unstable to axial xenon oscillations near end of life, in the absence of control action. These oscillations are slow (the period of oscillation being 25-30 hours). Figure 4.3-20 illustrates a free running, undamped axial xenon oscillation following a return to full power after a 2 hour period at 50 percent power near end of life. This divergent oscillation occurred in the absence of control action.

Of those load following maneuvers which are possible, a 90-30-90 daily load cycle is expected to be one of the most stringent. For this design basis maneuver, at 90% power, the peaking factor limit including all uncertainties and allowances for peaking factor uncertainty, augmentation effects, tilts, power measurement uncertainty, and shape index uncertainties is 3.10. This implies an upper limit on the allowable unaugmented axial peaking factor of 1.61.

Calculations of expected time dependent axial peaks and corresponding power level history during a 90-30-90 daily cycling maneuver are presented in Figure 4.3-20A. The information presented in Figure 4.3-20A was for a 3 hour ramp down to 30% of full power, 6 hours at 30% power, a 3 hour ramp increase to 90% power, followed by 12 hours at this higher power level. These calculations were run at the end of cycle when the axial power distribution is most sensitive to perturbations and the axial power distribution can be most severely distorted. Also, the power defect and xenon redistribution effects were compensated on rods alone. Control actions would be required to maintain the axial shape index within limits so that the results can be considered as conservative during the first 12 hour period at high power. In practice, the operator would optimize initial conditions if he were planning to perform such a cyclic maneuver on a routine basis.

With reference to Figure 4.3-20A one observes that the axial peak is never higher than 1.56. This is below the allowable limit even though the initial portion of the maneuver was not optimized. Focusing attention on the equilibrium cyclic portion of the maneuver, one observes that the axial peak at high power is never higher than about 1.40, well below allowable limits.

The results described above demonstrate that the peaking factors expected during one of the most stringent maneuvers are within acceptable limits. Further assurance is provided by the fact that the combination of power dependent insertion limits, rod sequencing and overlap and axial shape index monitoring limits will be established such that peaking factor limits are not exceeded at any power level.

4.3.2.3 Reactivity Coefficients

Reactivity coefficients relate changes in core reactivity to variations in core or moderator conditions.

Section 4.3.3 presents a comparison of calculated and measured moderator temperature coefficients and power coefficients for operating reactors. The good agreement provides confidence that the data presented in this section adequately characterizes this reactor. Values of the various reactivity coefficients used in accident analyses are given in Chapter 15. In general, these values are chosen in a conservative manner for each analysis and the values may fall outside the ranges of the data presented in this section whenever appropriate to allow for uncertainties in calculated values.

a) Fuel Temperature Coefficient

The fuel temperature coefficient is the change in reactivity per unit change in fuel temperature. A change in fuel temperature affects not only the thermal expansion of the fuel pellet but, in addition, the reaction rates in both the thermal and epithermal neutron energy regimes. Epithermally, the principal contributor to the change in reaction rate with fuel terrperature is the Doppler effect arising from the increase in absorption widths of the resonances with an increase in fuel temperature. The ensuing increase in absorption rate with fuel temperature causes a negative fuel temperature coefficient. In the thermal energy regime, a change in reaction rate with fuel temperature arises from the effect of temperature dependent scattering properties of the fuel matrix on the thermal neutron spectrum. The contribution of this effect to the fuel temperature coefficient can make the coefficient less negative, depending on the fuel composition and the energy dependence of the thermal neutron spectrum. In typical PWR fuels containing strong resonance absorbers such as U-238 and Pu-240, the magnitude of the component of the fuel temperature coefficient arising from the Doppler effect is more than a factor of ten larger than the magnitude of the thermal energy component. Since it is very difficult to analytically predict average fuel temperatures because of uncertainties in the behavior of fuel pellets, e.g., pellet cracking and fuel-clad interactions, an empirical model is used to determine effective fuel temperatures, as described in (f) below.

Figure 4.3-21 shows the dependence of the calculated fuel temperature coefficient on effective fuel temperature. Figure 4.3-21A shows the variation with burnup. The coefficient is more negative at the end of cycle because of the presence of Pu-240 which has a substantial resonance capture cross section. Where a heatup of the fuel occurs, the coefficient is conservatively decreased by an allowance, and where a cooldown of the fuel occurs, the coefficient is conservatively increased

by an allowance. These allowances are discussed in Chapter 15 and are used to take into account the variation of the fuel temperature coefficient with burnup, or uncertainty in the calculated fuel temperature coefficient.

b) Moderator Temperature Coefficient

The moderator temperature coefficient relates changes in reactivity to uniform changes in moderator temperature, including the effects of moderator density changes with changes in moderator temperature. One objective in the core design is to limit the moderator temperature coefficient to values that are acceptable from the standpoint of all accident situations treated in Chapter 15. In the first core, burnable poison rods (shims) are provided in the form of cylindrical pellets of alumina with uniformly dispersed boron carbide particles in order to limit the dissolved boron concentration, thereby making the moderator temperature coefficient more negative. The number of shims and their distribution in the core is shown for one quadrant in Figure 4.3-1. The distribution is identical for the other three quadrants. The reactivity control provided by the shims is given in Table 4.3-1. This control makes possible a reduction in the dissolved boron concentration to the values given in Table 4.3-1.

The calculated moderator temperature coefficient for various core conditions is given in Table 4.3-3. As shown in the table, the least negative value at full power conditions occurs in the beginning of life with a clean, unrodded core when the dissolved boron content is at its maximum. When in the core, the CEAs provide a negative contribution to the moderator temperature coefficient. The moderator temperature coefficient becomes more negative with burnup, due mainly to the reduction in the dissolved boron content with burnup. The contribution to this negative effect of the neutron spectral effect of plutonium and fission products is small. The buildup to equilibrium xenon supplies a positive contribution to the moderator temperature coefficient of about $0.05 \times 10^{-4} \Delta\rho/F$. However, when the dissolved boron concentration is reduced by the reactivity equivalent of xenon, the coefficient becomes more negative than the beginning of life value as shown in Table 4.3-3. Moderator temperature coefficient as a function of moderator temperature over the entire range from cold conditions to hot operating conditions is shown in Figure 4.3-22.

The current Technical Specifications/COLR require that the moderator temperature coefficient be less than +7 pcm/°F at or below 70% of rated thermal power, less than +2 pcm/°F above 70% power and greater than -32 pcm/°F at 100% of rated thermal power. Table 4.3-16 lists the MTC for the current cycle.

c) Moderator Density Coefficient

The moderator density coefficient is the change in reactivity per unit change in the average core moderator density (at constant moderator temperature). The density coefficient is opposite in sign to the moderator temperature coefficient, since an increase in moderator temperature means a decrease in moderator density. The density coefficient is always positive in the operating range but the magnitude is reduced in the presence of dissolved boron because an increase in water density (a positive reactivity effect) is accompanied by an increase in the soluble boron content of the core (a negative reactivity effect). The magnitude of the density coefficient is shown in Table 4.3-3 and a curve of density coefficient near operating conditions is shown in Figure 4.3-23.

d) Moderator Pressure Coefficient

The moderator pressure coefficient is the change in reactivity per unit change in reactor coolant system pressure. Since an increase in pressure increases the water density the pressure coefficient is opposite in sign to the temperature coefficient. The reactivity effect of increasing the pressure is reduced in the presence of dissolved boron because an increase in water density adds boron to the core. The calculated pressure coefficient for the beginning and end of the first cycle at full power are shown in Table 4.3-3.

e) Moderator Void Coefficient

During full power operation, some local subcooled boiling occurs which results in a predicted average steam (void) volume fraction in the moderator of substantially less than 1 percent. Charges in reactivity are associated with the appearance of these voids in the moderator and are reflected in the void coefficient of reactivity. The presence of boron has a positive effect on the coefficient since an increase in voids results in a reduction in the boron content of the core. The calculated values of moderator void coefficient at the begining and end of the first cycle are shown in Table 4.3-3. Figure 4.3-23A illustrates the estimated moderator void coefficient over the range of 0 to 100 percent void and is typical of beginning of life conditions without xenon.

f) Power Coefficient

The power coefficient is the change in reactivity per unit change in core power level. All of the previously mentioned coefficients contribute to the power coefficient, but only the moderator temperature coefficient and the fuel temperature coefficient contributions are significant. The contributions of the pressure and void coefficients are negligible due to their small magnitude and the small changes in pressure and void fraction per unit change in power level.

In order to determine the change in reactivity with power, it is necessary to know the changes in the average fuel and moderator temperatures with power. The average moderator (coolant) temperature $\underline{T}m$ is controlled to be a linear function of power. The analytical determination of average fuel temperature is extremely complex. Thus, the current model employs an empirical function based on power coefficients that have been determined experimentally for operating cores. The following functional relationship is used throughout the burnup cycle.

$$\underline{T}f = 2793 \left(1 - 0.7995\, e^{-0.1062\underline{P}}\right)$$

Where $\underline{P}$ is power level given in terms of average core thermal power per unit of fuel rod length, kw/ft, and $\underline{T}f$ is the average or effective fuel temperature (°F). Differentiating this with respect to power:

$$\frac{d\,\underline{T}_f}{d\,\underline{P}} = 237.2\, e^{-0.1062\,\underline{P}}$$

Using this relationship together with the fuel and moderator temperature coefficients of reactivity, the power coefficient can be obtained from the following equation:

$$\frac{d\rho}{d\underline{\underline{P}}} = \left[\frac{d\rho}{d\underline{\underline{T}}_f}\right] \left[\frac{d\underline{\underline{T}}_f}{d\underline{P}}\right] + \left[\frac{dp}{d\underline{\underline{T}}_m}\right] \left[\frac{d\underline{\underline{T}}_m}{d\underline{P}}\right]$$

A plot of the fuel temperature contribution to the power coefficient as a function of power (kw/ft) is shown in Figure 4.3-24. The full power value of the overall power coefficient for the unrodded core is shown in Table 4.3-3. The power coefficient becomes more negative with burnup due to the increasingly more negative moderator temperature coefficient. The insertion of CEAs into the core at constant power makes the power coefficient more negative due to a reduction in the soluble boron concentration as well as the spectral effects of the CEAs.

4.3.2.4 CEA Patterns and Reactivity Worths

CEAs designated as regulating rods and CEAs designated as shutdown rods are divided into groups, where all members of a group are withdrawn or inserted simultaneously and groups are moved in a specified sequence. Figure 4.3-25 shows the CEA group identification as selected for the first cycle. The order of insertion of the regulating banks, and the degree of overlap of successive banks of regulating rods are illustrated in Figure 4.3-26. The basis for the Power Dependent Insertion Limits (PDILs) shown on Figure 4.3-26 are that at any power level and any time in life:

a) there is sufficient reactivity worth in withdrawn CEAs to meet the shutdown margin and accident analysis allowance requirements shown in Table 4.3-5 plus the stuck rod worth shown in Table 4.3-6.

b) the amount of CEA insertion be such that an ejected rod accident would be no worse than the results specified in the safety analysis of the accident (Section 15.4.5.)

c) the power peaking factors are consistent with those assumed in setting the trip and monitoring limits.

Shutdown banks are normally inserted after the regulating banks and are withdrawn before the regulating banks. The reactivity worths of individual CEA groups at beginning of life and end of first cycle are shown in Table 4.3-4. CEA group worth depends on the CEA location in the core and the insertion of other CEA groups. Adherence to the relationship between power level and CEA insertion limit shown in Figure 4.3-26 ensures that shutdown margin requirements and maximum individual inserted CEA worth (ejected CEA) requirements are met.

Planar radial peaking factors for the core with successive regulating groups of CEAs inserted are shown in Table 4.3-2A. Data is presented at BOL and EOC and reflects the presence or absence of a PLR bank.

The reactor will be operated with the CEAs essentially withdrawn for steady state operation at full power, and with partial insertion of regulating banks (See Section 4.3.2.5-d, e) in order to compensate for minor variations in moderator temperature and boron concentration and to compensate for xenon reactivity effects that accompany load changes. The reactor can be brought to at least 10 percent subcritical in the cold or hot standby conditions, using the soluble boron control system with any insertion of the CEAs, including fully withdrawn.

The maximum worth of any individual CEA and the associated change in power distribution which would result in the event that a CEA was ejected from the core is presented in Section 15.4.5.

Predicted values of ejected CEA worths are always lower than the values assumed in the Chapter 15 safety analyses by at least the 10% allowance for calculation uncertainties noted in Chapter 15. This requirement will be enforced by the final power dependent insertion limit (PDIL) relationship. One design basis of the PDIL relationship is that the consequences of the CEA ejection are not more severe than the results shown in Chapter 15 for any power level and any time in life.

The amount of reactivity and associated change in power distribution in the event of a dropped CEA is discussed in Section 15.2.3 and the CEA withdrawal accident is discussed in Section 15.2.1.

Typical reactivity addition rates that could result from sequential CEA bank withdrawal are shown in Figures 4.3-26C, 26D, 26F, and 26H. These figures illustrate the effects of burnup and bank insertion (power level) on reactivity addition rates. The CEA bank withdrawal incident analyses described in Chapter 15 were conducted parametrically in reactivity insertion rate. Curves of the type illustrated in the above listed figures formed the bases for the range of reactivity insertion rates considered, with due regard for anticipated power dependent insertion limits and time-averaging of reactivity insertion rates. Experimental verification of the calculated CEA worths associated with the accident analyses will be accomplished during startup testing of the reactor. Scram reactivity as a function of time after scram signal is discussed in Section 15.1.3. CEA worths predicted for St. Lucie Unit 1 are verified during startup testing. With the implementation of the Startup Test Activity Reduction (STAR) program, measurements of a CEA worths may be skipped on a cycle specific basis with CEA worths verification being performed with an alternate method.

The allowable CEA misalignment from any bank is specified in the Technical Specifications. The magnitude of the allowable misalignment is based on three dimensional calculations of the power distribution in a model of the core in which CEA misalignment has been explicitly represented.

Three dimensional calculations have been run in which a single rod in a given rod group has been misaligned more than 8 inches above and below the tip positions of the remaining rods in the group. Misalignment of both the center rod and side rods has been investigated. In all cases, the change in the magnitude of the 3-D peak relative to the symmetric situation is no more than a fraction of a percent. Since analysis has shown the degradation in 3-D peak to be only a fraction of a percent, we feel that there is enough conservation inherent in the shape analyses to accommodate misalignments of this magnitude.

Cases have been run where a single rod is misaligned above and below the remaining rods in the group. In general, the affects of this misalignment can be thought of as a small tilt. In the case of the center rod, there is a slight shift in power toward the center of the core when the rod is misaligned upward and a slight shift toward the periphery when the rod is misaligned downward. When a side rod is misaligned upward the power shifts slightly toward the vicinity of the core where the rod is removed, but not into the assembly where the misaligned rod is located. When the side rod is misaligned downward, the power is suppressed slightly in the vicinity of the misaligned rod and the power in the remainder of the core redistributes to compensate. All of the calculations show that the 3-D peak is below the tips of the rods in an unrodded plane both before and after the misalignment.

Figure 4.3-26A presents normalized shutdown reactivity worth versus time after initial CEA motion to illustrate on a parametric basis the effect of CEA position and the effect of initial axial power distribution on scram reactivities which demonstrates:

a) Scramming the reactor which has CEAs positioned in the core Provides a faster shutdown (curves A & B).

b) Axial power distributions which are peaked towards the core bottom provide a slower shutdown than those peaked higher in the core (curves B & C).

The most significant factors affecting the initial rate of shutdown reactivity insertion are the initial axial power distribution and the rodded condition of the core. The analyses of scram reactivities assume a minimum available worth, the scram analysis shows that the unrodded core with a bottom peaked axial power distribution provides the most conservative negative reactivity insertion function for all times in life and power levels.

Power level is considered a factor only as it relates to the axial power distributions permitted within the monitoring band since the reactivity analysis conservatively assumes no power feedback effects during the scram. The curves presented in Figure 4.3-26A are expected to be outside this monitoring band.

Figures 4.3-26B through 4.3-26H provide integral and differential rod worth data. The initial conditions assumed in generating these data correspond to axial power distributions expected for equilibrium full power core conditions. Integral and differential rod worths are shown at BOL and EOL for (1) an unrodded core and (2) a core which is rodded to 0.6% bite. Since the rod worths do not change significantly from BOL to EOL, the integral and differential rod worth at MOL are bounded by the BOL and EOL curves presented.

Reactivity control in the reactor is accomplished by adjusting both the position of the regulating CEA banks and the concentration of boric acid dissolved in the reactor coolant. The CEAs permit rapid changes in reactivity, as required for reactor trip and to compensate for changes in moderator and fuel temperature and void formation associated with changes in power level.

During power operation, the shutdown CEA groups are fully withdrawn while the position of the regulating groups is adjusted to meet reactivity and power distribution requirements.

Adjustment of the boric acid concentration is used to control relatively slow reactivity changes associated with plant heatup and cooldown, fuel burnup, and certain xenon variations. Also, additional boric acid is used to provide a large shutdown margin for the initial loading and for refueling. The use of boric acid dissolved in the reactor coolant makes it possible to maintain most of the regulating control rod groups in a withdrawn position during full power operation, thus minimizing the distortions in power distribution.

The excore detectors are used to monitor incore axial power distributions by use of the interrelationship between the three different axial shape indices defined in Table 4.3-4a. The external shape index (Ie) is measured by four axially segmented ion chambers located around the periphery and external to the core. These safety channels are sensitive primarily to the flux distribution produced by peripheral fuel bundles in the vicinity of the detectors. If the excore detectors were located “against” the core, they would sense the source distribution of that segment of the core immediately opposite the detector segment. That is, the external shape index Ie would equal the peripheral axial shape index Ip. However, since these detectors are located on the inside face of the biological shield some distance from the core, the axial distribution they “see” is flattened or annealed due to the fact that each axial segment of the detector can sense the whole axial length of the core. In the model used to determine the relationship between axial shape index and the calculated values of peaking factors, shape annealing functions are input and corresponding values of Ip and Ie determined for each different axial power distribution. From the relationship between Ip and Ie, the gain adjustment that must be made to the signal to the reactor protective system (RPS) so that it senses Ip, is determined. Since this signal is later verified, and since the annealing effect is accounted for in setting the monitoring band, the relationship between peaking factors and shape index is evaluated in terms of Ip.

As mentioned above, the peripheral axial shape index (Ip) is determined from those fuel assemblies which contribute to the ex-core detector response. When the core is unrodded, and the axial power distribution is similar in all fuel assemblies, the peripheral axial shape index (Ip) equals the internal axial shape index (Ii). The insertion of CEAs into the core distorts the power distribution at the periphery of the core relative to the unrodded radial power distribution in that region. To account for this effect, the model includes as input, an array of rod shadowing (distortion) factors calculated for each possible combination of CEA configurations. The model has a routine which selects the CEA shadowing factors appropriate to the configuration of interest and determines the Ip corresponding to given Ii.

To determine the relationship between calculated peaking factors and peripheral axial shape index (Ip), many combinations of CEA group insertions, and xenon distributions are considered. The power distributions investigated include those for both steady state and transient conditions. For each configuration, the maximum three dimensional peaking factor in the limiting fuel pin in the core is calculated according to the relationship.

$$F_q^N = F_r^{HP} \cdot \hat{F}_z \cdot F_A \cdot F_e$$

where $F_r^{HP} \cdot \hat{F}_z \cdot F_A =$ the maximum product of the hot pin planar radial peaking factor, the core average normalized axial peaking factor, and a peaking augmentation factor to account for the effects of postulated axial gaps formed in densified fuel.

$F_e =$ an engineering factor to account for statistical variations of as built fuel parameters within specified manufacturing tolerances.

For each CEA Group insertion investigated, the ordered pairs (F_q^N , Ip) are plotted and an upper bound curve such as that illustrated in Figure 4.3-27A is generated. The upper bound curve so defined establishes the relationship between the three dimensional peaking factors (F_q^N) and peripheral axial shape index (Ip).

The setpoints for protective action (trip) are determined such that if the plant is operated within limiting conditions for operation with the actual safety system settings no less conservative than the limiting safety system settings then

1) no anticipated operational occurrence will result in violation of specified acceptable fuel design limits and
2) no other accident will result in consequences more severe than those reported in the accident analyses

To generate a safety limit curve such as that shown in Figure 4.3-27, curves of power-to-fuel design limits on linear heat rate and DNB are determined. The power-to-fuel design limit on linear heat rate (P_{fdl}) is that the peak linear heat rate in the limiting fuel pin in the core shall not be greater than the value at which centerline fuel melt would be predicted to occur. The power-to-fuel design limit on DNB (P_{fdl}) is that the DNBR in the hot channel shall not be less than 1.3.

To establish the power-to-fuel design limit curve on linear heat rate, the power at which centerline fuel melt would be predicted to occur is calculated for each of the configurations described above according to the relationship

$$P_{fdl} = \frac{W_{CLM} \cdot 100}{F_q^N \cdot \gamma \cdot W_{Avg}}$$

where W_{CLM} = deposited linear heat rate (in kw/ft) at which centerline fuel melt would be predicted to occur

W_{Avg} = core average generated heat energy which is deposited directly in the fuel.

γ = fraction of generated heat energy which is deposited directly in the fuel.

Ordered pairs (P_{fdl}, Ip) are then plotted for each CEA group insertion considered as illustrated in Figure 4.3-27B. It should be noted that Figure 4.3-27B is just the reciprocal of Figure 4.3-27A. The lower bound curve of Figure 4.3-27B establishes the relationship between the power-to-fuel design limit on linear heat (P_{fdl}) and peripheral axial shape index (Ip).

The variation due to burnup in the plots of peaking factors versus axial shape index is best explained with reference to Figures 4.3-27C through 4.3-27F. Figures 4.3-27C and 4.3-27D are plots of ordered pairs of axial peak versus shape index (F_z,I) for the unrodded core and for a configuration with a rod group inserted about 50% near beginning-of-cycle. The corresponding plots for similar rod configuration near end-of-cycle are displayed in Figures 4.3-27E and 4.3-27F. Plots of 3-D peaking factors for each point on these plots are obtained from the product of the worst radial peaking factor at any time during the burnup and the axial peaks shown on the figures. Appropriate radials and axials are combined in each distinctly rodded region of the core. The same matrix of radial peaking factors are applied at each burnup point for which axial peaking factor variations, such as those shown, are generated. Thus, these figures in effect display the variation in the 3-D peaking factors over the burnup cycle. The power-to-fuel design limit plots are simply mirror images of these plots.

With reference to Figures 4.3-27C to -27F one observes the relatively V-shaped nature of the envelope curve formed by the ordered pairs.

Near beginning-of-cycle (BOC), the axial peaks tend to be of greater magnitude near the center of the core. That is, the curve has a shallow valley and broad base. After end-of-cycle (EOC), the maximum axial peaks occur closer to the top and bottom of the core. Thus, the envelope curve tends to have a narrower base and a deeper valley. To obtain the data points used in setting local power density trip and monitoring limits, the most restrictive of these sets of curves for any given rod configuration are used. The resultant set of data points for all rod configurations allowed at any given power level are then combined and the most restrictive set of points are used to determine the axial shape index band on which trip and monitoring limits are based. Appropriate allowances and uncertainties are applied in determining these setpoints so that the final shape index band is not that implied by these figures.

It is not likely that the St. Lucie core would be operated for substantial periods of time with rods deeply inserted. However, the axial shape analyses results are sufficiently conservative to accommodate depletion with substantial amounts of rod insertion for periods of several thousand MWD/T in core average burnup.

The maximum radial peaking factors for various rod configurations over the entire burnup cycle are used in the shape analyses. When the core is depleted with rods inserted, the radial peaks in the rodded region decrease relative to the radial peak assumed for that rod configuration in the shape analysis. If the rods were to be pulled following depletion with them inserted the unrodded radial peak could be increased relative to that assumed in the shape analyses. However, since the worst combination of peaking factors for all allowable rod configurations at a given power level are used in setting local power density trip and monitoring limits, the analysis would remain conservative so long as the degraded unrodded peak following the rod withdrawal is no greater than the higher values in the matrix of radial peaks used to determine the setpoints.

Depletion with deeply inserted rods also changes axial inventory distributions. However, the correspondence between axial peaking factor and shape index for a wide range of axial power distributions is essentially unchanged, Thus, the net effect of the axial and radial effects is accommodated in the shape analysis technique for generating setpoints over a large portion of the burnup cycle. Beyond the point in time for which the degraded radial peak would exceed the values of the matrix of radial peaks used to determine the setpoints, continued operation could require an adjustment of the setpoints.

The same matrix of planar radial peaking factors versus rodded configuration is used at each burnup point during the cycle for which an axial shape analysis is run. Thus, in axial planes where group 7 is inserted, the worst group 7 planar radial peak at any time during the burnup cycle is used.

Figure 4.3-27G displays the time dependent variation in the group 7 and unrodded planar radial peaking factors over the entire burnup cycle. The planar radial peaking factors assumed in the shape analysis for each of these configurations is indicated on Figure 4.3-27G. Thus, a 1.32 unrodded radial and group 7 rodded radial peak of 1.47 are used in the shape analysis. One observes with reference to Figure 4.3-27G that the maximum rodded radial peaks occur at the same time during the burnup cycle as the maximum unrodded radial peak. By virtue of having used the worst radial peaking factors in the shape analyses, the resultant trip and monitoring limits conservatively account for peaking factor variations during most of the cycle. As a result, a single set of local power density trip and monitoring limits are applicable for the entire cycle.

The model used to calculate three dimensional peaking factors $\left(F_q^N\right)$ is also used to calculate the intergrated radial peak in the hottest pin axial power distribution $\left(F_z\right)$. This information along with the corresponding peripheral axial shape index $\left(I_p\right)$ for each of the configurations described previously is stored on files. These files are accessed directly by COSMO (a code employing the W-3 correlation) and calculations of the power-to-fuel design limit on DNBR $\left(P_{fdn}\right)$ performed for each hot pin axial power distribution investigated. Plots are made of the ordered pairs $\left(P_{fdn}, I_p\right)$ similar to those described above for P_{fdl}. The lower bound curve of these plots establishes the relationship between the power-to-fuel design limits on DNBR and peripheral axial shape index $\left(I_p\right)$ at fixed pressure, coolant inlet temperature and flow.

The safety limit curve, such as that shown in Figure 4.3-27 is obtained by combining the most limiting lower bound curves of P_{fdl} *and* P_{fdn} versus $\left(I_p\right)$ at any power level for regulating CEA group insertions allowed at that power level.

The trip limits based on centerline fuel melt considerations are established by reducing the power-to-fuel design limit curve on linear heat rate $\left(P_{fdl}\right)$ by uncertainties and allowances deemed necessary to account for the fact that process variables (e.g., peaking factors) used in the calculations are not known precisely. The uncertainties and allowances considered in establishing axial trip and monitoring limits are listed below.

A. <u>In Percent of Indicated Power</u>

1) Physics Calculation to Measurement Uncertainty. (See Section 4.3.3.1.2f)

2) Azimuthal Tilt Allowance

3) Power Measurement Uncertainty

B. <u>In Shape Index Units (SIU)</u>

1) Calibration Uncertainty of Excores Using Incores and Uncertainty in Applying Shape Annealing Correction to RPS signal

Rod shadowing and out-of-core detector decalibration effects are taken into account in the model. Coolant inlet temperature decalibration effects are taken into account by using the higher of the auctioneered ΔT and nuclear flux power indicated power.

The trip limits based on DNBR considerations are established in essentially the same fashion as the trip limits on linear heat rate. The same allowances and uncertainties are taken into account in reducing the power-to-fuel design limit curve $\left(P_{fdn}\right)$ and, in addition, uncertainties due to processing, coolant inlet temperature, primary system pressure and core flow rate signals are included. The resultant $P_{fdn}\ vs\ I_p$ limits constitute part of the thermal margin/low pressure trip where variations in cold leg temperature, reactor coolant system pressure, core power and axial shape index during operation are taken into account.

The monitoring (operational) limits on peripheral axial shape index $\left(I_p\right)$ are determined by reducing the trip limits by the amount of the required overpower margin. The required overpower margin on linear heat rate is the difference between the allowable full power peak linear heat rate determined by the LOCA analysis and the peak linear heat rate at which centerline fuel melt would be predicted to occur. The required overpower margin to a DNBR of 1.3 is that determined by the loss of flow analysis.

The maximum allowable axial and radial peaking factors are established as a product of the axial shape analysis. The full power axial shape index monitoring limits in conjunction with the power dependent insertion limits (PDIL's) given in the Technical Specifications / Core Operating Limits Report assure that (1) allowable full power three dimensional peaking factors (Fq's), including the effects of uncertainties, are no higher than Fq inferred from the design axial and radial peaking factors, and that (2) allowable axial power distributions do not result in DNBR overpower margins less conservative than that associated with the design axial power distribution. The allowances and uncertainties are accounted for in the axial shape analysis. Alarms are set to alert the operator when the axial shape index exceeds the monitoring limits defined as described above. Alarms are also set on pertinent NSSS parameters assumed in setting the axial shape index monitoring limits (e.g., power dependent rod insertion limits, quadrant power tilt, and CEA misalignment and sequencing).

There is no single radial peaking factor which can be classified as "expected". Radial peaking factors observed during operation will be those associated with the actual rodded configurations employed. In practice, the radial peaking factor is monitored by maintaining control rod insertions within the power dependent insertion limits (PDIL's) specified in the Technical Specifications / Core Operating Limits Report in conjunction with axial shape index monitoring limits. This mode of operation assures that radial peaking factors are no less conservative than those assumed in setting the monitoring limits. This is tantamount to restricting the allowable full power radial peaking factors to values less than the design radial peak even if all uncertainties combined in an adverse way.

Quadrant power tilt limits provide for action to be taken in the event of x-y power distribution anomalies not caused by CEA misplacement. CEA misplacement can cause abnormal quadrant power tilt indication, but corrective action for CEA malfunction is covered in the Technical Specifications on CEA misalignment and dropped CEA. When maintaining linear heat rate within acceptable limits using out-of-core detectors, limits on quadrant power tilt are imposed to account for the increase in linear heat rate which could be caused by a quadrant power tilt. The analysis to determine trip and monitoring limits accounts for possible margin degradation which could result from quadrant power tilts allowed by the Technical Specifications without corrective action. It should also be noted that equipment capable of sensing tilt consists not only of out-of-core power range neutron detectors, but also includes incore neutron detectors and the core exit thermocouples. For quadrant power tilts, determined by the excore detectors, in excess of prescribed values the Technical Specifications validation is required using incore detectors or thermocouples.

Data from tests at Palisades in which quadrant power tilts were deliberately imposed have been analyzed to determine the extent to which operating margin is reduced as a result of an azimuthal tilt. This analysis included an evaluation of data from both incore and excore detectors, and specifically accounted for the fact that the principle axis of the tilt was not necessarily coincident with a diameter passing through the detectors. This analysis showed that excore detectors are capable of monitoring quadrant power tilt and that there is a direct correspondence between the tilt determined from excore and incore detectors. It was also determined that margin degradation associated with an excore tilt indication of 1% is no greater than 1% for tilts associated with anomalies other than rod misalignments (e.g., with xenon redistribution effects).

4.3.2.5 Control Requirements

Core reactivity data, including reactivity changes associated with core temperature and power changes, the reactivity worth of equilibrium xenon and samarium, and the reactivity available to compensate for burnup and fission product poisoning are shown in Table 4.3-2. Soluble boron concentrations required for criticality at various core conditions are shown in Table 4.3-1 and as a function of core average burnup at full power with all CEAs withdrawn on Figure 4.3-26l. The maximum reactivity addition rates resulting from deboration with all three charging pumps running are given in Table 4.3-1. These values occur at beginning of life and decrease throughout the cycle.

Burnable poison rods are provided as described in Section 4.3.1-d to ensure that the moderator temperature coefficient has the required magnitude and algebraic sign. The reactivity controlled by these burnable poison rods is given in Table 4.3-1. At end of cycle, the reactivity worth of the residual burnable poison is small (typically 1 percent or less), and the soluble boron concentration is near zero.

Soluble boron is used to compensate for slow reactivity changes, for example, reactivity effects due to burnup and changes in xenon worth. Furthermore, soluble boron is used as a mechanism to shut the core down at cold conditions to as much as 10 percent $\Delta\rho$ subcritical. The regulating CEA groups are used to compensate for the changes in reactivity associated with routine power level changes. In addition, these CEAs may be used to compensate for minor variations in moderator temperature and boron concentrations at operating conditions. The reactivity worth requirements for the full complement of CEAs (regulating plus shutdown CEAs) are shown in Table 4.3-6 and are discussed below. These data are limiting requirements for any time in the cycle. The total worth of all CEAs, including shutdown CEAs, covers these requirements and provides adequate shutdown capability with the most reactive CEA stuck in the fully withdrawn position as shown in Table 4.3-6, at any time in the cycle.

a) Fuel Temperature Variation

The increase in reactivity that occurs when the fuel temperature decreases from a full power value to a zero power value is due primarily to the Doppler narrowing effect of the absorption cross-section of U238 and plutonium 240. The CEA reactivity allowance for fuel temperature variation shown in Table 4.3-5 contains some additional margin over the expected reactivity change for the first cycle shown in Table 4.3-2.

b) Moderator Temperature Variation

An increase in reactivity occurs when the moderator temperature decreases from the full power value to the zero power value. This reactivity increase, which is due to the negative moderator temperature coefficient, is largest at end of cycle when the soluble boron concentration is near zero and the moderator coefficient is strongly negative. At beginning of life, when the moderator temperature coefficient is less negative, the reactivity increase is smaller. The CEA reactivity allowance for moderator temperature variation given in Table 4.3-5 includes an allowance for this effect plus an allowance for reduction in CEA worth due to increased moderator density in going from full power to zero power.

Table 4.3-6 shows the reactivity worths of the full complement of CEAs, with and without the highest worth CEA in the fully withdrawn position, at beginning and end of cycle. This table also compares the available net shutdown worth (including the effects of the stuck CEA) to the reactivity worth requirements from Table 4.3-5. Ample margin is available to accommodate uncertainties in the calculated CEA worth. A comparison between calculated and measured CEA worths is discussed in Section 4.3.3.

c) Moderate Voids

In going from full power to zero power, an increase in reactivity results from the collapsing of steam bubbles caused by local boiling at full power. The amount of voids in the core is very small and is estimated to be substantially less than one percent at full power. As with the moderator temperature effect, the maximum increase in reactivity from full to zero power occurs at end of cycle, when the least amount of dissolved boron is present. This reactivity effect is very small, and the allowance for this effect is shown in Table 4.3-5.

d) Transient Xenon Reactivity

The allowance shown in Table 4.3-5 is designed to compensate for CEA worth that may be inserted at full power to compensate for xenon reactivity changes due to changes in reactor power level. When the CEAs reach the insertion limit, any additional reactivity adjustment is made by adjusting the dissolved boron concentration in the moderator. The Technical Specifications / Core Operating Limits Report require that the CEA insertion does not exceed specified limits. CEA motion-inhibiting features are discussed in Section 7.7.1.1.

e) CEA Bite and Boron Deadband

The CEA bite is the amount of reactivity worth in CEAs that can be inserted in the core at full power to initiate ramp changes in reactivity associated with load changes, and to compensate for minor variations in moderator temperature and boron concentration. The boron deadband allowance is used to compensate for fuel depletion effects between adjustments of the dissolved boron concentration.

f) Shutdown Margin and Accident Analysis Allowance

The allowance shown in Table 4.3-5 for shutdown margin and accident analysis is consistent with that assumed under various postulated accident conditions addressed in Chapter 15, which result in predicted acceptable consequences.

Table 4.3-6 shows the reactivity worths of the full complement of CEAS, with and without the highest worth CEA in the fully withdrawn position, at beginning and end of cycle. This table also compares the available net shutdown worth (including the effects of the stuck CEA) to the reactivity worth requirements from Table 4.3-5. Ample margin is available to accommodate uncertainties in the calculated CEA worth. A comparison between calculated and measured CEA worths is discussed in Section 4.3.3.

Figure 4.3-26 shows typical CEA insertion limits as a function of power level. Adherance to these limits, which is required by the Technical Specifications and enforced by the features described in Chapter 7, assures that the available shutdown margin at any power level will not be less than that given in Table 4.3-6.

4.3.2.6 Control and Monitoring of the Power Distribution

Methods of reactor control include (a) use of regulating bank 7 to shape the axial power distribution; (b) regulating CEA motion or dissolved boron concentration charges to change power level or to improve the radial power distribution; and (c) correcting off-optiumm conditions with cause margin degradation (e.g. control rod misalignments). In using these methods of control, it is required that, at any power level and any time in life:

a) there is sufficient reactivity worth in withdrawn control rods to meet the shutdown margin and accident analysis allowance requirements shown in Table 4.3-5 plus the stuck rod worth shown in Table 4.3-6

b) the amount of control rod insertion be such that an ejected rod accident would be no worse than the results specified in the safety analysis of the accident (Section 15.4.5)

c) other limiting conditions for operation, including required margins to specified acceptable fuel design limits, be satisfied.

The first two of these restrictions are automatically met by maintaining the CEAs at or above the allowable position shown on the power dependent insertion limit (PDIL) curve of Figure 4.3-26. The zero power PDIL limits the CEA insertion allowed at criticality. The third restriction requires that during normal operation, the combination of power distribution and other variables (e.g. CEA positions, power level, and coolant conditions) be maintained within the limiting conditions for operation.

These limiting conditions for normal operation are such that, when the entire system is considered, no anticipated operational occurrence will result in violation of specified acceptable fuel design limits or other safety limits and no other postulated accident will result in consequences more severe than the specified acceptable predicted consequences reported in Chapter 15.

Power distributions are continuously monitored by measuring (a) CEA positions which affect radial and axial power distributions, (b) quadrant power tilt, and (c) either axial shape index determined from the out-of-core neutron detector responses which provide a measure of the axial power distribution, or incore detector signals which are compared to local power density alarms.

The power range out-of-core neutron detectors described in Section 7.2.1 are used to monitor the symmetry of power distributions by means of parameters derived from the relative responses of detectors located at distinct azimuthal and axial positions. The out-of-core detectors are sensitive primarily to the power density variations within two to three

assembly widths of the fuel assembly nearest the detector. All possible xenon induced spatial oscillations affect the outer assemblies of the reactor. The functions of incore instrumentation are to provide a means of calibrating the individual out-of-core detectors relative to one another and to provide backup indication of power distribution asymmetrics.

Each of the four split ion chambers described in Section 7.2.1 constitutes a channel of axial shape monitoring capability. The parameter of interest, derivable from an axial channel, is external axial shape index. External axial shape index is related to internal axial shape index through a relationship which depends mainly on CEA position, and burnup. There is also a dependence upon out-of-core detector location both azimuthally and radially. Furthermore, a correspondence can be established between internal axial-shape index and the three dimensional nuclear peaking factor Fq. The nature of this relationship has been established through a large number of calculations of Fq. Field measurements at startup will confirm these relationships at key points. Relationships also exist between the power level for a specified margin to the limiting DNBR and internal and external shape index readings at given coolant conditions. A typical core safety limit curve as a function of internal axial shape index is shown in Figure 4.3-27.

It is possible to establish limits on the external axial shape index such that the maximum achievable Fq and the minimum margin to the limiting DNBR at any power level are within specified acceptable limits for normal operation. This monitoring limit band is the range of values of external shape index allowed during steady state operation as a function of power level. It is specified such that the limiting conditions for operation shall not be exceeded at any power level provided that coolant conditions are normal and that the Technical Specifications on CEA insertion, CEA misalignment, azimuthal tilt and detector calibration are observed (these are enforced separately). Typical radial and unrodded axial power distributions which would be allowed by such operation are discussed in Section 4.3.2.2. Figures 4.3-2 through 4.3-18 illustrate conditions expected at full power at various times during the fuel cycle as specified on the figures.

An alternate means of monitoring power distribution and maximum Fq is by means of the incore detectors. Alarms on the my signal of each fixed incore detector segment are set to activate whenever the peak linear heat rate approaches an allowable limit as determined by the ECCS analysis. These incore alarm setpoints are determined as follows:

1. The core is considered to be divided into four axial regions, each approximately one fourth the core height, and each encompassing the axial region monitored by one segment level of the incore detectors.

2. Each of the four axial regions is further subdivided into several axial nodes. For each of these axial nodes, in each bundle, the local burnup and peak to average local power is determined.

3. Local nodal overpower ratios are then established as follows:

    a) The local peak linear heat rate (kw/ft) for the node is calculated as the product of the peak local power times the uncertainties described in the Technical Specifications Bases to obtain the local augmented peak linear heat rate in the node.

b) Based on the local burnup in the node, the license limit linear heat rate is determined from the kw/ft versus local burnup curve.

c) The local nodal overpower ratio is the calculated ratio of the license limit linear heat rate to the local augmented peak linear heat rate for the node.

4. For each of the four axial regions defined in Step 1 above, an alarm factor is defined as the minimum local modal overpower ratio for any node in that region.

5. The incore detector alarm setpoint for each segment of each incore detector string is simply the product of the detector segment signal which served as the input to the determination of power distribution (Step 2) and the alarm factors (Step 4) for each level of incore detector segments.

The rationale for resetting the incore alarms as often as every thirty days is to optimize power capability. The procedures described above result in setting the incore alarms so that all detector segments at a given elevation will alarm when the limiting linear heat rate for the peak node in that region is achieved, assuming the power distribution is the same as when the alarms were set. For any other power distribution, some alarm limits will be reached before the peak node reaches its linear heat rate limit. Since some variation in the power distribution is to be expected with burnup, the alarms are reset every thirty days to obviate having spurious alarms and thus optimize power capability.

During maneuvering situations, when rods are inserted and withdrawn, the power distribution changes relative to the one used in setting the alarms. The technique employed to set the incore alarms, as described above, assures that alarm settings in fuel bundles not containing the peak power are more conservative than required since they allow for only the margin available in the bundle containing the power peak. Therefore, changes in the power distribution that would cause the peak power to occur in any of these fuel bundles would cause alarms well before local limits are exceeded. Since these alarms are conservatively set, a reduction in core power would be required to clear the alarms. Analytic studies to date have confirmed the conservative nature of the technique employed in setting the incore alarms for power distributions other than that used to fix the alarm settings.

The above procedures for setting the incore alarms are implemented by processing the incore detector signals to determine the power distribution and to generate the corresponding alarm setpoints.

External axial shape index is also input to the trips on linear heat rate and DNBR, as discussed in Section 7.2.1. These trips are provided to protect against exceeding specified acceptable fuel design limits on linear heat rate and DNBR.

If fewer than three power range protective channels are operable, the maximum allowed power level is reduced.

The out-of-core detectors are adequate for monitoring azimuthal tilt. The reactor will not be operated under conditions which would imply azimuthal instability. Measurements on a similar operating reactor indicate that this reactor will be azimuthally stable. Currently, it is planned to use the out-of-core detector indication as one means of determining azimuthal tilt. Other methods include utilization of incore neutron detectors and incore thermocouples.

4.3.2.7 Reactivity of Individual Assemblies

The maximum k_{eff} value of a single fuel assembly, when moderated and completely reflected by unborated water at room temperature, is 0.91 based enrichment of 3.7 wt % U-235. The minimum critical mass, with or without xenon and samarium poisoning, may be specified in terms of the number of assemblies in various geometric arrays that can produce criticality. A single assembly enrichment of 3.7 wt % U-235 is subcritical when immersed in room temperature unborated water. Two such assemblies with optimum spacing in water could be supercritical.

4.3.2.8 Xenon Stability

4.3.2.8.1 General

Xenon induced spatial oscillations in large PWRs fall into three classes or modes. These are referred to as axial oscillations, azimuthal oscillations and radial oscillations. An axial oscillation is one in which the axial power distribution periodically shifts upward and downward in the core. An azimuthal oscillation is one in which the X-Y power distribution periodically shifts from one side of the reactor to the other (Figure 4.3-28). A radial oscillation is one in which the X-Y power distribution shifts inward and outward from the center of the core to the periphery (Figure 4.3-29).

Stability of a reactor to a particular mode of oscillation is characterized by a damping factor. When the damping factor is positive, the reactor is unstable to that mode of oscillation. This means that when the power distribution is perturbed, i.e., altered in any manner, the magnitude of the oscillatory mode will increase with time in the absence of operator intervention. When the damping factor is negative, the reactor is stable and the magnitude of the oscillatory mode decreases with time.

A linear stability criterion, employing only the fundamental and first harmonic modes, has been used to judge the stability of the reactor to xenon-induced spatial oscillations. This criterion has been shown to be adequate (Reference 39) when:

a) the reactor is stable to xenon-induced oscillations, since the second harmonic modes contribute little to either the periods or the decay constants of the first harmonic mode oscillations

b) the reactor is unstable to xenon-induced oscillations, since the first harmonic modes excite the second harmonic modes without affecting the periods of the first harmonic modes.

Xenon oscillation studies indicate that a number of general statements can be made.

a) The damping factor for an oscillatory mode depends primarily upon the power coefficient and the time in the burnup cycle.

b) The time scale on which any oscillations occur is long, the period of oscillation being generally between 25 and 30 hours.

c) As long as the initial power peaking associated with an oscillation-inducing perturbation is within limiting conditions for operation, specified acceptable fuel design limits will not be approached for a period of hours.

d) The reactor will be stable to radial mode oscillations at all power levels at all times in the burnup cycle.

e) The reactor is predicted to be stable to azimuthal mode oscillations at all times in the burnup cycle. The azimuthal mode damping factor becomes more negative as burnup increases.

f) The reactor is expected to be naturally unstable to axial mode oscillations before the end of the first cycle.

g) All possible modes of undamped oscillations can be detected by both out-of-core and incore instrumentation.

4.3.2.8.2 Detection of Oscillations

The power range out-of-core neutron detectors are used to monitor the symmetry of power distributions by means of parameters derived from the relative responses of detectors located at distinct azimuthal and axial positions.

A discussion of the neutron detectors used to detect axial xenon oscillations by monitoring the variations in axial shape index is contained in Section 4.3.2.6. The adequacy of the out-of-core detectors for monitoring azimuthal tilt (horizontal plane symmetry) in the predicted absence of azimuthal instability is explained in Section 4.3.2.5. A discussion of the analytical and experimental bases of these predictions is given in Section 4.3.3.

A minimum of three separate responses from distinct azimuthal locations is needed for a single tilt measurement.

Out-of-core detector indication is one means of determining azimuthal tilt. Other methods include utilization of incore thermocouples and incore neutron detectors.

4.3.2.8.3 Control of Oscillations Required by Xenon Instability

The reactor protective system described in Section 7.2.2 is designed to prevent exceeding acceptable fuel design limits and to limit the consequences of postulated accidents. It is clear that to guarantee the effectiveness of the protective system, there must be provided a means to assure that under all allowed operating modes the state of the reactor is confined to conditions not more severe than the initial conditions assumed in the design and analysis of the protective system.

4.3.2.8.4 Control of Oscillations

Since the reactor will not be operated under conditions that imply instability with respect to azimuthal xenon oscillation, no special protective system features are needed to accommodate azimuthal mode oscillations. Nevertheless, a maximum quadrant tilt is prescribed in the Technical Specifications along with prescribed operating restrictions in the event that this tilt is exceeded. To satisfy the foregoing requirements, the maximum allowed azimuthal (quadrant) tilt is considered in design and analysis of the reactor protective system. Section 4.3.2.8.2 describes the means provided for monitoring azimuthal tilt.

The axial shape monitoring system provides assurance that fuel design limits are not exceeded due to abnormal axial power distributions, provided that all other major plant parameters are maintained within specified bounds. These limits represent the initial conditions assumed in the design and analysis of the balance of the protective system. Such means are provided by:

a) administrative procedures, including the specification of monitoring limits on external axial shape index

b) instrumentation to inform the operator of the status of the reactor relative to these limits

The features provided for azimuthal xenon control are:

a) administrative limits on quadrant power tilt

b) instrumentation for monitoring quadrant power tilt.

The features provided for axial xenon control and protection are:

a) administrative limits on axial power distribution, external axial shape index

b) Technical Specification power distribution limits on linear heat rate and DNB parameters that rely upon axial shape index limits

c) equipment for monitoring axial shape index

d) a variety of methods, including RCS boration / dilution, RCS temperature, and use of regulating bank 7 for control of axial power distribution.

The out-of-core detectors are used to monitor the axial power distribution and to detect deviations from the equilibrium distribution such as those which would occur during an axial xenon oscillation. This is done by monitoring variations in external axial shape index, a parameter derived from the out-of-core detector readings which is related to the axial power distribution. Induced axial oscillation tests carried out during startup testing at both Maine Yankee and Palisades have confirmed that the out-of-core detectors can be used to monitor axial xenon oscillations. Control of axial xenon oscillation is accomplished by a variety of methods, including RCS boration / dilution, RCS temperature, and utilizing regulating bank 7. When it is determined that the axial shape index may exceed the boundaries of a specified control band about the equilibrium value, then a method of control is selected to dampen the axial xenon oscillation.

4.3.2.9 Vessel Irradiation

The design of the reactor internals and of the water annulus between the active core and vessel wall is such that the peak vessel neutron fluence at 60 years at 2700 MWth is calculated to be less than 4.7×10^{19} n/cm^2(E > 1MeV). The neutron fluence at the limiting vessel material at 60 years is less than 3.1×10^{19} n/cm^2.

The EPU would normally result in an increase to the neutron fluence on the reactor pressure vessel. There was actually a small decrease in the projected 60-year fluence based on 52 EFPH; this is seen in Table 4.3-17. This decrease occurred because the EPU fluence analysis used more recent core power histories that enabled removal of excess conservatism from the pre-EPU 60-year fluence analysis, while adding a 10% factor of conservatism to the EPU fluence projections beginning with Cycle 25. The effect of the projected changes in operating conditions on reactor vessel integrity was evaluated. The vessel fluence projections for the St. Lucie Unit 1 plant life of 60 years are presented in Table 4.3-18. The 0° and 15° azimuths correspond to the peak fluence locations for the base metal and circumferential weld (0°) and the axial welds (15°). Vessel fluence is provided for the vessel inside surface (cladbase metal interface) and for the ¼ and ¾ thickness (t) locations. (Reference 9)

The limiting material is the longitudinal weld seam 3-203 at the 15°, 135° and 255° azimuthal locations with a maximum adjusted RT_{NDT} at 60 years that is below the 10 CFR 50.61 screening limit.

4.3.2.10 References for Section 4.3.2

1. XN-75-27(A), Supplement 1, September 1976.
2. XN-75-27(A), Supplement 2, December 1977.
3. XN-75-27(A), Supplement 3, November 1980.
4. XN-NF-84-12, "St Lucie Unit 1 Cycle 6 Safety Analysis Report Reload Batches XN-1 and XN-lA", Exxon Nuclear Company, February 1984.
5. XN-CC-28, Revision 5, "XTG - A Two Group Three-Dimensional Reactor Simulator Utilizing Coarse Mesh Spacing", Exxon Nuclear Company, July 1979.
6. XN-75-27(A), "Exxon Nuclear Neutronics Design Methods for Pressurized Water Reactors", Exxon Nuclear Company, June 1975.
7. XN-75-27(A), Supplement 4, December 1985
8. WCAP-11596-P-A, “Qualification of the PHOENIX-P/ANC Nuclear Design System for Pressurized Water Reactor Cores, “ June 1988 (Westinghouse Proprietary)
9. WCAP-17389-P, “St. Lucie Unit 1 Extended Power Uprate (EPU) Engineering Report”, February 2011, (Westinghouse Proprietary)

4.3.3 COMBUSTION ENGINEERING ANALYTICAL METHODS (CYCLES 1-5)

4.3.3.1 Reactivity and Power Distribution

4.3.3.1.1 Method of Analysis

The nuclear design analysis for low enrichment PWR cores is based on a combination of multigroup neutron spectrum calculations, which provide cross sections appropriately averaged over a few broad energy groups, and few-group one, two, and three dimensional diffusion theory calculations of integral and differential reactivity effects and power distributions. The multigroup calculations include

spatial effects in those portions of the neutron energy spectrum where volume homogenization is inappropriate, e.g., the thermal neutron energy range. Most of the calculations are performed with the aid of computer programs embodying analytical procedures and fundamental nuclear data consistent with the current state of the art.

A summary of the analytical tools employed is given below. Comparisons between calculated and measured data which validate the design procedures are presented in Section 4.3.3.1.2. As improvements in analytical procedures are developed and improved nuclear data become available, they will be added to the design procedures, but only after validation by comparison with related experimental data.

Few group constants for subregions of the spatial diffusion theory codes, e.g., fuel pin cells, moderator channels, structural member cells, etc., are calculated by the CEPAK lattice program. This program is the synthesis of a number of computer codes, many of which were developed at other laboratories, e.g., FORM[(l)]- THERMOS[(2)], and CINDER[(3)]. These programs are interlinked in a consistent way with inputs from differential cross section data from an extensive library.

The entire neutron spectrum is represented by 83 neutron groups between 0 and 10 Mev. Neutron leakage in a single Fourier mode is represented by either P-1 or B-1 approximations to transport theory throughout this entire range. Resonance shielding is determined analytically; the Hellstrand correlation (4) is employed for U-238, with appropriate adjustments guided by Monte Carlo calculations of

resonance capture in U-238 so as to provide agreement with selected measurements of the conversion ratio. ZUT-TUZ[5] calculations are employed for other resonance absorbers to define analytic expressions of the resonance integral as a function of pertinent variables. Appropriate Dancoff correction factors are determined for uniform lattices by a three-region model of the unit cell to provide a better description of the effect of scattering in the clad on resonance capture. For heterogeneous lattices this calculation is extended to include heterogeneities by nearest neighbor approximations. Included also in the resonance shielding calculation is an appropriate account of resonance overlap effects between different uranium and plutonium isotopes. In the thermal energy range, the effects of cell environment on the spatially dependent neutron spectrum within the lattice cell can be included in those cases where such effects are important. Anisotropic scattering and temperature dependent effects associated with the hydrogenous moderator are approximated by the use of transport corrected, temperature dependent scattering kernels generated by the GAKER[6] program. A major subroutine provides depletion calculations in the reactor cell to describe the evolution of the reactor spectrum and the appropriate cross section averages, the production of fission products, including xenon and samarium, and the production of conversion products such as plutonium isotopes. Various criticality search options are available to approximate the effects of reactivity control on the neutron spectrum and thus on the few group cross section averages over energy.

Boundary conditions and equivalent diffusion theory constants for CEAs are calculated by the CERES program. For a one region CEA, in cylindrical geometry, boundary conditions are calculated in each multigroup by the method of successive generations, with capture probabilities based on the tabulations of Stuart and Woodruff [7] . In slab geometry, the multigroup boundary conditions are obtained from analytical fits to the extensive transport calculations of Schiff and Stein[8]. Two region CEAs are transformed to fictitious homogeneous CEAs by matching extrapolation lengths on the outer surface, as defined by Kear and Ruderman [9];the homogeneous CEAs are then treated as above. Fictitious few group diffusion parameters for use in multidimensional diffusion theory calculations are calculated by methods defined by Wachspress [10] and Henry[11].

Effective diffusion theory constants for burnable poison rod (shim) cells are calculated by a sequence of programs consisting of HAMMER[12], DTF-IV [13], and MO-807 [14]. HAMMER is employed as a few group regionwise cross section generator for the shim cell; DTF-IV is employed in a one dimensional representation of the shim cell and environment to define relative reaction rates between shim and fuel cells; and MO-807 is employed to calculate the effective diffusion theory constants.

Static and depletion dependent reactivities and power distributions in one, two, and three dimensional representations of the core are determined by the diffusion-depletion programs PDQ-7[15] and HARMONY[16]. These calculations employ macroscopic (static) or microscopic (depletion) cross section data generated by the methods described in the preceding paragraphs.

Depletion dependent reactivities and power distributions in a one dimensional (axial) representation of the core are determined by the diffusion depletion program PDQ-ONDE. This program contains all the basic capabilities of HARMONY and the one dimensional option of PDQ-7 plus optional capabilities in carrying out CEA boundary and poison content criticality searches as well as spatial feedback on the power distribution with fuel and moderator temperature.

Static and time dependent reactivities and power distributions in a one dimensional (axial) representation of the core are determined by the diffusion theory program QUIX. This program solves the neutron flux and associated eigenvalue for problems containing up to 140 distinct regions or compositions with variable mesh intervals. In addition to the eigenvalue problem, OUIX will perform four types of search calculations to attain a specified eigenvalue, viz., a poison search, buckling search, CEA boundary search, and a moderator density dependent poison search; the effect of moderator and fuel temperature feedback on the power distribution can be employed. Provisions have been made in the program to allow the user to request two separate flux weighting edits. For a given flux weight edit, the program computes average cross sections and buckling for the set of regions specified in the input. The output consists of a complete restatement of the input, a summary of the eigenvalues and search quantities obtained for each iteration, a listing of the fission source and few group fluxes for each point, the integrated and averaged fluxes for each group, fluxes for each point, the integrated and averaged fluxes for each group and region, the longitudinal buckling for each group and region, a plot of the neutron source distribution vs radius, and the flux weighted quantities.

The following additions and improvements have been made to the nuclear design analytical methods:

1. Extended pointwise Doppler feedback technique.*

2. Improved prediction of power peaking in fuel pins adjacent to water holes.*

3. Improved correlation between fuel temperature and local power density.*

4. Use of coarse mesh computer program ROCS along with standard fine mesh PDQ.**

5. Use of the DIT assembly spectrum code to generate cross sections for both ROCS and PDQ.***

* Added in Cycle 2, see Cycle 2 RSE P.13 for more information. (Reference 42)

** Added in Cycle 3, see Cycle 3 RSE p. 14 for more information. (Reference 41)

*** Added in Cycle 5, see Cycle 5 RSE, Section 2.4.8 for more information.

4.3.3.1.2 Comparisons with Experiments

a) Reactivity

The nuclear analytical design methods in use at Combustion Engineering have been checked against a variety of critical and subcritical experiments. Table 4.3-7 summarizes the properties of the fuel, rods employed in the lattices analyzed; Tables 4.3-8 and 4.3-9 summarize pertinent characteristics of the lattice and the eigenvalues calculated with the design package.

The average eigenvalue for the critical uranium lattices of Table 4.3-8 (numbers 1 through 23) is 0.9987 $\pm$ 0.0019 and for the mixed oxide lattices of Table 4.3-9 the corresponding number is 1.0080 $\pm$ .0053. The UO_2 experiments cover a wide range of core dimensions, boron concentrations, temperature, enrichment, water-to-fuel ratios, and clad materials, thus giving confidence in the validity of the design package to predict beginning-of-life fuel properties with an acceptable accuracy. The analysis the mixed oxide lattices exhibits larger deviations than for the UO_2 lattices. This result is not surprising in view of the limited amount of data compared with UO_2 systems, the relatively large experimental buckings, and uncertainties is the same.

The rods-out, beginning-of-life, cold and hot zero power reactivities of the Obrigheim, [28] Maine Yankee and Connecticut Yankee[29] reactors were also calculated to demonstrate the validity of the model in large multiregion cores. The results are summarized below:

	Reactor	Temperature	Dissolved Boron Concentration (ppm)	K eff
a)	Obrigheim	cold	1727	0.9964
		hot	1962	0.9989
b)	Connecticut Yankee	260F	2040	1.0025
		560F	2305	1.0002
c)	Maine Yankee	260F	948	1.0009
		525F	988	1.0005

Reaction Rates

Reaction rates were measured in some of the lattices noted in the previous section and are shown, along with definitions of the measured quantities, in Table 4.3-10. It will be noticed that measurements of ρ28, the epicadmium-to-subcadmium capture ratio in U-238, all lie 4 percent or so below the calculations except for the most recent B&W case (lattice 6) and the Bettis measurements where the trend is reversed. Thus, the spread of available information from Cd ratio measurements in U-238 is about ±4 percent, with the quoted errors suggesting a slight underestimation of the resonance capture. Measurements of ρ28 have been plagued, however, by uncertainties in the effect of the Cd covers and by systematic errors in counting technique so that these measurements seem to be basically inadequate for a precise determination of resonance capture in U-238.

The single modified conversion ratio (MCR) in U-235 for the B&W lattice 6 agrees well with calculation. The ρ28 measurements are scattered on either side. The fission in U-238 relative to U-235 fissions, called δ28, is consistently underestimated as it should be since a homogeneous model is employed. The differences in an oxide lattice are about 1 percent in total fissions. In depletion calculations one can expect a slight overestimate of U-235 consumption from this error.

The Winfrith measurements of Pu-239 to U-235 fission ratio are consistently overestimated by about 2 percent. In the power reactor, further spatial depletion effects occur within a fuel rod which are not described in the design model, and which will tend to decrease this small discrepancy. Thus, the depletion calculations will underestimate slightly the U-235 burnup and the content of Pu-239.

c) Depletion Calculation

Over 50 spent fuel samples from Yankee Rowe Core I were subjected to isotopic and radio-chemical analyses which were performed in the Tracerlab Laboratory at Richmond, California and by the Vallecitos Atomic Laboratory of the General Electric Company[30]. Depletion calculations were performed on the Yankee core for comparison with the above measurements. Figure 4.3-30 compares measured and calculated values of the Pu/U mass ratio versus exposure, and Figure 4.3-31 shows a comparison for the relative isotopic composition of plutonium as a function of fractional U-235 depletion.

The inventory changes for the 74 fuel assemblies from Yankee Rowe Core I are compared with measured results[31] in Table 4.3-11; the calculations were carried out using both one-dimensional and three-dimensional representations.

d) Fuel Temperature and Power Coefficients

The fuel temperature coefficient of reactivity is the change in reactivity per unit change in fuel temperature. A change in fuel temperature affects not only the thermal expansion of the fuel pellet but, in addition, the reaction rates in both the thermal and epithermal energy regimes. In the thermal energy regime, a change in reaction rate with fuel temperature arises from the effect of the temperature dependent scattering properties of the fuel matrix on the thermal neutron spectrum. Epithermally, the principal contributor to the change in reaction rate with fuel temperature is the Dopper effect arising from the increase in absorption widths with fuel temperature. In typical PWR fuels containing strong resonance absorbers such as U-238 and Pu-240, the magnitude of the Doppler component is more than a factor of ten larger than the thermal energy component and the net fuel temperature coefficient is negative.

The fuel temperature coefficient is determined via spatial diffusion theory calculations for the reactor using fuel temperature dependent epithermal and thermal microscopic cross sections derived by the CEPAK lattice code.

The power coefficient of reactivity is the change in reactivity per unit change in core power level. The principal contributors to this coefficient are the fuel and moderator temperature coefficients combined with the appropriate changes in fuel and moderator temperature with power. The change in average moderator temperature with power is controlled and thus known for a given reactor.

The model used to compute the power coefficient employs the empirical relationship given in Section 4.3.2.3 (f) which is based on evaluations of power defects measured in reactors such as Obrigheim and Connecticut Yankee. This empirical relationship has been employed in the analysis of several burnup cycles of the San Onofre I, Obrigheim, and Connecticut Yankee reactors and has yielded agreement with measured power defects to within approximately 0.2 percent $\Delta\rho$.

The validity of the fuel temperature dependence on linear heat rate has been demonstrated by three dimensional calculations of the fuel temperature power coefficient for the startup tests of San Onofre Cycle 1 (Figure 4.3-32). The agreement with measured data is seen to be good for this air filled, steel clad fuel. Similar comparisons with data from reactors utilizing He filled fuel, namely Maine Yankee, Omaha, Obrigheim and Stade also show that the fuel temperature expression is satisfactory for predicting power defects, power escalation reactivity loss, and tends to under predict somewhat

the fuel temperature component of the power coefficient. It should be noted that all of these reactors have fuel pellet diameters close to 0.38 inches although the clad and fill gas compositions and pressures are different. The fuel temperature model apparently underestimates the Doppler coefficient most noticeably in He filled, Zr clad fuel.

Uncertainties applied to the fuel temperature coefficient used in accident analyses are estimated by performing statistical analyses of comparisons between calculations and measurement. The application of a $\pm$15% uncertainty in the conservative direction ensures that a conservative value of this parameter will be employed to within 2σ or 95% confidence limits.

e) Moderator Temperature Coefficient

Analyses of moderator temperature coefficients for the Connecticut Yankee and Maine Yankee reactors have been compared with measurements made during the course of the startup experiments. Table 4.3-12 shows that the agreement between the calculated and experimental values is good. It can be seen from the data given that the current analysis predicts a coefficient more than 0.23×10^{-4} Δρ/F more negative than measured at cold conditions and no more than 0.16×10^{-4} Δρ/F more negative than measured at hot conditions.

f) Power Distribution

Comparisons have been made between the measured and calculated power distribution for the Maine Yankee and Connecticut Yankee reactors. These comparisons for Maine Yankee were made at 50 percent and 75 percent of full power for both rodded and unrodded operating conditions and are shown in Figures 4.3-33 through 4.3-36. The measured power distributions shown on Figures 4.3-33 through 4.3-36 were obtained from Rh self powered fixed

incore detector signals used in conjunction with 1) algorithms consisting of power to signal ratios calculated by PDQ for various burnup and rod configurations, and 2) axial fitting routines. The sources of the uncertainty error associated with this measurement are:

1) instrument calibration and reproducibility

2) short range power distribution

3) axial power shape generation

4) global power distribution.

Comparisons for Connecticut Yankee were made at hot operating conditions at a core average burnup of 1525 MWD/MTU, with rods partially inserted. Figures 4.3-37 and 4.3-38 show the measured and calculated power distributions for the unrodded axial region and for the rodded axial region. Data points at each plane were normalized to a core average of unity. The indicated favorable agreement between calculation and measurement, even with significant rod insertion, lends confidence to the ability of the calculational techniques to predict power distributions under operating conditions.

The physics uncertainty allowance applied to the power distribution calculations performed as part of the shape analysis for monitoring purposes, is currently set at 8 percent. Comparison of predicted to measured incore detector signals from operating plants indicate values lower than 8 percent can be justified for this allowance.

Data being acquired from operating CE reactors will form the basis for continuing appraisal of the uncertainty allowance.

The design of the incore detector cable utilized in St. Lucie Unit 1 reactors differs from that employed in the earlier plants. The difference is the incorporation of an integral sheath for the detector-signal cable. This change resulted in the elimination of the detector-signal cable weld which was the cause of occasional failures on the earlier plants. The reliability of the incore detector assemblies in the St. Lucie reactor is significantly improved compared to that of the earlier system.

Performance of the incore detectors in the early plants has been such that at least 75 percent of the detector strings have been operable (no more than 1 of 4 segments failed) to date. This experience has led to the design improvement mentioned above. Even so, the failures experienced to date have not significantly affected the assessment of measurement accuracy since sufficient redundancy is present in the incore system to make up for the inoperable detectors.

g) CEA Reactivity Worth

Comparisons were made between the predicted and measured CEA worth for individual banks inserted sequentially, and for the total rod worth for Maine Yankee, whose CEA design is virtually identical to the CEA design of this reactor. Table 4.3-13 summarizes this comparison between calculation and experiment. The good agreement gives confidence in the methods used to predict CEA worths.

Table 4.3-14 presents a comparison between calculated and measured worths of simulated ejected and dropped control rods in Palisades, Maine Yankee, and Omaha.

Measurements made during startup testing confirm that the values of ejected CEA accident parameters assumed in the Chapter 15 safety analyses were conservative, and thus verify the adequacy of the final power dependent insertion limit (PDIL) relationship.

The ability of the calculational techniques to predict power distributions under anomalous rod configurations has been experimentally confirmed in the CE Fort Calhoun reactor. Figure 4.3-38A illustrates a comparison between calculated and measured changes in power distribution resulting from a dropped rod test in that reactor. After achieving a rods out, equilibrium xenon condition, a dual element shutdown rod (B-17) was "dropped" by driving it to its fully inserted position, and criticality was maintained by adjustment of the soluble boron concentration. The ratio of incore detector signals after the insertion to those before the insertion represents a measure of the change in power distribution due to the "dropped" rod.

These are compared on Figure 4.3-38A to the changes resulting from the insertion of rod B-17 as predicted by a full core 2-D PDQ calculation performed without fuel or moderator temperature feedbacks. Incore signals at detector level 2 (the axial region from 34 to 46% from core bottom) were used in the comparison, as they are at conditions most closely represented in the 2-D calculation. As can be seen on Figure 4.3-38A, the overall agreement between calculation and measurement is quite good. The calculations overpredict the power increase in peak bundles, as would be expected with the lack of feedback in the calculation.

4.3.3.2 Spatial Stability

4.3.3.2.1 Methods of Analysis

An analysis of xenon induced spatial oscillations may be done by two classes of methods: time dependent spatial calculations and linear modal analysis. The first method is based on a computer simulation of the space, energy, and time dependence of neutron flux and power density distributions. The second method calculates the damping factor based on steady state calculations of flux, importance (adjoint flux), xenon and iodine concentrations, and other relevant variables.

The time dependent calculations are indispensable for studies of the effects of CEA, overpower margin, out of core and incore detector responses, etc. and are performed in one, two, and three dimensions with few group diffusion theory using tested computer codes and realistic modeling of the reactor core.

The linear modal analysis methods are used to calculate the effect on the damping factors of changes in fuel zoning, enrichment, CEA patterns, operating temperature, and power levels. These methods, using information at a single point in time, are particularly suited to survey type calculations. Methods are based on the work of Randall and St. John[33] as extended by Stacey [34]. These methods have been checked against time dependent calculations.

4.3.3.2.2 Radial Xenon Oscillations

To confirm that the radial oscillation mode is extremely stable, a space-time calculation was run for a reflected, zoned core 11 feet in diameter without including the damping effects of the negative power coefficient. The initial perturbation was a poison worth of 0.4 percent in reactivity placed in the central 20 percent in the core for 1 hour. Following removal of the perturbation, the resulting oscillation was followed in 4-hour time steps for a period of 80 hours. As shown in Figure 4.3-29, the resulting oscillation died out very rapidly with a damping factor of about -0.06 per hour. When this damping coefficient is corrected for a finite time mesh by the formula in Reference 35, it is more strongly convergent. On this basis, it is concluded that radial oscillation instability will not occur.

This conclusion is of particular significance because it means that there is no type of oscillation where the inner portions of the core act independently of the peripheral portions of the core whose behavior is most closely followed by the out-of-core flux detectors. Radial mode oscillations, even though highly damped, would be manifested as periodic variation in the out-of-core flux power signal while the delta-T power signals remained constant. Primary reliance is placed on out-of-core flux detectors for the detection of any xenon oscillation.

4.3.3.2.3 Azimuthal Xenon Oscillations

Figures 4.3-39 and 4.3-40 indicate that the eigenvalue separation between the first azimuthal harmonic and the fundamental is about 0.86 percent in λ. The calculated damping coefficient for the first azimuthal mode is -0.016 per hour, and the higher modes will be even more strongly damped. This calculation assumed a moderator coefficient of zero, about 0.7×10^{-4} Δρ/F more positive than for the reactor at full power with equilibrium xenon at BOL. Furthermore, the Doppler coefficient is calculated to be approximately -1.36×10^{-3} Δρ/(kw/ft) which is sufficiently negative to ensure stability of all higher azimuthal modes.

4.3.3.2.4 Axial Xenon Oscillations

To check and confirm the predictions of the linear modal analysis approach numerical space time calculations have been performed for both beginning and end of cycle. The fuel and poison burnup distributions were obtained by depletion with soluble boron control so that the power distribution was strongly flattened. Spatial Doppler feedback was included in these calculations. In Figure 4.3-41, the time variation of the power distribution along the core axis is shown near end of life with reduced Doppler feedback. The initial perturbation used to excite the oscillations was a 50 percent insertion into the top of the core of a 1.5 percent reactivity CEA bank for 1 hour. The damping factor for this case was calculated to be about +0.02 per hour; however, when corrected for finite time mesh intervals by the methods of Reference 35, the damping factor is increased to approximately +0.04. When this damping factor is plotted on Figure 4.3-39 at the appropriate eigenvalue separation for this mode at end of cycle, it is apparent that good agreement is obtained with the modified Randall-St. John prediction (See Figure 4.3-40 for nomenclature).

Calculations performed with both Doppler and moderator reactivity feedback have resulted in damping factors which are essentially the same as those obtained with Doppler feedback alone. This result suggests that the constant power condition which applies to the axial oscillations results in a very weak moderator feedback since the moderator density is fixed at the top and bottom of the core and only the density distribution in between can change.

For the calculated Doppler coefficient of -1.36×10^{-3} Δρ/(kw/ft), it can be seen from Figure 4.3-39 that the damping factor toward the end of the burnup cycle is positive. Thus, within the uncertainties in predicting power coefficients and uncertainties in the analyses, there is a prediction of unstable axial xenon oscillations in the absence of any control action. These oscillations are sufficiently slow (the period of oscillation being 25-30 hours) so that there would be sufficient time to control the oscillations. In addition, automatic protection is provided if operator action is not taken to remedy the situation.

4.3.3.3 Reactor Vessel Fluence Calculational Model

The neutron flux at the inner wall surface of the reactor vessel calculated by combining the results of ANISN[36] and SHADRAC[37] in the equation:

$$\phi(E) = \phi\,(\text{ANISN}) \quad \frac{\phi\,A\ (\text{SHADRAC})}{\phi\,B\ (\text{SHADRAC})}$$

ϕ (E) = the neutron flux at energy E at the inner surface of the vessel

ϕ (ANISN) = the neutron flux calculated by ANISN using a cylindrical model of the reactor

ϕ_A(SHADRAC) = the neutron flux as calculated by SHADRAC in which the exact source geometry and a three dimensional time averaged power distribution are used.

ϕ_B(SHADRAC) = the neutron flux as calculated by SHADRAC using a cylindrical source geometry and the power distribution obtained from ANISN.

The neutron flux as calculated by the above method has uncertainty limits of +20 percent, -40 percent. The total uncertainty is composed of +10 percent, -30 percent in the calculational method and a +10 percent uncertainty in, the combined radial and axial power distribution. The calculational uncertainty factors are obtained by comparing the ANISN-SHADRAC results with measurements [38] from various operating reactors.

4.3.3.4 Axial Peaking Augmentation Factor

The augmentation factor calculational model is discussed in detail in Reference 40, Section 3.0.** Treatment of the augmentation factor for the St. Lucie Plant Unit No. 1 is given in Section 15.1.5.3.

4.3.4 TESTS AND INSPECTIONS

The program of tests and inspections on fuel has been described in Amendment 8 to San Onofre 2 and 3 PSAR (AEC Docket Nos. 50-361 and 362). Preoperational testing is outlined in Chapter 14.

** For Cycle 3 and latter cycles the model was changed. A statistical combination of gaps due to small densification effects near the peak pin and gaps due to large densification effects for the peak pin is now performed. See Cycle 3 RSE p. 13, Reference 41.

REFERENCES FOR SECTION 4.3.3

1. FORM - A Fourier Transform Fast Spectrum Code for the IBM-7090, McGoff, D. J., NAA-SR-Memo 5766 (September- 1960).

2. THERMOS - A Thermalization Transport Theory Code for Reactor Lattice Calculations, Honeck, H., BNL-5816 (July 1961).

3. CINDER - A One Point Depletion and Fission Product Program, England T.R., WAPD-TM-334 (Revised, June 1964).

4. Measurement of Resonance Integral, Hellstrand, Proceedings of National Topical Meeting of the Ans, San Diego, February 7-9, 1966, The M.I.T. Press.

5. ZUT - A Program for the Calculations of Resonance Integrals, Kuncir, G. F., GA-2525 (August 1961).

6. Honeck, H., Description of the Code GAKER , BNL Meirorandum, January 6, 1964.

7. Method of Successive Generations, Stuart, G. W. and Woodruff, R. W., Nuclear Science and Engineering, Vol. 3, P.339 (1958).

8. Escape Probability and Capture Fraction for Grey Slabs, Schiff, D. and Stein, S., WAPD-149 (June 1956).

9. An Analysis of Methods in Control Rod Theory and Comparison with Experiment, Kear, G. N. and Ruderman, M. J., GEAP-3937 (May 1962).

10. Thin Regions in Diffusion Theory Calculations, Wachspress, E. L., Nuclear Science and Engineering, Vol. 3, P. 186 (1958).

11. A Theoretical Method for Determining the Worth of Control Rods, Henry, A. F., WAPD-218 (August 1959).

12. The HAMMER System, Suich, J. E. and Honeck, H.C., DP-LO64, January 1967.

13. DTF-IV, A Fortran-IV Program for Solving the Multigroup Transport Equation with Anisotropic Scattering, Lathrop, K. D., LA-3373, July 15, 1965.

14. MO-807 - A Diffusion Theory Fitting Program Using Fortran-IV, Rutherford, C. N., WAPD-TM-671, September 1967.

15. PDQ-7 Reference Manual, Cadwell, W. R., WAPD-TM-678, (January, 1968).

REFERENCES FOR SECTION 4.3.3 (Cont'd)

16. Breen, R. J., et al, HARMONY - System for Nuclear Reactor Depletion Computation, WAPD-TM-478 (January 1965).

17. Engelder, T. C., et al, Spectral Shift Control Reactor, Basic Physics Program, B&W-1273 (November 1963).

18. Clark, R. H., et al, Physics Verification Program, Final Report B&W-3647-3 (March 1967).

19. Davison, P. W.,et al, Yankee Critical Experiments, YAEC-94 (April 1959).

20. Eich, W. J. and Rocacik, W. P., Reactivity and Neutron Flux Studies in Multi-Region Loaded Cores, WCAP-1433 (1961).

21. Fayer, F. J., et al, An Evaluation of Some Uncertainties in the Comparison Between Theory and Experiments for Regular Light Water Lattices, Brit. Nuc. En. Soc. J., 6 (April 1967).

22. Brown, J. R., et al, Kinetic and Buckling Measurements on Lattices of Slightly Enriched Uranium and UO_2 Rods in Light Water, WAPD-176 (1958).

23. Price, G. A., Uranium-Water Lattice Compilation, Part I, BNL 50035 (T-449) (December 1966).

24. Barrett, L. E., Spectral Shift Control Reactor, Basic Physics Program B&W-1233 (March 1962).

25. Schmid, L. C., et al, Critical Masses and Buckling of PuO_2-UO_2-H_2O Systems, ANS Trans, 1, 216 (1964).

26. Dawson, F. G., Plutonium Utilization Program Annual Report, BNWL-624 (December 1964).

27. Leamer, R. D., PuO_2-H_2O Fueled Critical Experiments, WCAP-3726-1 (July 1967).

28. Bronner, G., et al, Neutronenphysikalische Untersuchungen Bei Inbetriebnahme des KWO, Atomwirtschaft, December 1968, p. 618.

29. Hemmelwright, J. R., The Start-up Test Program of the Conn. Yankee Reactor (September 1967).

30. Chison, L., et al, Yankee Core Evaluation Program - Quarterly Report for the Period Ending September 30, 1963, WCAP-6056, (October 1963).

31. Peck, C. C., AEC-NFS Measurement Data Comparison - Yankee Reactor Fuel, (January 1968).

REFERENCES FOR SECTION 4.3.3 (Cont'd)

32. Sha, W. T., An Experimental Evaluation of the Power Coefficients in Slightly Enrichment PWR Cores, WCAP-3269-40 (1965).

33. Randall, D., "Xenon Spatial Oscillations," Nucleonics, 16, 3, P. 82-86 (1958).

34. Stacey, Jr., W. M., "Linear Analysis of Xenon Spatial Oscillations," Nuc. Sci. Eng., 30, p. 453-455 (1967).

35. Poncelet, C. G., "The Effect of a Finite Time Step Length on Calculated Spatial Xenon Stability Characteristics in Large PWR's," Trans. ANS, 10, 2, p. 571 (1967).

36. Ward W. Engle Jr., "A User's Manual for ANISN, A One-Dimensional Discrete Ordinates Transport Code With Anisotropic Scattering," K-1693, March 30, 1967.

37. SHADRAC, "Shield Heating and Dose Rate Attenuation Calculation," G30-1365, March 25, 1966.

38. D. W. Stephen, "Fast Neutron Attenuation by the P3MG" C-17 Shielding Method," CEND 302, July, 1967.

39. R. A. Rydin, "Higher Flux Mode Effects in Xenon Spatial Oscillations," Nuclear Science and Engineering, 50, 147 (1973).

40. "CE Fuel Evaluation Model," CENPD-139-P-A, (Proprietary) and CENPD-139-A (Non Proprietary), July 1, 1974.

41. Letter R. E. Uhrig (FPL) to V. Stello, Jr. (NRC) Re: St. Lucie Unit 1, Docket No. 50-335, Cycle 3 Reload Safety Evaluation, L-79-45 dated 2/22/79.

42. Letter R. E. Uhrig (FPL) to V. Stello, Jr. (NRC) Re: St. Lucie Unit 1, Docket No. 50-335, Cycle 2 Reload Safety Evaluation, L-78-99 dated 3/22/78.

TABLE 4.3-1
NUCLEAR DESIGN PARAMETERS
(Historical Information)

General	Cycle 1
Fuel Management	3-Batch, Mixed Central Zone
First cycle average burnup, Mwd/MTU	12,800
First cycle lifetime, full power hours	9,940
U-235 enrichments, w/o	
Batch A (69 assemblies)	1.93
Batch B (80 assemblies)	2.33
Batch C (68 assemblies)	2.82
Core average	2.35
H_2/UO_2volume ratio, core (hot, 1st cycle)	2.05
Number of control element assemblies	
Full Length	73
Burnable Poison Rods (shims)	
Number	1296
Material	B_4C-Al_2O_3
Worth, %Δρ (at BOL)	
Hot (568.6F)	8.5
Cold (68F)	7.0
Dissolved Boron	
Dissolved boron content for criticality, ppm, (CEA's withdrawn, beginning-of-life)	
Cold (68F)	945
Hot, zero power, clean (532F)	965
Hot, full power, (568.6F)	820
Hot, equilibrium xenon, full power	590
Dissolved boron content provided for refueling, ppm, (first cycle/later cycles)	1720/2150
Boron worth, ppm/%Δρ	
Hot (568.6F)	82
Cold (68F)	65
Maximum Reactivity Addition Rates (%Δρ/min) at beginning of life	
Hot Full Power	0.024
Hot Zero Power	0.027

TABLE 4.3-1 (Con't)

Plutonium Buildup (at end of 1st cycle)

Gms Fissile Pu (final) / Kg U (original)	4.2
Gms Pu (final) / Kg U original)	5.4

Neutron Lifetime

Beginning of Life (BOL) 29.05 μ seconds
End of Life (EOL) 31.4 μ seconds

TABLE 4.3-2
Cycle 1
(Historical Information)

EFFECTIVE MULTIPLICATION FACTORS AND REACTIVITY
(No Control Element Assemblies or Dissolved Boron, Initial Core)

	k_{eff}	ρ	ρ
Cold (68F)	1.170	0.145	-
Hot, 532F, Zero Power	1.134	0.118	-
Hot, Full Power, No Xe or Sm (568.6F)	1.111	0.100	-
Hot, Full Power, Equilibrium Xe	1.078	0.072	-
Hot, Full Power, Equilibrium Xe, Sm (Reactivity available for depletion)	1.073	0.068	-
Reactivity Decrease, Hot			
Zero to Full Power, BOL	-	-	0.018
Fuel Temperature	-	-	0.014
Moderator Temperature	-	-	0.004
Reactivity Decrease, Hot			
Zero to Full Power, EOC	-	-	0.020
Fuel Temperature	-	-	0.014
Moderator Temperature	-	-	0.006

TABLE 4.3-2A

PLANAR PEAKING FACTORS FOR SEQUENTIAL INSERTION
OF CEA GROUPS AT HOT FULL POWER - CYCLE 1
(Historical Information)

		BEGINNING OF LIFE	END OF FIRST CYCLE
Bank	7	1.43	1.42
	7+PLR	1.42	1.40
	7+6	1.45	1.41
	7+6+PLR	1.65	1.57
	7+6+5	1.75	1.68
	7+6+5+PLR	-	1.82
	7+6+5+4	1.55	1.52
	7+6+5+4+PLR	-	1.64
	7+6+5+4+3	1.78	1.79
	7+6+5+4+3+PLR	-	1.84
	7+6+5+4+3+2	1.77	1.79
	7+6+5+4+3+2+PLR	-	2.27
	7+6+5+4+3+2+1	2.22	2.21
	7+6+5+4+3+2+1+PLR	-	2.60

TABLE 4.3-3
REACTIVITY COEFFICIENTS - CYCLE 1 (CEA's WITHDRAWN)
(Historical Information)

Moderator Temperature Coefficient,Δρ /F	
Beginning-of-Life, 820 ppm Boron	
Cold, (68F)	-0.1×10^{4}
Hot Zero Power, (532F)	-0.2×10^{4}
Hot Full Power, (563.6F)	-0.4×10^{4}
Hot Full Power, Equilibrium Xe	-0.7×10^{-4}
End-of-Cycle, 0 ppm Boron	
Cold, (68F)	-0.4×10^{4}
Hot Zero Power, (532F)	-1.4×10^{-4}
Hot Full Power Equilibrium Xe	-2.1×10^{-4}
Moderator Density Coefficient,Δρ/(gm/cc)	
Hot, Operating (568.6F)	
Beginning-of-Life, 820 ppm Boron	+0.04
End-of-Life, 0 ppm Boron	+0.19
Fuel Temperature Contribution to Power Coefficient, Δρ(kw/ft)	
Hot, Zero Power	$-3.34\ 10^{-3}$
Full Power (BOL)	-1.36×10^{-3}
Moderator Void Coefficient,Δρ/% Void	
Hot, Operating (568.6F)	
Beginning-of-Life, 820 ppm Boron	-0.26×10^{-3}
End-of-Cycle, 0 ppm Boron	-1.35×10^{-3}
Moderator Pressure Coefficient,Δρ/psi	
Hot, Operating (568.6F)	
Beginning-of-Life, 820 ppm Boron	$+0.49 \times 10^{-6}$
End-of-Cycle, 0 ppm Boron	$+2.55 \times 10^{-6}$
Overall Power Coefficient,Δρ/ (kw/ft)	
Hot, Operating (568.6F)	
Beginning-of-Life, 820 ppm Boron	-1.60×10^{-3}
End-of-Cycle, 0 ppm boron	-2.65×10^{-3}

TABLE 4.3-4

WORTHS OF CEA GROUPS, %Δρ Cycle 1
(Historical Information)

	Beginning of Life		End of First Cycle	
	260F Hot, Full Power		260F Hot, Full Power	
Shutdown CEAs				
Group A	3.39	4.41	3.31	4.36
Group B	0.07	0.46	0.07	0.49
Regulating CEAs				
Group 1	0.29	0.78	0.30	0.80
Group 2	0.82	1.60	0.83	1.61
Group 3	1.13	0.59	1.13	0.59
Group 4	1.22	1.46	1.19	1.43
Group 5	0.07	0.40	0.06	0.37
Group 6	0.20	0.58	0.20	0.58
Group 7	0.60	0.74	0.62	0.77

TABLE 4.3-4A

AXIAL SHAPE INDICES

INTERNAL AXIAL SHAPE INDEX: $I_I = \frac{P_L - P_U}{P_L + P_U}$

WHERE P_L = TOTAL POWER GENERATED IN THE LOWER HALF CORE

P_u = TOTAL POWER GENERATED IN UPPER HALF OF CORE

$P_L + P_U$ = TOTAL POWER

PERIPHERAL AXIAL SHAPE INDEX: $I_P = \frac{P_{PL} - P_U}{P_{PL} + P_{PU}}$

WHERE P_{PL} = TOTAL POWER GENERATED IN LOWER HALF OF PERIPHERAL FUEL BUNDLES ADJACENT EX-CORE DETECTORS

P_{PU} = TOTAL POWER GENERATED IN UPPER HALF OF PERIPHERAL BUNDLES ADJACENT EX-CORE DETECTORS

EXTERNAL AXIAL SHAPE INDEX: $I_E = \frac{D_L - D_U}{D_L + D_U}$

WHERE D_L = DETECTOR RESPONSE IN LOWER EX-CORE DETECTOR SEGMENTS

D_U = DETECTOR RESPONSE IN UPPER EX-CORE DETECTOR SEGMENTS

$D_L + D_U$ = TOTAL EX-CORE DETECTOR RESPONSE

TABLE 4.3-5
Cycle 1

CEA REACTIVITY ALLOWANCES,%Δρ
HOT FULL POWER TO HOT ZERO POWER
(Historical Information)

Fuel Temperature Variation	1.6
Moderator Temperature Variation (including loss in CEA worth)	1.6
Moderator Voids	0.1
Transient Xenon Reactivity	0.4
CEA Bite and Boron Leadband	0.2
Shutdown Margin and Accident Analysis Allowance	2.45
Total Reactivity Allowance	6.35

TABLE 4.3-6
Cycle 1
COMPARISON OF CALCULATED CEA WORTHS AND REQUIREMENTS,%Δρ
(Historical Information)

	Beginning of Life	End of First Cycle
All Standard CEAs Inserted, Cold (68F)	6.4	6.4
All Standard CEAs Inserted, Hot (568.6F) Full Power	11.0	11.0
Maximum Stuck Rod Worth, Hot (568.6F) Full Power	2.8	2.8
CEA Worth for the Case of the Highest Worth CEA Withdrawn, Hot (568.6F) Full Power	8.2	8.2
Total Reactivity Requirement (TAble 4.3-5)	6.65	6.65
Excess Over Nominal Design Requirement	1.55	1.55

TABLE 4.3-7

FUEL ROD DESCRIPTION
(Historical Information)

Laboratory	Clad OD (in.)	Clad Thickness (in.)	Clad Material	Fuel Pellet OD (in.)	Fuel Density (gm/cc)	Fuel Enrichment w/o U-235	w/o PuO_2
B&W	0.4755	0.016	SS 304	0.440	9.46	4.020	0
B&W	0.4748	0.032	AL 6061	0.4054	10.24	2.459	0
Yankee	0.3383	0.0161	SS 304	0.3000	10.18	2.700	0
Winfrith	0.4301	0.01051	SS 304	0.3984	10.44	3.003	0
Brookhaven	0.499	0.02743	SS 304	0.4441	9.30	3.006	0
Bettis	0.453	0.028	Al	0.3830	10.53	1.311	0
Hanford	0.426	0.027	Zr-2	0.372	9.646*	0.22	1.50
Battelle N. W. Westinghouse	0.568	0.030	Zr-2	0.508	9.869*	0.72	2.20

*effective fuel density

TABLE 4.3-8

RESULTS OF ANALYSIS OF CRITICAL AND SUBCRITICAL $U0_2$ SYSTEMS
(Historical Information)

Lattice		w/o U-235	Pitch (in.)	H_20/UO_2	Boron (ppm)	K_{eff}	Ref
B&W-1273	1	4.020	0.595	1.137	0	0.9998	17
	2	4.020	0.595	1.137	3390	1.0018	17
	3	4.020	0.571	0.956	0	0.9963	17
	4	2.459	0.595	1.371	0	1.0009	17
	5	2.459	0.595	1.371	1675	1.0016	17
B&W-3467	6	2.459	0.644	1.846	0	1.0004	18
	7	2.459	0.644	1.846	864	1.0014	18
	8	2.459	0.644	1.846	1536	0.9997	18
Yankee	9	2.700	0.405	1.048	0	0.9965	19
	10	2.700	0.435	1.405	0	0.9979	19
	11	2.700	0.470	1.853	0	0.9990	19
	12	2.700	0.493	2.166	0	1.0004	*20*
Winfrith	13(20C)	3.003	0.520	1.001	0	0.9987	*21*
	14(80C)	3.003	0.520	1.001	0	0.9977	*21*
	15	3.003	0.735	3.164	0	1.0009	21
	16	3.003	0.492	0.779	0	0.9992	21
Bettis	17	1.311	0.6133≠	1.429	0	0.9963	22
	18	1.311	0.6133≠	1.429	0	0.9963	22
	19	1.311	0.6133≠	1.429	0	0.9970	22
	20	1.311	0.6504≠	1.781	0	0.9962	22
	21	1.311	0.6504≠	1.781	0	0.9975	22
	22	1.311	0.7110≠	2.401	0	0.9968	22
	23	1.311	0.7110≠	2.401	0	0.9975	22
BNL[(a)]	24	3.006	0.6767≠	1.319	0	0.9997	23
	25	3.006	0.6767≠	1.319	1363	0.9932	23
	26	3.006	0.7163≠	1.632	0	0.9964	23
	27	3.006	0.7163≠	1.632	470	0.9950	23
	28	3.006	0.7163≠	1.632	992	0.9931	23
	29	3.006	0.7163≠	1.632	1345	0.9940	23
	30	3.006	0.7706≠	2.091	0	0.9981	23
	31	3.006	0.7706≠	2.091	1141	0.9931	23
B&W[(a)]	32 (66F)	4.020	0.595	1.137	0	1.0046	24
	33 (103F)	4.020	0.595	1.137	0	1.0036	24
	34 (203F)	4.020	0.595	1.137	0	1.0003	24
	35 (308F)	4.020	0.595	1.137	0	0.9992	24
	36 (406F)	4.020	0.595	1.137	0	1.0010	24

≠ Triangular Pitch

(a) Subcritical Measurements

TABLE 4.3-9

RESULTS OF ANALYSIS OF PuO_2-UO_2 FUELED LATTICES
(Historical Information)

Lattice	w/o U-235	w/o PuO_2	Pitch (in.)	H_2O/Fuel	Boron (ppm)	K_{eff}	Ref
Hanford	0.22	1.50	0.55≠	1.099	0	1.0027	25
			0.60≠	1.557	0	1.0056	25
			0.71≠	2.705	0	1.0108	25
			0.80≠	3.788	0	1.0094	25
BNWL	0.72	2.2(1)	0.85≠	1.837	0	1.0056	26
			0.93≠	2.445	0	1.0099	26
WCAP	0.72	2.2(1)	0.69	1.099	0	0.9994	27
			0.75	1.525	0	1.0058	27
			0.67	1.099	261	0.9998	27
			0.9758	3.448	261	1.0122	27
			0.69	1.099	526	1.0005	27
			0.9758	3.448	526	1.0099	27
BNWL	0.72	2.2(2)	0.93≠	2.445	0	1.0112	26
			1.05≠	3.461	0	1.0068	26
BNWL	0.72	2.2(3)	0.85≠	1.837	0	1.0113	26
			0.93≠	2.445	0	1.0123	26
WCAP	0.72	2.2(3)	0.9758	3.448	0	1.0206	27

≠ Triangular Pitch

(1) 7.654 w/o Pu-240 in Pu
(2) 16.54 w/o Pu-240 in Pu
(3) 23.503 w/o Pu-240 in Pu

TABLE 4.3-10
REACTION RATES
(Historical Information)

Babcock and Wilcox

Lattice	ρ_{28}		δ_{25}	
	Meas.	Calc.	Meas.	Calc.
1	4.12±.31	4.28	.254±.006	.276
3	5.08±.10	5.11	.307±.002	.333
4	2.28±.03	2.31	.151±.001	.152

Lattice	ρ_{28}		δ_{25}		MCR	
	Meas.	Calc.	Meas.	Calc.	Meas.	Calc.
6	1.85±.02	1.77	.063±.006	.0516	.484±.011	.488

Winfrith

Lattice	RCR		δ_{28}		Pu239/U235	
	Meas.	Calc.	Meas.	Calc.	Meas.	Calc.
13	4.158±.03	4.156	.0845±.0009	.0830	1.589±.009	1.623
14	4.293±.047	4.263	.0881±.0027	.0848	1.637±.009	1.631
16	4.789±.053	4.810	.1050±.0018	.0988	1.661±.009	1.702

Definitions:

ρ_{28} = epicadmium captures in U-238/subcadmium captures in U-238

δ_{25} = epicadmium fissions in U-235/subcadmium fissions in U-235

δ_{28} = total fissions in U-238/total fissions in U-235

MCR = captures in U-238/fissions in U-235

RCR = MCR in lattice/MCR in thermal column

TABLE 4.3-10 (Cont'd)

Bettis

Lattice	ρ_{28}		δ_{28}		δ_{25}	
	Meas.	Calc.	Meas.	Calc.	Meas.	Calc.
17	.143±.01	1.375	.078±.004	.0718	.089±.002	.0913
20	1.15±.01	1.146	.070±.004	.0612	.072±.001	.0744
23	.934±.01	.893	.057±.003	.0491	.055±.001	.0571

Brookhaven

Lattice	ρ_{28}		δ_{28}	
	Meas.	Calc.	Meas.	Calc.
24	2.92±.09	3.01	.065	.0626
26	2.41±.04	2.46	.056	.0535
30	1.81±.06	1.96	.048	.0443

TABLE 4.3-11

YANKEE ROWE CORE I

INVENTORY CHANGE COMPARISON

	U-235 Dep. (kg)	Total Pu. (kg)	Fiss. Pu. (kg)	Fissile Consumption (g/Mwd)
NFS Meas.	171.0±4.7	91.1±1.0	80.27±0.88	0.535±0.028
1-D	170.8	91.0	80.88	0.530
3-D	169.0	89.9	79.48	0.528

TABLE 4.3-12

MODERATOR TEMPERATURE COEFFICIENTS IN
THE CONNECTICUT YANKEE AND MAINE YANKEE
REACTORS AT START OF LIFE

Reactor	Moderator Temperature °F	Dissolved Boron Concentration, PPM	Rod Worth Inserted %	Moderator Temperature Coefficient 10^{-4} Δρ/F	
				Calculated	Measured
Connecticut Yankee	260	2,040	Unrodded	0.46	0.57
	560	2,305	Unrodded	0.84	1.00
	560	2,045	1.8	0.37	0.47
	560	1,730	4.5	-0.23	-0.25
	560	1,610	5.6	-0.30	-0.30
Maine Yankee	270	910	Unrodded	-0.03	0.20
	525	910	Unrodded	0.26	0.18

TABLE 4.3-13

MAINE YANKEE SEQUENTIAL CEA GROUP WORTH

CEA GROUP INSERTED	INCREMENTAL WORTH, %Δρ(at 525F) MEASURED	CALCULATED
5	0.55	0.58
4	0.35	0.38
3	0.89	0.93
2	0.83	0.95
1	0.77	0.80
C	1.16	1.23
B	0.73	0.75
A	4.04	3.76
TOTAL	9.32	9.38

TABLE 4.3-14

COMPARISON OF CALCULATED AND
MEASURED DROPPED AND
EJECTED ROD WORTHS, %Δρ

		Measured	Calculated
A.	Palisades		
	Ejected Rods		
	1. corner Rod from 9 rod pattern*	0.27	0.25
	2. corner Rod from 13 rod pattern	0.64	0.71
B.	Maine Yankee		
	Ejected Rods		
	1. center Rod from 9 rod pattern	0.13	0.15
	2. corner Rod from 29 rod pattern	0.33	0.27
	Dropped Rods		
	3. central dual with bank 5 in	0.14	0.15
C.	Omaha		
	Ejected Rod		
	1. peripheral rod from zero power PDIL	0.28	0.29
	Dropped Rod		
	2. peripheral dual from full power PDIL	0.15	0.14
	3. more central dual from full power PDIL	0.19	0.18

* 5 rods inserted 50%, others bottomed

TABLE 4.3-17

Comparison of Peak 0° and 15° Azimuth Vessel ID Fluence Values at 52 EFPY		
Source	Azimuthal Location	Surface (n/cm2, E > 1.0 MeV)
Pre-EPU	0°	4.24E+19
EPU analysis	0°	4.036E+19
Pre-EPU	15°	2.81E+19
EPU Analysis	15°	2.630E+19

TABLE 4.3-18

EFPY	Azimuthal Location	Fluence at Clad-Base Metal Interface (n/cm2, E>1.0 MeV)	¼ t Fluence (n/cm2,E>1.0 MeV)	¾ t Fluence (n/cm2,E>1.0 MeV)
35	0°	2.573E+19	1.534E+19	5.448E+18
35	15°	1.659E+19	9.888E+19	3.512E+18
52	0°	4.036E+19	2.405E+19	8.545E+18
52	15°	2.630E+19	1.567E+19	5.568E+18
54	0°	4.208E+19	2.508E+19	8.909E+18
54	15°	2.744E+19	1.635E+19	5.810E+18

4.3.5 SIEMENS NUCLEAR POWER ANALYTICAL METHODS (CYCLES 6-13)

The methods used in the core analysis are described in References 1 through 6. In summary, the reference neutronic design analysis of the reload core was performed using the XTGPWR reactor simulator code. The input isotopics data were based on quarter core depletion calculations performed using the XTGPWR code. The fuel shuffling between cycles was accounted for in the calculations.

Calculated values of LHR and F, were determined with the XTGPWR reactor model. The calculational thermal-hydraulic feedback and axial exposure distribution effects on power shapes, rod worths, and cycle lifetime are explicitly included in the analysis.

4.3.5.1 References for Section 4.3.5

1. XN-CC-28(A), Revision 3, "XTG-A, Two Group Three Dimensional Reactor Simulator Utilizing coarse Mesh Spacing," Exxon Nuclear Company, January 1975.

2. XN-75-27(A), "Exxon Nuclear Neutronics Design Methods for Pressurized Water Reactors," Exxon Nuclear Company, June 1975.

3. XN-75-27(A), Supplement 1, September 1976.

4. XN-75-27(A), Supplement 3, November 1980.

5. XN-75-27(A), Supplement 3, November 1980.

6. XN-75-27(A), Supplement 4, December 1985.

THIS PAGE INTENTIONALLY BLANK

4.3.6 CORE DESCRIPTION

The St. Lucie Unit 1 reactor consists of a combination of fresh and burned fuel for a total of 217 assemblies, each having a 14x14 fuel rod array. The assemblies are composed of up to 176 fuel rods, a number (0, 4, 8, 12, 16 or 20) of Gd bearing burnable poison rods and 5 control rod guide tubes or 4 control rod guide tubes and 1 instrument tube. The fuel rods consist of pellets inserted into zirconium alloy. The control rod guide tubes and instrument tubes are also made of zircaloy. Each fuel assembly contains nine zircaloy spacers with Inconel springs. A description of fuel design and design methods is contained in References 1 and 2. EC292529 EC292529 EC292529

The assemblies consist of enriched UO_2 fuel rods and UO_2-Gd_2O_3 bearing rods (gadolinia burnable absorber fuel rods.) UO_2 fuel rods have a central zone enrichment of ≤4.6 U-235 (with radically zoned rods reduced by 0.4 w/o U-235), whereas the UO_2-Gd_2O_3 rods have a central zone of 2, 4, 6, and 8 w/o Gd_2O_3 dispersed in reduced w/o U-235 carriers. The axial blankets (UO_2 fuel rods) and cutback regions (UO_2-Gd_2O_3 bearing rods) are enriched with 2.6 w/o U-235. EC292529

Typical reload enrichments and burnable absorber characteristics are given in Table 4.1-2. The core contains only Framatome fuel assemblies. EC292529

A low radial leakage fuel management plan is used for St. Lucie Unit 1. The fresh assemblies loaded in the core interior contain gadolinia-bearing fuel in order to control power peaking and reduce the initial boron concentration to maintain the MTC within its Technical Specifications and Core Operating Limits Report limits. The exposed fuel is also loaded in a manner to control the power peaking.

4.3.6.1 References for Section 4.3.6

1. XN-NF-82-09(A), "Generic Mechanical Design Report Exxon Nuclear 14x14 Fuel Assemblies for Combustion Engineering Reactors," Exxon Nuclear Company, November 1982.

2. XN-NF-82-97, "St Lucie Unit 1 Addendum to Generic Mechanical Design Report Exxon Nuclear 14x14 Fuel Assemblies for Combustion Engineering Reactors,"-.Exxon Nuclear Company, December 1982.

4.3.7 CONTROL ROD REACTIVITY REQUIREMENTS

Table 4.3-6 (Cycle 1) shows the reactivity worths of the full complement of CEAs, with and without the highest worth CEA in the fully withdrawn position, at beginning and end of cycle. This table also compares the available net shutdown worth (including the effects of the stuck CEA) to the reactivity worth requirements from Table 4.3-5 (Cycle 1). Ample margin is available to accommodate uncertainties in the calculated CEA worth. A comparison between calculated and measured CEA worths is discussed in Section 4.3.3.

Shutdown margin evaluation is shown in Table 4.3-15.

The control rod groups and insertion limits are specified in the Technical Specifications/COLR. The impact of the CEA changeout at Cycle 9 was evaluated and addressed in Reference 1. The implementation of the redesigned CEAs in Cycle 20 is evaluated as part of the reload PCM for that cycle.

4.3.7.1 References for Section 4.3.7

1. Letter, T J Helbling (ANF) to A R Morse, TJH:048:88, dated March 8, 1988.

TABLE 4.3-15

TYPICAL SHUTDOWN MARGIN

Control Rod Worth (pcm)	EOC HZP
ARI	9483
N-1	7338
Power Dependent Insertion Limit (PDIL)	1362
[(N-1) - PDIL] (0.9)	5378
Shutdown Margin (pcm)	
Required Shutdown Margin	3600
Excess Shutdown Margin	1778

TABLE 4.3-16

TYPICAL ST. LUCIE UNIT 1 NEUTRONICS CHARACTERISTICS

	BOC	EOC
Critical Boron (ppm)		
HFP, ARO, Equilibrium Xenon	985	0
HZP, ARO No Xenon	1501	--
Moderator Temperature Coefficient (pcm/°F)		
HFP	-8.8	-29.9
HZP	2.4	-10.6
Doppler Coefficient (pcm/°F)	-1.2	-1.4
LHR, HFP (kW/ft)[(a)] Eq. Xe.	13.6	--
Control Rod Worth, N-1, HZP (pcm)	6688	7338
Excess Shutdown Margin, HZP (pcm)	1387	1778

(a) Including Uncertainties

Batch	No. Assemblies	Shims/ Assembly
A	69	0
B	80	12
C	40	0
C•	12	12(Low Conc)
C+	16	12(High Conc)

	A	B	C	D	E	F	G	J	L	
1								C	C	1
2					C	C	C+	C+	B	2
3				C	C•	B	A	B	A	3
4				C•	B	A	B	A	B	4
5			C	C•	B	A	B	A	B	A	5
6			C	B	A	B	A	B	A	B	6
7			C+	A	B	A	B	A	B	A	7
8		C									
9			C+	B	A	B	A	B	A	B	9
10		C									
11			B	A	B	A	B	A	B	A	11

Shimmed Fuel Assembly

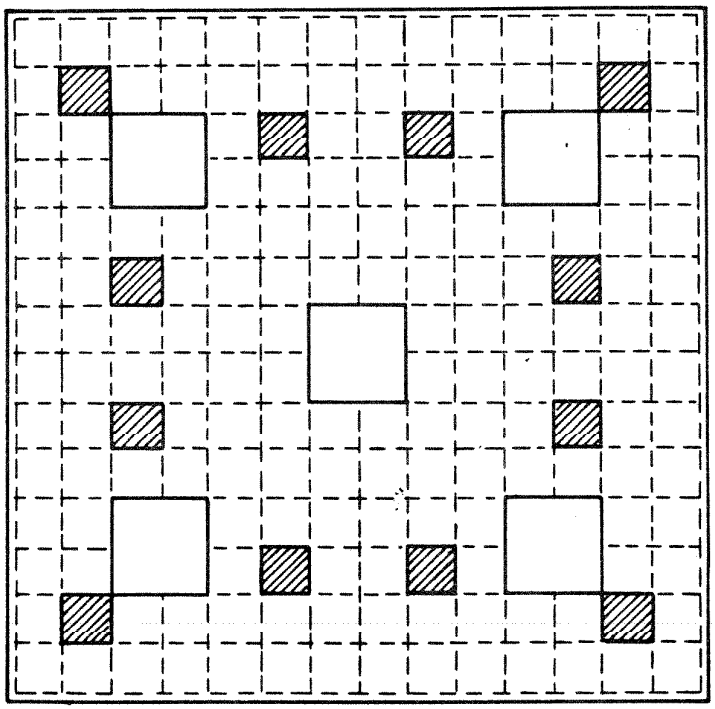

POISON ROD

FUEL ROD

CEA GUIDE TUBE

Am. 3-7/85

FLORIDA POWER & LIGHT CO. St. Lucie Plant Unit 1	Cycle 1 BURNABLE POISON ROD DISTRIBUTION	Figure 4.3-1

Note: See Section 4.3.5, Table 4.3.5-1 & Figure 4.3.5-2.

FLORIDA POWER & LIGHT CO.
St. Lucie Plant
Unit 1

Planar Average Core Power Distribution
2560 Mwt 1st Core
Beginning of Life, No Xenon

Figure 4.3-2

Am. 3-7/85

ENRICHMENT TYPE

X
0.80 — BOX PEAKING FACTOR
0.80 — ENTHALPY RISE FACTOR
0.80 — PIN PEAKING FACTOR

MAXIMA

BOX PEAKING FACTOR	1.20
ENTHALPY RISE FACTOR	1.27
PIN PEAKING FACTOR	1.30

	A	B	C	D	E	F	G	H	J	K	L	
								C 0.59 0.99 1.01		C 0.78 1.07 1.09		1
					C 0.58 0.95 0.98	C 0.80 1.09 1.12	C+ 0.95 1.24 1.24	C+ 1.09 1.20 1.23		B 0.95 1.06 1.08		2
				C 0.68 1.06 1.09	C. 1.01 1.17 1.20	B 0.95 1.07 1.09	A 1.01 1.08 1.11	B 1.04 1.13 1.15		A 1.03 1.10 1.14		3
			C 0.68 1.06 1.09	C. 1.05 1.20 1.23	B 0.99 1.10 1.11	A 1.02 1.09 1.16	B 1.07 1.16 1.18	A 1.07 1.14 1.18		B 1.10 1.17 1.20		4
		C 0.58 0.95 0.98	C. 1.01 1.17 1.20	B+ 0.99 1.10 1.11	A 1.03 1.10 1.14	B+ 1.09 1.17 1.20	A 1.09 1.17 1.20	B 1.13 1.21 1.23		A 1.11 1.19 1.22		5
		C 0.80 1.09 1.12	B 0.95 1.07 1.09	A 1.02 1.09 1.13	B 1.09 1.17 1.19	A 1.10 1.17 1.21	B 1.15 1.22 1.25	A 1.14 1.21 1.25		B 1.17 1.24 1.26		6
		C+ 0.95 1.24 1.24	A 1.01 1.08 1.11	B 1.07 1.16 1.18	A 1.09 1.17 1.20	B 1.15 1.22 1.25	A 1.15 1.22 1.26	B 1.19 1.26 1.28		A 1.17 1.24 1.28		7
8	C 0.59 0.99 1.01											
		C+ 1.09 1.20 1.23	B 1.04 1.13 1.15	A 1.07 1.14 1.18	B 1.13 1.21 1.23	A 1.14 1.21 1.25	B 1.19 1.26 1.28	A 1.18 1.25 1.29		B 1.20 1.27 1.30		9
10	C 0.78 1.07 1.09											
		B 0.95 1.06 1.08	A 1.03 1.10 1.14	B 1.10 1.17 1.20	A 1.11 1.19 1.22	B 1.17 1.24 1.26	A 1.17 1.24 1.28	B 1.20 1.27 1.30		A 1.19 1.26 1.30		11

℄

FLORIDA POWER & LIGHT CO.
St. Lucie Plant
Unit 1

Planar Average Core Power Distribution
2560 Mwt 1st Core
Beginning of Life, Equilibrium Xenon

Figure 4.3-3

Am. 3-7/85

ENRICHMENT TYPE

X
0.00 ← BOX PEAKING FACTOR
0.00 ← ENTHALPY RISE FACTOR
0.00 ← PIN PEAKING FACTOR *

MAXIMA

BOX PEAKING FACTOR 1.22
ENTHALPY RISE FACTOR 1.29
PIN PEAKING FACTOR 1.32 *

	A	B	C	D	E	F	G	H	J	K	L	
								C 0.58 0.96 0.98		C 0.76 1.04 1.06		1
					C 0.57 0.94 0.96	C 0.78 1.07 1.10	C+ 0.94 1.22 1.23		C+ 1.07 1.18 1.21		B 0.93 1.05 1.07	2
			C 0.67 1.04 1.07		C 0.99 1.16 1.19	B 0.94 1.07 1.09	A 1.00 1.08 1.11		B 1.04 1.13 1.15		A 1.03 1.10 1.14	3
			C 0.67 1.04 1.07	C 1.04 1.18 1.22	B 0.98 1.10 1.12	A 1.02 1.10 1.13	B 1.08 1.17 1.19		A 1.08 1.15 1.19		B 1.11 1.19 1.21	4
		C 0.57 0.94 0.96	C 0.99 1.16 1.19	B 0.98 1.10 1.12	A 1.04 1.11 1.15	B 1.10 1.19 1.21	A 1.11 1.18 1.22		B 1.14 1.23 1.25		A 1.13 1.21 1.24	5
		C 0.78 1.07 1.10	B 0.94 1.07 1.09	A 1.02 1.10 1.13	B 1.10 1.19 1.21	A 1.11 1.19 1.23	B 1.16 1.25 1.27		A 1.16 1.24 1.27		B 1.18 1.26 1.28	6
		C+ 0.94 1.22 1.23	A 1.00 1.08 1.11	B 1.08 1.17 1.19	A 1.11 1.18 1.22	B 1.16 1.25 1.27	A 1.17 1.24 1.28		B 1.20 1.28 1.30		A 1.19 1.26 1.30	7
8		C 0.58 0.96 0.98										
		C+ 1.07 1.18 1.21	B 1.04 1.13 1.15	A 1.08 1.16 1.19	B 1.14 1.23 1.25	A 1.15 1.24 1.27	B 1.20 1.28 1.30		A 1.20 1.27 1.31		B 1.22 1.29 1.32	9
10		C 0.76 1.04 1.06										
℄		B 0.93 1.05 1.07	A 1.03 1.10 1.14	B 1.11 1.19 1.21	A 1.13 1.21 1.24	B 1.18 1.26 1.28	A 1.19 1.26 1.30		B 1.22 1.29 1.32		A 1.21 1.28 1.32	11

FLORIDA POWER & LIGHT CO.
St. Lucie Plant
Unit 1

Planar Average Core Power Distribution
2560 Mwt 1st Core
End of Cycle, Equilibrium Xenon

Figure 4.3-4

Am. 3-7/85

ENRICHMENT TYPE

X

0.00 BOX PEAKING FACTOR

0.00 ENTHALPY RISE FACTOR

0.00 PIN PEAKING FACTOR *

MAXIMA

BOX PEAKING FACTOR 1.17
ENTHALPY RISE FACTOR 1.26
PIN PEAKING FACTOR 1.30 *

	A	B	C	D	E	F	G	J	L	
							H	K		
							C 0.57 0.91 0.92	C 0.72 0.99 1.00		1
					C 0.56 0.90 0.92	C 0.76 1.04 1.05	C+ 0.95 1.18 1.22	C+ 1.11 1.26 1.30	B 1.07 1.17 1.21	2
			C 0.65 1.01 1.02	C. 1.01 1.21 1.24	B 1.05 1.16 1.20	A 1.00 1.08 1.09	B 1.15 1.21 1.25	A 1.05 1.09 1.11		3
		C 0.65 1.01 1.02	C. 1.05 1.23 1.27	B 1.12 1.19 1.23	A 1.04 1.09 1.11	B 1.16 1.21 1.25	A 1.06 1.09 1.11	B 1.17 1.21 1.25		4
	C 0.56 0.90 0.92	C. 1.01 1.21 1.24	B 1.12 1.19 1.23	A 1.05 1.10 1.12	B 1.17 1.21 1.25	A 1.06 1.09 1.11	B 1.17 1.21 1.25	A 1.05 1.09 1.11		5
	C 0.76 1.04 1.05	B 1.05 1.16 1.20	A 1.04 1.09 1.11	B 1.17 1.21 1.25	A 1.06 1.10 1.12	B 1.16 1.20 1.24	A 1.04 1.08 1.10	B 1.15 1.19 1.23		6
	C+ 0.95 1.18 1.22	A 1.00 1.08 1.09	B 1.16 1.21 1.25	A 1.08 1.09 1.11	B 1.16 1.20 1.24	A 1.04 1.08 1.10	B 1.14 1.18 1.22	A 1.03 1.07 1.08		7
8	C 0.57 0.91 0.92									
	C+ 1.11 1.26 1.30	B 1.15 1.21 1.25	A 1.06 1.09 1.11	B 1.17 1.21 1.25	A 1.04 1.08 1.10	B 1.14 1.18 1.22	A 1.02 1.06 1.08	B 1.13 1.16 1.20		9
10	C 0.72 0.99 1.00									
℄	B 1.07 1.17 1.21	A 1.05 1.09 1.11	B 1.17 1.21 1.24	A 1.05 1.09 1.11	B 1.15 1.19 1.23	A 1.03 1.07 1.08	B 1.13 1.16 1.20	A 1.02 1.05 1.07		11

FLORIDA POWER & LIGHT CO.
St. Lucie Plant
Unit 1

Planar Average Core Power Distribution
2560 Mwt 1st Core, Rod Bank 7 Fully Inserted
Beginning of Life, No Xenon

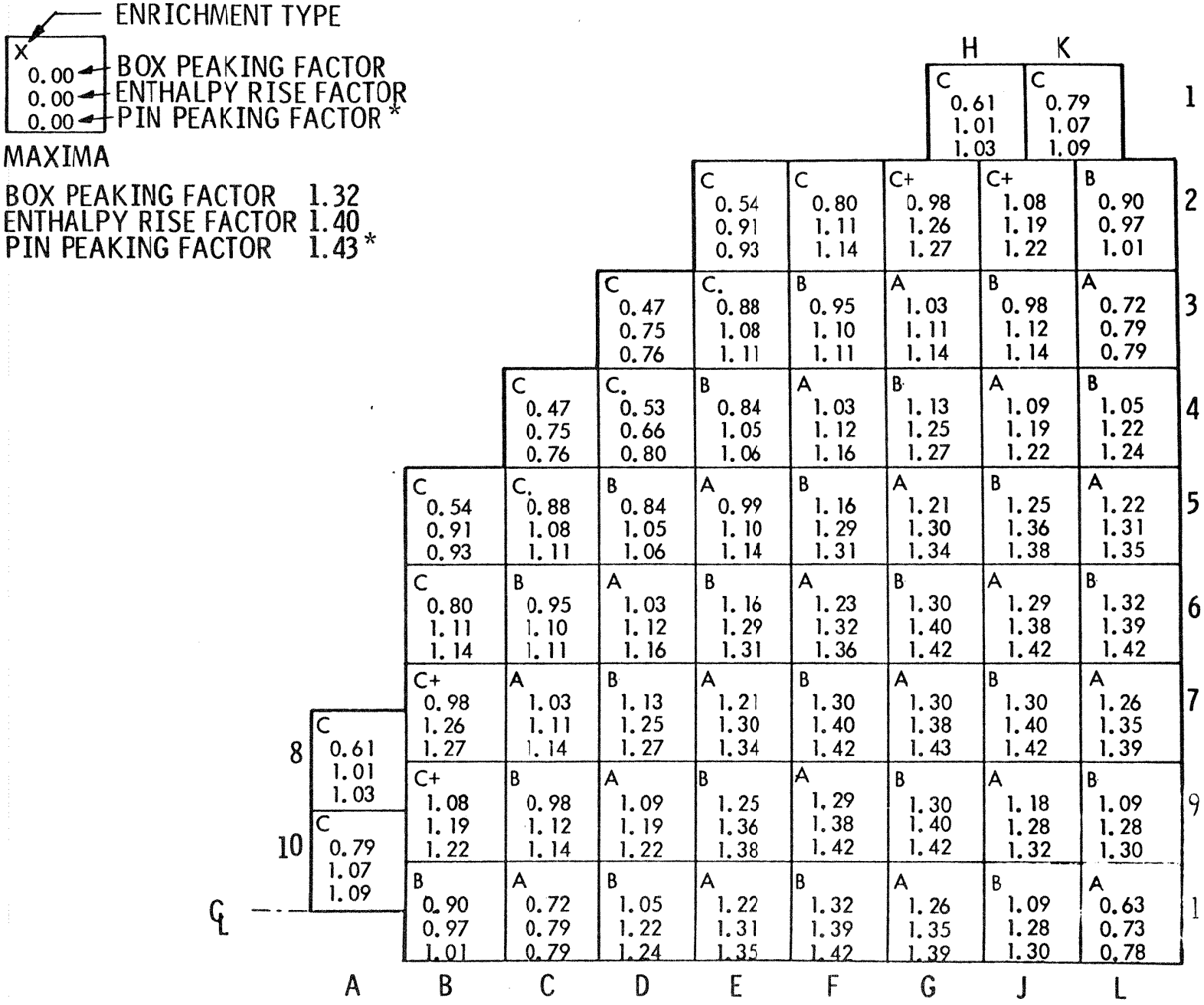

Am. 3-7/85

Figure 4.3-5

FLORIDA POWER & LIGHT CO.
St. Lucie Plant
Unit 1

Planar Average Core Power Distribution
2560 Mwt 1st Core, Rod Bank 7 Fully Inserted
Beginning of Life, Equilibrium Xenon

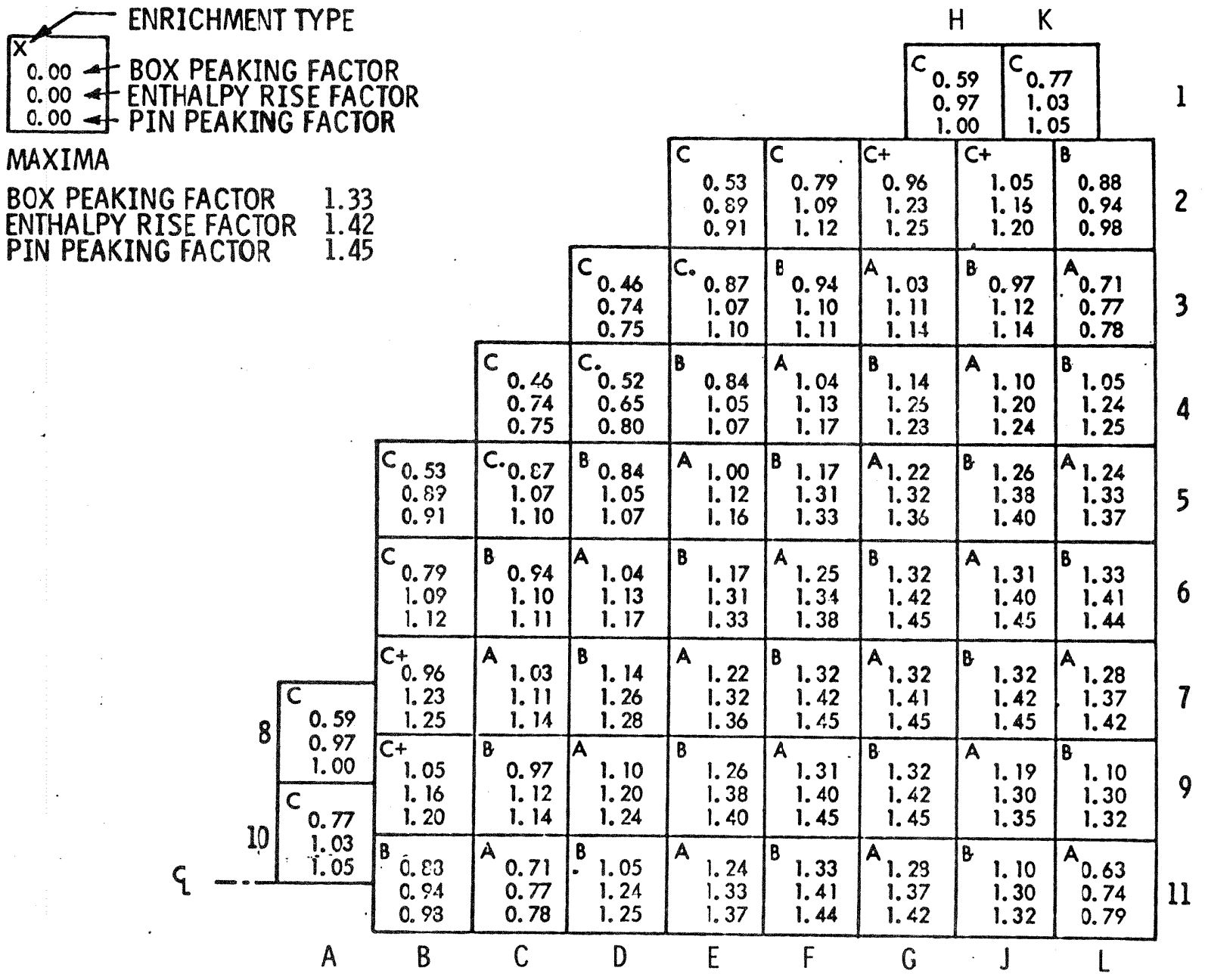

Am. 3-7/85

Figure 4.3-6

FLORIDA POWER & LIGHT CO.
St. Lucie Plant
Unit 1

Planar Average Core Power Distribution
2560 Mwt 1st Core, Rod Bank 7 Fully Inserted
End of Cycle, Equilibrium Xenon

Figure 4.3-7

Am. 3-7/85

ENRICHMENT TYPE

X
0.00 — BOX PEAKING FACTOR
0.00 — ENTHALPY RISE FACTOR
0.00 — PIN PEAKING FACTOR *

MAXIMA

BOX PEAKING FACTOR 1.33
ENTHALPY RISE FACTOR 1.37
PIN PEAKING FACTOR 1.42 *

	A	B	C	D	E	F	G	J	L	
							H	K		
							C 0.58 0.91 0.92	C 0.72 0.98 0.98		1
					C 0.53 0.87 0.88	C 0.76 1.06 1.06	C+ 0.97 1.19 1.22	C+ 1.09 1.21 1.24	B 1.00 1.06 1.09	2
				C 0.45 0.71 0.72	C. 0.89 1.12 1.15	B 1.05 1.18 1.22	A 1.02 1.10 1.12	B 1.08 1.19 1.23	A 0.73 0.87 0.90	3
			C 0.45 0.71 0.72	C. 0.52 0.68 0.86	B 0.95 1.14 1.17	A 1.05 1.15 1.17	B 1.23 1.30 1.34	A 1.07 1.17 1.19	B 1.11 1.25 1.29	4
		C 0.53 0.87 0.88	C. 0.89 1.12 1.15	B 0.95 1.14 1.17	A 1.01 1.14 1.16	B 1.25 1.34 1.38	A 1.17 1.23 1.25	B 1.29 1.36 1.40	A 1.15 1.22 1.24	5
		C 0.76 1.06 1.06	B 1.05 1.18 1.22	A 1.05 1.15 1.17	B 1.25 1.34 1.38	A 1.18 1.24 1.26	B 1.33 1.37 1.42	A 1.19 1.24 1.26	B 1.31 1.35 1.40	6
		C+ 0.97 1.19 1.22	A 1.02 1.10 1.12	B 1.23 1.30 1.34	A 1.17 1.23 1.25	B 1.33 1.37 1.42	A 1.19 1.24 1.27	B 1.28 1.35 1.40	A 1.13 1.21 1.22	7
8	C 0.58 0.91 0.92	C+ 1.09 1.21 1.24	B 1.08 1.19 1.23	A 1.07 1.17 1.19	B 1.29 1.36 1.40	A 1.19 1.24 1.26	B 1.28 1.35 1.40	A 1.05 1.17 1.18	B 1.05 1.21 1.24	9
10	C 0.72 0.98 0.98	B 1.00 1.06 1.09	A 0.73 0.87 0.90	B 1.11 1.25 1.29	A 1.15 1.22 1.24	B 1.31 1.35 1.40	A 1.13 1.21 1.22	B 1.05 1.21 1.24	A 0.57 0.72 0.78	11

℄

FLORIDA POWER & LIGHT CO.
St. Lucie Plant
Unit 1

Planar Average Core Power Distribution
In the Region Containing Part Length Rods
2560 Mwt 1st Core, Beginning of Life, No Xenon

Figure 4.3-8

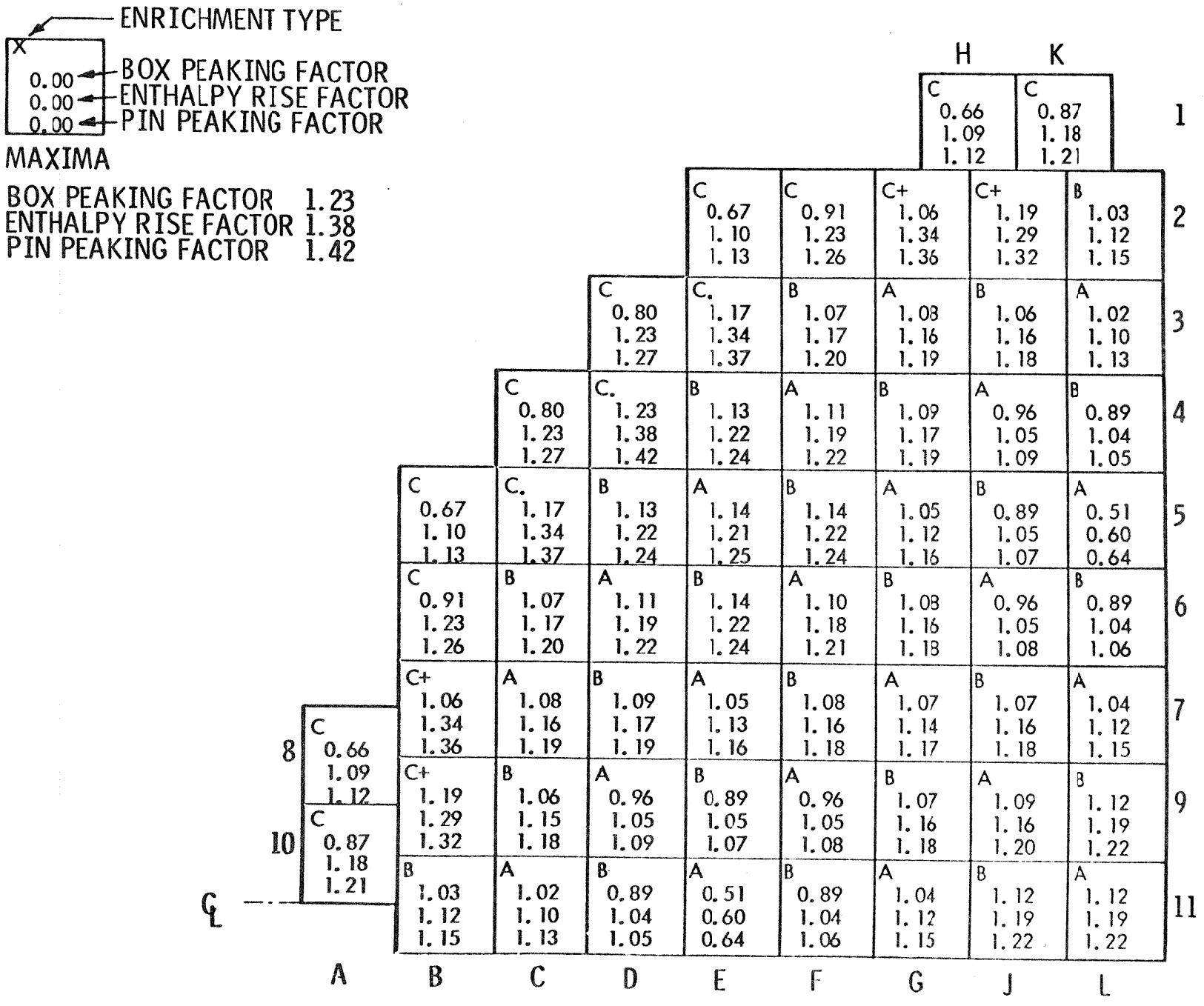

FLORIDA POWER & LIGHT CO.
St. Lucie Plant
Unit 1

Planar Average Core Power Distribution
In the Region Containing Part Length Rods
2560 Mwt 1st Core, Beginning of Life, Equilibrium Xenon

Figure 4.3-9

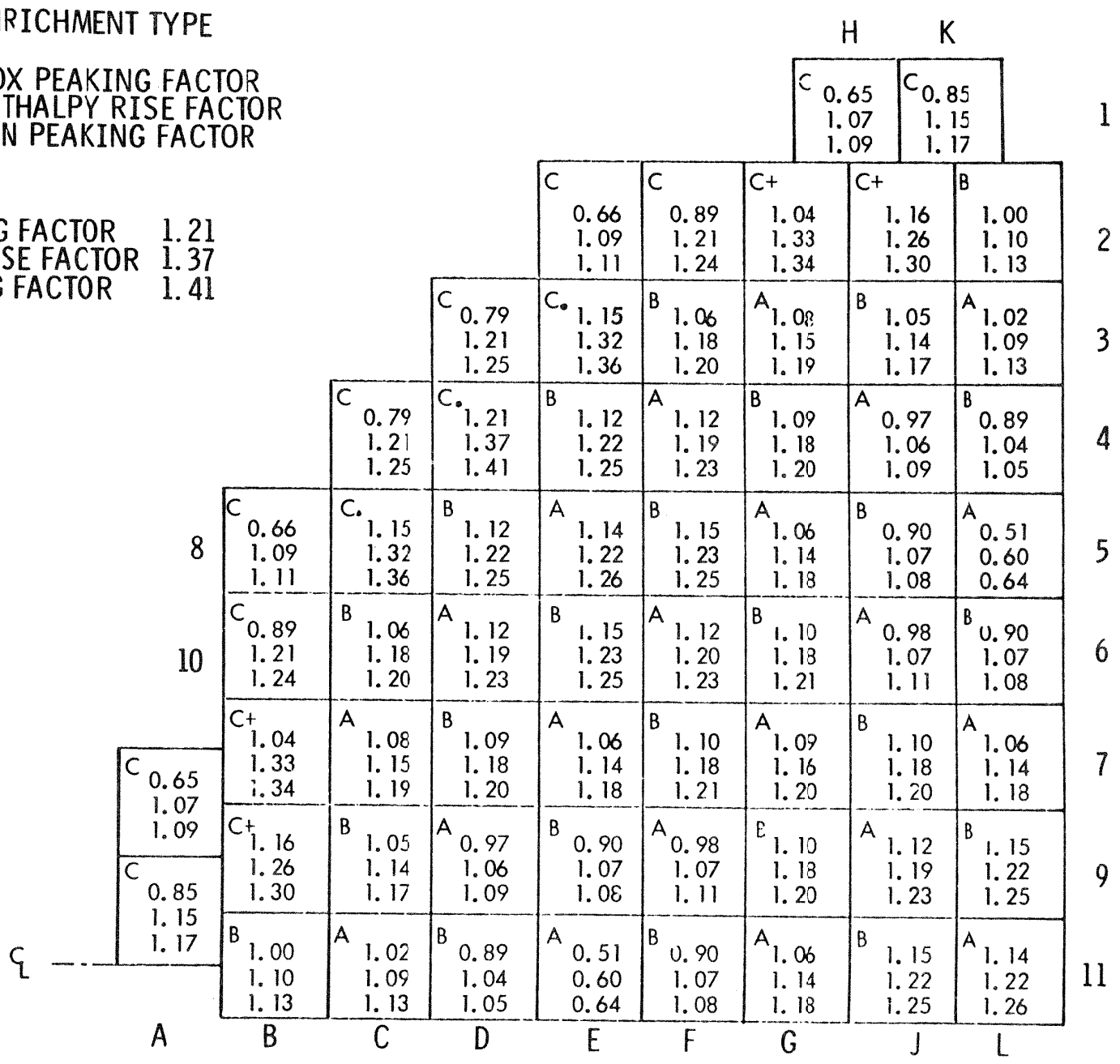

FLORIDA POWER & LIGHT CO.
St. Lucie Plant
Unit 1

Planar Average Core Power Distribution
In the Region Containing Part Length Rods
2560 Mwt 1st Core, End of Cycle, Equilibrium Xenon

Figure 4.3-10

X — ENRICHMENT TYPE

0.00 — BOX PEAKING FACTOR
0.00 — ENTHALPY RISE FACTOR
0.00 — PIN PEAKING FACTOR

MAXIMA

BOX PEAKING FACTOR	1.26
ENTHALPY RISE FACTOR	1.41
PIN PEAKING FACTOR	1.45

	A	B	C	D	E	F	G	H	J	K	L
1								C 0.63 1.00 1.01		C 0.79 1.09 1.09	
2					C 0.64 1.04 1.04	C 0.85 1.16 1.17	C+ 1.05 1.28 1.31	C+ 1.20 1.33 1.37		B 1.14 1.23 1.27	
3				C 0.76 1.17 1.18	C 1.16 1.37 1.41	B 1.17 1.28 1.32	A 1.07 1.13 1.15	B 1.17 1.23 1.27		A 1.05 1.11 1.13	
4			C 0.76 1.17 1.18	C 1.21 1.41 1.45	B 1.26 1.33 1.37	A 1.13 1.19 1.21	B 1.18 1.26 1.30	A 0.96 1.07 1.09		B 0.96 1.11 1.14	
5			C 0.64 1.04 1.04	C 1.16 1.37 1.41	B 1.26 1.33 1.37	A 1.16 1.21 1.23	B 1.23 1.31 1.35	A 1.02 1.11 1.13	B 0.93 1.08 1.12	A 0.50 0.64 0.70	
6			C 0.85 1.16 1.17	B 1.17 1.28 1.32	A 1.13 1.19 1.21	B 1.23 1.31 1.35	A 1.06 1.14 1.16	B 1.10 1.18 1.22	A 0.88 0.97 0.98	B 0.88 0.99 1.02	
7			C+ 1.05 1.28 1.31	A 1.07 1.13 1.15	B 1.18 1.26 1.30	A 1.02 1.11 1.13	B 1.10 1.18 1.22	A 0.97 1.03 1.04	B 1.03 1.08 1.11	A 0.91 0.96 0.98	
8		C 0.63 1.00 1.01									
9			C+ 1.20 1.33 1.37	B 1.17 1.23 1.27	A 0.96 1.07 1.09	B 0.93 1.08 1.12	A 0.88 0.97 0.98	B 1.03 1.08 1.11	A 0.94 0.98 0.99	B 1.05 1.08 1.12	
10		C 0.79 1.09 1.09									
11			B 1.14 1.23 1.27	A 1.05 1.11 1.13	B 0.96 1.11 1.14	A 0.50 0.64 0.70	B 0.88 0.99 1.02	A 0.91 0.96 0.98	B 1.05 1.08 1.12	A 0.95 0.98 1.00	

℄

FLORIDA POWER & LIGHT CO.
St. Lucie Plant
Unit 1

PLANAR AVERAGE CORE POWER DISTRIBUTION IN THE REGION CONTAINING BOTH PART LENGTH RODS AND ROD BANK 7
2560 Mwt 1st CORE, BEGINNING OF LIFE, NO XENON

Figure 4.3-11

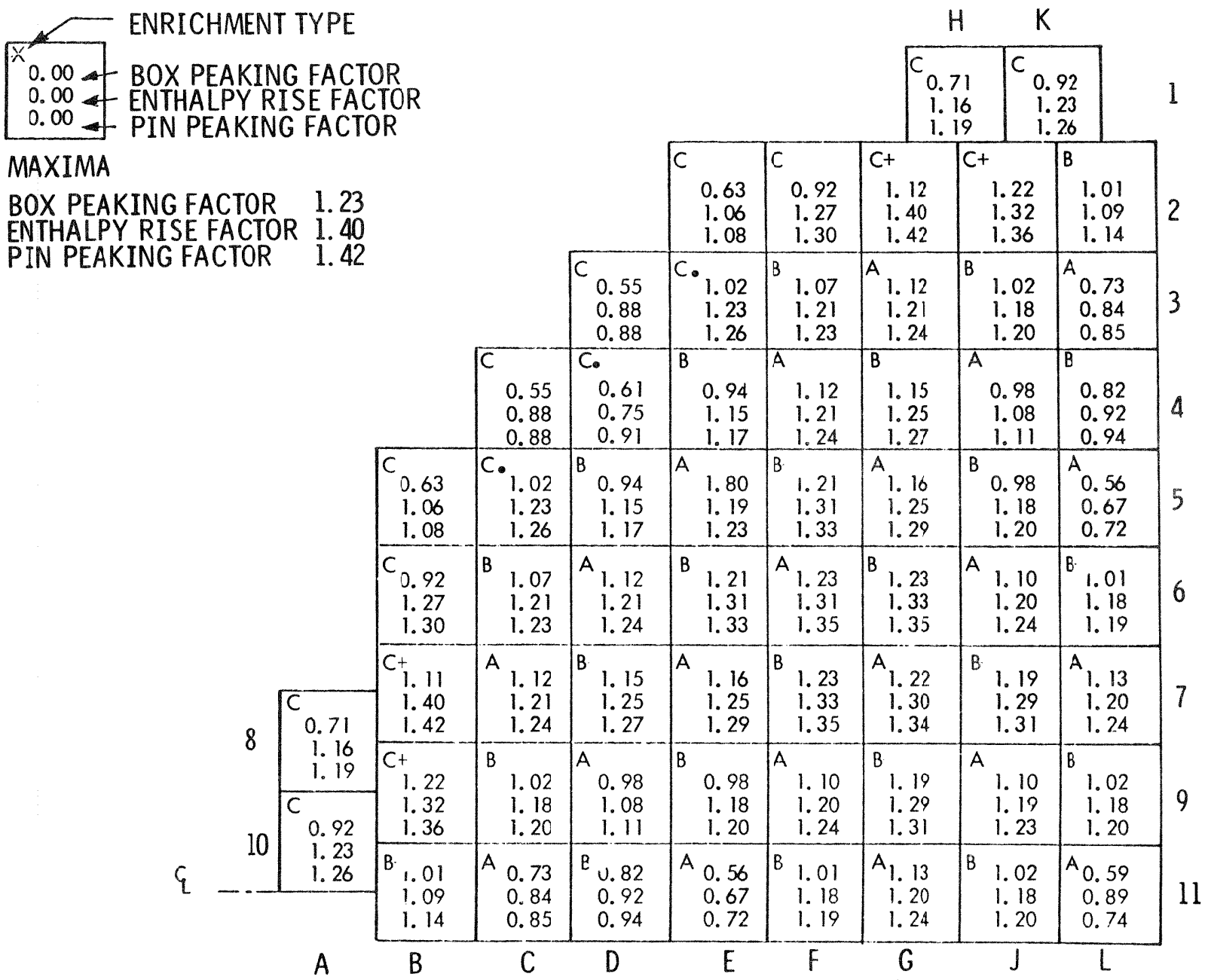

FLORIDA POWER & LIGHT CO.
St. Lucie Plant
Unit 1

PLANAR AVERAGE CORE POWER DISTRIBUTION IN THE REGION CONTAINING BOTH PART LENGTH RODS AND ROD BANK 7
2560 Mwt 1st CORE, BEGINNING OF LIFE, EQUILIBRIUM XENON

Figure 4.3-12

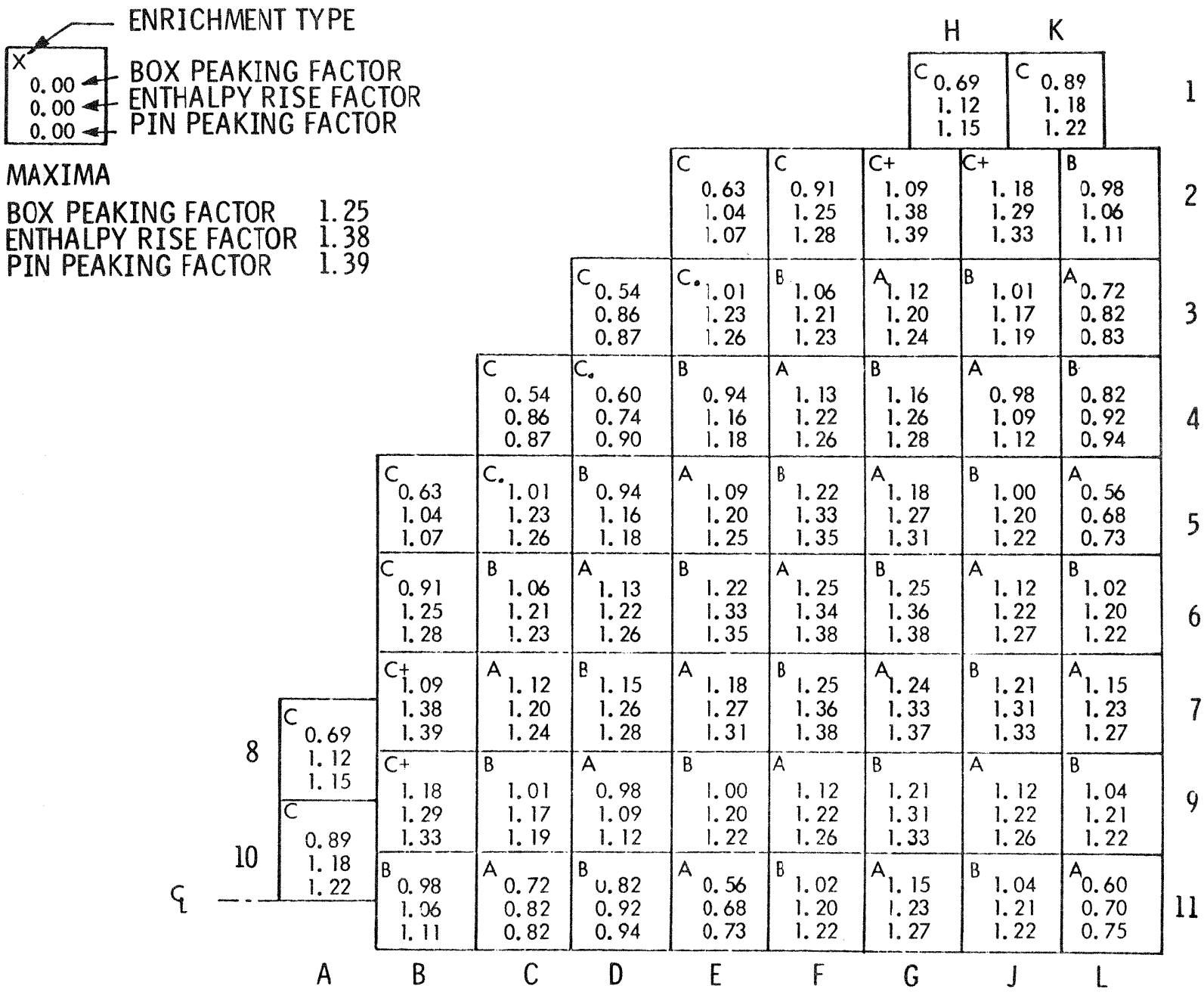

FLORIDA POWER & LIGHT CO.
St. Lucie Plant
Unit 1

PLANAR AVERAGE CORE POWER DISTRIBUTION IN THE REGION CONTAINING PART LENGTH RODS AND ROD BANK 7
2560 Mwt 1st CORE, END OF CYCLE, EQUILIBRIUM XENON

Figure 4.3-13

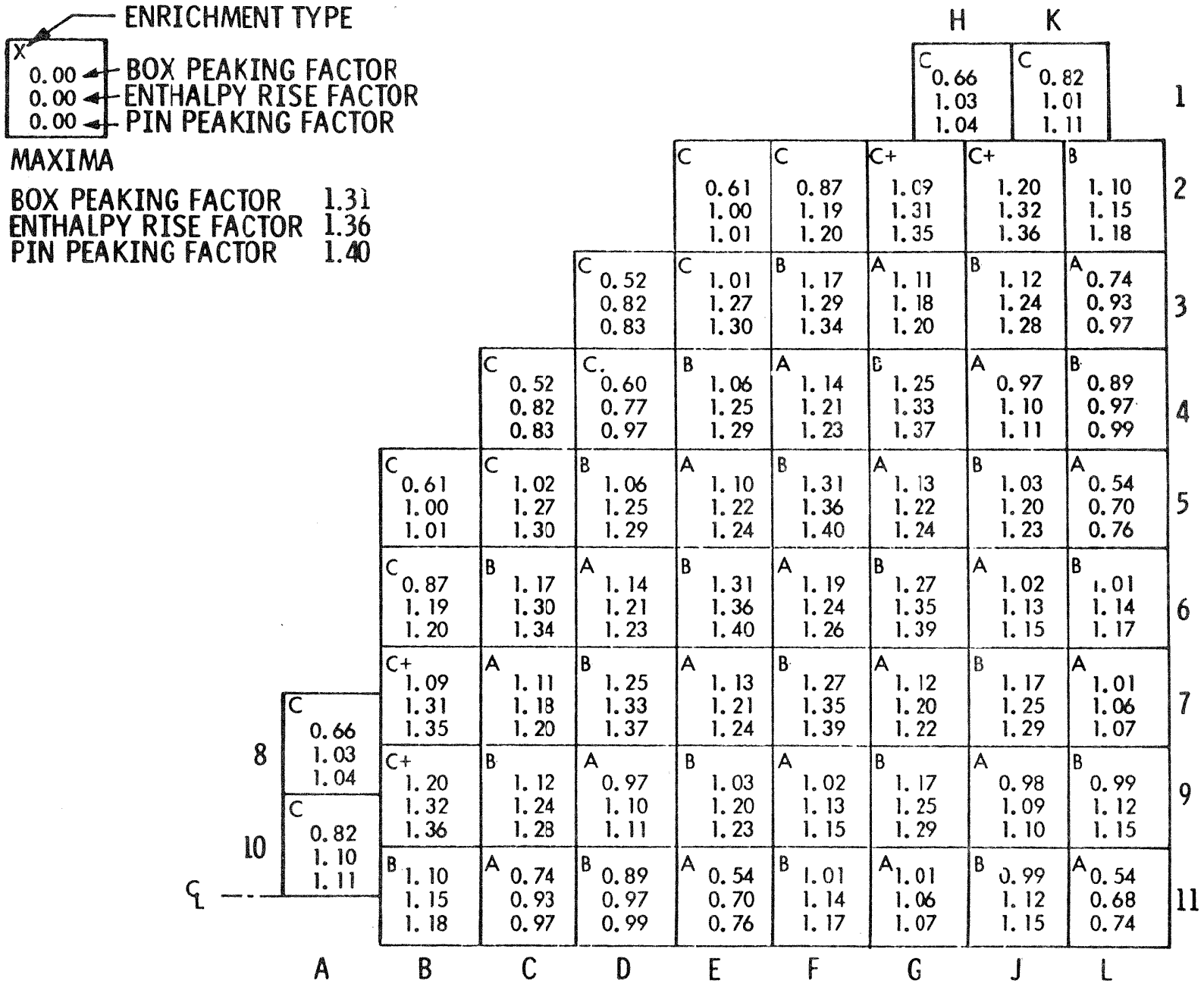

FLORIDA POWER & LIGHT CO.
St. Lucie Plant
Unit 1

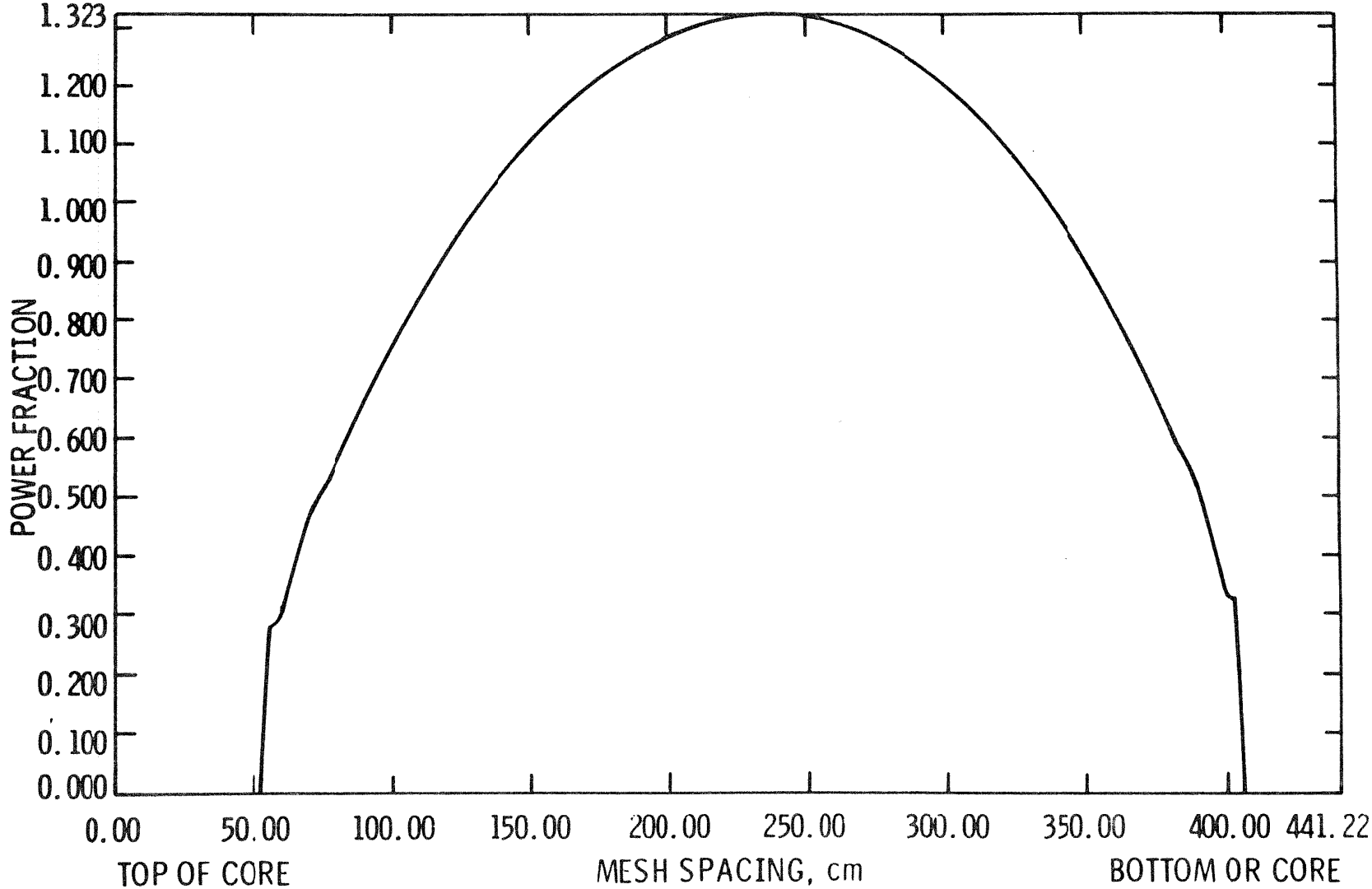

Cycle 1
Axial Power Shape
Beginning of Life

Figure
4.3-14

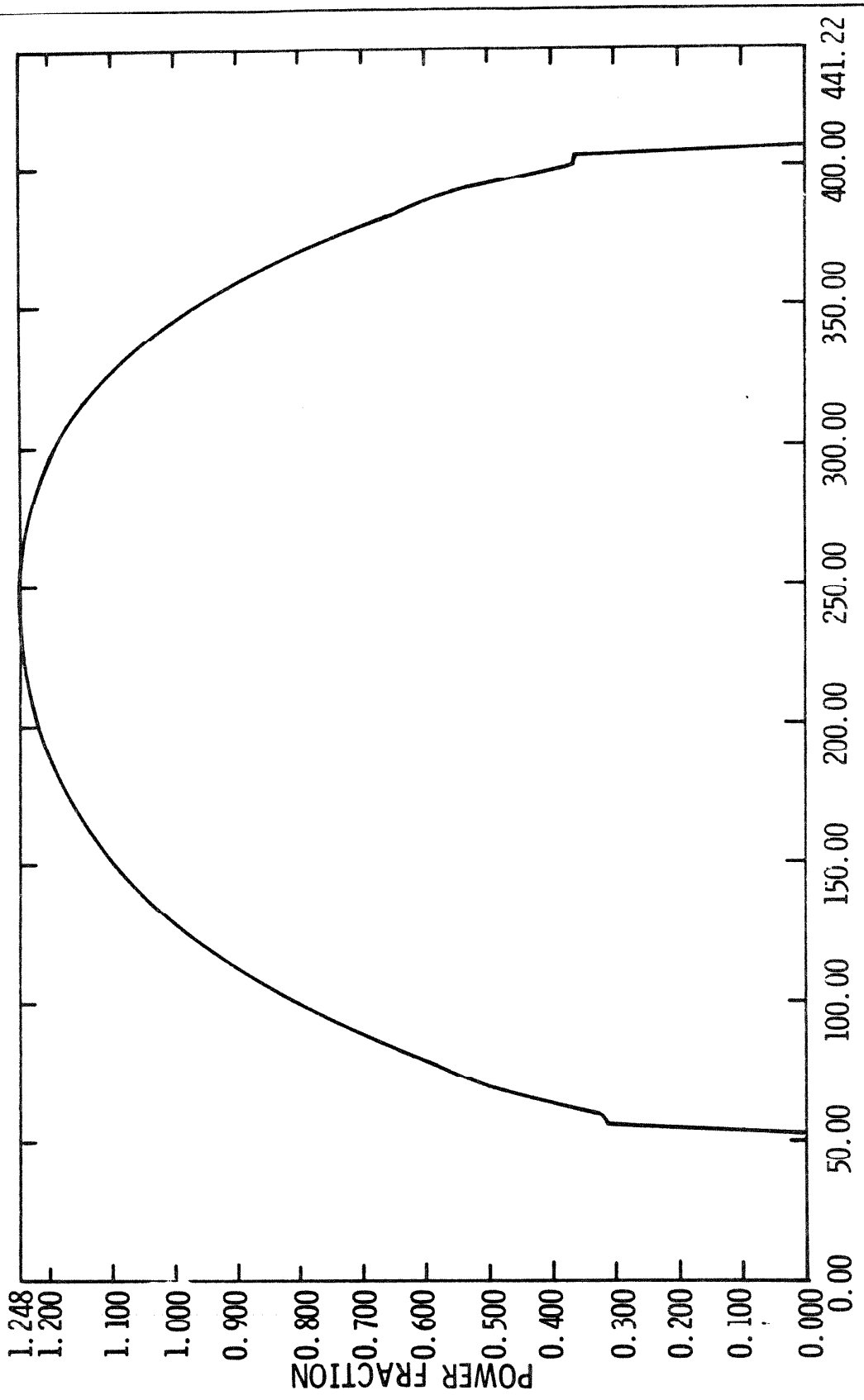

FLORIDA POWER & LIGHT CO. St. Lucie Plant Unit 1	Cycle 1 Core Axial Power Shape 3,200 Mwd/MTU	Figure 4.3-15

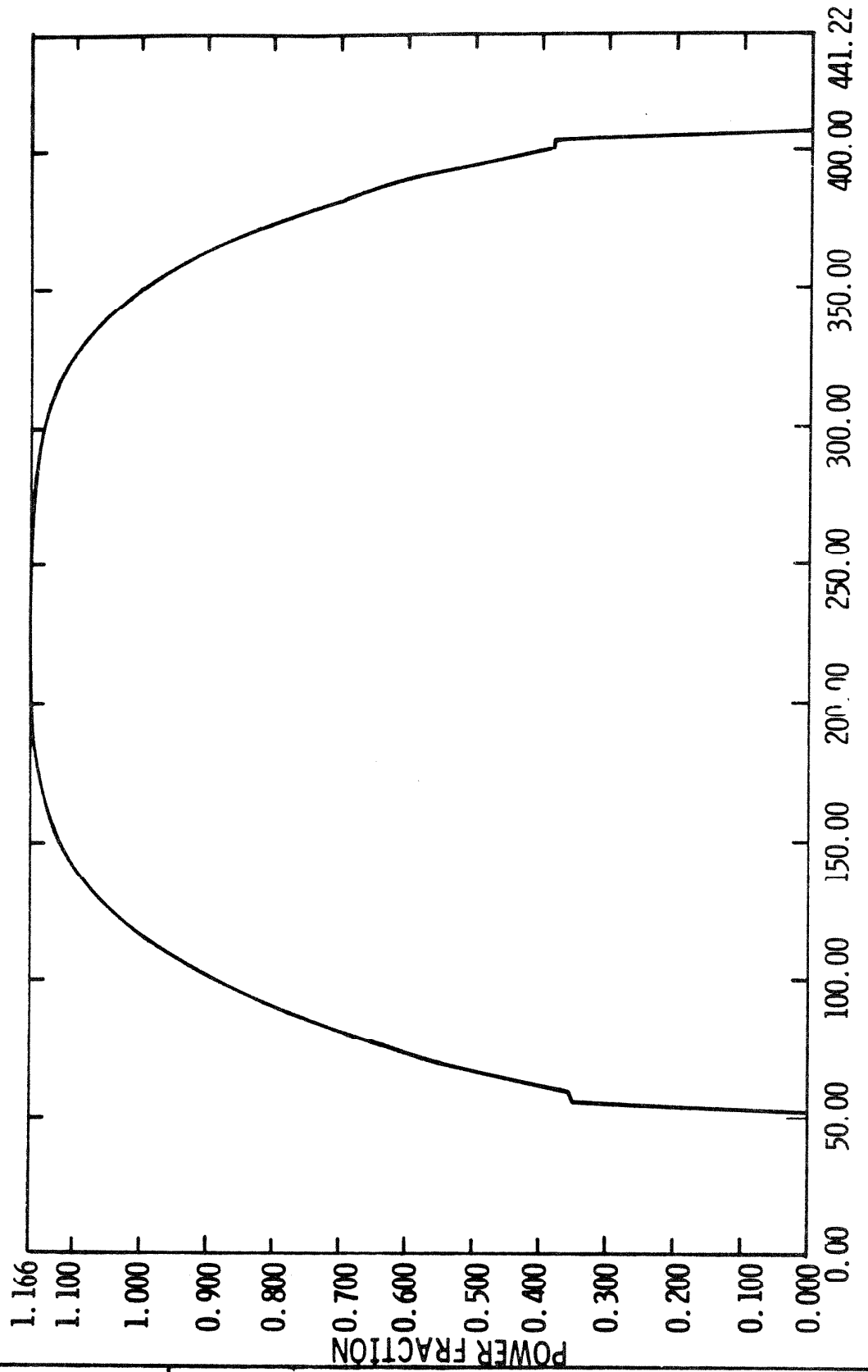

FLORIDA POWER & LIGHT CO. St. Lucie Plant Unit 1	Cycle 1 Core Axial Power Shape 6400 Mwd/MTU	Figure 4.3-16

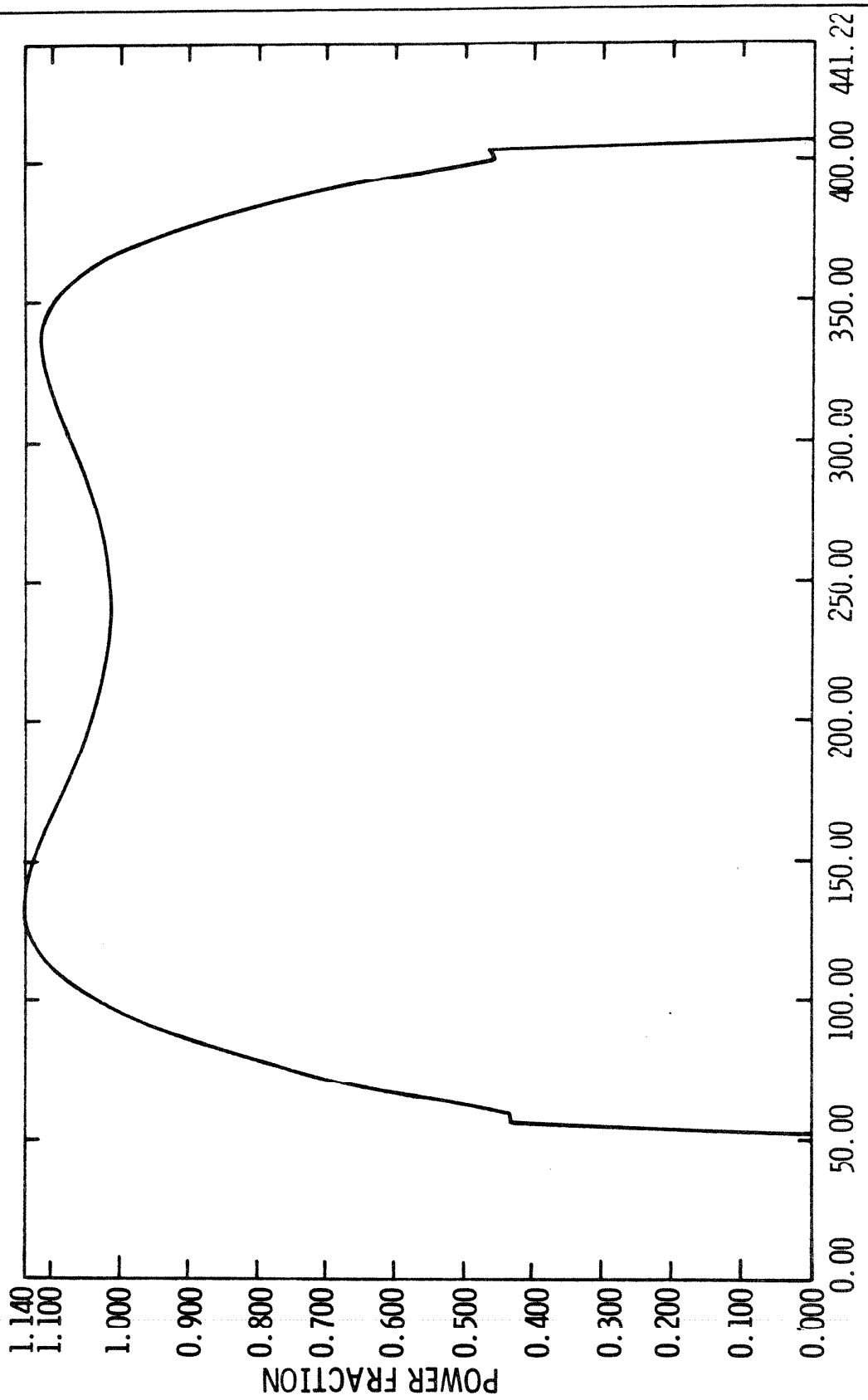

FLORIDA POWER & LIGHT CO. St. Lucie Plant Unit 1	Cycle 1 Core Axial Power Shape 9600 Mwd/MTU	Figure 4.3-17

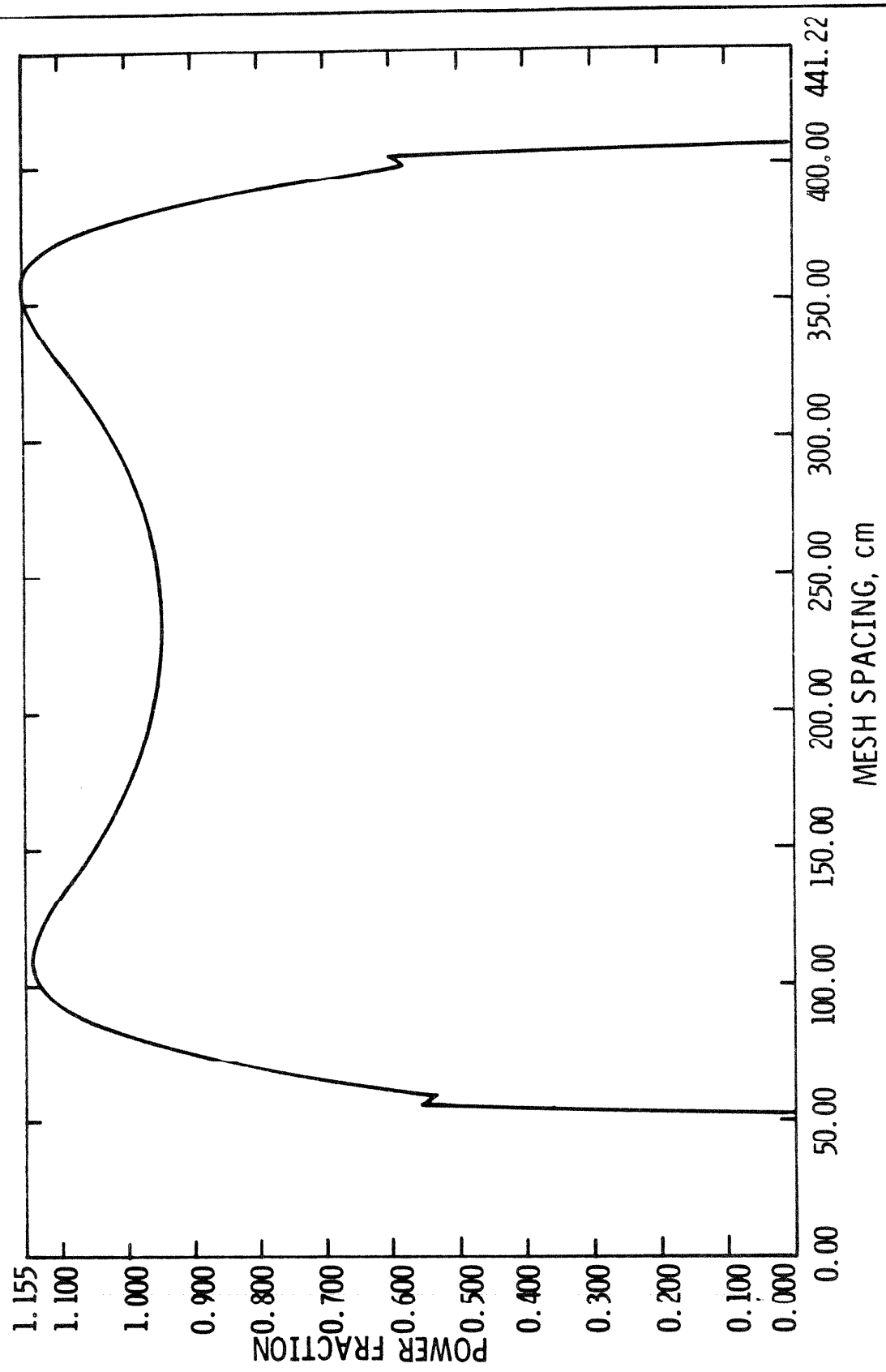

FLORIDA POWER & LIGHT CO. St. Lucie Plant Unit 1	Cycle 1 Core Axial Power Shape 12,700 Mwd/MTU	Figure 4.3-18

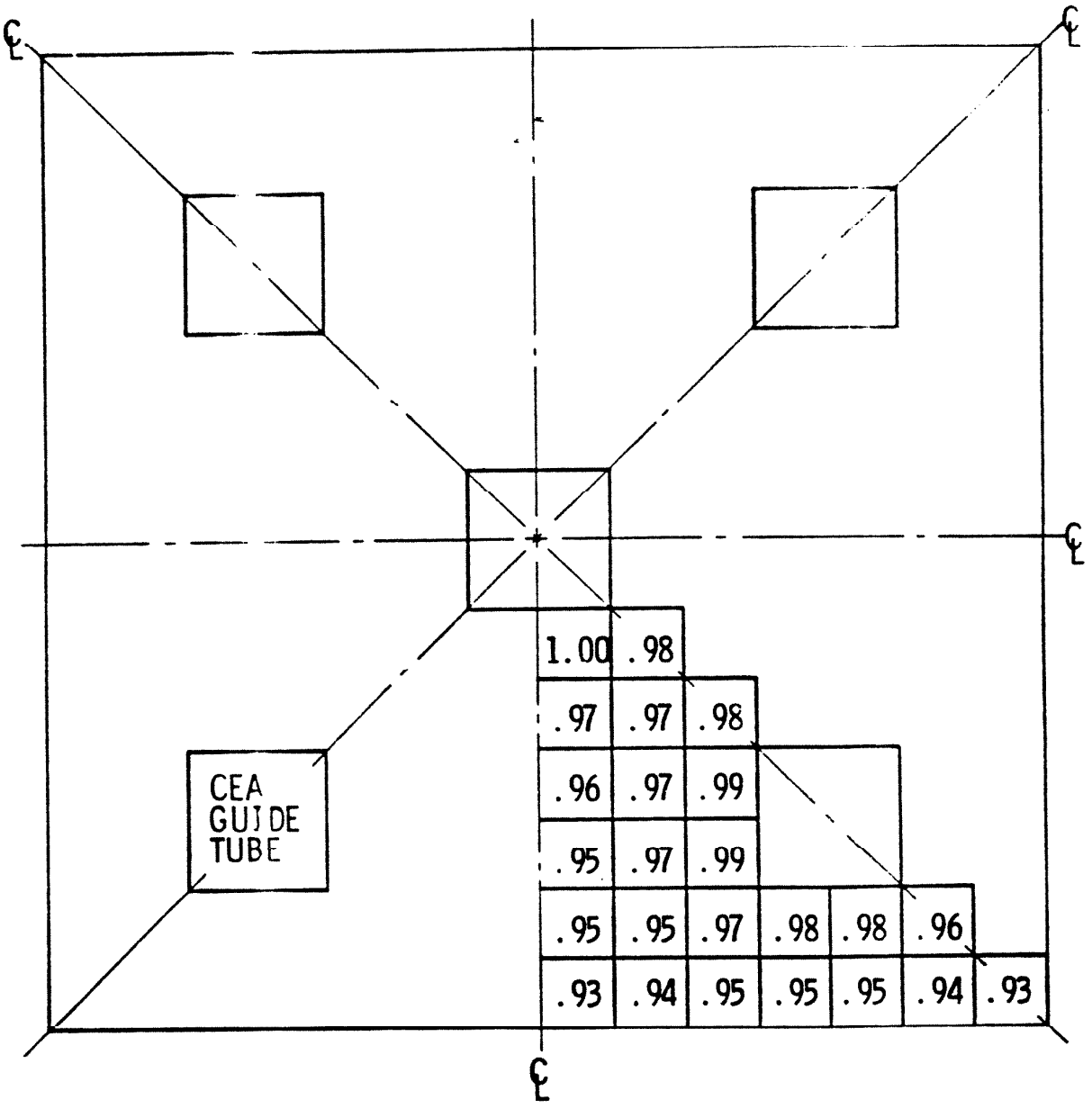

FLORIDA POWER & LIGHT CO. St. Lucie Plant Unit 1	Normalized Power Distribution Within Typical Assembly	Figure 4.3-19

FLORIDA POWER & LIGHT CO.
St. Lucie Plant
Unit 1

Cycle 1
Core Average Axial Peaking Factor vs Time, hrs

Figure 4.3-20

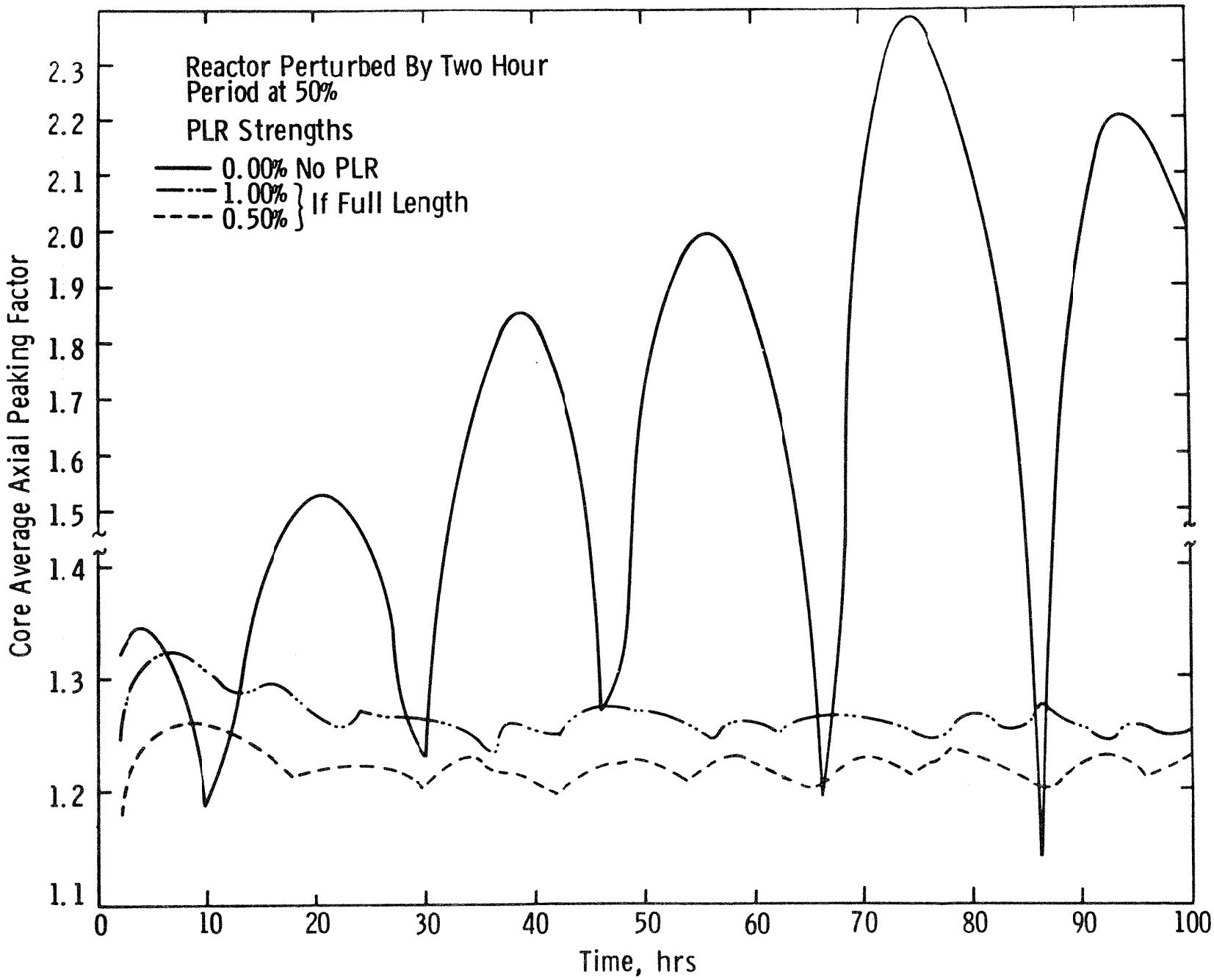

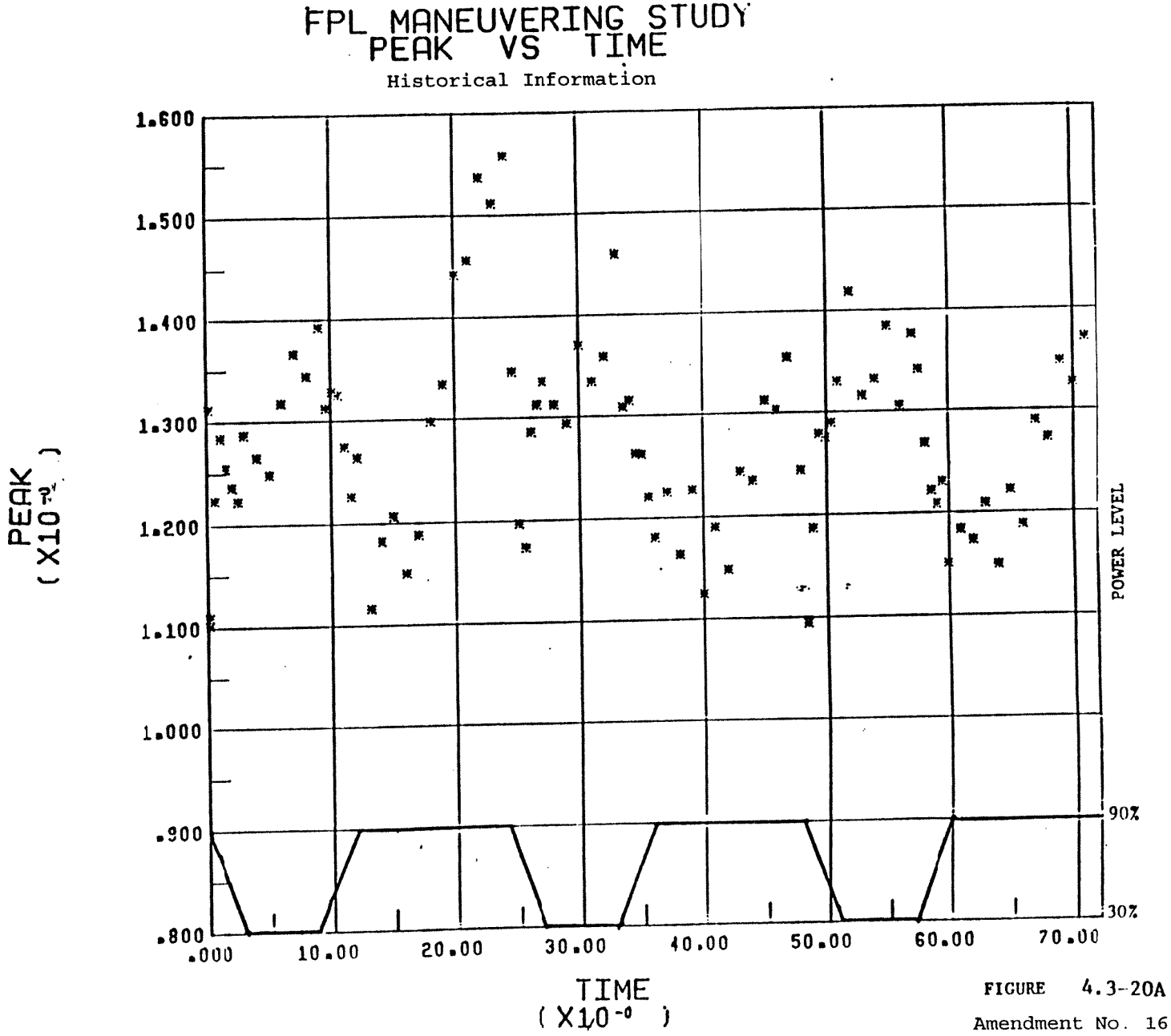

FIGURE 4.3-20A

Amendment No. 16, (1/98)

FLORIDA POWER & LIGHT CO.
St. Lucie Plant
Unit 1

Cycle 1

Fuel Temperature Coefficient
vs Average Fuel Temperature

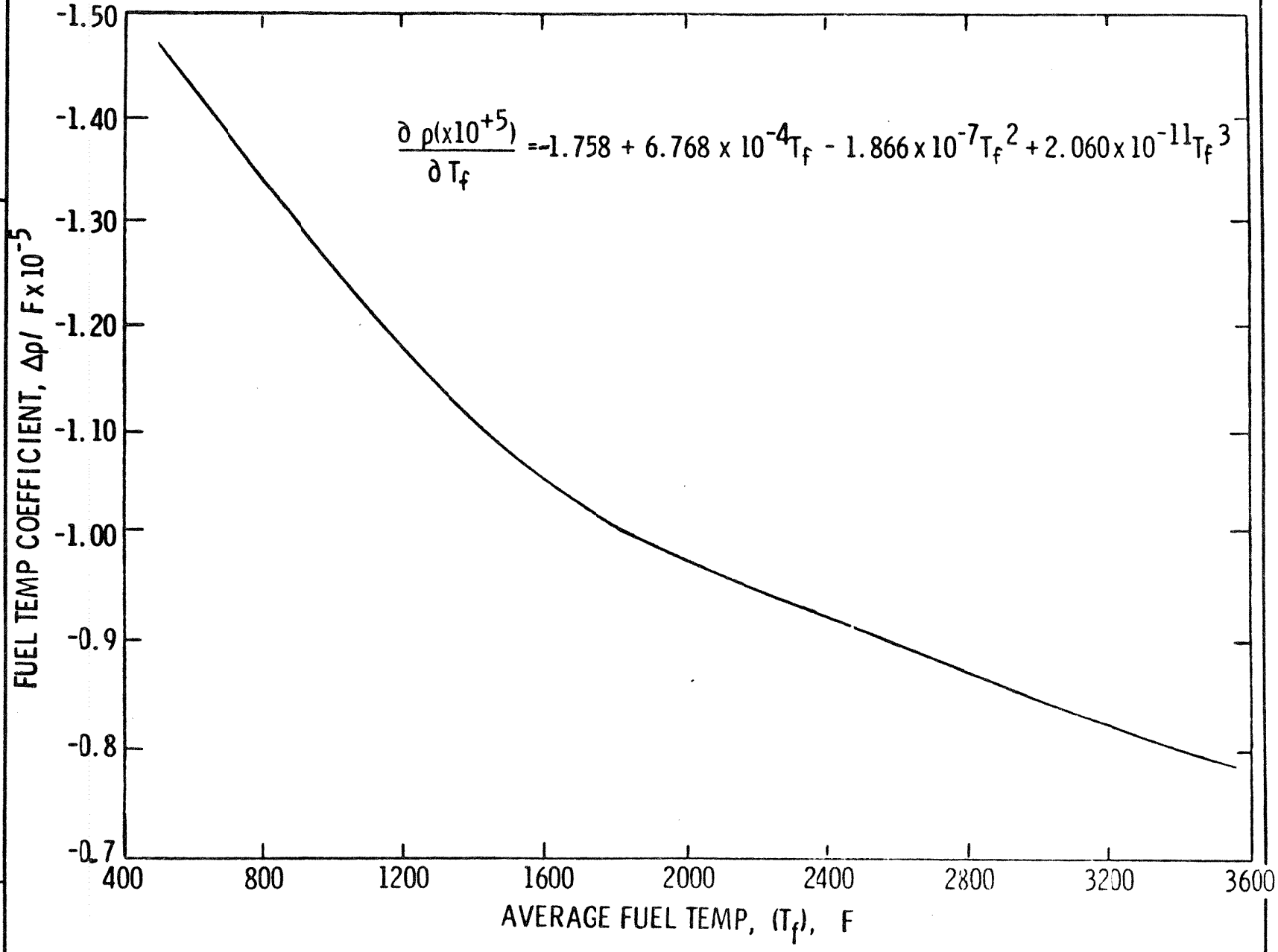

Figure 4.3-21

FIGURE 4.3-21A
Doppler Coefficient
Cycle 1

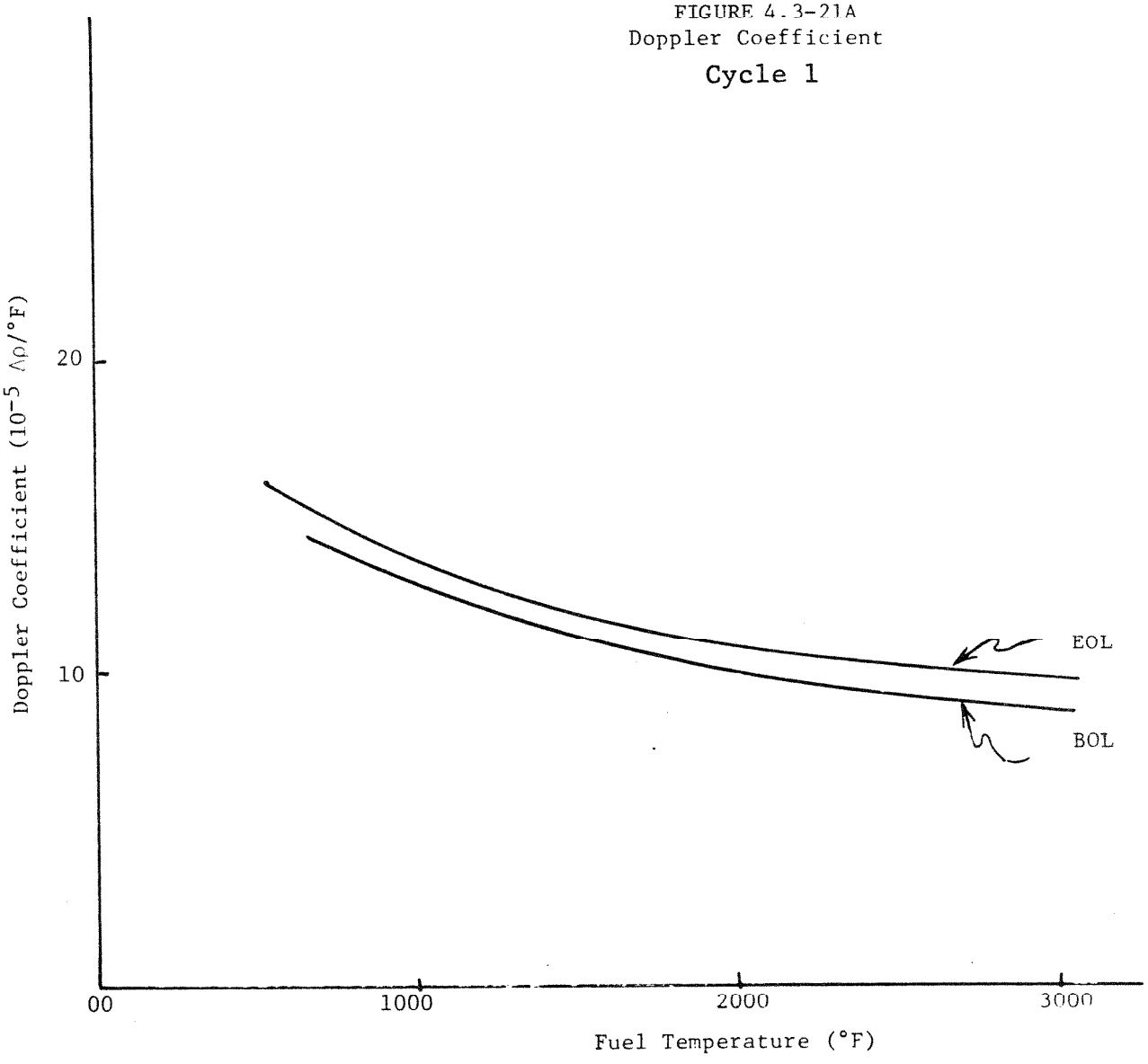

Note: See Cycle 6 RSE Table 6.1 for current doppler coefficients

Am. 3-7/85

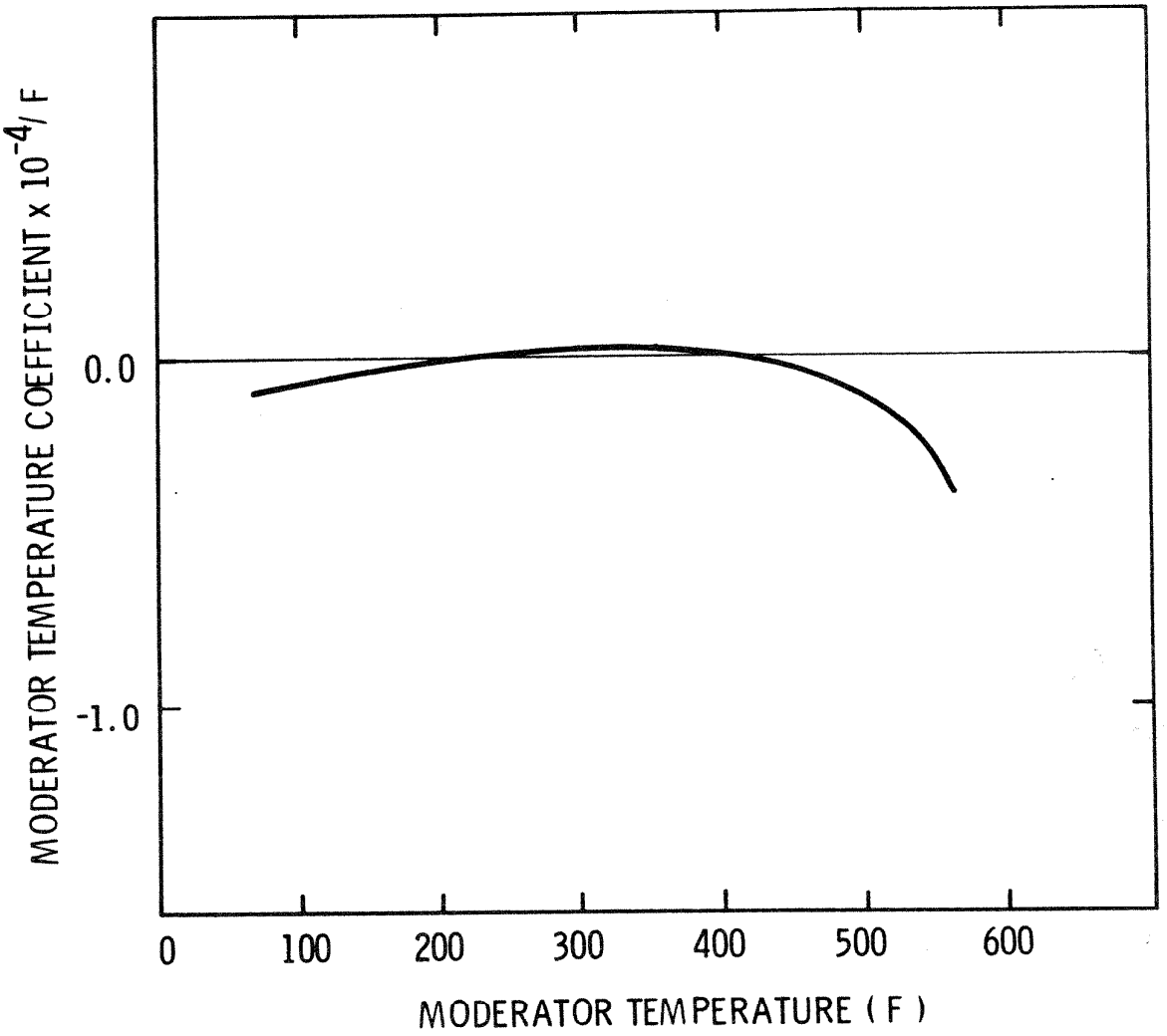

Note: See Cycle 6 RSE Table 6.1 for current moderator temperature coefficients

Am. 3-7/85

FLORIDA POWER & LIGHT CO. St. Lucie Plant Unit 1	MODERATOR TEMPERATURE COEFFICIENT, BOL No Xenon, 820 PPM Boron Cycle 1	Figure 4.3-22

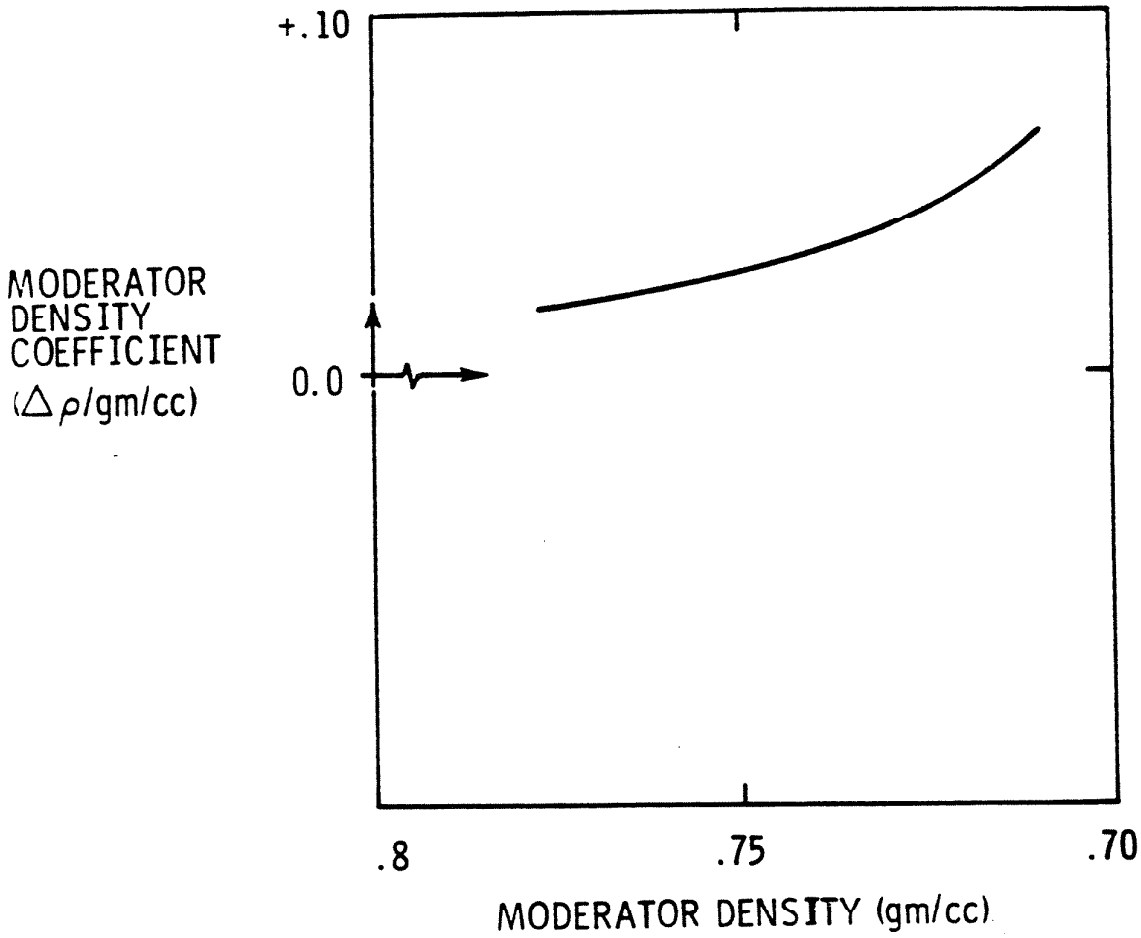

FLORIDA POWER & LIGHT CO. St. Lucie Plant Unit 1	Moderator Density Coefficient, BOL No xenon, 820 PPM Boron	Figure 4.3-23

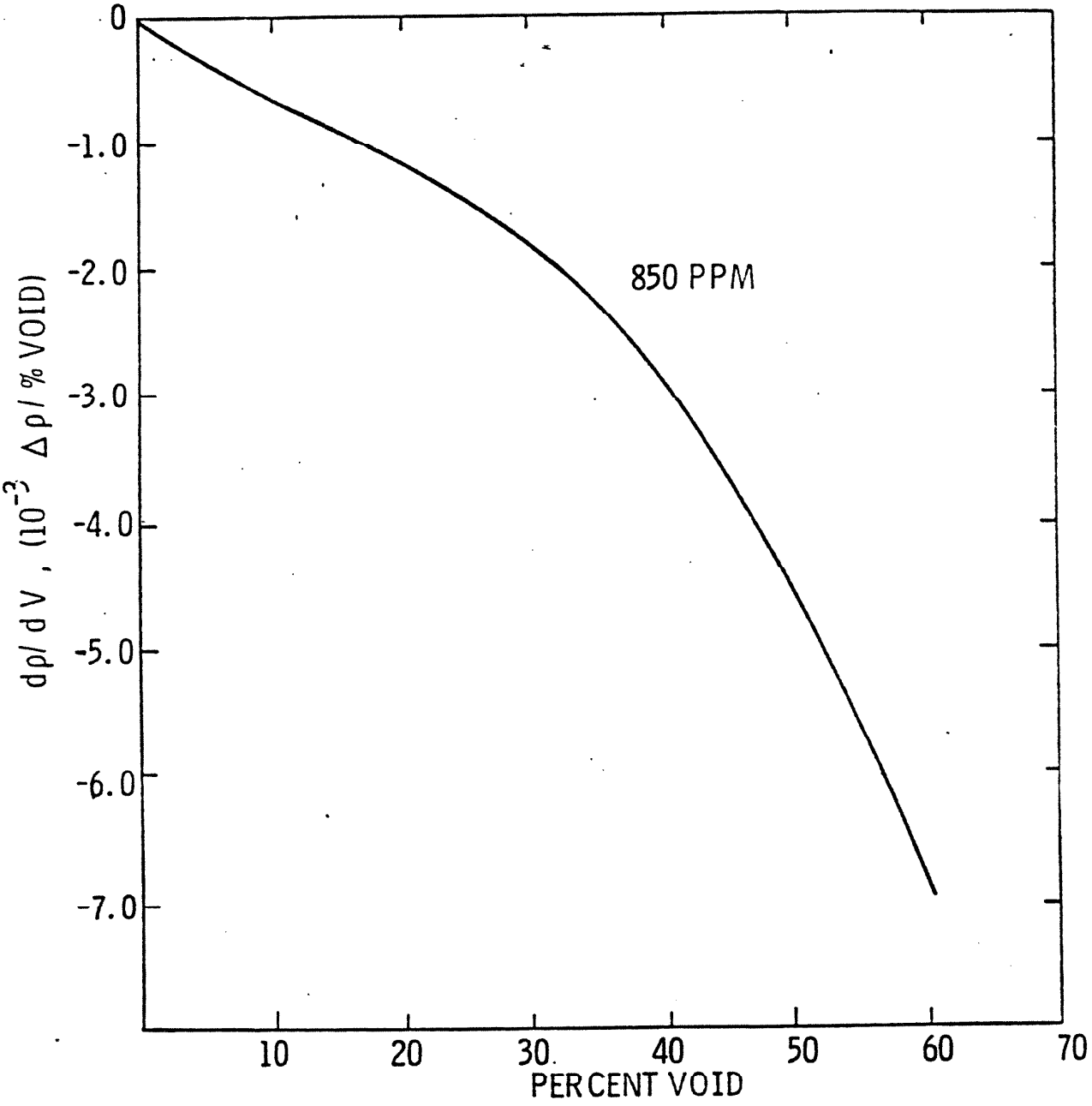

Amendment No. 16, (1/98)

Historical Information

FLORIDA POWER & LIGHT COMPANY ST. LUCIE PLANT UNIT 1	
MODERATOR VOID COEFFICIENT vs PERCENT VOID	FIGURE 4.3-23A

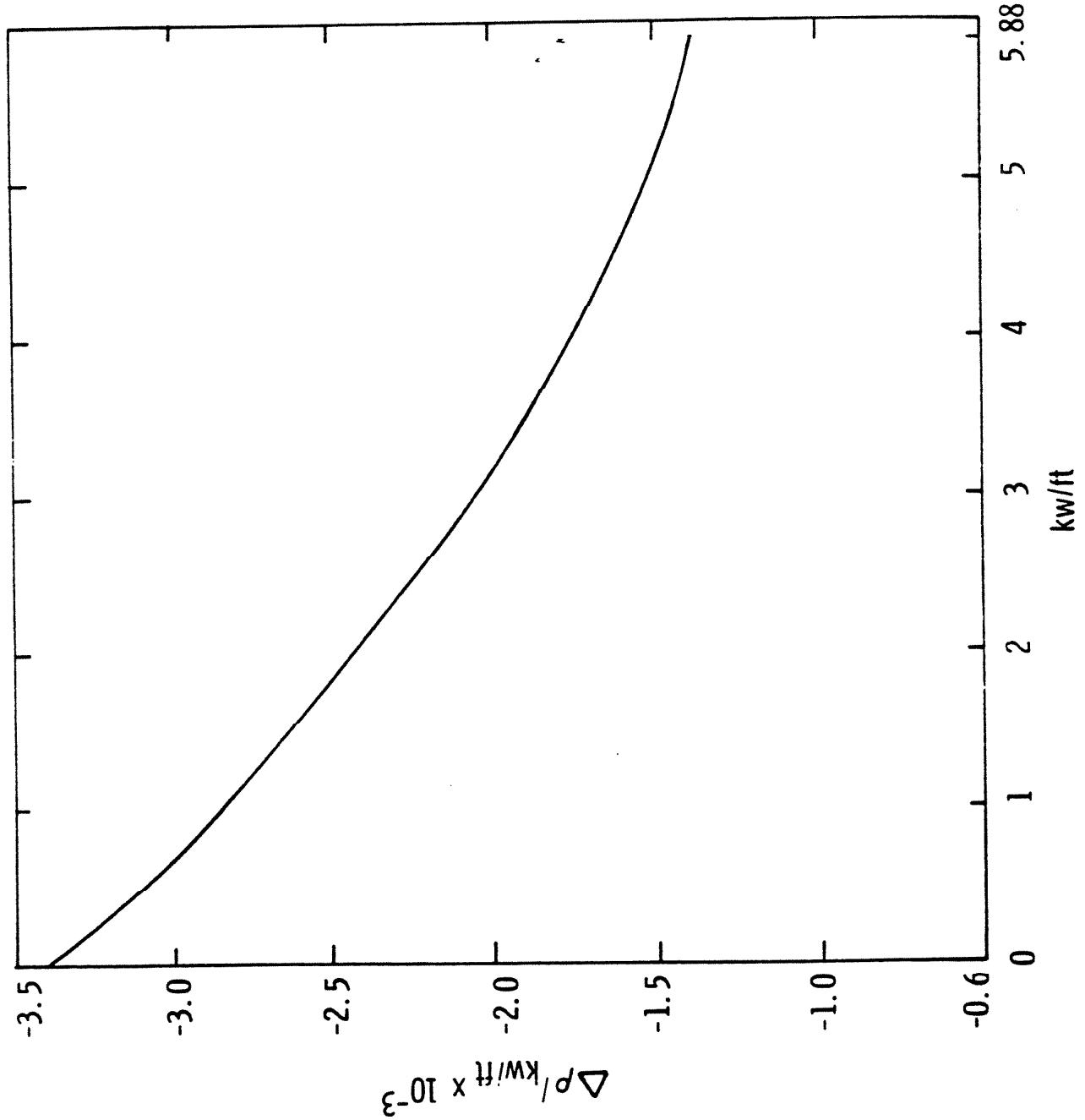

Historical Information

Amendment No. 16, (1/98)

FLORIDA POWER & LIGHT CO. St. Lucie Plant Unit 1	Fuel Temperature Contribution to Power Coefficient vs kw/ft	Figure 4.3-24

FLORIDA POWER & LIGHT CO.
St. Lucie Plant
Unit 1

Cycle 1

CEA Group Identification

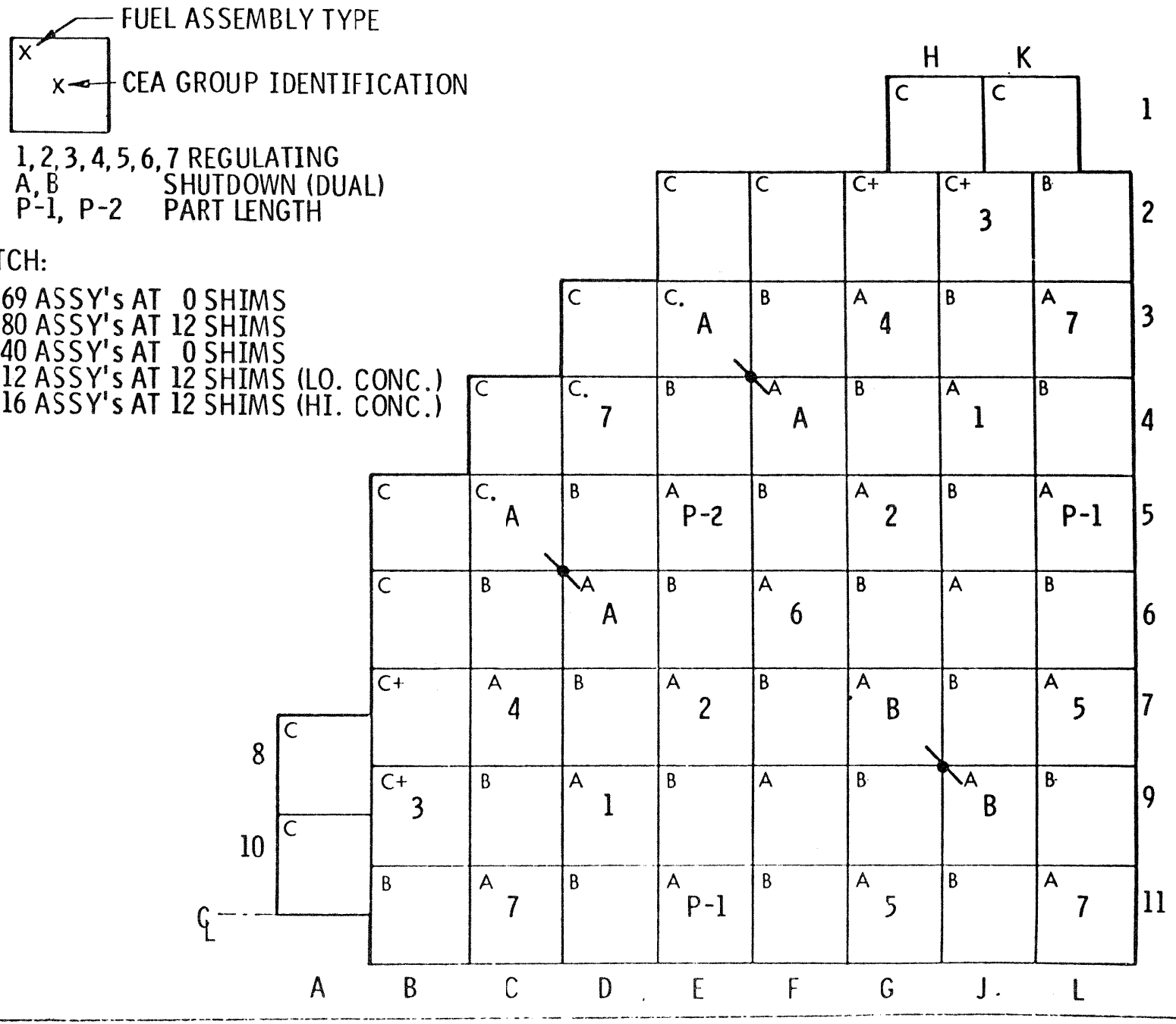

Am. 3-7/85

Figure 4.3-25

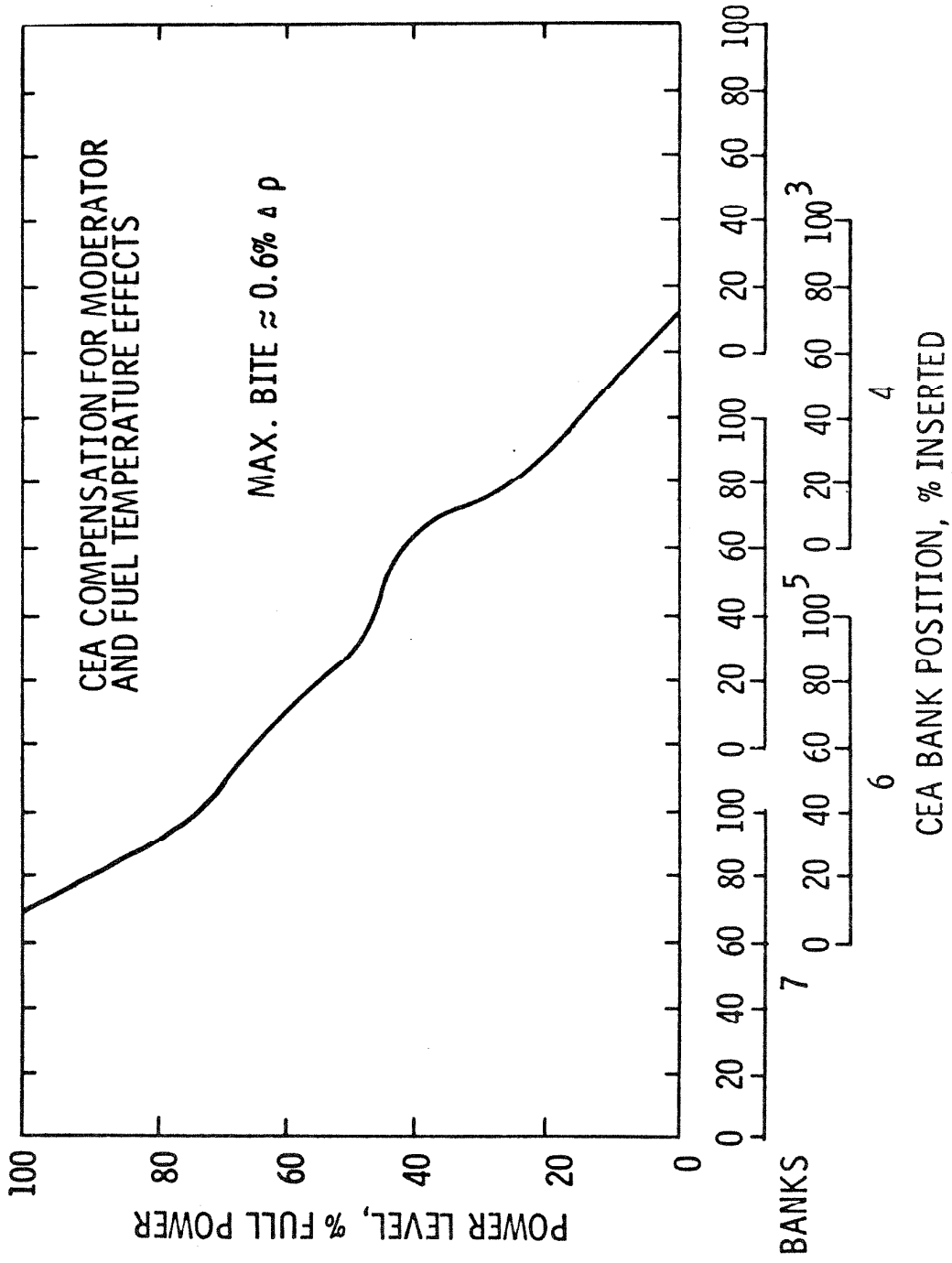

Note: See St. Lucie Unit 1 Technical Specifications

Am. 3-7/85

FLORIDA POWER & LIGHT CO. St. Lucie Plant Unit 1	Cycle 1 Power Dependent CEA Insertion Limits	Figure 4.3-26

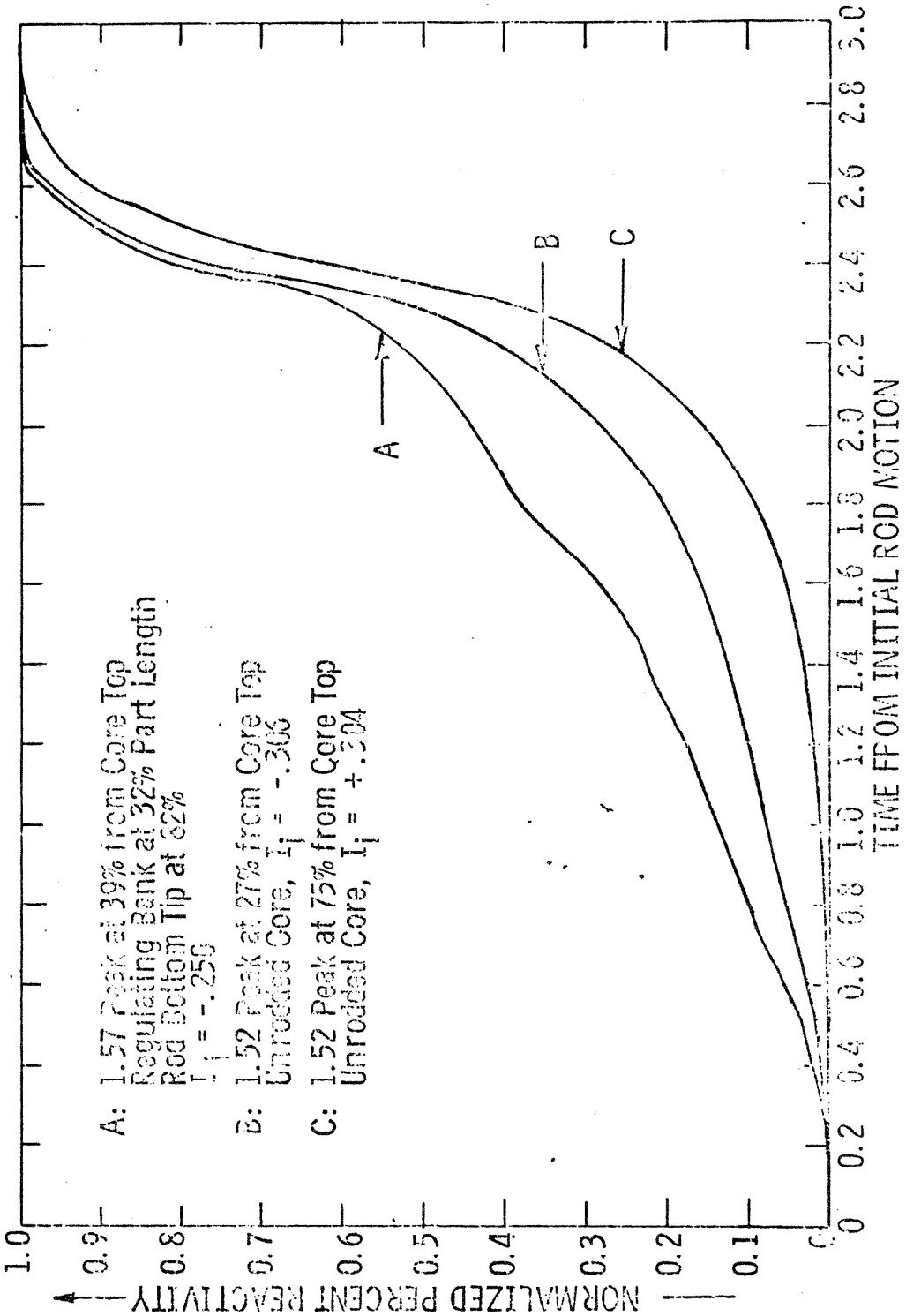

Cycle 1

Am. 3-7/85

FLORIDA POWER & LIGHT CO. St. Lucie Plant	SHUTDOWN BANK WORTH vs TIME FROM INITIAL ROD MOTION	Figure 4.3-26A

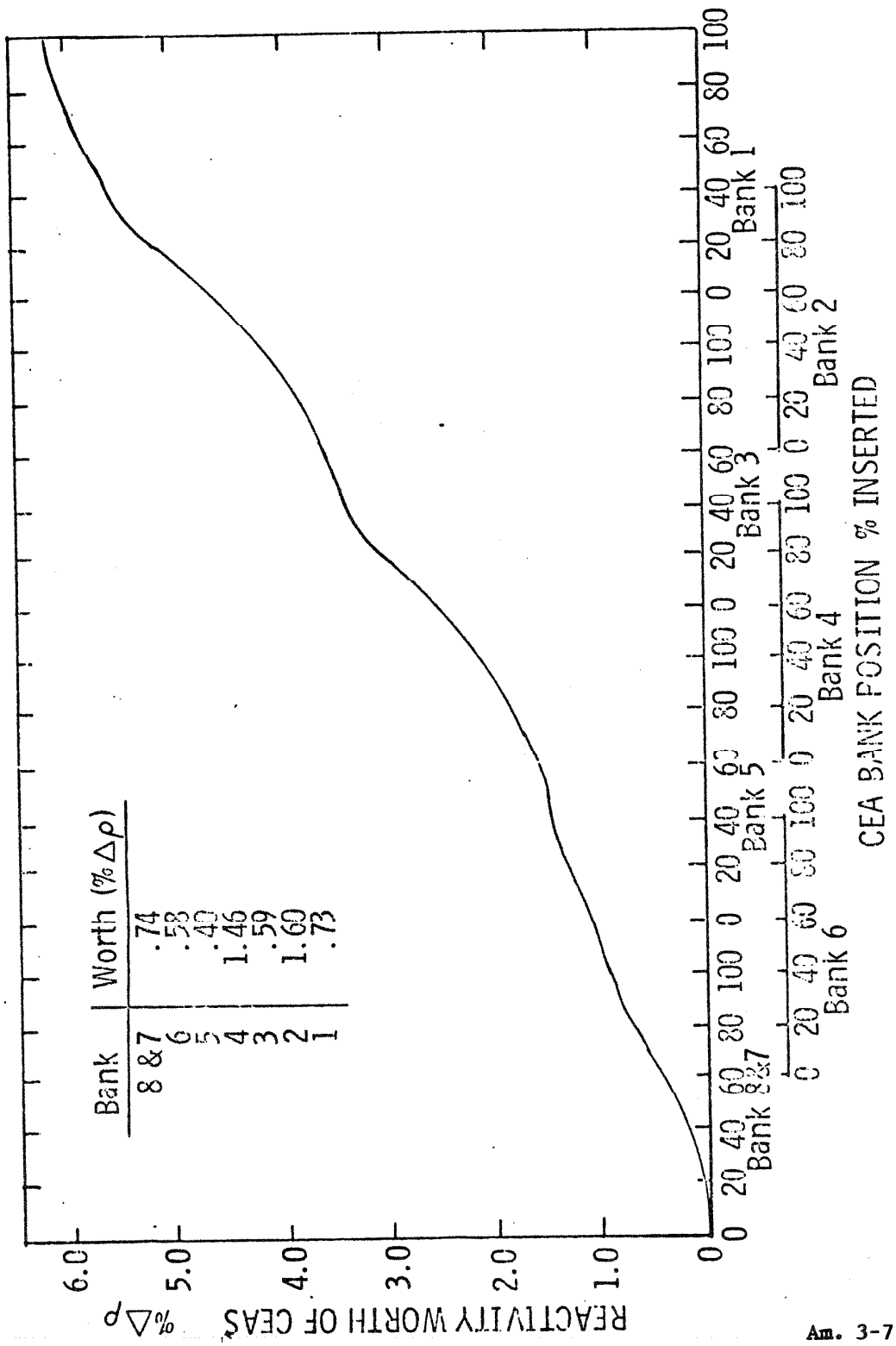

Am. 3-7/85

FLORIDA POWER & LIGHT CO. St. Lucie Plant	INTEGRAL WORTH vs INSERTION AT BOL (WITHOUT PLRS) Cycle 1	Figure 4.3-26B

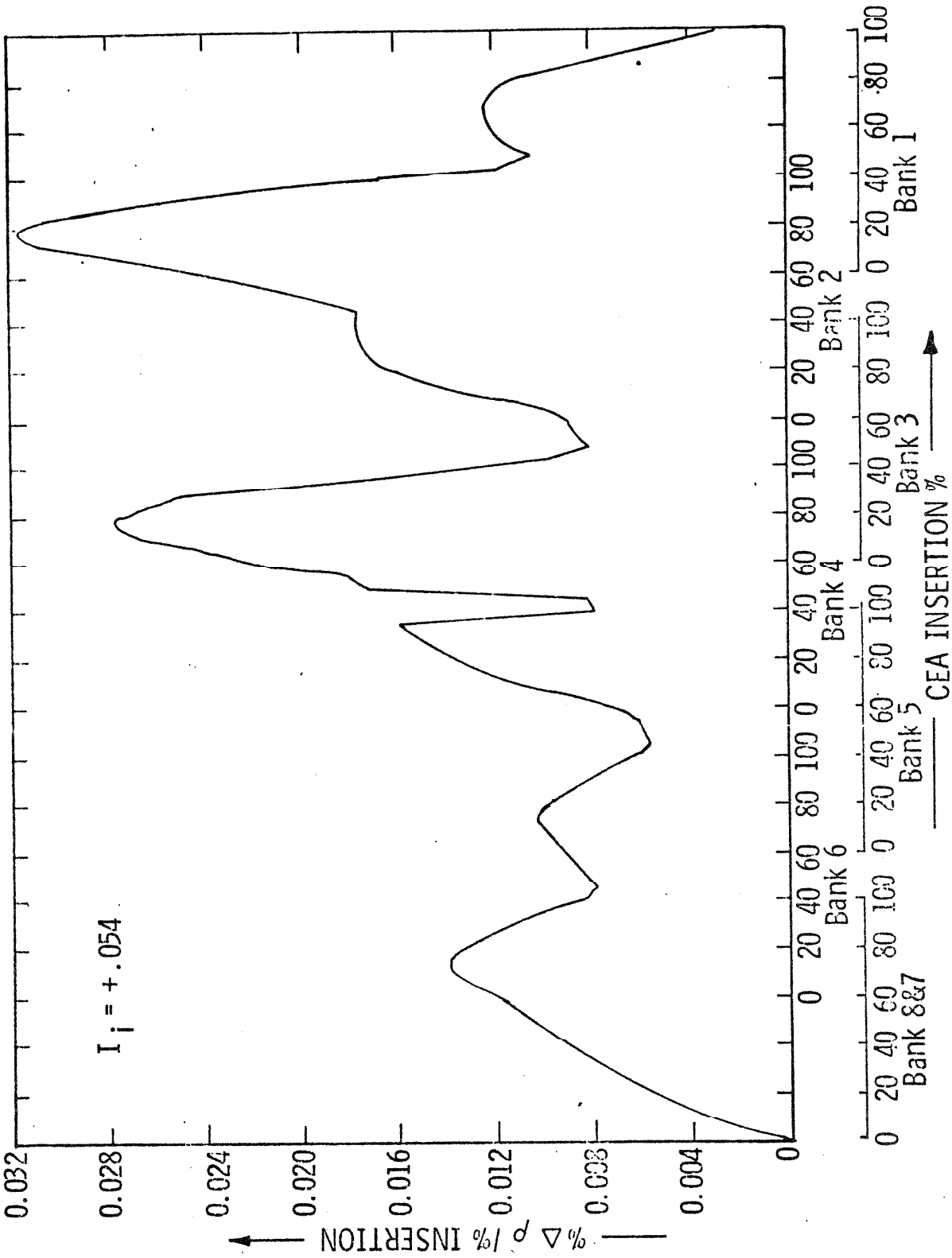

Am. 3-7/85

FLORIDA POWER & LIGHT CO. St. Lucie Plant	DIFFERENTIAL WORTH vs INSERTION AT BOL SEQUENTIAL INSERTION OF ROD GROUPS WITH 40 PERCENT OVERLAP - NO PLRS Cycle 1	Figure 4.3-26C

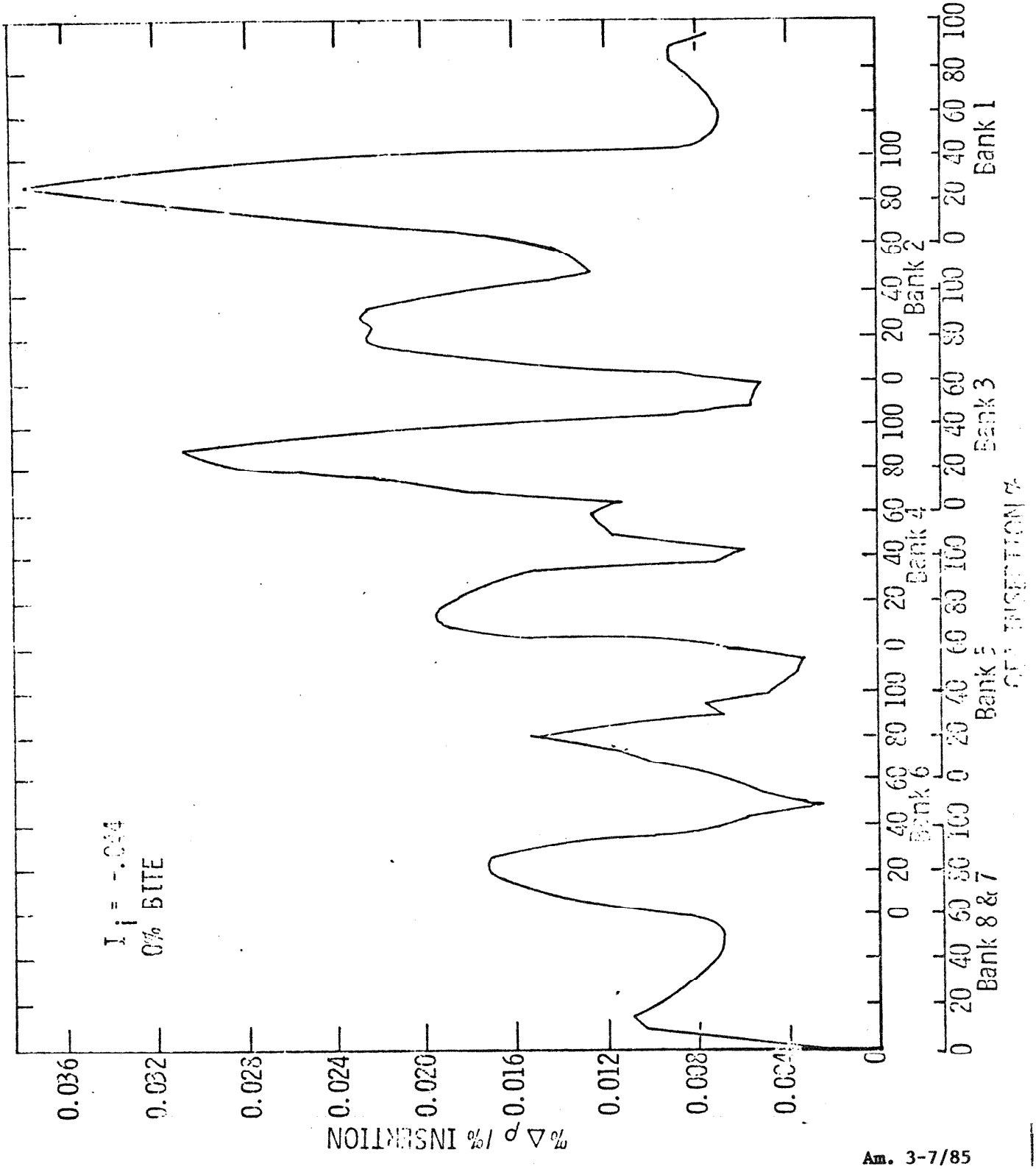

Am. 3-7/85

FLORIDA POWER & LIGHT CO. St. Lucie Plant	DIFFERENTIAL WORTH vs INSERTION AT EOL SEQUENTIAL INSERTION OF ROD GROUPS WITH 40 PERCENT OVERLAP - NO PLRS Cycle 1	Figure 4.3-26D

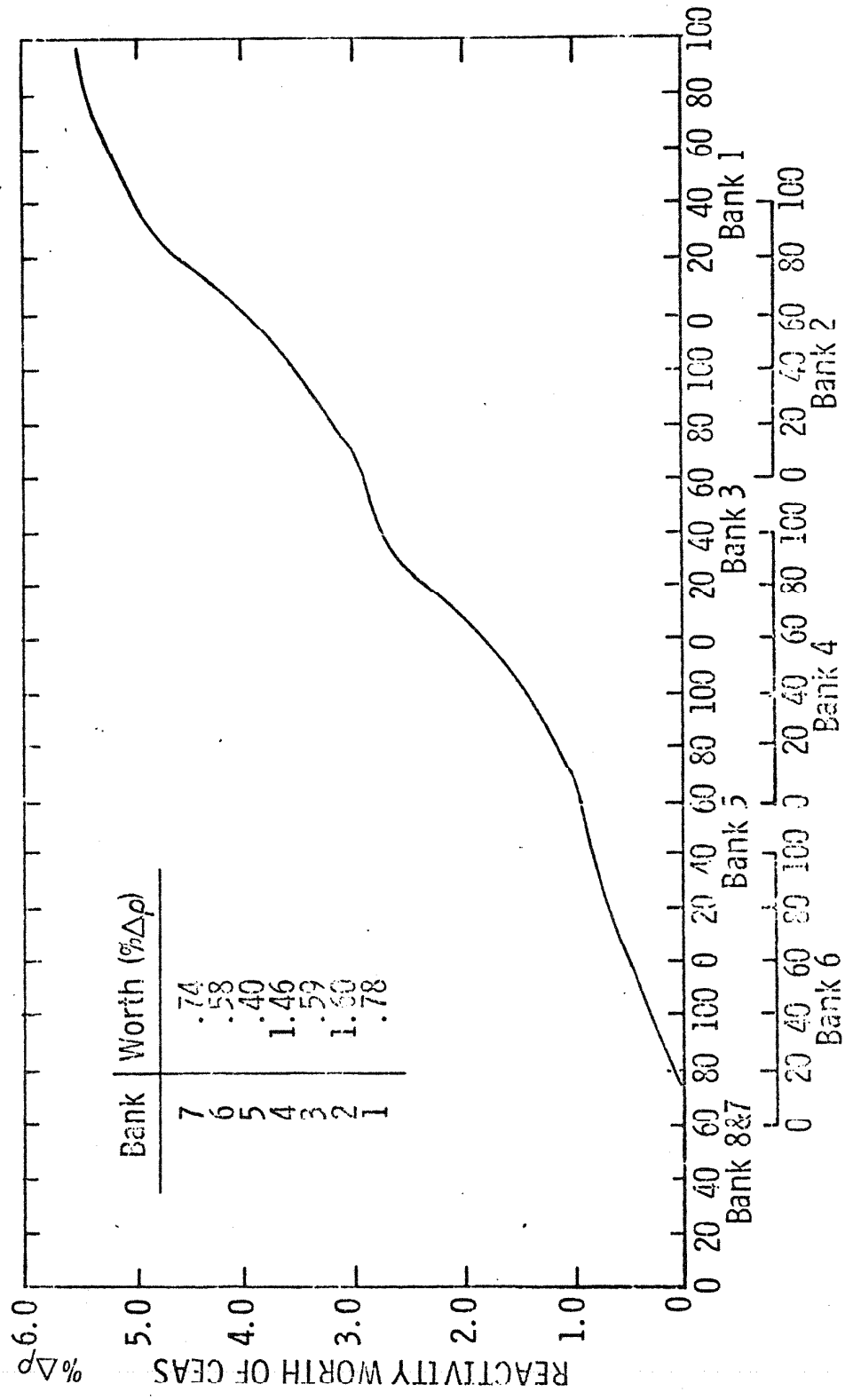

Am. 3-7/85

FLORIDA POWER & LIGHT CO. St. Lucie Plant	INTEGRAL WORTH vs INSERTION AT BOL (WITH 0.6% Δ ρ BITE) (WITHOUT PLRS) Cycle 1	Figure 4.3-26E

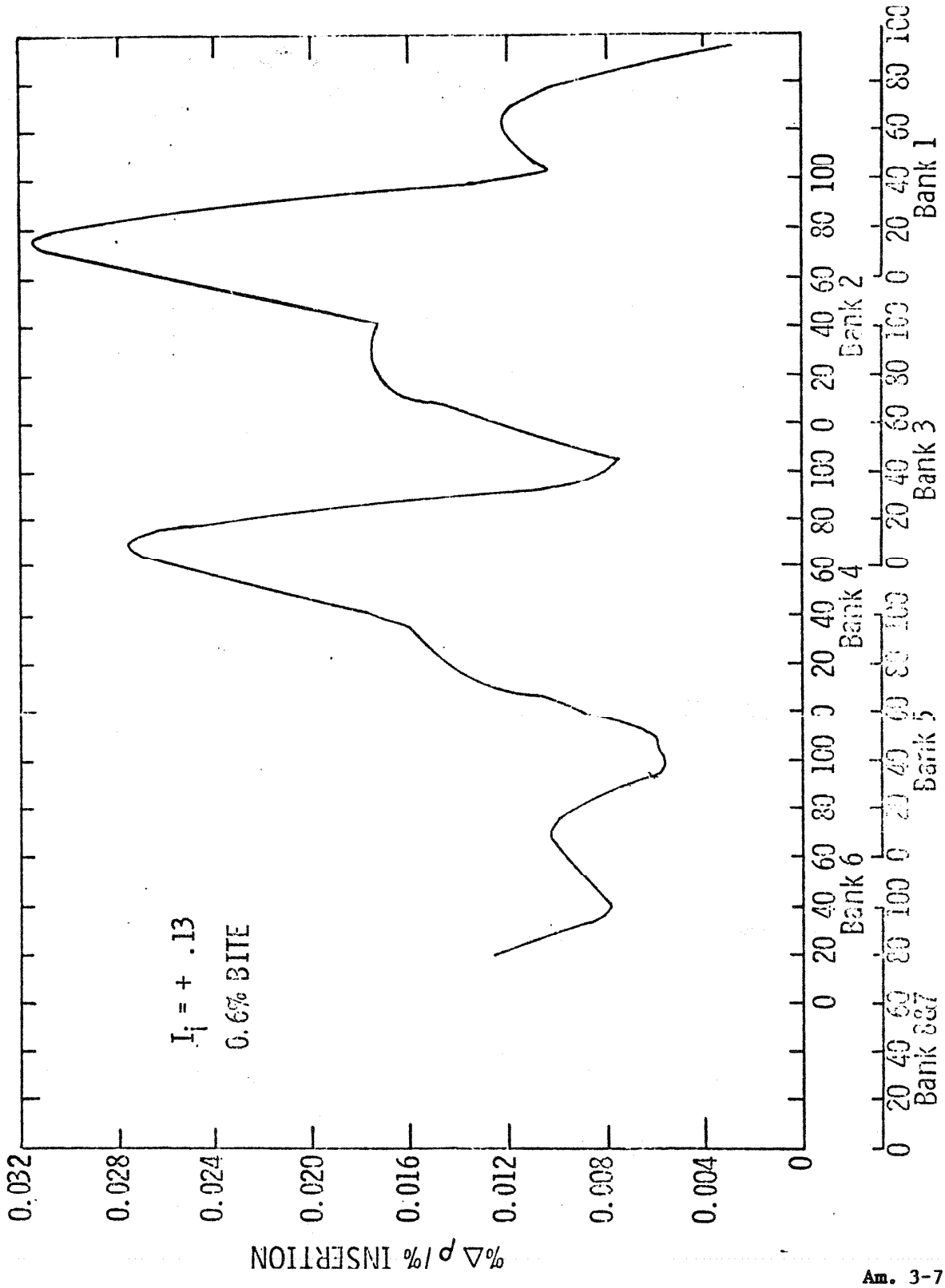

Am. 3-7/85

FLORIDA POWER & LIGHT CO. St. Lucie Plant	DIFFERENTIAL WORTH vs INSERTION AT BOL SEQUENTIAL INSERTION OF ROD GROUPS WITH 40 PERCENT OVERLAP - NO PLRS Cycle 1	Figure 4.3-20F

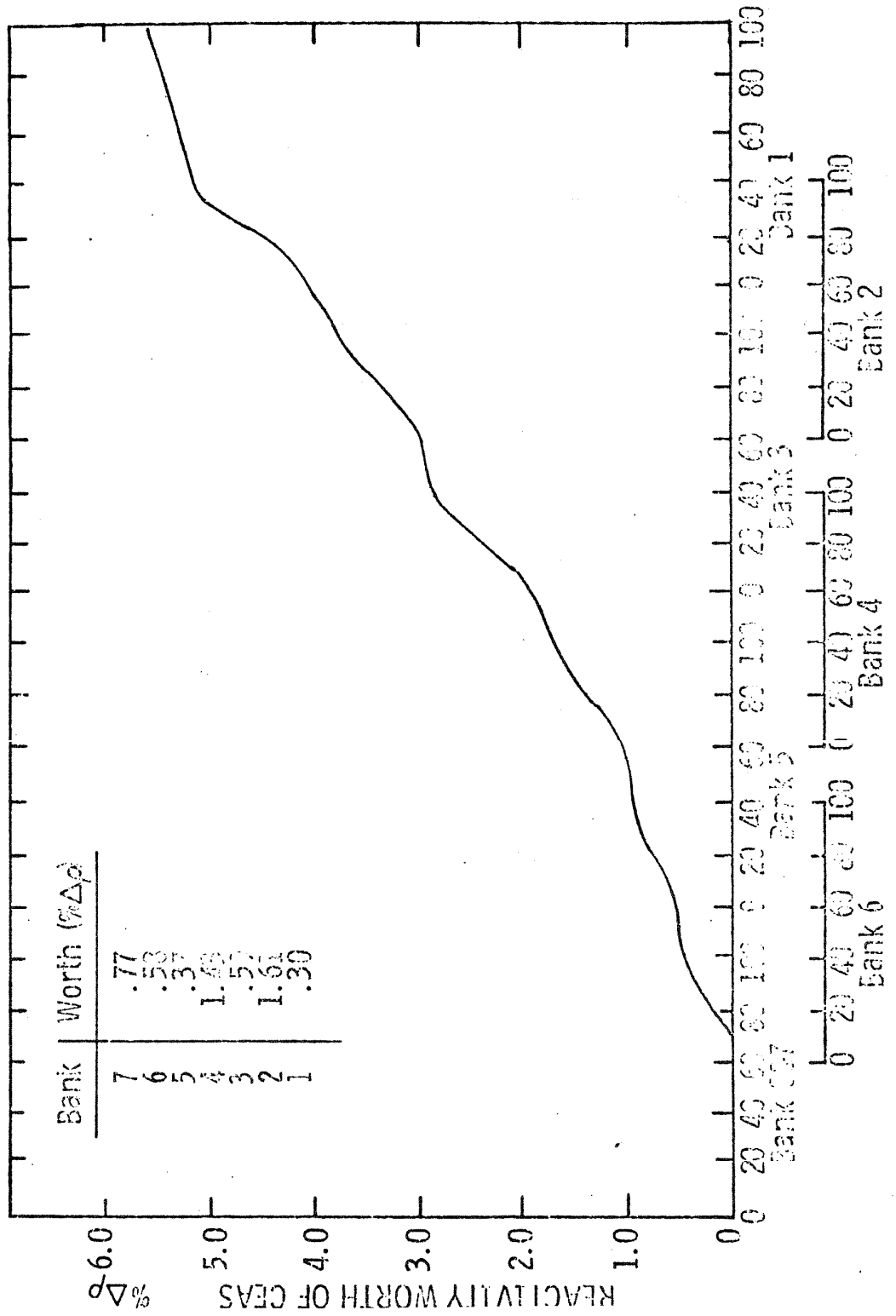

Am. 3-7/85

FLORIDA POWER & LIGHT CO. St. Lucie Plant	INTEGRAL WORTH vs INSERTION AT EOL (WITH 0.6 %Δρ BITE) (WITHOUT PLRS) Cycle 1	Figure 4.3-26G

FLORIDA POWER & LIGHT CO.
St. Lucie Plant

DIFFERENTIAL WORTH vs. INSERTION AT EOL
SEQUENTIAL INSERTION OF ROD GROUPS
WITH 40 PERCENT OVERLAP - NO PLRS
Cycle 1

Figure 4.3-26H

Am. 3-7/85

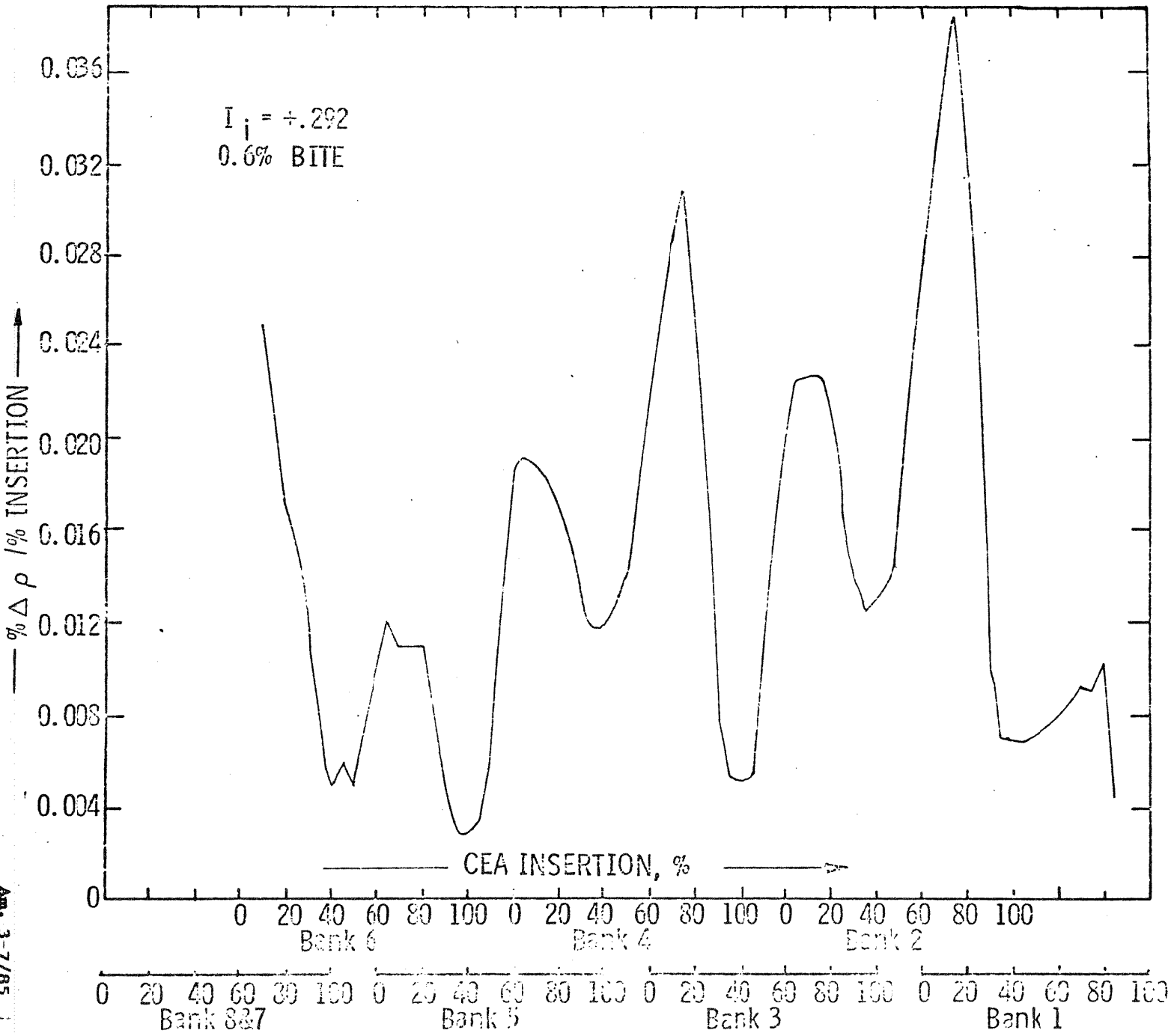

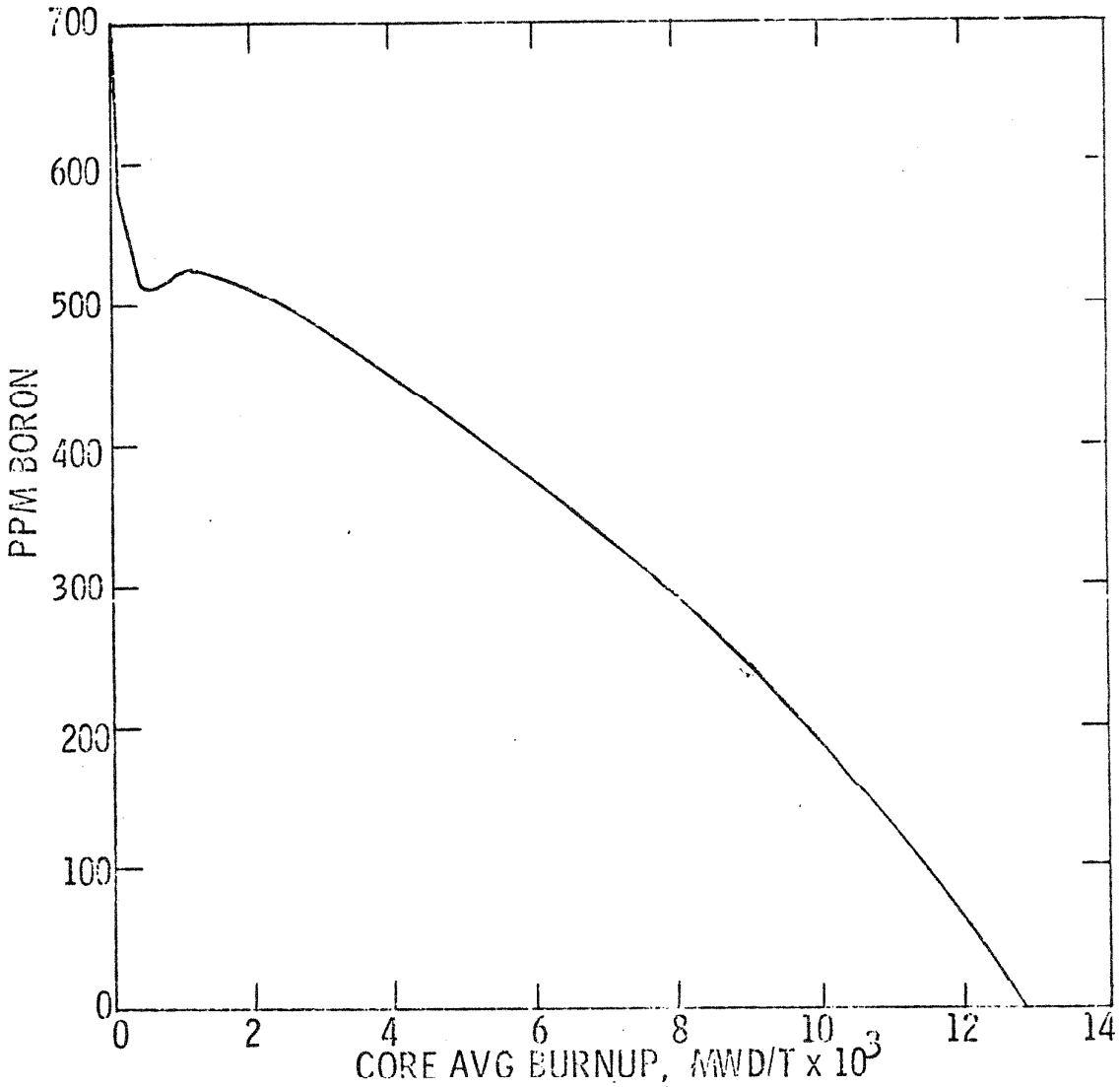

Am. 3-7/85

FLORIDA POWER & LIGHT CO. St. Lucie Plant	CRITICAL BORON CONCENTRATION PPM vs BURNUP AT FULL POWER ALL CEAs WITHDRAWN Cycle 1	Figure 4.3-26I

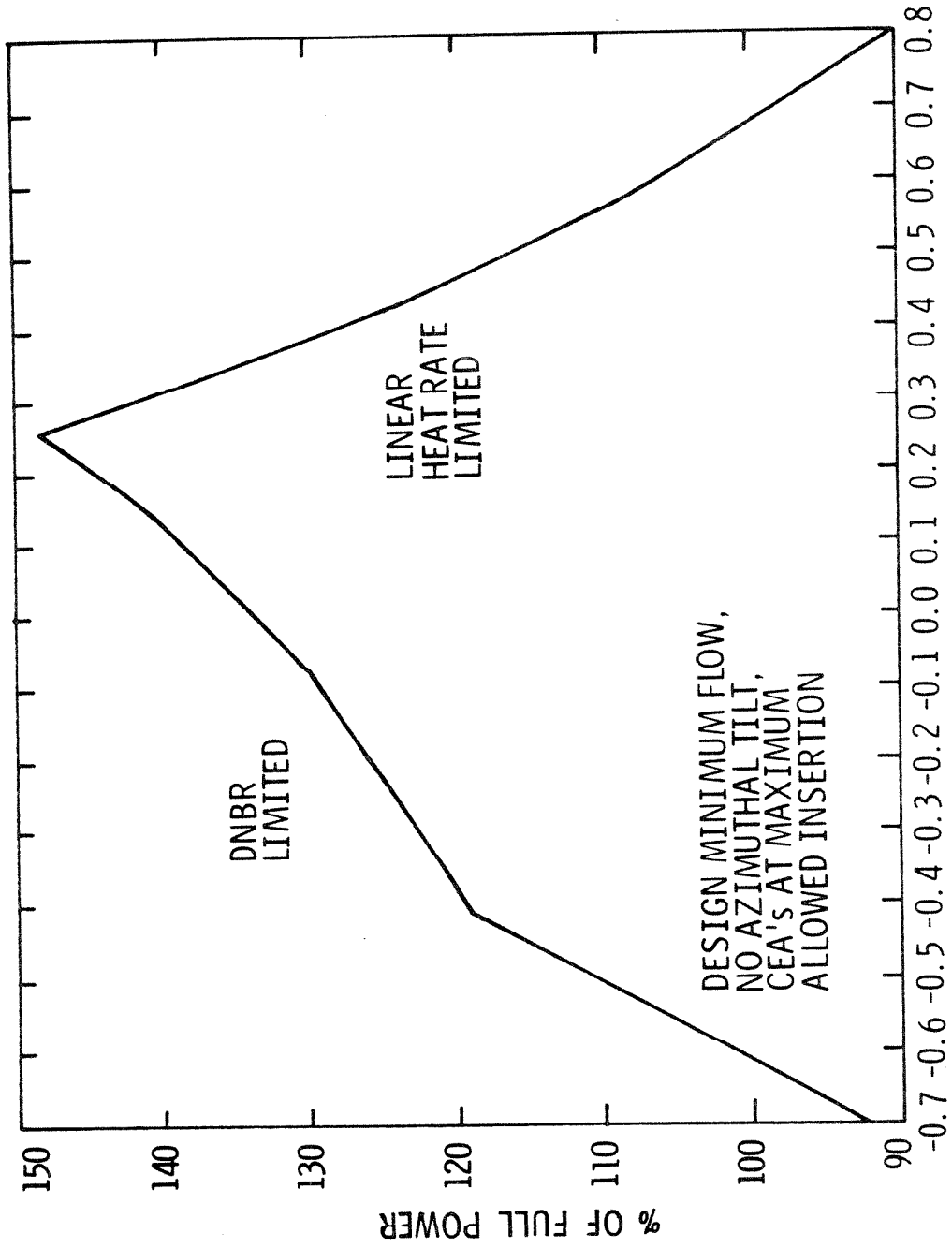

FLORIDA POWER & LIGHT CO. St. Lucie Plant Unit 1	Typical Core Safety Limit Curve % of Full Power vs Internal Axial Shape Index	Figure 4.3-27

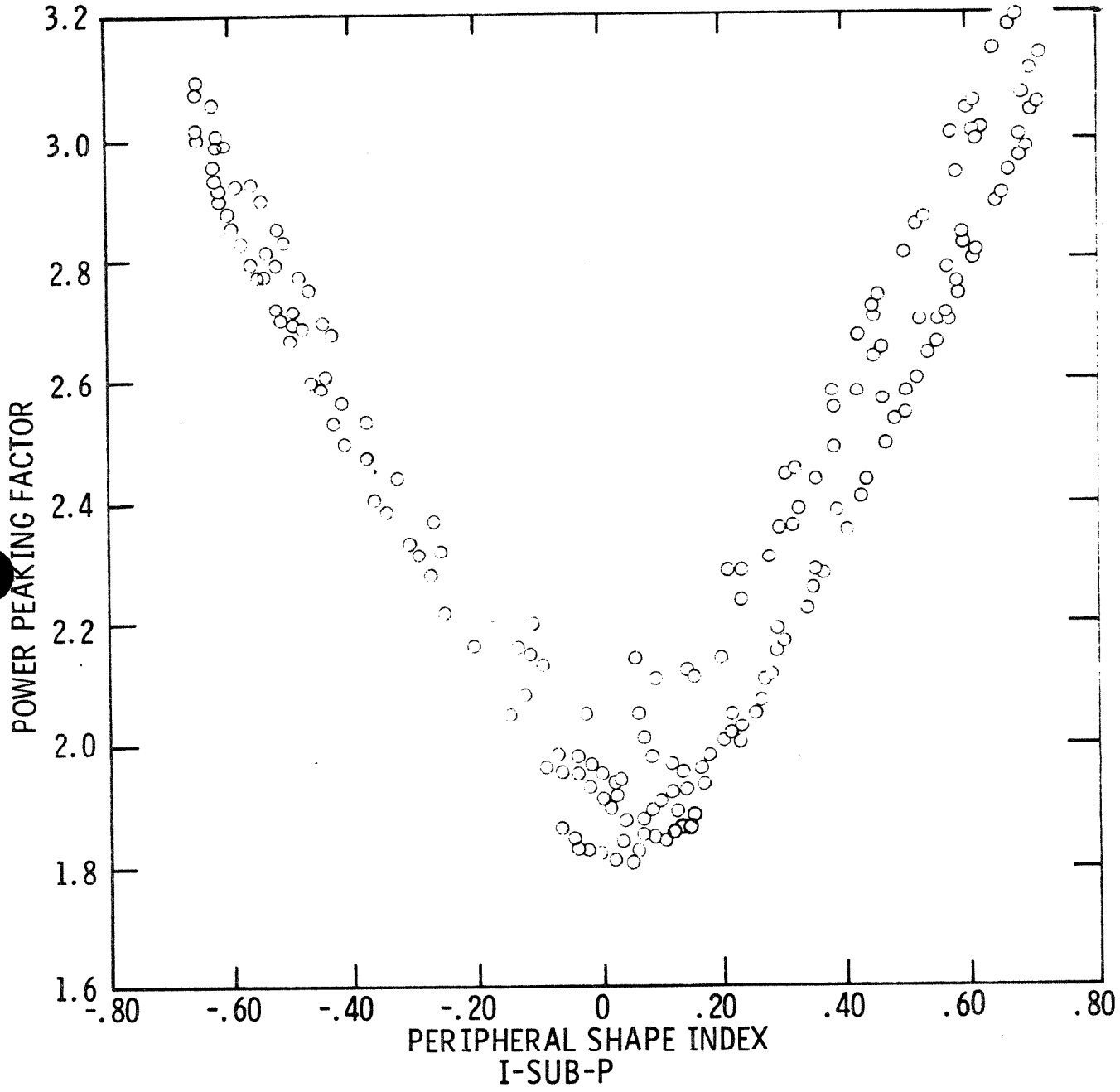

Cycle 1

FLORIDA POWER & LIGHT CO. St. Lucie Plant	TYPICAL AXIAL ANALYSIS RESULTS BANK IN 50%, ALL PLR's	Figure 4.3-27A

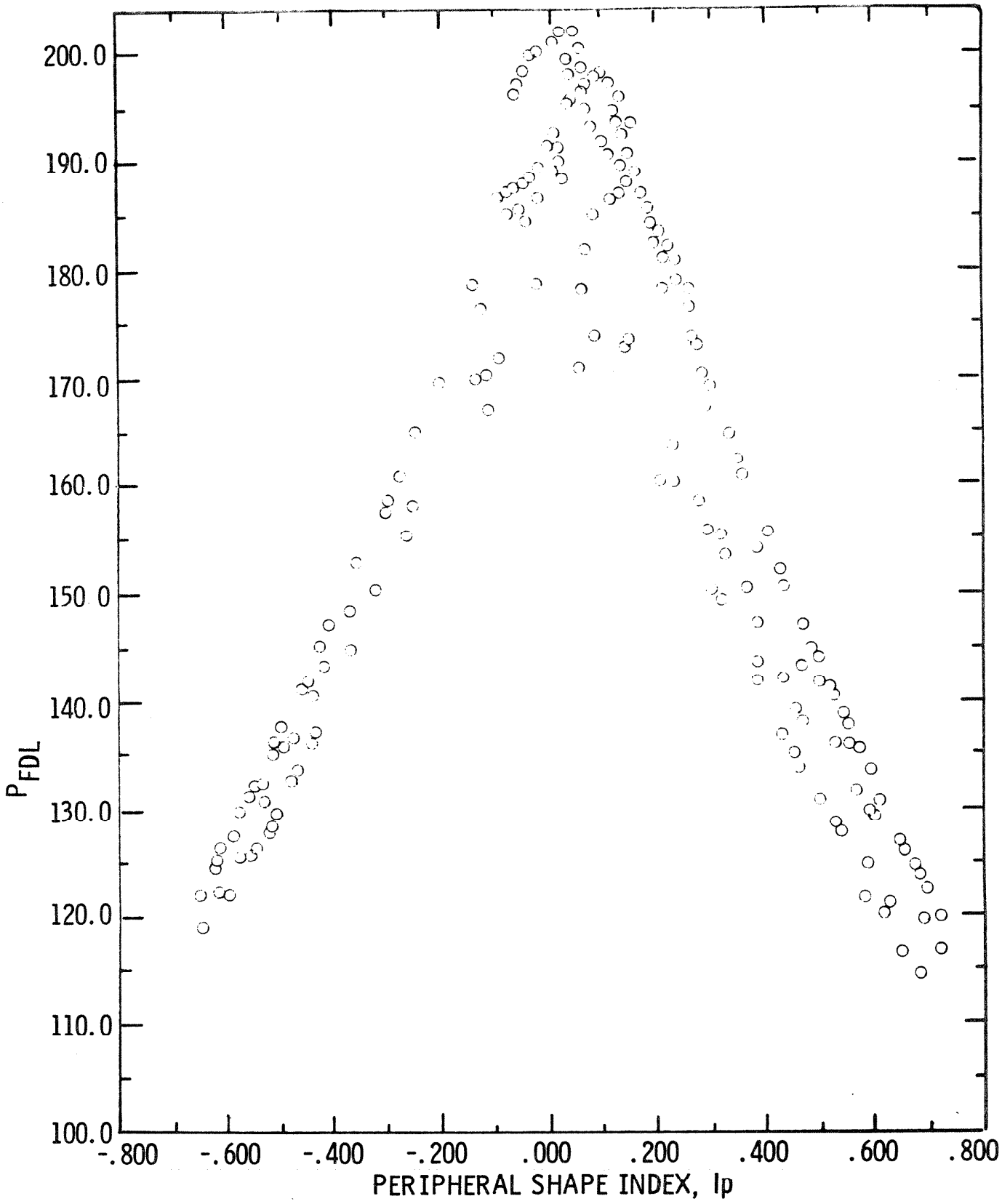

FLORIDA POWER & LIGHT CO. St. Lucie Plant	TYPICAL AXIAL ANALYSIS RESULTS BANK IN 50%, ALL PLR's Cycle 1	Figure 4.3-27B

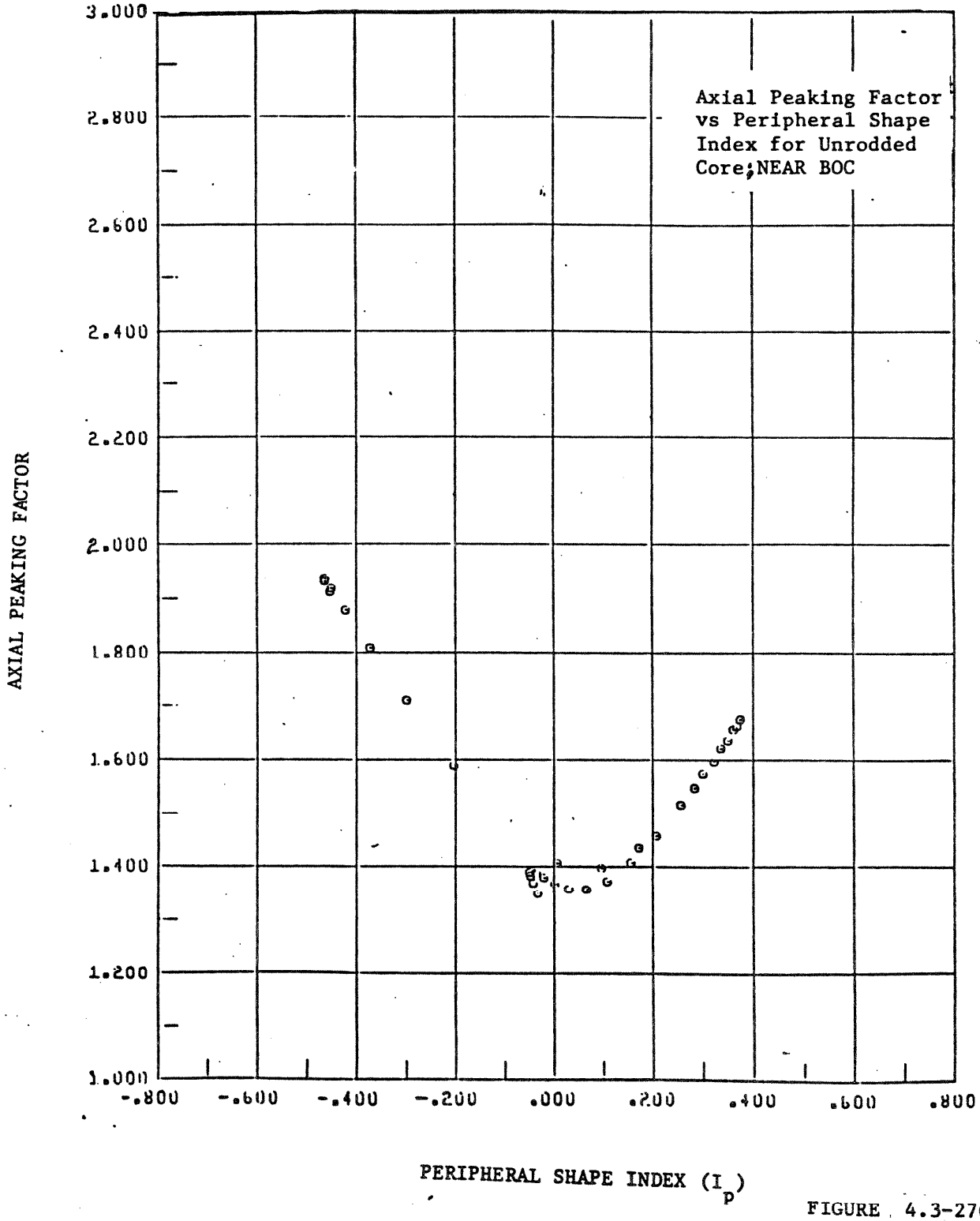

FIGURE 4.3-27C

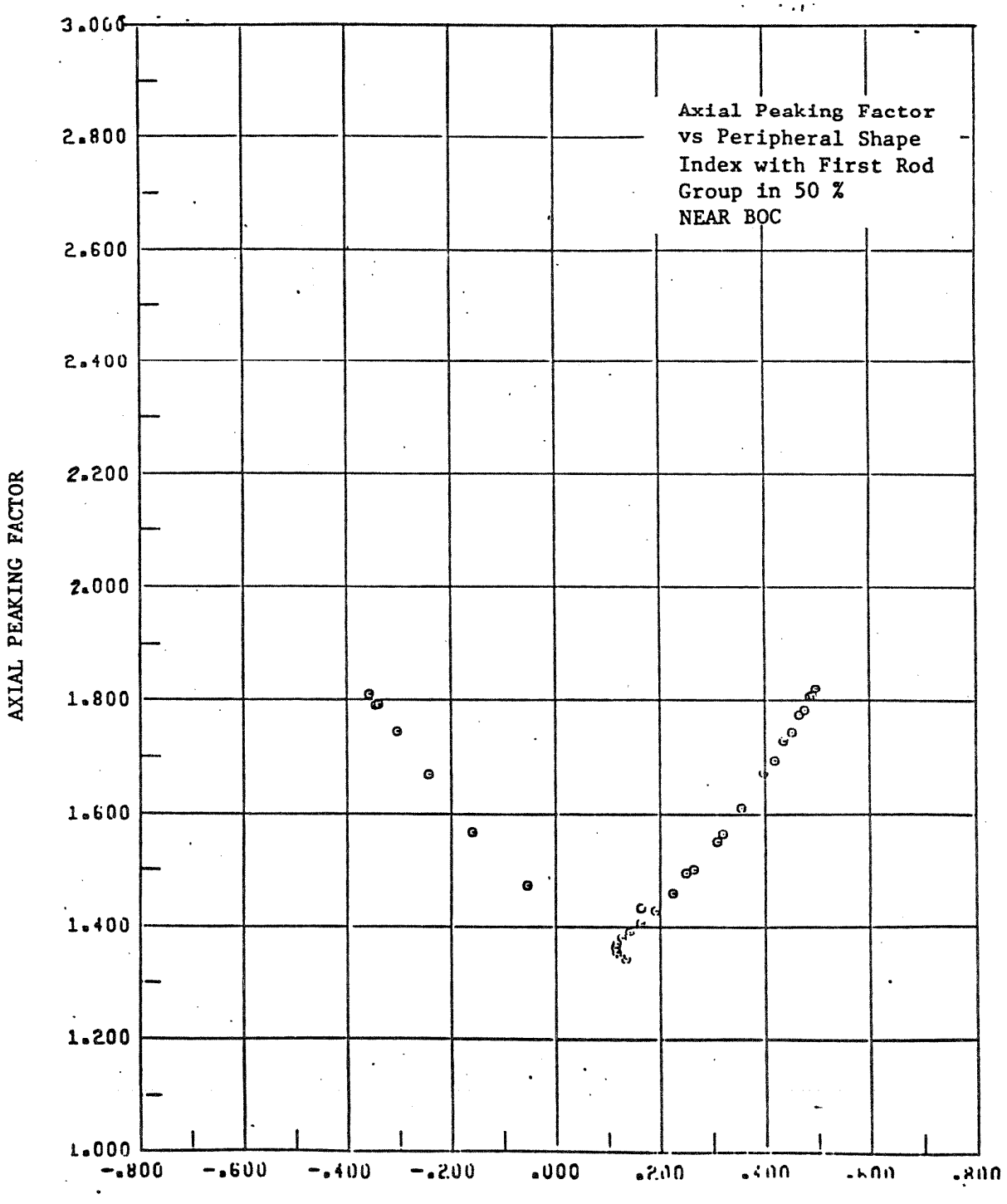

FIGURE 4.3-27D

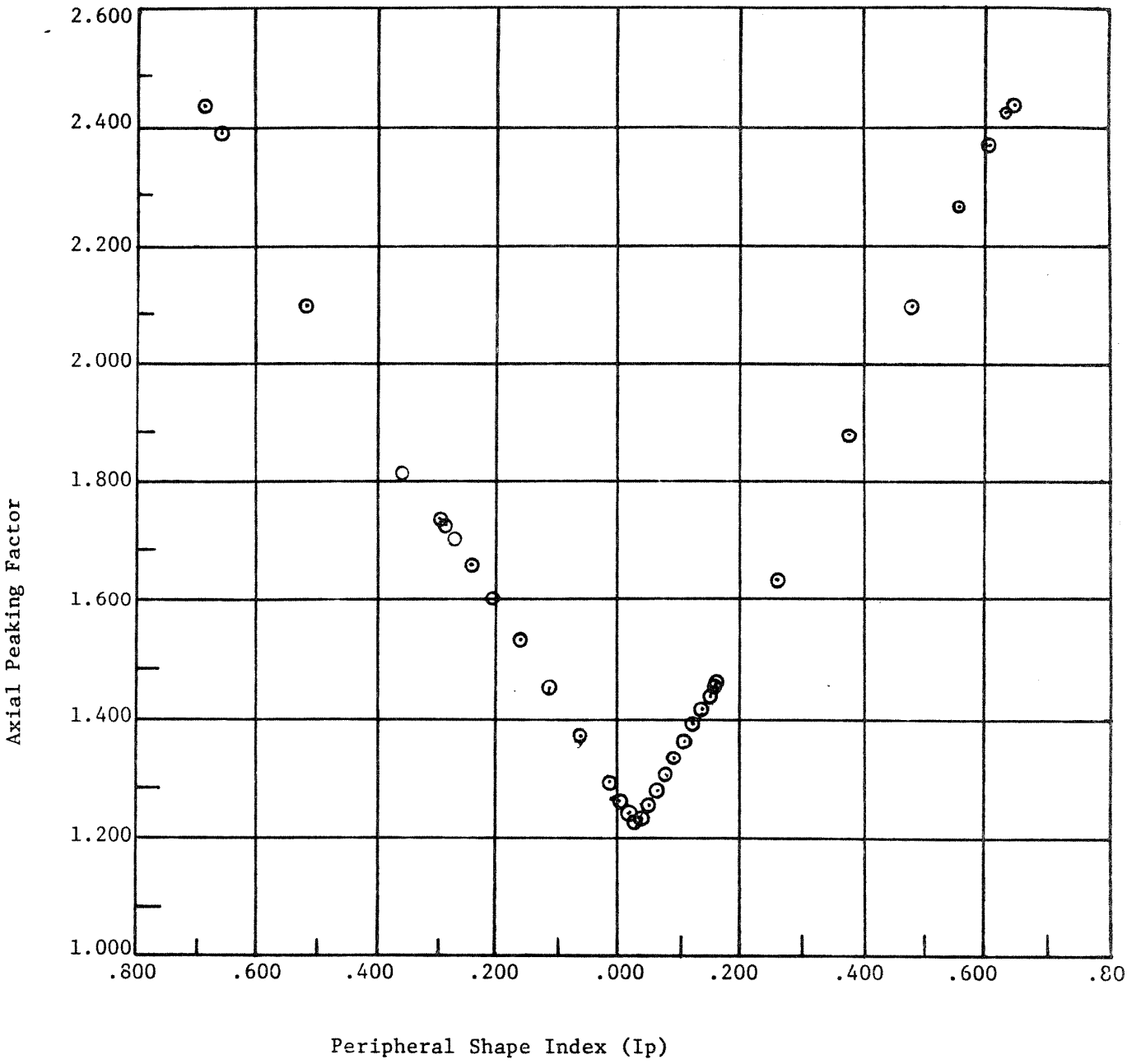

FLORIDA POWER & LIGHT CO. St. Lucie Plant Unit 1	Axial Peaking Factor vs Peripheral Shape Index for Unrodded Core NEAR EOC	Figure 4.3-27E

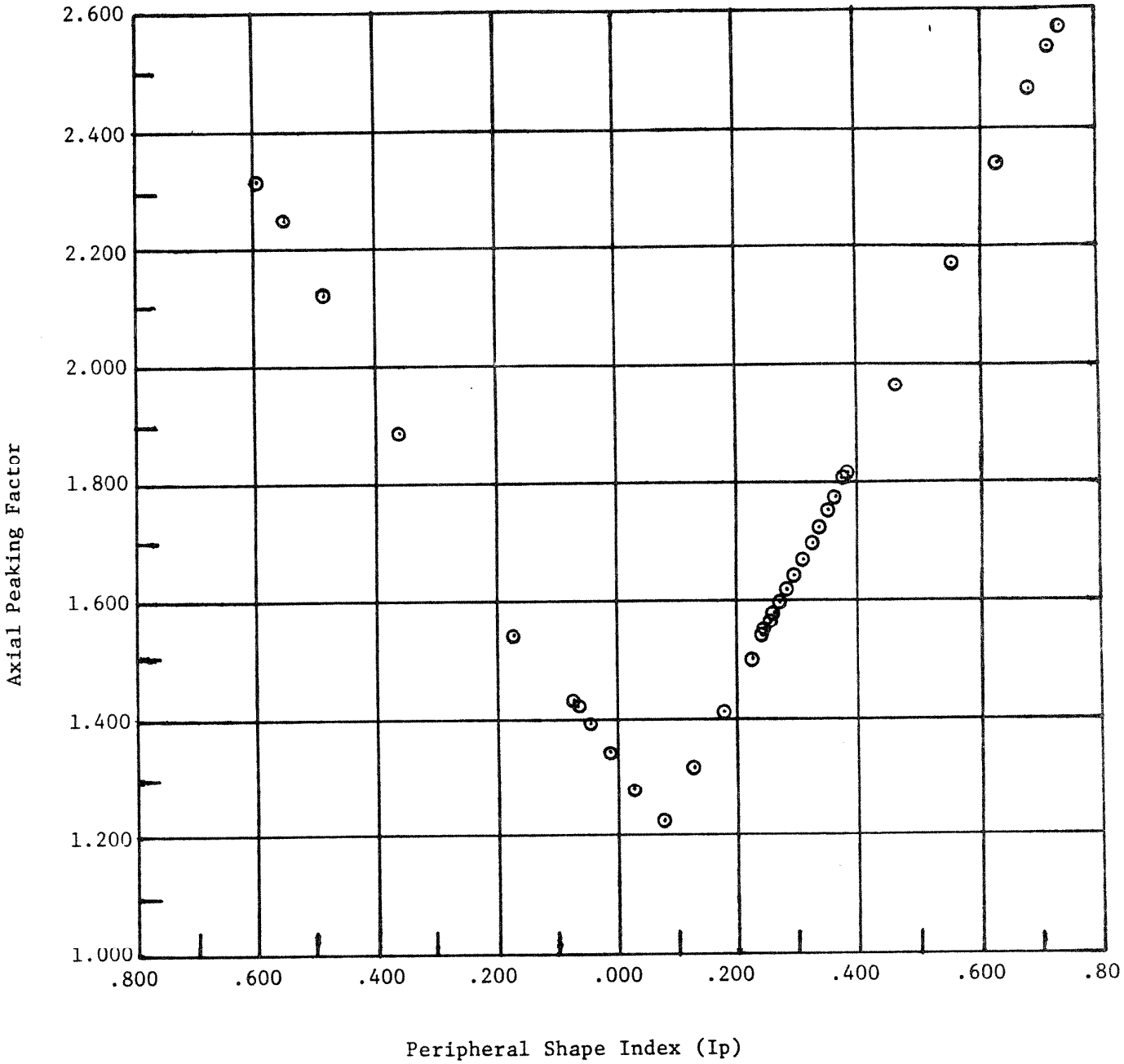

FLORIDA POWER & LIGHT CO. St. Lucie Plant Unit 1	Axial Peaking Factor vs Peripheral Shape Index with First Group Inserted 50% NEAR EOC	Figure 4.3-27F

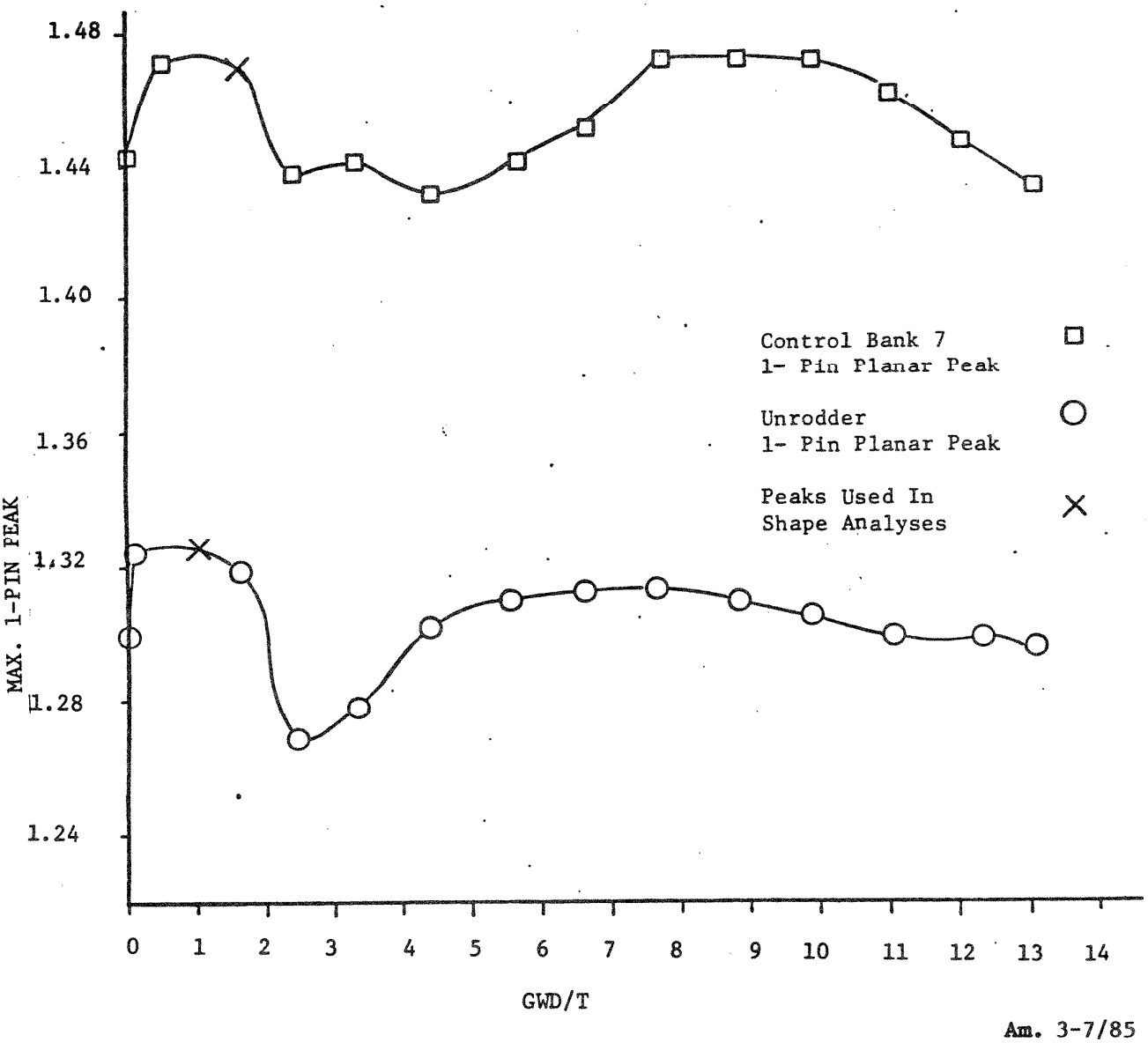

Am. 3-7/85

Note: See Cycle 6 RSE Figures 6.2 & 6.3 for current 1-pin peak information

FLORIDA POWER & LIGHT COMPANY
ST. LUCIE PLANT UNIT 1

Cycle 1
UNRODDED AND GROUP 7 RADIAL PEAKING FACTORS VERSUS BURNUP

FIGURE
4.3-27G

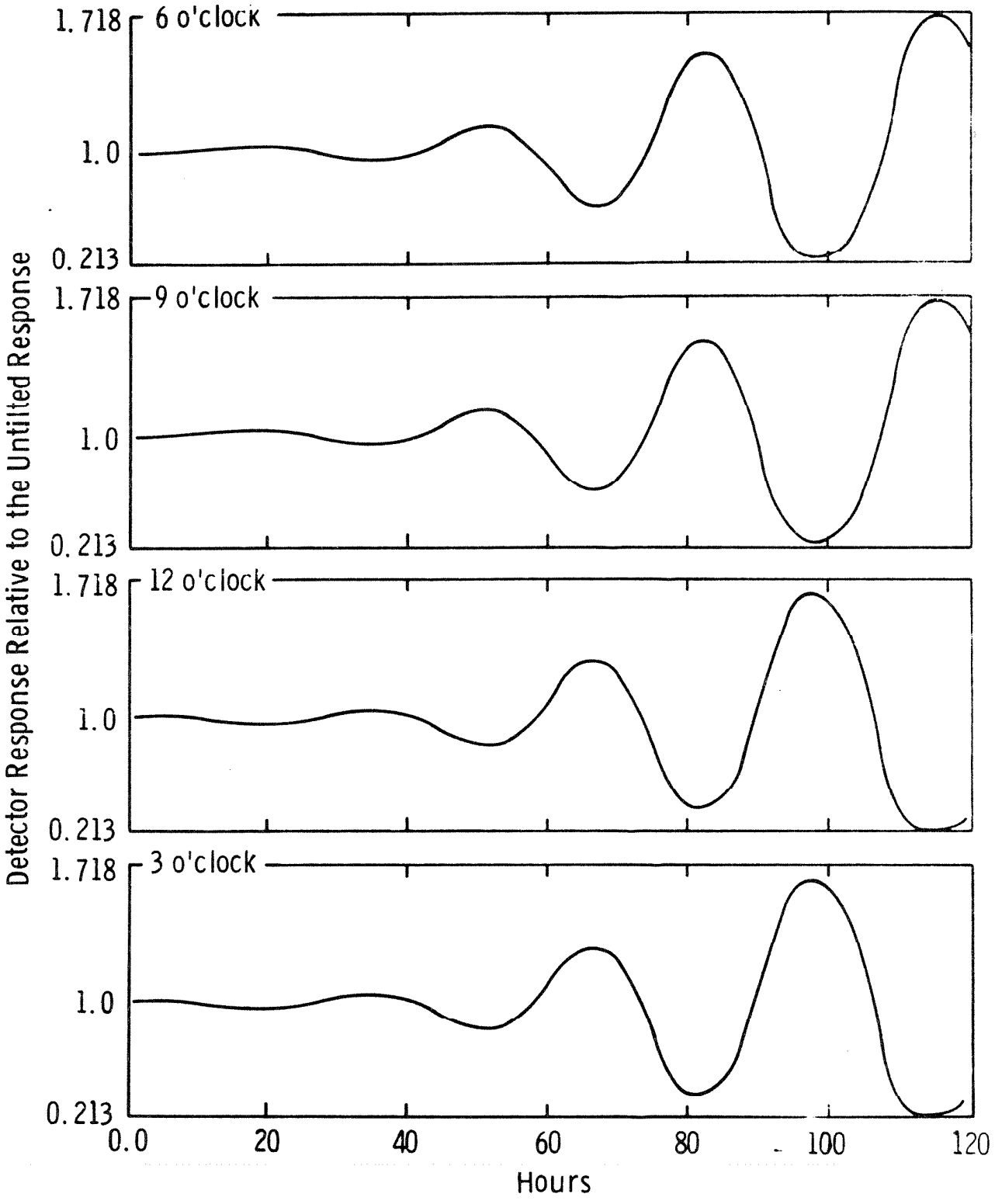

FLORIDA POWER & LIGHT CO. St. Lucie Plant Unit 1	Free Oscillation Response of Detectors at Various Azimuthal Locations	Figure 4.3-28

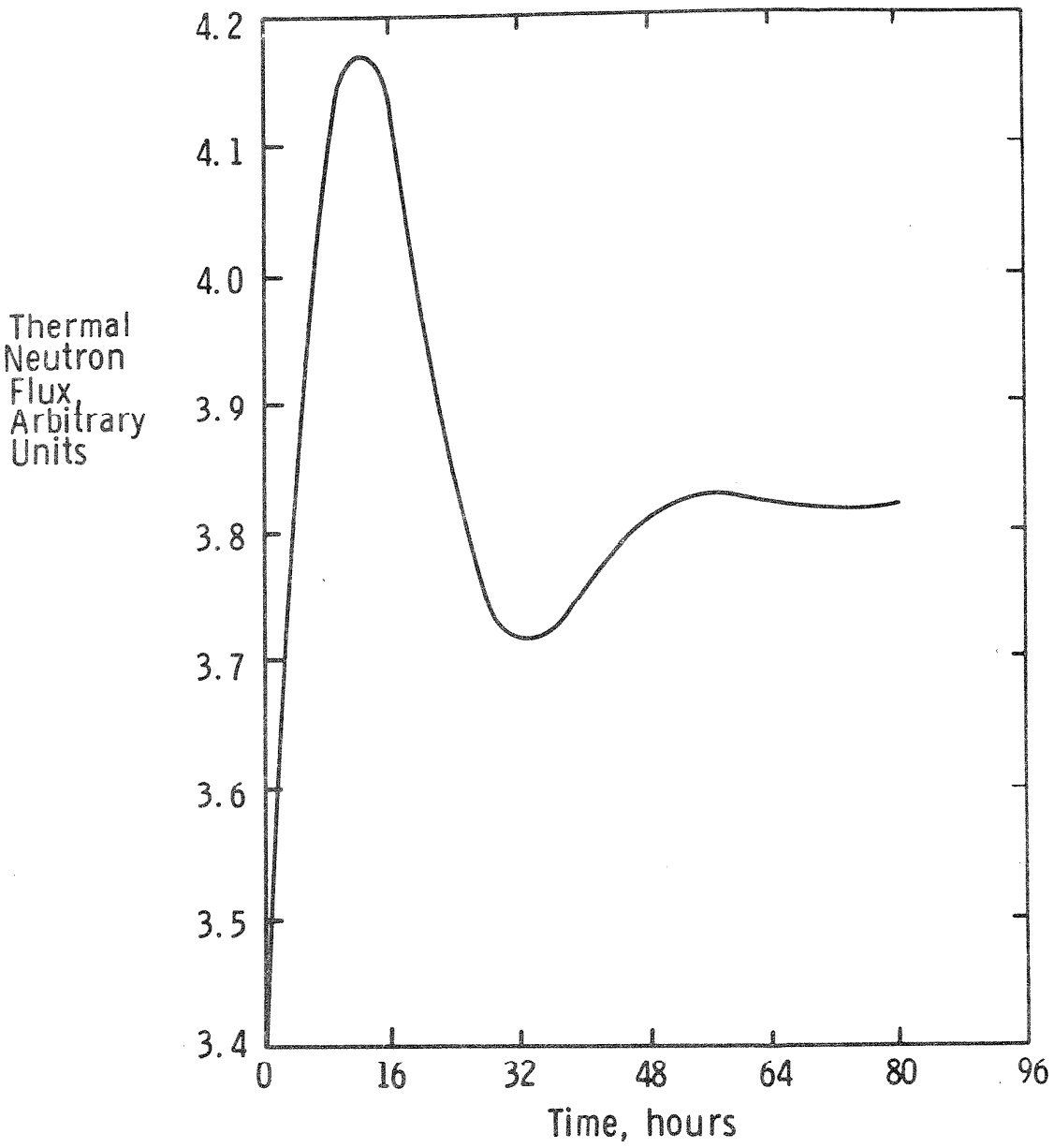

FLORIDA POWER & LIGHT CO. St. Lucie Plant Unit 1	Thermal Neutron Flux at the Center of the Core vs Time	Figure 4.3-29

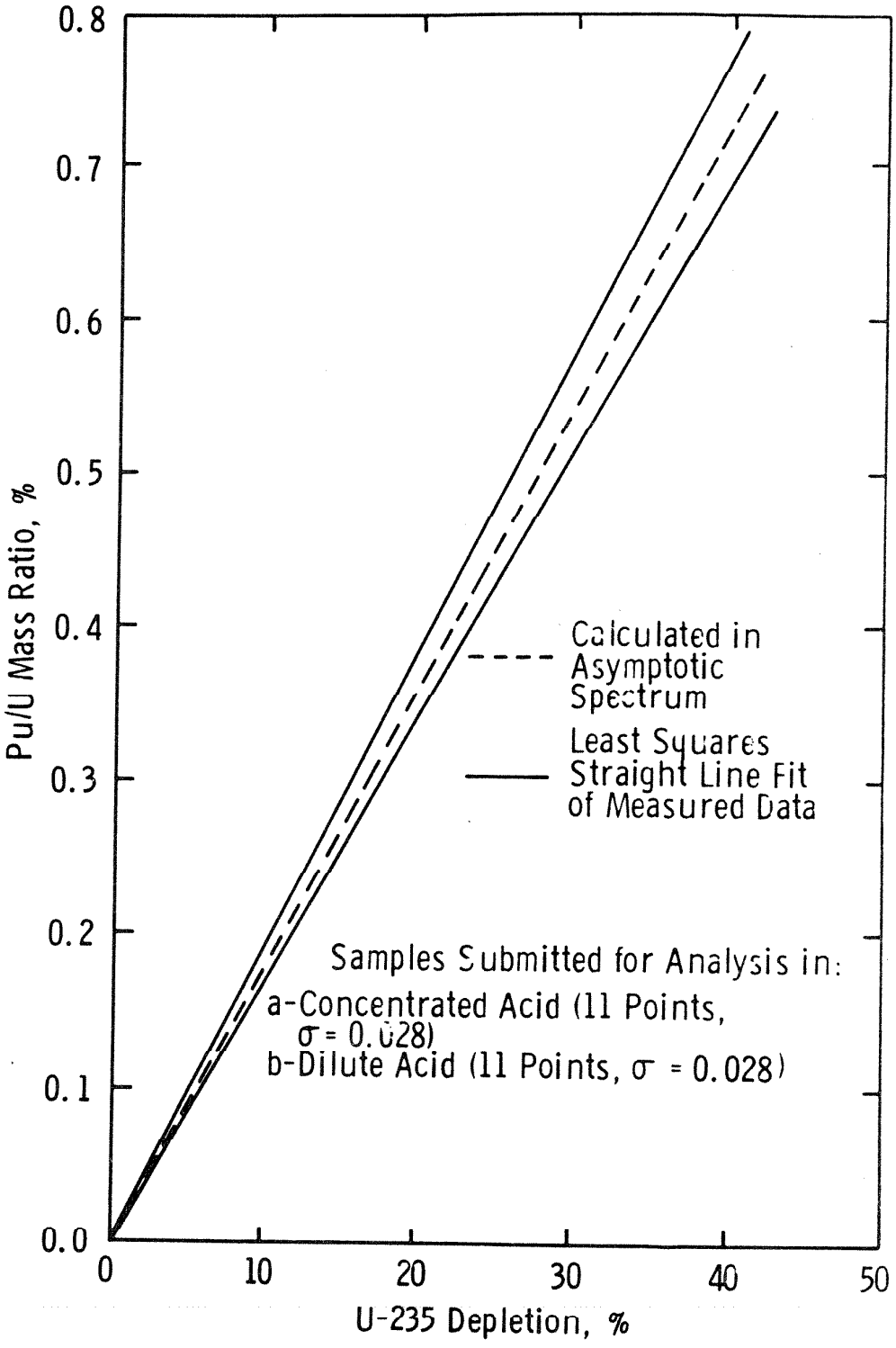

FLORIDA POWER & LIGHT CO. St. Lucie Plant Unit 1	Comparison of Calculated and Measured Plutonium to Uranium Mass Ratio in the Asymptotic Neutron Spectrum for Yankee Rowe	Figure 4.3-30

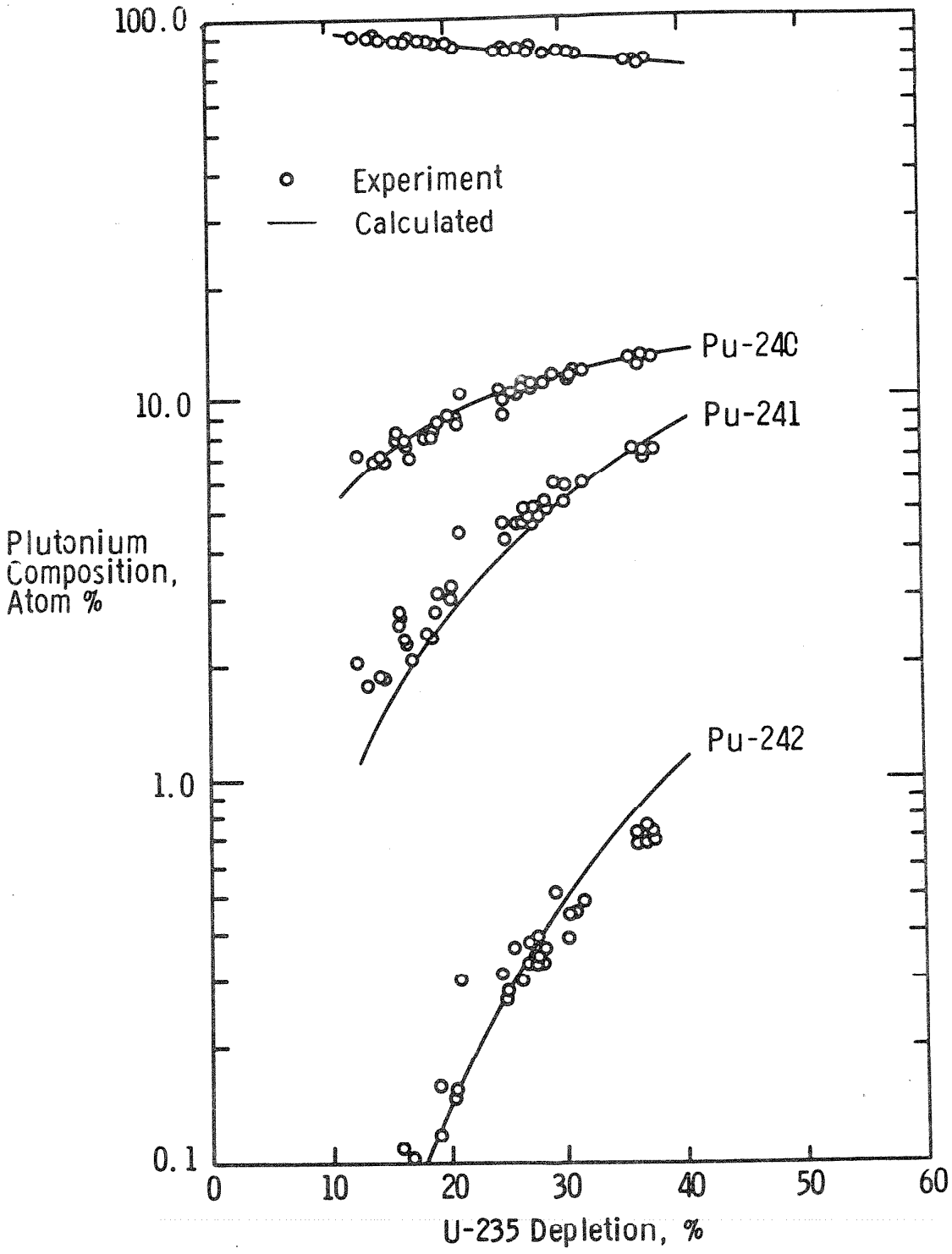

FLORIDA POWER & LIGHT CO. St. Lucie Plant Unit 1	Plutonium Isotopic Composition vs Fuel Depletion in the Asymptotic Spectrum for Yankee Rowe	Figure 4.3-31

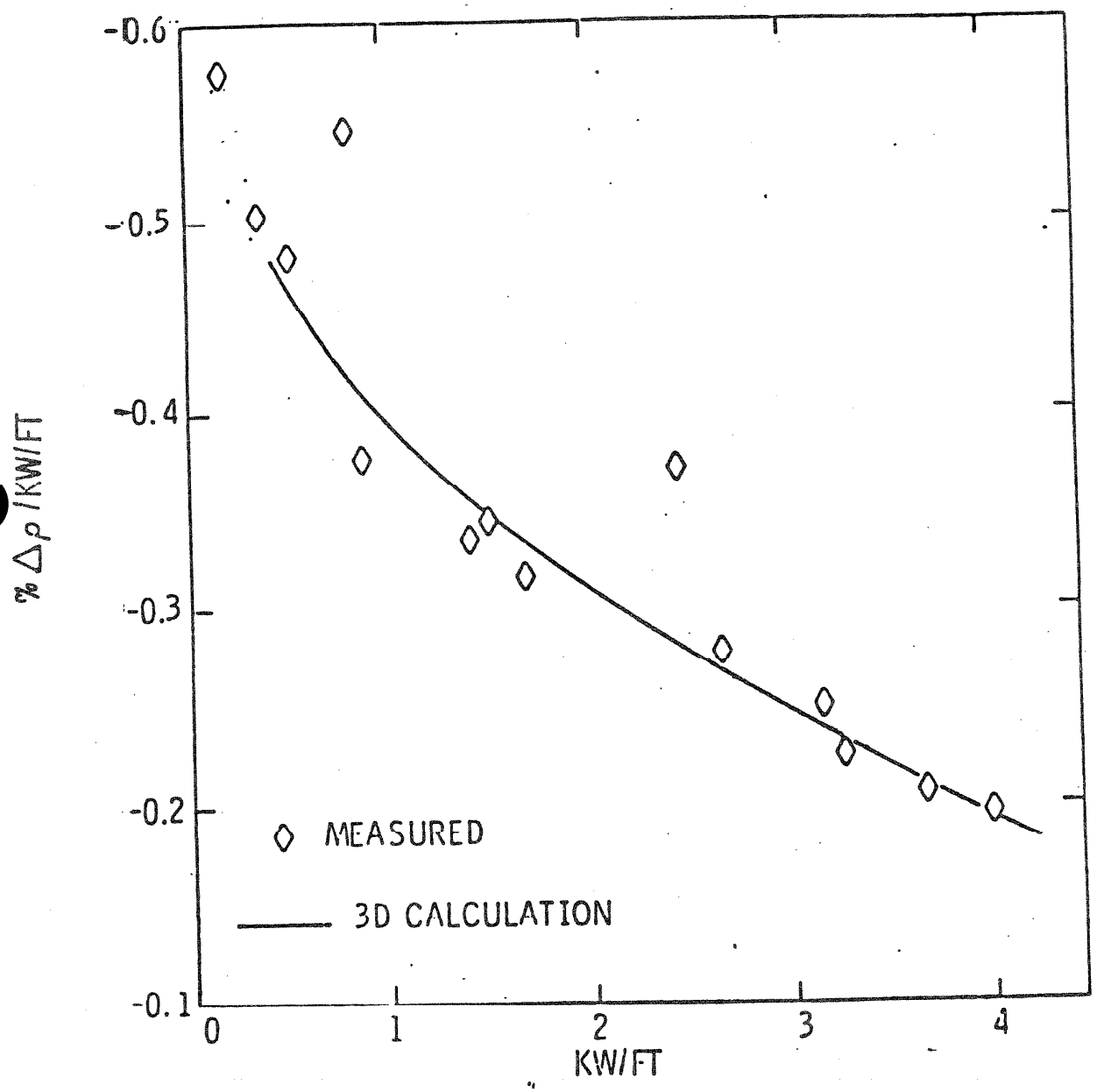

SAN ONOFRE CYCLE 1

FUEL TEMPERATURE CONTRIBUTION TO THE

POWER COEFFICIENT AT STARTUP

FIGURE

4.3-32

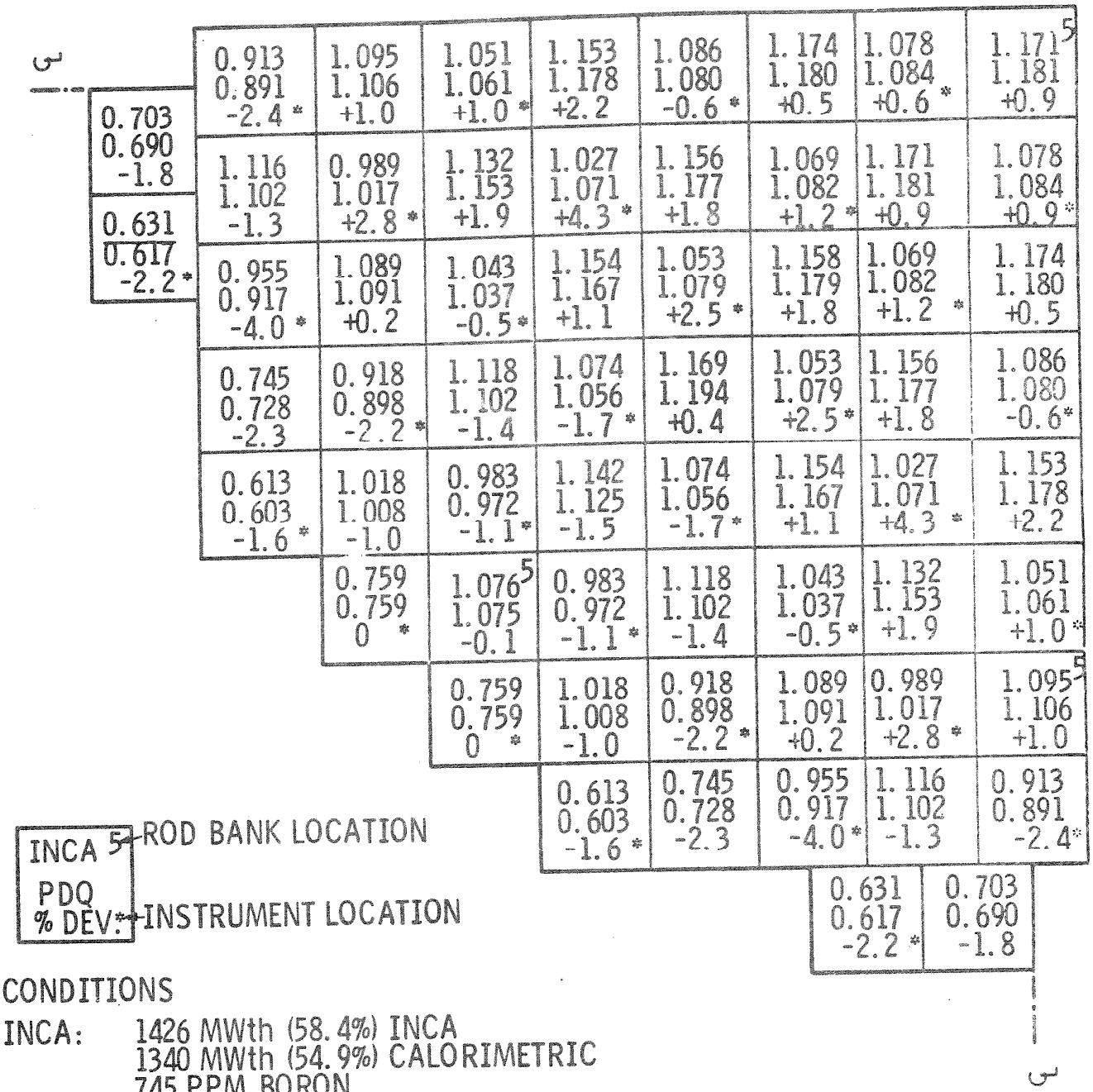

CONDITIONS

INCA: 1426 MWth (58.4%) INCA
1340 MWth (54.9%) CALORIMETRIC
745 PPM BORON
BANK 5 IN 4%

PDQ: 1220 MWth (50%)
743 PPM BORON
BANK 5 IN 4%

RMS DEVIATION = 1.8%

FLORIDA POWER & LIGHT CO. St. Lucie Plant Unit 1	Maine Yankee Power Escalation Tests Power Distribution, 50% Power, Unrodded Equilibrium Xenon	Figure 4.3-33

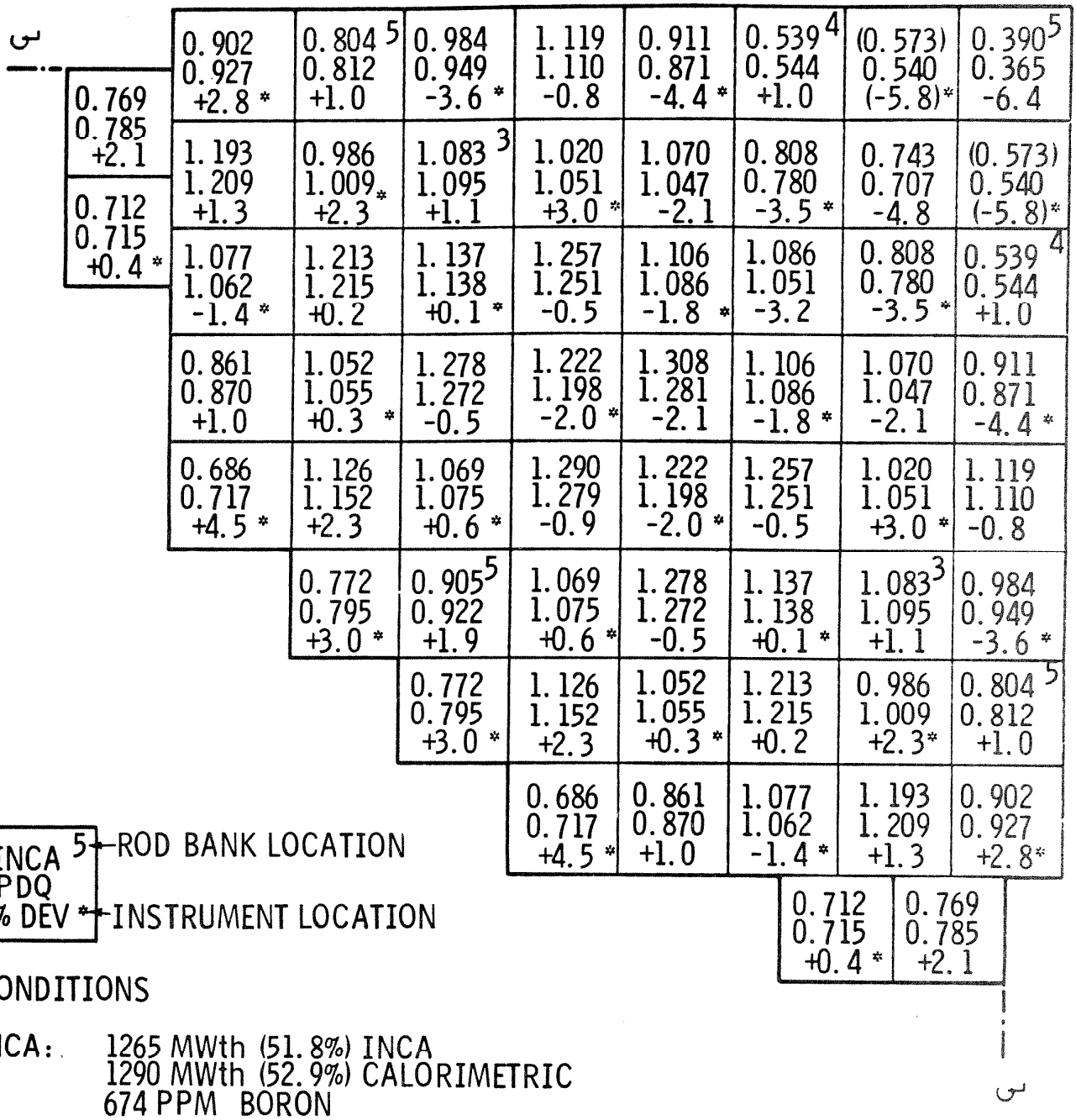

CONDITIONS

INCA: 1265 MWth (51.8%) INCA
1290 MWth (52.9%) CALORIMETRIC
674 PPM BORON

BANKS IN	5	4	3
	98%	85%	25%

PDQ-QUIX-CEPIA:
1220 MWth (50%) RMS DEVIATION = 2.3%
743 PPM BORON

BANKS IN	5	4	3
	98%	85%	25%

FLORIDA POWER & LIGHT CO. St. Lucie Plant Unit 1	Maine Yankee Power Escalation Tests Power Distribution, 50% Power, rodded Equilibrium Xenon	Figure 4.3-34

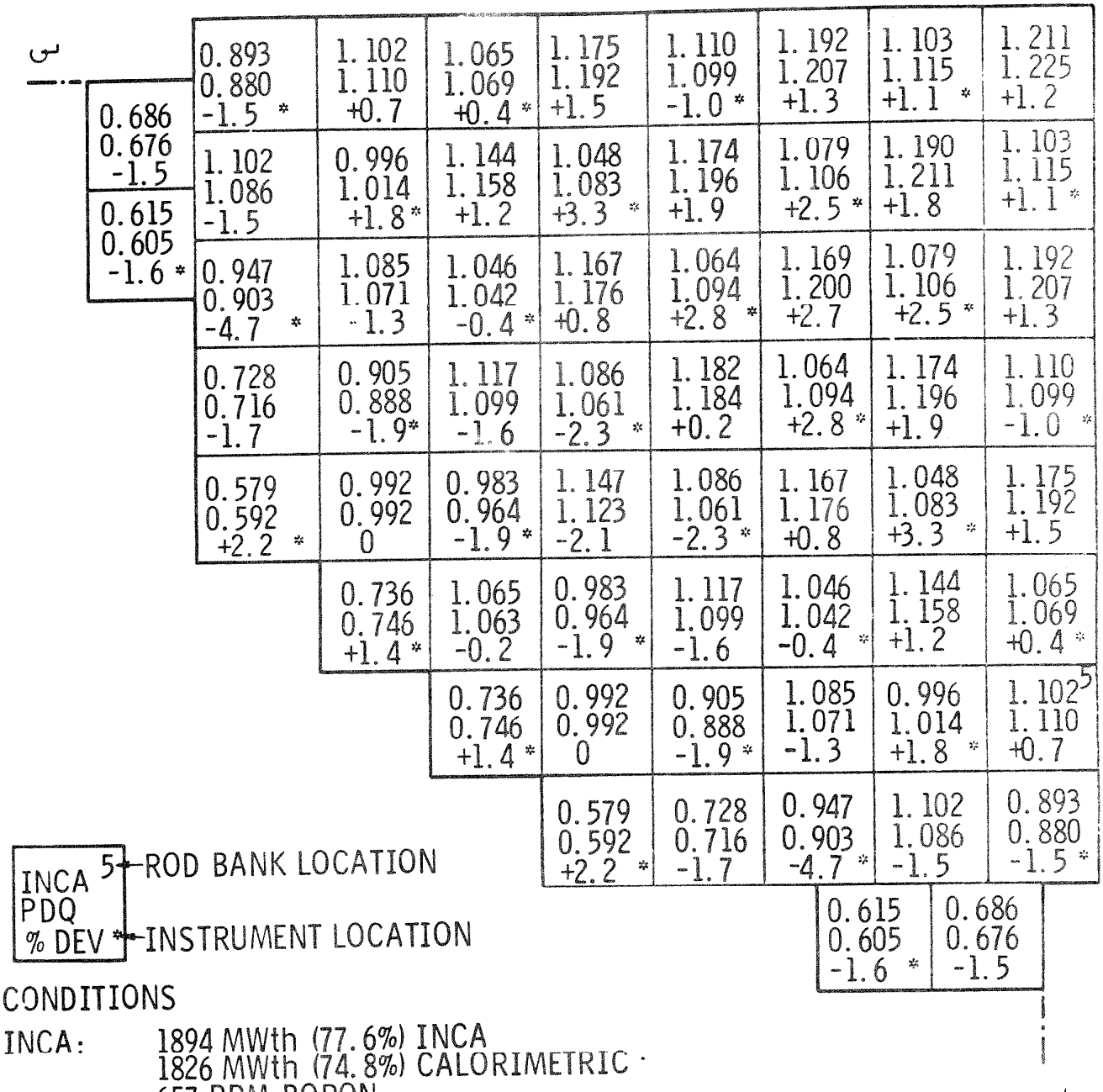

INCA 5 ← ROD BANK LOCATION
PDQ
% DEV * ← INSTRUMENT LOCATION

CONDITIONS

INCA: 1894 MWth (77.6%) INCA
1826 MWth (74.8%) CALORIMETRIC
657 PPM BORON
447.6 MWD/T
BANK 5 IN 1%

PDQ: 1952 MWth (80%)
700 PPM BORON
NO BURN UP
ALL RODS OUT

RMS DEVIATION = 1.8%

FLORIDA POWER & LIGHT CO. St. Lucie Plant Unit 1	Maine Yankee Power Escalation Tests Power Distribution, 75% Power, Unrodded Equilibrium Xenon	Figure 4.3-35

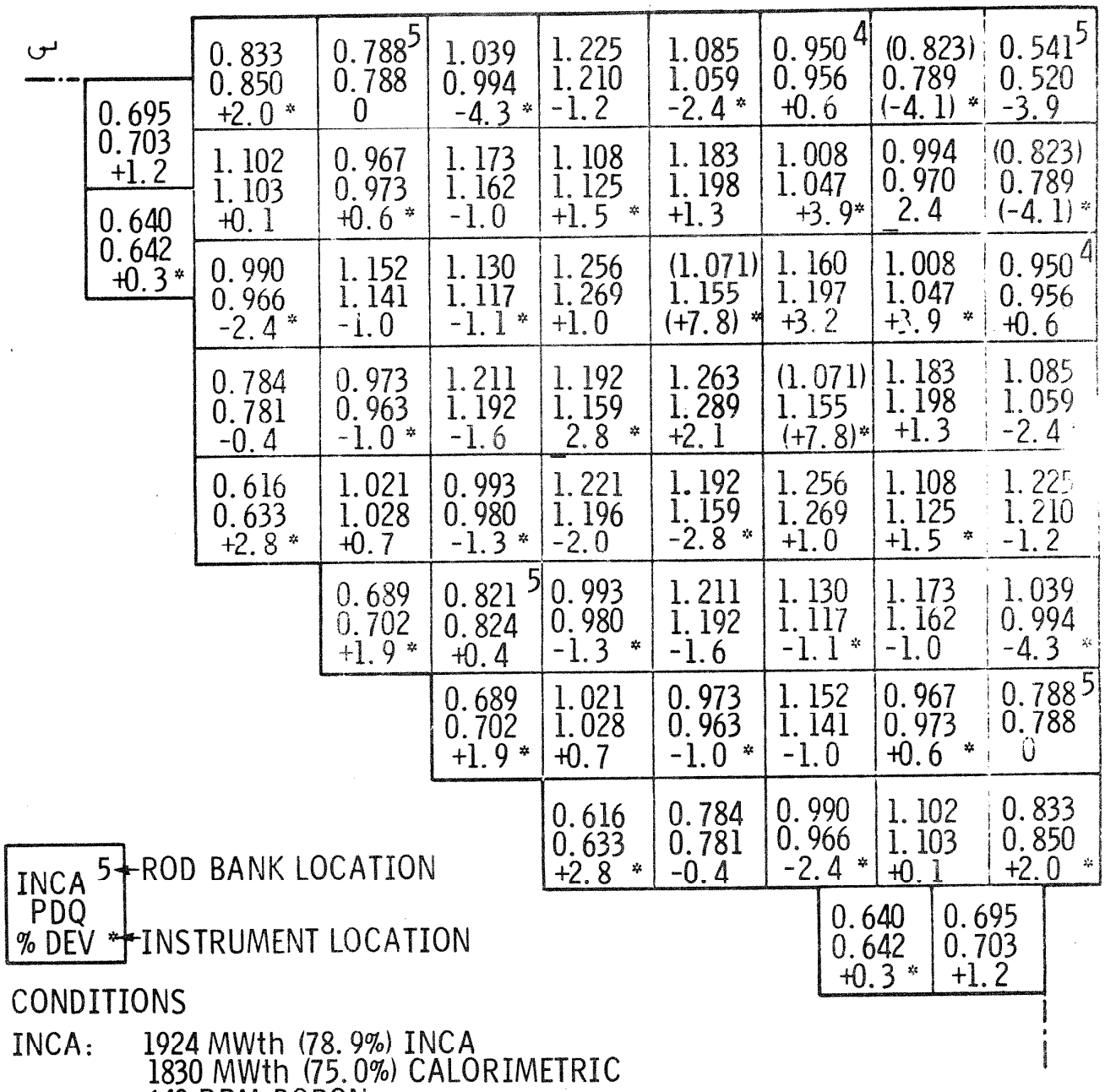

CONDITIONS

INCA: 1924 MWth (78.9%) INCA
1830 MWth (75.0%) CALORIMETRIC
640 PPM BORON
378 MWD/T

BANKS	5	4
IN	98%	43%

PDQ-QUIX-CEPIA: 1952 MWth (80%)
700 PPM BORON
NO BURN UP

BANKS	5	4
IN	98%	43%

RMS DEVIATION 2.3%

FLORIDA POWER & LIGHT CO. St. Lucie Plant Unit 1	Maine Yankee Power Escalation Tests Power Distribution, 75% Power, Rodded Equilibrium Xenon	Figure 4.3-36

Measurement 1 at 20 cm. from Bottom of Fuel

Measurement 2 at 50 cm. from Bottom of Fuel

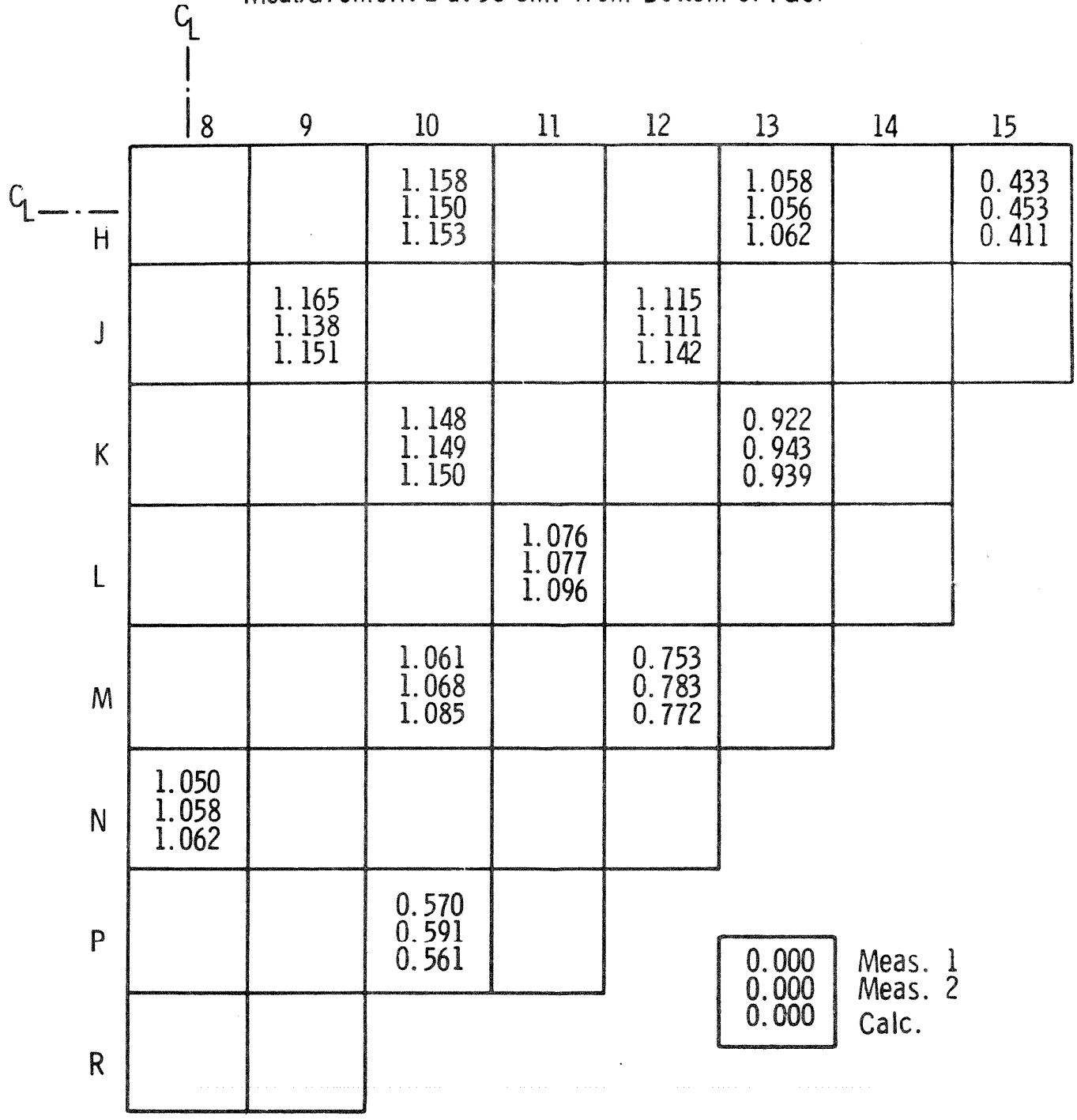

FLORIDA POWER & LIGHT CO. St. Lucie Plant Unit 1	Comparison Between Calculated and Measured Relative Fission Chamber Readings at Center of Fuel Assy's in Unrodded Portion of Conn. Yankee Core	Figure 4.3-37

Rodded Assemblies: K10, H12, M12, M8
Measurement at 45 cm from Top of Fuel

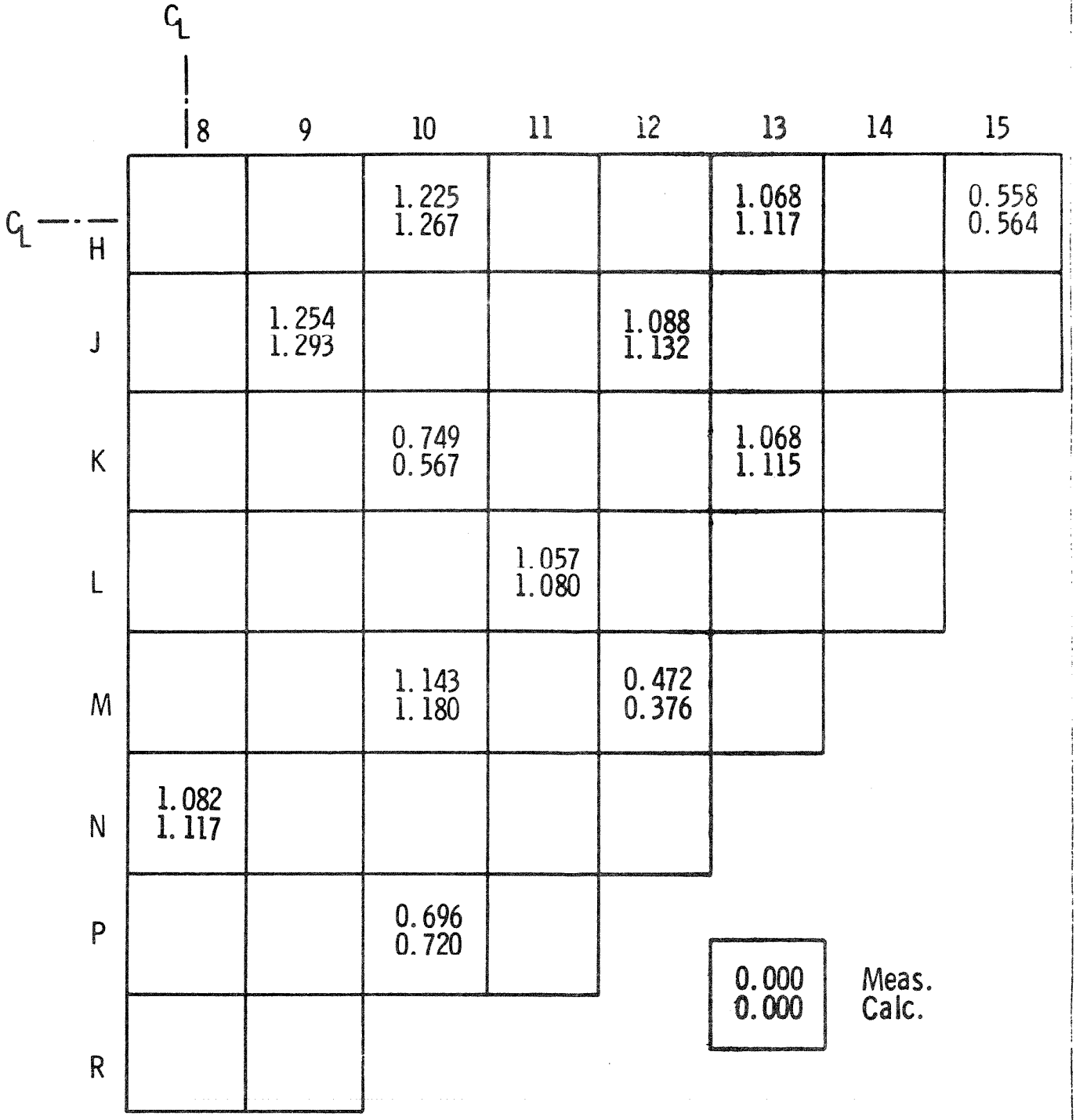

FLORIDA POWER & LIGHT CO. St. Lucie Plant Unit 1	Comparison Between Calculated and Measured Relative Fission Chamber Readings at Center of Fuel Assy's in Rodded Portion of Conn. Yankee Core	Figure 4.3-38

CHANGE IN POWER DISTRIBUTION DUE TO

DROPPED ROD IN THE FORT CALHOUN REACTOR

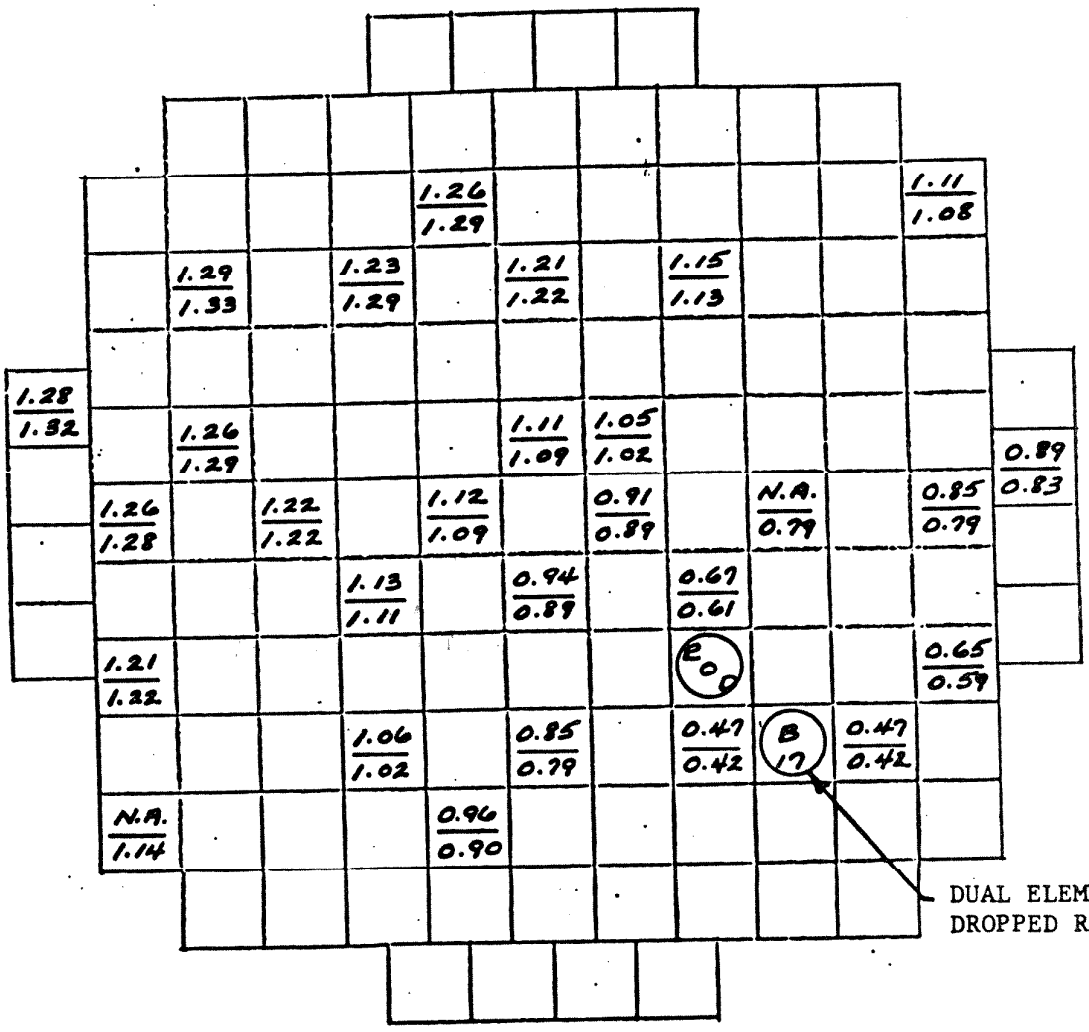

LEGEND

$\frac{W}{X}$

W — AFTER / BEFORE — RATIO OF — IN-CORE DETECTOR SIGNALS (MEASUREMENT)

X — AFTER / BEFORE — RATIO OF — PDQ FUEL BUNDLE POWERS (CALCULATION)

FIGURE 4.3-38A

FLORIDA POWER & LIGHT CO.
St. Lucie Plant
Unit 1

Damping Coefficient vs Reactivity Difference Between Fundamental and Excited State

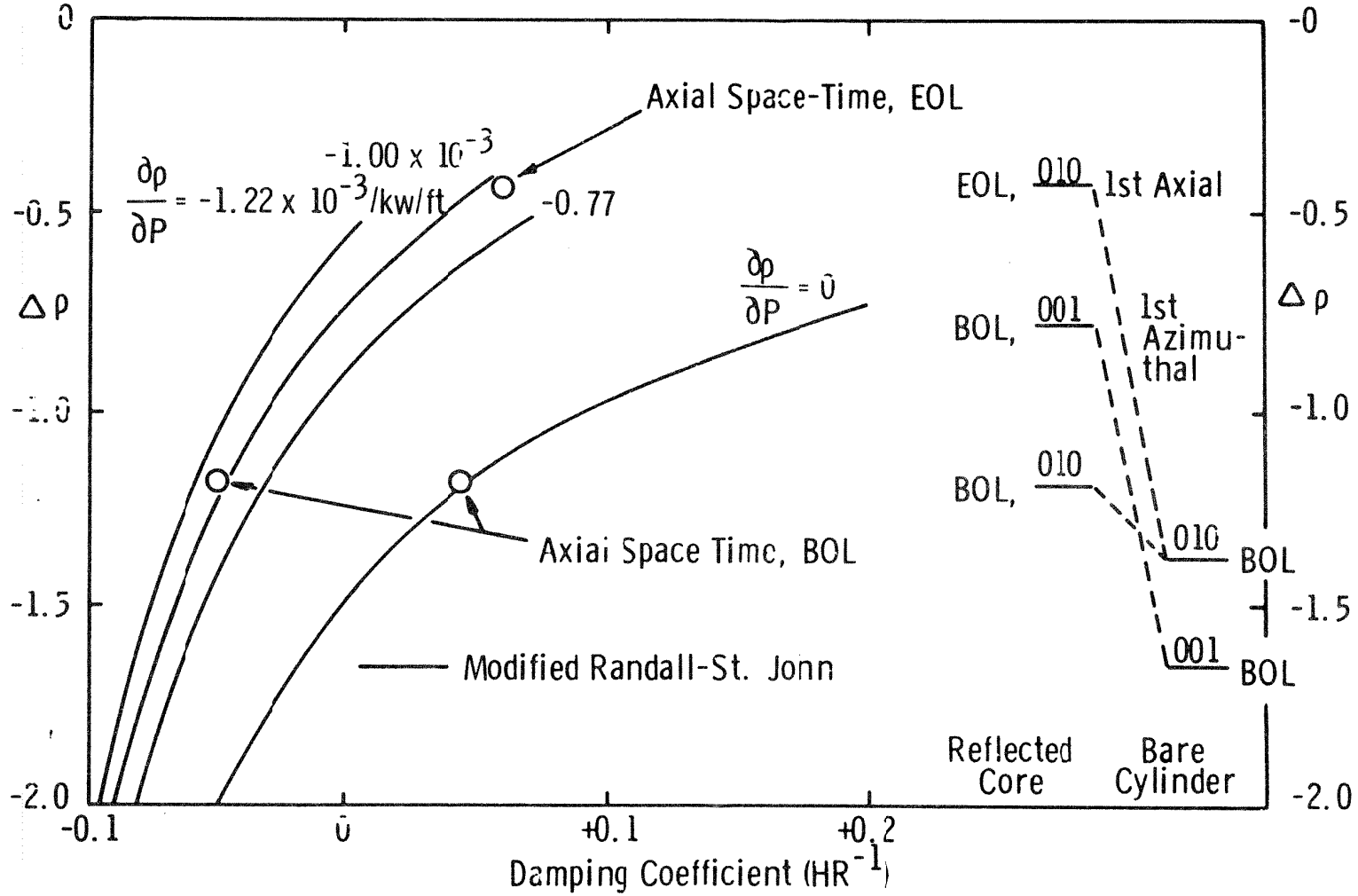

Figure 4.3-39

FLORIDA POWER & LIGHT CO.
St. Lucie Plant
Unit 1

Reactivity Difference Between Fundamental and Excited States of a Bare Cylindrical Reactor

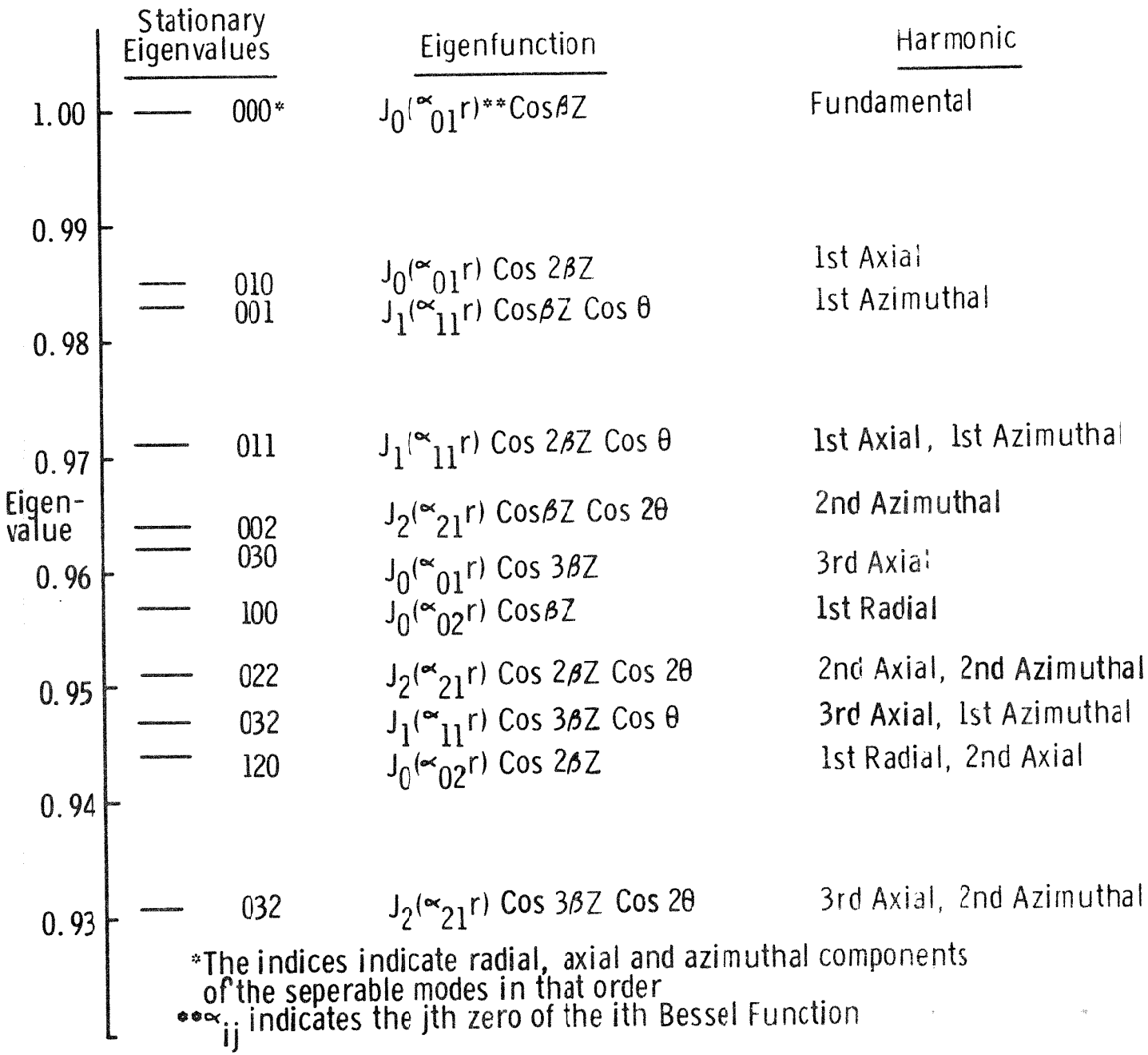

*The indices indicate radial, axial and azimuthal components of the seperable modes in that order

**α_{ij} indicates the jth zero of the ith Bessel Function

Figure 4.3-40

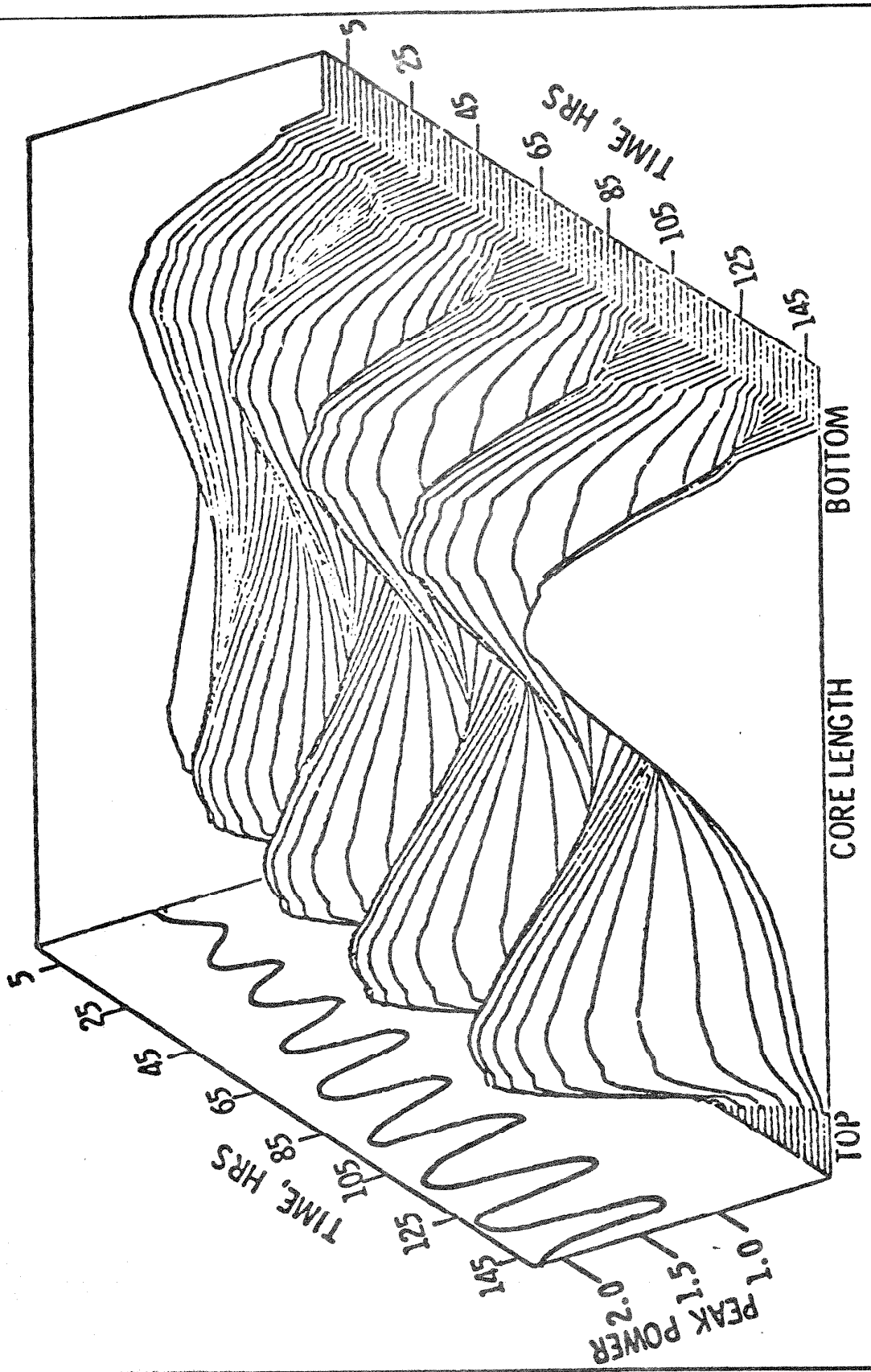

FLORIDA POWER & LIGHT CO. St. Lucie Plant Unit 1	Divergent Axial Oscillation in an EOC Core With Reduced Power Feedback ($\alpha c = 0.96 \times 10^{-4}\ \Delta\rho/kw1^{-1}$)	Figure 4.3-41

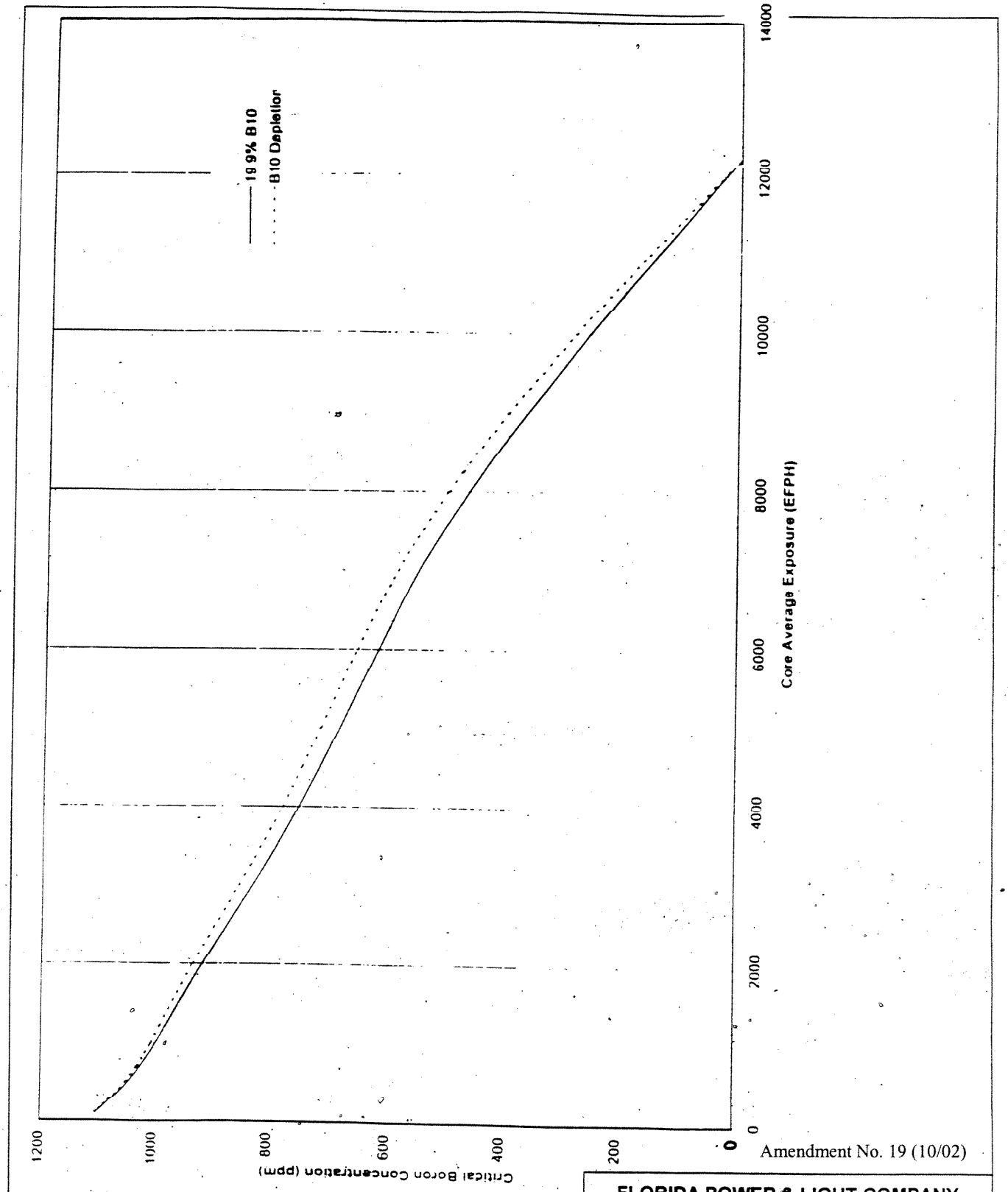

Amendment No. 19 (10/02)

FLORIDA POWER & LIGHT COMPANY
ST. LUCIE PLANT UNIT 1

ST. LUCIE UNIT 1, TYPICAL
BORON LETDOWN CURVE, ARO, HFP

FIGURE 4.3-42

DELETED

Florida Power & Light Company
St. Lucie Plant Unit 1

St. Lucie Unit 1, Cycle 26
Relative Power Densities,
HFP, ARO 100 EFPH
Figure 4.3-43

DELETED

Florida Power & Light Company
St. Lucie Plant Unit 1

St. Lucie Unit 1, Cycle 26
Relative Power Densities,
HFP, ARO 12,084 EFPH
Figure 4.3-44

DELETED

Florida Power & Light Company
St. Lucie Plant Unit 1

St. Lucie Unit 1, Cycle 26
Core Loading Pattern
Figure 4.3-45A

THIS FIGURE HAS BEEN DELETED

Amendment 17, (10/99)

FLORIDA POWER & LIGHT COMPANY
ST. LUCIE PLANT UNIT 1

FIGURE 4.3-46

This figure has been deleted

Florida Power & Light Company
St. Lucie Plant Unit 1

Figure 4.3-47

4.4 THERMAL AND HYDRAULIC DESIGN

This section presents thermal and hydraulic analysis of the reactor core, analytical methods utilized, and experimental work for supporting the analytical techniques. The prime objective of the thermal and hydraulic design of the reactor is the assurance that the fuel and supporting structures can meet normal steady state and transient performance requirements without exceeding the design bases. A summary of the significant thermal and hydraulic parameters is presented in Table 4.4-2. Section 4.4.6 contains a description of the current Thermal and Hydraulics design for EPU conditions. EC292529

4.4.1 DESIGN BASES

4.4.1.1 Thermal Design

Thermally Induced fuel damage during normal steady state and anticipated transient operation is prevented by the thermal and hydraulic design bases. The following are designed for normal operation, anticipated transients and operating occurrences:

a) A minimum allowable limit of 1.30 is set on the Departure from Nucleate Boiling Ratio (DNBR) during normal operation and any anticipated transients as calculated according to the W-3 correlation*.

b) A peak centerline fuel temperature below the melting point.

c) A maximum core void fraction to prevent premature DNB.

The primary thermal-hydraulic criteria for ANF reload fuel assure that fuel rod integrity is maintained during normal operation and anticipated operational occurrences. Specific criteria are:

1) Avoidance of boiling transition for the limiting fuel rod in the core with at least a 95% probability confidence level.

2) Fuel centerline temperatures remain below the melting point of the fuel pellets with at least a 95% probability confidence level.

Observance of these criteria during anticipated operational transients is considered conservative relative to the requirement that anticipated operational transients not produced fuel rod failures or loss of functional capability.

Beginning with Cycle 17

The Cycle 17 core consists of both bi-metallic and High Thermal Performance (HTP) SPC assemblies. Since the hydraulic loss coefficients are not the same for the different assembly types, a thermal hydraulic compatibility analysis was performed for Cycle 17, which indicates that the two fuel types are thermal-hydraulically compatible (Reference 47).

---

*For stretch power the CE-1 correlation was used with a corresponding limit of 1.23. See Stretch Power Application Section 6.1, Reference 25.

4.4.1.2 Coolant Flow Rate and Distribution

A low limit on the total reactor coolant flow rate, called "design" flow, assures that the fuel assemblies are adequately cooled when uncertainties in system flow resistance, pump head, and core bypass flow are taken to minimize effective core flow. (See Section 5.5.5 for pump design). The hydraulic loads for the design of the internals are based on the upper limit of the flow. The upper limit is obtained in a similar manner as the design minimum flow but with the uncertainties taken to maximize the coolant flow rate.

4.4.1.3 Fuel Design Bases

The fuel design bases are given in Section 4.2.1. Thermal and hydraulic parameters which influence the fuel rod integrity include maximum linear heat rate, core coolant velocity, clad temperature, and UO_2 temperature. Values of these parameters given in the following sections are consistent with those used in Section 4.2.1 and show that the fuel design bases are satisfied.

4.4.2 DESCRIPTION

4.4.2.1 Plant Parameters for Thermal Hydraulic Design

The plant parameters considered include total reactor coolant flow rate, reactor vessel inlet temperature, reactor coolant system pressure, and core thermal power. Two sets of thermal-hydraulic conditions are defined: nominal conditions and design conditions. Nominal plant conditions represent the best estimate for the reactor coolant flow rate, pressure, and vessel inlet temperature and do not include allowances for instrument errors. Design plant conditions represent the lower limit on reactor coolant flow rate when uncertainties in system resistance and pump head are included, and represent the upper limit on reactor vessel inlet temperature when design margins on steam generator performance are included. Furthermore, the variations which occur during steady state operation in the power, pressure, and inlet temperature due to controller deadband and instrument error are considered with the design plant parameters. During steady state operation, the possible variations in these parameters define an operating envelope. One combination of these parameters gives the minimum DNBR and this combination is utilized in Chapter 15 as the initial conditions in transient and accident analysis. Table 4.4-1 lists the nominal and design plant parameters.

4.4.2.2 Summary of Thermal and Hydraulic Parameters

The thermal and hydraulic parameters for the reactor are listed in Table 4.4-2.

4.4.2.2.1 Comparison of ANF Assembly Hydraulic Parameters

The reload ANF-4 fuel assembly is characterized by hydraulic loss coefficients that are essentially the same as those for reload XN-3. A minor spacer design change was reviewed for the ANF-4 fuel. In each interior spacer, 18 nonfunctional dimples will project 20 mils further than in the XN-3 spacer. Some 70 dimples are changed in this manner in the top and bottom spacers. The effect on spacer projected area of the increased dimple height is offset by a compensating change in the profile of the formed dimple. The effect of this minor design change on spacer loss coefficient is, therefore, insignificant. No other design changes which might impact hydraulic performance were made.

The XN-3 fuel and the ANF-4 fuel have a slightly greater hydraulic resistance than the co-resident XN-2 fuel. A full core of XN-3/ANF-4 fuel will reduce vessel flow by less than 0.15% relative to a full core of XN-2 fuel. Reactor coolant flow rate is monitored at intervals to ensure conformance to the Technical Specifications limits.

4.4.2.2.2 Thermal-Hydraulic Compatibility of Co-Resident ANF Assemblies

The Cycle 9 core will consist of 176 XN-3/ANF-4 type assemblies and 41 XN-2 type assemblies. Assembly hydraulic loss coefficients for co-resident ANF fuel types in Cycle 9 agree within 1.6%, providing better hydraulic compatibility than existed in the Cycle 6 core, where the assembly loss coefficient for the limiting ANF fuel exceeded that of the co-resident CE fuel by slightly less than 4%. Diversion cross flow effects of the XN-3/ANF-4 spacer in Cycle 9 will therefore be smaller than those considered in the Cycle 6 thermal hydraulic design analysis[30,44]. The MDNBR performance impact of the spacer redesign for reloads XN-3/ANF-4 is thus less than that evaluated for previous mixed cores at St. Lucie Unit 1.

The ANF-4 assembly design employs a longer, solid lower end cap. This results in a reduction of the fuel pellet stack length by 2.64 inches relative to the 136.7 inch stack length which characterized XN-2 and earlier reloads. The ANF-4 fuel is identical to XN-3 fuel in this respect. The effect of the active length reduction is to increase the hot rod clad surface heat flux and reduce calculated MDNBRs. The active length reduction is explicitly modeled in the Cycle 9 setpoint verification analyses discussed in Sections 4.4.5 and 15.6.

4.4.2.3 Core Hydraulics

4.4.2.3.1 Core Flow Distribution and Bypass Flow

The total coolant flow entering the four reactor vessel inlet nozzles is given in Table 4.4-2 for full power at design and nominal operating conditions. This flow proceeds into the annular space between the reactor vessel and the core support barrel as shown in Figure 4.1-1. From this inlet region, two secondary flow paths bypass coolant into the vessel outlet region. One path is through the clearance between the core support barrel sleeve and the reactor vessel nozzle directly into the vessel outlet nozzle. The other is through the alignment keyways into the vessel head region and then through flow areas in the upper guide structure support plate into the vessel outlet region.

The main flow path is down the annulus between the vessel wall and the core support barrel, through the flow skirt, and then, turning upwards in the lower plenum, up through the bottom plate past the lower support structure.

Above the bottom plate, openings in the inner support cylinder provide a bypass route into the space between the cylinder and the core support barrel, up past the edge of the core support plate, and into the irregular annulus reflector region between the core shroud and the core support barrel. The main stream flows axially through the core support plate and the lower end fittings of the fuel assemblies into the fuel region. Holes in the fuel assembly guide tubes permit a portion of the flow to pass into the guide tubes and bypass the active core. At locations where CEAs are not present, the fuel assembly alignment plate has no penetrations and therefore, core bypass flow is limited in these guide tubes. As a result of core support barrel repairs in 1983, (Section 4.2.2.2) plugged holes and patches installed in the upper section of the barrel have created other sources of bypass leakage. Table 4.4-3A is an inventory of these plugs and patches. Additionally, an analysis was made for bypass leakage assuming worst case failure of a patch assembly. Bypass flow inventory for this case is given on Table 4.4-3B.

The main flow proceeds through the fuel region where a portion of the flow may enter the radial reflector region through joints between the segments of the core shroud. For design purposes, all of this bypass flow is assumed to occur at the bottom of the fuel region. Table 4.4-3 lists the bypass flow channels and the percent of the total vessel flow rate entering these channels. After leaving the fuel region, the coolant continues through the fuel alignment plate into the outlet region where it flows past the control element assembly shrouds out through the core support barrel sleeves into the vessel outlet nozzle.

The effective flow rates for core heat transfer is therefore 96.1 percent of the total vessel flow rate. The amount bypassing the core is termed the core bypass leakage. Internal leakage and flow redistribution factors in the core are calculated using the COSMO code and the effective core flow rate, as discussed in Section 4.4.2.4.7.

4.4.2.3.2 Pressure Drop

Irrecoverable pressure losses from the inlet to the outlet nozzles are calculated using standard loss coefficient methods and results from model tests. Pressure losses for 100 percent power at 2250 psia and the nominal coolant inlet temperature are listed in Table 4.4-4 together with the effective coolant temperature associated with each pressure loss.

4.4.2.3.3 Hydraulic Loads on Internal Components

The design hydraulic loads for the internal components for steady state operating conditions are listed in Table 4.4-4A. These loads were derived from analysis and from reactor flow model and components test results (see Sections 4.4.3 and 4.4.4, respectively). All hydraulic loads in the table are based on the maximum expected system flow rate and a coolant temperature of 500°F. When these hydraulic loads are used in the structural analysis, they are adjusted for the worst conditions of coolant temperature for each component.

The types of loads included in the analysis are steady state frictional drag and flow impingement loads, and fluctuating loads induced by pump pressure pulsations, turbulence, and vortex shedding. All of these loads are not exerted on each internal component, but each component sees at least one of the loads. The components and type of loads that are exerted on them are listed. Design hydraulic loads for accident conditions are discussed in Chapters 6 and 15.

4.4.2.3.4 Reactor Vessel Coolant Volumes and Flow Path Dimensions

Plant configuration data, as it relates to the flow and containment of the reactor cooling water, is divided into the reactor vessel and internals coolant data, discussed below, and the primary system components coolant data presented in Section 5.3. Table 4.4-4B provides the volume, flow path length, height and elevation of the reactor vessel and internals regions shown in Figure 4.4-21. Table 4.4-4C gives the flow areas for each of the major reactor vessel and internals components, shown in Figure 4.4-21. Total coolant flow through the various reactor internal flow paths is given in Table 4.4-3. Steady state pressure and temperature distributions are provided in Tables 4.4-2 and 4.4-4.

4.4.2.4 Hot Channel Factors

4.4.2.4.1 Application of Hot Channel Factors

The thermal design of the reactor core takes into account nuclear effects, manufacturing tolerances in the fuel assembly, fuel rod and UO_2 pellets, flow thermal mixing, flow distribution. These effects are superimposed in the nominal channel in order to determine the conditions in the hot channel. The effects are taken into account in the hot channel heat flux and enthalpy rise factors.

The heat flux and enthalpy rise hot channel factors are ratios of the maximum to core average of these quantities. Each of these factors is divided into subfactors to account for specific physical effects. A subfactor is identified as a nuclear factor or as an engineering factor.

Nuclear factors are of three types: the nuclear enthalpy rise factor; the rod radial nuclear factor; and the axial peaking factor. The nuclear enthalpy rise factor is the ratio of one-fourth the total power from the four rods that enclose a flow channel to the core average fuel rod power. The rod radial nuclear factor is the ratio of the total power from a fuel rod to the core average fuel rod power. The maximum value of the normalized axial power distribution is the axial peaking factor. The local heat flux is determined by multiplying the core average heat flux by the rod radial nuclear peaking factor and the local

axial peaking factor. A small fraction of the power is generated external to the fuel rod. This fraction, which is given in Table 4.4-2, is not included in the heat flux. However, it is included in the calculation of hot channel enthalpy rise. All nuclear factors are based upon nominal dimensions and nominal pellet enrichment,

Engineering factors account for physical differences between the hot channel and a nominal channel, other than those differences due to nuclear effects. The engineering hot channel factors can be further classified as statistical or nonstatistical factors. Statistical factors are those that result from the effects of manufacturing tolerances on heat flux or enthalpy rise. They are termed statistical-factors because manufacturing tolerances are randomly distributed about a mean value. It is assumed that the functional combination of tolerance data into a subfactor results in a normally distributed value for the subfactor. This assumption is appropriate for the small tolerance deviations in fuel assemblies. Nonstatistical engineering factors are those that are due to physical effects, such as the flow distribution at the core inlet.

The maximum design values of the factors used for the channel when investigating minimum DNB ratios differ from those used to determine maximum centerline fuel temperatures, since both quantities are used as limiting criteria.

4.4.2.4.2 Nuclear Power Factors

The heat flux factor is the ratio of the peak heat flux in the core to the core average heat flux. It is the product of the rod radial nuclear factor, the axial peaking factor and the engineering heat flux factor. Departure from nucleate boiling is dependent on the local heat flux along the channel and on the local fluid enthalpy in the channel. Therefore, the heat flux factor and the maximum nuclear enthalpy rise factor cannot be treated as independent variables. Table 4.4-2 gives the design values for each of these factors, and Figure 4.4-1 shows the axial power distribution that is used in conjunction with the nuclear enthalpy rise factor.

The minimum thermal margin in the core is calculated f.or the most limiting channel or rod. All other fuel rods in the core will have greater thermal margin. Figure 4.4-2 is a typical cumulative distribution of the fraction of the rods above a given radial peak.

The effect of asymmetries in core power distribution (specifically azimuthal or quadrant power tilt) is not directly taken into account in the COSMO thermal-hydraulic calculations. An allowance for the azimuthal tilt is factored into the generation of the DNBR and kw/ft trip and monitoring setpoints. The tilt allowance is used to degrade the available thermal margin by an amount proportional to the azimuthal tilt allowed by the Technical Specifications. A detailed discussion of quadrant power tilt is given in Section 4.32.

4.4.2.4.3 Engineering Heat Flux Factor

The effect on local heat flux due to deviations from nominal design dimen sions and specifications is accounted for by the engineering heat flux factor. Design variables that contribute to this engineering factor are pellet density, fuel enrichment, pellet diameter, and clad outside diameter. These variables may be combined statistically to obtain the engineering heat flux factor. The design value used for the engineering heat flux factor has been shown to be appropriate based on deviations obtained from fuel manufacturing inspection data for the Palisades Reactor (AEC Docket No. 50-255) and the Maine Yankee reactor (AEC Docket No. 50-309). Similar tolerances and quality control procedures are used for this reactor, and inspection data is expected to confirm that the factor given in Table 4.4-2 is appropriate.

Variations in clad outside diameter will directly change the rod surface heat flux but will not significantly change the rod linear heat rate. Therefore, variations in clad outside diameter are omitted in the calculation of fuel temperatures. Statistical evaluation of the fuel manufacturing inspection data for Maine Yankee (AEC Docket No. 50-309) yields a value of less than 1.03 for the effect on local linear heat rating due to variations in fuel density, fuel enrichment, and pellet diameter. The value of 1.03 is used as a design limit and will be substantiated for this reactor. Table 4.4-5 gives the fuel inspection data for the Palisades and Maine Yankee reactors.

4.4.2.4.4 Engineering Enthalpy Rise Factor

The enthalpy rise factor accounts for the effects of deviations in fuel fabrication from nominal dimensions or specifications on the enthalpy rise in the hot channel. Tolerance deviations, averaged over the length of the four fuel rods that enclose the hot channel, for fuel density, enrichment, pellet diameter, clad outside diameter, and rod pitch and bowing contribute to this factor.

The engineering enthalpy rise factor is divided into two components. One component is the subfactor due to the increased heat input resulting from higher than nominal U-235 content and the other is the subfactor due to the decreased flow rate resulting from a smaller than nominal channel flow area. These subfactors are called the engineering heat input subfactor, and the

engineering pitch, bowing, and clad diameter subfactor. The two components of the engineering enthalpy rise factor are computed individually, using statistical methods, and are then multiplied to give the engineering enthalpy rise factor. The subfactor due to pitch, bowing and clad diameter, is based on inspection data in a manner analogous to the engineering heat flux factor. The value of the engineering enthalpy rise factor is 1.12.

The engineering factors on the enthalpy rise and the heat flux are applied to the hot channel and to the hottest rod within the channel, respectively. The engineering enthalpy rise factor increases the enthalpy rise within the hot channel to show the effect of increased heat input and, consequently, a reduction in the subchannel flow rate. The engineering heat flux factor has the effect of increasing the local heat flux along the hottest rod within the hot channel when calculating DNBR, without further increasing the enthalpy rise in the channel.

4.4.2.4.5 Inlet Flow Distribution Factor

The inlet flow distribution factor accounts for the effect of nonuniform flow at the core inlet on the hot channel enthalpy.

Tests were conducted with scale models for the Palisades (AEC Docket No. 50-255), Maine Yankee (AEC Docket No. 50-309), Fort Calhoun (AEC Docket No. 50-285), and Calvert Cliffs Unit 1 (AEC Docket No. 50-317) reactors to determine the hydraulic performance for normal and part-loop reactor configurations. The models were geometrically similar to each of the reactors except for the core regions, where each fuel assembly was simulated by cylindrical tubes with orifices to provide the proper axial flow resistance. Air was used as the test medium for the Palisades and Omaha flow models, while water was used for the Maine Yankee and Calvert Cliffs models. Core flow distribution measurements and reactor pressure loss coefficients were obtained for the various pumping configurations. The flow model programs are further discussed in Section 4.4.3. Taking into consideration the similarities between this reactor and other C-E reactors in conjunction with the experimental data from the flow model programs, the following flow distribution factors for the various pumping configurations were established.

Pump Configuration	Inlet Flow Distribution Factor
Normal Four-Pump Operation	1.05
Three-Pump Operation	1.06
Two-Pump Operation, One Pump in Each Loop, Diametrically Opposed Inlet Nozzles	1.08
Two-Pump Operation, Both on the Same Steam Generator	1.14

4.4.2.4.6 Flow Mixing Factor

The effect of turbulent flow mixing between channels on the hot channel enthalpy rise is calculated by the INTHERMIC[1] computer code which uses as input an experimental correlation for turbulent flow mixing between neighboring channels, and the fuel assembly rod power distribution. Results from the INTHERMIC calculation are expressed as the "mixing hot channel factor," defined as the ratio of hot channel mixed to unmixed enthalpy rise. The mixing hot channel factor is not constant, but varies axially along the length of the channel. It has a value of unity at the channel inlet, where no lateral enthalpy gradient exists, and decreases progressively up the channel as the lateral enthalpy gradient builds up. The design value for the mixing hot channel factor at the channel outlet is 0.88. At the location of the minimum DNB ratio (about 60 percent of the core height above the inlet when the DNB ratio is 1.3) and mixing hot channel factor is 0.93.

The turbulent flow mixing factor between neighboring channels is based on experiments (described in Section 4.4.4) conducted at the Combustion Engineering Laboratories. These experiments determined the inverse Peclet number, ξ/VDe, where ξ is the turbulent mixing flow rate per unit length (volumetric basis), De is the channel hydraulic diameter, and V is the channel coolant velocity. The value of inverse Peclet number from these experiments is 0.0035.

The geometry and the rod power distribution of the array of channels surrounding the hot channel, the axial and radial power distribution, and the presence of statistical engineering factors on the hot channel all affect the lateral enthalpy distribution and, hence, the mixing hot channel factor. The design value for the mixing hot channel factor is a conservative estimate based on the results from a number of INTHERMIC calculations for various local power distributions.

4.4.2.4.7 Internal Leakage and Flow Redistribution Factor

When the preceding enthalpy rise factors are utilized as input to the core and hot channel analysis computer program COSMO[2], the resulting hot channel enthalpy rise factor always exceeds the product of the input factors. The residual factor, which is the ratio of the total enthalpy rise factor to the product of the input enthalpy rise factors, represents the effect of internal leakage and flow redistribution. Internal leakage and flow redistribution refer to a reduction in hot channel flow rate relative to the average flow rate per fuel rod. The average flow rate per fuel rod is defined as the total core flow rate divided by the total number of fuel rods. Because of the presence of unheated guide tubes, poison rods, and larger than nominal gaps between fuel assemblies, the flow rate for a nominal fuel matrix channel (i.e., a channel of nominal geometry with unity peaking and enthalpy rise factors) is less than the core average flow rate per fuel rod. This reduction in flow is called "internal leakage" and its effect on enthalpy rise is the internal leakage enthalpy rise factor. As nuclear peaking and enthalpy rise factors are imposed on the nominal matrix channel, a further reduction in flow occurs due to increase in flow resistance caused by local boiling. This reduction in flow is called flow

redistribution and its effect on enthalpy rise is called the flow redistribution enthalpy rise factor. At 100 percent power and for nominal coolant conditions, the product of the internal leakage factor and the flow redistribution factor for the hot channel is given in Table 4.4-2.

4.4.2.5 Core Temperatures

4.4.2.5.1 Fuel Cladding Temperatures

The surface temperature of the cladding is dependent on the heat flux, the surface heat-transfer coefficient, and the temperature of the ambient coolant. The surface heat-transfer coefficient for nonboiling forced convection is obtained from the Dittus-Boelter relation:

$$h = \frac{0.023k}{D_e} (N_{Re})^{0.8} (N_{Pr})^{0.4} \quad Btu/hr - ft^2 - F$$

where fluid properties are evaluated at the bulk conditions.

In the nucleate boiling regime, the surface temperature of the cladding is determined from the Jens and Lottes(3) correlation:

$$T_{wall} = T_{saturation} + 60(q'' \times 10^{-6})^{0.25} \exp(-P/900)$$

where q" = Surface heat flux, Btu/hr-ft ^{2}
P = Pressure, psia
T_{sat} = Saturation temperature, F

The steady state radial temperature difference through the cladding, assuming constant internal volumetric heat generation rate and variable cladding conductivity is calculated from the general one-dimensional differential heat conduction equation.

The thermal conductivity of Zircaloy-4 clad material in the range of 100F to 1000F is determined from:[4]

$$k_c = 7.97 + 0.00316(T)$$

where T = F
k_c = Btu/hr-ft-F

The axial profile of the temperature at the clad mean radius over the active fuel length for an average and a hot fuel rod is shown in Figure 4.4-3. The distinction between these rods is that the hot rod experiences the design axial and radial peaking while the average rod experiences the design axial peak with a radial peak of unity. The local coolant temperature surrounding these rods depends on the location of the rod within the reactor and the axial distance along the rod from the channel inlet.

4.4.2.5.2 Fuel Thermal Performance

Steady state fuel temperatures are determined by the FATES computer program. The calculational procedure considers the effect of linear heat rate, fuel relocation, fuel swelling, densification, thermal expansion, fission gas release, and clad deformations. The model for predicting fuel thermal performance is discussed in detail in Reference 23.

Two sets of burnup and axially dependent linear heat rate distributions are considered in the calculation. One is the hot rod, time averaged, distribution expected to persist during long term operation, and the other is the envelope of the maximum linear heat rate at each axial location. The long term distributions are integrated over selected time periods to determine burnup, which is in turn used for the various burnup dependent behavioral models in the FATES computer program. The envelope accounts for possible variations in the peak linear heat rate at any elevation which may occur for short periods of time and is used exclusively for fission gas release calculations.

The power history used assumes continuous 100% reactor power from Beginning of Life (BOL). Using this history, the highest fuel temperatures occur very early in life. It has been shown that fuel temperatures for a given power level at any burnup are insensitive to the previous history used to arrive at the given power level.

Fuel thermal performance parameters for any other rod in the core can be obtained by using the axial location in the hot rod, whose local power and burnup corresponds to the local power and burnup in the rod being examined. This procedure will yield conservatively high stored energy in the fuel rod under consideration.

Significant parameters such as cold pellet and clad diameters, gas pressure and composition, burnup and void volumes are calculated and used as initial conditions for subsequent calculations for stored energy during ECCS analysis. The coupling mechanism between FATES calculations and the ECCS analysis is described in detail in Reference 24.

4.4.2.6 Departure from Nucleate Boiling Analysis

4.4.2.6.1 Design Approach to Departure from Nucleate Boiling

The margin to departure from nucleate boiling (DNB) at any point in the core is expressed in terms of the departure from, nucleate boiling ratio The DNBR is defined as the ratio c)f the heat flux required to produce departure from nucleate boiling at specific local coolant conditions to the actual local heat flux. At some point in the core, the DNBR is a minimum and it is at this point that the margin to DNB for the core is evaluated. The following items are important in predicting the core margin to DNB:

a) The coolant inlet conditions

b) The power level

c) The nuclear power distribution.

d) The analytical methods utilized to predict local coolant conditions

e) The correlation used to predict DNB heat flux.

The conventional approach to DNB ratio concentrates on the most limiting location in the core and does not consider the nearness to DNB of the core taken as a whole. Alternatively, typical distributions of DNBR for a larger group of channels can be calculated to show the number of rods which approach the DNB limit.

Correlations for DNB are intended only to predict actual DNB and, therefore, the concept of DNB ratio can be misleading if a physical meaning rather than a statistical meaning is attached to the ratio. Because of the uncertainties associated with correlating DNB, there is a finite probability that if a channel is operated at a specified DNB ratio, based on a particular correlation, it will be at or above the DNB heat flux. Therefore, the proper interpretation of DNB ratio is that it is a measure of the probability that DNB will occur in the particular design situation to which the DNB correlation is applied. This interpretation assumes, of course, that all operating parameters are known precisely and that the probability being evaluated is only that associated with the correlation. It is customary to esatablish the relationship between DNB ration and probability of DNB by statistically evaluating the scatter between actual values of DNB heat flux, as measured experimentally for many test geometries and operating conditions,

and the corresponding values that are predicted by the correlation.
Uncertainties associated with prediction of the operating conditions in the channel are subject to separate interpretation. The approach used in design is to select core operating conditions and analytical methods in such a way that there is a very small probability that the actual hot channel coolant conditions are more severe than the calculated conditions used as input to the DNB correlation.

The W-3 DNB* correlation presented in Reference 11 is used for reactor design and is reiterated below:

W-3 DNBR Correlation

$$q'' \text{ DNB} = \frac{q''_{DNB,EU}}{F}$$

$$\frac{q''_{DNB,EU}}{10^6} = \left[(2.022 - 0.0004302p) + (0.1722 - 0.0000984p) \exp (18.177 - 0.004129p)X\right] \left[\frac{G}{10^6}(0.1484 - 1.596X + 0.1729X|X|) + 1.037\right] (1.157 - 0.869X) \left[0.2664 + 0.8357 \exp(-37.812D_h)\right] \left[0.8258 + 0.000794 (h_f - h_i)\right]$$

$$F = \frac{C}{q''(1-e^{-Cz})} \int_o^z q''(y) \exp\left[-C(z-y)\right] dy$$

$$C = \frac{5.28(1-X)^{7.9}}{\left[\frac{G}{10^6}\right]^{1.72}} \qquad ft^{-1}$$

Where q" DNB = Predicted Burnout Heat Flux (Btu/hr-ft^2)
q" DNB,EU = Equivalent Uniform Heat Flux (Btu/hr-ft^2)
q"(y) = Axial Heat Flux Distribution (Btu/hr-ft^2)
p = Pressure, psia
X = Quality
G = Mass Flow Rate, lbs/hr-ft^2
D_h = Hydraulic Diameter, ft
z = Axial Distance from Inlet, ft
h_f = Enthalpy of Saturated Liquid, Btu/lb
h_i = Inlet Enthalpy, Btu/lb
y = Distance along Channel, ft

*For Stretch Power, the CE-1 correlation is used; see Cycle 4 Stretch Power Applications Section 6.1, Reference 25.

The correlation consists of an equivalent uniform DNB heat flux correlation and a correction factor, F, to adapt the uniform DNB heat flux correlation to a channel having a nonuniform axial heat flux profile. The ranges of parameters used to develop the correlation encompass the range used in the design of the reactor. Although the correlation was developed from circular tube and rectangular channel DNB data, the equivalent uniform correlation also predicts DNB for rod bundles having uniform axial and radial heat flux and simple spacer grids. To apply the correlation to a reactor fuel bundle, it is necessary to determine local conditions in the channels using a digital computer code, COSMO* (see Section 4.4.3.2) and to correct the equivalent uniform DNB heat flux for the non-uniform axial flux profile by using the correction factor, F.

EXPERIMENTAL DATA CORRELATION

Parameter	W-3* Correlation Limits
System Pressure	1000 - 2300 psia
Mass Velocity of Coolant	$1 \times 10^6 - 5 \times 10^6$ lb/hr-ft^2
Equivalent Diameter Based on Wetted Perimeter	0.2 - 0.7 inch
Local Quality	-0.15 - +0.15
Inlet Enthalpy	≥400 Btu/lb
Heated Length	10 - 144 inch

Since the correlation was based on experimental DNB data, it applies most directly to values of the DNBR near 1.0, which represents the condition of DNB. Values of DNBR far from 1.0 may not have significant meaning. Therefore, the increase in the reactor power which is required to reach the design basis limit is frequently used as a measure of thermal margin. The core power distribution is held constant and the overpower ratio to reach 1.30 DNBR is calculated. Table 4.4-2 gives the resultant overpower ratio.

4.4.2.6.2 Partial Loop Operation

Partial loop pumping configurations are designed normal modes of reactor operation but actual part loop operation is not permitted by the Technical Specifications.

* For the stretch power analysis the TORC Code and the CE-1 correlation are used in place of COSMO and the W-3 correlation; for information, see Cycle 4 Stretch Power Application Section 6.1, Reference 25.

4.4.2.6.3 Distribution of DNB Ratio in the Core

The previous discussion focused on the effect of coolant conditions and power level on a hypothetical limiting hot channel or fuel rod in the core and with all statistical factors applied. It is also of interest to examine the distribution of DNB ratios for a number of high power density fuel rods. It is not valid to apply the statistical factors to large numbers of fuel rods and the analyses which are described in the following discussion do not include the effect of the statistical factors. Figure 4.4-7 shows the number of rods in the reactor which have a DNB ratio less than the value indicated on the abscissa for the design coolant conditions, design power distribution, and 112 percent power.

4.4.2.6.4 Coolant Void Fraction in Core

The core average void fraction and the maximum void fraction are calculated in the COSMO* program using the Maurer Method[12] which includes subcooled void fraction. The care average void fraction at 112 percent power is less than 0.1 percent for design conditions. The maximum local void fraction is 25 percent which occurs at the exit of the design hot channel.

The distribution of void fraction as a function of nuclear enthalpy rise factor is shown in Figure 4.4-8. The axial distribution of the void fraction for the design hot channel and design axial shape is shown in Figure 4.4-9. The average void fraction for the hot channel is 7.6 percent.

*See note on COSMO in Subsection 4.4.2.6.1.

4.4.3 EVALUATION

4.4.3.1 Hydraulics

4.4.3.1.1 Reactor Flow Model Tests

Flow model testing using reactor scale models is part of the Combustion Engineering reactor development program. Such testing began in 1966 by Combustion Engineering and is a continuing activity. Past test programs have provided information on flow distribution in various regions of the reactor, on pressure loss coefficients, on hydraulic loads on vessel internal components, and on turbulence-induced pressure and velocity fluctuations. Much of this information is not amenable to direct calculation, and can only be obtained from operating reactor data or from scale model tests. Scale model tests possess the advantage, relative to actual reactor tests, of providing the information early in the design stage, of being more suitable for extensive instrumentation, and of being flexible so that proposed design modifications can be investigated.

The reactor flow models used by Combustion Engineering are approximately 1/5th true scale models, with the exception of the core region. Because of the difficulties in modeling an open lattice type core, the model cores to date have consisted of closed core tubes which simulate the fuel bundles. Each core tube contains an orifice or nozzle to provide the proper axial flow resistance and to measure the local flow rate. Hydraulically, Combustion's PWR designs fall into five basic geometric configurations as shown below.

Configuration	Reactor(s)	Distinguishing Hydraulic Features
1	Palisades	Four inlets, two outlets, cruciform control rods, 204 fuel assemblies.
2	Fort Calhoun	Four inlets, two outlets, CEA control elements, 133 fuel assemblies.
3	Maine Yankee	Three inlets, three outlets, CEA control elements, 217 fuel assemblies.
4	Calvert Cliffs (1&2) St. Lucie (1&2) Millstone (Unit 2) San Onofre (Units 2&3) Forked River Waterford (Unit 3) Pilgrim (Unit 2)	Four inlets, two outlets, CEA control elements, 217 fuel assemblies.
5	Arkansas Nuclear One (Unit 2)	Four inlets, two outlets, CEA control elements, 177 fuel assemblies.

Flow model tests have been conducted on the first four configurations. The Palisades and Fort Calhoun flow tests were performed by Battelle Memorial Institute using air as the test medium. The Maine Yankee and the configuration 4 reactor flow model tests were performed in a 15,000-gpm cold water facility in the Combustion Engineering Laboratory. The configuration 4 flow model simulated the core length that is characteristic of the Calvert Cliffs, St. Lucie

and Millstone reactors. The San Onofre, Forked River, Waterford, and Pilgrim designs have a longer core, higher power level, and higher flow rate than the other reactors in configuration 4; however, their hydraulic behavior in terms of dimensionless flow distributions, heat loss coefficients, and hydraulic loading coefficients, is similar from a scale model standpoint. Corrections for the longer core and downcomer are derived analytically. The data required for configuration 5 will be interpolated from the experimental results from tests on the other configurations.

Other minor geometric differences among the configuration 4 and 5 reactors are accounted for by utilizing the experience gained from the earlier tests, during which numerous investigations were made of the effect of various internal components on flow distribution and pressure drop. For example, the Palisades tests were run with and without a flow skirt, with the core barrel concentric and eccentric in the vessel, and with the lower core support plates in place and removed. The Fort Calhoun tests were run with and without the thermal shield, with the lower core support structure removed and in place, and with the upper guide structure and fuel alignment plate removed and in place. Earlier flow model test programs also investigated the effects of part-loop operation and the degree of mixing of the coolant in the vessel upstream and downstream of the core.

Accordingly, the configuration 4 tests were restricted to obtaining data, with all loops operating, on core flow distribution, segmental flow path pressure drop, and hydraulic loads on several vessel internal components. The flow path segments comprised the inlet region, the annular downcomer, the lower plenum, the core, and the upper plenum. Since the designs of the upper plenum differ somewhat among the reactors in configuration 4, tests were run on the two most different designs.

Data evaluation has enabled the following conclusions:

a) The core flow distribution for normal operation is similar to that observed in the preceding tests for reactors with four inlets and two outlets, in that there is quadrantal symmetry and the lowest core tube flows are found on the periphery between the outlet nozzles. In general, the distribution is flatter than for configurations 1 and 2, and this is attributed to the upper plenum possessing a higher flow resistance. Thus, the minimum and maximum deviations from the average core tube flow ratio, $(W_i\text{-}W)/W$, observed in these latest tests, are ±0.05. The measurement uncertainty associated with these values is 0.006 and includes instrument and replication error.

   In utilizing the flow distributions to determine the inlet flow maldistribution enthalpy rise factor (or plenum factor), it is assumed that the design value of the rod radial peaking factor can occur in any fuel assembly. However, since the assembly power is significantly lower for the peripheral fuel assemblies, the maximum permissible plenum factor is larger for peripheral assemblies than for those in the interior. This fact is taken

into account through a combination of the experimental flow distribution and the most conservative physics power distribution envelope to yield a single design value for plenum factor. That value, when used with the designated design values for assembly power and rod peaking factor, results in the most limiting thermal margin. It is equal to or less than the thermal margin that would be calculated for each individual fuel assembly location using the local values of plenum factor and power. Further information on this subject is given in Reference 13.

Based upon the core power distributions which are available for the various cores and upon the previous flow model tests, a design value of 1.05 had been chosen for the plenum factor for the

Calvert Cliffs, St. Lucie and Millstone units, prior to the configuration 4 tests. It is obvious, even without considering the power distribution, that the new flow distribution data have established the conservatism of the 1.05 value.

Apart from plenum factor determination, the core flow distribution yields information on an input datum necessary in the analysis of fuel assembly uplift: the maximum local flow rate ratio. In the present case, the experimental value of 1.05 confirms the 1.05 value assumed in the calculation of the uplift hydraulic load noted in Section 4.4.2.3.

b) In a range of 50 to 100 percent of full flow (where full flow in the model was defined as the value that gave reactor pressure drops), experimental segmental flow path pressure drop values agreed with model predictions to within 15 percent, while nozzle-to-nozzle values agreed to within 10 percent, with the predicted value generally being the larger. The current reactor predictions (noted in Section 4.4.2.3) include a correction for the systematic difference. The measurement uncertainty in the experimental results is 5 percent and includes instrument and replication error.

c) The experimental flow model information substantiating the hydraulic loads (other than fuel assembly uplift) listed in Section 4.4.2.3 is that obtained during configuration 1, 2, and 3 testing. The data obtained during configuration 4 testing are comparable with the earlier data.

Further discussion of the philosophy of C-E flow model testing appears in Reference 14.

4.4.3.1.2 Core Pressure Drop Correlations

The total pressure drop along the active fuel region of the core is computed as the sum of the individual losses resulting from friction, acceleration of the fluid, change in elevation of the fluid, and spacer grids. The individual losses are computed using the momentum equation and the set of empirical correlations presented in Reference 15.

In the following paragraphs, the correlations used are summarized and the validity of the scheme is demonstrated with a comparison of measured and predicted pressure drop for single-phase and two-phase flow in rod bundles with CEA type geometry.

For isothermal, single phase flow, the pressure drop due to friction for flow along the rods is based on the equivalent diameter of the rod assembly and the Blasius friction factor:

$$F = 0.184\ N_R^{-0.2}$$

The pressure drop associated with the spacer grids is computed using a grid loss coefficient (K_{SG}) given by:

$$K_{SG} = 2.94\ N_R^{-0.141}$$

The coefficients were determined from pressure drop data obtained for a wide range of Reynolds number for isothermal flow through CEA type rod bundles fitted with production spacer grids. The data came from the DNB Program (Section 4.4.4.2) and from the Fort Calhoun Components Test (Section 4.4.4.3). The standard error of estimate associated with the loss coefficient relation is 0.054 and includes replication and instrument error.

To compute pressure drop either for heating without boiling or for subcooled boiling, the friction factor given above for isothermal flow is modified through the use of the multipliers given in Reference 15. It is important to recognize that the multipliers were developed in such a way as to incorporate the effects of subcooled voids on the acceleration and elevation components of the pressure drop as well as the effect on the friction losses. Consequently, it is not necessary to compute specifically either a void fraction for subcooled boiling or the individual effects of subcooled boiling on the friction, acceleration, or elevation components of the total pressure drop.

The effect of bulk boiling on the friction pressure drop is computed using a curve fit to the Martinelli-Nelson data (Reference 16) above 2000 psia or the Martinelli-Nelson correlation (Reference 16 with the modification given in Reference 15) below 2000 psia. The acceleration component of the pressure drop for bulk boiling conditions is computed in the usual manner for the case of two-phase flow where there may be a nonunity slip ratio (see Reference 17). The elevation and spacer grid pressure drops for bulk boiling are computed as for single phase flow except that the bulk coolant density (ρ) is used, where:

$$\bar{\rho} = \alpha\rho_v + (1-\alpha)\,\rho_\ell$$

and α = Bulk boiling void fraction.

ρ_v = Density of saturated vapor.

ρ_ℓ = Density of saturated liquid.

The bulk boiling void fraction used in computing the elevation, acceleration, and spacer grid losses is calculated by assuming a slip ratio of unity if the pressure is greater,than 1850 psia or by using the Martinelli-Nelson void fraction correlation[16] with the modifications presented in Reference 15, if the pressure is below 1850 psia.

To verify that the scheme described above accurately predicts pressure drop for single-phase and two-phase flow through the fuel assembly, comparisons have been made of measured pressure drop and the pressure drop predicted by design code COSMO, for the rod bundles used in the DNB test program at Columbia University (see Section 4.4.4.2). Figure 4.4-10 shows typical results for a 21 rod bundle (5x5 array with four rods replaced by a control rod guide tube). The agreement demonstrates the validity of the methods described above.

4.4.3.2 Analytical Model

In order to evaluate the core thermal margin an analytical model has been established which defines a hypothetical hot channel containing the design radial peak rod and having all factors applied to it which cause it to be the most limiting channel in the core. This channel is open and therefore, has the same axial pressure distribution as the fuel assembly. The pressure drop from inlet to exit of the hot assembly is controlled by the pressure drop through the core. There are three segmental phases to the calculation of the DNBR.

a) Calculation of the core flow distribution and pressure drop.

b) Calculation of the hot subchannel coolant conditions.

c) Calculation of the DNBR.

4.4.3.2.1 Core Flow Distribution

The core flow distribution is calculated by considering the core as an array of parallel closed flow paths, called zones. The thermal and hydraulic characteristics of each zone are used to calculate the core flow distribution with the provision that the pressure drops across all zones are equal. In this phase of the calculation each zone is separate from the others and there is no energy or mass interchange between zones. The hot assembly, which contains the hot channel is included as one of the zones in this first phase of the calculations. The equations used are described in COSMO[2].*

*See note on COSMO in Subsection 4.4.2.6.1.

Twelve zones are used in the COSMO* calculations to represent the core. Because of quadrantal symmetry in the core inlet flow distribution and in the core wide fuel assembly power distribution, this is equivalent to forty-eight zones representing the entire core. The heat flux in each zone is dependent on the normalized radial peak for the zone and on the core power level being analyzed. The following gives the core average heat flux at 100% power and the radial peaks of the zones. The core average heat flux shown includes the energy deposited directly in the moderator, so that the zone enthalpy is properly calculated by the code.

Zone No.	Radial Peak	
1	1.08	
2	1.02	
3	0.93	
4	1.11	
5	1.05	
6	1.12	
7	1.12	
8	0.76	
9	0.60	
10	0.96	
11	1.00	
12	1.59 -	Assembly containing Hot Subchannel

Core average heat flux
at 2700 mwt = 183,843 Btu/hr-ft^2

Zone heat flux = (Core Average Flux) x (Radial Peak)

The overall core pressure drop is determined using the best estimate of assembly peaking distribution which is much flatter than the distribution which accompanies the design peaking condition. Since the more peaked distribution would be accompanied by increased two-phase flow and higher core pressure drop, the flow is higher in the hot channel and hot assembly.

* See note on COSMO in Subsection 4.4.2.6.1.

4.4.3.2.2 Hot Subchannel Coolant Conditions

In the second phase of the calculations, the coolant conditions are determined in the hot subchannel of the core. A subchannel is defined as the coolant flow area bounded by four adjacent fuel rods. Since the subchannel is open to the hot assembly, the flow rate in the hot channel will be increased or decreased along the axial length such that the axial pressure distribution in the subchannel is made equal to that of the hot assembly.

As has been discussed in the section on hot channel factors, several factors are applied to the hot channel to account for uncertainties due to manufacturing tolerances and core behavior. All these factors are applied simultaneously to the hot channel to ensure that it is the most limiting channel in the core. These factors include (see Section 4.4.2.4):

a) Engineering Enthalpy Rise Factor

b) Heat Flux Factor

c) Pitch and Bow Factor

d) Inlet Flow Distribution Factor.

In addition, a turbulent interchange thermal mixing factor, deternined by INTHERMIC code,(1) is applied to account for energy transferred from the hot channel to cooler surrounding channels. This is discussed in Section 4.4.4.

4.4.3.2.3 Calculation of DNBR

The final phase of the calculations uses the hot channel coolant conditions and the local heat flux in conjunction with the W-3DNBR*correlation discussed in Section 4.4.2.6 to determine the minimum DNBR in the core. The design criteria of 1.3 minimum DNBR using the W-3*correlation gives at least 95 percent certainty that burnout will not occur in the hot channel. Verification of the applicability of the W-3*correlation to predict DNB in the fuel assembly is given in Section 4.4.4.

4.4.3.2.4 Void Fraction Calculation

The analytical model, in addition to the 1.3 DNBR criterion, further ensures no fuel damage by imposing void fraction limitations. If unstable flow should occur in a heated channel, premature DNB can occur. The design criterion is that the void fraction may not exceed 20 percent when the mass velocity is less than 1.2×10^6 lb/hr-ft^4 or 60 percent with mass velocities greater than 1.2×10^6 lb/hr-ft^2. These limits ensure that unstable flow cannot occur in the core and, therefore, DNB cannot occur.

When determining void fraction limitations in the core, the statistical factors which are applied to the hot channel when considering DNBR limitations are not applied to the void fraction limit calculations.

*See note on COSMO in Subsection 4.4.2.6.1.

Since we are considering an array of channels in the void fraction analysis, it is not correct to assume worst factors occur on every channel in the array. The inlet flow distribution factor can apply to an array of channels and is included.

4.4.3.2.5 Sensitivity of DNBR to Analytical Model

Some of the fundamental parameters for determining the DNBR are varied from design values to show the sensitivity of the variation on the core thermal margin. The core overpower ratio to 1.30 DNBR is used as a measure of the thermal margin. In these comparisons, the design core power distribution is assumed constant.

The hot assembly power, relative to the hot channel power, influences the openness of the core to divergent crossflow. The hot assembly is assumed to be a closed channel in parallel with other closed channels representing the entire core. The hot subchannel is considered open within the hot assembly. Hence, when the hot assembly has a radial peak equal to that of the hot channel, the hot channel essentially has no divergent crossflow. As the hot assembly radial peak is reduced from the design value, the hot subchannel effectively becomes more open to the core. Figure 4.4-11 shows the change in the percent overpower from the design value as the hot assembly radial peak is varied about the design value. The change in overpower ratio varies from a 4 percent increase if the hot assembly is open to the core to about 1 percent decrease if the hot assembly is assumed to have the same radial peak as the hot subchannel.

The enthalpy rise factors due to rod pitch and bow, turbulent interchange, and core inlet flow distribution (see Table 4.4-2) are all multiplied together within the analytical model. They effectively increase the hot subchannel enthalpy rise over that due only to the heat input from the surroundings fuel rods. Figure 4.4-12 shows the change in the percent overpower from the design value as the enthalpy rise factors are varied about the design value. The percent change in enthalpy rise factor can be thought of as a change in any one or in the product of the factors. Two lines are shown in the figure for two axial power distribution the design distribution which peaks at 35 percent from the core inlet and a typical, flat, end-of-life distribution which peaks at about 90 percent from the inlet (see Figure 4.4-14 for the axial shapes). At the design value of the enthalpy rise factor, there is a maximum of about 2/3 percent decrease in overpower ratio for each percent increase in the enthalpy rise factors.

The Inverse Peclet number (see Section 4.4.4.4) is a basic parameter in determining the amount of turbulent interchange and hence the value of the mixing enthalpy rise factor. Figure 4.4-13 shows the change in overpower ratio as the Inverse Peclet number is varied about the design value of 0.0035. At the design conditions the overpower decreases about 1/3 of 1 percent for a 10 percent decrease in the value of the Inverse Peclet number. Other axial shapes have about the same sensitivity as the design shape.

4.4.3.3 Thermal Response

4.4.3.3.1 Power Distribution

The design power distribution discussed in Section 4.4.2.4 was used for calculations of thermal margin presented herein. Other combinations of axial and radial distributions will occur during operation of the plant. Typical axial distributions are shown in Figure 4.4-14 along with the values of nuclear enthalpy rise factor which give the same thermal margin as the design curve, for the same core power and coolant conditions. As discussed in Section 4.4.2.4, the control system will restrict operation of the plant such that the core power distributions which are permitted to occur will have at least as much thermal margin as the distributions shown in Figure 4.4-14.

4.4.3.3.2 Thermal Margin Limit Curves

Other combinations of temperature, power, and pressure are also likely to occur during reactor operation. The limit curves, in Figures 4.4-15, -16, -17, and -18 show the sensitivity of the reactor to various operating conditions. For a given power and pressure, the thermal margin limit curves show the maximum permissible temperature to reach the design basis limits for DNBR or void fraction. (See Sections 4.4.1 and 4.4.3.4). The reactor protective system trips the reactor before these limits are reached.

In calculating these limits, assumptions were made on the variation in the radial peaking factor with power level. For powers at or above 100 percent, the radial peak was heal constant of the value given in Table 4.4-2. For the normal mode of operation, four pump flow, the radial peak was varied with powers less than 100% to indicate the radial peak variation when maneuvering the plant. The assumption has been made that between 100% and 82% power, the peak increased such that the hot channel power remained constant. For powers below 82%, the radial peak was held constant at the 82% power value.

For three and two pump operation the assumption was made that the radial peak remained constant for all powers, an assumption which limits maneuvering.

The differences in the two modes of operation are seen in the difference between the curved portion of the limit lines shown in Figure 4.4-15 for four pump operation and the straight lines shown for three and two pump operation in Figures 4.4-16 to 4.4-18.

The limit curves are valid for the axial power distributions shown in Figure 4.4-14 when the radial peak at 100% power is as given in Figure 4.4-14 and when it varies with power as described above.

For the four pump curves in Figure 4.4-15, all points on the curves are calculated for a DNBR = 1.3. For the three pump lines in Figure 4.4-16, some of hie lines are calculated for a DNBR of 1.3* and some are calculated for the limiting void fraction criteria given in Section 4.4.3.2.4 and discussed further in Section 4.4.3.4. The more limiting of void or DNBR is used to plot the lines. In Figure 4.4-16, the line for 2400 psia is calculated for a DNBR'= 1.3.* The line for 1750 psia is calculated for the void limit. The line for 2200 psia is calculated for DNB below 575 F and the line for 2000 psia is calculated for DNB below 550 F. Above these two temperatures, these two lines are calculated for the void limit. For both two pump configurations represented in Figures 4.4-17 and 4.4-18, the lines are calculated for the void limit.

The limit curves shown in Figures 4.4-15 to 4.4-18 are not used in obtaining the setpoints for the reactor protective system. They are given to show the sensitivity of the reactor for the typical conditions stipulated above. The method used in developing hie setpoints is described in Section 7.2.1.

The limit curves are based on the design value of coolant volumetric flow rated. The mass flow then varies accordingly with coolant temperature and pressure.

4.4.3.4 Hydraulic Stability

Flow oscillations that lead to premature DNB have been observed during critical heat flux experiments. As a result of these observations, it is necessary to consider the possibility of flow oscillations which would exceed the normal levels associated with two-phase flow. The following types of flow oscillations are to be avoided for a boiling channel in the reactor core:

a) Parallel channel pressure drop-flow instabilities

b) Density wave oscillations

c) Flow pattern instability.

For Stretch Power the CE-1 correlation was used with a corresponding limit of 1.23. See Stretch Power Application Section 6.1, Reference 25.

Pressure drop-flow instabilities and density wave oscillations have been studied for a single channel by Stenning and Veziroglu,[18] and for two parallel channels with and without cross-connections by Veziroglu and Lee[19]. It was found that pressure drop-flow oscillations occur when the pressure drop across the test section decreases with increasing flow. Density wave oscillations occurred at lower flow rates than did the pressure drop-flow oscillations and the cross-connected parallel channels were more stable than the parallel channel system without cross connections. Since the hydraulic conditions in pressurized water reactor channels are typically in a range where the pressure drop increases with increasing flow, pressure drop-flow oscillations will not occur. Density wave oscillations are also unlikely since they tend to occur at even lower flow velocities than do pressure drop-flow oscillations. Consequently, the principal type of flow instability to be considered in a PWR core are oscillations caused by flow pattern instability.

Flow pattern instability can occur when a two-phase flow undergoes a transition from one flow regime to another such as from bubbly to annular flow. Flow regime transition is a necessary but not a sufficient condition for flow pattern instability. Nevertheless the thermal hydraulic design includes conservative limits on hydraulic conditions which might lead to bubbly-slug and bubbly-annular flow regime transitions. Limits are imposed on local void fraction in a small array of hot channels that include the design hot channel. These limits are based on the flow regime transition data of Bengles and Suo.[20] The limits are:

$$\alpha_{max} = 20\% \text{ if } G \leq 1.2 \times 10^6 \text{ lb/hr-ft}^2 \text{ max}$$

$$\alpha_{max} = 60\% \text{ if } G > 1.2 \times 10^6 \text{ lb/hr-ft}^2 \text{ max}$$

These limits are conservative for an open lattice array because crossflow and mixing will tend to damp tendencies toward local flow instability and because local pressure drop fluctuations due to flow regime transitions are not reflected back to the channel inlet.

The procedure for applying the void fraction limits is to compute the void fraction in a non-statistical hot channel using the COSMO*/INTHERMIC thermal and hydraulic method. A non-statistical hot channel is one which has all the normal hot channel peaking factors except the statistical engineering factors. These are omitted since the void fraction limits are intended to be applicable to an array of channels rather than a single channel. Then the most limiting condition (void fraction or W-3 DNBR)* is assumed to define the core thermal margin. For normal four pump operation the W-3 DNBR* is generally the limiting condition. Void fraction can become limiting for certain part loop pumping configurations.

4.4.3.5 Fuel Model Evaluation

The following sections present an evaluation of the UO_2 thermal conductivity, UO_2 melting temperature, and pellet-clad gap conductance for C-E fuel. For an evaluation of the effects of thermal bowing, fuel waterlogging rupture, and cladding stresses during normal and accident conditions refer to Section 4.2.1.4.

See note on COSMO in Subsection 4.4.2.6.1.

4.4.3.5.1 UO_2 Thermal Conductivity

A detailed discussion of the model used for UO_2 Thermal Conductivity is given in Reference 23.

4.4.3.5.2 UO_2 Melting Point

An examination of the published data on the variation of the melting point of UO_2 with burnup, shows a decrease at a nearly linear rate of -56°F per 10,000 MWD/MTU.[21]. This rate results in a UO_2 melting point of 4800°F after a maximum local burnup of 50,000 MWD/MTU is achieved.

4.4.3.5.3 Pellet-Clad Gap Conductance

A detailed discussion of the model for pellet-clad gap conductance is given in Reference 23.

4.4.3.5.4 Fuel Centerline Temperature

The power level required to produce centerline melt in Zirconium alloy clad urania fuel rods is typically $\geq$ 21 kW/ft. Loss-of-coolant accident considerations for St. Lucie Unit 1 limit the steady-state peak LHR to a maximum of 15 kW/ft. The minimum 40% margin between 21 kW/ft and 15 kW/ft (which is the peak LHR allowed) is large enough that fuel centerline melt is not a limiting factor for anticipated operational transients.

4.4.3.6 Coolant Flow Blockage

An experimental and analytical program has been conducted on the effects of fuel assembly coolant flow maldistribution during normal reactor operation. In the experimental phase, velocity and static pressure measurements were made in cold, flowing water in an oversize model of a fuel assembly in order to determine the three-dimensional flow distributions in the vicinity of several types of flow obstruction. The effect of the distributions on thermal behavior were evaluated, where necessary, with the use of CORAL, a C-E version of the COBRA I subchannel thermal and hydraulic code. Subjects investigated included:

a) The assembly inlet flow maldistribution caused by the core support plate and lower end fitting. In the study, the flow distribution was measured at several axial positions downstream of the lower end fitting, and the data were used with CORAL to evaluate the effect on thermal margin of the inlet flow maldistribution. It was concluded that the effect was small enough so that no special allowance for it need be made in the calculational techniques.

b) The assembly inlet flow maldistribution caused by blockage of a core support plate flow hole. CORAL evaluation of the flow recovery data indicated that even the complete blockage of a core support plate flow hole during 120 percent of full-power operation would not produce a W-3 DNBR of less than 1.0.

c) The flow maldistribution within the assembly caused by complete blockage of one to nine subchannels. Flow distributions were measured at positions upstream and downstream of a blockage of one to nine channels. The influence of the blockage diminished very rapidly in the upstream direction. A CORAL analysis of the downstream data for a single subchannel blockage indicated that it would not produce a W-3 DNBR of less than 1.0 downstream of the blockage, even during 120 percent of full-power operation.

d) The flow distribution below the top end fitting, is effected by the end fitting and alignment plate flow hole geometry and by the presence of the CEA shroud. Measurement of the upstream flow pattern, in what would be the active core region, showed no appreciable effect of an artificial exit flow distribution which was even more non-uniform than that characteristic of the geometry of the end fitting, alignment plate, and CEA shrouds. Because of this result, a CORAL thermal margin analysis was considered unnecessary.

Additional information on the assembly flow distribution tests appears in Reference 22.

4.4.4 TESTING AND VERIFICATION

4.4.4.1 Introduction

This section describes several Combustion testing and verification programs which yield thermal and hydraulic information germane to Combustion reactors. These are Departure from Nucleate Boiling (DNB) Tests, Components Tests, Turbulence Interchange Measurements, and Reactor Testing and Verification. Two other programs, Reactor Flow Model Tests, and Assembly Flow Distribution Tests, are discussed in Sections 4.4.3.1 and 4.4.3.6, respectively.

4.4.4.2 DNB Testing

In 1969, Combustion Engineering initiated a series of tests at Columbia University on the Departure from Nucleate Boiling (DNB) phenomenon. One purpose of the tests was to obtain experimental DNB and pressure drop data for verifying the combined accuracy of our thermal and hydraulic COSMO/INTHERMIC design code and the empirical W-3 DNB correlation in predicting the DNB condition for the CEA fuel assembly. (Discussions of the two codes appear in References 1 and 2.)

The tests were conducted on an exact scale model of a CEA fuel assembly, consisting of one guide tube and twenty-one electrically heated "fuel" rods arranged five-by-five. Parts of production spacer grids were used to support the rods; vertical spacing of the grids was 16 inch center-to-center, with the end of the heated length just upstream of the last grid. Three distinct test sections were tested: one with a 7-ft heated length and a uniform lateral power distribution, one with a 7-ft heated length and a nonuniform lateral power distribution, and one with a 4-ft heated length and a nonuniform lateral power distribution. The axial power distribution was uniform for all test sections. Test conditions comprised a coolant inlet temperature range of 450F to 650F, a mass velocity range of $1x10^6$ to $3x10^6$ lb/hr-ft^2 and a system pressure range of 1500 to 2200 psia.

Approximately ninety DNB data points were obtained from all three test sections. The COSMO/INTHERMIC/W-3 combination was used for predicting the corresponding critical heat flux values for the experimental conditions of inlet temperature, mass velocity, and system pressure. A necessary part of the COSMO input is the mixing factor, which was calculated by INTHERMIC for the design. Inverse Peclet Number of 0.0035. The measure of the accuracy of prediction was defined as the average value of the ratio of experimental to predicted critical heat flux. As indicated in Figure 4.4-19, the overall value was 0.983 with a sample standard deviation of 0.058 and compare satisfactorily with corresponding values in the literature. The results show that COSMO/INTHERMIC/W-3 is acceptable for describing DNB in the CEA geometry, and, by inference, that the Inverse Peclet Number was accuratley determined in the turbulent interchange measurements described in Section 4.4.4.4.

Since 1969, the following additional subjects have been investigated:

a) Data reproducibility was demonstrated through repetition of the 7 ft nonuniform lateral power distribution test.

b) For several tests, the testing envelope was expanded to cover a mass velocity range of 0.5×10^6 to 4×10^6 lb/hr-ft^2 and a system pressure range of 900 to 2300 psia, and some data were also obtained at still lower mass velocities and pressures, down to 0.05 lb/hr-ft^2 and 100 psia. The data are used in the evaluation of the adequacy of design methods for nonstandard operating and accident conditions.

c) Tests were run which showed that the spacer grid has no local adverse effect on DNB and that there is no effect on DNB for spacer grid center-to-center vertical spacings greater than 16 inches. The latter result therefore demonstrated the applicability of the 1969 test data to later fuel assembly designs, in which the grid spacing varies between 17 and 19 inches.

In the more recent tests, coolant exit temperature distribution data have been obtained, in addition to the segmental and total test section pressure drop information. As with the DNB data, predictions of those quantities are made using the thermal and hydraulic computer codes. The temperature data show reasonable agreement with the predictions, considering the technical difficulties of measuring "average" subchannel temperatures, particularly near the cold test section shroud wall. Agreement of predicted and experimental pressure drop data for subcooled and bulk boiling conditions is good. Isothermal pressure drop data have been used as a source for spacer grid loss coefficient information, described in Section 4.4.3.1.

Current and future DNB program work is concentrated in the following activities.

a) Verification of the absence of test rig bias in the Columbia data by repeating a test at a second facility, the Winfrith Laboratory of the UKAEA.

b) Determination of the DNB effect on nonuniform axial power distributions through experiment and prediction, thus completing the assessment of the applicability of the W-3 correlation.

c) Improvement in experimental test section design and in the accuracy of the codes and DNB correlations in predicting DNB under steady state, transient, and accident conditions. The objective is to assure an adequate DNB thermal margin under all conditions without excessive conservatism arising either from test section idiosyncrasies or from insufficiently precise correlations.

Additional information on the DNB program is presented in Reference 13.

4.4.4.3 Components Testing

Component test programs have been conducted in support of all Combustion designed reactors. The tests subject a full scale reactor core module comprising one to four fuel bundles and a control element assembly and drive mechanism to the hydraulic environment of the reactor under all normal operating conditions. The objectives of the programs are to confirm the basic hydraulic characteristics of the components and to verify that fretting and wear will not be excessive during the component lifetime. When the reactor design has changed sufficiently to make questionable the continuing applicability of the results of earlier programs, a new program embodying the important aspects of the latest design is conducted. Thus, components tests have been run on the Palisades design, with cruciform control rods, on the Fort Calhoun CEA design,

with rack-and-pinion Control Drive Mechanisms and on the Maine Yankee and later designs, with dual CEA's and magnetic jack CEDM'S.

During the course of the tests, information is obtained on wear, on CEA/CEDM scram behavior, and on fuel assembly uplift and pressure drop. The first two subjects are discussed in Chapter 4.2.1 and 4.2.3. The third is discussed below.

As part of the assessment of fuel assembly margin to uplift in the core, measurements are made of fuel assembly net weight, to the point of lift-off, for an isothermal temperature range of 150F to 600F at a system pressure of 2100 to 2250 psia. To obtain the desired information, one of the fuel assemblies of the module is mounted on load beams so that the assembly net weight can be measured as a function of flow rate and temperature. Data reduction involves the calculation of an uplift coefficient, which describes the hydraulic uplift force acting on the assembly. The coefficient is defined as follows:

$$K_{UP} = \frac{W_o}{\frac{\rho V^2 A}{2_g}}$$

where W_o = Wet weight of assembly with no flow.

V = Flow velocity in assembly at the point of lift-off.

A = Envelope area of assembly.

A plot of the K_{UP} data shows that they can be fitted by the relation:

$$K_{UP} = AN_R^{-B}$$

where A and B are 40.1 and 0.117, respectively, with a standard deviation of 3.7 percent which includes replication and instrument error.

The uplift coefficient is employed in the analysis to the uplift forces on the fuel assemblies in the reactor. The force is determined for the most adverse assembly location for startup and normal operating conditions. Additional input to the calculation includes analytical corrections to the coefficient for the absence of the CEA, for crud formation, and for small geometrical differences among the fuel assemblies for the different reactor designs.

A characteristic uplift load derived from the experimental work and subsequent analysis appears in Section 4.4.2.3.

Pressure measurements are also made to verify the accuracy of the calculated loss coefficients for various fuel assembly components. Direct reduction of the pressure drop data yields the loss coefficients for the lower-and upper end fitting region, while the spacer grid loss coefficient is evaluated by subtracting a calculated fuel rod friction loss from the measured pressure drop across the fuel rod region.

The experimental end fitting loss coefficients are essentially independent of Reynolds Number and, with their sample standard deviations, are in reasonable agreement with the predicted values used in the calculation of core pressure drop (Section 4.4.2.3). The experimental spacer grid loss coefficient from the Components Tests for Maine Yankee and later CEA designs is in close agreement with the design value for that parameter, which is based upon experimental results from the Fort Calhoun Components Test and the applicable tests of the DNB Program (Section 4.4.4.2).

4.4.4.4 Turbulent Interchange Testing

In 1966, a series of single phase tests on coolant mixing through turbulent interchange was run on a "prototype" fuel assembly which was geometrically similar to the Palisades assembly. The model enabled determination of vertical subchannel flow rates using pressure instrumentation and the average level of turbulent interchange using dye injection and sampling equipment. The tests yielded the value of Inverse Peclet number characteristic of turbulent interchange in the prototype geometry. The Inverse Peclet Number is a dimensionless parameter defined by the relation:

$$\hat{\mathrm{P}}_e \equiv \frac{\omega'}{\bar{G}\bar{D}_e}$$

where ω' = Turbulent interchange between subchannels, lb/hr-ft

$\bar{D}_e$ = Average equivalent diameter of two neighbor subchannels between which turbulent interchange occurs, ft

$\bar{G}$ = Average mass velocity of two neighbor subchannels, lb/hr-ft^2

In the test geometry, the value of $\hat{\mathrm{P}}_e$ was found to be 0.00366, with a sample standard deviation of 16 percent. The value was shown during the course of the tests to be insensitive to coolant temperature and mass velocity. The best estimate value of the Inverse Peclet Number was established at 0.0035 on the basis of the experimental results, and is the value used in core thermal and hydraulic calculations.

As part of a C-E sponsored research and development program, a new series of single-phase dye injection mixing tests was conducted in 1968. The tests were performed on a model of a portion of a CEA type fuel assembly which was sufficiently instrumented to enable measurement, via a data reduction computer program, of the individual lateral flow across the boundaries of twelve subchannels of the model. The Inverse Peclet Number calculated from the average of 56 individual turbulent interchange flow values (two across each subchannel boundary) was 0.0034. With respect to general turbulent interchange, therefore, the more recent study on the CEA assembly verifies the constancy of the Inverse Peclet number for moderately different fuel assembly geometries and confirms the design value of that characteristic. Additional indirect verification appears in the agreement between predicted and measured values of critical heat flux obtained in the DNB Program (Section 4.4.4.2).

More detailed information on this subject appears in Reference 14.

4.4.4.5 Reactor Testing

During reactor startup, data descriptive of thermal and hydraulic conditions within the reactor vessel will be obtained. These will include core exit temperature distribution, hot and cold leg temperature, loop flow rates, and core power distributions. The data will be evaluated and compared with design calculations and parameters to assure that the reactor thermal and hydraulic behavior is normal.

4.4.5 FUEL THERMAL-HYDRAULIC DESIGN METHODOLOGY (ENC)

This section presents the thermal and hydraulic analysis of the reactor core as performed by Exxon Nuclear Company in justification for use of their 14x14 Pressurized Water Reactor reload fuel in St. Lucie Unit 1.

4.4.5.1 Design Bases and Criteria

The primary thermal-hydraulic design basis for reload fuel is that fuel rod integrity should be maintained during normal operation and anticipated operational occurrences. Specific criteria are:

1) Avoidance of boiling transition for the limiting fuel rod in the core with at least a 95% probability at a 95% confidence level. The margin to boiling transition for ENC and CE fuel is assessed with ENC's XNB critical heat flux correlation. See Reference 13 and the following section on Statistical Combination of Uncertainties.

2) Fuel Centerline temperatures should be below the melting point of the fuel pellets. (See Section 4.4.5.2.4)

Observance of these criteria during anticipated operational transients is considered conservative relative to the requirement that anticipated operational transients not produce fuel rod failures or loss of functional capability.

4.4.5.2 Methods of Analysis

4.4.5.2.1 Core Flow Distribution Analysis (Modeling CE and ENC Fuel)

The core flow distribution analysis is performed to assess crossflow between assemblies in the core for use in subsequent MDNBR subchannel analysis. This is particularly important for mixed fuel loading where hydraulically different fuel types are co-resident in the core.

The hydraulic analysis was conducted using the XCOBRA-IIIC computer code and a 1/8 core symmetry model which allowed crossflow between adjacent assemblies. The single phase loss coefficients given in Reference 30 (based on pressure drop tests performed in ENC's Portable Loop Hydraulic Test Facility) were used to characterize the ENC and CE fuel types. Three separate core flow distribution calculations were made to establish limiting assembly mass, energy, and momentum crossflows for the MDNBR subchannel analysis to follow. In the first, an ENC fuel assembly was assumed to be limiting during Cycle 6 with a significantly higher power level relative to the remainder of the core.

In the second calculation a CE fuel assembly was assumed to be limiting during Cycle 5 operation with a high assembly power level. In the third analysis, an ENC fuel assembly was assumed to be limiting in Cycle 6 with reload batches XN-1 and XN-1A (8 extra ENC fuel assemblies). For the relative DNB performance analysis a maximum F_r limit of 1.70 was assumed and imposed on the limiting assembly power for both the ENC and CE limiting cases. From these calculations two limiting assembly axially varying crossflow boundary conditions were established to be used in respective MDNBR evaluations for CE and ENC fuel types. In each case, a 5% inlet flow maldistribution factor is assumed for the limiting and surrounding assemblies.

4.4.5.2.2 MDNBR Subchannel Analysis

For the reactor setpoint analyses, a subchannel model is required to predict core flow and enthalpy distributions, transient heat fluxes, and, finally MDNBR. The XCOBRA-IIIC computer code(41) and the XNB DNB correlation[42] were used to calculate MDNBR. The applicability of the XNB critical heat flux correlation to ANF fuel in St . Lucie Unit 1 is demonstrated in Reference 38.

The XCOBRA-IIIC 1/8 core model employed in the analysis is shown in Figure 4.4-22. Each assembly is represented as a single hydraulic channel having hydraulic characteristics and power appropriate to that assembly. The MDNBR performance of the loading pattern modeled is conservative with respect to that of the final loading pattern for Cycle 9. The model contains a greater number of the lower resistance XN-2 type assemblies than will be loaded for Cycle 9. The hot assembly is a higher resistance XN-3/ANF-4 type. The difference in hydraulic resistanced between the hot assembly and the average core is thus exaggerated in the model. Simulated flow diversion from the hot assembly is, therefore, greater than will be the actual flow diversion in Cycle 9. The Cycle 9 loading pattern will thus display a slight increase In hot assembly mass flux which will improve DNBR performance relative to that modeled. The radial power distribution for the final loading pattern will differ slightly from that modeled. The impact of this minor difference on calculated hot assembly MDNBR is negligible because it produces no change in hot assembly local coolant conditions. The loading pattern modeled and depicted in Figure 4.4-22 will thus conservatively represent the Cycle 9 core as it is finally constituted.

A pin-by-pin subchannel model of a 1/8 segment of the limiting assembly was developed. The 1/8 core model described above provided cross flow boundary conditions to the 1/8 assembly model at the assembly boundaries. A diagram of the 1/8 assembly model is shown in Figure 4.4-23. The local power distribution at end-of-life conditions was chosen because it provided the maximum assembly power with the hot rod at the Technical Specification limit. This resulted in a larger hot channel enthalpy rise and lower MDNBR than would normally be expected. An inlet flow maldistribution factor of 5% was applied to the subchannel model. Also, the local peaking factors were arbitrarily increased such that the highest power rod in the assembly had a peaking factor equal to the Technical Specification / Core Operating Limits Report limit of 1.70.

In the XCOBRA-IIIC model, all of the core power was assumed to be generated in the fuel rods to obtain the correct subchannel enthalpy rise. In reality, 2.5% of the power is deposited directly in the moderator due to gamma heating. Therefore, MDNBRs predicted by XCOBRA-IIIC were divided by 0.975 to account for the fact that rod heat flux corresponds to 97.5% of the power.

The model used in the statistical setpoint analysis consisted of 4 channels representing the hot subchannel, the remainder of the limiting assembly, the assemblies surrounding the limiting assembly, and the rest of the core. This 4-channel model was benchmarked against the 1/8 core and 1/8 assembly model over a wide range of off-normal conditions which enveloped those expected during operational plant transients. The bare rod friction coefficients and the turbulent mixing coefficient were adjusted so that the model conservatively predicted MDNBR when compared to the detailed 1/8 assembly model.

The application of the 4-channel XCOBRA-IIIC model for the statistical verification of trip setpoints and limiting conditions of operation is described in Section 15.6.

4.4.5.2.3 Statistical Combination of Uncertainties

The determination of Limiting Conditions of Operation (LCOs) and Limiting Safety System Settings (LSSSs) related to fuel centerline melt, departure from nucleate boiling (DNB) and Specified Acceptable Fuel Design Limits (SAFDLs), are discussed in this sub-section. The limits in all cases include compensation for uncertainties. Historically, uncertainties have been included in a "deterministic" fashion; that is, each uncertain parameter was always selected to be at its most unfavorable limit. This approach of stacking uncertainties provide for uncertainties in a very conservative fashion that required only a single analysis.

The approved ENC setpoint methodology for CE reactors (Ref 4) provides the basis for the statistical setpoint analyses here described. In the statistical analyses, the uncertainties are accounted for by statistical convolution rather than by using the deterministic approach. Thus, the approved deterministic analyses procedures have been modified to statistically, rather than deterministically, account for uncertainties, thereby providing a better estimate of the limits. The generic statistical uncertainty analysis methodology (GSUAM) employed by ENC to statistically combine the uncertainties is discussed in Ref 4. GSUAM provides an accurate method for accounting for uncertainties. It does however, require a larger number of calculations relative to the deterministic approach.

The uncertainties which must be accounted for are basically from two sources: Measurement and calculations. The latter category includes model structural deficiencies and parameter uncertainties. Axial Shape Index (ASI) measurement drift and power measurement are pure measurement uncertainties and can be applied directly to the results of an uncertainty analysis in which they are not varied.

An example of an analysis in which GSUAM can be applied is the derivation of the Thermal Margin/Low Pressure (TM/LP) trip, which involves calculations of DNBR over a range of powers, inlet temperatures, pressures and Axial Shape Indices (ASI). In order to reduce the number of calculations used in the analysis, the statistical combination of uncertainties is performed at only a single nominal point and the calculational uncertainty thus derived is applied to every nominal point. The nominal point at which GSUAM is used is conservatively chosen to provide the greatest uncertainty in the calculated results and, therefore, a conservative estimate at all other points.

Choice of the nominal point is based on finding the location where the difference between the nominal point and the deterministic calculation is maximum. The point selected by this criterion will result in a conservative estimate of the uncertainties in the calculated result for all applicable points.

Tables 2.1 & 2.2 (Ref. 29) have identified parameter uncertainties and some of their values that are treated with the methodology described above. The parameters for which uncertainties are identified generally are CE plant system parameters, and the uncertainty values correspond to those appearing in publicly available documents such as the St. Lucie accident and transient analysis reports. The uncertainties associated with sources such as the rod insertion speed, pump coast down rate and the DNBR correlation were established from measurement data.

4.4.5.2.4 Fuel Performance

Steady state fuel temperatures are determined by the RODEX 2 computer program (Ref. 9). The calculational procedure considers the effect of linear heat rate, fuel relocation, fuel swelling, densification, thermal expansion, fission gas release, and clad deformations. The model for predicting fuel thermal performance is discussed in Section 4.4.5.3.2. The following are some of the most important considerations included in the fuel thermal performance evaluation.

a) INTERNAL PRESSURE: The fuel rod internal pressure was calculated the RODEX2 code with the ENC developed physically based model for fission gas release. The rod was analyzed at 85 to 100% of the design peak power of 15.0 Kw/ft to the design burnup of 44,500 MWD. The calculated EOL internal pressure is below the reactor system pressure.

b) CLADDING TEMPERATURE: The cladding temperature was conservatively obtained from the fuel rod internal pressure analysis. The rod was analyzed at 85 to 100% of the maximum allowable power. The calculated cladding ID, cladding OD, and volumetric average temperatures were found to be within the design limits.

c) FUEL PELLET TEMPERATURE: Prevention of fuel failure from overheating of the fuel pellets is accomplished by ensuring that the peak LHGR during normal operation and anticipated transients does not result in calculated centerline melt. The power level required to produce centerline melt in Zirconium alloy clad urania fuel rods is typically $\geq$ 21 Kw/ft. Loss of Coolant accident considerations for St. Lucie Unit 1 limit the steady state LHGR to 15 Kw/ft. The 40% margin between 21 Kw/ft and 15 Kw/ft is large enough that fuel centerline melt is not a limiting factor for anticipated operational transients.

d) ROD BOW CONSIDERATIONS: Fuel rod bow is determined throughout the life of the fuel assembly so that reactor operating thermal limits can be established. These limits include the minimum critical heat flux ratio associated with protection against boiling transition and the maximum fuel rod LHGR associated with protection of metal-water reaction and peak cladding temperature limits for a postulated loss of coolant accident (LOCA).

ENC's rod bow measurements have been used to establish an empirical model for determining rod bow as a function of burnup which is used to calculate thermal limits. (References 31 & 32). This model was used to estimate the magnitude of rod bow for St. Lucie Unit 1 fuel. The calculations indicate that 50% closure of rod-to-rod gap occurs at an assembly exposure of about 85,000 MWD/MTM for ENC's 14 x 14 design. Significant impact to MDNBR due to rod bow does not occur until gap closure exceeds 50%. Since the maximum design exposure for ENC fuel in the St. Lucie Unit 1 unit core is significantly less, rod bow does not limit MDNBR for ENC fuel. A further consequence of the small amount of rod bow for ENC fuel is that total power peaking is not significantly impacted.

e) CREEP COLLAPSE: Creep collapse calculations are performed with RODEX2 and COLAPX (Ref. 36) codes in accordance with the method described in Ref. 37. RODEX2 determines the cladding temperature and internal pressure history based on a model which accounts for changes in fuel rod volumes, fuel densification and swelling, and fill gas absorption. Minimum fill gas pressure, maximum fuel densification, mimimum statistical cladding wall thickness and nominal pellet dimensions are assumed. The reactor coolant, fuel rod internal temperature, and pressure histories generated by RODEX2 are input to the COLAPX code along with the maximum statistical initial cladding ovality and the fast flux history. The power and flux histories for the peak burnup rod are utilized. The COLAPX code calculates, by large deflection theory, the ovality of the cladding as a function of time while the uniform cladding creepdown is obtained from the RODEX2 analysis. The cladding creepdown and ovality increase are then summed and at a rod average burnup of 6000 MWD/MTU, the combined creep down of 0.003 inch is less than the initial minimum diametral fuel-cladding gap. This will prevent pellet hangups due to cladding creep, allowing the plenum springs to close axial gaps until densification is substantially complete, and thus assures that clad collapse will not occur. The power histories utilized in the fuel performance evaluation correspond to the peak discharge burnup fuel rod and are illustrated in Tables 6.3 & 6.4, Ref. 28.

4.4.5.3 Computer Codes

4.4.5.3.1 XCOBRA-IIIC

This computational procedure is designed to evaluate subchannel thermal hydraulic conditions during steady and transient state, in boiling and nonboiling conditions. One-dimensional, two phase separated, slip flow is assumed in the COBRA calculation. These assumptions are valid only if the cross-flow between connecting subchannels is small compared to the axial velocities in the individual subchannels. Because small cross-flow does exist mathematical models have to be postulated for both turbulent and diversion cross-flow mixing. Models of two-phase state are also defined in terms of void fraction, which is a function of enthalpy, flow rate, heat flux, pressure, axial position and time. The program is not applicable when large blockages exist in the fuel bundles since this leads to considerable crossflow which cannot be adequately represented by the one-dimensional analysis (see Ref. 33).

4.4.5.3.2 RODEX 2

The RODEX2 code (Ref. 34) is an interactive calculational procedure that considers the thermal hydraulic environment at the cladding surface, the pressure inside the cladding, and the thermal, mechanical and compositional state of the fuel and cladding.

In addition to evaluation of the fuel rod steady-state cladding strain, RODEX2 determines the initial conditions for fuel rod power ramping analyses and the minimum fuel rod internal pressures for cladding creep analyses. Pellet density, swelling, densification, and fission gas release or absorption models, and cladding and pellet diameters are input to RODEX2 to provide the most conservative subsequent ramping or collapse calculations for the reference fuel rod design.

The fuel rod performance characteristics modelled by the RODEX2 code are:

- Gas Release and Absorption
- Radial Thermal Conduction and Gap Conductance
- Free Rod Volume and Gas Pressure Calculation
- Pellet-Cladding interaction
- Fuel Swelling, Densification, Cracking and Crack Healing
- Cladding Creep Deformation and Irradiation Induced Growth

In the RODEX2 model, calculations are performed on a time incremental basis with conditions updated at each calculated increment so that the power history and path dependent processes can be modelled. The axial dependence of the spatial power and burn up distributions are handled by dividing the fuel rod into a number of fuel segments which are modelled as radially dependent regions whose axial deformations and gas release are summed. Power distributions can be changed at any desired time and the coolant and cladding temperatures are readjusted at all axial nodes. Deformations of the fuel and cladding and gas release are incrementally calculated during each period of assumed constant power generation. Gap conductance is calculated for each of these incremental calculations based on gas release throughout the rod and the accumulated deformation at the center of each axial region within the fueled region of the rod. These deformation calculations consider fuel densification, swelling and

cracking, thermal expansion, cladding creepdown, irradiation induced growth, and fuel creep and crack healing.

4.4.5.4 Mixed (Transition) Core Configuration

Because of the higher grid spacer loss associated with the ENC fuel (See Ref. 30) compared to the resident CE fuel, ENC suffers a flow diversion penalty-since cycle 6 is the first cycle in which ENC fuel will be loaded, Cycle 6 will have a lower ratio of ENC to CE fuel assemblies than future cycles, and therefore, a larger penalty. Succeeding cycles will experience decreasing penalties until all the fuel in the core is ENC fuel, at which point there will be no flow penalty and the thermal margin for ENC fuel will be significantly improved. For this reason, it is anticipated that the Cycle 6 core will be more thermal hydraulically limiting than future cycles, and thus the present analysis will be bounding for Cycle 7 and subsequent cycles at St. Lucie Unit 1. A preliminary evaluation of future cycles has indicated that as the number of ENC fuel assemblies in the core increases there will be slight increases in assembly flow for both ENC and CE fuel, and thereby a higher limiting assembly MDNBR for both fuel types.

Beginning with Cycle 17

The Cycle 17 core consists of both bi-metallic and High Thermal Performance (HTP) SPC assemblies. The XCOBRA-IIIC computer code along with the XNB correlation for bi-metallic assemblies and the HTP correlation (Reference 48) for HTP assemblies were used to calculate MDNBR. Due to the increase in thermal performance of the HTP assemblies, and the fact that the maximum assembly power of the limiting bi-metallic assembly is close to the power of the peak assembly, a bi-metallic assembly is limiting from the standpoint of DNBR (Reference 47).

4.4.5.5 Cycle 6 Thermal Margin Evaluation

Table 4.4-6 summarizes thermal hydraulic parameters used in the core flow distribution calculations and subsequent MDNBR analyses. The calculations were performed at a 130% overpower condition (1.30 x 2700 MWt) in order to maximize potential differences in limiting assembly MDNBR between ENC, reload batches XN1 and XN-1A, and CE Cycle 5 fuel and they provided MDNBR's which are representative of those that may be expected during a severe operational transient event (i.e. MDNBRs near the XNB 95:95 correlation limit).

The relative impact of ENC fuel assemblies on existing core thermal margins is about a 7% decrease in MDNBR relative to results for a limiting CE assembly in Cycle 5. In the Cycle 6 reload Batches XN-1 and XN-1A analysis, the limiting ENC assembly was assumed to consist of 164 active fuel rods, while the CE limiting assembly is composed of 168 active rods.

Due to a slight difference in the number of active fuel rods in Cycle 6 and Cycle 5, ENC rods have about a 1% higher heat flux which yields a proportionate decrease in MDNBR. The remaining 6% difference in MDNBR between ENC and CE fuel is due to hydraulic dissimilarities between the two fuel designs.

4.4.6 THERMAL AND HYDRAULIC DESIGN EVALUATION FOR EXTENDED POWER UPRATE (EPU)

4.4.6.1 Introduction

This section describes the Thermal-Hydraulic (T-H) analysis supporting the extended power uprate (EPU), which increases the reactor core thermal power from 2700 MWt to 3020 MWt. The current licensing basis for T-H design includes the prevention of DNB on the limiting fuel rod with a 95% probability at a 95% confidence level and criteria to avoid fuel centerline melting. The EPU analysis
is based on this licensing basis analysis, incorporating the increased core power. The analysis

addresses the DNB performance, including the effect of fuel rod bow and bypass flow. The EPU analyses have considered the CE14 HTP fuel design with the standard guide tube design and the MONOBLOC™ guide tube design. The MONOBLOC™ guide tube has been evaluated to have no significant impact on the pressure drop and T-H characteristics of the core. Thus, the fuel assembly flow area and hydraulic resistance are considered unchanged between the pre-EPU and post-EPU fuel design, so there will be no T-H compatibility or stability issues typically associated with a transition core.

4.4.6.2 Input Parameters, Assumptions, and Acceptance Criteria

XCOBRA-IIIC is the core T-H sub-channel analysis code that was used for the EPU analysis. NRC approval of the XCOBRA-IIIC code was issued in the safety evaluation report (SER) attached to Reference 41.

For the EPU analysis, fuel-related safety and design parameters of the CE14 HTP fuel design with standard guide tubes and with MONOBLOC™ guide tubes have been used. These parameters have been used in safety and design analyses discussed in this section.

Table 4.4-8 lists the T-H parameters for the current design at 2700 MWt, as well as for the EPU design at 3020 MWt with the CE14 HTP fuel design with MONOBLOC™ guide tubes. Some of the parameters listed in Table 4.4-8 are used in the analysis basis as XCOBRA-IIIC input parameters, while others are provided since they are listed in UFSAR Table 4.4-2. This section identifies those parameters that are used as input parameters to the XCOBRA-IIIC model and also identifies the limiting direction of each parameter. The following parameters from Table 4.4-8 are used in the XCOBRA-IIIC model:

- Reactor core heat output (MWt)
- Heat generated in fuel (%)
- Nominal vessel/core inlet temperature (°F)
- F_r, enthalpy rise hot channel factor
- Pressurizer/core pressure (psia)
- RCS minimum flow rate (gpm)

Biases were applied to input parameters according to the approved methodology (Reference 52). For the transient analyses, uncertainties were deterministically applied. Thus, steady-state measurement and instrumentation errors were taken into account in an additive fashion to ensure a conservative analysis. For statistical DNB calculations, uncertainties were statistically treated according to the approved methodology (Reference 50). The system related uncertainties bounded by the non-loss of coolant accident (LOCA) safety analyses are listed in Table 4.4-9.

Control grade equipment was modeled in such a way that it does not mitigate the effects of an event. For example, the pressurizer power operated relief valves and pressurizer spray system were assumed operable while the pressurizer heaters were assumed inoperable for DNBR transient events where suppressing primary side pressure is conservative.

The reactor trip setpoints and time delays modeled in the transient analyses were conservatively applied to provide bounding simulations of the plant response. To the extent that the reactor protection system and engineered safety features system is credited in the accident analyses, the setpoints have been verified to adequately protect the plant for EPU operation.

The reactor core is designed to meet the following limited T-H criteria:

- There is at least a 95% probability at a 95% confidence level that DNB will not occur on the limiting fuel rods during Modes 1 and 2, operational transients, or any condition of moderate frequency.
- No fuel melting during any anticipated normal operating condition, operational transients, or any conditions of moderate frequency.

The ratio of the heat flux causing DNB at a particular core location, as predicted by a DNB correlation, to the actual heat flux at the same core location is the DNBR. Analytical assurance that DNB will not occur is provided by showing the calculated DNBR to be higher than the 95/95 limit DNBR for conditions of normal operation, operational transients and transient conditions of moderate frequency.

4.4.6.3 Description of Analyses and Evaluations

The T-H analysis of the CE14 HTP fuel is based on the approved methodologies for performing DNB calculations (References 49 and 52). The S-RELAP5 code was used for the transient analysis. The XCOBRA-IIIC code was used to calculate minimum DNBR (MDNBR) using the HTP and Biasi critical heat flux (CHF) correlations. EC292761
RODEX2-2A (References 55 and 56) was developed to perform calculations for a fuel rod under normal operating conditions. For non-LOCA applications, RODEX2-2A was used to validate the gap conductance used in the analyses and to establish the fuel centerline melt linear heat rate (LHR) as a function of exposure.

The HTP DNB correlation is based entirely on rod bundle data and takes credit for the significant improvements in DNB performance due to the flow mixing nozzles effects. NRC acceptance of a 95/95 HTP correlation safety limit DNBR of 1.141 for the 14x14 HTP fuel assemblies is documented in Reference 48. The Biasi CHF correlation EC292761
(Reference 53) is used to calculate the DNBR for post-scram reactor conditions. The ranges of parameters used in the EPU design have been verified to fall within the range of applicability for these correlations. A 2% mixed-core penalty is typically applied to DNBR safety limits as required by the SER in Reference 49. The power EC292761
distribution effects are discussed in the specific analyses presented in UFSAR Chapter 15.

The approved methodology for performing DNB calculations using the XCOBRA-IIIC code is described in Reference 49. The SER for the Reference 41 topical report states that the use of XCOBRA-IIIC is limited to the “snapshot” mode. This, MDNBR calculations were performed using a steady-state XCOBRA-IIIC model with core boundary conditions at the time of MDNBR from the S-RELAP5 transient analyses.

The Reference 50 topical report describes the method for performing statistical DNB analyses. Two conditions were noted in the SER for the Reference 50 methodology:

- The methodology is approved only for Combustion Engineering (CE) type reactors which use protection systems as described in the Reference 50 topical report.
- The methodology includes a statistical treatment of specific variables in the analysis; therefore, if additional variables are treated statistically, Framatome should re-evaluate the methodology and EC292529
document the changes in the treatment of the variables. The documentation will be maintained by Framatome and will be available for NRC audit. EC292529

Protection against the fuel centerline melting (FCM) SAFDL is expressed as a limit on LHR allowed in the core. The FCM limit was explicitly calculated for the EPU. Due to the reduced thermal conductivity of gadolinia fuel rods, the FCM limit may be set by gadolinia fuel. A FCM limit is established for UO_2 fuel rods such that, FCM is precluded for all fuel rod types.

The approved methodology for calculating the enthalpy deposition for a control element assembly (CEA) ejection accident is given in Reference 51. No restrictions or requirements were identified in the SER for the Reference 51 methodology.

The impact of rod bowing on the MDNBR and peak LHR was evaluated using the rod bow methodology described in References 31 and 32. The objective was to determine the threshold burnup level at which a rod bow penalty must be applied to either the MDNBR or peak LHR results. The results show that the threshold burnups are beyond the current licensing limit of 55 GWd/MTU, therefore no rod bow penalty is required for DNB or LHR calculations Fuel rod bow measurements recently taken on contemporary CE 14 HTP fuel designs show better than predicted bow

performance. Further evidence of acceptable fuel rod bow performance is provided by recent poolside evaluations at Millstone Unit 2 and St. Lucie Unit 1. These show the rod to rod gaps on discharged fuel are not significantly changed due to rod bow based on visual observations.

The impact on the guide tube heating was evaluated. The XCOBRA-IIIC code was used to provide the necessary boundary conditions. The uprated conditions were determined to have sufficient margin to boiling in the guide tubes.

4.4.6.4 Results

USFAR Chapter 15 summarizes the analysis limits and results for non-LOCA events that were reanalyzed for EPU. The results of the analyses demonstrate that the event-specific acceptance criteria are met for EPU operation. The compliance with the acceptance criteria is verified on a cycle-by-cycle basis as part of the cycle specific reload evaluation.

A mixed core penalty was conservatively included in the DNB analysis limit, even though the EPU core design used in the analyses was not a mixed core.

A rod bow penalty was not required for DNB and LHR calculations.

The 14x14 HTP design allows power operation at a radial peaking limit of 1.65. The T-H design criteria are satisfied for the EPU. The anticipated reduction in margin has been offset by the following major contributions:

- A reduction in the radial peaking limit, and
- An increase in the TS minimum flow rate.

4.4.6.5 Conclusions

FPL has reviewed the analyses related to the effects of the proposed EPU on the thermal and hydraulic design of the core and the RCS. FPL concludes that the analyses have adequately accounted for the effects of the proposed EPU on the thermal and hydraulic design and demonstrated that the design:

- Has been accomplished using acceptable analytical methods,
- Is equivalent to proven designs,
- Provides acceptable margins of safety from conditions that would lead to fuel damage during normal reactor operation and AOOs, and
- Is not susceptible to T-H instability.

FPL further concludes that it has adequately accounted for the effects of the proposed EPU on the hydraulic loads on the core and RCS components. Based on this, FPL concludes that the thermal and hydraulic design will continue to meet its current licensing basis with respect to the requirements of GDCs –10 and -12 following implementation of the proposed EPU. Therefore, FPL finds the proposed EPU acceptable with respect to thermal and hydraulic design.

REFERENCES FOR SECTION 4.4

1. CENPD-8, INTHERMIC: A Computer Code for Analysis of Thermal Mixing, January 1971, (C-E PROPRIETARY).

2. CENPD-9, COSMO IV: A Thermal and Hydraulic Steady State Design Code for Water Cooled Reactors, January 1971, (C-E PROPRIETARY).

3. Jens, W. H., and Lottes, P. A., Analysis of Heat Transfer, Burnout, Pressure Drop, and Density Data for High Pressure Water, ANL-4627, May 1, 1951.

4. C-E Materials Manual, Figure 2.

11. Tong, L. S., Prediction of Departure from Nucleate Boiling for an Axially Non-Uniform Heat Flux Distribution, Journal of Nuclear Energy, 1967, Vol. 21, pp. 241 to 248.

12. Maurer, G. W., A Method of Predicting Steady Static Boiling Vapor Fractions in Reactor Coolant Channels, Bcttis Technical Review, WAPD-BT-19, Reactor Technology, June 1960.

13. CENPD-7, Response to AEC Questions Related to San Onofre No. 2 and 3 Cores, (C-E PROPRIETARY REPORT).

14. CENPD-12, Additional Thermal Hydraulic Information on Combustion Engineering 3390 Mwt Reactor Cores, (C-E PROPRIETARY REPORT).

15. STDY-3, A Program fro the Thermal Analysis of a Pressured Water Nuclear Reactor During Steady-State Operation, Pyle, R. S., WAPD-TM-213, June, 1960.

16. Martinelli, R. C. and Nelson, D. B., Prediction of Pressure Drop During Forced Circulation Boiling of Water, ASME Trans,. August, 1948.

REFERENCES FOR SECTION 4.4 (Cont'd)

17. Mendler, 0. J., et.al., Natural-Circulation Tests with Water at 800 to 200 psia under Non-Boiling, Local Boiling, and Bulk Boiling Conditions, Jour. of Heat Transfer, August, 1961.

18. Stenning, A. H., and Veziroglu, T. N., Flow Oscillation Modes in Forced-Convection Boiling, Proceedings of the 1965 Heat Transfer and Fluid Mechanics Institute, p. 301.

19. Veziroglu, T. N., and Lee, S. S., Boiling-Flow Instabilities in a Cross-Connected Parallel-Channel Upflow System, ASME Chapter 71-HT-12.

20. Bangles, A. E., and Suo, M., Investigation of Boiling Water Flow Regimes at High Pressure, NYO-3304-8 (February 1966).

21. Christensen, J. A., et.al., Melting Point of Irradiated Uranium Dioxide, WCAP-6065, February, 1965.

22. Response to AEC Questions Related to Waterfor Steam Electric Station Units 3 and 4 Cores, CENPD-30.

23. CE Fuel Evaluation Model, CENPD-139-P-A (Proprietary) and CENPD-139-A (Non-Proprietary), July, 1974.

24. Strikin-II A Cylindrical Geometry Fuel Rod Heat Transfer Program, ENPD-135P (Proprietary), CENPD-135 (Non-Proprietary), August, 1974.

25. Letter R. E. Uhrig (FPL) to D. G. Eisenhut (NRC) Re: St. Lucie Unit 1 Docket No. 50-335, Proposed Amendment to Facility Operating License DPR-67, L-80-381 dated 11/14/80.

REFERENCES

26. XN-NF-82-99, "Plant Transient Analysis For St. Lucie Unit 1," Exxon Nuclear Company, Inc. January, 1983

27. XN-NF-84-11, "St. Lucie Unit 1 Transient and Setpoint Analysis For Cycle 6," Exxon Nuclear Company, Inc. April 1984

28. XN-NF-82-09, "Generic Mechanical Design Report, Exxon Nuclear 14 x 14 Fuel Assemblies For Combustion Engineering Reactors," Exxon Nuclear Company, November 1982

29. XN-NF-507 (Supplement 1), "ENC Setpoint Methodology For C.E. Reactors Statistical Setpoint Methodology," Exxon Nuclear Company, Inc. September 1982

30. XN-NF-84-12, "St. Lucie Unit I Cycle 6 Safety Analysis Report Reload Batches XN-1 and XN-1A," Exxon Nuclear Company, Inc. February, 1984

31. XN-75-32 (P), Supplement 4, "Computational Procedure For Evaluating Fuel Rod Bowing," Exxon Nuclear Company, May 1982.

32. XN-75-32 (NP), Supplements 1 through 3, "Computational Procedure For Evaluating Fuel Rod Bowing," Exxon Nuclear Company, July 1979.

33. XN-NF-75-21 (P), Revision 2, "XCOBRA-IIIC: A Computer Code To Determine The Distribution of Coolant During Steady-State and Transient Core Operation," Exxon Nuclear Company, September 1982.

34. XN-NF-81-58 (P), “RODEX2 Fuel Rod Thermal-Mechanical Response Evaluation Model,” K. R. Mercx, August 1981

35. XN-NF-573, “RAMPEX Pellet-Clad Interaction Evaluation Code For Power Ramps,” May 1982

36. K.R. Mercx, “Cladding Collapse Calculational Procedure JN-72-23,” November 1972

37. XN-NF-82-06, “Qualification of Exxon Nuclear Fuel For Extended Burnup,” June 1982.

38. XN-NF-83-08 (P), "Justification of the XNB Departure From Nucleate Boiling Correlation For St. Lucie Unit 1," Exxon Nuclear Company, Inc. February 15, 1983

39. XN-NF-75-21(A), Revision 2, "XCOBRA-IIIC: A Computer Code to Determine the Distribution of Coolant During Steady-State and Transient Core Operation,” Exxon Nuclear Company, September 1982

40. XN-NF-612(A), Revision 1, "XNB DNB Correlation for PWR Fuel Designs,” Exxon Nuclear, April 1982

References (cont'd)

41. XN-NF-75-21(P)(A), Revision 2,"XCOBRA-III C: A Computer Code to Determine the Distribution of Coolant During Steady - State and Transient Core Operation," Exxon Nuclear Company, January 1986.

42. XN-NF-621(P)(A), Revision 1, "XNB DNB Correlation for PWR Fuel Designs," Exxon Nuclear Company, September 1982.

43. XN-NF-169, Revision 1, February 1987, "St Lucie Unit 1 Cycle 8 Safety Analysis Report".

44. XN-NF-82-81, Revision 1, "St Lucie Unit 1 Cycle 6 Safety Analysis Report", Exxon Nuclear Company, January 1983.

45. ABB-CENO Letter ST-97-509 dated October 22, 1997, Evaluation of High RCS Flowrate Limits for St. Lucie Unit 1.

46. ABB-CENO Letter ST-97-609 dated December 15, 1997, Results of Engineering Evaluation of Reactor Vessel Internals for RCS Flowrates 135% of Design Value.

47. Siemens Report EMF-2504, Rev. 0, “St. Lucie Unit 1 Cycle 17 Safety Analysis Report (USFSAR Chapter 15 Review and Mechanical).”

48. Siemens Report EMF-92-153 (P)(A) Revision 1, “HTP: Departure from Nucleate Boiling Correlation for High Thermal Performance Fuel,” January 2005.

49. XN-NF-82-21(P)(A) Revision 1, Application of Exxon Nuclear Company PWR Thermal Margin Methodology to Mixed Core Configurations, Exxon Nuclear Company, September 1983.

50. EMF-1961(P)(A) Revision 0, Statistical/Transient Methodology for Combustion Engineering Type Reactors, Siemens Power Corporation, July 2000.

51. XN-NF-78-44(NP)(A), A Generic Analysis of the Control Rod Ejection Transient for Pressurized Water Reactors, Exxon Nuclear Company, October 1983.

52. EMF-2310(P)(A) Revision 1, SRP Chapter 15 Non-LOCA Methodology for Pressurized Water Reactors, Framatome ANP, Inc., May 2004. (as modified by the EPU approval.)

53. Energia Nucleare, Volume 14, No. 9, September 1967, "Studies on Burnout, Part 3 - A New Correlation for Round Ducts and Uniform Heating and its Comparison with World Data, L. Biasi et al." EC292761

54. DELETED EC292761

55. XN-NF-81-58(P)(A) Revision 2 and Supplements 1 and 2, RODEX2 Fuel Thermal-Mechanical Response Evaluation Model, Exxon Nuclear Company, March 1984.

56. ANF-81-58(P)(A) Revision 2 and Supplements 3 and 4, RODEX2 Fuel Thermal-Mechanical Response Evaluation Model, Advanced Nuclear Fuels, June 1990.

TABLE 4.4-1

PLANT PARAMETERS FOR THERMAL & HYDRAULIC DESIGN
STEADY STATE

	Nominal Conditions	Design Conditions (Steady State)
Pressure, psia	2250	2250 ± 50
Vessel Inlet Temperature, F	538.9	539.7 ± 4.3**
Vessel Outlet Temperature, F	591	599 max**
Total Primary Coolant Flow Rate, x 10^6 lb/hr	129.6	122.0 min**
Reactor Power, percent	100	100 ± 2**
Maximum Analyzed RCS Flow, GPM		438,500*** ($135\%Q_D$)

** These values have changed for stretch power. See Cycle 4 Stretch Power Application Table 6-1, Reference 25. Values for Cycle 15 operation with Replacement Steam Generators are provided in ABB-CENO 007-ST97-C-008 Rev 0.

*** References 45 & 46

TABLE 4.4-2
THERMAL-HYDRAULIC PARAMETERS AT FULL POWER

Note: This data is provided as an historical comparasion of pre-stretch and stretch power thermal hydraulic parameters.

General Characteristics	Unit	Cycle 3	Cycle 4
Total Heat Output (core only)	MWt	2,560	2,700
	10^6 BTU/hr	8,735	9,215
Fraction of Heat Generated in Fuel Rod		.975	.975
Primary System Pressure			
Nominal	psia	2,250	2,250
Minimum in steady state	psia	2,200	2,200
Maximum in steady state	psia	2,300	2,300
Design Inlet Temperature	°F	544	549
Total Reactor Coolant Flow	gpm	370,200	370,000
(minimum steady state)	10^6lb/hr	140.2*	139.3*
Hydraulic Diameter (nominal channel)	ft	0.044	0.044
Average Mass Velocity	10^6lb/hr-ft^2	2.53*	2.51*
Pressure Drop Across Core (minimum steady state flow irreversible Δp over entire fuel assembly)	psi	10.3	10.4
Total Pressure Drop Across Vessel (based on nominal dimensions and minimum steady state flow)	psi	33.5	33.6
Core Average Heat Flux (accounts for above fraction of heat generated in fuel rod and axial densification factor)	BTU/hr-ft^2	174,400	183,843
Total Heat Transfer Area (accounts for axial densification factor)	ft^2	48,860	48,872

*Calculated at design inlet temperature, nominal primary system pressure.

TABLE 4.4-2 (Cont'd)

General Characteristics	Unit	Cycle 3	Cycle 4
Film Coefficient at Average Conditions	BTU/hr-ft^2 °F	5,820	5,820
Maximum Clad Surface Temperature	OF	657	657
Average Film Temperature Difference	OF	31	33
Average Linear Heat Rate of Undensified Fuel Rod (accounts for above fraction of heat generated in fuel rod)	kw/ft	5.83	6.14
Average Core Enthalpy Rise	BTU/lb	65*	68.7*

*Calculated at design inlet temperature, nominal primary system pressure.

TABLE 4.4-2 (Cont'd)

Calculational Factors	Cycle 3	Cycle 4
Engineering Heat Flux Factor**	1.03	1.03
Engineering Factor on Hot Channel Heat Input**	1.03	1.02*
Inlet Plenum Nonunifom Distribution	1.05	Not applicable
Rod Pitch, Bowing and Clad Diameter**	1.065	1.065
Fuel Densification Factor (axial)	1.01	1.002
Fuel Rod Bowing Augmentation Factor on Fr	1.018	1.018

*Based on "As built" information.
**These factors have been combined statistically with our uncertainty factors at 95/95 confidence/probability level (Ref - 12) to define a new design limit on CE-1 minimium OMBR when iterating on power as discussed in Reference 12.

TABLE 4.4-3
St. Lucie Unit I

Best Estimate Core Bypass Flow Distribution
With All Core Support Barrel Plugs and
Lug Patch Assemblies Installed
Normal Operation

	Leakage Path (Figure 4.4-20)	Bypass Flow Rate (% of Vessel Flow Rate)
1.	Alignment Keys	0.09
2.	Outlet Nozzle Gap	1.18
	Core Shroud:	
3.	Holes	0.27
4.	Seams	0.23
5.	Guide Tubes	1.61
6.	Surveillance Holes in Core Support Barrel Flange (6)	0.08
7.	Core Support Barrel Plugs/Patch Assembly and Crack Clearances	0.19
	Total Bypass Flow	3.65*

* Total bypass flow decreased approximately 0.25% due to use of HVFR in 8 periphery fuel assemblies.

Table 4.4-3A

St. Lucie Unit 1

Inventory, Areas, and Perimeters of
Core Support Barrel Holes

Device	Hole Size (in)	No. of Holes	Total Area (in^2)	Total Plug Perimeter (in)	Patch Perimeter (in)
Plug	8.0D	8	402.1	201.1	-
Plug	5.0D	2	39.3	31.4	-
Plug	3.1D	2	15.1	19.5	-
Patch Lug No. 1		1	85.2(2)	-	40.0
with Plugs 3.1D(1)		4	30.2(2)	39.0	-
Patch Lug No. 3		1	26.3	-	27.6
with Plugs 3.1D(1)		3	22.6	29.2	-
Patch Lug No. 4		1	46.1	-	29.7
with Plugs 3.1D(1)		4	30.2	39.0	-
Patch Lug No. 5		1	55.3	-	34.4
with Plugs 3.1D(1)		4	30.2	39.0	-
Patch Lug No. 6		1	53.1	-	37.2
with Plugs 3.1D(1)		3	22.6	29.2	-
				427.4	168.9

(1) Plugs used to anchor lug patch plate

(2) Maximum credible size of repair failure (requires simultaneous failure of all four plugs holding in the patch and loss of the patch itself)

85.2 in^2
30.2 in^2

115.4 in^2

Table 4.4-3B

St. Lucie Unit 1

Best Estimate Core Bypass Flow Distribution
with Failure of Lug No. 1 Patch Assembly
Cycle 6
(Historical Information)

Leakage Path	Bypass Flow Rate (% of Vessel Flow Rate)
Alignment Keys	0.09
Outlet Nozzle Gap	1.17
Core Shroud:	
Holes	0.25
Seams	0.19
Guide Tubes	1.56
Surveillance Holes in Core Support Barrel Flange (6)	0.08
Core Support Barrel Plugs/Patch Assembly and Crack Clearances	0.14
Failed Lug No. 1 Patch Assembly	3.45
Total Bypass Flow	6.93

TABLE 4.4-4

ORIGINAL DESIGN
REACTOR VESSEL BEST ESTIMATE
PRESSURE LOSSES AND COOLANT TEMPERATURES

	Pressure Loss psi	Temperature Degree F
Inlet Nozzle and 90 Degree Turn	5.3	544
Downcomer, Lower Plenum, and Support Structure	7.3	544
Fuel Assembly	8.1	572.3
Fuel Assembly Outlet to Outlet Nozzle	6.4	600.6
Total Nozzle-to-Nozzle	27.1	

(WITH REPLACEMENT STEAM GENERATORS)
REACTOR VESSEL BEST ESTIMATE
PRESSURE LOSSES AND COOLANT TEMPERATURES

	Pressure Loss psi	Temperature Degree F
Inlet Nozzle & 90 Degree Turn	6.8	543.5
Downcomer, Lower Plenum, Support Structure & Fuel Assembly	21.5	571
Fuel Assembly Outlet to Outlet Nozzle	7.1	594 (Bulk)
	35.4	

Source: ABB-CENO 007-ST97-C-008 Rev 0
Based on 413,508 GPM @ HFP

TABLE 4.4-4A

DESIGN OPERATING HYDRAULIC LOADS ON VESSEL INTERNALS*

Component	Load Description	Load Value
1. Core Support Barrel	Radial pressure differential directed inward opposite inlet nozzle	40 psi
2. Core Support Barrel and Upper Guide Structure	Uplift load	480,000 lb
3. Flow Skirt	Radial pressure differential directed inward over 40° sector	6.0 psi average 10.2 psi maximum
4. Bottom Plate	Pressure differential load directed upward	43,400 lb
5. Core Support Plate	Pressure differential load directed upward	43,100 lb
6. Fuel Assembly	Uplift load	1080 lb at 120 flow an 50^{O}F CEA location crudded core
7. Core Shroud	Radial load directed outward	20.8 psi at bottom, 0.0 psi at top
8. Upper Guide Structure	Pressure differential load directed upward	148,000 lb
9. Fuel Alignment Plate	Pressure differential load directed upward	89,600 lb
10. Upper Guide Plate	Pressure differential load directed downward	132,000 lb
11. CEA Shrouds	Frictional drag load	4,200 lbs (dual) 1,100 lbs (single CEA)

* Data Reflects Cycle 6 Conditions

TABLE 4.4-4B

REACTOR VESSEL & INTERNALS COOLANT DATA

	Region	Volume (ft^3)	Flow Path Length (ft)	Height (ft)	Elevation (ft)
V_I	(Inlet nozzles; annulus from CSB flange to Flow Skirt base; lower head to bottom of active core region)	1,990(3)	38.1	29.7 Annulus 10.0 Lower Plenum	-27
V_2	(Active Core Region)	644	11.4	11.4	-17
V_3	(Active Core Region Bypass)	167	12.7	12.7	-17
V^4	(Top of Active Core Region to top of Fuel Alignment Plate)	81	1.3	1.3	-5.6
V^5	(Outlet Nozzles; Volume between top of Fuel Alignment Plate and top of UGS support plate)	1,210	14.8	10.6	-4.2
V^6	(Closure Head, from top of UGS support plate including CEDM and Instrument Nozzles)	699	--	6.6	+6.4

Notes: (1) Refer to Figure 4.4-21 for arrangement of coolant volumes.

(2) Elevation measured from bottom of coolant volume region to center line of vessel nozzles.

(3) Calculated value with thermal shield removed. (Exxon Reports XN-NF-82-98 & XF-NF-84-11)

TABLE 4.4-4C

REACTOR INTERNALS COMPONENT FLOW AREAS, FT^2

1.	Vessel inlet nozzle entry (total)	20
2.	Vessel outlet nozzle exit (total)	19
3.	Core support barrel to vessel annulus	35
4.	Thru and around flow skirt	46
5.	Lower support plate	28
6.	Core support plate	28
7.	Core shroud to core support barrel bypass gap	1.1
8.	Active core region	54
9.	Thru and around fuel alignment plate	28
10.	Upper guide structure outlet plenum at nozzle elevation	80
11.	Inside single CEA shrouds	20
12.	Inside dual CEA shrouds	12
13.	From vessel head region into upper guide structure outlet plenum	1.0

TABLE 4.4-5

ENGINEERING FACTORS
PALISADES AND MAINE YANKEE MEASURED VALUES

Engineering Heat Flux Factor	Mean Value	o'	Subfactor $1o'$ Value	Subfactor $3o'$ Value
Pellet Diameter, Inches	0.35908	0.00016	1.0009	1.0027
Pellet Density, % TD	93.43	0.0059	1.0063	1.0190
Enrichment, Palisades			1.0051	1.0153
Enrichment, Maine	2.0232	0.0131	1.0065	1.0194
Clad Diameter, inches	0.4168	0.0014	1.0034	1.0102
		TOTAL FACTOR =		1.027
Pitch and Bow Enthalpy Rise Factor				
Rod Spacing, Axial Average, inches	0.1350	0.0012	1.012	1.036
		TOTAL FACTOR =		1.036
Engineering Factor on Channel Heat Input				
Fuel Column Weight, gm, Palisades	2201	10.67	1.002	1.007
Fuel Column Weight, gm, Maine	2543	15.49	1.003	1.009
Enrichment, Palisades			1.0051	1.0153
Enrichment, Maine	2.0232	0.0131	1.0065	1.0194
(Palisades		TOTAL FACTOR =		1.017
(Maine)		TOTAL FACTOR =		1.022

Engineering Factor on Linear Heat Rate (Maine)	Design Value	Confidence	Max/Mean	$3o'$ Subfactor
Pellet Diameter, inches	0.3795±.0005	100%	--	1.0026
Pellet Density, % TD	93.0±1.5	2±	--	1.0242
Enrichment, %	2.01±.05	100%	1.0111	1.0111
		TOTAL FACTOR =		1.027

TABLE 4.4-6

Thermal-Hydraulic Design Data*

(Historical Information)

Operating Conditions	
Rated Power (Core)	2,700MWt
Fraction of Heat Generated in Fuel	.975
Pressurizer Pressure	2,250 psia
Core Inlet Temperature	549.0°F
Total Reactor Coolant Flow	139.4×10^6 lb/hr
Active Coolant Flow	134.0×10^6 lb/hr
Limiting Assembly Peaking Factors	
Axial	1.60
Engineering	1.03
F_r	1.70
Total Nuclear	2.80

* Reflects Cycle 6 Conditions

TABLE 4.4-7

Assembly Component Loss Coefficients

	ENC		CE	
	Nominal	+Uncertainties	Nominal	- Uncertainties
Lower Tie Plate*	5.197 $R_e^{-0.0356}$	5.252 $R_e^{-0.0356}$	3.55	3.51
Spacer	1.752 $R_e^{-0.067}$	1.771 $R_e^{-0.067}$	1.019 $R_e^{-0.04}$	1.008 $R_e^{-0.04}$
Upper Tie Plate*	7.42	7.5	7.45	7.37
Bare Rod Friction	0.1987 $R_e^{-0.2}$	0.2008 $R_e^{-0.2}$	0.1987 $R_e^{-0.2}$	0.1966 $R_e^{-0.2}$

* Includes reversible losses due to change in area and losses due to core support hardware.

TABLE 4.4-8

Comparison of Thermal-Hydraulic Design Parameters for EPU

Thermal-Hydraulic Design Parameters	Pre-EPU Value	Current (EPU) Value
Reactor core heat output, MWt	2,700	3,020
Reactor core heat output, 10^6 BTU/hr	9,215	10,307
Heat generated in fuel, %	97.5	97.5
Nominal Pressurizer/core pressure, psia	2,250	2,250
Nominal vessel/core inlet temperature, °F	548	551
RCS minimum flow rate (including bypass), gpm	365,000	375,000
RCS minimum flow rate (including bypass), 10^6 lb_m/hr	137.5	140.76
Core bypass flow, %	3.9	4.2
Core flow area, ft^2	53.15	53.15
Core inlet mass velocity (excluding bypass, based on TS minimum flow rate), 10^6 lb_m/hr-ft^2	2.49	2.54
Core average heat flux, BTU/hr-ft^2	183,843	206,277.8
Total heat transfer surface area, ft^2	50,116.5	50,116.5
Average linear power, kW/ft	6.14	6.96
Enthalpy rise hot channel factor (radial peaking)	1.7	1.65

TABLE 4.4-9

System Related Uncertainties for EPU Analyses

Parameter	Uncertainty
Reactor Thermal Power	+0.3% (at 100% RTP)
RCS Flow	-15,000 gpm
RCS Pressure	±40.0 psi
Core Inlet Temperature	±3.0 °F

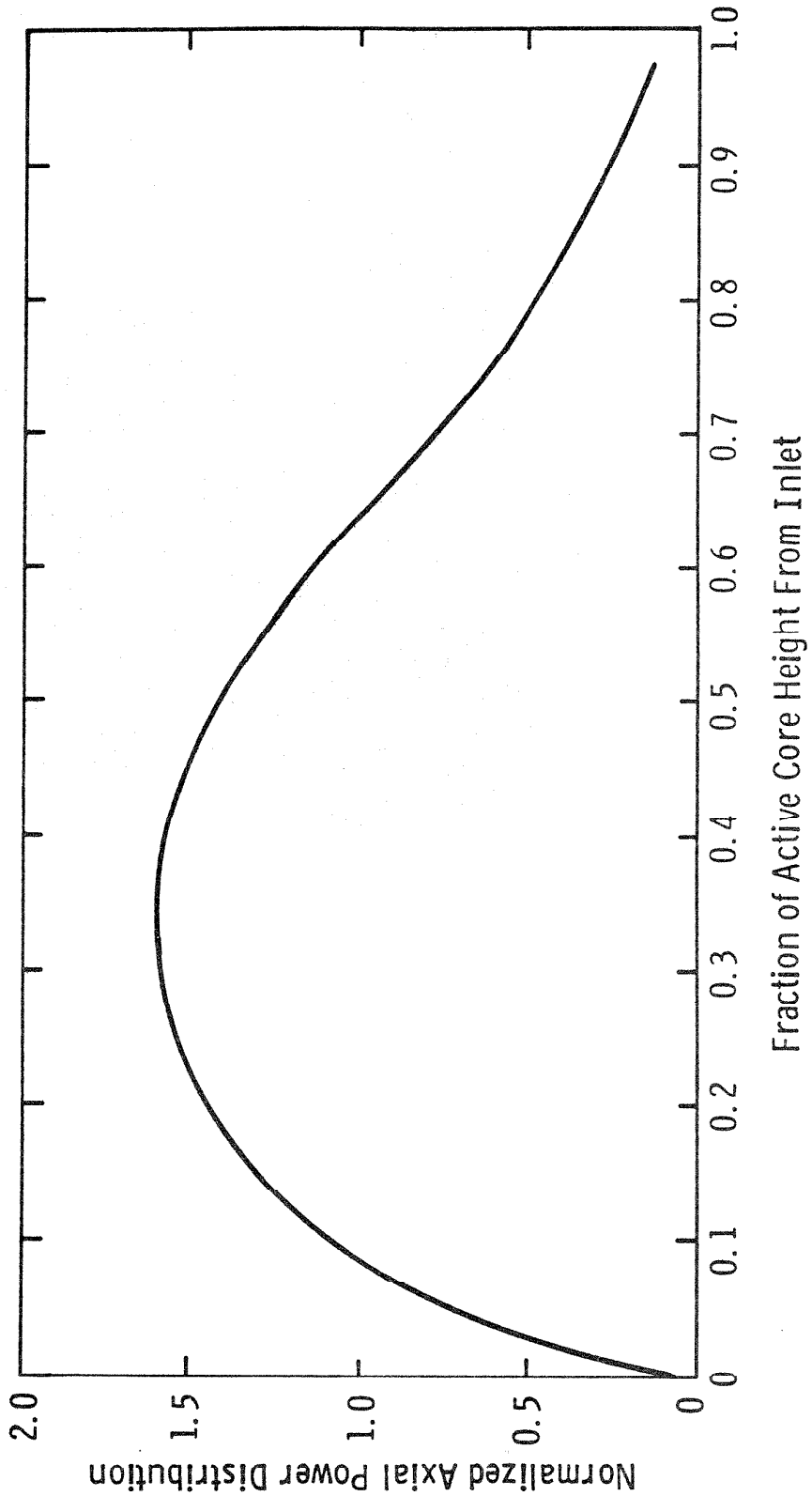

FLORIDA POWER & LIGHT CO. St. Lucie Plant	Design Axial Power Distribution	Figure 4.4-1

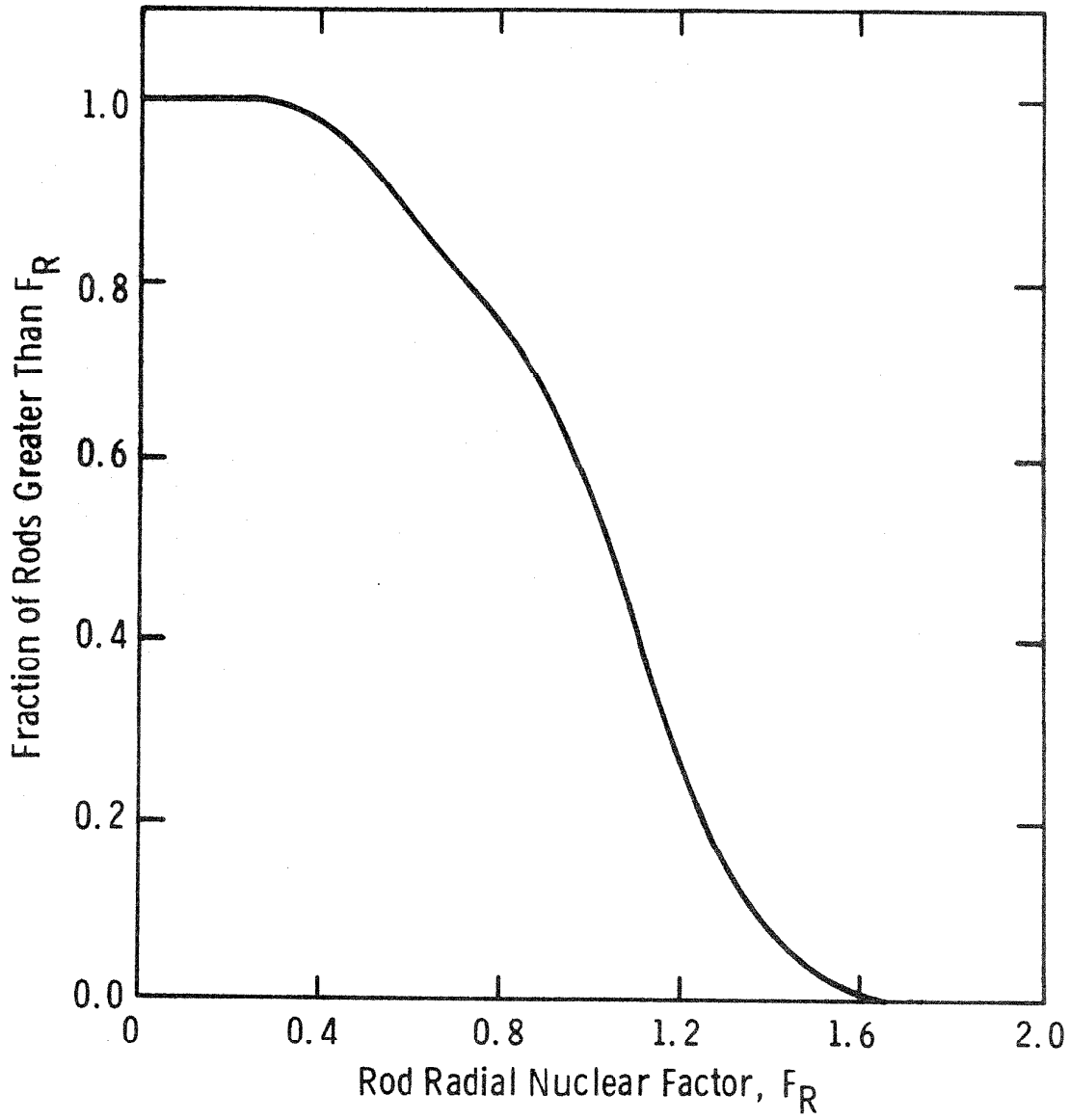

FLORIDA POWER & LIGHT CO. St. Lucie Plant	Cumulative Distribution of Rod Radial Factor For Design Coolant Conditions	Figure 4.4-2

FLORIDA POWER & LIGHT CO.
St. Lucie Plant

Clad Average Temperature vs
Fraction of Active Core Height From Inlet

Figure
4.4-3

13-112

FLORIDA POWER & LIGHT CO. St. Lucie Plant	Thermal Conductivity of Densified UO_2	Figure 4.4-4

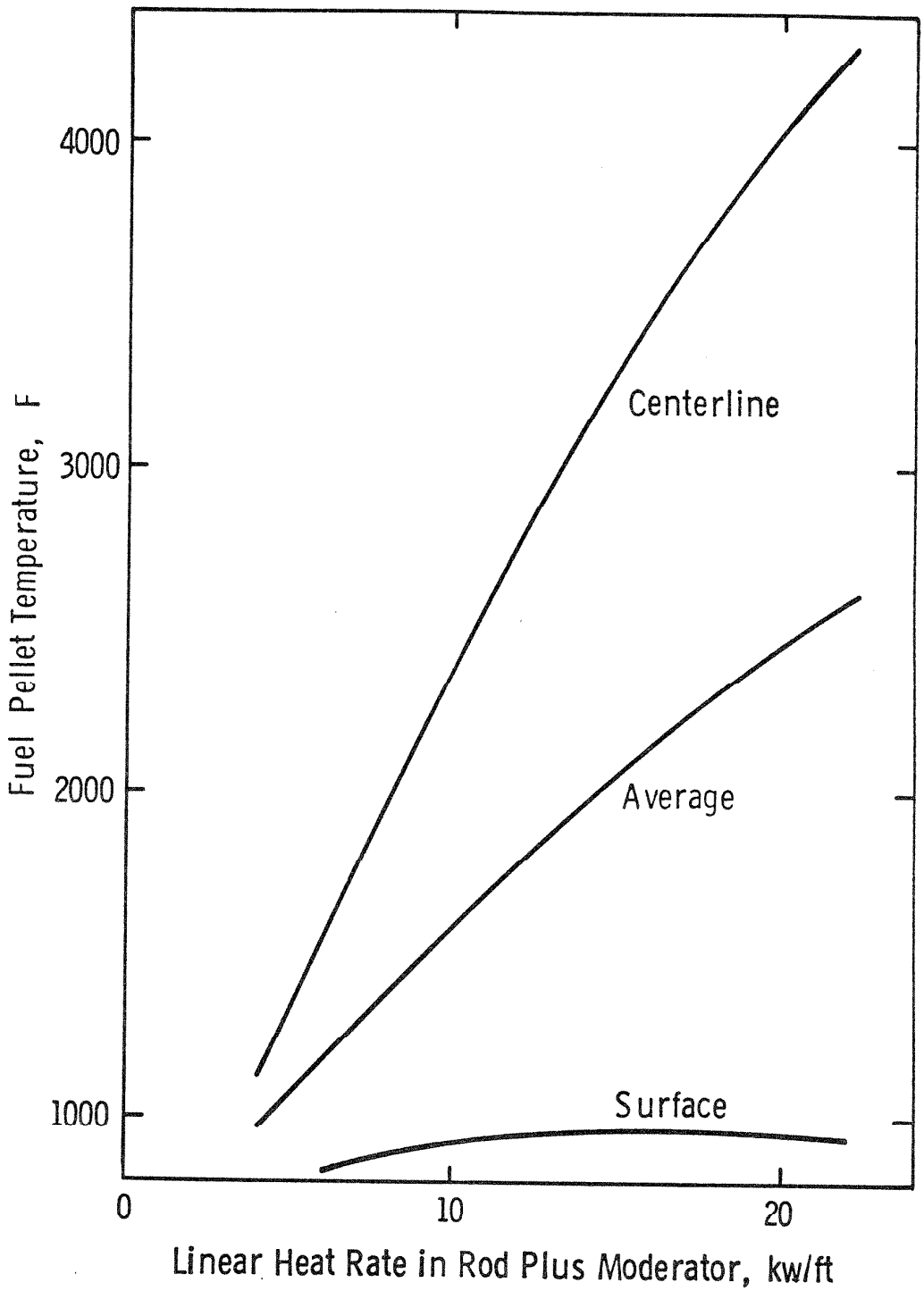

FLORIDA POWER & LIGHT CO. St. Lucie Plant	Fuel Pellet Temperature at BOL	Figure 4.4-5

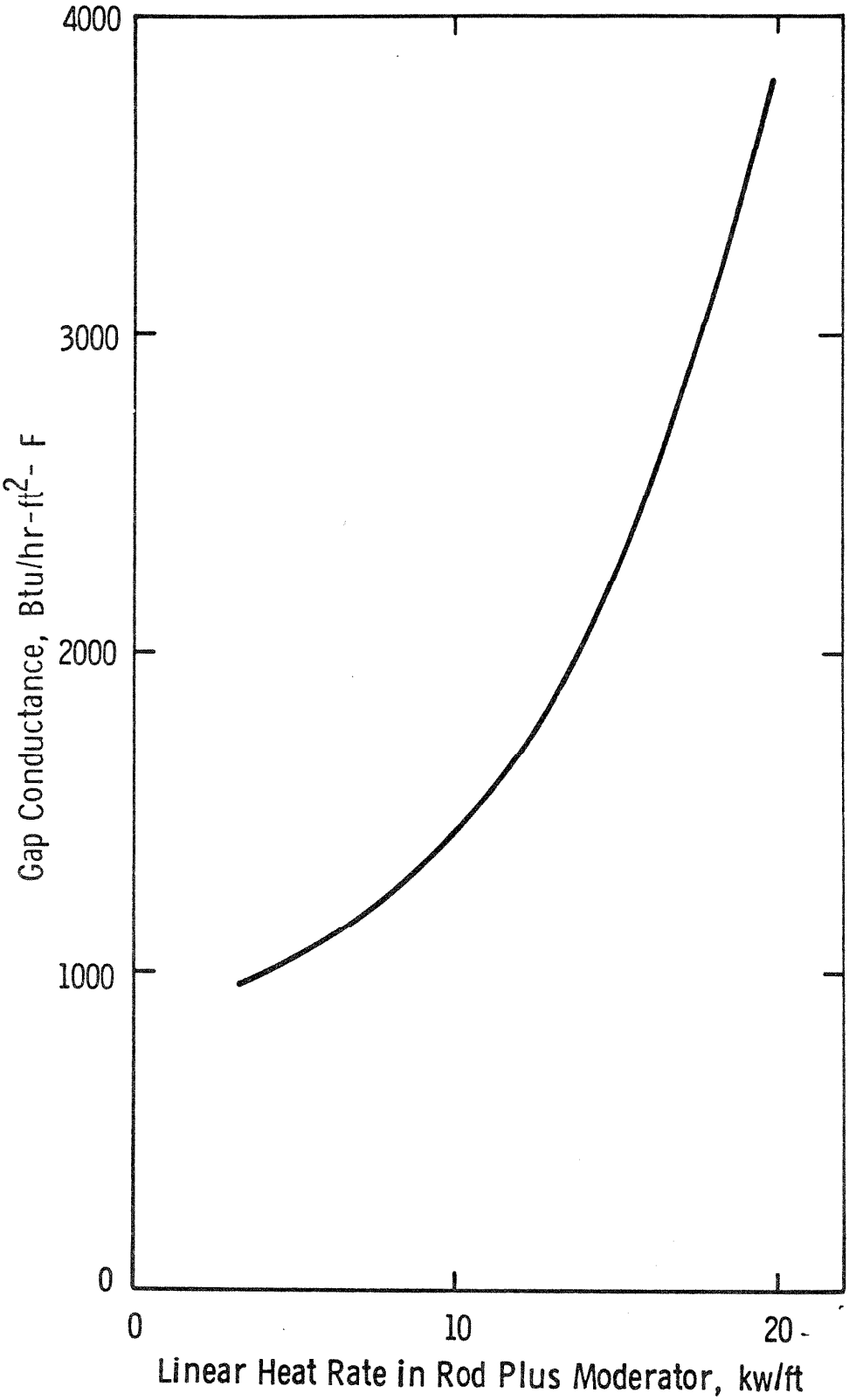

FLORIDA POWER & LIGHT CO. St. Lucie Plant	Pellet-Clad Gap Conductance at BOL	Figure 4.4-6

FLORIDA POWER & LIGHT CO. Hutchinson Island Plant	Cumulative Distribution of Number of Fuel Rods vs DNB Ratio at 112 Percent Power and Design Coolant Conditions	Figure 4.4-7

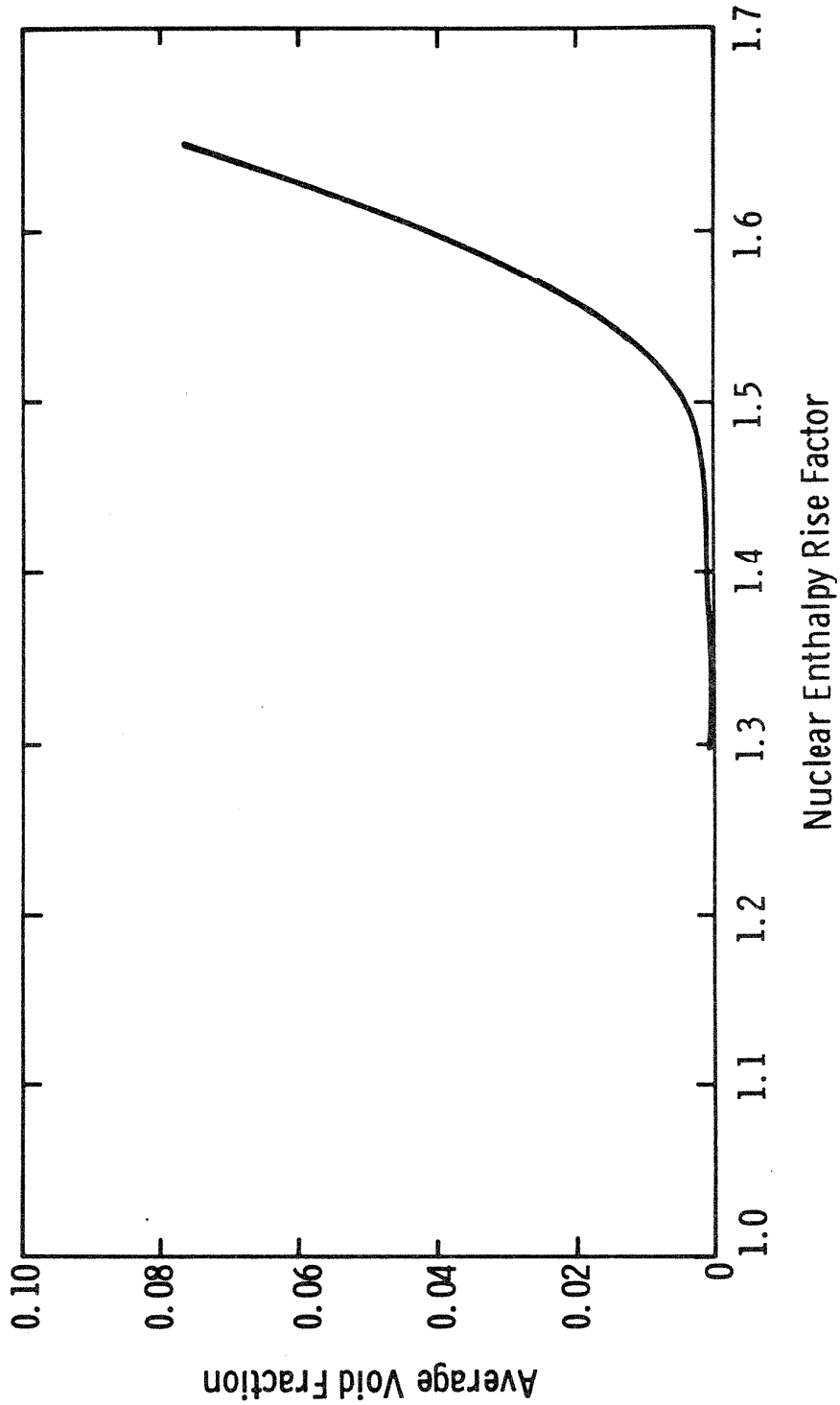

FLORIDA POWER & LIGHT CO. St. Lucie Plant	Void Fraction vs Nuclear Enthalpy Rise Factor at 112 Percent Power and Design Coolant Conditions	Figure 4.4-8

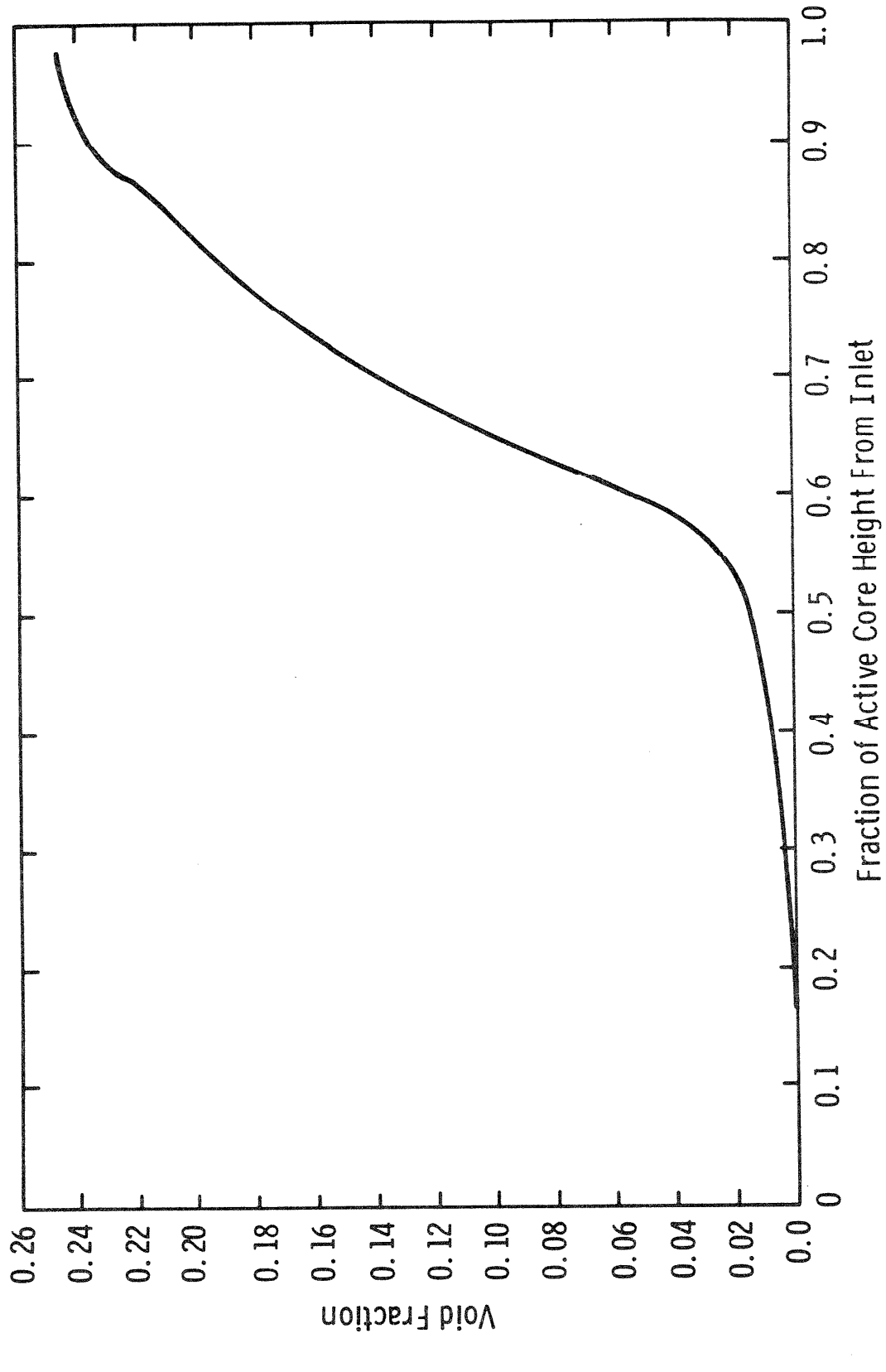

FLORIDA POWER & LIGHT CO. St. Lucie Plant	Void Fraction vs Height in Design Hot Channel at 112 Percent Power and Design Coolant Conditions	Figure 4.4-9

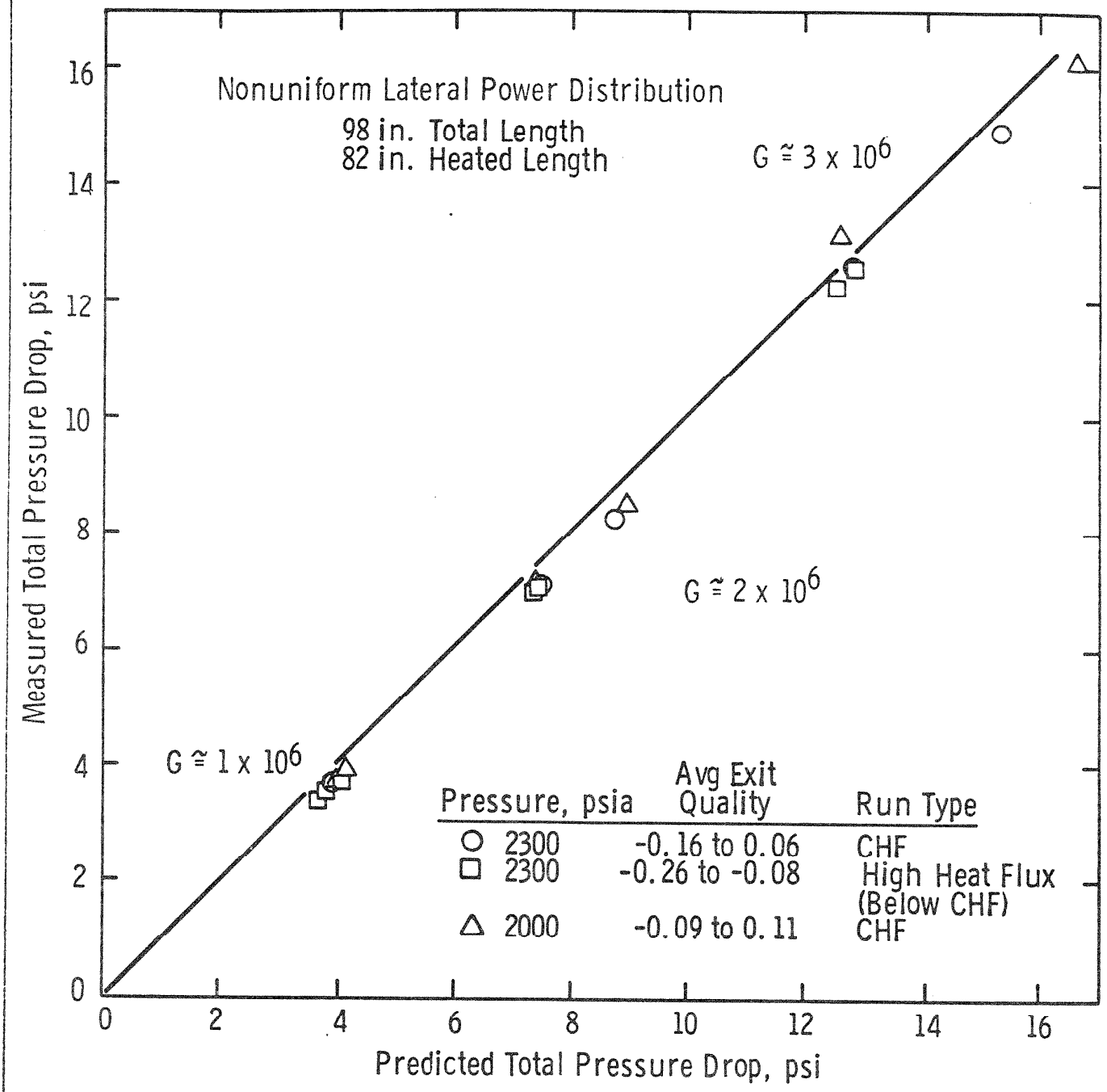

FLORIDA POWER & LIGHT CO. St. Lucie Plant	Cosmo Pressure Drop Predictions For a Twenty-One Rod Bundle	Figure 4.4-10

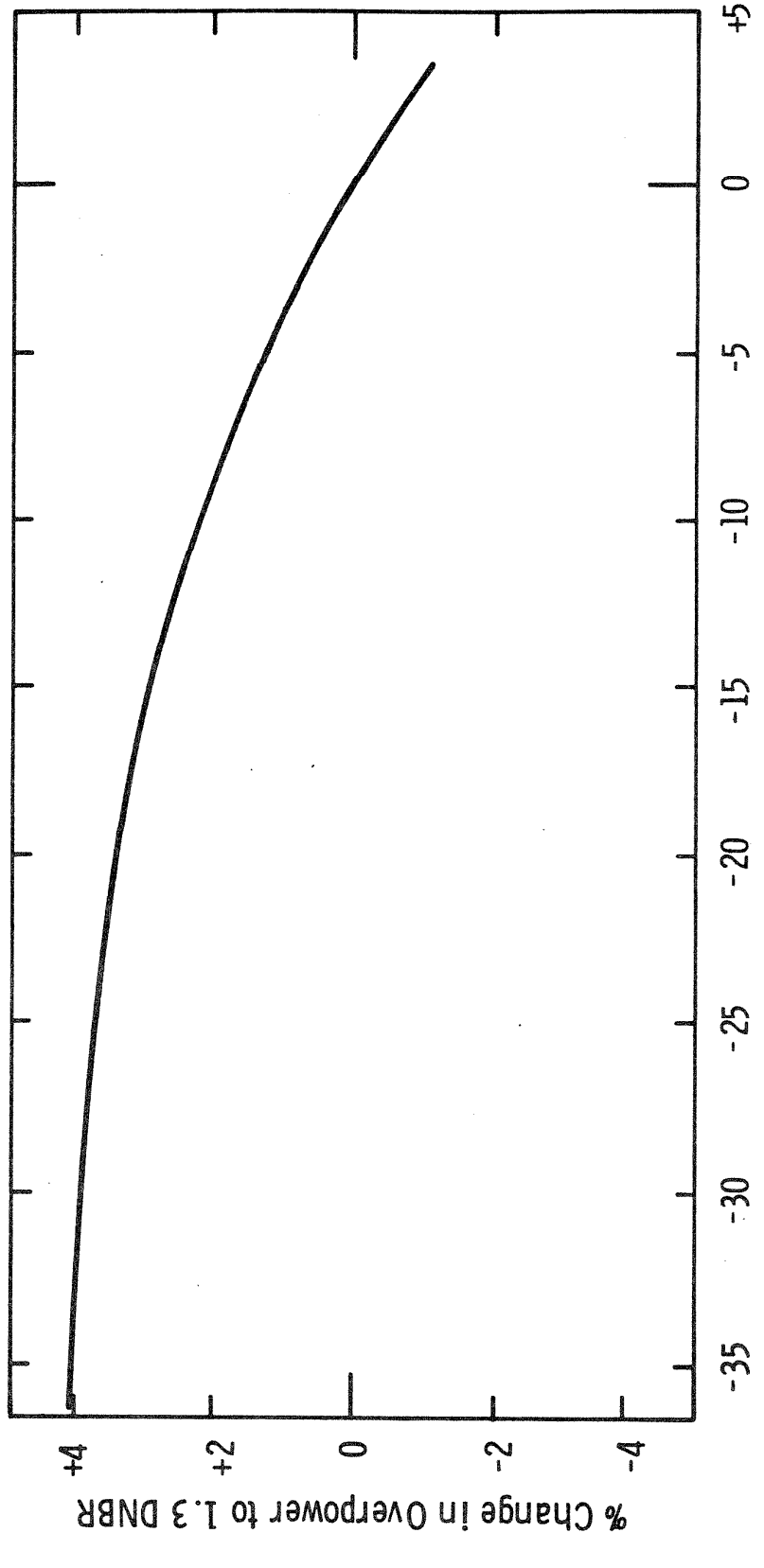

FLORIDA POWER & LIGHT CO. St. Lucie Plant	Percent Change in Overpower vs Percent Change in Reference Assembly Peak	Figure 4.4-11

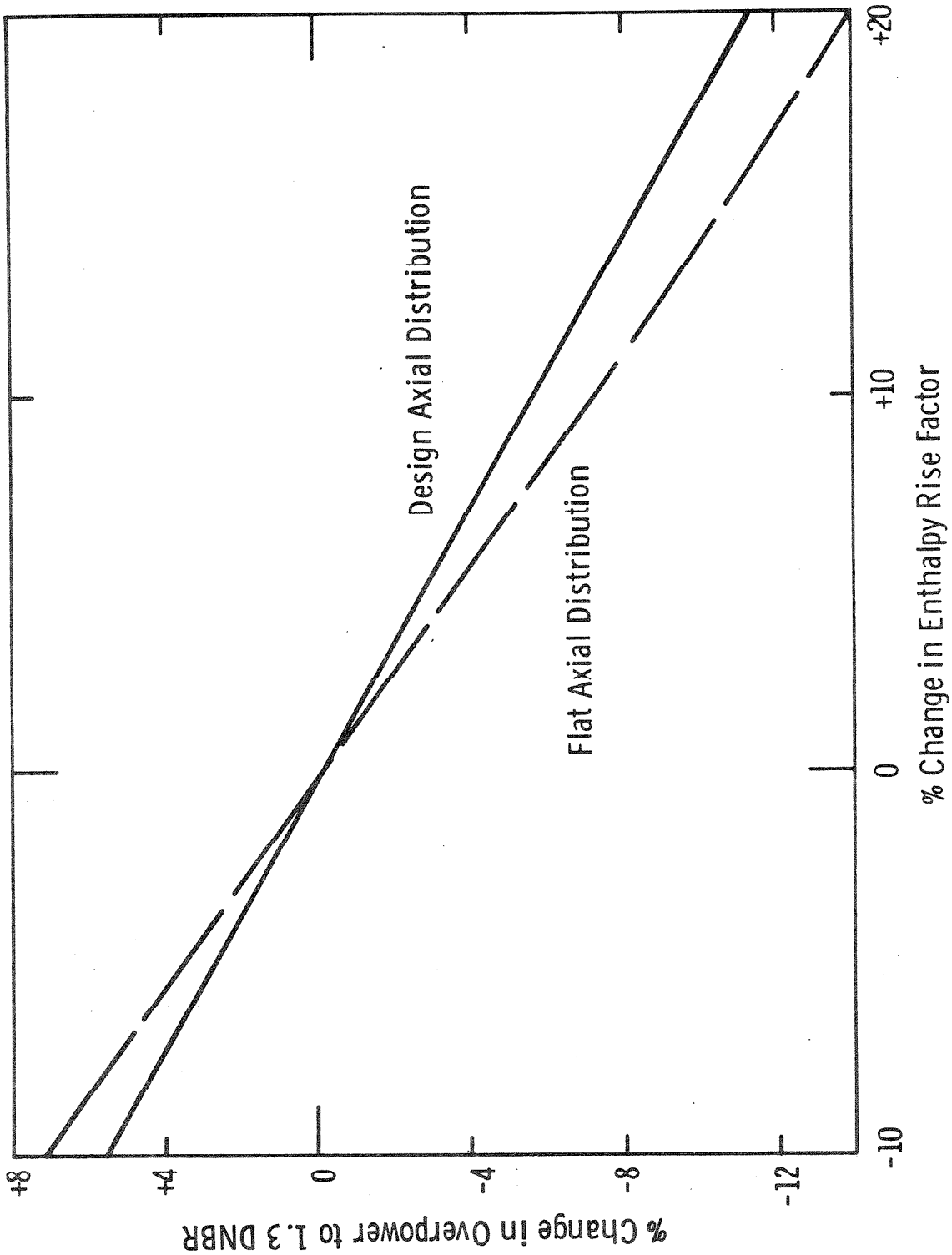

FLORIDA POWER & LIGHT CO. St. Lucie Plant	Percent Change in Overpower vs Percent Change in Enthalpy Rise Factor	Figure 4.4-12

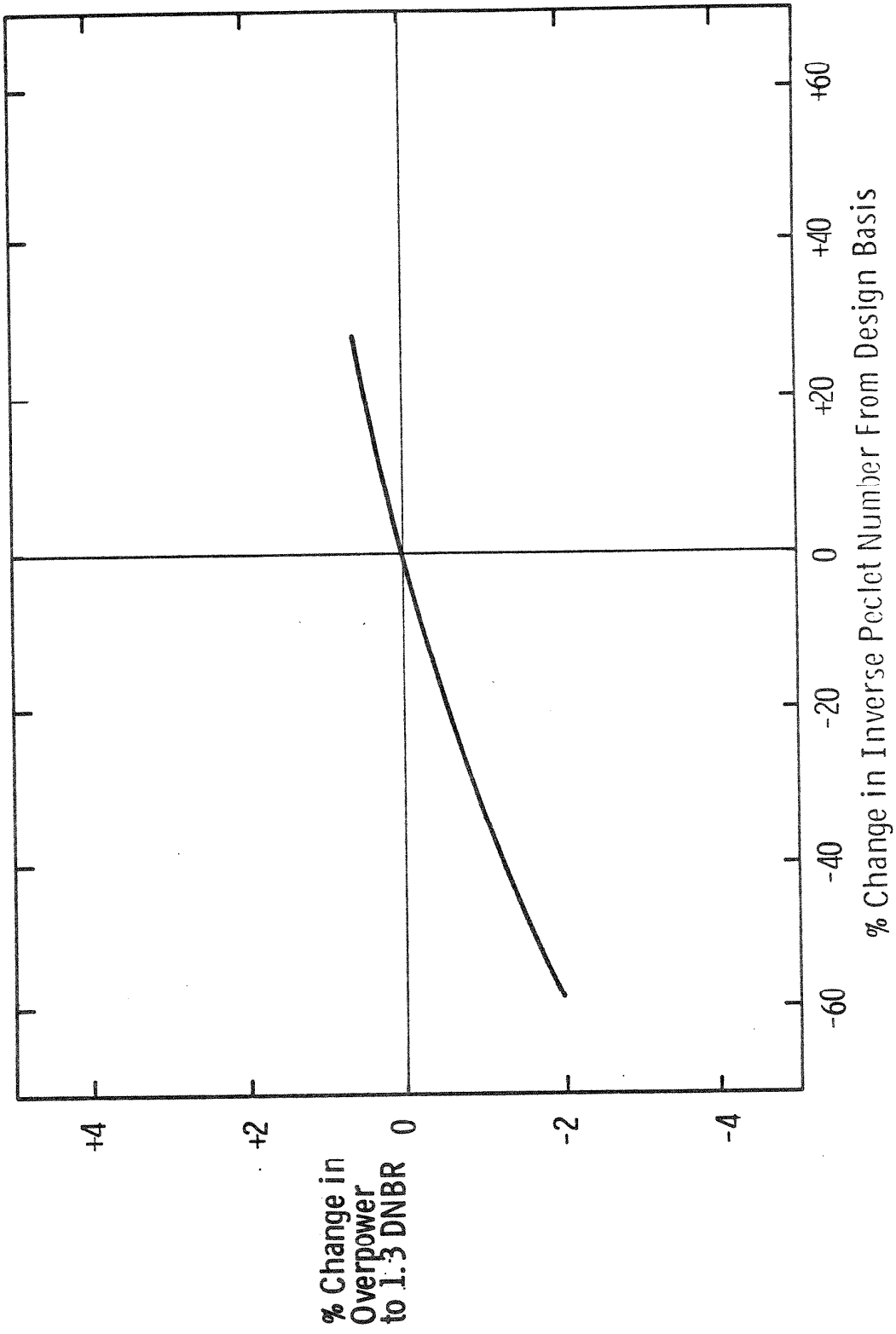

FLORIDA POWER & LIGHT CO. St. Lucie Plant	Percent Change in Overpower vs Percent Change in Inverse Peclet Number	Figure 4.4-13

FLORIDA POWER & LIGHT CO.
St. Lucie Plant

Axial Power Distributions

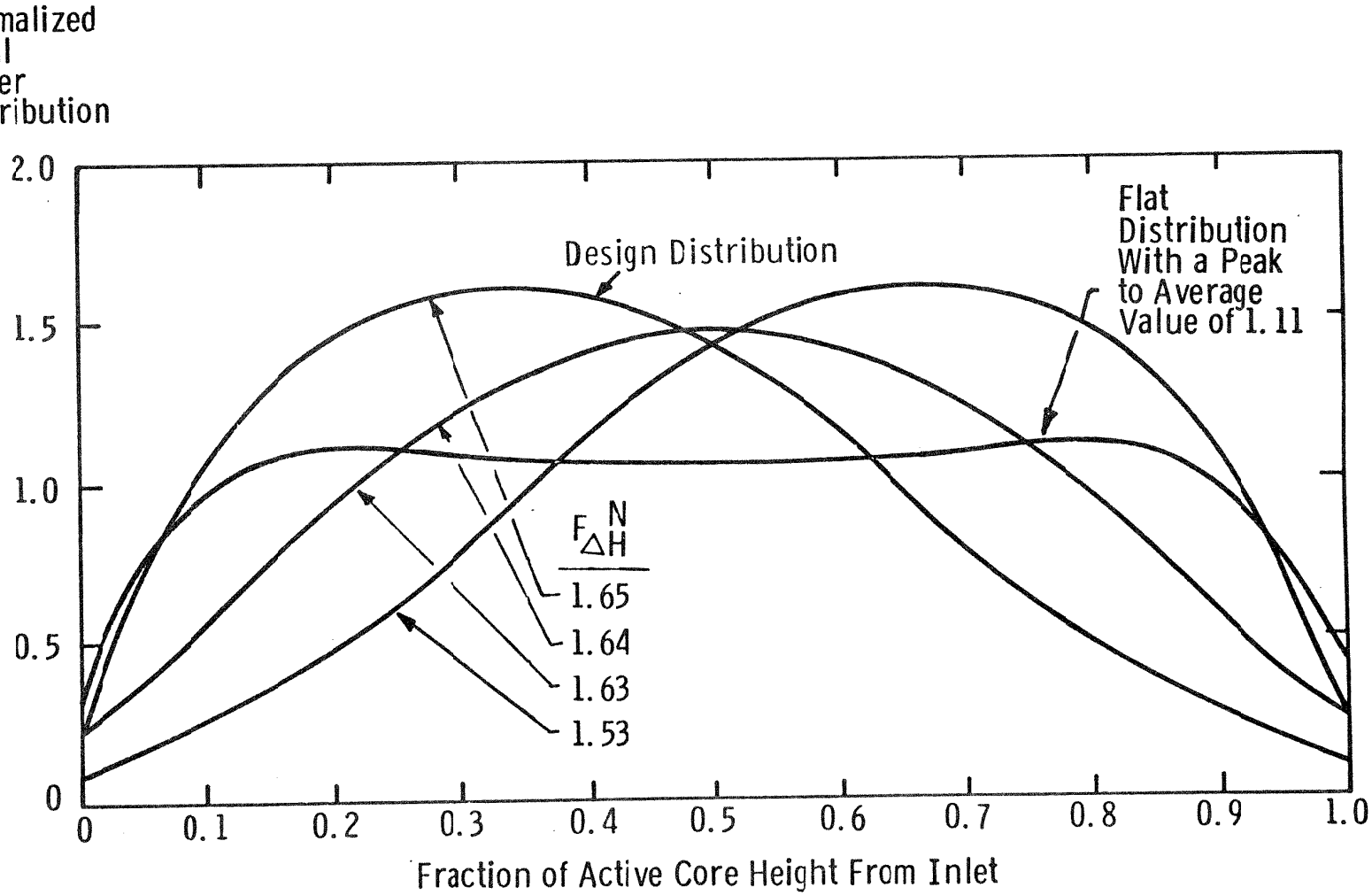

Figure 4.4-14

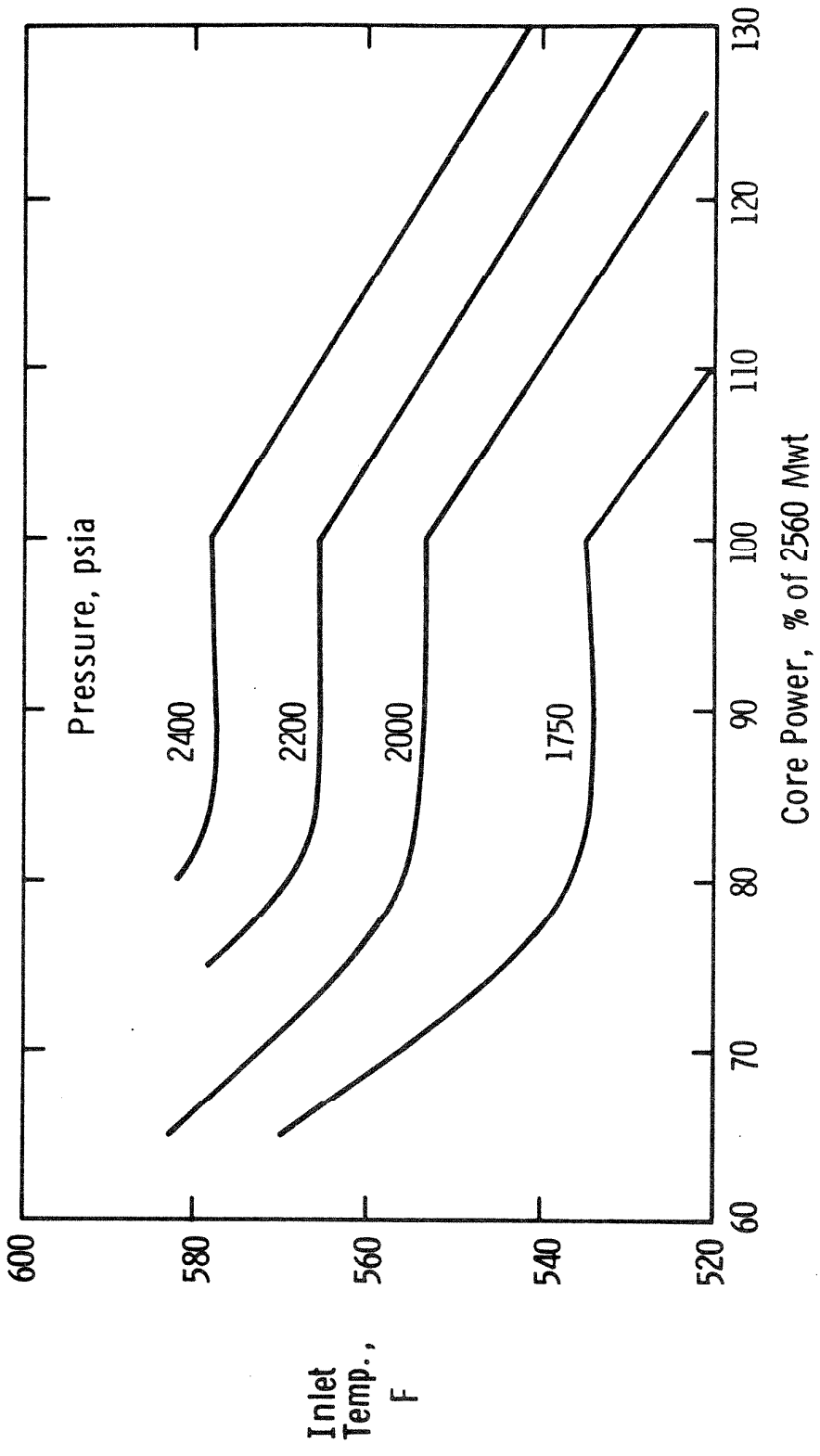

FLORIDA POWER & LIGHT CO. St. Lucie Plant	Thermal Margin Limit Curves For 4 Pump Operation	Figure 4.4-15

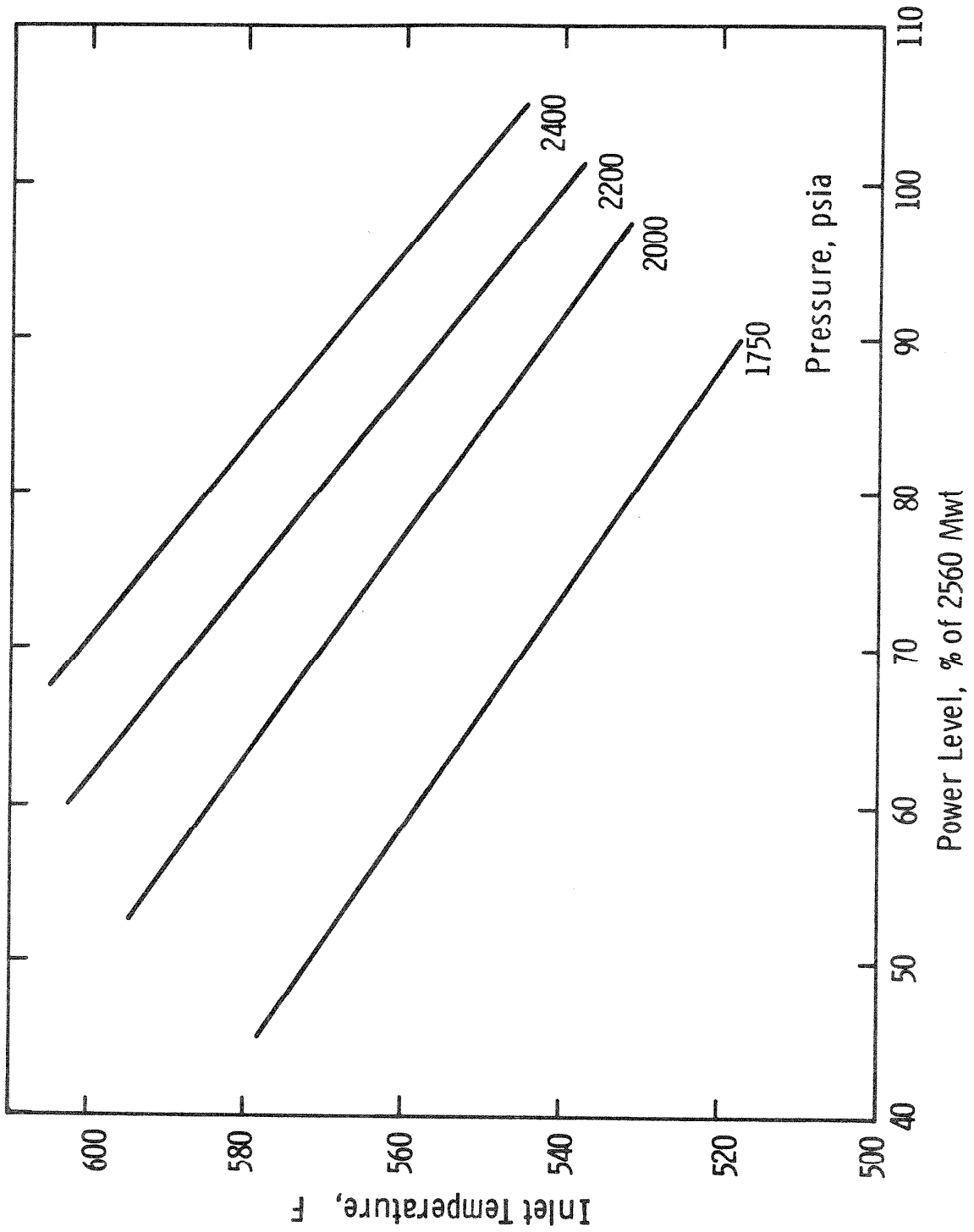

FLORIDA POWER & LIGHT CO. St. Lucie Plant	Thermal Margin Limit Curves for 3-Pump Operation	Figure 4.4-16

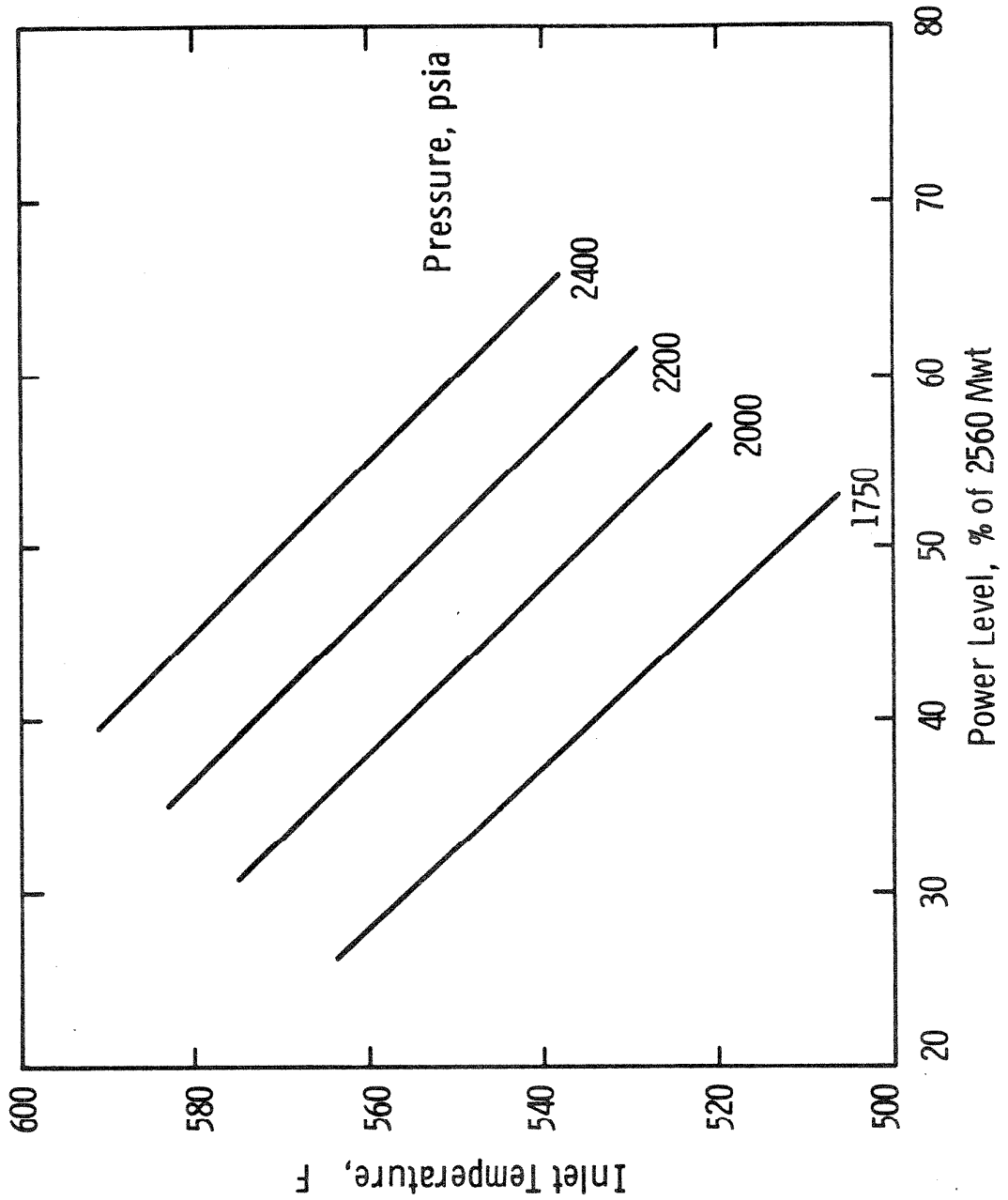

FLORIDA POWER & LIGHT CO. St. Lucie Plant	Thermal Margin Limit Curves 2 Pumps in the Same Loop	Figure 4.4-17

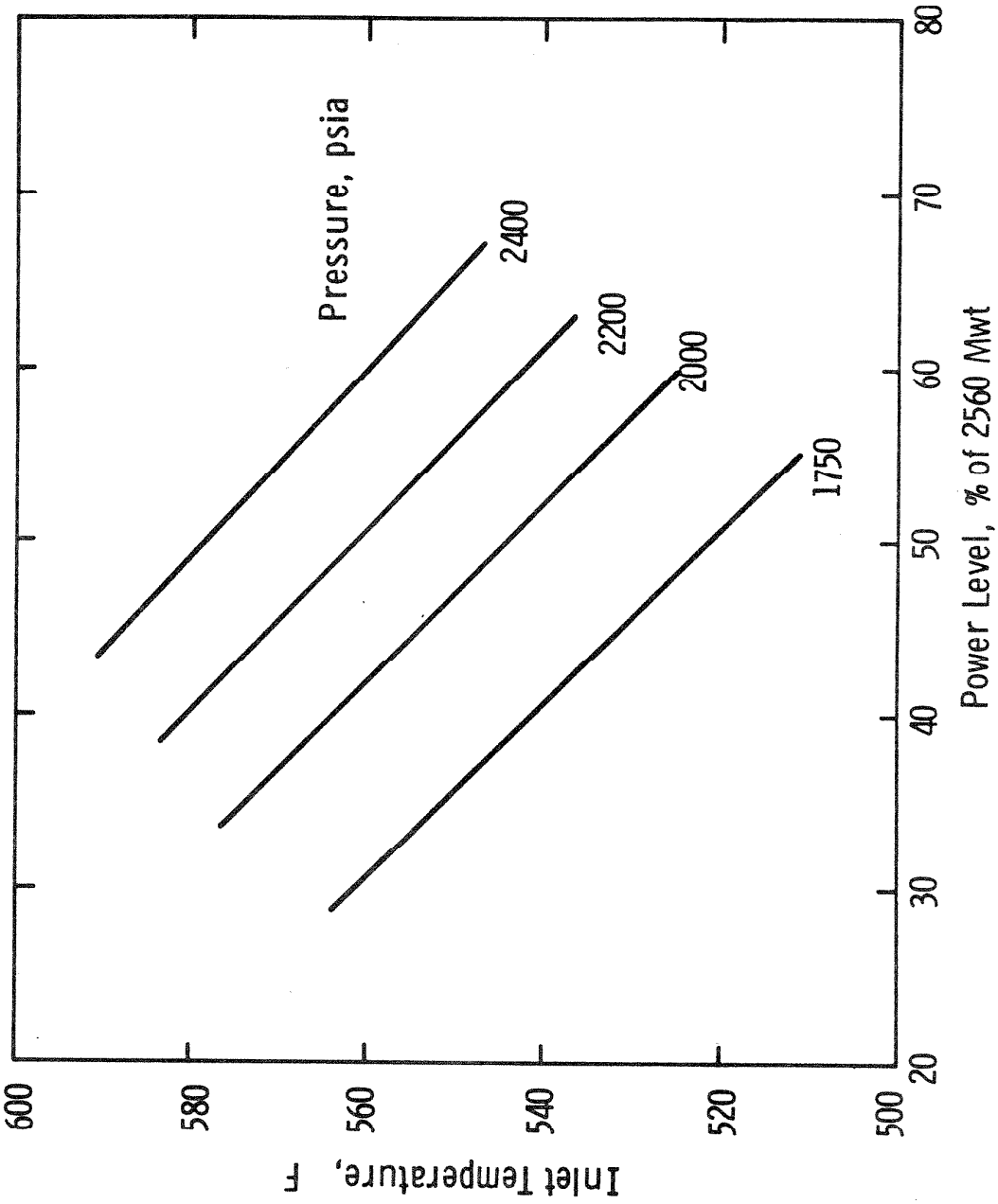

FLORIDA POWER & LIGHT CO. St. Lucie Plant	Thermal Margin Limit Curves Two Pump Opposite Loop Operation	Figure 4.4-18

FLORIDA POWER & LIGHT CO. St. Lucie Plant	Ability to Predict Critical Heat Flux Using COSMO and the W-3 Correlation	Figure 4.4-19

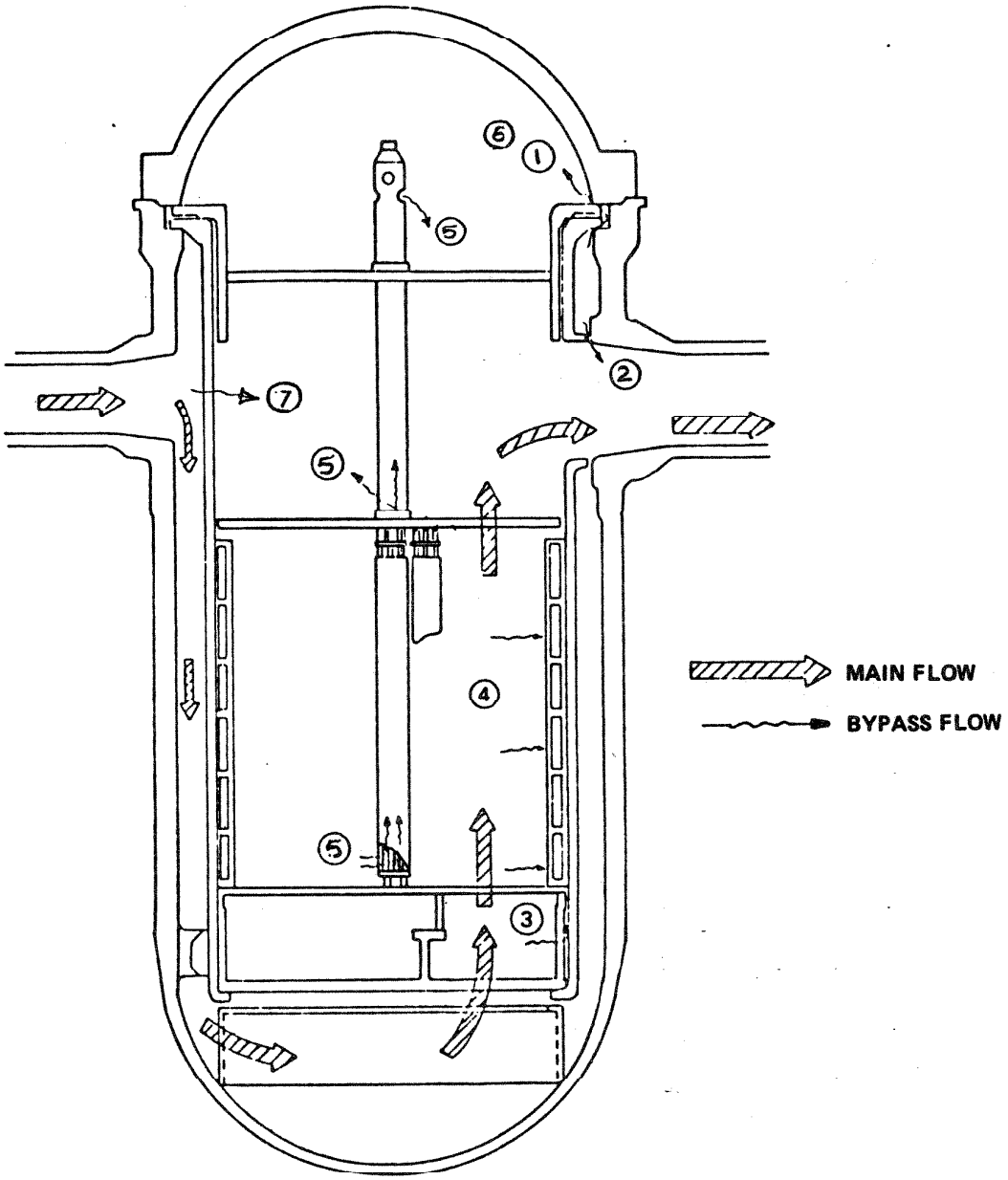

Am. 3-7/85

FLORIDA POWER & LIGHT COMPANY
ST. LUCIE PLANT UNIT 1

REACTOR VERTICAL ARRANGEMENT
SHOWING BYPASS FLOW PATHS
FIGURE 4.4-20

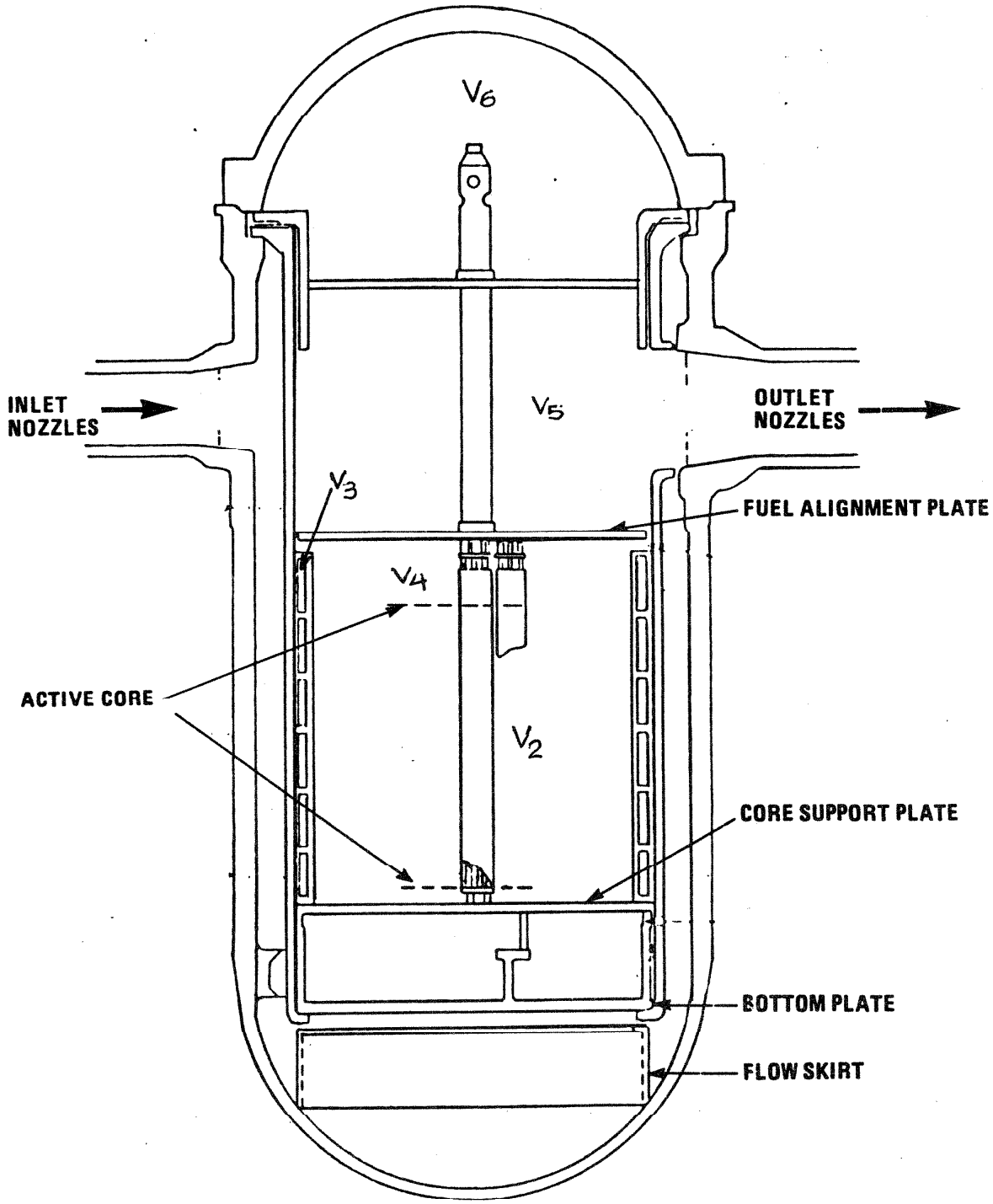

Am. 3-7/85

FLORIDA POWER & LIGHT COMPANY
ST. LUCIE PLANT UNIT 1

REACTOR STATIONS

FIGURE 4.4-21

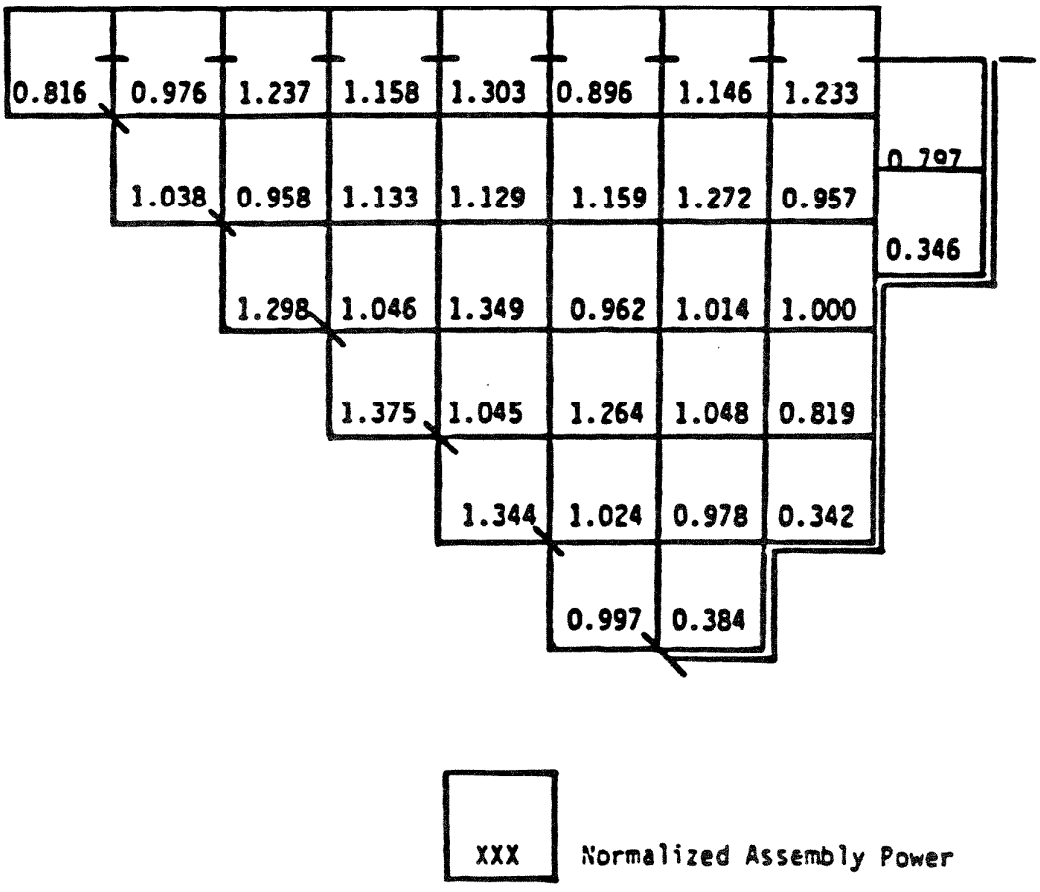

AMENDMENT NO. 8 (7/89)

FLORIDA POWER & LIGHT COMPANY
ST. LUCIE PLANT UNIT 1

ST. LUCIE UNIT 1, NORMALIZED ASSEMBLY POWER DISTRIBUTION

FIGURE 4.4-22

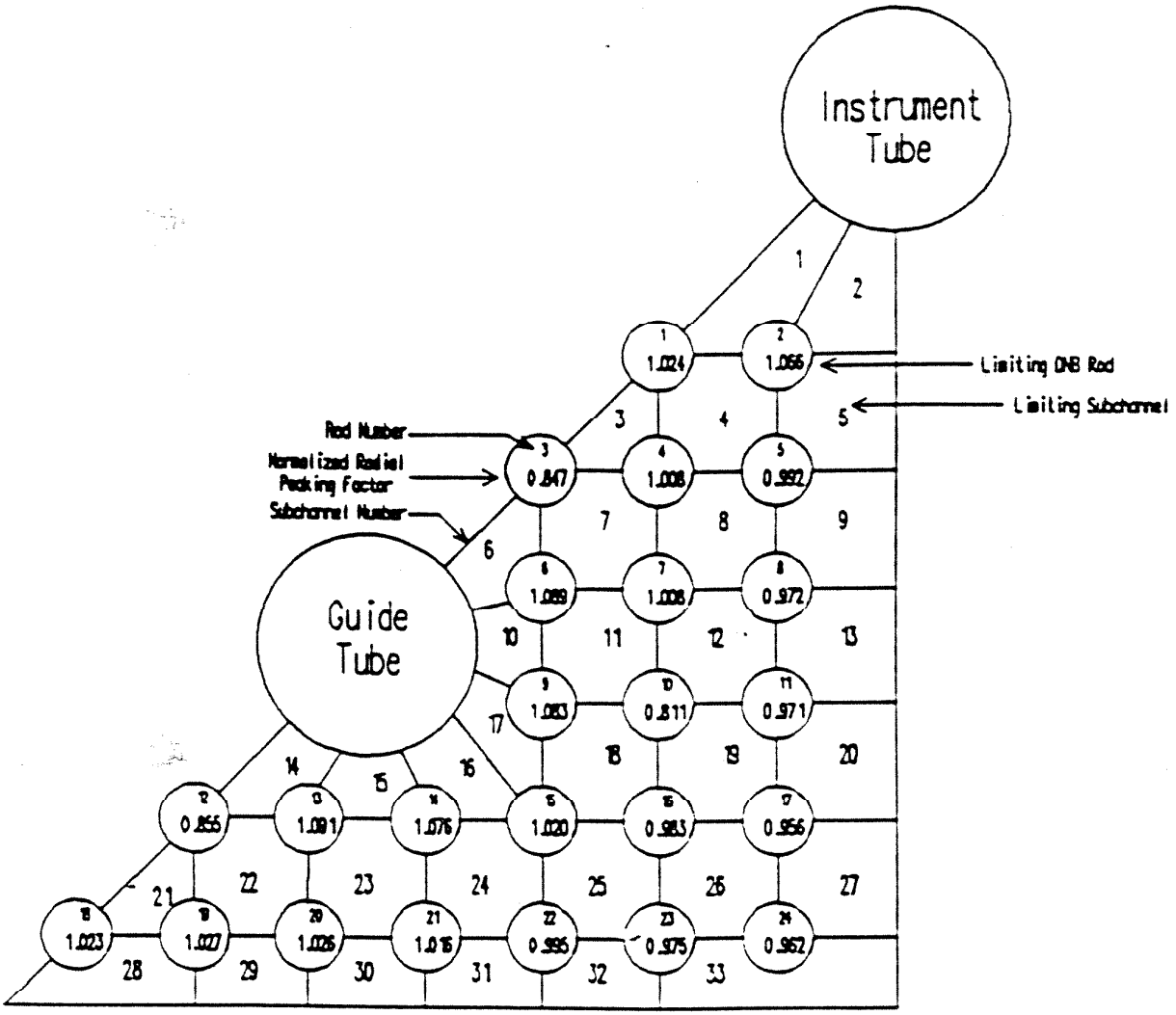

20 GWd/MTU Burnup

FLORIDA POWER & LIGHT COMPANY ST. LUCIE PLANT UNIT 1
ANF 1/8 ASSEMBLY SUBCHANNEL MODEL
FIGURE 4.4-23

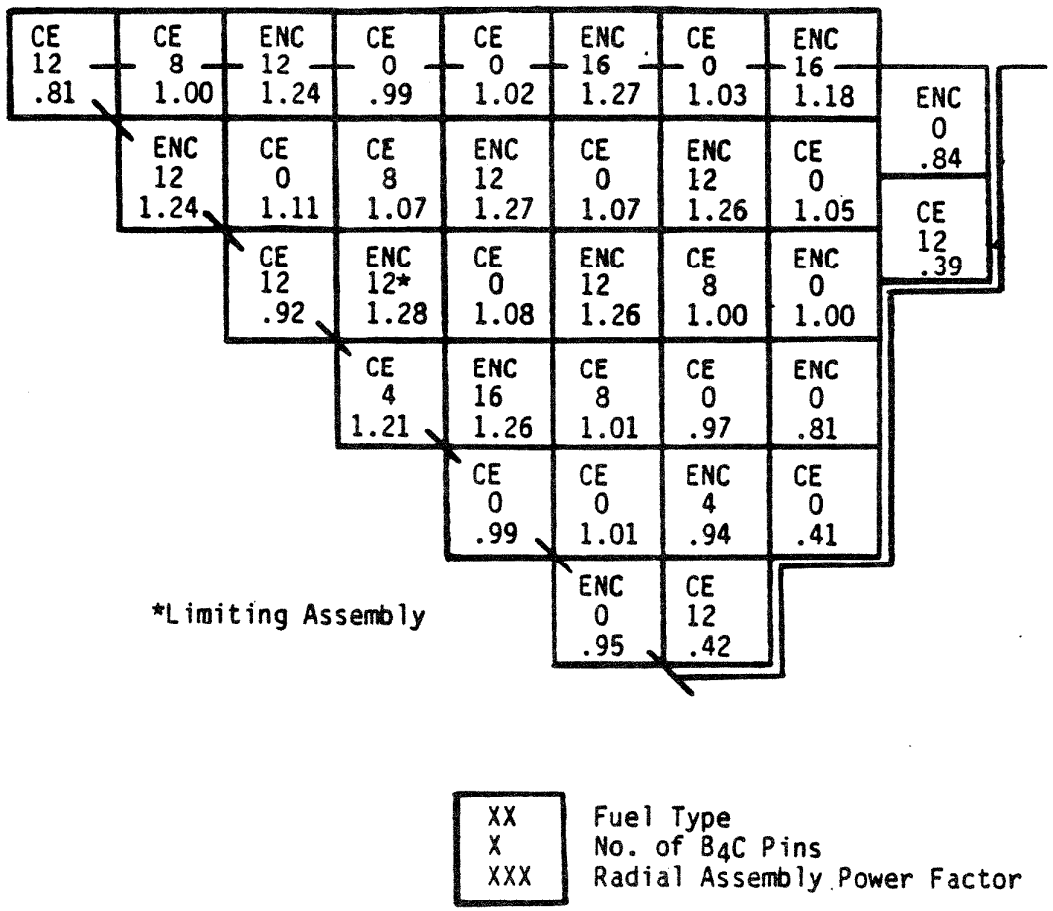

Figure4.4-24Cycle 6 1/8 Core Model
Reload Batches XN-1 and XN-1A

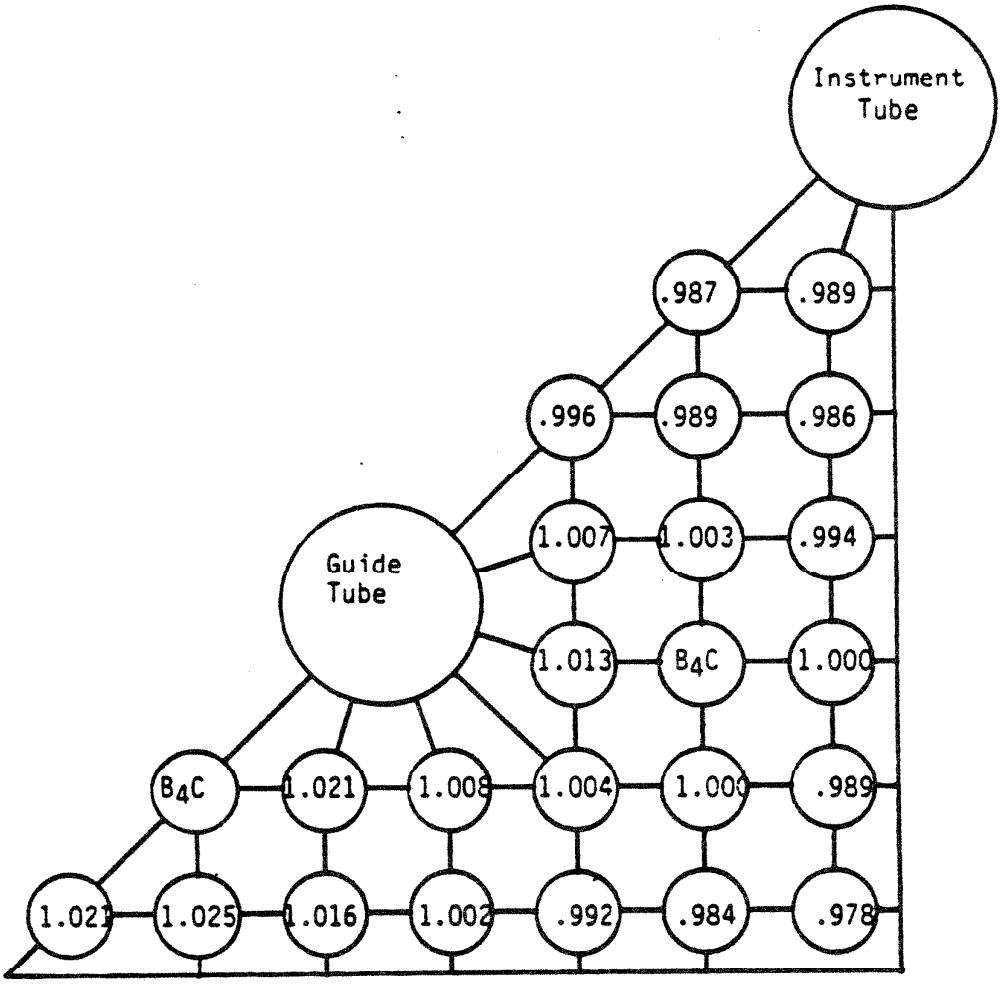

Figure 4.4-25 ENC 1/8 Assembly Subchannel Model

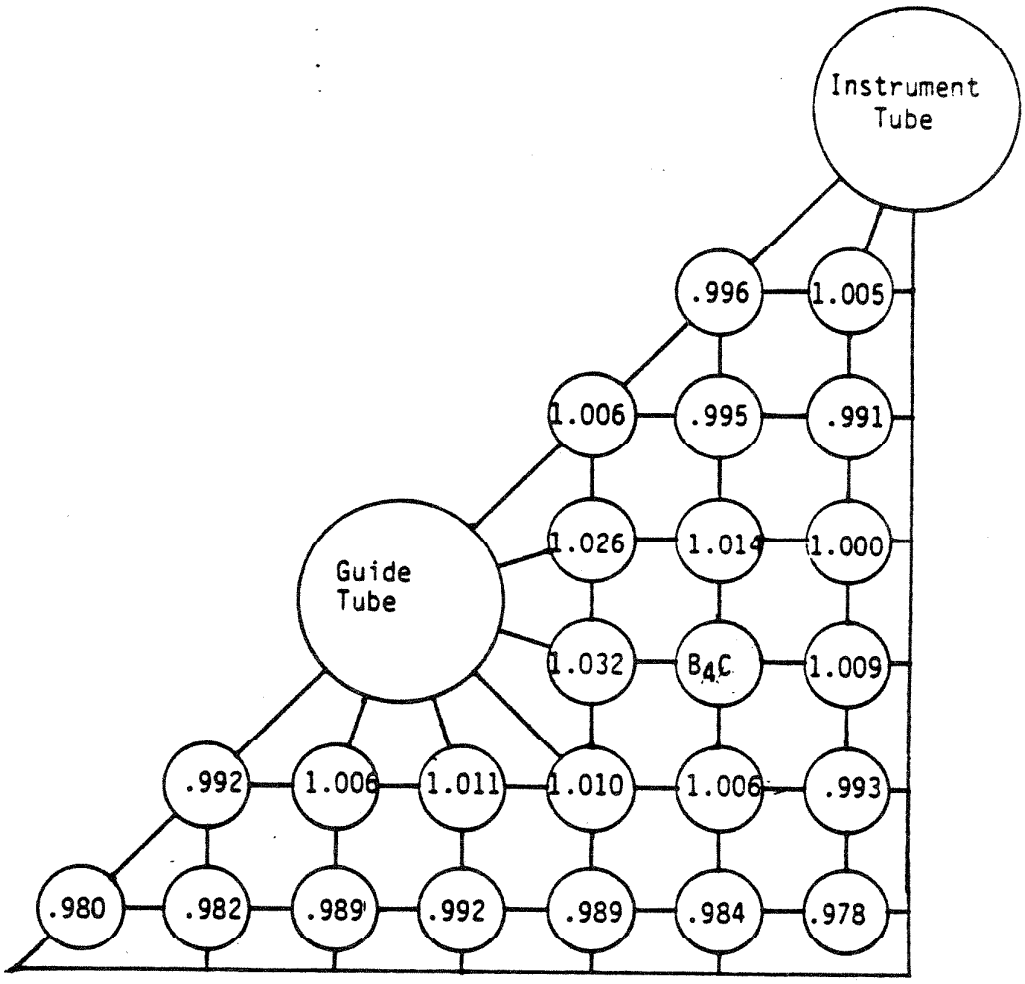

Figure 4.4-26 CE 1/8 Assembly Subchannel Model

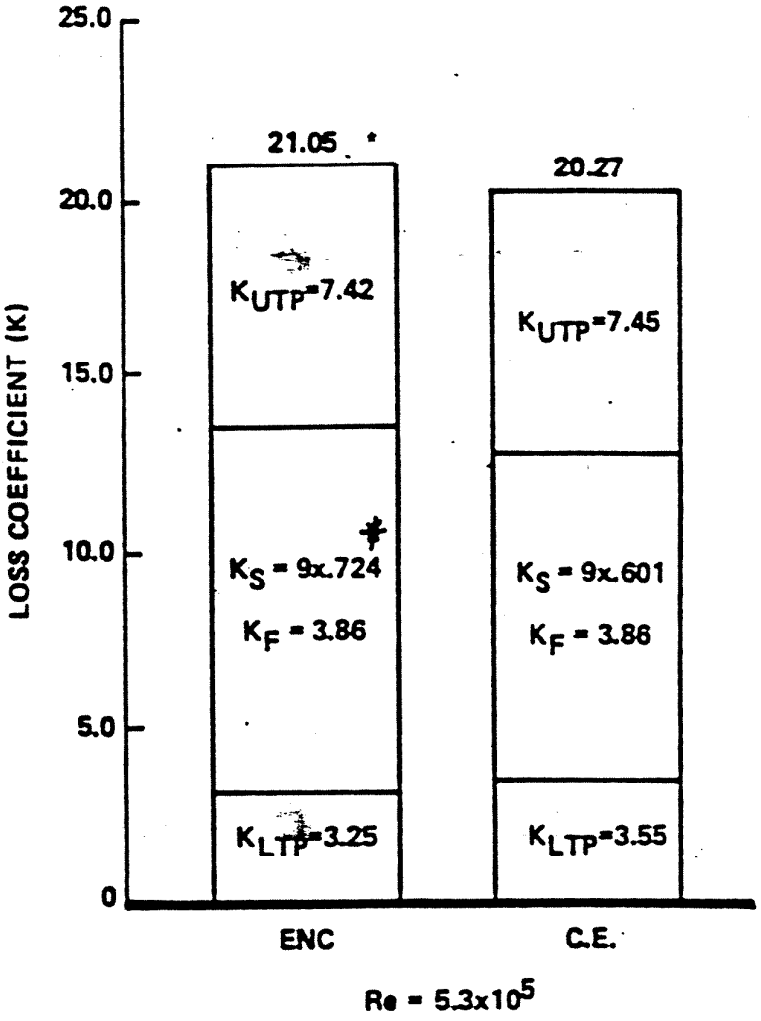

* Loss coefficient for the spacers increased for Cycle 8 due to the spacer redesign. The overall assembly loss coefficient increased by 1.6% to give ~ 21.05 * 1.016 = 21.39

FLORIDA POWER & LIGHT COMPANY
ST. LUCIE PLANT UNIT 1

COMPARISON OF NOMINAL ENC AND CE COMPONENT LOSS COEFFICIENTS

FIGURE 4.4-27

THIS FIGURE HAS BEEN DELETED

Amendment No. 16, (1/98)

FLORIDA POWER & LIGHT COMPANY
ST. LUCIE PLANT UNIT 1

ST. LUCIE UNIT 1, CYCLE 7
NORMALIZED ASSEMBLY
POWER DISTRIBUTION AT 6,000 EFPH,
HFP, ARO

FIGURE 4.4-28

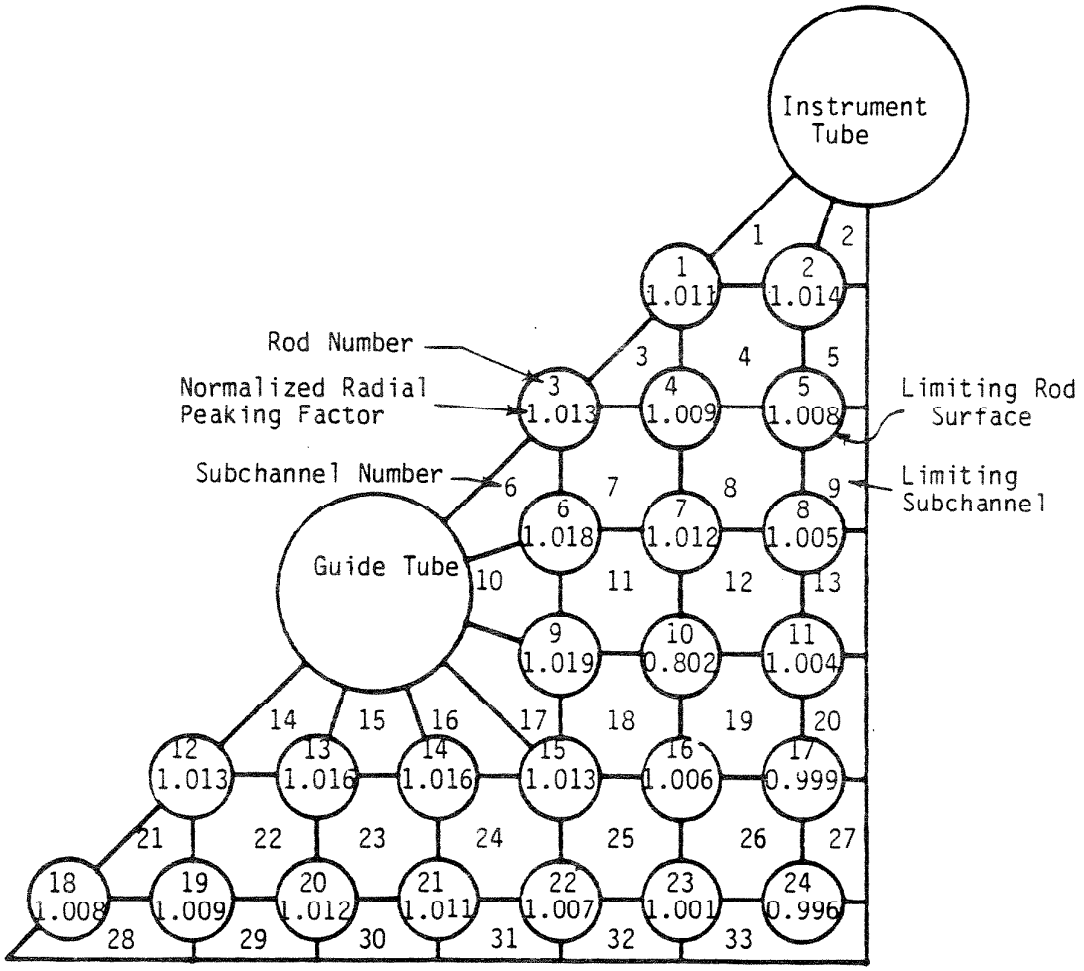

40 GWd/MTU Burnup

AMENDMENT NO. 4 (7/86)

FLORIDA POWER & LIGHT COMPANY
ST. LUCIE PLANT UNIT 1

ENC 1/8 J2 ASSEMBLY SUBCHANNEL MODEL

FIGURE 4.4-29